Physics of Shock Waves and High-Temperature Hydrodynamic Phenomena

Volume II

Physics of Shock Waves and High-Temperature Hydrodynamic Phenomena

BY

Ya. B. Zel'dovich
Astronomical Soviet

Yu. P. Raizer
Institute of Mechanical Problems

Academy of Sciences, U.S.S.R.
Moscow

EDITED BY

Wallace D. Hayes
Department of Aerospace and Mechanical Sciences
Princeton University
Princeton, New Jersey

Ronald F. Probstein
Department of Mechanical Engineering
Massachusetts Institute of Technology
Cambridge, Massachusetts

Volume II

Translated by Scripta Technica, Inc.

ACADEMIC PRESS
New York and London
1967

ACADEMIC PRESS, INC.
111 Fifth Avenue, New York, New York 10003

United Kingdom Edition published by
ACADEMIC PRESS, INC. (LONDON) LTD.
Berkeley Square House, London W.1

LIBRARY OF CONGRESS CATALOG CARD NUMBER: 66-29390

Second Printing, 1968

PRINTED IN THE UNITED STATES OF AMERICA

Editors' foreword

The lack of a comprehensive book on high-temperature physical gasdynamics has been felt for a long time. Since we wrote the first edition of "Hypersonic Flow Theory" we have particularly felt the need for a complementary text covering this field. A few books in the field have appeared, treating some of the pertinent topics. The brilliant text of Zel'dovich and Raizer first appeared early in 1964, and was not only outstanding but completely unique. The revised and updated second edition of this text is presented here in English, shortly after the Russian version. We hope that these two volumes together with the second edition of our own "Hypersonic Flow Theory" will serve to present a comprehensive picture of high-temperature high-speed flows in both their physical and hydrodynamical aspects. Our second edition will be in two volumes, the first on Inviscid Flows already published, and the second on Viscous and Rarefied Flows planned for 1969.

Zel'dovich and Raizer's text is truly comprehensive in the field of high-temperature gasdynamics, dealing thoroughly with all the essential physical aspects and their influence on the dynamics and thermodynamics of continuous media. The authors bring a deep physical insight to bear in explaining the nature of seemingly most complicated phenomena. Mathematical and formal treatments are kept to a minimum, while the results of such treatments are reported and compared with those of simplified approaches. The actual scope of the text is discussed in the authors' prefaces.

The standard approach of the theoretical physicist for many of the subjects treated here is quite formal, and not readily connected in the student's mind with physical ideas. Relatively rare are approaches which are correct in essentials and which are based upon sound physical reasoning from fundamental concepts. It is here that this text excels and is unduplicated. The authors consistently explain the physical phenomena of interest on the simplest correct physical basis, using classical instead of quantum physics where this is possible.

As an inevitable consequence of the comprehensive nature of the text, it is a large one. In the English version we have been forced to split the work

into two volumes. This split is a fairly natural one, however, as the first volume covers primarily the fundamental hydrodynamic, physical, and chemical processes involved; the second volume covers primarily the application and interaction of these processes in a multitude of important problems. However, the two volumes together certainly constitute a fully integrated and interrelated work.

It is truly difficult to qualify the audience to which this work is directed. Our physicist colleagues who have used parts of the book in class have found it exceptionally well adapted to teaching in graduate courses. At the same time, they, like the editors, have learned from the book and have obtained a better appreciation for the subject as a whole. The book is also ideally suited for engineers, presenting for them not only the basis for acquiring the physical understanding they need, but also specific formulas, methods, and experimental results for use in making practical calculations. Thus, without exaggeration, we can say that it is well suited to researchers, engineers, students, and professors. In a word, the authors have succeeded in the aims set forth in their original preface.

The authors are thoroughly acquainted with the world literature, and the references cited are comprehensive. The Soviet journals cited are mostly those now regularly translated into English, so that very few of the references cited in this edition are to be found only in Russian.

The editors are grateful for the close and friendly cooperation of the authors. We have exchanged comments, clarifications, and lists of errata. Some editorial changes have been incorporated with the authors' consent. Where it was thought helpful to indicate a different point of view on a topic, to discuss terminology, or occasionally to amplify a statement, we have added an editors' footnote. Subject and author indexes have been added, covering Volume I at the end of that volume, and covering both volumes at the end of Volume II.

The editors gratefully acknowledge the financial support and assistance of the Advanced Research Projects Agency through a contract technically administered by the Fluid Dynamics Branch of the Office of Naval Research with the Massachusetts Institute of Technology. Without this support the editors would not have been able to carry out this project. For the main part of the translating we are indebted to Scripta Technica, Inc. We wish to thank Miss Margaret Gazan for her skillful handling of the secretarial work and of many editorial details. A number of our colleagues have given us valuable comments and corrections, for which we express our sincere thanks.

We also wish to thank Mezhdunarodnaya Kniga for furnishing us the figures. We express our most sincere appreciation to our publishers for their cooperative attitude in this endeavor.

Our warmest thanks go to the authors for their wholehearted cooperation in this undertaking.

September, 1966

WALLACE D. HAYES
RONALD F. PROBSTEIN

Preface to the English edition

This book considers a large variety of problems of modern physics and engineering, which deal with shock waves, high temperatures and pressures, plasmas, strong explosions, very strong electrical discharges, interaction of intense laser radiation with a medium, etc. We have attempted not only to present the clearest possible interpretation of the physical bases of the phenomena arising in these fields, but also to give practical guidance to those who work with these subjects in science and modern technology.

The content of this book is determined to a large extent by the tastes of the authors. In particular, we have considered in more detail those phenomena and problems which were investigated by us personally. Naturally, more attention has been given to the work of Soviet authors. However, we have attempted to reflect in a sufficiently complete manner the work of American and British scientists, which has led to important advances in the solutions of the problems considered.

The text prepared by us for the English edition is almost identical with that of the second Russian edition, which is to be published in 1966. It contains important additions (and corrections) not contained in the first Russian edition of 1963.

We are very glad that this book has been translated into English and will become accessible to many foreign scientists and engineers. We are grateful to the translators for their work and value most highly the initiative of Professors Hayes and Probstein, who have undertaken the editorship of the translation, have shown great care and thoroughness, and have made a number of valuable comments.

October, 1965

YA. B. ZEL'DOVICH
YU. P. RAIZER

Preface to the first Russian edition

The requirements of modern technology have made it necessary for scientific research to penetrate into the domain of very high values of the state variables, such as with high concentrations of energy, very high temperatures and pressures, and extreme velocities. In practice, such conditions are encountered in strong shock waves, in explosions, in hypersonic flight of bodies in the atmosphere, in very strong electrical discharges, etc.

A great variety of physical and physical-chemical processes can occur in gases at high temperatures: excitation of molecular vibrations, dissociation, chemical reactions, ionization, and radiation of light. These processes affect the thermodynamic properties of gases, while at high velocities and with sufficiently rapid changes in the state of the fluid the rates of these processes also affect the motion of the fluid. Of special importance at very high temperatures are processes related to the emission and absorption of light and radiative heat transfer. The enumerated processes are of interest not only from the point of view of their energetic effect on the motion of the gas, but also frequently lead to changes in the composition of the gas and its electrical properties, to the emission of radiation from the gas and many optical phenomena, etc. An appreciable portion of this book is devoted to the study of all of these problems, comprising the newly-arisen branch of science termed "physical gasdynamics."

Of great scientific and practical interest is the study of strong shocks in solids. Recent achievements, which have permitted the compression of solid bodies by means of shock waves to pressures of millions of atmospheres, have opened new paths for the investigation of solid media at ultra-high pressures. Considerable attention has, therefore, been devoted to these problems in the present book.

Many scientific disciplines are interwoven here, including gasdynamics, shock wave theory, thermodynamics and statistical physics, molecular physics, physical and chemical kinetics, physical chemistry, spectroscopy, the general theory of radiation, the elements of astrophysics, and solid state physics. Many of the physical processes and phenomena considered are of differing character and are not directly related to each other. The result of such diversity in the material is the absence of obvious continuity in the

contents of the book. Certain chapters are quite independent, and deal with completely different areas of physics or mechanics, so that not all chapters are related to each other. Hence, the reader interested in one or another particular topic will find it sufficient to become acquainted only with the corresponding chapters.

In examining the most diverse problems, even those of mathematical character, we endeavored primarily to explain the physical essence of the phenomena using the simplest mathematical tools, frequently resorting to estimates and semiqualitative analysis. At the same time, we attempted to help those physicists, fluid mechanicians, and engineers who work in the corresponding areas of applied physics and engineering, and to supply them with practical tools for independent analysis of many different and complex physical phenomena. For this purpose, the treatment of the majority of the phenomena examined is carried through to specific numerical results, the formulas for the calculation and evaluation of various quantities are presented in a convenient form for practical work, a large amount of useful experimental data and reference material is cited, etc.

The book is of a theoretical character and the description of experimental apparatus and methods is kept to a minimum. However, the presentation and comparison of experimental results with theoretically predicted values has been given an appropriate amount of attention.

The journal literature in "physical gasdynamics" is immense. As far as we know, however, no attempt has been made, either in the Soviet Union or elsewhere in the world, to present a systematic and generalized exposition — in a single book and from a single point of view — of the material in this new area of science. Apparently this book is the first attempt in this direction.

The literature cited in the text reflects the fact that the book was written during 1960 and 1961. However, references to more recent works and brief additions were added in those sections dealing with problems which are being developed at an especially rapid pace. This refers primarily to Chapters V, VI and VII.

The great variety of the phenomena and the large scope of the material forced us to limit the presentation to far from all the problems related to the vast area under consideration. We have not considered the more mathematical aspects of hydrodynamics, nor such problems as that of supersonic flow past bodies. We have only barely touched upon electromagnetic phenomena, and have not dealt at all with thermonuclear fusion, behavior of a plasma in a magnetic field, nor magnetohydrodynamics and magnetogasdynamics, combustion, detonation, etc. A great many books dealing with such problems are already available.

The selection of the material for the book has been to some extent a subjective one. A significant place in the text is devoted to phenomena which were investigated by the authors in their own studies. Thus, the authors' original works have served as a basis for part of the text — almost completely in Chapters VIII and IX, to a considerable extent in Chapters VII, X and XII, and partially in Chapter XI. Chapter I represents a complete revision of an earlier book by one of the authors, "Theory of Shock Waves and Introduction to Gasdynamics," published by the Academy of Sciences of the USSR in 1946.

We should like to express our especial gratitude to A. S. Kompaneets, who is responsible for working out a number of problems dealt with in the book and for many useful criticisms and remarks on the manuscript. We are grateful to L. B. Altshuler and S. B. Kormer for their remarks on the manuscript for Chapter XI, which is based on their work to a large extent. We are also grateful to M. A. El'yashevich who read the manuscript carefully and made valuable comments.

YA. B. ZEL'DOVICH
YU. P. RAIZER

Preface to the second Russian edition

The general structure of the book and the major part of the text in this second edition were retained without change. At the same time, certain chapters were thoroughly revised and a considerable amount of new material was added. Chapter V now contains a part devoted to breakdown (high-intensity ionization) processes and to the heating of gases by a focused laser beam. This is one of the most interesting phenomena connected with the interaction between an intense light beam and a medium. It was discovered experimentally several years ago, shortly after the development of lasers, which produce high pulse intensities measured in tens of megawatts and higher, and immediately attracted the attention of many physicists (including the authors of this book, who have published works on the theory of this phenomenon).

In connection with problems of gas ionization by laser radiation we have added sections to Chapter V in which emission and absorption of light by free electrons on collision with neutral atoms is considered. The lively interest which is now shown toward lasers has induced us to write a special section (in Chapter II) devoted to the semiclassical treatment of induced emission and of the laser effect.

Extensive changes were made in Part 3 of Chapter VI, in which we consider problems of ionization, recombination, and electronic excitation. This part has been virtually rewritten and extensively expanded in order to take into account modern views on these processes. According to these views an important role is played by stepwise ionization of atoms (first excited and then ionized) and electron capture into upper atomic levels through three-body collisions with subsequent deexcitation of the excited atoms through electron impact and radiative transition. Ionization in air has been considered in more detail. The presentation of the closely related problem of ionization of a gas in a shock wave (in Chapter VII) was also changed.

Sections of Chapter VIII, pertaining to the rate of change in the degree of ionization and of the "freezing" accompanying a sudden expansion of an ionized gas into a vacuum have been rewritten. This problem has been recently reexamined with account taken of electron capture into upper

atomic levels as a result of recombination through three-body collisions.

On the basis of material which was contained in the first edition and of more recent results we have added in Chapter XII a part dealing with the propagation of shock waves in an inhomogeneous atmosphere with an exponential density distribution. We have added an appendix wherein are collected certain constants, relations between atomic constants, and relations between units and formulas which are frequently encountered in practice when dealing with the subject matter of this book.

We have here mentioned only the principal, but by far not all of the changes and additions which were made (we also note that mistakes and printing errors which were found in the first edition have been corrected).

Topics of physics and mechanics which were touched upon in the book are developing at an extremely rapid rate, with the consequent discovery of more and more new fields of application (an example of this is the phenomenon of breakdown and heating of gases in the focus of a laser beam).

As an evidence of the interest shown toward these scientific disciplines we cite the fact that immediately after publication of this book, an English translation was undertaken in the United States, and a need for a new edition very soon arose. We hope that this second revised and supplemented edition will be of use to specialists already working in the above fields of science and engineering and to those who are about to enter these fields.

YA. B. ZEL'DOVICH
YU. P. RAIZER

Contents

VIII. Physical and chemical kinetics in hydrodynamic processes

IX. Radiative phenomena in shock waves and in strong explosions in air

Condensed Contents of Volume I

Chapter I

Elements of gasdynamics and the classical theory of shock waves

1. Continuous flow of an inviscid nonconducting gas
2. Shock waves
3. Viscosity and heat conduction in gasdynamics
4. Various problems

Chapter II

Thermal radiation and radiant heat exchange in a medium

Chapter III

Thermodynamic properties of gases at high temperatures

1. Gas of noninteracting particles
2. Gases with Coulomb interactions

Chapter IV

Shock tubes

Chapter V

Absorption and emission of radiation in gases at high temperatures

1. Continuous spectra
2. Atomic line spectra
3. Molecular band spectra
4. Air
5. Breakdown and heating of a gas under the action of a concentrated laser beam

Chapter VI

Rates of relaxation processes in gases

Physics of Shock Waves and High-Temperature Hydrodynamic Phenomena

Volume II

VII. Shock wave structure in gases

§1. Introduction

The basic ideas on shock waves have been presented in Chapter I. It was shown that the hydrodynamic equations for an ideal fluid admit the existence of discontinuous solutions describing shock waves. The flow parameters, i.e., the density, pressure, and velocity on each side of the discontinuity surface, are connected by finite difference equations which correspond to the differential equations describing the continuous flow regions. Both the hydrodynamic and the difference equations are expressions of the general laws of conservation of mass, momentum, and energy. It follows from the conservation laws that the entropy of the fluid also undergoes a jump (increases) at the discontinuity surface. The increase in entropy across a shock wave is determined only by the conditions of conservation of mass, momentum, and energy and by the thermodynamic properties of the fluid, and is entirely independent of the dissipative mechanisms causing this increase.

It is somewhat paradoxical that the adiabatic equations of motion for a fluid admit the existence of surfaces where the entropy undergoes a jump. The irreversibility of a shock compression indicates the presence of dissipative processes, such as viscosity and heat conduction, which lead to the increase in the entropy. It is precisely the viscosity which results in the irreversible conversion into heat of a major part of the kinetic energy of the stream crossing the discontinuity, in a coordinate system in which the discontinuity is at rest. Thus, if we are interested in the mechanism of shock compression, in the internal structure and thickness of the transition layer in which the fluid is transformed from the initial to the final state and which, within the framework of the hydrodynamics of an ideal fluid, is replaced by a mathematical surface, we must turn to a theory which includes a description of the dissipative processes. In Chapter I this problem was considered for the case of weak shock waves. In this chapter we shall not impose any limitations on the strength of the shock.

Usually in hydrodynamic processes changes in the macroscopic parameters in regions of continuous flow occur very slowly in comparison with the rates of the relaxation processes which lead to the establishment of thermodynamic equilibrium. Each gas particle at any instant of time is in the state of thermodynamic equilibrium which corresponds to the slowly changing macroscopic variables, as though the particle "follows" the changes in the variables.

Therefore, when considering shock discontinuities within the framework of the hydrodynamics of an ideal fluid, it is entirely permissible to assume the state of the gas on both sides of the discontinuity to be in equilibrium.

The density, pressure, etc. change very rapidly in the thin transition layer, through which the gas passes from its initial state of thermodynamic equilibrium into its final, also equilibrium, state. The thermodynamic equilibrium inside this region, called here the shock front, can be appreciably disturbed. Therefore, in studying the internal structure of a shock front it is necessary to consider the kinetics of relaxation processes and to investigate in detail the mechanism of the establishment of the final state of thermodynamic equilibrium in the fluid which is attained behind the shock front.

The study of the internal structure of shock fronts is of interest for many reasons. At first this problem attracted attention as purely a theoretical one, the solution of which aided in understanding the physical mechanism of shock compression, as a truly remarkable phenomenon in gasdynamics. Later shock waves were employed in laboratories with the aim of obtaining high temperatures and of studying various processes which take place in gases at high temperatures, as for example, vibrational excitation in molecules, molecular dissociation, chemical reactions, ionization, and radiation (see Chapter IV). Theoretical considerations of the shock front structure enable one to deduce from the experimental data a good deal of valuable information about the rates of these processes. Finally, the study of the structure of very strong shock fronts in which radiation plays an important role helps to clarify the problem of such an important characteristic as the luminosity of the shock front and makes it possible to explain some interesting optical effects observed in strong explosions in air (see Chapter IX).

The mathematical theory of shock front structure is based on the assumption that the structure is steady. The time it takes the fluid in a shock wave to go from the initial to the final state is very short, much shorter than the characteristic times over which the flow variables change in the continuous flow region behind the shock front. In exactly the same way, the front thickness is much less than the characteristic length scale over which the state of the gas behind the front changes significantly, for example, the distance from the shock front to the piston "pushing" the wave (the piston moves with a nonuniform speed, in general). In the short time during which the shock wave traverses a distance of the order of the front thickness, its propagation velocity, pressure, and the other flow variables behind the front remain practically unchanged. However, the kinetics of the internal processes which take place within a shock front propagating through a gas with given initial conditions depend only on the wave strength. Therefore over some relatively long period, each of the gas particles flowing into the shock discontinuity passes through the same sequence of states as the preceding ones. In other

words, the distribution of the various variables across the shock front forms a "frozen" picture which moves during this period as an entity together with the front (Fig. 7.1).

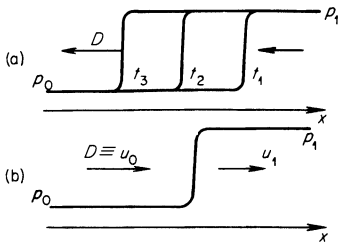

Fig. 7.1. Pressure distributions across a shock wave: (a) propagation of the shock in a laboratory coordinate system; (b) the shock in a coordinate system moving with the front.

If we denote the front velocity by D ($D = |D| > 0$), and the coordinate normal to the front surface at a given point by x, then we can say that all the state variables of the gas inside the wave depend on position and time only in the combination $x + Dt$. In a coordinate system moving with the front the process is steady and is independent of time. This fact (which has already been used in deriving the relationships across the discontinuity) greatly simplifies the study of the problem from a mathematical point of view, since all the flow variables in the coordinate system moving with the wave are functions not of the two variables x and t, but only of a single coordinate, and the process can be described by ordinary differential equations.

In considering the thickness of weak shock fronts in §23 of Chapter I, we have shown that the molecular mean free path serves as a characteristic scale of the shock thickness. As the wave strength increases, the thickness decreases, and when the increase in the pressure behind the front over the initial pressure becomes comparable with the initial pressure, the front thickness is of the order of a molecular mean free path. It is physically clear that the thickness of a strong shock wave, where the compression takes place in the presence of "viscous" forces, is always of the order of a molecular mean free path*. This can be most simply explained by considering a shock wave in a coordinate system in which the gas behind the front is at rest (in a coordinate system moving with the piston) or, equivalently, by considering the bringing

* We wish to emphasize the particular way in which we use the concept of "viscosity" in the case being considered. When referring to viscosity, it is usually understood that the velocity gradients are small and that the velocity changes significantly only over distances much greater than a molecular mean free path. In other words, viscosity in hydrodynamics is a "macroscopic" concept. If a sharp change in gas velocity and density takes place over a distance of the order of a mean free path, then this "microscopic" phenomenon may not be considered from the point of view of hydrodynamics but must be treated on the basis of the kinetic theory of gases. As applied to the case of very large gradients, the term "viscosity" in the shock wave front denotes the mechanism by which the directed velocity of the molecules is changed to a random velocity by molecular collisions.

to rest of a high-velocity gas stream incident on a stationary wall. The kinetic energy of the directed molecular motion (the kinetic energy of hydrodynamic motion) is converted into kinetic energy of random motion, i.e., into heat when the fluid is brought to rest. In order to "brake" the fast molecules, whose directed velocity is much greater than the initial thermal velocity (in the case of a strong wave, with a hypersonic shock speed), several gaskinetic collisions are sufficient, since on the average each collision changes the direction of motion of a molecule through a large angle. Therefore, the directed momentum of the molecules is almost entirely scattered after several collisions and the velocities become random.

The distribution of energy over the various internal degrees of freedom, in particular vibrational excitation of the molecules, dissociation, and ionization, usually requires many collisions. The thickness of the relaxation layer in which the final thermodynamic equilibrium is established is much greater than the thickness of the initial shock wave. Hence the entire transition layer of the shock front can be divided into two regions with appreciably different thicknesses, a very thin "viscous" shock front and an extended relaxation layer.

In a sufficiently strong shock front in which the gas is heated to high temperatures, an important role is played by radiation and radiative heat transfer. The structure of the front in this case becomes even more complex. The total front thickness is determined by the largest scale characterizing the transition process associated with radiant heat exchange, namely the radiation mean free path, which ordinarily is many times greater than the gaskinetic mean free path.

In the following sections we shall consider in detail the characteristic properties of the structure of shock fronts. We start by considering relatively weak shock waves, after which we shall consider increasingly stronger waves.

1. The shock front

§2. Viscous shock front

Since the compression shock in a shock front takes place over distances comparable with the gaskinetic mean free path, we should actually begin our study of shock front structure on the basis of the kinetic theory of gases. As a first step in this direction, however, it is natural to consider the problem in the framework of the hydrodynamics of a real fluid, in which dissipative processes are taken into account, i.e., with viscosity and heat conduction. Here, in contrast to §23 of Chapter I, we do not impose any limitations on the strength

of the shock wave. To provide continuity of presentation we repeat here some conclusions and calculations of that section. In order not to complicate the presentation by unnecessary detail connected with the slow excitation of nontranslational degrees of freedom, we regard the gas as monatomic and neglect ionization.

The one-dimensional flow equations for a viscous and heat conducting gas flow which is steady in a coordinate system moving with the wave front are

$$\begin{aligned} &\frac{d}{dx}\rho u = 0, \\ &\rho u \frac{du}{dx} + \frac{dp}{dx} - \frac{d}{dx}\frac{4}{3}\mu\frac{du}{dx} = 0, \\ &\rho u T \frac{d\Sigma}{dx} = \frac{4}{3}\mu\left(\frac{du}{dx}\right)^2 - \frac{dS}{dx}. \end{aligned} \tag{7.1}$$

Here Σ is the specific entropy*, μ the coefficient of viscosity†, and S is a

* *Editors' note.* The reader is cautioned to note that the symbol S used elsewhere in the book to denote specific entropy is going to be consistently used for energy flux, particularly for radiant energy flux, and therefore a new symbol had to be used for entropy in this chapter.

† For the case considered the concepts of first and second viscosities are indistinguishable.

Editors' note. More specifically, their effects are combined into a single term. As in the analysis of §23, Chapter I, we may include second or bulk viscosity by replacing $\frac{4}{3}\mu$ by the longitudinal coefficient $\mu'' = \frac{4}{3}\mu + \mu'$.

Dilute monatomic gases have $\mu' = 0$, and the usual physical origin of bulk viscosity is in rotational relaxation. As discussed in §2 of Chapter VI, the rotational relaxation time τ_{rot} is extremely short, though it may be appreciably larger than the characteristic translational or gaskinetic collision time of (6.1), Chapter VI.

On the assumptions that τ_{rot} is large compared with τ_{gas} but small compared with a characteristic macroscopic time scale, and that vibrational modes are unexcited, a relation between μ' and τ_{rot} may be established. The quantity $\bar{p}$ of (1.95), Chapter I, is given by $\bar{p} = \rho R T_{\text{trans}}$, while p_{st} is given by $p_{\text{st}} = \rho(\gamma - 1)(c_{\text{trans}} T_{\text{trans}} + c_{\text{rot}} T_{\text{rot}})$, with $c_{\text{trans}} + c_{\text{rot}} = c$ and $(\gamma - 1)c_v = R$. Thus we identify

$$\bar{p} - p_{\text{st}} = \mu' \frac{D\rho}{\rho Dt} = \rho R(T_{\text{trans}} - T_{\text{rot}})\frac{c_{\text{rot}}}{c_v}.$$

With $\tau_{\text{rot}} \gg \tau_{\text{trans}}$ and the rotational mode governed by a relaxation law, we have

$$\frac{DT_{\text{rot}}}{Dt} = \frac{T_{\text{trans}} - T_{\text{rot}}}{\tau_{\text{rot}}}.$$

Finally, with τ_{rot} small in comparison with the macroscopic time scale, we may approximate

$$\frac{DT_{\text{rot}}}{Dt} \approx \frac{DT_{\text{trans}}}{Dt} \approx (\gamma - 1)T_{\text{trans}}\frac{D\rho}{\rho Dt} \approx \frac{(\gamma - 1)^2\varepsilon}{R}\frac{D\rho}{\rho Dt}.$$

nonhydrodynamic energy flux, equal according to the ordinary heat conduction law to

$$S = -\kappa \frac{dT}{dx}, \tag{7.2}$$

where κ is the coefficient of thermal conductivity. To the system of equations (7.1) must be added the boundary conditions expressing the absence of any gradients ahead of and behind the wave front, and also the fact that the flow variables must approach their initial (for $x = -\infty$) and final (for $x = +\infty$) values.

Rewriting the third equation in (7.1) by means of the relation

$$T\, d\Sigma = d\varepsilon + p\, dV = dh - \frac{1}{\rho}\, dp$$

and integrating each equation in (7.1), we obtain the first integrals of the system

$$\begin{aligned} \rho u &= \rho_0 D, \\ p + \rho u^2 - \frac{4}{3}\mu \frac{du}{dx} &= p_0 + \rho_0 D^2, \\ h + \frac{u^2}{2} + \frac{1}{\rho_0 D}\left(S - \frac{4}{3}\mu u \frac{du}{dx}\right) &= h_0 + \frac{D^2}{2}. \end{aligned} \tag{7.3}$$

The constants of integration are expressed here in terms of the initial values of the flow variables, distinguished by the subscript "0" and by the front velocity $D \equiv u_0$.

If we refer the system (7.3) to the final state (denoted by the subscript "1")

Eliminating $T_{\text{trans}} - T_{\text{rot}}$ and $D\rho/Dt$ yields the result

$$\mu' = (\gamma - 1)^2 \rho\varepsilon \frac{c_{\text{rot}}}{c_v} \tau_{\text{rot}}.$$

See Kohler [100].

If τ_{rot} is not much larger than τ_{gas}, the relaxation analysis above does not apply. The relation above then may be considered to indicate correct orders of magnitude. For either diatomic or polyatomic molecules,

$$\frac{\mu'}{\mu} \approx 0.16 \frac{\tau_{\text{rot}}}{\tau_{\text{gas}}}.$$

The quantity τ_{rot} is the relaxation time for a process in which T_{trans} is kept fixed. For a process in which $\varepsilon = c_{\text{trans}} T_{\text{trans}} + c_{\text{rot}} T_{\text{rot}}$ is kept fixed, the relaxation time is $c_{\text{trans}} \tau_{\text{rot}}/c_v$. The distinction between these two definitions of the relaxation time should be kept in mind.

we obtain the already well-known relations across a discontinuity, which we repeat here for convenience

$$\begin{aligned} \rho_1 u_1 &= \rho_0 D, \\ p_1 + \rho_1 u_1^2 &= p_0 + \rho_0 D^2, \\ h_1 + \frac{u_1^2}{2} &= h_0 + \frac{D^2}{2}. \end{aligned} \tag{7.4}$$

It follows from these equations that the entropy jump across a shock wave $\Sigma_1 - \Sigma_0 = \Sigma(p_1, \rho_1) - \Sigma(p_0, \rho_0)$ is entirely independent of both the dissipative mechanisms involved, or in this case of the values of the coefficients of viscosity and thermal conductivity μ and κ. The latter determine only the internal structure of the wave front and its thickness δ. The thickness δ of the viscous shock front is proportional to the coefficients μ and κ, which in turn are proportional to the molecular mean free path l. In the limit $l \to 0$ the hydrodynamics of a real fluid becomes, in the continuous flow regions, the hydrodynamics of an ideal fluid. The shock front in the limit $l \to 0$ becomes a mathematical surface, since $\delta \sim l \to 0$. In this case, the gradients of all the flow variables across the front tend to infinity as $1/l$ but their jumps remain finite.

Specifying the coefficients of viscosity and thermal conductivity and also the thermodynamic relation $h(p, \rho)$ (in a monatomic gas $h = c_p T = \frac{5}{2} p/\rho$), we can numerically integrate the system (7.3) and (7.2) with the given boundary conditions. However, it is much more convenient to have an analytic solution, since it illustrates graphically all the relationships governing the phenomenon. Unfortunately, it is not possible in general to find an analytic solution to the system. The equations can be integrated analytically if we limit ourselves to weak waves and expand the solution in a series with respect to the small change in one of the flow variables. This method was used in §23 of Chapter I for estimating the front thickness (the complete solution is given in the book by Landau and Lifshitz [1]). An exact analytic solution for a wave of arbitrary strength can be found in one special case. This solution, first obtained by Becker [2] and subsequently investigated by Morduchow and Libby [3], describes all of the physical laws governing the structure of a shock front, and is both simple and graphic. Let us describe this solution in more detail.

Usually the transport coefficients in gases, that is, the values of the kinematic viscosity $\nu = \mu/\rho$ and of the thermal diffusivity $\chi = \kappa/c_p\rho$, are close to each other and to the diffusion coefficient $l\bar{v}/3$. Let us set the dimensionless group $Pr = \mu c_p/\kappa = \nu/\chi$, called the Prandtl number, equal to 3/4. In this case the expression in parentheses in the last of equations (7.3) becomes a total

differential of the quantity $h + u^2/2$, and the equation becomes

$$\left(h + \frac{u^2}{2}\right) - \frac{4}{3}\frac{\mu}{\rho_0 D}\frac{d}{dx}\left(h + \frac{u^2}{2}\right) = h_0 + \frac{D^2}{2}.$$

In writing the integral of this linear equation, it is evident that $h + u^2/2$ can be finite at $x = +\infty$ only if it is independent of x,

$$h + \frac{u^2}{2} = h_0 + \frac{D^2}{2}\ *. \tag{7.5}$$

Thus, for a Prandtl number equal to 3/4, (7.5) is satisfied not only behind the shock front (see (7.4)), but also at any intermediate point x.

Equation (7.5) gives a curve in the p, V plane along which the gas changes from the initial to the final state. Noting that for the monatomic gas under consideration $h = \frac{5}{2}pV$, and introducing the dimensionless velocity or specific volume

$$\eta = \frac{u}{D} = \frac{V}{V_0} = \frac{\rho_0}{\rho},$$

we find the equation of this curve is

$$\frac{p}{p_0} = \frac{1 + \frac{1}{3}M^2(1 - \eta^2)}{\eta} = \frac{4\eta_1 - \eta^2}{(4\eta_1 - 1)\eta}. \tag{7.6}$$

Here η_1 refers to the final state behind the shock front

$$\eta_1 = \frac{1}{4} + \frac{5}{4}\frac{p_0}{\rho_0 D^2} = \frac{1}{4} + \frac{3}{4}\frac{1}{M^2}, \tag{7.7}$$

and M is the Mach number $M = D/c_0$, where c_0 is the speed of sound in the initial state ($c_0^2 = \frac{5}{3}p_0V_0$). In deriving (7.6) and (7.7) we have made use of the equations relating the variables on both sides of the shock front. The Hugoniot equation in terms of the variables p_1/p_0 and η_1 is

$$\frac{p_1}{p_0} = \frac{4 - \eta_1}{4\eta_1 - 1}.$$

Figure 7.2 shows the Hugoniot curve and the curve along which the state of a particle changes through the wave (and also the characteristic straight line connecting the initial and the final states).

Using (7.6) and the first two equations of (7.3), let us write a differential equation describing the velocity and specific volume distributions through

* This equation is analogous to the Bernoulli equation in steady flow theory.

the shock front $\eta(x)$

$$\frac{5}{3}\frac{\mu}{\rho_0 D}\eta\frac{d\eta}{dx} = -(1-\eta)(\eta-\eta_1). \tag{7.8}$$

For simplicity, the coefficient of viscosity is assumed to be independent of temperature and equal to $\mu = \rho_0 l_0 \bar{v}_0/3$ (it is independent of density, since

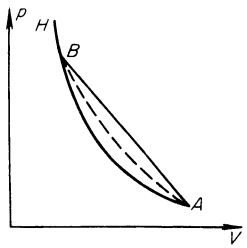

Fig. 7.2. Shock transition $A \to B$ on a p,V diagram. H is the Hugoniot curve. The point describing the state inside the wave front passes from A to B along the dashed line.

$\mu \sim \rho l$, and $l \sim 1/\rho$). The integral of (7.8) contains an additive constant consistent with the arbitrariness in the choice of the coordinate origin. Locating the origin at the point of inflection of the velocity profile (in the "center" of the wave) and using (7.7), we find for $\eta(x)$ the expression

$$\frac{1-\eta}{(\eta-\eta_1)^{\eta_1}} = \frac{1-\sqrt{\eta_1}}{(\sqrt{\eta_1}-\eta_1)^{\eta_1}}\exp\left[a\frac{M^2-1}{M}\frac{x}{l_0}\right] \qquad \left(a = \frac{27}{40}\sqrt{\frac{5\pi}{6}} = 1.1\right). \tag{7.9}$$

Knowing the velocity profile $u = D\eta$, it is easy to determine the distributions of the other variables. Thus, for the temperature we have from (7.5) $T/T_0 = 1 + \frac{1}{3}M^2(1-\eta^2)$; the pressure is defined in terms of η by (7.6) and the entropy is

$$\Sigma - \Sigma_0 = c_p \ln\frac{T}{T_0} - R\ln\frac{p}{p_0} \qquad \left(R = \frac{p}{\rho T}\right).$$

It is evident from (7.9) that as $x \to -\infty$, $\eta \to 1$ and as $x \to +\infty$, $\eta \to \eta_1$, with the initial and final values being approached asymptotically in an exponential manner. All the flow variables velocity, density, pressure, and temperature change monotonically across the wave from their initial to the final values, which are approached asymptotically as $x \to \mp\infty$*. The entropy, on the other hand, does not change monotonically, and has a maximum within the wave (this has already been shown in §23, Chapter I). We can easily satisfy

* The inflection points for the various variables in the wave front do not coincide.

ourselves that this is so by rewriting the entropy equation (the third of equations (7.1)) with the aid of the second law, the "Bernoulli equation" (7.5), and the second of equations (7.1). We find

$$\rho u T \frac{d\Sigma}{dx} = \rho u\left(\frac{dh}{dx} - V\frac{dp}{dx}\right) = \rho u\left(-u\frac{du}{dx} - V\frac{d}{dx}\frac{4}{3}\mu\frac{du}{dx} + V\rho u\frac{du}{dx}\right)$$

$$= -u\frac{d}{dx}\frac{4}{3}\mu\frac{du}{dx} = -\frac{4}{3}\mu u\frac{d^2u}{dx^2}.$$

It is evident that the entropy has an extremum at the inflection point in the velocity, that is, at the wave "center". The existence of an entropy maximum in the wave is connected with the presence of heat conduction. One of the dissipative processes, viscosity, produces only an entropy increase, proportional to $(du/dx)^2$. Heat conduction, however, produces an irreversible transfer of heat from the hotter to colder gas layers. Here the increase in entropy of fluid particles through heat conduction in the colder layers (where $dS/dx \sim -d^2T/dx^2 < 0$) is positive, and in the hotter layers (where $dS/dx \sim -d^2T/dx^2 > 0$) is negative.

The entropy decrease in the more heated layers does not in any way contradict the second law. The entropy of the gas as a whole or of an individual particle increases across the whole shock discontinuity as a result of the process of shock compression. However, an individual layer of gas passing through the wave is no longer an isolated system. Its entropy increases at the beginning, when it is supplied heat through heat conduction and the work of the viscous forces, and then decreases when the heat loss due to heat conduction in the direction of the colder gas layers behind it exceeds the heat supplied by the work of the viscous forces.

The front thickness, as in §23 of Chapter I, is given by

$$\delta = \frac{D - u_1}{(du/dx)_{\max}}.$$

It is evident from (7.9) that the order of magnitude of the front thickness is

$$\delta \sim l_0 \frac{M}{M^2 - 1}.$$

In a weak shock wave when $M - 1 \ll 1$, $\delta \sim l_0/(M-1)$, in agreement with the results presented in §23 of Chapter I. In this case, the front thickness can be equal to many molecular free paths. In the case when $M = 2$, shown in Fig. 7.3, the front thickness is approximately equal to three molecular free paths l_0. In the limiting case of a strong wave, when $M \to \infty$, $\delta \sim l_0/M \to 0$. The statement that the front thickness vanishes as the wave strength increases

should, of course, not be taken literally*. The fact is simply that when the front thickness becomes of the order of a mean free path, the hydrodynamic theory loses its meaning, since it is based on the assumption that the gradients are small, that the mean free path is small in comparison with the distance over which appreciable changes in the flow variables take place. Hence the theory

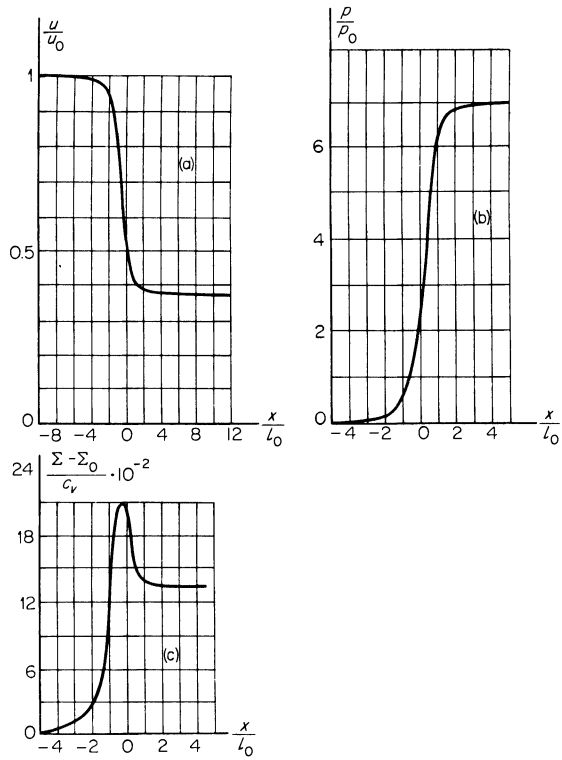

Fig. 7.3. Distributions of (a) velocity, (b) pressure, and (c) entropy through a viscous shock front with Mach number $M = 2$ in a gas with a specific heat ratio $\gamma = 7/5$ and a temperature-independent viscosity coefficient. The abscissa is in units of molecular mean free path in the undisturbed gas (the graphs were taken from [3]).

* *Editors' note.* The result that $\delta \sim l_0/M \to 0$ as $M \to \infty$ is somewhat artificial. It is based on the assumption that μ is constant through the wave. Since $\mu \sim \rho\bar{v}l$ and $\rho_0/\rho_1 \sim 1$, $\bar{v}l$ remains of the same order through the wave. But $\bar{v}_1 \sim M\bar{v}_0$, and $l_1 \sim l_0/M \to 0$ as $M \to \infty$ if l_0 is kept fixed. But $\delta \sim l_1$ in the same limit, and δ remains finite if l_1 does.

The conclusion $\delta \sim l_1$, that the shock front thickness is of the order of a few mean free paths in the flow *behind* the shock, is a general one for strong shocks. Even though the Navier–Stokes equations are invalid for strong shocks, they nevertheless give not only correct order-of-magnitude results, but also quite faithful numerical results for the macroscopic flow variables except in the upstream part of the shock front.

is simply inapplicable for sufficiently strong waves. It is evident physically that the thickness of the shock front for a wave of any strength cannot become smaller than the mean free path, since the gas molecules flowing into the discontinuity must make at least several collisions in order to scatter the directed momentum and to convert the kinetic energy of the directed motion into the kinetic energy of random motion (into heat). At the same time, the thickness of the shock front in the case of a strong wave cannot include many mean free paths, since the molecules of the incident stream lose, on the average, an appreciable fraction of their momentum during each collision.

The problem of the structure of strong shock fronts must be treated on the basis of the kinetic theory of gases, and hence the many numerical studies concerned with the improvement of the simple theory presented above, by taking the dependence of the transport coefficients on temperature into account, by calculating the effect of the Prandtl number on the front structure, and so forth [4–13], do not contribute anything new in principle beyond the particular case considered above, and at best are of interest for the case of weak waves only*.

Tamm [101], and independently Mott-Smith [16], applied the Boltzmann kinetic equation to the problem of the structure of a shock front. An approximate solution to the Boltzmann equation in the neighborhood of the shock front is constructed as a superposition of two Maxwellian distributions corresponding to the temperature and macroscopic velocity in the initial and final states. The relative weight of each function varies over the width of the wave from 0 to 1. The front thickness for an infinite strength shock wave tends to a finite limit. Sakurai [17], who has somewhat refined Mott-Smith's method on the basis of a hard-sphere model for the molecular interactions, obtained shock thicknesses in units of mean free path based on the initial conditions, of† $\delta/l_0 = 2.11$, 1.68, 1.46, and 1.42 for Mach numbers of $M = 2.5$, 4, 10, and ∞, respectively. We note several other papers which have developed

* An attempt to refine the hydrodynamic approximation by taking into account second derivatives in the expressions for the transfer terms (the so-called Burnett approximation), undertaken by Zoller [14], somewhat improves the results for weak waves and, essentially, only points out the limits of applicability of the hydrodynamic theory. For a wave strength $p_1/p_0 = 1.5$, the thickness of the front, according to Zoller, is equal to 17 mean free paths, and for $p_1/p_0 = 4$ is equal to 6 mean free paths. The front thickness of weak shock waves in monatomic gases was measured by Greene, Cowan, and Hornig [15] using a method based on the reflection of light (see §5 of Chapter IV). The thickness was found equal to 30, 19, and 13 mean free paths for Mach numbers $M = 1.1$, 1.5, and 2.5, respectively. Zoller's calculations are in not too bad agreement with these results. See also [56].

† The front thickness δ is defined in the following manner. If f_α and f_β are the molecular distribution functions in the initial and final states, then the distribution function at an intermediate point x in the wave is, according to the theory, $f = \nu(-x)f_\alpha + \nu(x)f_\beta$, where $\nu(x) = \frac{1}{2}(1 + \tanh(2x/\delta))$.

Mott-Smith's method and treated the shock front on the basis of the Boltzmann equation [52–55].

§3. The role of viscosity and heat conduction in the formation of a shock front

Despite the fact that the values of the transport coefficients—kinematic viscosity and thermal diffusivity, or the corresponding dissipative terms in the energy equation—are close to each other, the contribution of each of these dissipative processes to the formation of a shock are far from equal. Physically, it is clear that the principal role in the mechanism of shock compression is played by viscosity rather than heat conduction, since it is the viscous mechanism which causes the scattering of the directed momentum of the incident gas and the conversion of the kinetic energy of the directed molecular motion into the kinetic energy of random motion, i.e., the conversion of mechanical energy into heat. Heat conduction, on the other hand, only indirectly affects the conversion of mechanical energy as a result of the redistribution of pressure. In order to satisfy ourselves of this, it is useful to consider the problem of a one-dimensional steady flow of a gas through a shock front under the assumption that viscosity is completely absent and that the dissipation is caused by heat conduction only. An investigation of this problem (first carried out by Rayleigh [18]) is of considerable interest, since it illustrates the features of the structure of a shock front in the presence of other mechanisms of heat exchange, e.g., radiative heat transfer or electron heat conduction (in a plasma).

By neglecting viscosity, the first integrals in the hydrodynamic equations for one-dimensional steady flow (7.3) take the form

$$\begin{aligned} \rho u &= \rho_0 D, \\ p + \rho u^2 &= p_0 + \rho_0 D^2, \\ h + \frac{u^2}{2} + \frac{S}{\rho_0 D} &= h_0 + \frac{D^2}{2}. \end{aligned} \tag{7.10}$$

It follows from the first two equations of (7.10) that in the process of shock compression, in the absence of viscosity, the state of a gas particle must change continuously along a straight line in the pressure-specific volume diagram

$$p = p_0 + \rho_0 D^2(1 - \eta), \qquad \eta = \frac{V}{V_0}. \tag{7.11}$$

This important property of inviscid gas flow is illustrated in Fig. 7.4, which shows a Hugoniot curve and a straight line connecting the initial and final states of the gas.

We shall attempt to solve the system of equations (7.10) where, as before, we shall eliminate all variables except the dimensionless velocity or relative specific volume η. For generality, we shall not restrict our problem to a

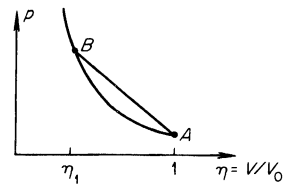

Fig. 7.4. Straight line shock transition for an inviscid gas.

monatomic gas and shall retain an arbitrary constant specific heat ratio. Noting the equation of state

$$p = \frac{\mathscr{R}}{\mu_0}\rho T = R\rho T, \qquad R = \frac{\mathscr{R}}{\mu_0} \tag{7.12}$$

(μ_0 is the molecular weight), and the thermodynamic relation $h = [\gamma/(\gamma-1)]p/\rho$, we express by means of the third equation of (7.10) and (7.11) the nonhydrodynamic energy flux and temperature in terms of η,

$$\frac{T}{T_0} = 1 + \gamma M^2(1-\eta)\left(\eta - \frac{1}{\gamma M^2}\right), \tag{7.13}$$

$$S = -\frac{\rho_0 D^3}{2}\frac{\gamma+1}{\gamma-1}(1-\eta)(\eta-\eta_1). \tag{7.14}$$

Here, as before, the quantity

$$\eta_1 = \frac{\gamma-1}{\gamma+1} + \frac{2}{\gamma+1}\frac{1}{M^2}$$

is the dimensionless velocity in the final state and $M = D/c_0$ is the Mach number.

The function $T(\eta)$ passes through a maximum at the point

$$\eta = \eta_{\max} = \frac{1}{2} + \frac{1}{2\gamma M^2}.$$

Two cases can be encountered in considering shock waves of different strengths. If the shock is sufficiently weak, then $\eta_1 > \eta_{\max}$. Indeed, for a Mach number close to unity ($M - 1 \ll 1$), we find $\eta_1 \approx 1 - [4/(\gamma+1)](M-1)$, so that it is also close to unity, while $\eta_{\max} \approx (\gamma+1)/2\gamma < 1$. In this case, a monotonic compression of the gas from the initial to the final volume (from $\eta = 1$ to $\eta = \eta_1$) results in a monotonic increase in the temperature from the

initial value T_0 to the final value T_1, given (under the assumed conditions) by

$$\frac{T_1}{T_0} = 1 + \frac{2\gamma(\gamma-1)}{(\gamma+1)^2}(M^2-1)\left(1+\frac{1}{\gamma M^2}\right).$$

The curves of $T(\eta)$ and $S(\eta)$ in this case have the shape illustrated in Fig. 7.5.

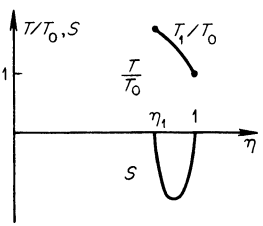

Fig. 7.5. T,η and S,η diagrams for the case when a continuous shock transition with heat conduction only is possible, without considering viscosity.

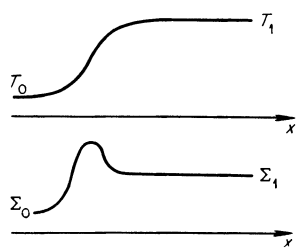

Fig. 7.6. Temperature and entropy distributions in a shock wave with heat conduction only (without viscosity) in the case when a continuous transition is possible.

By eliminating η from (7.13) and (7.14) and substituting (7.2) for S, we obtain a differential equation of the type $dT/dx = f(T)$ which has a continuous solution. The temperature and entropy distributions in such a wave are represented schematically in Fig. 7.6. They are quite similar to the distributions found in the preceding section. It is evident from the entropy equation (7.1) with $\mu = 0$, that the entropy has a maximum at the point where $d(\kappa\, dT/dx)/dx = 0$, or in the case of $\kappa = const$ where the temperature in the wave $T(x)$ has an inflection point, i.e., where $d^2T/dx^2 = 0$. Therefore, a weak shock wave with a continuous distribution of flow variables across the front can also exist in the absence of viscosity, with only heat conduction present.

Let us now consider a sufficiently strong shock wave. In this case the specific volume for which the temperature assumes its maximum value lies between the initial and final values: $\eta_1 < \eta_{max} < 1$. Actually, for $M \gg 1$, $\eta_{max} \approx 1/2$, and $\eta_1 = (\gamma-1)/(\gamma+1) < 1/4$, since the specific heat ratio cannot exceed 5/3. Thus, for a continuous monotonic compression of the gas from its initial to its final volume, the temperature across the wave front must necessarily pass through a maximum. Plots of the functions $T(\eta)$ and $S(\eta)$ for this case are given in Fig. 7.7. Let us investigate the possibility of the existence of a continuous solution of (7.13) and (7.14) in this case. It

can be seen from (7.14) and Fig. 7.7 that the heat flux S caused by heat conduction does not change sign over the entire range in which the relative volume changes from $\eta = 1$ to $\eta = \eta_1$ and it is opposite to the direction of gas flow, i.e., $S < 0$. In accordance with the definition of the flux $S = -\kappa\, dT/dx$, the temperature can only increase as the volume changes from its

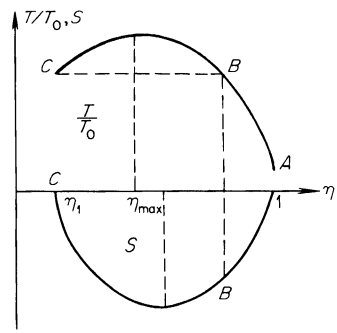

Fig. 7.7. T,η and S,η diagrams for the case of an isothermal jump, taking into account heat conduction alone but without taking viscosity into account.

initial to its final value: $dT/dx > 0$. Consequently, the region behind the temperature maximum, where $dT/d\eta > 0$, is not realized. In this region the specific volume has not yet reached its final value and must decrease, with $d\eta/dx < 0$; the temperature, however, also decreases with decreasing volume, with

$$\frac{dT}{dx} = \frac{dT}{d\eta}\frac{d\eta}{dx} < 0,$$

and the heat flux would have to be directed in the opposite direction ($S > 0$), in contradiction to (7.14).

Thus, a continuous distribution of temperature and density with respect to position is impossible in the case of a strong wave in which only heat con-

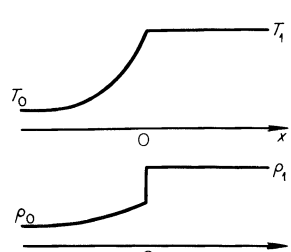

Fig. 7.8. Temperature and density profiles in a shock wave with an isothermal jump.

duction is taken into account. Starting from the initial state, the final state can be reached without passing through the temperature drop region caused by the increased compression only if a discontinuity is allowed in the solution.

In particular, there is a continuous change from the initial state (point A on Fig. 7.7) to point B, and then there is a jump to the final point C. The formation of a density jump indicates that viscous forces must be present, and that a strong discontinuity can disappear only through the action of viscosity but not of heat conduction. The temperature in the jump remains constant, and only its derivative, i.e., the flux, changes. The temperature and density profiles in such a wave, which is called an "isothermal" shock, are shown in Fig. 7.8*.

It is easy to find the largest strength for which a continuous solution in the absence of viscosity is still possible. This strength corresponds to the case in which the maximum of the function $T(\eta)$ coincides with the final state, when $\eta_{\max} = \eta_1$. In this case, the Mach number and the pressure ratio across the front are given by

$$M' = \left(\frac{3\gamma - 1}{\gamma(3 - \gamma)}\right)^{1/2}, \qquad \frac{p_1'}{p_0} = \frac{\gamma + 1}{3 - \gamma}.$$

For example, for $\gamma = 5/3$, $M' = 1.35$ and $p_1'/p_0 = 2$, while for $\gamma = 7/5$, $M' = 1.2$ and $p_1'/p_0 = 1.5$.

If we consider the other limiting case, when there is only viscosity and heat conduction is absent, we obtain a continuous solution for the flow variables across the shock wave which does not differ basically from the solution of the preceding section, with the single exception that the entropy in this case also increases monotonically (see the third equation of (7.1) without the term dS/dx). The behavior of the entropy in both limiting cases can be clarified by considering a p, V or a p, η diagram (Fig. 7.9). In the absence of viscosity

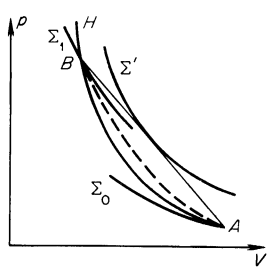

Fig. 7.9. p, V diagram for a shock wave, taking viscosity into account. H is the Hugoniot curve; Σ_0, Σ_1, and Σ' are isentropes; the transition from the initial to the final state takes place along the dashed curve.

the state in the wave changes along the straight line AB and the entropy (as is evident from a comparison of the Hugoniot curve with the isentropes) first

* We note that the "isothermal" character of the shock, i.e., the continuity of temperature across the shock front, is a consequence of the assumption that the heat flux is proportional to the temperature gradient. In the third part of this chapter, in considering radiant heat exchange in a shock front, we shall see that without this assumption the temperature will also have a discontinuity.

increases, reaching a maximum at the point of tangency of the straight line and the isentrope Σ', and then decreases. In the absence of heat conduction the state changes along the dashed curve which passes below the straight line AB (the equation of this curve is $p = p_0 + \rho_0 D^2(1 - \eta) + \frac{4}{3}\mu\, du/dx$, where $du/dx < 0$), and it is nowhere tangent to the isentropes. The situation here is completely analogous to that which exists in the weak waves considered in §23 of Chapter I.

§4. Diffusion in a binary gas mixture

The presence of gradients in the thermodynamic quantities of a gas mixture gives rise to diffusional fluxes in the components of the mixture, which results in a redistribution of their concentrations. In general, diffusion tends to equalize the spatial concentrations of the components. However, the existence of pressure and temperature gradients or of an external force field such as gravity, centrifugal forces in rotating mixtures, or the presence of an acceleration results in component separation in an initially homogeneous mixture. In particular, such a situation arises in a shock wave propagating through a gas mixture. The concentrations of the components behind and ahead of the front are uniform and constant in space. In the region of the front, where gradients are present, these concentrations change. As with viscosity and heat conduction, diffusion represents an irreversible molecular mass transfer of a specific component (viscosity is responsible for momentum transfer and heat conduction for internal energy transfer) and is one of the sources for the dissipation of mechanical energy.

The diffusional flux is defined as follows. Let the mass concentration of one of the components in a binary gas mixture, for example, of the light component whose molecular mass is m_1, be equal to α. The concentration of the second, heavy component whose molecular mass is $m_2 (m_2 > m_1)$ is $1 - \alpha$*. As a result of the diffusion of one gas with respect to the other the gases have different macroscopic velocities, which we denote by $\mathbf{u}_1$ and $\mathbf{u}_2$. If ρ is the density of the mixture, then the total flux of the first component is $\rho\alpha\mathbf{u}_1$, and the flux of the second component is $\rho(1 - \alpha)\mathbf{u}_2$. The macroscopic or hydrodynamic velocity of the mixture $\mathbf{u}$ is defined in such a way that the total mass flux of the gas is equal to $\rho\mathbf{u}$ ($\mathbf{u}$ is the momentum per unit mass). Thus, $\rho\mathbf{u} = \rho\alpha\mathbf{u}_1 + \rho(1 - \alpha)\mathbf{u}_2$ or $\mathbf{u} = \alpha\mathbf{u}_1 + (1 - \alpha)\mathbf{u}_2$. Within the framework of the

* The mass concentration α is equal to the mass of the first, light component, per unit mass of the mixture. If the number of molecules per unit mass of mixture is N_1 and N_2 ($N_1 + N_2 = N$), then $\alpha = N_1 m_1$ and $1 - \alpha = N_2 m_2$. The molar concentrations are

$$\frac{N_1}{N} = \frac{\alpha}{Nm_1}, \qquad \frac{N_2}{N} = \frac{1 - \alpha}{Nm_2}.$$

hydrodynamics of an ideal fluid (without diffusion), the velocities of both components of the mixture are the same and equal to $\mathbf{u}$. The fluxes of the components are equal to $\rho\alpha\mathbf{u}$ and $\rho(1-\alpha)\mathbf{u}$.

In the next approximation there appear in the hydrodynamic theory viscosity, heat conduction, and diffusion (in the mixture). The diffusional flux $\mathbf{i}$ refers to the difference between the total and the hydrodynamic fluxes of one component, say the first component, $\mathbf{i} = \rho\alpha\mathbf{u}_1 - \rho\alpha\mathbf{u} = \rho\alpha(\mathbf{u}_1 - \mathbf{u})$. The total flux of the first component is equal to the sum of the hydrodynamic and diffusional fluxes $\rho\alpha\mathbf{u} + \mathbf{i}$. The total flux of the second component is, obviously, $\rho(1-\alpha)\mathbf{u}_2 = \rho(1-\alpha)\mathbf{u} + \rho(1-\alpha)(\mathbf{u}_2 - \mathbf{u}) = \rho(1-\alpha)\mathbf{u} - \mathbf{i}$. The diffusional fluxes of the two components in a binary mixture are of the same magnitude but of opposite direction.

As pointed out above, diffusion arises as a result of the presence of concentration, pressure, and temperature gradients in a gas*. In the one-dimensional case the gradients are simply equal to derivatives with respect to x, and the vector $\mathbf{i}$ has only an x component which will be denoted simply by i. The diffusional flux is given by (see [1])

$$i = -\rho D\left(\frac{d\alpha}{dx} + \frac{k_p}{p}\frac{dp}{dx} + \frac{k_T}{T}\frac{dT}{dx}\right). \tag{7.15}$$

Here D is the diffusion coefficient, k_pD is the pressure diffusion coefficient, and k_TD is the thermal diffusion coefficient. The dimensionless quantity k_p is determined only by the thermodynamic properties of the mixture and is given by (see [1]†)

$$k_p = (m_2 - m_1)\,\alpha(1-\alpha)\left(\frac{1-\alpha}{m^2} + \frac{\alpha}{m_1}\right)^{\ddagger}. \tag{7.16}$$

For $m_2 > m_1$, $k_p > 0$ and the pressure diffusional flux of the light component is in the direction of decreasing concentration. The flux caused by the concentration gradient is also in the direction of decreasing concentration (for either component). The thermal diffusional flux of the light component for

* The state of a binary mixture is characterized by three thermodynamic variables: the concentration and any two of the usual variables such as temperature, pressure, and density. In studying diffusion, it is convenient to choose pressure and temperature as the independent variables.

† In the absence of viscous momentum transfer (see below).

‡ The quantity k_p is most simply derived by considering an equilibrium binary mixture in a gravity field at constant temperature. In equilibrium the molecular number densities n_1 and n_2, from the Boltzmann equation, are expressed in proportional form as $n \sim \exp(-m_1gx/kT)$, and $n_2 \sim \exp(-m_2gx/kT)$, where g is the acceleration of gravity and x is the altitude. Since the equilibrium diffusional flux is equal to zero, $d\alpha/dx + (k_p/p)\,dp/dx = 0$. Using the relationship between the concentration α and the particle number densities n_1 and n_2 and noting that $p = (n_1 + n_2)kT$, we find the above equation for k_p.

most mixtures is in the direction of increasing temperature (for $m_2 > m_1$, $k_T < 0$).

In contrast to k_p, the thermal diffusion ratio k_T depends not only on the component concentrations (for $\alpha = 0$ or 1, $k_T = 0$) and the molecular masses, but also on the law governing the molecular interactions. The quantity k_p is determined purely by the thermodynamic properties of the gas, since thermodynamic equilibrium is possible even in the presence of a pressure gradient in an external force field. If a temperature gradient is also present, then the gas is no longer in a state of equilibrium. If only repulsive forces varying as $1/r^n$ are acting between the molecules, then for $n > 5$, which is usually the case, $k_T < 0$: the light gas will diffuse in the direction of increasing temperature. For $n < 5$, which is rarely encountered, the light gas diffuses in the direction of decreasing temperature (the case of $n < 5$ includes the Coulomb law for the interaction of charged particles, for which $n = 2$). When $n = 5$ thermal diffusion is absent and $k_T = 0$. Usually, when the relative gradients $\nabla p/p$ and $\nabla T/T$ are comparable, the importance of thermal diffusion is small in comparison with pressure diffusion. For further details on thermal diffusion see [19]. With the diffusional flux is connected an additional irreversible energy flux $\mathbf{q}$, which is proportional to the diffusional flux $\mathbf{i}$ (see [1]).

Zhdanov, Kagan, and Sazykin [19a] have introduced an important correction to the classical diffusion concepts presented above. These authors derived an expression for the diffusional flux from the kinetic equation, using the Grad "thirteen moment" method. This method of approximation has a number of advantages over the Chapman–Enskog method used to obtain (7.15), whenever it is necessary to take into account higher approximations in the expansion of the distribution function. It is found that equation (7.15) for the diffusional flux is valid only in the absence of viscous momentum transfer in the gas. Under conditions when viscous momentum transfer is present (that is, when there is a velocity gradient) equation (7.15) must also include terms proportional to the viscous forces. In spite of the fact that these forces are determined by second-order derivatives of macroscopic quantities (such as velocity), they can be of the same order as terms proportional to first-order derivatives such as the term with pressure gradient. For example, in the case of a purely viscous steady flow without acceleration, the pressure gradient is simply balanced by the viscous forces. In the case of unsteady flow, the inclusion of viscous forces in the expression for the diffusional flux actually introduces into this expression terms proportional to the accelerations of the gas.

In the case of purely viscous flow, the replacement of the viscous force by the pressure gradient which balances it results in a change in the pressure diffusion constant k_p in comparison with its purely thermodynamic value (7.16). The pressure diffusion constant is no longer a thermodynamic quantity

in a viscous flow; it depends on the character of the molecular interaction. The pressure diffusion constant under some conditions can become negative (in the case when the molecular weights of the components differ very slightly from each other and when the molecular cross sections are appreciably different). When viscous momentum transfer is taken into account, the thermal diffusion ratio k_T also changes.

§5. Diffusion in a shock wave propagating through a binary mixture

Let us consider what happens when a shock wave is propagated through a binary gas mixture. Large gradients in the thermodynamic quantities are present in the shock front and, as a result, conditions for diffusion are favorable. Physically, it is clear that the light component will concentrate in the shock front. Indeed, in the heated gas behind the shock front the molecules of the light component have a higher thermal velocity than the molecules of the heavy component ($\bar{v} \sim (T/m)^{1/2}$). Therefore, the light molecules "pull ahead" and leave the heavy molecules slightly behind (in the laboratory coordinate system, where the original mixture is at rest).

Let the heavy gas have a small admixture of the light gas. Then the density distributions of both the heavy and light gases (ρ_2 and ρ_1) in a strong shock wave have the form shown in Fig. 7.10. This figure also shows the concentration distribution of the light component $\alpha = \rho_1/(\rho_2 + \rho_1)$. The thickness of the

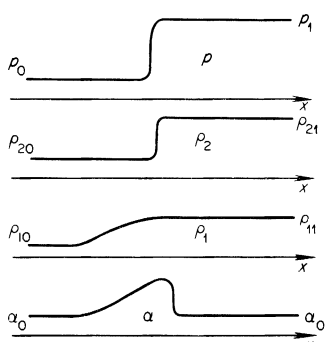

Fig. 7.10. Pressure and density distributions of the heavy (ρ_2) and light (ρ_1) components and concentration of the light component (α) in a shock wave propagating through a binary gas mixture.

region containing the higher concentration of the light component is of the order of $\Delta x \sim D/u_0$, where D is the diffusion coefficient and u_0 here denotes the shock velocity*. The diffusion coefficient D is of the order of $l\bar{v}_1$, where

* This follows from the condition that the total flux of the light component is steady in a coordinate system moving with the front. Approximately $\rho_1 u_0 \sim D\, d\rho_1/dx$, from which $\rho_1 = \rho_{11} \exp(-u_0|x|/D)$. Here we have used an approximate boundary condition according to which we can assume that the density of the light component at the point $x = 0$, where the viscous shock front is located, is equal to its final value ρ_{11}.

$\bar{v}_1$ is the thermal speed of the light gas heated by the shock wave and l is the molecular mean free path. The velocity of the front u_0 is of the order of the thermal speed of the heated heavy gas, $u_0 \sim \bar{v}_2$. But $\bar{v}_1/\bar{v}_2 \approx (m_2/m_1)^{1/2}$, so that $\Delta x \approx (m_2/m_1)^{1/2} l$. The thickness of the viscous shock front is of the order of l. Consequently, the thickness of the region in which the light component is concentrated is greater by a factor of $(m_2/m_1)^{1/2}$ than the thickness of the shock front. The components are most sharply separated when the particle masses are appreciably different ($m_2/m_1 \gg 1$).

This effect would be most pronounced in the case of a plasma, owing to the very large difference between the electron and ion masses. In a plasma, however, an important role is played by the electrostatic interaction between the electrons and ions, which strongly limits the diffusion process (for a discussion of this see §13).

Together with viscosity and heat conduction, diffusion affects the structure of a shock front. To describe this structure we must set up the equations for the planar steady flow case, in a manner similar to that of §2 for treating the viscous shock front. The equations for the conservation of mass and momentum and the first two equations of (7.3) remain unchanged (μ is now understood to represent the coefficient of viscosity of the mixture). To the equation of conservation of energy (the last equation of (7.3)), we must add the molecular heat flux resulting from diffusion and replace the molecular flux due to heat conduction S by the sum $S + q$. The system of equations will now include the diffusional flux i (to which the heat flux q is proportional), and the system will contain a new unknown function, the concentration α. Therefore an additional equation must be added to the system. This is the equation of continuity (conservation of mass) for one of the components (the existence of an equation of continuity for the entire mass of gas automatically ensures the conservation of the second component). The condition of constancy of mass flux of the light component in the planar steady flow case is

$$\rho\alpha u + i = const = \rho_0\alpha_0 u_0$$

(the diffusional flux disappears ahead of the wave). The general equation of continuity for one of the components [1] is

$$\frac{\partial \rho\alpha}{\partial t} + \nabla \cdot (\rho\alpha \mathbf{u} + \mathbf{i}) = 0.$$

It is evident then that behind the wave, where the diffusional flux also vanishes, the concentration is equal to its initial value $\alpha_1 = \alpha_0$ (since $\rho_1 u_1 = \rho_0 u_0$).

The system of equations for one-dimensional steady flow in a binary mixture can be solved, in principle, in the same manner as for a single-component gas (see §2). The solution will yield a distribution of all quantities in the wave front. This problem was considered by D'yakov [20] for the case of a weak

shock, when it is possible to expand all quantities in powers of a small parameter (see §23, Chapter I)*. As was shown in §§18 and 23 of Chapter I, if we regard the pressure change in a weak shock $\Delta p = p_1 - p_0$ as a first-order quantity, then the volume and temperature changes will also be first-order quantities. The total entropy change in the transition from the initial to the final state $\Sigma_1 - \Sigma_0$ is a third-order quantity and the entropy change inside the wave front, let us say, $\Sigma_{max} - \Sigma_0$ is a second-order quantity. The thickness of the shock wave front is of the order of $\Delta x \approx l p_0/\Delta p$, where l is the molecular mean free path. From the conservation equation for one of the components, which can be rewritten as

$$\alpha - \alpha_0 = -\frac{i}{\rho_0 u_0},$$

and from the expression for the diffusional flux, it is evident that the changes in concentration in the wave $\Delta\alpha$ and the flux i are second-order quantities, with

$$\alpha - \alpha_0 \sim i \sim \frac{dp}{dx} \sim \frac{\Delta p}{\Delta x} \sim (\Delta p)^2.$$

Consequently, the term containing the concentration gradient in the expression for the diffusional flux can be neglected ($d\alpha/dx \sim \Delta\alpha/\Delta x \sim (\Delta p)^3$, while $dp/dx \sim (\Delta p)^2$).

D'yakov [20] obtained an analytic solution for the concentration distribution in the front of a weak shock wave. This solution will not be given here (the distribution has the form shown in Fig. 7.11), but we shall estimate the

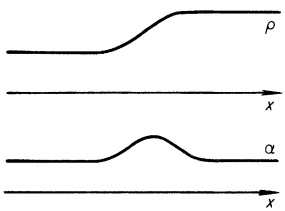

Fig. 7.11. Density and concentration distributions in a weak shock propagating through a binary gas mixture.

order of magnitude of the change in concentration. If we neglect thermal diffusion, which normally plays a less important role than pressure diffusion (since the value of k_T is usually lower than that of k_p), then we may write

$$\Delta\alpha = \alpha - \alpha_0 \sim \frac{|i|}{\rho_0 u_0} \sim \frac{D}{u_0}\frac{k_p}{p}\frac{\Delta p}{\Delta x}.$$

* For another treatment of this problem (including a numerical integration for shocks of arbitrary strength, *eds.*) see also the article by Sherman [21].

The diffusion coefficient $D \sim l\bar{v}$, where the thermal speed of the molecule $\bar{v}$ is of the order of the speed of sound, that is, of the order of u_0. Noting that $\Delta x \sim (p/\Delta p)l$, we find $\Delta\alpha \sim k_p(\Delta p/p)^2$. The excess amount of the light component collected by the shock wave (per unit area of front surface) is of the order of

$$M = \rho \int_{-\infty}^{\infty} (\alpha - \alpha_0)\, dx \sim \rho\, \Delta\alpha \cdot \Delta x \sim \rho k_p \frac{\Delta p}{p}\, l.$$

In a sufficiently strong shock, where $\Delta p \sim p$, we have $\Delta\alpha \sim k_p$, $M \sim \rho k_p l$. If the difference between the molecular masses is comparatively large ($k_p \sim (m_2 - m_1)$), then the change in concentration in a strong wave is of the order of the concentration itself and the excess mass of one component is of the order of the mass of the component itself in a layer of thickness of a molecular mean free path.

We have noted above that diffusion, like viscosity and heat conduction, results in the dissipation of mechanical energy and in an increase in the entropy of the gas (for a discussion of this point see [1])*. We know that with dissipative processes excluded, in the framework of the hydrodynamics of an ideal fluid a shock wave is represented as a mathematical discontinuity. The discontinuity vanishes and becomes a layer of finite thickness with a continuous distribution of flow variables only if dissipative processes are considered. Here heat conduction by itself can ensure a continuous transition in the shock wave only in the case when the wave strength is not too great (see §3). It is interesting to consider whether a dissipation of diffusional origin, without taking into account viscosity or heat conduction, can ensure a continuous transition in a shock wave propagating through a binary mixture. This question was investigated by Cowling [22] (neglecting thermal diffusion). It was found that, as in the case when there is only heat conduction, a continuous solution is possible only for shock strengths below a certain limit which depends on the difference between the molecular masses and the concentration of the components. In the limiting cases, when the concentration of one of the components tends to zero ($\alpha \to 0$ or $\alpha \to 1$), that is, when the gas becomes a single-component fluid, or when the relative difference of the masses tends to zero, the upper limit of the allowable shock strength also tends to zero. When the difference between the molecular masses is large and the numbers of molecules of both species are comparable, diffusion provides a continuous transition up to quite high shock strengths, being more effective

* Like heat conduction, diffusion can also cause a local entropy decrease (see §2). Diffusion does, however, increase the entropy of the entire system as a whole, and of a particle taken over the transition from the initial to the final state in a shock wave. Unlike heat conduction and diffusion, viscosity can only cause a local increase of entropy, and can only result in an increase in the entropy of a particle.

in this respect than heat conduction. Thus, for example, in a mixture of hydrogen and oxygen ($m_1/m_2 = 1/8$) with a 10% molar concentration of oxygen (N_2/N), a continuous compression of the mixture by a shock is possible up to a density ratio of 4.78 (the limiting density ratio for $\gamma = 7/5$ of 6 was used in the calculations). Heat conduction alone can provide a continuous compression to a density ratio of no more than $(3\gamma - 1)/(\gamma + 1) = 4/3$.

2. *The relaxation layer*

§6. Shock waves in a gas with slow excitation of some degrees of freedom

Often the excitation of certain degrees of freedom of a gas* requires many molecular collisions, with the necessary number of collisions (or the relaxation times) appreciably different for different degrees of freedom. The time required to establish complete thermodynamic equilibrium in a shock front and, consequently, the front thickness, is determined by the slowest of the relaxation processes. Here, of course, we should consider only those processes which result in the excitation of degrees of freedom which make an appreciable contribution to the specific heat for finite values of the flow variables. If τ_{max} is the longest relaxation time, and u_1 is the gas velocity behind the front with respect to the front, then the front thickness is of the order of $\Delta x \sim u_1 \tau_{max} = D(\rho_0/\rho_1)\tau_{max}$†.

The translational degrees of freedom of a particle are those which are "excited" most rapidly. Therefore the mechanical energy of a gas flowing into a discontinuity is primarily converted into thermal energy of translational motion of the gas atoms and molecules. As shown in §2, the thickness of a viscous shock front for strong shocks is of the order of one or several gaskinetic mean free paths. At room temperatures molecular rotations are also rapidly excited as a result of a small number of collisions, while vibrations are ordinarily unimportant at these temperatures. Consequently, the front thickness for weak shocks propagating through a molecular gas heated to room temperature is of the order of several gaskinetic mean free paths‡.

At temperatures of the order of 1000°K, when kT is comparable with the energy $h\nu_{vib}$ of the vibrational quanta of molecules, excitation of the vibrational modes requires many thousands and sometimes tens and hundreds of thousands of collisions. The thickness of a shock front of corresponding

* Let us recall that for the sake of brevity we include within the term "degree of freedom" also the potential energy of dissociation, of chemical reactions, and of ionization.

† In what follows, we shall continue to denote the shock front velocity by D.

‡ Exceptions are molecular hydrogen and deuterium, which require hundreds of gaskinetic collisions for rotational excitation (see §2, Chapter VI).

strength is determined by the relaxation time of the vibrational degrees of freedom.

The rates of relaxation processes always increase rapidly with increasing temperature; thus, for example, at temperatures of the order of 8000°K, when $kT \gg h\nu_{\text{vib}}$, several collisions are sufficient for the excitation of the vibrational modes. Those processes which took place rather slowly for certain shock strengths and which determined the front thickness become rapid in a strong wave and are replaced by other processes. For example, in a diatomic gas at temperatures of the order of 4000–8000°K, the establishment of thermodynamic equilibrium is delayed principally by the slow molecular dissociation (the vibrational modes are excited comparatively fast and ionization is not yet important). At temperatures of the order of 20,000°K a small number of collisions is sufficient to dissociate the molecules, and the front thickness is determined by the rate for single ionization (double ionization is still unimportant). At $T \sim 50{,}000$°K single ionization is replaced by double, and so forth.

Obviously, the limit of the temperature region in which one or another relaxation process is slow is not clearly defined. In exactly the same manner, the front thickness at a given temperature is not always determined by only one of the processes. However, as an approximation for a shock wave of a given strength it is always possible to subdivide the excitation processes for the different degrees of freedom which make significant contributions to the heat capacity into rapid and slow processes. Here the term rapid is understood to refer to processes whose relaxation times τ_{rel} are comparable with the gaskinetic relaxation times and for which the characteristic lengths $\Delta x = u_1 \tau_{\text{rel}}$ are of the order of a moderate number of gaskinetic mean free paths and thus are comparable with the thickness of the viscous shock front. It follows that slow refers to those processes which require a very large number of gaskinetic collisions.

The problem of the structure of a shock front in a gas with slow excitation of part of the specific heat was first analyzed by one of the present authors in 1946 [23, 24] using a reversible chemical reaction and excitation of molecular vibrations as examples.

Let us consider qualitatively the process of shock compression in a gas with slow excitation of some of the degrees of freedom. We shall not as yet specify the kinds of degrees of freedom and we divide them only into two categories: those which are excited rapidly and those which require many gaskinetic collisions. The principal dissipative processes—viscosity and heat conduction—play a role only in the region where there are large gradients of the flow variables, in the region where the rapidly relaxing degrees of freedom are excited. This region coincides to a certain degree with the viscous shock front region. In the slow relaxation region, extending over a distance of many

gaskinetic mean free paths, the gradients are small and this dissipation can be neglected.

We shall not consider the structure of the narrow region in which the rapid processes take place. In principle, it does not differ from the structure of the viscous shock front treated in §2. The increase in specific heat due to the rapid excitation of the nontranslational degrees of freedom introduces only some quantitative changes in the structure of the viscous front without changing the basic qualitative relations. Since the thickness of this region is not large, of the order of several mean free paths, we can consider it approximately as infinitesimally thin and relate the quantities on both sides of it by conservation equations which are in all respects similar to equations (7.4). In what follows, for the sake of definiteness, we shall term the region of rapid relaxation the "compression shock" to differentiate it from the concept of the "shock wave front" which includes the entire transitional region from the initial to final thermodynamic equilibrium state.

Denoting the flow variables directly behind the compression shock by a prime, we can write the equations defining these quantities

$$\rho' u' = \rho_0 D; \qquad p' + \rho' u'^2 = p_0 + \rho_0 D^2; \qquad h' + \frac{u'^2}{2} = h_0 + \frac{D^2}{2}.$$

The enthalpy $h' = h'(p', \rho') = h'(T', \rho')$ includes only the rapidly excited degrees of freedom of the gas (with the slowly excited degrees of freedom frozen at the state ahead of the shock, *eds.*). The extended region of slow relaxation is described by integrals of the one-dimensional steady flow equations of the type (7.3), in which the dissipation terms can be neglected. Considering ρ, p, ε, h, and u as functions of the coordinate x, we can write the integrals of the equations in this region as

$$\begin{gathered} \rho u = \rho_0 D = \rho' u', \\ p + \rho u^2 = p_0 + \rho_0 D^2 = p' + \rho' u'^2, \\ h + \frac{u^2}{2} = h_0 + \frac{D^2}{2} = h' + \frac{u'^2}{2}. \end{gathered} \tag{7.17}$$

It is convenient to place the coordinate origin $x = 0$ on the "infinitesimally thin" compression shock. In exactly the same manner, if we follow the change of state of a given particle passing through the shock front with respect to time, then it is convenient to let $t = 0$ be the time of rapid compression in the compression shock. The boundary or initial conditions for the flow variables $\rho(x)$, $u(x)$ have the form $\rho(0) = \rho'$, $u(0) = u'$, and so forth. When $x \to +\infty$ we have as before $\rho(\infty) = \rho_1$, $u(\infty) = u_1$, and so forth.

Shown on the p, V diagram of Fig. 7.12 are two Hugoniot curves originating

from a point A corresponding to the initial state of the gas. One of them (II) corresponds to complete thermodynamic equilibrium, that is, it corresponds to the final state of the gas behind the shock front. The other curve (I)

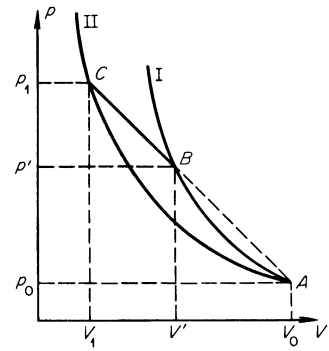

Fig. 7.12. p, V diagram for a shock propagating through a gas with slow excitation of some of the degrees of freedom.

corresponds to the excitation of only the rapidly relaxing degrees of freedom and to the "frozen" state of slowly relaxing degrees of freedom. In calculating curve I the specific internal energy of the slowly excited degrees of freedom is taken to be the same as in the initial state, in spite of the fact that the density and pressure of the gas change. As may be seen from the figure, curve I is steeper than curve II. Indeed, at the same density, the temperature and pressure are greater when some of the degrees of freedom are frozen, since, roughly speaking, the same compression energy is distributed among a smaller number of degrees of freedom*.

Let us draw a straight line AC, connecting the initial and final states of the gas. As is well known, the slope of this line determines the propagation velocity of the shock wave through the undisturbed gas D. It follows from the first two equations of (7.17) that the state of the gas particles in the relaxation region changes along this straight line:

$$p = p_0 + \rho_0 D^2\left(1 - \frac{V}{V_0}\right) = p' + \rho' u'^2\left(1 - \frac{V}{V'}\right). \tag{7.18}$$

Thus, the point describing the successive states of a gas particle for a given front velocity jumps from the initial state $A(p_0, V_0)$ to the intermediate state $B(p', V')$ behind the compression shock and then moves to the final state $C(p_1, V_1)$ along the straight line (7.18). In this case the pressure and density ratio increase as the final state is approached and the gas velocity relative to

* In this case, numerical calculations show that the increase in the number of particles due to dissociation or ionization cannot compensate for the temperature decrease caused by the expenditure of energy in dissociation and ionization at constant volume. Therefore, the pressure in case II is still lower than in case I.

the front decreases. In the case of a wave so weak that its velocity is smaller than the speed of sound corresponding to the frozen degrees of freedom, the straight line AC passes below the tangent to the Hugoniot curve I at point A (Fig. 7.13). In this case, the state changes continuously along the straight line AC from point A to point C, and the gas experiences from the very beginning a gradual excitation of the lagging part of the specific heat.

It is evident from (7.18) that the pressure in the relaxation region of a strong shock increases by only a small amount. Indeed, even if in the rapid compression zone only the translational degrees of freedom are excited, so that

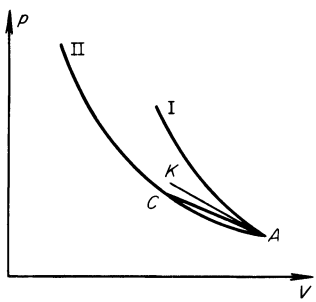

Fig. 7.13. p, V diagram for a weak shock propagating through a gas with slow excitation of some of the degrees of freedom. AK is the tangent to the Hugoniot curve I at the point A.

$V'/V_0 = 1/4$, then the pressure in the relaxation layer can increase by not more than 25% of its final value, since the quantity $1 - V/V_0$ to which the pressure change $p - p_0$ is proportional lies in the range $1 > 1 - V_1/V_0 > 1 - V'/V_0 \geqslant 3/4$. If, however, other degrees of freedom are also rapidly excited, then $V'/V_0 < 1/4$ and the pressure change in the relaxation region is even smaller. The enthalpy increase in the relaxation region is extremely small. It follows from the third and first equations of (7.17) that

$$h = h_0 + \frac{D^2}{2}\left(1 - \frac{V^2}{V_0^2}\right). \tag{7.19}$$

The quantity $(V'/V_0)^2 < 1/16$ for a strong shock, so that the enthalpy increase in the relaxation region does not in any case exceed 5–6%. Since the specific enthalpy is almost constant in the relaxation region and the specific heats increase as the previously frozen degrees of freedom are excited, the temperature in this region will decrease. The temperature decrease can be appreciable if the lagging part of the specific heat is large and makes a large contribution to the final specific heat of the gas. The final temperature T_1 can be one half or one third as much as the temperature T' behind the compression shock. In exactly the same manner, the gas density can also increase appreciably (roughly speaking, $p \sim \rho T$; p changes slightly and T changes appreciably). The profiles of p, ρ, u, and T in a shock front propagating through a gas with slow excitation of part of the specific heat are shown

schematically in Fig. 7.14. For specific calculations of the distributions, the rate equations for the corresponding relaxation processes must be used. This will be done for several cases in the following sections.

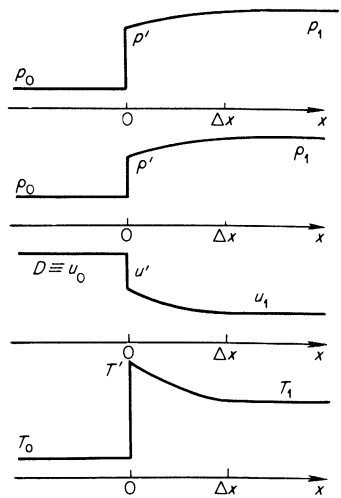

Fig. 7.14. Pressure, density, velocity, and temperature profiles in a shock front propagating through a gas with slow excitation of some of the degrees of freedom; $\Delta x \approx u\tau_{rel}$ is the front thickness.

We note that if the shock wave is generated by a piston moving with a constant velocity u, then the velocity with which the gas moves behind the compression shock relative to the undisturbed gas $D - u'$ is not the same as the piston velocity (it is lower); only the relative velocity of the gas in the final state behind the wave front, $D - u_1$, is the same as the piston velocity.

§7. Excitation of molecular vibrations

At temperatures of the order of 1000–3000°K (depending on the type of molecule) behind the shock front, molecular dissociation is very small and the contribution made by the chemical energy to the internal energy of the gas may be neglected. In this case the front thickens basically as a result of the slow vibrational excitation of the molecules. Molecular rotations at these temperatures are excited very rapidly, in only a few collisions, so that the rotational energy at each point of the wave front is in equilibrium and corresponds to the "translational" temperature of the gas.

We shall consider a diatomic gas composed of molecules of the same species initially heated to room temperature of the order of $T_0 \approx 300$°K. At this temperature the vibrational energy is extremely small and the specific heat ratio is equal to 7/5. The flow variables behind the compression shock can be calculated from the ordinary equations for a perfect gas with constant specific heats, corresponding to the participation of only the translational

and rotational degrees of freedom of the molecules, with a specific heat ratio of $\gamma' = 7/5$. We shall write these equations, characterizing the strength of the shock wave by the Mach number ($M = D/c_0$; $c_0^2 = \frac{7}{5}p_0V_0$), as is conventional in laboratory studies:

$$\frac{\rho'}{\rho_0} = \frac{6}{1 + 5M^{-2}},$$

$$\frac{p'}{p_0} = \frac{7}{6}M^2 - \frac{1}{6},$$

$$\frac{T'}{T_0} = \frac{1}{36}(7 - M^{-2})(M^2 + 5).$$

The flow variables in the final state behind the shock front can be calculated from the general relations at the front by specifying the functions $h_1(T_1)$ or $\varepsilon_1(T_1)$, taking into account the vibrational energy.

In general, the final values of the flow variables are not expressed by simple equations, since the vibrational energy in the region where quantum effects must be considered is a complicated function of temperature (see (3.19)). If we consider sufficiently strong shock waves with temperatures behind the front greater than the energy of vibrational quanta divided by the Boltzmann constant ($T_1 > h\nu/k$), then the vibrational energy per molecule is equal to its classical value kT and $\varepsilon = [1/(\gamma - 1)]p/\rho$, where the specific heat ratio $\gamma = 9/7$. In this limiting case $\varepsilon_1 = \frac{7}{2}p_1V_1$ and the Hugoniot relation takes the simple form*

$$\frac{p_1}{p_0} = \frac{6 - V_1/V_0}{8V_1/V_0 - 1} \quad \text{or} \quad \frac{V_1}{V_0} = \frac{p_1/p_0 + 6}{8p_1/p_0 + 1}. \tag{7.20}$$

From the general relation (1.67) it follows that

$$\frac{7}{5}M^2 = \frac{p_1/p_0 - 1}{1 - V_1/V_0}. \tag{7.21}$$

One can also easily express p_1/p_0, as well as V_1/V_0 and $T_1/T_0 = p_1V_1/p_0V_0$ in terms of the Mach number M. It should be noted that the region of applicability of the above simple equation for the Hugoniot of a diatomic gas is very limited. If $T_1 < h\nu/k$, then the vibrational energy is not equal to kT, while at temperatures appreciably greater than $h\nu/k$, molecular dissociation becomes important.

As an example, let us consider a shock wave at a Mach number $M = 7$ in oxygen with an initial temperature $T = 300°\text{K}$. If the initial pressure is

* We emphasize that these equations are not the same as the equations for a gas with the constant specific heat ratio $\gamma = 9/7$, since in the initial state $\gamma = 7/5$ and $\varepsilon_0 = \frac{5}{2}p_0V_0$.

atmospheric and the speed of sound $c_0 = 350$ m/sec, then the shock velocity $D = 2.45$ km/sec. The flow variables behind the compression shock are $\rho'/\rho_0 = 5.45$, $p'/p_0 = 57$, $T'/T_0 = 10.5$, $T' = 3150°\text{K}$. The parameters in the final state behind the shock front are $\rho_1/\rho_0 = 7.3$, $p_1/p_0 = 60$, $T_1/T_0 = 8.2$, and $T_1 = 2460°\text{K}$. The value of $h\nu/k$ for oxygen is $2230°\text{K}$; since T_1 is slightly larger than this value it is possible to use the simple equation for calculating T_1 (dissociation of oxygen at this temperature and not too low a density is sufficiently small that it can be neglected).

Let us find the distribution of the flow variables in the relaxation region and estimate its thickness. The specific internal energy of the gas at any point x consists of the energy of the translational and rotational degrees of freedom, equal to $\frac{5}{2}RT$, with T the "translational" temperature at the point x and R the gas constant per gram, and of the nonequilibrium vibrational energy which will be denoted by ε_{vib}: thus, $\varepsilon = \frac{5}{2}RT + \varepsilon_{\text{vib}}$. As was pointed out above, the specific enthalpy remains practically constant in the relaxation region (in our numerical example the change amounts to only 1 %), and hence

$$h = \tfrac{7}{2}RT + \varepsilon_{\text{vib}} \approx const \approx h_1 \approx h'.$$

This equation relates the nonequilibrium vibrational energy to the temperature at the point x. Directly behind the compression shock the vibrational modes are not excited (in the initial state at $T = T_0 \approx 300°\text{K}$ the vibrational energy is very small), so that at the point $x = 0$ behind the compression shock $\varepsilon_{\text{vib}} = 0$. Behind this point a gradual excitation of the vibrational modes takes place, ε_{vib} increases, and the temperature decreases from T' to the final value T_1, at which value the vibrational energy attains its equilibrium value corresponding to this temperature.

The temperature distribution with respect to x may be found from the rate equation for vibrational excitation (6.9):

$$\frac{D\varepsilon_{\text{vib}}}{Dt} = \frac{\varepsilon_{\text{vib}}(T) - \varepsilon_{\text{vib}}}{\tau_{\text{vib}}}.$$

Here $\varepsilon_{\text{vib}}(T)$ is the equilibrium vibrational energy corresponding to the translational temperature T, and τ_{vib} is the relaxation time. Let us for simplicity consider only strong shocks where the temperature is sufficiently high and the equilibrium vibrational energy is expressed by the classical formula $\varepsilon_{\text{vib}}(T) = RT$. In this case $\varepsilon_{\text{vib}} = h_1 - \frac{7}{2}RT = \frac{9}{2}RT_1 - \frac{7}{2}RT$. Substituting these expressions into the rate equation and replacing the material derivative with respect to time by a derivative with respect to position by taking into account the fact that the process is steady, $D/Dt = \partial/\partial t + u\,\partial/\partial x = u\,d/dx$, we obtain the equation

$$\frac{dT}{dx} = \frac{9}{7}\frac{T_1 - T}{u\tau_{\text{vib}}}.$$

The relaxation time τ_{vib} depends on the temperature and density (or pressure). This dependence can be approximately described by (6.19), which was derived in §4 of Chapter VI, namely

$$\tau_{vib} \approx \frac{const}{\rho} e^{const/T^{1/3}}.$$

In order to make these considerations physically clearer we shall assume that $u\tau_{vib}$ is approximately constant in the relaxation region and corresponds to some average temperature and density between T' and T_1 and ρ' and ρ_1 ($u = D\rho_0/\rho$). This approximation is meaningful since the temperature and density changes are not large. In our numerical example, the temperature changes by a factor of 1.28, $T^{1/3}$ by a factor of 1.08, and the density and the velocity change by a factor of 1.34. Integrating the temperature equation with the initial condition $T = T'$ at $x = 0$, and noting that since $h' = h_1$, $T' = \frac{9}{7}T_1$, we obtain the temperature distribution

$$T = T_1\left(1 + \frac{2}{7} e^{-9x/7u\tau_{vib}}\right) = T'\left(\frac{7}{9} + \frac{2}{9} e^{-9x/7u\tau_{vib}}\right).$$

Recalling that the pressure is almost constant ($p \sim \rho T \approx const$), and that the temperature variation is also not too rapid, we find the approximate density distribution

$$\rho = \rho_1 - (\rho_1 - \rho') e^{-9x/7u\tau_{vib}} = \rho' + (\rho_1 - \rho')(1 - e^{-9x/7u\tau_{vib}}). \quad (7.22)$$

Thus, as $x \to \infty$ the temperature and density asymptotically approach their final values T_1 and ρ_1, and the effective thickness of the relaxation region and of the shock front is approximately given by

$$\Delta x = \tfrac{7}{9} u\tau_{vib}. \quad (7.23)$$

Equations (7.22) and (7.23) can serve for an experimental determination of the vibrational relaxation time. Ordinarily for this purpose, interferometric methods are used to measure the density distribution behind the compression shock and the thickness of the shock front (see Chapter IV). To extract from the experiment better data than can be obtained using the above simple theory one can refine the simple theory by taking into account the quantum dependence of the vibrational energy on temperature, the change in velocity $u = u(x)$, etc. Of course, all of these refinements do not change either the qualitative picture of the distributions or the order of magnitude of the front thickness.

The theory presented above can also be extended to vibrational relaxation in polyatomic molecules if the strength of the shock wave is such that only the

lowest-frequency vibrational mode is excited*. Calculations and measurements for CO_2 and N_2O may be found in [25]. Table 7.1 gives several values of shock front thicknesses in oxygen and nitrogen as determined by vibrational relaxation (from the experiments of Blackman [26]). These data are reduced to

Table 7.1

SHOCK FRONT THICKNESS IN OXYGEN AND NITROGEN WITH VIBRATIONAL RELAXATION [26]

M	D, km/sec	T_1°	ρ_1/ρ_0	$\tau_{vib} \cdot 10^6$, sec	Δx, cm
			Oxygen		
5.95	2.08	2000	6.3	5	0.165
8.0	2.8	3300	7.1	0.8	0.031
			Nitrogen		
7.42	2.43	3000	6.55	30	1.11
9.97	3.26	5000	7.14	5	0.23

correspond to a pressure behind the front $p_1 = 1$ atm ($\Delta x \sim \tau_{vib} \sim 1/p_1$), and an initial temperature $T_0 = 296°K$.

The most detailed summary of all theoretical work devoted to the calculation of the structure of the vibrational relaxation region in a shock front is to be found in the review by Blythe [57]. This paper considers a large variety of approximate solutions and also presents the results of exact solutions obtained with the aid of digital computers (see also [58]). We also note several experimental papers which describe studies of the vibrational relaxation in a shock front and determine the corresponding relaxation times and rates of vibrational excitation. Oxygen was studied in [59, 60], nitric oxide in [61], carbon monoxide in [62], and carbon dioxide in [63, 64]. A detailed survey of the experiments relating to this problem along with numerous references is given in the book of Stupochenko, Losev, and Osipov [90].

§8. Dissociation of diatomic molecules

At temperatures of the order of 3000–7000°K behind a shock front in a diatomic gas there is still no ionization, molecular vibrations are excited relatively quickly, and the thickness of the wave front is connected with the slowest relaxation process—molecular dissociation. Estimates show that the

* In the case of nonlinear polyatomic molecules the numerical coefficient 9/7 in (7.21) and (7.22) must be replaced by 5/4, corresponding to the different rotational specific heat ($\frac{3}{2}k$ per molecule instead of k).

vibrational relaxation time in the above temperature range is approximately an order of magnitude less than the time required for establishing dissociative equilibrium. Approximately, therefore, one may take the vibrational, as well as the rotational, energies at each point of the relaxation region to have their equilibrium values. The flow variables behind the compression shock correspond to an intermediate value of the specific heat ratio $\gamma' = 9/7$ (the vibrations at such high temperatures are completely "classical"). They can be calculated from (7.20) and (7.21).

Appreciable dissociation appears only in sufficiently strong shocks, where the density ratio across the compression shock is close to its limiting value of 8 corresponding to the specific heat ratio of $\gamma = 9/7$ (we assume that the shock wave propagates through a gas at room temperature $T \approx 300°\text{K}$). In this case (7.20) and (7.21) simplify to give, approximately,

$$\frac{\rho'}{\rho_0} = 8, \qquad \frac{p'}{p_0} = \frac{49}{40} M^2, \qquad \frac{T'}{T_0} = \frac{49}{320} M^2,$$

where M is the Mach number (defined with $\gamma = 7/5$ ahead of the shock, *eds.*). The flow variables behind the shock front, with dissociation taken into account, cannot be expressed by simple formulas (see §9, Chapter III); they are calculated from the general relationships at the shock front.

Let us find the distribution of the flow variables in the relaxation region. The specific internal energy of the gas taking dissociation into account is (see (3.21))

$$\varepsilon = \frac{7}{2}(1-\alpha)RT + 2\alpha\frac{3}{2}RT + \alpha U = \left(\frac{7}{2} - \frac{\alpha}{2}\right)RT + \alpha U,$$

where U is the dissociation energy per unit mass of gas and α is the degree of dissociation (which may be out of equilibrium). Since the density ratio just behind the compression shock is already very large (almost 8), the pressure change in the relaxation region is small and the enthalpy change is negligibly small. From this it follows that

$$p = R(1+\alpha)\rho T \approx const = p' = R\rho' T', \tag{7.24}$$

$$h = \left(\frac{9}{2} + \frac{\alpha}{2}\right)RT + \alpha U \approx const = h' = \frac{9}{2}RT'. \tag{7.25}$$

These equations allow us to express the density and degree of dissociation at a point x of the wave in terms of the temperature, or the temperature and density in terms of the degree of dissociation. Thus, for example, neglecting α ($\alpha < 1$) in comparison with 9, we find from (7.25) that

$$\alpha = \frac{9}{2}\frac{R}{U}(T' - T) = \frac{9}{2}\frac{T' - T}{T_{\text{dis}}}, \tag{7.26}$$

where $T_{dis} = U/R$ (for example, for oxygen $T_{dis} = 59{,}400°K$). There is still no dissociation at the point $x = 0$ behind the compression shock: $\alpha = 0$ and $T = T'$. Beyond that point dissociation begins; the degree of dissociation increases and the temperature decreases on account of the energy lost in dissociation. This process continues until dissociative equilibrium corresponding to the gas temperature is attained.

To find the distribution of the flow variables with respect to x we shall use the rate equation for dissociation (see §5, Chapter VI). We shall consider here shock waves which are not very strong, in which the degree of dissociation reached behind the front is small, i.e., $\alpha_1 \ll 1$. In this case we can neglect molecular dissociation due to collisions with atoms and retain in the rate equation (6.21) only those terms which correspond to dissociation as a result of collisions with molecules and recombination of atoms by three-body collisions (with a molecule acting as the third body). When replacing in the rate equation (6.21) the atom number density by the degree of dissociation according to the relation $N_A = 2\alpha N_0$ (N_0 is the original molecule number density) only the degree of dissociation and not the gas density (i.e., N_0) should be differentiated with respect to time, since (6.21) does not contain any term describing the density change. If such a term is added to (6.21), it cancels out with the term $2\alpha\, dN_0/dt$, obtained by differentiating N_0 in the expression

$$N_A = 2N_0\alpha.$$

Neglecting α in comparison with unity in all terms, using the definition of the relaxation time τ given by (6.25), and replacing the material derivative with respect to time by a derivative with respect to position, we can rewrite the rate equation in the form

$$\frac{d\alpha}{dx} = \frac{(\alpha)}{2u\tau}\left[1 - \frac{\alpha^2}{(\alpha)^2}\right],$$

where (α) is the equilibrium degree of dissociation corresponding to the temperature and density of the gas at the point x (see (6.23)).

As in the preceding section we shall take both the relaxation time $\tau(T, \rho)$ and the velocity of the gas with respect to the compression shock $u = D\rho_0/\rho$ to be constant, corresponding to some average value of the temperature and density in the relaxation region. If the final degree of dissociation is very small, and the temperature and density changes are not too large, then this approximation may be used for a rough estimate. The equilibrium degree of dissociation (α) which depends on T and ρ will also be taken constant and equal to the degree of dissociation in the final state α_1. Integrating the rate

equation under these assumptions and imposing the initial condition $\alpha = 0$ at $x = 0$, we obtain

$$\frac{\alpha_1 - \alpha}{\alpha_1 + \alpha} = e^{-x/u\tau}. \tag{7.27}$$

Substitution of the degree of dissociation α calculated from this expression into (7.26) gives the temperature distribution $T(x)$ (for $\alpha = \alpha_1$, $T = T_1$), from which (7.24) will give the density distribution $\rho(x)$. We shall not write out the equations for the $T(x)$ and $\rho(x)$ distributions. It is obvious from these distributions as well as from (7.27) that T and ρ asymptotically approach their final values behind the wave front T_1 and ρ_1. The effective thickness of the relaxation region and of the shock front, as should have been expected, is approximately equal to

$$\Delta x \approx u\tau,$$

where τ is some average relaxation time in the nonequilibrium region.

Nonequilibrium dissociation in a shock front has been studied experimentally by many authors. A large number of these studies were carried out in oxygen. Matthews [27] used an interferometer to measure the density distribution in the nonequilibrium region behind the compression shock in a shock tube. The experimental data were compared with the theoretical calculations based on a solution of the rate equation for the dissociation. Matthews calculated a number of distributions with different values of the reaction rate constants; the constants were selected to obtain the closest agreement with the experimental data. (The distributions were calculated more exactly than in the method presented above.) The experimentally determined dissociation

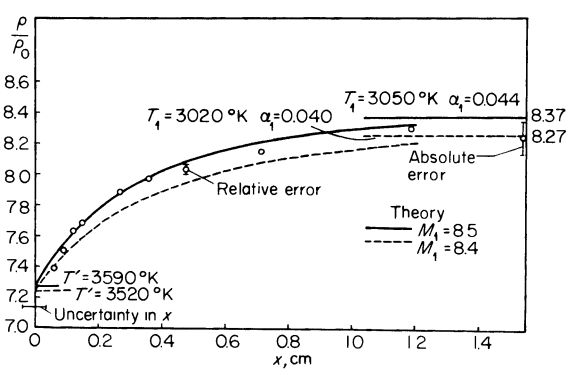

Fig. 7.15. Density distribution across a compression shock in oxygen according to the data of [27]. The initial pressure $p_0 = 19.6$ mm Hg and the initial temperature $T_0 = 300°K$.

rate for oxygen was given in §6, Chapter VI. Figure 7.15 shows the density distribution in the nonequilibrium region of a shock wave in oxygen according to the data of Matthews. It is evident from Fig. 7.15 that the thickness of the shock front under experimental conditions is of the order of $\Delta x \approx 1$ cm. Losev [28] and Generalov and Losev [29] measured the temperature distribution behind a compression shock in the region in which oxygen was out of equilibrium by means of the temperature-dependent absorption of ultraviolet radiation in the Schumann–Runge bands of O_2 molecules. Light absorption was used to study the dissociation rate of bromine and iodine in a shock wave [30].

In the papers by Camac and Vaughan [65], Rink *et al.* [66], and Wray and Freeman [91], the dissociation of oxygen in a shock wave was investigated; in [67] the dissociation of hydrogen was studied and in [68] the dissociation and recombination of nitrogen were studied. For a survey of the literature and a detailed bibliography see the book [90].

§9. Shock waves in air

Air is a mixture of two diatomic gases: nitrogen and oxygen (79 and 21% with respect to the number of molecules). In shock waves with strengths corresponding to final temperatures $T_1 \sim 3000$–$8000°K$ a considerable broadening of the shock front is observed as a result of the dissociation of nitrogen and oxygen molecules. Besides the dissociation reactions at high temperature, oxidation of nitrogen also takes place. The determination of the distributions of the flow variables in the wave front and the thickness of the front requires the simultaneous solution of the rate equations for all of these reactions. Such calculations have been carried out by Duff and Davidson [32] and also by a number of other authors. A number of experimental papers are devoted to the study of the nonequilibrium region in air using shock tubes. References to these articles may be found in the review [31] and in the book [90].

For illustration let us present the results of the calculations reported in [32] (the calculations were carried out with the use of an electronic computer). The calculations included the following basic chemical reactions:

$$\begin{aligned} O_2 + M &\rightleftarrows O + O + M, \\ N_2 + M &\rightleftarrows N + N + M, \\ NO + M &\rightleftarrows N + O + M, \\ O + N_2 &\rightleftarrows NO + N, \\ N + O_2 &\rightleftarrows NO + O. \end{aligned}$$

In all of these reactions M denotes any atom or molecule. The following recombination rate constants were taken for the three dissociation reactions:

$3 \cdot 10^{14}$, $3 \cdot 10^{14}$, and $6 \cdot 10^{14}$ $\text{mole}^{-2} \cdot \text{cm}^6 \cdot \text{sec}^{-1}$, respectively. The forward rates of the fourth and fifth reactions were taken in the following form:

$$k_4 = 5 \cdot 10^{13} \exp\left(-\frac{75{,}500}{\mathscr{R}T}\right) \text{ mole}^{-1} \cdot \text{cm}^3 \cdot \text{sec}^{-1},$$

$$k_5 = 1 \cdot 10^{11} T^{1/2} \exp\left(-\frac{6200}{\mathscr{R}T}\right) \text{ mole}^{-1} \cdot \text{cm}^3 \cdot \text{sec}^{-1}$$

(cf. the data of §8, Chapter VI).

Two assumptions were made in these calculations: (1) the vibrational degrees of freedom at each point of the nonequilibrium region are in equilibrium and (2) the rate of vibrational excitation was calculated simultaneously with the rates of the chemical reactions. The temperature and density distributions behind the compression shock in a shock wave with a Mach number $M = 14.2$ propagating through air with $p_0 = 1$ mm Hg and $T_0 = 300°\text{K}$ are shown in Fig. 7.16. The temperature behind the compression shock T' is

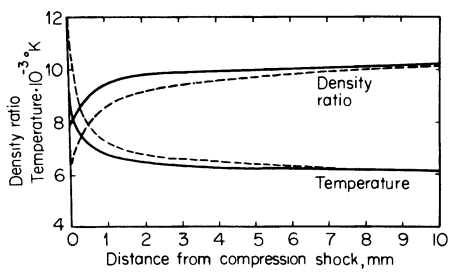

Fig. 7.16. Temperature and density distributions in a shock front in air at a Mach number $M = 14.2$. The ordinate gives the temperature and the density ratio ρ/ρ_0. The initial pressure $p_0 = 1$ mm Hg, and the temperatue $T_0 = 300°\text{K}$. The solid curves correspond to instantaneous excitation and the dashed curves to a finite rate of excitation of the vibrational modes.

9772°K if the vibrational modes are taken to be in equilibrium and 12,000°K if they are unexcited there. Results obtained under the assumption of vibrational equilibrium are shown by the solid lines and those obtained from the assumption of no vibrational excitation behind the compression shock by the dashed lines. The difference between these curves, although not very large, is still significant, since the chemical reaction rates do not strongly exceed the vibrational excitation rate. The front thickness under these conditions, as can be seen from Fig. 7.16, is of the order of 5 mm.

The thickness of the relaxation layer in air in the dissociation region was measured by Losev and Generalov [33]. The temperature change in the relaxation layer was measured from the change in the absorption of light

from an external source in the Schumann–Runge bands of oxygen molecules. The pressure behind the shock front was very close to atmospheric. For $D = 3.7$ km/sec, $\Delta x \approx 0.5$ cm (the average temperature in the layer $\bar{T} \approx 4500°K$); for $D = 2.8$ km/sec, $\Delta x \approx 1.3$ cm ($\bar{T} \approx 3200°K$). Comparison with the Duff and Davidson calculations presented above indicates the correctness of the reaction rate constants chosen for these calculations.

Wray, Teare, Kivel, and Hammerling [69] list rate constants for chemical reactions in high temperature air. The constants were chosen by the authors on the basis of analysis of the available experimental data and are recommended by them for the calculation of nonequilibrium processes in shock waves. Calculations carried out by the authors on the front structure in air are in agreement with the shock tube measurements of Lin [70]. The list of the rate constants is given below. The last two lines give the reaction rate

Table 7.2

RECOMBINATION RATE CONSTANTS [69]

Reaction	Recombination rate constant, $cm^6/mole^2 \cdot sec$	Third body
$O+O+M \rightarrow O_2+M$	$2.2 \cdot 10^{20} T^{-3/2}$	O
	$8.0 \cdot 10^{19} T^{-3/2}$	O_2
	$2.5 \cdot 10^{15} T^{-1/2}$	N_2, N, NO, A
$N+N+M \rightarrow N_2+M$	$5.5 \cdot 10^{20} T^{-3/2}$	N
	$2.0 \cdot 10^{20} T^{-3/2}$	N_2
	$6.0 \cdot 10^{15} T^{-1/2}$	O_2, O, NO, A
$N+O+M \rightarrow NO+M$	$2.0 \cdot 10^{21} T^{-3/2}$	NO, O, N
	$1.0 \cdot 10^{20} T^{-3/2}$	O_2, N_2, A

Reaction	Rate constant, $cm^3/mole \cdot sec$
$NO+N \rightarrow O+N_2$	$1.3 \cdot 10^{13}$
$NO+O \rightarrow N+O_2$	$1.0 \cdot 10^{12} T^{1/2} e^{-3120/T}$
$N+O \rightarrow NO^+ + e$	$3 \cdot 10^{13} T^{-1/2} e^{-32,500/T}$
$NO^+ + e \rightarrow N+O$	$1.8 \cdot 10^{21} T^{-3/2}$

constants for ionization and electron recombination which play an important role in establishing ionization equilibrium in air at comparatively low temperatures. The rate constants for the reverse chemical reactions can be expressed in terms of the rate constants for the forward reactions and the corresponding equilibrium constants. A detailed summary of the rates of various reactions which take place in air, including those involving charged particles, is given in Chapter 11 of the collection [92]. We note also [71–75],

which have reported studies on the relaxation layer in a shock wave in air and related problems. A more detailed survey with respect to shock waves in air is given in the book [90].

§10. Ionization in a monatomic gas

For temperatures behind the shock front of the order of 15,000–20,000°K the gas is appreciably ionized. The establishment of ionization equilibrium at these temperatures is the slowest of the relaxation processes and therefore determines the thickness of the wave front*.

From the point of view of experimentally studying ionization in a shock tube it is most attractive to deal with monatomic gases. Due to the absence of a number of the degrees of freedom possessed by molecular gases it is easier in monatomic gases to obtain high temperatures $\sim$15,000–20,000°K. Monatomic gases are also very suitable for checking the theory of the phenomenon, since ionization (single) is the only relaxation process responsible for broadening the shock front. The first detailed study of this kind was carried out by Petschek and Byron [35] for argon.

Let us consider a shock wave in a monatomic gas. Appreciable ionization is attained only for rather strong waves, where the limiting density ratio reached across the compression shock is 4, since the specific heat ratio $\gamma' = 5/3$. The flow variables behind the compression shock are expressed in terms of Mach number by the simple relations

$$\frac{\rho'}{\rho_0} = 4, \quad \frac{p'}{p_0} = \frac{5}{4} M^2, \quad \frac{T'}{T_0} = \frac{5}{16} M^2.$$

For example, for $M = 18$ and an initial temperature $T_0 = 300°\text{K}$, which corresponds to a shock velocity $D = 5.75$ km/sec, the temperature behind the compression shock $T' = 30{,}000°\text{K}$. At equilibrium behind the shock front in argon for an initial pressure $p_0 = 10$ mm Hg, the gas is approximately 25% ionized and the temperature $T_1 = 14{,}000°\text{K}$.

The thickness of the compression shock is approximately two to three gaskinetic atomic mean free paths. If the gas is ionized ahead of the shock front and thus also immediately behind the compression shock, it is only weakly so. Ionization occurs after the shock compression and rapid heating of the gas particles. The basic ionization mechanism is ionization by electron impact (see Chapter VI). However, ionization by electron impact with the formation of an electron avalanche requires the presence of some initial "priming" electrons. One of the mechanisms which can lead to this initial ionization is ionization by atom-atom collisions. As was noted in Chapter VI,

* Molecular dissociation at these temperatures proceeds very rapidly, with a small number of collisions.

the cross section for this process is extremely small. Therefore, the formation of the "priming" electrons by atom-atom collisions requires an appreciable time. Correspondingly, the region behind the compression shock where the flow variables correspond to a negligibly small degree of ionization and are simply equal to ρ', p', and T', etc., extends over a rather large distance.

Avalanche ionization begins when the rate of ionization by electron impact becomes greater than the rate of ionization by atom collisions, or of ionization due to other processes. Possible mechanisms for the formation of the priming electrons will be discussed below. Since the rate of ionization by atomic collisions is extremely low, avalanche ionization begins with only very few "priming" electrons, when the degree of ionization $\alpha \sim 10^{-5}$–10^{-3}. We shall not examine here the formation of the "priming" electrons but shall consider the basic process of ionization from the very low to the equilibrium values ($\alpha_1 = 0.25$ in our example).

At a constant electron temperature T_e the avalanche increases exponentially as $n_e \sim \alpha \sim e^{t/\tau}$ (see §11 of Chapter VI), until recombination begins to compensate appreciably for the ionization. Thereafter, the degree of ionization gradually approaches its equilibrium value at which the recombination exactly balances ionization. In actuality, the formation of an avalanche proceeds in a more complex manner. Each act of ionization results in the electron gas losing an amount of energy equal to the ionization potential I (which in argon is equal to 15.8 ev). On the other hand, the temperature of the electron gas is of the order of 10,000°K, that is, the thermal energy of a single electron is of the order of 1.5 ev. Thus, the formation of a single new electron requires an energy equal to the thermal energy of approximately ten electrons. If the thermal energy of the electrons were not replenished, the electron temperature would drop very rapidly. This would also result in a drop in the rate of ionization which depends very strongly on the electron temperature through a Boltzmann factor of the type e^{-I/kT_e} (see §11, Chapter VI). The electron energy loss in ionization is compensated for by energy transfer to the electrons from the atom gas heated by the compression shock. However, the energy exchange between the heavy particles and the electrons, due to the great difference in their masses, progresses extremely slowly and it is just this exchange process which limits the rate of development of the electron avalanche and determines the time required to reach equilibrium ionization.

For small degrees of ionization, very few ions are present and the electrons acquire their energy by collisions with neutral atoms. However, the effectiveness of such collisions for electron temperatures $T_e \sim 1$ ev $\approx 10^4$°K is approximately 10^3 times less effective than the electron-ion collisions. Therefore, the transfer of energy from atoms to electrons is important only at the very beginning of the process; already at a low degree of ionization $\alpha \sim 10^{-3}$, the

energy exchange between the ions and electrons is of primary importance. The temperature of the ions is equal to that of the atoms since the energy exchange between them proceeds very rapidly as a result of their equal masses. Thus, a small number of ions serves in this case as an "intermediary" in the energy exchange from the atoms to the electrons. In the electron gas the energy is distributed very quickly, so that we can speak of an electron temperature T_e which is, naturally, different from the temperature T of the heavy particles (atoms and ions).

The electrons not only ionize the atoms but also excite them. The energy of the first excited level of an argon atom is $E^* = 11.5$ ev. In the case of appreciable electron concentrations the excited atoms are deexcited by electron collisions of the second kind. In this case the excitation energy is again returned to the electron gas. However, when the electron temperatures are of the order of and, in particular, higher than 1 ev, electron impact ionization of an excited atom becomes more probable than deexcitation (only a moderate amount of energy $I - E^* = 4.3$ ev is required for ionization). The ionization in this case takes place in two stages, the atom is first excited and then it is ionized. The energy expended for ionization in this two-stage process still remains equal to the ionization potential: $E^* + (I - E^*) = I$. Other multistage processes in which an atom is not immediately ionized by electron impact, but is first subjected to several increases in the degree of excitation, are also possible (see Chapter VI).

If the rate of ionization of excited atoms is high in comparison with those of deexcitation and of the excitation of unexcited atoms, then the ionization rate is essentially determined by the excitation rate only (in accordance with (6.79)). This is precisely the assumption made by Petschek and Byron [35], who assumed that each atom is "instantaneously" ionized following the excitation. The excited atoms emit part of their energy. The photon generated as a result of this emission is absorbed by a neighboring unexcited atom (the absorption cross section for the resonant photons is very large), which, in turn, reemits and so forth*.

Let us set up a system of equations which approximately describes the ionization process and the distributions of flow variables in the shock wave. For simplicity we restrict ourselves to the case of a small degree of ionization

* Resonant photons born in the heated zone behind a shock front may leave the heated region by diffusing through the gas and penetrating the front surface. After that they diffuse through the unexcited gas and leave the propagating shock wave behind. The diffusion of resonance radiation at a large distance ahead of the front results in a significant concentration of excited atoms. This process was considered by Biberman and Veklenko [34]. They have shown that at a distance of 1 m ahead of the wave front in argon with $p_0 = 10$ mm Hg, $M = 18$, and $T_1 = 14{,}000°\mathrm{K}$, the concentration of excited atoms reaches $5 \cdot 10^{13}\ \mathrm{cm}^{-3}$, which corresponds to an excitation "temperature" of $\sim 13{,}500°\mathrm{K}$, only slightly lower than the temperature of resonance radiation passing through the front surface and equal to T_1.

$\alpha \ll 1$. For convenience we shall refer to the energy and all other thermodynamic quantities not per unit mass but per original gas atom.

The enthalpy per original atom is equal to

$$h = \tfrac{5}{2}kT + \tfrac{5}{2}\alpha kT_e + \alpha I.$$

From the condition that the enthalpy is approximately constant in the relaxation zone and that $\alpha \ll 1$ we obtain a relationship between the degree of ionization and the atom temperature analogous to that of (7.26)

$$\alpha = \frac{5}{2}\frac{T' - T}{T_{\text{ion}}}, \tag{7.28}$$

where $T_{\text{ion}} = I/k$ (in argon $T_{\text{ion}} = 1.83 \cdot 10^5 ^\circ\text{K}$).

The gas pressure is $p = nkT + n\alpha kT_e \approx nkT$, where $n = n_a + n_i = n_a + n_e$ is the total number of atoms and ions per unit volume. It can be expressed in terms of the atom temperature and the degree of ionization from (7.18). It can be determined less exactly from the condition that the pressure in the relaxation zone is approximately constant: $p \approx nkT \approx n'kT'$. This yields

$$n = 4n_0\left(1 - \frac{2}{5}\alpha\frac{T_{\text{ion}}}{T'}\right)^{-1}, \tag{7.28'}$$

where n_0 is the atom number density ahead of the front.

The rate equation for the degree of ionization $\alpha = n_e/n$ is

$$\frac{D\alpha}{Dt} = u\frac{d\alpha}{dx} = \frac{q}{n}. \tag{7.29}$$

Here q is the algebraic sum of all terms which describe the appearance and disappearance of free electrons per unit volume per unit time. Over the main region q is determined by electron impact ionization. Within the framework of the Petschek–Byron assumptions, for example, q in this region represents the rate of atom excitation $q = \alpha_e^* n_e n_a$, where the rate constant α_e^* is given by (6.79). In the very beginning of the process, immediately behind the compression shock, q is determined by processes which result in the formation of "priming" electrons (atom-atom collisions, etc., see below). In the final stage, in the region where equilibrium is approached, recombination must also be included in q.

The rate of ionization by electron impact depends on the temperature of the electron gas, which is governed by the equation of electron energy balance. We denote the entropy and enthalpy of the free electrons per original atom by Σ_e and $h_e = \frac{5}{2}\alpha kT_e$, and the electron pressure by $p_e = n\alpha kT_e$. Remembering

that $D/Dt = u\,d/dx$, we may write the energy balance equation

$$uT_e \frac{d\Sigma_e}{dx} = u\left(\frac{dh_e}{dx} - \frac{1}{n}\frac{dp_e}{dx}\right) = \frac{1}{n}(\omega_{ea} - \omega_i), \tag{7.30}$$

where ω_{ea} is the heat inflow per unit volume per unit time due to the energy exchange from the ions and atoms to the electrons, and ω_i is the energy lost by the electrons in ionization (per unit volume per unit time)*. According to (6.121)

$$\omega_{ea} = \frac{3}{2}k\left(\frac{DT_e}{Dt}\right)_{\text{exch}} n_e = \frac{3}{2}kn_e\frac{T - T_e}{\tau_{\text{exch}}}, \tag{7.31}$$

where $1/\tau_{\text{exch}} = 1/\tau_{ei} + 1/\tau_{ea}$; τ_{ei} is the characteristic time for energy exchange between ions and electrons (equation (6.120)) and τ_{ea} is the characteristic time for energy exchange between atoms and electrons (equation (6.122)). The

* Equation (7.30) can also be derived from equations of the type of (1.10) and (1.6) written for an electron gas. In this case, however, we must take into account the fact that a small polarization (relative displacement of positive and negative electric charge, *eds.*) takes place in an ionized gas in the presence of gradients of the macroscopic quantities, as a result of which electric fields arise which prevent an appreciable charge separation (for more details, see §13). The polarization field $\mathbf{E}$ ensures a "rigid" connection between the electron and atom-ion gases. When this field is taken into account, additional terms appear in the electron equations of motion and energy

$$m_e n_e \frac{D\mathbf{u}_e}{Dt} = -\nabla p_e - en_e\mathbf{E}$$

$$\frac{\partial}{\partial t}\left[n_e\left(\frac{3}{2}kT_e + \frac{m_e u_e^2}{2}\right)\right] + \nabla\cdot\left[n_e\mathbf{u}_e\left(\frac{5}{2}kT_e + \frac{m_e u_e^2}{2}\right)\right] = \omega_{ea} - \omega_i - en_e\mathbf{E}\cdot\mathbf{u}_e.$$

Because the mass of the electrons is extremely small, the inertia term in the equation of motion of the electron gas is extremely small, and the gradient of the electron pressure is balanced by the action of the polarization field; thus, $-en_e\mathbf{E} = \nabla p_e$. We now substitute this quantity into the energy equation, neglecting the small kinetic energy of the electron gas, and consider the one-dimensional steady-state case. Noting also that the electron gas velocity $\mathbf{u}_e$ is practically the same as that of the atom-ion gas $\mathbf{u}$, using the integral of the continuity equation $nu = const$ and the definition $n_e = \alpha n$, we arrive at (7.30). We also write the equations of motion and energy for the atom-ion gas in the form:

$$m_a n\frac{D\mathbf{u}}{Dt} = -\nabla p + en_i\mathbf{E}, \qquad p = p_a + p_i, \qquad n = n_a + n_i,$$

$$\frac{\partial}{\partial t}\left[n\left(\frac{3}{2}kT + \frac{m_a u^2}{2}\right)\right] + \nabla\cdot\left[n\mathbf{u}\left(\frac{5}{2}kT + \frac{m_a u^2}{2}\right)\right] = -\omega_{ea} + en_i\mathbf{E}\cdot\mathbf{u}.$$

energy expended in ionization is equal to

$$\omega_i = Iq = Inu\frac{d\alpha}{dx}. \tag{7.32}$$

The system of differential equations (7.29) and (7.30) for $\alpha(x)$ and $T_e(x)$ and the algebraic equations (7.28) and (7.28′) which give $T(\alpha)$ and $n(\alpha)$, together with the ionization rate q defined in an appropriate manner, can be used to find the distributions of all the quantities in the relaxation zone. In fact, the rates of exchange and of inelastic losses ω_{ea} and ω_i compensate one another to an appreciable extent, $\omega_{ea} - \omega_i \ll \omega_{ea}$, ω_i. Thus in by far the greatest part of the relaxation region the energy balance equation (7.30) reduces to the algebraic relation $\omega_{ea} \approx \omega_i$, which makes it possible to express α in the form of a function of T_e. This was the approach used by Petschek and Byron for calculating the width of the relaxation region.

The basic difficulty in considering ionization in the relaxation region is presented by the problem of the formation of the priming electrons. The cross sections for ionization by atom collisions are practically unknown (see §15, Chapter VI). The published experimental data for argon [37, 38] pertain to energies of several tens of ev. Therefore some reasonable estimate of the cross section must be assumed for calculation purposes. The structure of the relaxation region in argon was calculated by Bond [36] and Biberman and Yakubov [93]*. For illustration we show in Fig. 7.17 the distributions taken from [93] of the atom and electron temperatures and of the degree of ionization for a Mach number $M = 16$, $D = 5.1$ km/sec, and inital pressure $p_0 =$ 10 mm Hg. These curves were calculated on the assumption that the atoms are ionized by electron impact directly from the ground level, and that the cross section for ionization by atom collisions near the threshold as a function of the collision energy ε is approximated by a straight line with slope $C =$ $1.2 \cdot 10^{-20}$ cm^2/ev, so that when $\varepsilon = I + 1$ ev the cross section $\sigma = 1.2 \cdot 10^{-20}$ cm^2 (see Chapter VI). It can be seen from the figure that initially the ionization is extremely small and that it increases very slowly. The electron temperature rises quite rapidly to a value $T_e \approx 1.3$ ev, and then remains almost constant.

In this region the energy supplied by the ions is compensated by the energy lost in ionization. It should be noted that the time for accumulating priming electrons due to atom-atom collisions should depend only weakly on the cross section chosen. In the case of $T_e = const$ it is completely independent of the cross section of atom-atom ionization and is determined by the time of the succeeding electron avalanche development (this was shown at the end of §13, Chapter VI). As shown by calculations in [93], the taking into account of the step-wise character of electron impact ionization with preliminary

* In [35] only values of the total width of the region were obtained.

excitation of the atoms significantly reduces the ionization time and width of the relaxation region only for shock Mach numbers less than 12–13; for $M > 13$ this reduction is insignificant.

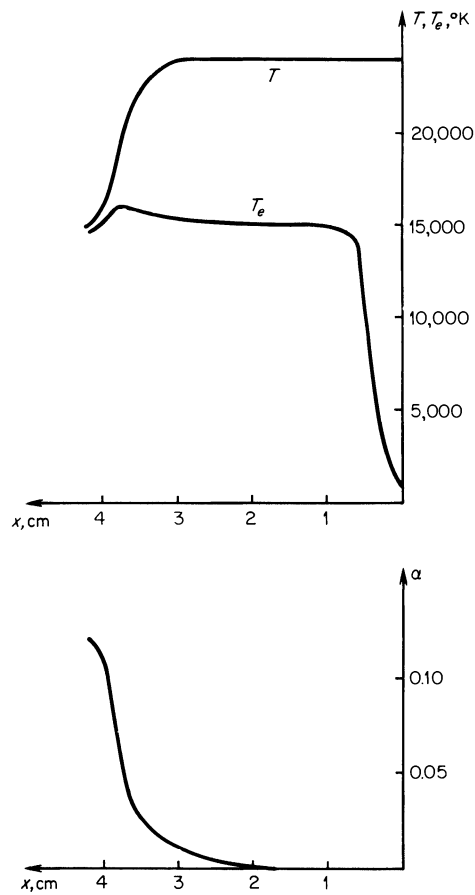

Fig. 7.17. Distribution of electron and atom temperatures and degree of ionization in a shock wave in argon on the assumption that the initial electrons are formed by atom-atom collisions. The Mach number is 16, the pressure ahead of the front 10 mm Hg, and the initial temperature 293°K.

Experiments in a shock tube on ionization relaxation in argon were carried out by Petschek and Byron [35]. In order to expand the nonequilibrium region and to increase the relaxation times so as to make them accessible to measurement, the experiments were carried out at quite low initial pressures of argon. The most reliable measurements were made at $p_0 = 2$ mm Hg. The

electron density distribution in the shock wave was determined by recording the continuous luminous spectrum which results from electron-ion recombination. The intensity in this spectrum, at a given cross section x of the shock wave, is proportional to the square of the electron density (the gas is transparent to radiation). In addition, probes were used to measure the electron density gradients, and these were in agreement with the luminosity measurements. The experiments showed that the width of the relaxation region, which is determined to an appreciable extent by the initial rate of ionization, is strongly dependent on the degree of purity of the argon; in the formation of priming electrons an important role is played by the impurities (with low ionization potentials).

We present the results of some measurements of the ionization relaxation time in argon. The relaxation times and approximate front thicknesses are reduced to the initial pressure condition $p_0 = 10$ mm Hg (they are inversely proportional to the gas density). The values are for a very pure gas, with an impurity content of $\sim 5 \cdot 10^{-5}$. The experiments show that, roughly speaking,

Table 7.3

IONIZATION RELAXATION TIME IN ARGON

M	T', °K	D, km/sec	$\tau \cdot 10^6$, sec	Δx, cm
10.3	10,000	3.3	100	~6.5
11.5	12,500	3.7	17	~1
13.4	16,700	4.3	3	~0.2
16.4	25,000	5.25	0.5	~0.032
20.3	40,000	6.5	0.1	~0.006

$\log \tau$ is a linear function of $1/T'$, that is, $\tau \sim \exp(const/T')$. The constant in this relation corresponds to an activation energy of approximately 11.5 ev.

Comparison of experimental data on electron density distributions with avalanche ionization calculations has shown that the avalanche is developed only after the initial ionization reaches a value of the order of 0.1 of the equilibrium ionization, or an absolute value of $\alpha \sim 10^{-2}$. The question of the nature of the initial ionization was not resolved in [35]. Estimates have shown that ionization as a result of atom-atom collisions or photoionization by photons born in the equilibrium region cannot ensure the rapid formation of the large number of priming electrons which are required to explain the experimental data. The evident insufficiency of the mechanism of atom-atom collisions is shown by the fact that calculations which take into account only this mechanism give relaxation times which are tens of times larger than the experimental relaxation times [93].

A number of authors have proposed different mechanisms for the initial ionization: in particular, it has been suggested that a role is played by the diffusion of electrons from a region with a high level of ionization into a region where the degree of ionization is low and even into the gas ahead of the shock front. (Electron diffusion in a shock wave is treated in [39, 76, 77].) The role of atom excitation ahead of the shock front by resonance radiation emerging from the equilibrium region was pointed out in [94].

An analysis of the various ionization mechanisms in a shock wave in argon (and in monatomic gases in general) is contained in the paper by Biberman and Yakubov [93] cited previously. The authors have investigated the effect of variations in the choice of ionization cross sections by electron and atom impacts, the role of step-wise and radiative processes. They have come to the conclusion that the decisive role in the rapid formation of the priming electrons must be played by the excitation of atoms by resonant radiation coming from the equilibrium region. This effect brings about a large increase in the concentration of excited atoms, which are easily ionized by electron impacts. Taking into account the above effect, the authors were able to considerably narrow the gap between calculated and experimental values of the relaxation times and to obtain satisfactory agreement.

We must note that the problem of ionization relaxation and, in particular, of the initial ionization mechanism is still not entirely clear. We also wish to note [95] in which relaxation in xenon is studied, and [96], which is concerned with the effect of radiation.

§11. Ionization in air

Ionization in shock waves in air was studied in the early papers [40, 41, 70, 78–80], and especially thoroughly in the experiments described in [87]. In the latter experiments waves with velocities of 4.5–7 km/sec (Mach numbers 14–20) were studied in shock tubes at initial pressures of 0.02–0.2 mm Hg. The measurements showed that the ionization develops very rapidly and reaches a value of the order of equilibrium ionization at distances from the shock equal to 10–40 gaskinetic mean free paths in the undisturbed air. Here the degree of ionization is of the order of 10^{-4}–10^{-3} at equilibrium, but the degree of ionization in the relaxation region passes through a maximum which can exceed the equilibrium value by several times.

It was already noted in Part 2 of Chaper VI that the ionization mechanism in a molecular gas such as air, for shock waves which are not too strong, differs appreciably from the ionization mechanism in monatomic gases. The free electrons in air are formed primarily by associative ionization, in which two atoms combine into a molecule with the simultaneous removal of an electron and formation of a molecular ion. The principal process requiring the lowest

activation energy is the reaction

$$N + O + 2.8 \text{ ev} \rightarrow NO^+ + e.$$

Since the ionization potentials of all the components of air are much higher than the amount of energy expended in this reaction, the latter (for not too high temperatures) takes place at a much faster rate than direct ionization of atoms and molecules by particle impacts. The rate constant of the above principal ionization reaction is given in Table 7.2 of §9. Since an appreciable role in the ionization of air is played by atoms, calculations of ionization rates in air are based on calculations of molecular dissociation (chemical reactions in general). These calculations were carried out by Lin and Teare [86], and they are in good agreement with measurements [87]. Calculations (for shock wave velocities not exceeding 9 km/sec) have shown that ionization occurs rapidly, even faster than the chemical reactions, so that the ionization in the relaxation region, to a certain extent, comes into equilibrium with the chemical composition of the gas and "follows" the change in the degree of molecular dissociation.

Ionization in air in shock waves with velocities somewhat greater than 10 km/sec (9–15 km/sec) was considered by Biberman and Yakubov [97]. They took into account the chemical composition of the air in the relaxation region and the excitation of the atoms and molecules. Unlike the case of low velocities, dissociation takes place more rapidly than does ionization and the ionization occurs mainly in the atom gas. Associative ionization plays the determining role in the creation of the initial electrons; as the electron density increases, the role of step-wise ionization by electron impacts becomes more important, with the energy of the electrons, as is also the case in a monatomic gas, replenished by energy transfer from the ions.

The ionization rate of atoms and molecules by electron impact was calculated in [97] using a method of combining the excited and ionized states into one group. This method, suggested by Biberman and Ul'yanov [99], may also be useful for other problems connected with the disturbance of ionization equilibrium. It consists of the following: It is assumed that impact excitation and ionization of atoms which are in the ground state, and also the inverse processes of deexcitation with the atom moving to the ground level and recombining by three-body collisions with capture of an electron into the ground level, take place at a relatively slow rate. At the same time it is assumed that the increase in the degree of excitation by electron impact and ionization of excited atoms, as well as the corresponding inverse processes, takes place at a relatively rapid rate.

The rates of actual processes behave in this manner to some extent, so that the above assumptions are reasonable. But if these assumptions hold we can assume approximately that a Boltzmann distribution is established among the

different excited states, while a Saha distribution is established between the excited and ionized atomic states. In other words, all the excited and ionized states can be combined into a single group, by assigning to this group of states the particular temperature equal to the temperature of the electron gas. On the other hand, the electron density, as well as the relation between the electron (or excited atom) densities and the densities of atoms in the ground state, is no longer described by the Saha equation, and is not an equilibrium relation. It is determined from the rate equation which describes the transition of atoms between the ground state and the excited and ionized states. If desired, this method can be refined by separating out from the excited and ionized states the lowest excited states, and writing separate rate equations for the atom concentrations in these states. Reference [99] has used the above method for considering the effect of radiation leaving a bounded gas volume when the state of the gas is disturbed from thermodynamic equilibrium.

Ionization in air for very high velocity shock waves, of the order of tens of km/sec (applied to the problem of the motion of meteors in the atmosphere) was considered by Bronshten [98]. One of the most characteristic properties of ionized gases is their ability to conduct an electric current. A rather large number of papers have been devoted to calculations and theoretical studies of the electrical conductivity of ionized air (and other gases). See, for example, [70, 81–84].

§12. Shock waves in a plasma

The structure of a shock front propagating through an ionized gas has a number of interesting features. These features were noted by one of the present authors [42]; quantitative calculations of the front structure have been made by Shafranov [43]; see also the papers by Imshennik [51], Jukes [44], Tidman [44a], and Pikel'ner [85]. The basic features of the structure are related to the slow character of the energy exchange between ions and electrons and to the high electron mobility, as a result of which the electron heat conduction greatly exceeds the ion heat conduction. Maxwellian distributions in the electron and ion gases are established quite rapidly, in a time of the order of the time between particle "collisions"*. On the other hand, the equilibration of the temperatures of both gases takes place much more slowly, because of the large difference between the electron and ion masses. This relaxation process determines the shock front thickness in a plasma.

For a qualitative discussion of the consequences of the low rate of energy exchange between the electrons and ions, we shall first assume that the electron heat conduction does not differ from the ion heat conduction. In

* For the concept of "collision" of charged particles interacting according to the Coulomb law see §20, Chapter VI.

addition, we shall assume that ionization does not take place in the shock wave, but that the wave is propagated through a gas which is already ionized. In a coordinate system moving with the wave, a considerable part of the kinetic energy of the gas entering the compression shock is irreversibly converted into heat through the action of ion viscous forces. The increase in ion temperature across the compression shock is of the order $\Delta T_i \sim m_i D^2/k$, where m_i is the mass of an ion and D is the velocity of the incident gas, equal to the shock front velocity. The thickness of the viscous shock is determined by the time between ion collisions τ_i; it is of the order of an ion mean free path $l_i \sim \bar{v}\tau_i$, where $\bar{v} \sim D$ is the thermal velocity of the ions in the compression shock (the definition of τ_i is given in §20, Chapter VI). During the compression time τ_i the ion gas does not succeed in transferring to the electron gas any appreciable thermal energy, since the characteristic exchange time $\tau_{ei} \sim (m_i/m_e)^{1/2} \cdot \tau_i$ is very large. For ions of average mass, τ_{ei} is hundreds of times larger than τ_i; for protons it is only 43 times larger than τ_i. The increase in electron temperature across the compression shock due to the conversion of the kinetic energy of the incident electron gas into heat through the action of electron viscous forces is negligibly small. It is of the order $\Delta T_e \sim m_e D^2/k$, that is, smaller by a factor of m_e/m_i than ΔT_i. The electron gas in the compression shock is heated by another process.

The electrons and ions are bound together by the forces of electric interaction and this bonding is very strong. The smallest separation of the electron and ion gases results in the formation of strong electric fields which prevent further separation. Hence, each small parcel of the plasma remains electrically neutral. The electron density n_e is always the same as the positive charge density Zn_i (Z is the ionic charge, n_e and n_i are the electron and ion number densities, respectively). In the compression shock the electron gas does not behave independently, but is compressed in the same manner as the ion gas. We can say that the electrons are "rigidly coupled" to the ions by the electric forces. These forces are "external" with respect to the electron gas and do not lead to any dissipation. Since the dissipation of energy due to electron viscous forces is negligibly small, the compression and heating of the electron gas in the compression shock is adiabatic. Thus, for example, when a hydrogen plasma is compressed by a strong shock wave the density across the compression shock increases by a factor of 4, corresponding to the specific heat ratio of 5/3. The ion temperature can increase very markedly if the wave is strong, while across the compression shock the electron temperature increases only by a factor of $4^{\gamma-1} = 4^{2/3} = 2.5$. Therefore in a strong shock wave propagating through a plasma with equal ion and electron temperatures, behind the compression shock there is a marked difference in the temperatures of the two gases. After a small parcel has undergone the shock compression it begins to transfer thermal energy from the ions to the electrons, and this

leads to an equilibration of the temperatures in a time of the order of the exchange time τ_{ei} (see §20, Chapter VI). The thickness of the relaxation region behind the compression shock in which the plasma approaches equilibrium (with equal temperatures $T_e = T_i = T_1$) is of the order of $\Delta x \sim u_1 \tau_{ei}$ ($u_1 = (\rho_0/\rho_1)D$). The final temperature T_1 is determined by the general equations of conservation for the shock front. Thus, in the absence of effects connected with the existence of increased electron heat conduction, the temperature distribution in the wave front would have the form shown in Fig. 7.18.

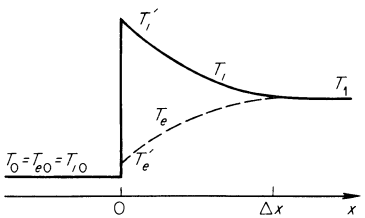

Fig. 7.18. Ion and electron (dashed line) temperature profiles in a shock front in a plasma without taking into account electron heat conduction.

If none of the other degrees of freedom other than the previously "frozen" translational degrees of freedom of the electron are excited (which is the situation in a fully ionized gas), then the density and pressure in the relaxation region remain strictly constant. Indeed, the specific heat ratios for a gas with "frozen" and equilibrium degrees of freedom are the same and equal to $\gamma = 5/3$, so that the compression across the compression shock takes place along a Hugoniot curve which coincides with the Hugoniot curve of the final state. The physical reason is, obviously, the fact that the pressure is only determined by the average translational energy of the particles, which remains constant during the exchange, the value being independent of its distribution among the particles.

Let us now consider the effect of electron heat conduction on the shock front structure. Up to this point we have assumed (with ample justification) that the dissipative processes, viscosity and heat conduction, are important only in the region of large gradients in the compression shock, where the macroscopic quantities change significantly over distances of the order of a gaskinetic mean free path. In the relaxation region, which extends over a distance of many mean free paths, the gradients are small and the dissipation processes can be neglected. Actually, the characteristic scale, which serves as a criterion for the smallness of the gradients, is a length scale based on the transport coefficients and the front velocity. The transport coefficient, for example, for the atom thermal diffusivity, is of the order of $\chi \sim l\bar{v}/3$ and the length scale $\lambda \sim \chi/D \sim l\bar{v}/D \sim l$ is of the order of a gaskinetic mean free path, since the thermal speed of the atoms in the front $\bar{v}$ is of the order of the front

velocity D. The coefficient of electron thermal diffusivity χ_e is approximately

$$\chi_e = \frac{l_e \bar{v}_e}{3} \approx \frac{\bar{v}_e^2 \tau_e}{3},$$

where l_e is the electron mean free path, $\bar{v}_e$ is the thermal speed of electrons, and τ_e is the time between the "collisions" of electrons with each other. As was shown in §20 of Chapter VI, the mean free path for charged particles is independent of their mass and depends only on the charge and temperature, i.e., $l \sim T^2/Z^4$.

At comparable temperatures and in light gases, for example, in hydrogen ($Z = 1$), the electron and ion mean free paths are of the same order, while the electron velocity is larger than the ion velocity by the factor $(m_i/m_e)^{1/2}$. Therefore the electron heat conduction coefficient is $(m_i/m_e)^{1/2}$ times larger than the ion heat conduction coefficient, and the characteristic scale over which the electron heat conduction takes place is

$$\lambda_e \sim \frac{\chi_e}{D} \sim \left(\frac{m_i}{m_e}\right)^{1/2} \frac{\chi_i}{D} \sim \left(\frac{m_i}{m_e}\right)^{1/2} l_i.$$

This length scale is of the same order as the thickness of the relaxation region in which the electron and ion temperatures equilibrate:

$$\Delta x \sim D\tau_{ei} \sim D\left(\frac{m_i}{m_e}\right)^{1/2} \tau_i \sim \frac{D}{\bar{v}} \left(\frac{m_i}{m_e}\right)^{1/2} l_i \sim \left(\frac{m_i}{m_e}\right)^{1/2} l_i.$$

Therefore, the gradients in the relaxation region are not small with respect to electron heat conduction and the heat exchange by conduction in this region is comparable to the heat exchange between ions and electrons. The electron heat conduction promotes more rapid equilibration of the temperatures behind the viscous shock, since it transports the heat from the layers which are further removed from the compression shock to the more forward layers where the electron temperature is lower. In addition, and this effect is extremely important, the electron heat conduction results in a preheating of the gas ahead of the viscous compression shock. While the "hot" ions cannot move away too far from behind the compression shock into the region ahead of the shock (their thermal velocity is comparable with the propagation velocity of the shock through the undisturbed gas), the "hot" electrons successfully move ahead and leave the compression shock behind, since their velocity is approximately $(m_i/m_e)^{1/2}$ times greater than the front velocity. A preheating layer is thus formed ahead of the compression shock. In this layer the electron temperature is higher than the ion temperature, since the electron gas is heated first and only then is the heat partially transferred to the ions. A sharp increase in the ion temperature takes place in the compression shock.

The electron temperature remains constant, since its tendency to a discontinuous increase is prevented by the "smoothing out" due to the large heat conduction. The compression shock has an "isoelectron-thermal" character. The temperature profiles in the wave front, taking into account electron heat conduction, are shown in Fig. 7.19.

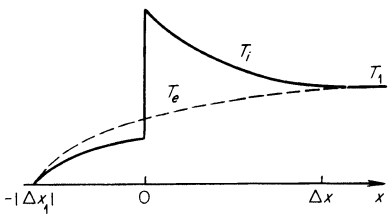

Fig. 7.19. Ion and electron (dashed line) temperature profiles in a shock front propagating through a cold plasma.

Let us estimate the thickness of the preheating layer ahead of the compression shock. We shall assume, for simplicity, that no energy is transferred from the electron gas which is being preheated to the ion gas, and also that the gas ahead of the compression shock is not compressed and not slowed down (in a coordinate system where the front is at rest). Exact calculations justify these simplifying assumptions. The electron heat conduction flux is

$$S = -\kappa_e \frac{dT_e}{dx} = -\chi_e c_e \frac{dT_e}{dx}, \tag{7.33}$$

where $\kappa_e = \chi_e c_e$ is the coefficient of thermal conductivity and c_e is the specific heat at constant volume of the electron gas per unit volume. The effective coefficient of electron thermal conductivity is

$$\kappa_e = \xi \frac{(kT_e)^{5/2} k}{m_e^{1/2} Ze^4 \ln \Lambda} = \xi \cdot 1.93 \cdot 10^{-5} \frac{T_e^{\circ 5/2}}{Z \ln \Lambda} \quad \frac{\text{erg}}{\text{cm} \cdot \text{sec} \cdot \text{deg}},$$

where $\ln \Lambda$ is the Coulomb logarithm (see §20 of Chapter VI), and ξ is a number which depends only weakly on Z; $\xi(1) = 0.95$, $\xi(2) = 1.5$, $\xi(4) = 2.1$*.

* We present, for reference purposes, the formula for the electrical conductivity of a plasma

$$\sigma = 2.63 \cdot 10^{-4} \gamma(Z) \frac{T^{\circ 3/2}}{Z \ln \Lambda} \quad (\text{ohm} \cdot \text{cm})^{-1},$$

$$= 2.38 \cdot 10^{8} \gamma(Z) \frac{T^{\circ 3/2}}{Z \ln \Lambda} \quad \text{sec}^{-1},$$

$$\gamma(1) = 0.58; \qquad \gamma(2) = 0.68; \qquad \gamma(4) = 0.78.$$

Since the process is steady, the heat conduction flux in the preheating layer is equal to the hydrodynamic flux of electron energy*

$$-S = Dc_e T_e = \chi_e c_e \frac{dT_e}{dx} \tag{7.34}$$

(the initial electron temperature ahead of the front is assumed to be zero; far ahead of the wave the flux S vanishes). Noting that $\chi_e \sim \bar{v}_e l_e \sim T_e^{5/2}$ or $\chi_e = aT_e^{5/2}$, where $a = const$, and integrating (7.34), we find

$$x - x_0 = \frac{2}{5}\frac{a}{D} T_e^{5/2}$$

or

$$T_e = \left[\frac{5}{2}\frac{D}{a}(x - x_0)\right]^{2/5}, \tag{7.35}$$

where x_0 is the coordinate of the leading edge of the preheating region, from which the temperature departs from the value zero. The temperature profile described by this equation is shown schematically in Fig. 7.19. If we place the coordinate origin $x = 0$ at the point of the compression shock and denote the temperature at this point by T_{e0} (the electron temperature does not change across the shock), then the expression for the thickness of the preheating layer can be written

$$|x_0| = \frac{2}{5}\frac{a}{D} T_{e0}^{5/2} = \frac{2}{5}\frac{\chi_e(T_{e0})}{D}. \tag{7.36}$$

When electron heat conduction is taken into account, the electron temperature at the shock is of the same order as behind the entire wave front, so that the thickness of the preheating layer is of the same order as the thickness of the relaxation region behind the shock

$$|x_0| \sim \frac{\chi_e(T_1)}{D} \sim \frac{\bar{v}_e l_e}{D} \sim \left(\frac{m_i}{m_e}\right)^{1/2} l_e \sim \left(\frac{m_i}{m_e}\right)^{1/2} l_i \sim \Delta x_{\text{exch}}.$$

The thickness of the preheating layer ahead of the compression shock increases rather rapidly with an increase in wave strength. If we consider the fact that $\chi_e \sim T_e^{5/2} \sim T_1^{5/2}$, and $D \sim T_1^{1/2}$, then we find from (7.36) that $|x_0| \sim T_1^2 \sim D^4$.

The temperature profile we have found is characteristic of nonlinear heat

* This is a first integral of the energy equation for the given case:

$$c_e \frac{dT_e}{dt} = -\frac{\partial S}{\partial x}; \qquad Dc_e \frac{\partial T_e}{\partial x} = -\frac{\partial S}{\partial x}; \qquad Dc_e T_e = -S.$$

conduction with the coefficient of thermal conductivity decreasing with decreasing temperature*. In the case of ordinary heat conduction with a constant coefficient of thermal conductivity $\kappa = const$, $\chi = const$ we would have found from the energy equation that the preheating extends exponentially to infinity:

$$T = T_1 e^{-|x|/x_1}, \qquad T_1 = T(x = 0),$$

where the characteristic scale is $x_1 = \chi/D$. In the case of ordinary heat conduction, the effective thickness of the preheating region x_1, in contrast to the nonlinear case, decreases with increasing wave strength: $x_1 \sim D^{-1} \sim T_1^{-1/2}$.

When electron heat conduction is taken into account in very strong shocks, the un-ionized gas is strongly preheated and ionized even before the compression shock, so that the qualitative features of the structure of a wave propagating through an ionized gas remain the same also in the case when the wave travels through an un-ionized gas.

For an exact calculation of the structure of a shock front in a fully ionized gas we must add to the hydrodynamic equations which account for electron heat conduction, such as (7.10), the entropy equation for an electron gas similar to (7.30)

$$n_i u T_e \frac{d\Sigma_e}{dx} = -\frac{dS}{dx} + \omega_{ei}, \tag{7.37}$$

where ω_{ei} is the energy transferred per unit volume per unit time from the ion to the electron gas; it is given by (7.31). The velocity and the charge density of both gases at any point are assumed to be equal ($n_e = Zn_i$). The enthalpy and pressure are

$$h = h_i + h_e = \tfrac{5}{2}kT_i + Z\tfrac{5}{2}kT_e,$$

$$p = p_i + p_e = n_i kT_i + n_e kT_e.$$

The entropy of the electron gas per ion is

$$\Sigma_e = Zk \ln \frac{T_e^{3/2}}{n_e} + const = Zk \ln \frac{T_e^{3/2}}{\rho} + const. \tag{7.38}$$

Let us find the condition which determines the electron temperature in the compression shock. To do this we integrate (7.37) over the region of the compression shock as its thickness tends to zero, noting that the electron temperature across the shock is continuous (it is equal to T_{e0}). Denoting

* More details on nonlinear heat conduction are given in Chapter X.

quantities ahead of and behind the shock by the subscripts 01 and 02, we can write the result of integration as

$$\rho_0 D T_{e0} \ln \frac{\rho_{02}}{\rho_{01}} = S_{02} - S_{01}. \tag{7.39}$$

The flux has a jump at the discontinuity: the difference between the fluxes on both sides of the discontinuity corresponds to the work to isothermally compress the electron gas by the "external" forces exerted by the ions.

The system of equations describing the front structure can be solved only by numerical integration. This was done by Shafranov [43] for the limiting case of a strong wave ($p_1/p_0 \gg 1$) in a hydrogen plasma ($Z = 1$) with zero initial temperature. The temperature and density distributions are shown in Fig. 7.20. The temperature T_1 here is arbitrary (it is proportional to the

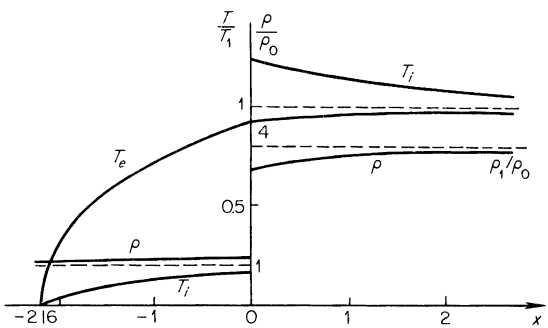

Fig. 7.20. Temperature and density distributions for a strong shock wave in a plasma (the figure is taken from [43]). The electron temperature at the compression shock is $T_{e0} = 0.93T_1$; the ion temperatures ahead and behind the compression shock are $T_{i_1} = 0.16T_1$ and $T_{i_2} = 1.24T_1$, respectively. The densities ahead and behind the compression shock are $\rho_{01}/\rho_0 = 1.13$ and $\rho_{02}/\rho_0 = 3.53$.

square of the wave velocity D). The unit of length that has been used is $0.019 D\tau_{ei_1}$, where τ_{ei_1} is the characteristic exchange time in the final state behind the shock wave front; for example, at an initial density $n_{i0} = n_{e0} = 10^{17}$ cm^{-3} and temperature behind the front $T_1 = 10^5$°K, $\tau_{ei_1} = 3.3 \cdot 10^{-9}$ sec, $D = 94$ km/sec, and the unit of length is $5.9 \cdot 10^{-4}$ cm.

§13. Polarization of a plasma and the creation of an electric field in a shock wave

In the preceding section we have assumed that the electrons and ions are rigidly bound to each other by electric forces, and that the plasma is electrically neutral at each point in the shock; the electron density changes from

point to point and is exactly proportional to the ion density. Actually, however, this assumption is not strictly fulfilled. Due to the presence of large electron density gradients in the compression shock, and to the high mobility of electrons resulting from their exceedingly small mass, conditions are favorable for the diffusion of the electron gas with respect to the ion gas, for changes in the electron concentration, and for the creation of space charges.

The effects of diffusion on the propagation of a shock wave in a binary gas mixture were considered in §5. Diffusion in a plasma, however, is substantially different from diffusion in a mixture of neutral gases. The point is that the smallest change in the relative concentration of the electrons and ions leads to the creation of space charges, i.e., to polarization of the plasma accompanied by the creation of a strong electric field. This field prevents further polarization and inhibits the diffusion electron current.

Let us estimate the order of magnitude of the polarization of a plasma in the presence of gradients of the macroscopic quantities, and the degree to which, on average, the condition of electrical neutrality is satisfied. For simplicity, let us consider a hydrogen plasma ($Z = 1$). We assume the electron temperature to be of the order of T and the electron and ion number density to be given approximately by $n_e = n_i = n$. Furthermore, let us also assume the presence of gradients in the macroscopic quantities, such as density, pressure, etc., such that the characteristic dimension of the region in which appreciable changes in these quantities take place is of the order of x. As a result of electron diffusion in a region of the order of x there will be a difference between the electron and ion densities, $\delta n = n_i - n_e$, which results in the creation of a space charge $e\delta n$. This gives rise to an electric field $E \sim 4\pi e \cdot \delta n \cdot x$* and to a potential difference across the boundaries of the region $\delta\phi \sim Ex \sim 4\pi e\delta n \cdot x^2$. But in the absence of external fields the separation of ions and electrons and the potential difference are maintained only by the thermal motion of the electrons; consequently, the potential energy of the electrons $e\delta\phi$ cannot exceed a value of the order of kT; $e\delta\phi \sim 4\pi e^2 \cdot \delta n \cdot x^2 \sim kT$. From this, the degree of polarization, that is, the extent of the departure from electrical neutrality in the region being considered, is of the order of

$$\frac{\delta n}{n} \sim \frac{kT}{4\pi e^2 n x^2}.$$

A strong separation of the ions and electrons, for which $\delta n/n \sim 1$, can come

* We recall that the electrostatic equations for the field intensity E and the potential ϕ are

$$\nabla \cdot \mathbf{E} = 4\pi e \cdot \delta n, \qquad \mathbf{E} = -\nabla\phi.$$

about only in a thin layer whose thickness d is determined by the condition $\delta n/n \approx 1 \approx kT/4\pi e^2 n d^2$. From this

$$d \approx \left(\frac{kT}{4\pi e^2 n}\right)^{1/2} = 6.9\left(\frac{T^\circ}{n}\right)^{1/2} \text{ cm}.$$

The length d is simply the Debye radius (see §11, Chapter III)*. It characterizes the distance over which the plasma screens the electric field of any charged body, that is, the thickness of the so-called double layer which forms around a charged body. In particular an individual ion can serve as the "charged body" (this is precisely the manner in which the concept of the Debye radius was introduced in §11, Chapter III).

Using the definition of d, the departure from electrical neutrality may be expressed as $\delta n/n \sim (d/x)^2$. The largest gradients in the plasma appear in the viscous compression shock of a propagating strong shock wave, when the macroscopic variables change appreciably over a distance of the order of the mean free path of the charged particles

$$l \sim \frac{(kT)^2}{ne^4 \ln \Lambda} \sim 3.5 \cdot 10^4 \frac{T^{\circ 2}}{n} \text{ cm}\dagger.$$

The average departure from electrical neutrality in the compression shock region ($x = x_{\min} \sim l$) is

$$\frac{\delta n}{n} \sim \left(\frac{d}{l}\right)^2 \sim \frac{e^6 n (\ln \Lambda)^2}{4\pi (kT)^3} \approx 3.9 \cdot 10^{-8} \frac{n}{T^{\circ 3}}.$$

This quantity is very small for all reasonable values of density and temperature; for example, at $T = 10^{5\circ}$K, $n = 10^{18}$ cm^{-3}, $d \approx 0.8 \cdot 10^{-6}$ cm, $l \approx 3.5 \cdot 10^{-4}$ cm, $\delta n/n \sim 4 \cdot 10^{-5}$, $\delta\phi \sim kT/e = 8.6$ volts‡, and $E \sim \delta\phi/l \sim 2.5 \cdot 10^4$ volts/cm.

We note that the compression of the electron gas in a strong compression shock whose thickness is of the order of a mean free path l is due only to the electric forces exerted by the ions (the compression of the ion gas is usually due to viscosity). Consequently, the potential difference in the compression shock is determined by the work done per electron in compressing the electron gas $e(\phi_{02} - \phi_{01}) = kT_{e0} \ln(\rho_{02}/\rho_{01})$. For a several-fold compression the logarithm is of the order of unity and, consequently, $e\delta\phi \sim kT$, as was stated above.

The distribution of charge, electric field, and potential in a shock front in a

* More precisely, the Debye radius multiplied by $\sqrt{2}$, since n in (3.78) is the total number of ions and electrons.

† The logarithmic factor in the mean free path (see §20, Chapter VI) is usually of the order $\ln \Lambda \sim 10$.

‡ The numerical value of $\delta\phi$ is of the order of the temperature in electron volts.

plasma are shown in Fig. 7.21. The significant difference between the distributions of the concentrations of the different components in a plasma and the distributions of the concentrations in a mixture of neutral gases lies in the fact that, together with the region of increased electron concentration in the

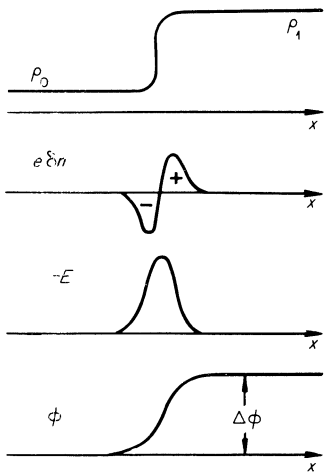

Fig. 7.21. Mass density, space charge density, electric field intensity, and electrostatic potential distributions in a shock front propagating in a plasma with electron diffusion taken into account.

forward part of the shock front, there arises a region of decreased concentration in the rear part of the wave. For a mixture of neutral gases only the light component concentrates in the shock front (the excess mass of the light component arrives from "infinity"). This situation is not possible in the case of a plasma. Concentration of electrons without a simultaneous concentration of positive ions in a neighboring region would lead to the appearance of an electric field at "infinity", that is, it would require the expenditure of an infinite amount of energy.

In [45], the structure of a weak shock front in a plasma was examined, taking into account only the effect of electron diffusion impeded by the electric forces and without taking into account either viscosity or heat conduction, in a manner similar to that of Cowling [22] for a mixture of electrically neutral gases (see §5)*. As in the electrically neutral case diffusion guarantees the spreading out of a shock discontinuity which is not too strong. Because of the restraining effect of the electric field the thickness of the transition layer is smaller than in the neutral gas mixture.

Jaffrin and Probstein [89] have considered the structure of a shock wave in a fully ionized plasma in a general form, simultaneously taking into account the viscosity, the thermal conductivity, and the polarization and charge separation

* See also [44, 46].

of the plasma. They have used as their starting point a system of hydrodynamic equations for a mixture of electron and ion gases and Poisson's equations for the electric field. The mass density, electron, and ion temperature distributions which were obtained in this paper agree with the distributions as described in the preceding section. The qualitative considerations given on the formation of a double electric layer, shown schematically in Fig. 7.21, in the region of the viscous shock are substantiated. However, in a strong shock wave there appears still another double electric layer of the same type, which is located at the leading edge of the region heated by electron thermal conduction, at the point where a sharp rise takes place in the electron temperature. The physical nature of this second layer is the same as that of the basic layer: the temperature rise at the edge of the heated layer is accompanied by a fairly small (in comparison with the inner viscous shock) but very sharp compression, and in this region the electrons diffuse relative to the ions and a charge separation results.

3. *Radiant heat exchange in a shock front*

§14. Qualitative picture

When a shock wave is propagated through a gas occupying a large volume, and the dimensions of the heated region are very large in comparison with the mean free path of a photon so that the gas temperature changes very little over a distance of the order of a mean free path, the thermal radiation in a wave is brought into local thermodynamic equilibrium with the fluid. Radiative equilibrium also exists immmediately behind the shock front.

The energy density and radiation pressure become comparable with the energy density and pressure of the fluid only at extremely high temperatures or extremely low gas densities. For example, in standard density air this occurs at a temperature of $\approx 2.7 \cdot 10^6$ °K. The radiation energy and pressure in shock waves of not too high a strength are much smaller than the energy and pressure of the fluid, and therefore have almost no effect on quantities behind the front. The relationship between the radiation energy flux and the energy flux of the fluid is, however, different, since the shock velocities encountered in practice are much smaller than the speed of light. The ratio of energy fluxes $\sigma T^4/D\rho\varepsilon \sim (U_{\text{rad}}/\rho\varepsilon)(c/D)$, is, roughly speaking, greater by a factor of c/D than the ratio of energy densities. Thus, for $D = 100$ km/sec, $c/D = 3 \cdot 10^3$. In atmospheric air, for example, both fluxes become equal already at a temperature $T \sim 300{,}000$°K, for which the radiation density is still very small.

It would seem that radiative transfer of energy away from the front of a

strong shock must play an important role, and that therefore in the third equation of (7.4) with the energy flux of the fluid we should also include the energy flux carried away from the surface of the front by radiation $S = \sigma T_1^4$. This could have an appreciable effect on the final state behind the shock front, and could lead to a high density behind the front similar to the high density obtained with increased specific heats. Actually, however, the energy lost by radiation from the front surface is rather limited and the effect of this loss is usually negligible. The point is that in a continuous spectrum gases are transparent only to the photons of comparatively low energy. Both atoms and molecules strongly absorb photons whose energies exceed the ionization potentials, giving rise to the photoelectric effect, while molecules, as a rule, absorb photons of even lower energies; for example, the boundary of the transparent region for cold air lies at $\lambda \sim 2000$ Å and $h\nu \sim 6$ ev. When the temperature behind the front is high, the energy contained in the low-frequency region comprises only a small fraction of the total energy in the spectrum. Thus, at a temperature behind the front of $T = 50{,}000°\text{K}$ only 4.5% of the energy of the Planck spectrum is concentrated in the transparent region of air $h\nu < 6$ ev. In this case the low energy photons are in the Rayleigh–Jeans region of the spectrum and their flux (and the corresponding possible energy losses) is in any case proportional not to the fourth but only to the first power of temperature.

The major part of the radiation from the shock front actually escapes to "infinity" only at temperatures for which the maximum of the Planck spectrum lies in the transparent region of the spectrum, at temperatures behind the front of the order of 1–2 ev. At such temperatures, however, the absolute magnitude of the radiation flux σT_1^4 is very small and the additional density increase resulting from radiation losses in air at standard density does not exceed one percent.

Thus, the presence of thermal radiation has only a very small effect on the flow variables behind the front of a not too strong shock. However, this is not the case for the effect of the radiation on the internal structure of the transition layer between the initial and final thermodynamic equilibrium states of the gas, on the structure of the shock front itself. Here the radiation in strong waves (which are of real interest) is found to play a very important role and, moreover, it is precisely the radiant heat exchange which determines the front structure. The problem of the structure of a shock front taking into account radiant heat exchange, to which §§14–17 of the chapter are devoted, has been studied by the present authors in [42, 47–49]. Although the flux of radiation going out from the wave front to "infinity" is very small and exerts no influence in terms of energy on the shock wave flow variables, the fact that it exists is of tremendous importance since it enables the observation of the wave by optical methods. The problem of shock wave luminosity and the

brightness of the front surface is closely interwoven with the problem of the front structure. It will be considered in Chapter IX.

Owing to the opaqueness of the cold gas, the radiation emanating from the surface of the shock discontinuity in strong waves is almost entirely absorbed ahead of the discontinuity and heats the layers of gas flowing into the discontinuity. The energy which goes into the heating is produced by emission from the gas layers which have already suffered a shock compression and which as a result are cooled by the radiation. The effect thus reduces to the transfer of energy from one gas layer to the others by radiation. Radiant heat exchange takes place in distances of the order of the absorption mean free path of the photons. Usually the photon mean free path is several orders of magnitude larger than the gaskinetic mean free path of the particles (see Chapter V) and is larger than the thickness of the relaxation layer in which thermodynamic equilibrium is established in the fluid. Thus, in air at standard density the mean free paths for photons with energies $h\nu \sim 10$–100 ev, corresponding to temperatures behind the front of $T_1 \sim 10^4$–10^5 °K, are of the order of 10^{-2}–10^{-1} cm, while the gaskinetic mean free path is of the order of 10^{-5} cm.

The shock front thickness, in which the radiant heat exchange plays an important role in the energy balance, is determined by the photon mean free path, which is the greatest length scale. In a sense we can speak about the relaxation of radiation in a shock front and about the establishment of equilibrium between the radiation and the fluid behind the front. Let us follow qualitatively the change in the front structure going from weak to strong waves. Here we shall consider the phenomenon on a "large scale", disregarding the "small scale" details related to the relaxation of the various degrees of freedom of the gas; we assume that the fluid at each point of the wave is in thermodynamic equilibrium. The viscous compression shock together with the relaxation region behind it will be considered as a mathematical discontinuity.

In the limiting case of a sufficiently weak wave when the role of the radiation on the energy balance is small, the profiles of all the variables across the

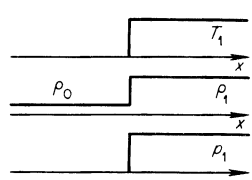

Fig. 7.22. Temperature, density, and pressure profiles in a "classical" shock wave.

shock wave have the "classical" step-like character (Fig. 7.22). As the strength increases, the radiation flux from the front surface σT_1^4 increases very rapidly.

The radiation is absorbed ahead of the discontinuity at a distance of the order of a photon mean free path and heats the gas; the heating drops off with distance from the discontinuity as a result of absorption of the radiation flux. The compression shock is now propagated not through a cold, but through a heated gas and the temperature behind the shock T_+ is higher than without heating, that is, it is higher than in the final state. The temperature behind the compression shock decreases from T_+ to T_1. In other words, a gas particle passing through the shock wave is first heated by radiation and, after being subjected to a shock compression, is then cooled by the emission of part of its energy as radiant flux. Heating of the gas ahead of the discontinuity leads to an increase in its pressure and to some density increase (and also to a slowing down, in a coordinate system in which the front is at rest). In the compression shock the gas is compressed to a density slightly lower than the final one. The cooling of the gas behind the compression shock helps to compress it further to the final density (as in the case of the decrease in temperature resulting from the excitation of additional degrees of freedom). In this process the pressure also increases. The profiles of temperature, density, and pressure for the wave described are shown schematically in Fig. 7.23.

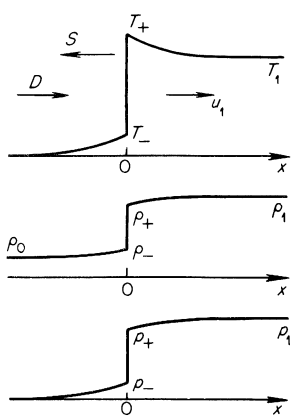

Fig. 7.23. Temperature, density, and pressure profiles in a shock front of not too large a strength, taking into account radiant heat exchange.

The preheating temperature ahead of the discontinuity T_- is proportional to the radiation flux emerging from the discontinuity surface $-S_0 \approx \sigma T_1^4$, and, therefore, increases rapidly with increasing wave strength. Thus, in air at standard density $T_- \approx 1400°\text{K}$ for $T_1 = 25{,}000°\text{K}$, $T_- = 4000°\text{K}$ for $T_1 = 50{,}000°\text{K}$, and $T_- = 60{,}000°\text{K}$ for $T_1 = 150{,}000°\text{K}$. The difference between the overshoot temperature behind the shock T_+ and the final temperature T_1 increases correspondingly (roughly speaking, $T_+ - T_1 \approx T_-$). At some temperature behind the front $T_1 = T_{cr}$, the preheating temperature T_- reaches the value of T_1 and the temperature profile assumes the shape

shown in Fig. 7.24. This temperature T_{cr} is approximately equal to 300,000°K for air, and can be called critical since it divides two rather different types of shock front structure.

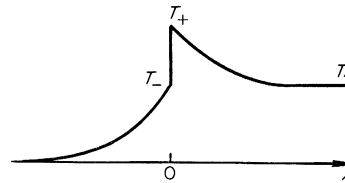

Fig. 7.24. Temperature profile in a shock wave of "critical" strength.

Let us consider a strong wave of supercritical amplitude, with a temperature behind the front $T_1 > T_{cr}$. The photon energy flux emitted by the gas behind the compression shock and emerging from the discontinuity surface toward the cold gas would be sufficient to heat a layer whose thickness is of the order of a photon absorption mean free path to a very high temperature, higher than T_1. Can such an intensive heating be actually achieved? Obviously, it cannot, since otherwise the preheating layer would begin to radiate strongly and cool down very rapidly to the temperature T_1. The formation of a state with $T_- > T_1$ would mean that in a closed system heat could be spontaneously transferred from the low- to high-temperature gas layers, in contradiction with the second law of thermodynamics*. Actually, the energy which the radiation removes from the gas heated in the compression shock is simply used up in heating the thicker layers ahead of the discontinuity. Photons emerging from behind the surface of the discontinuity are absorbed ahead of the discontinuity in a layer of thickness of the order of a mean free path and the fluid, heated to a temperature close to T_1, radiates and thus heats the neighboring layers, etc. We are dealing here with a typical case of preheating of the gas by radiation heat conduction. A heat-conduction wave is propagated ahead of the discontinuity, encompassing a thicker gas layer, the higher is the shock strength. The phenomenon is completely analogous to a shock wave with electron heat conduction considered in §12 (radiation heat conduction is also nonlinear).

The temperature and density profiles in a shock wave of supercritical strength are shown in Fig. 7.25. As before, behind the compression shock there is a temperature peak resulting from the shock compression. As before, the gas particles which have undergone the shock compression are cooled by emitting a part of their energy, which goes into developing a thermal wave ahead of the discontinuity. Unlike the subcritical case, however, the thickness of the peak is now less than a radiation mean free path and decreases with increasing wave strength (see also §17).

* Additional details on the impossibility of a state with $T_- > T_1$ will be presented in §17. A rigorous proof of this statement is given in [42].

In the radiation heat conduction approximation, where the details of the phenomena occurring at distances less than a mean free path are not considered, the peak is "cut off" as shown by the dashed line in Fig. 7.25, and

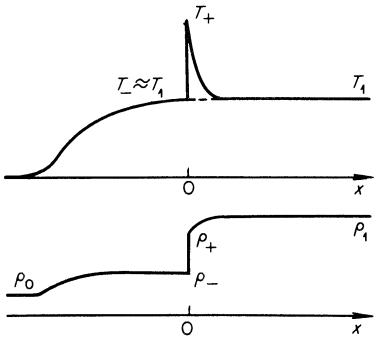

Fig. 7.25. Temperature and density profiles in a very strong shock front taking into account radiant heat exchange. The dashed line corresponds to the radiation heat conduction approximation (isothermal jump).

the shock takes on the character of an "isothermal" shock (see §3 of this chapter). In the following sections the physical picture whose general features have been outlined above will be justified mathematically.

§15. Approximate formulation of the problem of the front structure

As usual, we shall consider a one-dimensional steady flow in a coordinate system in which the front is at rest. A number of simplifications will be introduced to make clear the specific features of the front structure which are related to radiant heat exchange. The gas will be assumed to be a perfect one with constant specific heats, so that its pressure and specific internal energy may be expressed by the simple relations

$$p = R\rho T, \qquad \varepsilon = \frac{1}{\gamma - 1} RT.$$

The viscous compression shock, together with the relaxation layer in which thermodynamic equilibrium in the fluid is established, will be replaced by a mathematical discontinuity. We shall neglect relaxation phenomena, viscosity, heat conduction, and also electron heat conduction in the radiant heat exchange region*. The shock wave is taken to be strong (the initial pressure and energy of the fluid are small in comparison with the final values). We shall not consider, however, extremely strong waves; in our case we may neglect the energy and pressure (but not the flux!) of radiation. We also neglect the small flux of low energy photons escaping from the wave front to

* Estimates in a number of actual cases, including the practically important case of a shock wave in standard density air, show that electron heat conduction plays less of a role than that of the transfer of energy by radiation (see [48]).

"infinity" by assuming that the radiation flux ahead of the front is zero.

Using the above assumptions the system of integrals of the hydrodynamic equations (7.10) takes the following form:

$$\begin{aligned} \rho u &= \rho_0 D, \\ p + \rho u^2 &= \rho_0 D^2, \\ \varepsilon + \frac{p}{\rho} + \frac{u^2}{2} + \frac{S}{\rho_0 D} &= \frac{D^2}{2}. \end{aligned} \tag{7.40}$$

Here S is the radiation energy flux. We note that this flux is directed opposite to the gas flow moving in the positive x direction, so that $S < 0$ ($D, u > 0$). Ahead of the front, at $x = -\infty$, and behind the front, at $x = +\infty$, the flux $S = 0$, and all the variables take on their initial or final values; these will be denoted again by the subscripts "0" and "1". The x coordinate will be measured from the compression shock.

In order to determine the radiation flux, we must add to the hydrodynamic equation (7.40) the radiative transfer equation. We shall consider the angular distribution of photons within the framework of the diffusion approximation, replacing the rigorous kinetic equation for the intensity by two equations for the density and flux of radiation (see §10, Chapter II). We emphasize that the diffusion approximation does not formally make any assumptions regarding the proximity of the radiation density to its equilibrium value, and that the diffusion approximation is by no means equivalent to the radiation heat conduction approximation. The diffusion approximation can also be used to describe nonequilibrium radiation, by taking into account the angular distribution of photons only approximately (see the discussion of this point in §13, Chapter II). We shall use only the spectrally integrated values of the radiation density and flux U and S, introducing for this purpose a photon mean free path l appropriately averaged with respect to frequency. As noted in Chapter II, this approximation is, strictly speaking, possible only in definite limiting cases. It does not, however, alter the qualitative relations governing the radiative heat transfer and is, therefore, sufficient for our purposes.

The radiation equations in the above approximations (see (2.62) and (2.65)) can be written

$$\frac{dS}{dx} = \frac{c(U_p - U)}{l},$$

$$S = -\frac{lc}{3}\frac{dU}{dx}.$$

Here $U_p = 4\sigma T^4/c$ is the energy density of equilibrium radiation, corresponding to the temperature of the fluid at the given point x.

Since the hydrodynamic and radiative transfer equations do not explicitly contain x, we can transform to a new coordinate—the optical thickness τ, measured from the point $x = 0$ in the positive x direction

$$d\tau = \frac{dx}{l}, \qquad \tau = \int_0^x \frac{dx}{l}. \tag{7.41}$$

If the mean free path l is known as a function of the temperature and density, we can easily transform the various quantities in the final solution from distributions with respect to the optical coordinate to distributions with respect to x, by means of equations (7.41) (for $l = const$ both distributions are obviously the same). In terms of the optical thickness the transfer equations take the form

$$\frac{dS}{d\tau} = c(U_p - U), \tag{7.42}$$

$$S = -\frac{c}{3}\frac{dU}{d\tau}. \tag{7.43}$$

The hydrodynamic equations (7.40) and the radiative transfer equations (7.42) and (7.43), together with the natural boundary conditions expressing the absence of radiation in the cold gas ahead of the wave and the fact that the radiation behind the wave front is in thermodynamic equilibrium*

$$\tau = -\infty, \quad S = 0, \quad U = 0, \qquad T = 0, \tag{7.44}$$

$$\tau = +\infty, \quad S = 0, \quad U = U_{p_1} = \frac{4\sigma T_1^4}{c}, \qquad T = T_1, \tag{7.45}$$

completely describe the structure of the shock front within the present statement of the problem. The system of differential equations is of second order. The order can be decreased by eliminating τ from the system by dividing equations (7.42) and (7.43) by each other

$$\frac{dS}{dU} = \frac{c^2}{3}\frac{U - U_p}{S}. \tag{7.46}$$

The (p, V), (T, V), and (S, V) diagrams considered in §3 are very convenient for clarifying the physical meaning of the relations governing the front structure. Introducing again the relative specific volume $\eta = V/V_0$, equal to the reciprocal of the density ratio or to the velocity ratio

$$\eta = \frac{V}{V_0} = \frac{\rho_0}{\rho} = \frac{u}{D},$$

* Only two of these conditions are independent, the others follow from the equations.

we find from the first two equations of (7.40) that in the regions where the flow variables are continuous the pressure changes along the straight line

$$p = \rho_0 D^2(1 - \eta). \tag{7.47}$$

The dependence of temperature and flux on the density ratio is described by relations similar to (7.13) and (7.14). These relations are obtained from (7.40) for the case of a gas with constant specific heats. Replacing the Mach number in (7.13) and (7.14) by the temperature behind the shock front T_1, we obtain

$$T = \frac{T_1\eta(1 - \eta)}{\eta_1(1 - \eta_1)}, \tag{7.48}$$

$$S = -\frac{\rho_0 D R T_1(1 - \eta)(\eta - \eta_1)}{2\eta_1^2(1 - \eta_1)}, \tag{7.49}$$

where $\eta_1 = (\gamma - 1)/(\gamma + 1)$. Radiation in a shock wave plays an important role only at high temperatures, when the gas is strongly ionized. For numerical estimates the effective specific heat ratio in the ionization region can be taken equal to $\gamma = 1.25$. The corresponding density ratio across the wave front is $1/\eta_1 = 9$, $\eta_1 = 0.111$.

The functions $T(\eta)$, $S(\eta)$, and $p(\eta)$ are shown in Figs. 7.26 and 7.27.

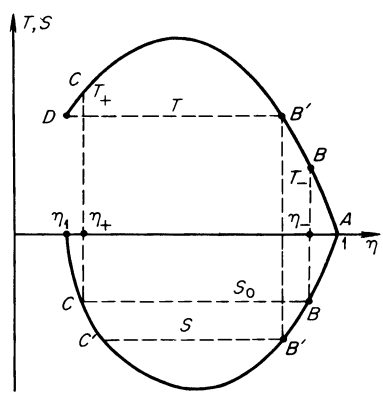

Fig. 7.26. T,η and S,η diagrams for a shock wave taking radiant heat exchange into account.

Figure 7.26 shows that the $T(S)$ curve, which can be obtained from (7.48) and (7.49), has two branches. One of them, which in the limit $S \to 0$ gives $T \to 0$ ($\eta \to 1$), corresponds to states close to the initial state, and thus to the preheating region ahead of the discontinuity; the other, which in the limit $S \to 0$ gives $T \to T_1$ ($\eta \to \eta_1$), corresponds to the states close to the final state, and thus to the region behind the discontinuity.

In the following two sections we shall find approximate solutions of the equations for the two limiting cases described in §14, i.e., for shock waves of

subcritical and supercritical strengths. It should be noted that the transition from the first to the second case is continuous. It is simply that for intermediate strengths, close to critical, it is not possible to find solutions in analytic form. Numerical integration for these intermediate strengths is not difficult. However, this is not really necessary, since the limiting analytic solutions found are valid for strengths very close to critical from either side.

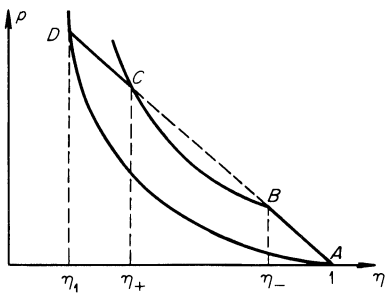

Fig. 7.27. p, η diagram for a shock wave taking radiant heat exchange into account.

§16. The subcritical shock wave

Let us consider a shock of moderate strength in which the radiation-induced effects are small. The temperature behind the compression shock will then be close to the final temperature and a radiation flux of absolute magnitude $|S_0| \approx \sigma T_1^4$ will come out from the surface of the discontinuity. Following the state of a gas particle incident on the wave, we note that the point representing the particle on the (T, η), (S, η), and (p, η) diagrams moves from the initial position A in the direction of increasing compression up to position B at which the flux is equal to S_0. The gas density, temperature, pressure, and radiation flux in the parcel increase monotonically as the discontinuity is approached. It follows from equations (7.48) and (7.49), and this is also evident from Fig. 7.26, that the increase in density on those branches of the curves which originate from the initial point A, in the preheating region, is very small. Even for $T = T_1$, the density ratio on this branch will be only $1/(1 - \eta_1) = 1.13$ (if $\gamma = 1.25$ and $\eta_1 = 0.111$), and for temperatures ahead of the discontinuity T_- smaller than T_1, the density ratio in the preheating region is even smaller. If we approximately eliminate η from (7.48) and (7.49) and express S in terms of T to second order in η_1, we obtain

$$-S = \frac{D\rho_0 RT}{\gamma - 1} = D\rho_0 \varepsilon. \tag{7.50}$$

This equation, which is obtained from the energy integral (7.40) if the terms p/ρ, $D^2/2$, and $u^2/2$ are dropped, has a simple physical meaning. It denotes the

fact that the radiant energy absorbed in the preheating region is used up only in raising the gas temperature. Actually, it is easy to show that the compression work p/ρ and the change in the kinetic energy $D^2/2 - u^2/2$, which are essentially proportional to η_1, balance each other to within order η_1^2.

The equation of conservation of energy in the case when the gas is neither slowed down nor compressed, written as

$$-S = D\rho_0\varepsilon(T, \rho_0), \tag{7.51}$$

is valid in general when the specific heats depend on temperature. If we evaluate this equation at the point $x = 0$ directly ahead of the discontinuity we find the maximum preheating temperature T_-

$$|S_0| \approx \sigma T_1^4 = D\rho_0\varepsilon(T_-). \tag{7.52}$$

In a gas with constant specific heats $D \sim \sqrt{T_1}$ and $T_- \sim T_1^{3.5}$, and the preheating rapidly increases with increasing wave strength.

We may use (7.52) to obtain an approximate estimate of the temperature behind the front for which the temperature ahead of the compression shock T_- reaches the value T_1 (we call such a wave critical). The approximation lies in the fact that the flux from the discontinuity surface is again assumed to be σT_1^4, although it is actually slightly greater, because the temperature behind the discontinuity is slightly higher than T_1. The approximate equation for the critical condition $T_1 = T_{cr}$ is

$$\sigma T_{cr}^4 = D(T_{cr})\rho_0\varepsilon(T_{cr}). \tag{7.53}$$

Table 7.4

TEMPERATURE AHEAD OF COMPRESSION SHOCK IN AIR AT STANDARD DENSITY

D, km/sec	T_1, °K	ε_-, ev/mol.	T_-, °K	D, km/sec	T_1, °K	ε_-, ev/mol.	T_-, °K
23.3	50,000	3.7	6,800	56.5	150,000	122	60,000
28.5	65,000	8.4	9,000	81.6	250,000	635	175,000
32.1	75,000	13.1	12,000	86.2	275,000	910	240,000
40.6	100,000	32.7	25,000	88.1	285,000	1020	285,000

In Table 7.4 are presented values of the temperature ahead of the compression shock in air at standard density calculated from (7.52), taking into account the actual variation of $\varepsilon(T)$. It is evident from the table that the critical temperature in air is approximately equal to 300,000°K (285,000°K according to (7.53)). As follows from (7.53), the critical temperature is the temperature for which the energy flux of the radiation and of the fluid become approximately equal (we recall the remark made at the beginning of §14).

Returning to the original equations for a gas with constant specific heats, let us find the approximate solution in the preheating region of a subcritical wave. If the temperature in the preheating region is small in comparison with the temperature behind the front ($T_- < T_1$), then the equilibrium radiation density, which is proportional to the fourth power of the gas temperature ($U_p \sim T^4$), is much less than the actual density U, which is determined by radiation passing through the gas and coming out from behind the surface of discontinuity at a temperature T_1 ($U \sim |S_0| \sim T_1^4$). The radiation born in the preheating region in this case makes only a small contribution to the total flux and density. The radiation density in the preheating region is therefore significantly out of equilibrium. Neglecting in (7.42) and (7.46) U_p in comparison with U, we find for the solution ahead of the discontinuity for $\tau < 0$

$$-S = \frac{cU}{\sqrt{3}} = -S_0 e^{-\sqrt{3}|\tau|}, \tag{7.54}$$

$$T = T_- e^{-\sqrt{3}|\tau|}, \tag{7.55}$$

$$\frac{\rho - \rho_0}{\rho_0} = \frac{\rho_- - \rho_0}{\rho_0} e^{-\sqrt{3}|\tau|}, \tag{7.56}$$

$$p = p_- e^{-\sqrt{3}|\tau|}. \tag{7.57}$$

All the quantities decrease exponentially with optical thickness with increasing distance from the discontinuity (Fig. 7.28). The values of T_-, ρ_-, and

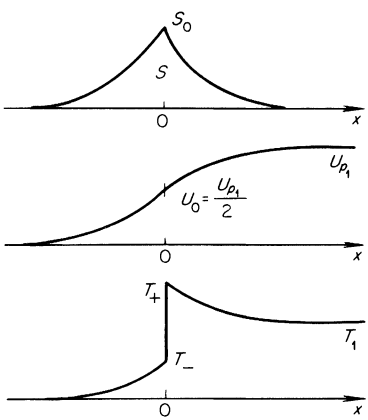

Fig. 7.28. Radiation flux, density of radiation, and temperature profiles in a subcritical shock wave.

p_- can be easily calculated with the aid of (7.52) and (7.48) and the equation of state.

The radiation density and flux at the shock discontinuity remain continuous. Actually, according to (7.43), a discontinuity in the radiation density would

correspond to an infinite value of the flux, which from conservation of energy must actually be finite. A discontinuity in flux would lead to an unsteady accumulation or loss of radiant energy at the discontinuity. Consequently, a representative point in the T, η and S, η diagrams on passing through the viscous shock jumps from a point B on one of the branches to position C on another branch, corresponding to the same flux S_0. (The derivative of the flux in this case, of course, is discontinuous.) The same is true on the p, η diagram: the gas is compressed through the compression shock following the Hugoniot curve CB passing through the point B. After the shock compression the state of the particle monotonically approaches its final position at the point D. Here, the temperature and radiation flux decrease and the gas density and pressure increase.

As is evident from the T, η diagram, in a wave of not too large strength the temperature difference between the value behind the discontinuity T_+ and the value behind the front T_1 is, like the volume change behind the discontinuity, not large. Eliminating η as before from (7.48) and (7.49) for the second branch, we find to second order in η_1 the relation between the flux and temperature behind the discontinuity

$$-S = \frac{1}{\eta_1(3-\gamma)} D\rho_0 R(T - T_1). \tag{7.58}$$

For an approximate solution of the radiative transfer equation in the region behind the discontinuity, we note that the temperature here changes very little and we can set $U_p \approx U_{p1} = 4\sigma T_1^4/c = const$. We obtain for $\tau > 0$

$$-S = \frac{c}{\sqrt{3}}(U_{p1} - U) = -S_0 e^{-\sqrt{3}\tau}, \tag{7.59}$$

$$T - T_1 = (T_+ - T_1)e^{-\sqrt{3}\tau}, \tag{7.60}$$

with $T_+ - T_1 = [(3-\gamma)/(\gamma+1)]T_- \approx 0.78T_-$ for $\gamma = 1.25$. The radiation density at the discontinuity is found by patching together at $\tau = 0$ the two branches of the curves $U(S)$ given by (7.54) and (7.59). We obtain*

$$U_0 = \tfrac{1}{2}U_{p1} = 2\sigma T_1^4. \tag{7.61}$$

The radiation density and flux profiles in a subcritical wave are illustrated in Fig. 7.28, in which for comparison the temperature profile is also shown.

Let us determine the limits of applicability of the approximate solution of the equations in the preheating region. Equation (7.50) is very accurate even in a wave of critical strength, since for $\gamma = 1.25$ the density ratio ahead of the

* We note that here another value $-S_0 = (2/\sqrt{3})\sigma T_1^4$ is obtained for the flux, which differs slightly from the preceding value $-S_0 = \sigma T_1^4$. The small discrepancy is a result of the inaccuracy of the diffusion approximation, and it disappears when the exact radiative transfer equation is used; for additional details see [47].

discontinuity is small: $\rho_-/\rho_0 \leqslant 1.13$. The solution of the radiative transfer equation (7.54), however, was obtained under the approximation $U_p \ll U$ and becomes invalid when the radiation density U is comparable with its equilibrium value. It follows from (7.54) and (7.50) that this occurs at a temperature T_c satisfying the equation

$$\frac{4\sigma T_c^4}{\sqrt{3}} = \frac{D\rho_0 R T_c}{\gamma - 1}. \tag{7.62}$$

Comparing this equation with (7.53) in which the specific heats are assumed constant [$\varepsilon = RT/(\gamma - 1)$], and noting that D has only a weak dependence on temperature ($D \sim \sqrt{T_1}$ with $\gamma = const$), we see that T_c is very close to the critical temperature T_{cr}. It follows from this that the radiation density in the preheating region is always out of equilibrium for temperatures below critical and that our approximate solution is valid for waves with strengths close to the critical.

Essentially, the radiation density becomes of the order of its equilibrium value when the radiant energy and the hydrodynamic fluxes are comparable. As can be seen from (7.54) to (7.57), the optical thickness of the preheating region in a subcritical wave is of the order of unity. The geometric thickness of the region is, consequently, of the order of a radiation mean free path averaged over the spectrum. In air at standard density this thickness is of the order of 10^{-2}–10^{-1} cm. The thickness is the greater, the higher is the temperature behind the front, since the radiation mean free path increases with increasing photon energies. The thickness of the region behind the compression shock where the gas and the radiation approach their final states is also of approximately the same order of magnitude.

§17. The supercritical shock wave

Let us consider a shock wave of large, supercritical strength when the temperature behind the front $T_1 > T_{cr}$. The temperature in the preheating region increases from zero to T_-, which is equal to the final temperature T_1 and thus also higher than T_{cr}. Since the temperature T_c defined by (7.62) is close to T_{cr}, T_- is greater than T_c. The density ratio in the preheating region is not large and (7.50) still applies.

At the leading edge of the region where the temperature is lower than T_c, the radiation is again out of equilibrium, and the solution is of the type of (7.54) and (7.55) in which T, S, and U decrease exponentially with the optical thickness. At the point where the temperature reaches the value T_c, the radiation density is of the order of its equilibrium value and the flux S is of the order of the Stefan–Boltzmann flux σT^4. Moving further toward the discontinuity, the radiation flux increases by virtue of the conservation relation

(7.50) in proportion to the temperature ($S \sim T$), so that it becomes smaller than the Stefan–Boltzmann flux. This means that in the temperature region where $T > T_c$, oppositely directed one-sided fluxes (which are of the order of σT^4) to a large extent balance each other, the generated radiation at each point is comparable to the absorption, and thus the radiation density is close to its thermodynamic equilibrium value. In other words, in this layer of the preheating region the radiation is in local equilibrium with the fluid and the radiative transfer has the character of radiation heat conduction. The flux S is now determined by the temperature gradient, and its smallness in comparison with the Stefan–Boltzmann flux is due to the fact that the temperature changes very little over a distance of the order of a photon mean free path.

A solution for the radiation heat conduction layer can be obtained by replacing the radiation density U in (7.43) by the equilibrium value $U_p \approx U$

$$S = -\frac{c}{3}\frac{dU_p}{d\tau} = -\frac{16\sigma c T^3}{3}\frac{dT}{d\tau}. \tag{7.63}$$

Solving this equation together with the algebraic equation (7.50), we find the temperature, flux, and radiation density profiles in the equilibrium layer of the preheating region. They should be patched together with the solution at the leading edge of the nonequilibrium layer at a point with temperature $T = T_c$, which effectively separates the two layers. The optical coordinate of this point will be denoted by τ_c. After some elementary calculations we obtain in the nonequilibrium layer, for $\tau < \tau_c$, $|\tau| > |\tau_c|$,

$$\frac{T}{T_c} = \frac{cU}{4\sigma T_c^4} = \frac{\sqrt{3}S}{4\sigma T_c^4} = e^{-\sqrt{3}|\tau - \tau_c|}, \tag{7.64}$$

and in the equilibrium layer for $\tau_c < \tau < 0$, $0 < |\tau| < |\tau_c|$,

$$\frac{T}{T_c} = \frac{\sqrt{3}S}{4\sigma T_c^4} = \left(\frac{cU}{4\sigma T_c^4}\right)^{1/4} = \left(1 + \frac{3\sqrt{3}}{4}|\tau - \tau_c|\right)^{1/3}, \tag{7.65}$$

where τ_c is expressed in terms of the temperature ahead of the discontinuity by

$$|\tau_c| = \frac{4}{3\sqrt{3}}\left[\left(\frac{T_-}{T_c}\right)^3 - 1\right]. \tag{7.66}$$

Since the temperature in the nonequilibrium layer decreases exponentially, decreasing by several times over an optical distance equal to unity, the value of $|\tau_c|$ in the case of a very strong wave, with $T_-^3 \gg T_c^3$, is effectively the optical thickness of the preheating region. We note that in the equilibrium layer the photon mean free path is taken to be the Rosseland mean value (see §12, Chapter II). The temperature ahead of the discontinuity in the supercritical wave almost coincides with the temperature T_1 behind the front.

The temperature ahead of the discontinuity T_- can never become higher than the final temperature behind the front T_1. Indeed, if $T_- > T_1$, then the radiation density in the preheating region ahead of the discontinuity, which is approximately equal to $U_- \approx 4\sigma T_-^4/c$, would become higher than the radiation density behind the front $U_{p_1} = 4\sigma T_1^4/c$. Consequently, the radiation density in the region between the discontinuity and the final state ($0 < \tau < +\infty$) would decrease in the direction away from the discontinuity. The flux $S \sim -dU/d\tau$ would be positive and directed in the direction of gas motion. However, this contradicts (7.48) and (7.49), which follow from the conservation laws and which show that the flux in the shock wave is everywhere negative and directed opposite to the gas motion. The temperature T_- is thus bounded above by the value of T_1. The impossibility of heating the gas ahead of the compression shock to a temperature exceeding the temperature behind the front T_1 attests at the same time to the fact that a discontinuity must necessarily arise in the solution (a representative point on the T, η and S, η diagrams, in order to reach the final position D, must "jump over" from a position B' on another branch). The above physical considerations on the impossibility of the temperature T_- exceeding T_1 and the necessity that a discontinuity must arise, are confirmed by a rigorous analysis of the equations for this regime (see [42]).

Since in a supercritical wave $T_- \approx T_1$, the radiation density ahead of the discontinuity is close to equilibrium and even ahead of the discontinuity it almost reaches its final value. Thus,

$$U_0 = U_- \approx \frac{4\sigma T_-^4}{c} \approx \frac{4\sigma T_1^4}{c} = U_{p_1}, \tag{7.67}$$

and in the region behind the discontinuity the radiation density remains practically constant

$$U(\tau) \approx U_{p_1} = \frac{4\sigma T_1^4}{c} \qquad \text{for} \quad \tau > 0. \tag{7.68}$$

It follows from (7.65) that the flux at the discontinuity is equal to

$$S_0 = \frac{4\sigma T_c^4}{\sqrt{3}} \frac{T_1}{T_c}. \tag{7.69}$$

On the T, η and S, η diagrams a representative point in a supercritical wave moves along the curves from the point A to the point B' and then jumps to the point C', where the flux is the same. The temperature behind the discontinuity T_+ can be obtained from (7.48) and (7.49). It is

$$T_+ = (3 - \gamma)T_1. \tag{7.70}$$

Using the radiation heat conduction approximation in the region behind the discontinuity together with the fact that the radiation density in this region is constant, we find that the temperature is also constant. The temperature across the compression shock is continuous and equal to T_1. A representative point on the T, η and S, η diagrams moves directly from the position B' ahead of the discontinuity to the final position D. Here the flux will obviously undergo a discontinuity, since it is different from zero and equal to S_0 ahead of the compression shock and in the final state (point D) is equal to zero. We are thus dealing with a typical case of an "isothermal shock" which has already been encountered in §§3 and 12.

The formation of the "isothermal shock" is a result of the mathematical approximation in which the flux is taken to be proportional to the temperature gradient. This excludes the possibility of a temperature jump, since a temperature discontinuity would result in an infinite flux. Actually, however, by virtue of the fact that the process in the compression shock is steady it is the flux which is continuous while the temperature undergoes a jump. This does not present any contradiction. It is simply that the radiation in the region immediately behind the discontinuity is out of equilibrium (the radiation density is lower than at equilibrium, since the density corresponds to the temperature $T_- \approx T_1$ while the gas temperature is $T_+ > T_1$) and the flux, which is determined by the gradient of the actual radiation density, is not expressed in terms of the gas temperature gradient. Again, a temperature peak exists behind the shock discontinuity and the temperature profile in a supercritical wave has the shape shown in Fig. 7.25.

Let us estimate the optical thickness of the temperature peak behind the discontinuity from simple physical considerations. The geometrical thickness of the peak Δx is such that radiation born in this region gives a flux S_0, coming out from the surface of the discontinuity and used up in preheating the gas entering the wave. The energy radiated per unit time in a layer Δx (per unit area of discontinuity surface) is of the order of

$$\frac{\sigma T_+^4}{l}\Delta x \sim \frac{\sigma T_1^4}{l}\Delta x.$$

This quantity is approximately equal to the flux S_0, which according to (7.69) is of the order of $S_0 \sim \sigma T_c^3 T_1$. From this we obtain the thickness of the temperature peak

$$\Delta\tau = \frac{\Delta x}{l} \sim \left(\frac{T_c}{T_1}\right)^3. \tag{7.71}$$

The thickness decreases rapidly with increasing wave strength and the peak in a very strong wave is much narrower than a radiation mean free path. It is for this reason that this peak is "cut off" in the radiation heat conduction

approximation, which disregards details related to distances shorter than a radiation mean free path.

In conclusion, let us cite some values of the thickness of the preheating region in a supercritical shock wave propagating through air at standard density. These values were estimated using (7.66) and the values of the Rosseland mean free path for real air calculated by the method presented in §8 of Chapter V. At $T_1 = 500{,}000°\mathrm{K}$, $\tau_c = 3.4$ and the thickness is of the order of 40 cm. At $T_1 = 750{,}000°\mathrm{K}$, $\tau_c = 14$ and the thickness is of the order of 2 m. Since the temperature peak is very narrow, these thicknesses represent at the same time the thickness of the entire shock front.

§18. Shock waves at high energy densities and radiation pressures

It was shown in §3 that in not too weak a shock wave, when heat conduction is present but viscosity is absent, the gas cannot make a continuous transition from the initial to final state. A discontinuity is necessarily formed, which corresponds to a viscous compression shock and which within the framework of the given approximation is infinitesimally thin (since the viscosity of the fluid was excluded from the very beginning). If the heat conduction flux is proportional to the temperature gradient, then all the flow variables, with the exception of temperature, undergo a discontinuous jump at the discontinuity and an "isothermal shock" takes place. In §§12 and 17 we have examined specific examples of "isothermal shocks" which are caused by electron and radiation heat conduction.

However, for extremely strong shock waves, when the energy density and the radiation pressure become sufficiently large in comparison with the energy and pressure of the fluid, the situation changes. The discontinuity disappears and the gas in the shock wave makes a continuous transition from the initial to the final state through radiation heat conduction alone, even if the fluid viscosity is not considered. This problem was treated by S. Z. Belen'kii and (later) by Belokon' [50].

We shall describe the internal structure of the shock front on the basis of equations (7.40), where S is the radiation heat conduction flux. The total pressure and energy are composed of quantities pertaining both to the fluid and to the radiation; here the radiation is taken to be in thermodynamic equilibrium. The point which describes the state in the wave on a p, V diagram moves along the straight line

$$p = \rho_0 D^2(1 - \eta), \qquad \eta = \frac{V}{V_0}, \tag{7.72}$$

where

$$p = R\rho_0 \frac{T}{\eta} + \frac{4}{3}\frac{\sigma T^4}{c}. \tag{7.73}$$

The temperature and the relative volume behind the wave front T_1 and η_1 are related by the Hugoniot equation (with temperature and volume as variables) including both the radiation energy and pressure. This equation was derived in §10, Chapter III (equation (3.76)). Let us rewrite it here in the form

$$\frac{R\rho_0 T_1}{\eta_1}\left(\frac{\eta_1}{\eta_{10}} - 1\right) = \frac{4\sigma T_1^4}{3c}(1 - 7\eta_1), \tag{7.74}$$

where $\eta_{10} = (\gamma - 1)/(\gamma + 1)$ is the final relative volume without taking into account the radiation density and pressure. It is evident from this equation that for $p_{rad} \gg p_{gas}$, $\eta_1 = 1/7$; and for $p_{rad} \ll p_{gas}$, $\eta_1 = \eta_{10}$.

The temperature as a function of the volume for the compression of the gas in the wave front is obtained by substitution of (7.73) into (7.72), and is

$$R\rho_0 \frac{T}{\eta} + \frac{4}{3}\frac{\sigma T^4}{c} = \rho_0 D^2(1 - \eta).$$

It is more convenient to write it in a somewhat different way by replacing $\rho_0 D^2$ by T_1 and η_1

$$R\rho_0 \frac{T}{\eta} + \frac{4}{3}\frac{\sigma T^4}{c} = \left(R\rho_0 \frac{T_1}{\eta_1} + \frac{4}{3}\frac{\sigma T_1^4}{c}\right)\frac{1 - \eta}{1 - \eta_1}. \tag{7.75}$$

The function $T(\eta)$ has a maximum in the interval $0 < \eta < 1$ (the coordinates of the maximum are denoted by T_{max} and η_{max}).

The radiation flux in the wave S, as in the case when both the radiation density and pressure are small, is always unidirectional and opposite to the gas flow. It vanishes only when $x = -\infty$ and $x = +\infty$, ahead and behind the wave front. Therefore, the temperature in the wave must increase monotonically from $T = 0$ to T_1, since otherwise the flux $S \sim -dT/dx$ would change sign within the wave.

If the radiation pressure is low, $p_{rad} \ll p_{gas}$, then as follows from (7.75) $\eta_{max} = 1/2 > \eta_1 \approx \eta_{10} = (\gamma - 1)/(\gamma + 1)$. In this case the point on the T, η diagram jumps from one branch of the $T(\eta)$ curve to the other without passing through the maximum, and this results in an isothermal shock (see §§3 and 17). If the radiation pressure is high, $p_{rad} \gg p_{gas}$, then the point η_{max} at which the function $T(\eta)$ passes through its maximum lies beyond the range of volumes actually encountered, $1/7 \approx \eta_1 < \eta < 1$: the value of η_{max} is close to zero (this is evident from (7.75)). Thus, in this case the gas density in the wave and the temperature change continuously and there is no discontinuity. This case is shown on a diagram of T^4 versus η (Fig. 7.29). Temperature, gas density, and radiation flux profiles in such a wave are shown schematically in Fig. 7.30.

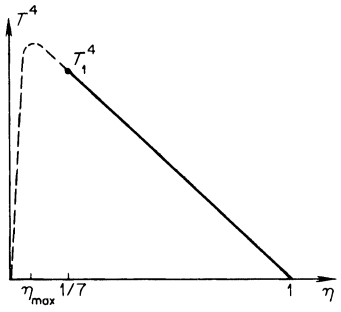

Fig. 7.29. T^4, η diagram for a shock wave with radiation and without a discontinuity.

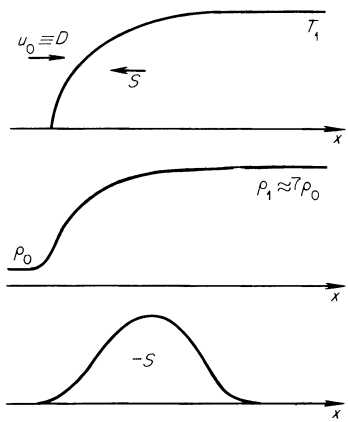

Fig. 7.30. Temperature, gas density, and radiation flux profiles in a shock wave taking into account the radiation energy and pressure in the case when a discontinuity is not present.

Let us find the wave strength at which the discontinuity disappears. Obviously, the strength corresponds to the case when the point of maximum temperature T_{max}, η_{max} coincides with the final point T_1, η_1 (exactly as in §3). Indeed, a discontinuity is present for $\eta_1 < \eta_{max}$ ("small" strengths), while for $\eta_{max} < \eta_1$ ("large" strengths) the discontinuity is absent. The front variables corresponding to the transition strength which separates the continuous solution and isothermal jump regions will be denoted by T^*, η^*. Differentiating (7.75) for the function $T(\eta)$ and setting $dT/d\eta = 0$, $T = T^*$, $\eta = \eta^*$, and also setting in this equation and in the Hugoniot equation (7.74) $T_1 = T^*$ and $\eta_1 = \eta^*$, we obtain a system of two equations for the unknowns T^* and η^*

$$\frac{R\rho_0 T^*}{\eta^{*2}} = \left(R\rho_0 \frac{T^*}{\eta^*} + \frac{4}{3}\frac{\sigma T^{*4}}{c}\right)\frac{1}{1-\eta^*},$$

$$\frac{R\rho_0 T^*}{\eta^*}\left(\frac{\eta^*}{\eta_{10}} - 1\right) = \frac{4\sigma T^{*4}}{3c}(1 - 7\eta^*).$$

Eliminating T^* from this system we obtain a quadratic equation for η^*, one of whose roots corresponds to the real state and is given by

$$\eta^* = \frac{1}{4 + (2 + 1/\eta_{10})^{1/2}}. \tag{7.76}$$

Thus, for example, for $\gamma = 5/3$, $\eta_{10} = 1/4$, $\eta^* = 1/6.45$ (this value is slightly higher than the limiting volume for $p_{\text{rad}} \gg p_{\text{gas}}$ which is equal to 1/7). The transition strength, according to (7.74), corresponds to a ratio of the radiation pressure to the fluid pressure in the final state equal to

$$\left(\frac{p_{\text{rad}}}{p_{\text{gas}}}\right)^* = \frac{4\sigma T^{*4}/3c}{R\rho_0 T^*/\eta^*} = 4.45.$$

Let us note that for this strength the gas velocity behind the front relative to the front is exactly equal to the isothermal speed of sound in the final state (while for strengths greater than the transition strength, for which there is no discontinuity, the gas velocity behind the front is higher than the isothermal speed of sound; the front moves with a supersonic velocity with respect to the gas behind it).

The temperature distribution in a shock wave without a discontinuity can be found in the usual manner from the hydrodynamic equations (7.40) and from the expression for the radiation heat conduction flux $S = -\frac{1}{3}cl\, d(4\sigma T^4/c)/dx$. We shall not discuss this further here.

The article by Imshennik [51] considers a shock wave in a two-temperature plasma with radiation taken into account (the electron and ion temperatures are not assumed to be equal). In [88] the structure of a shock front is studied, with radiant energy transfer taken into account on the basis of the equations of radiation hydrodynamics (in the nonrelativistic approximation).

VIII. Physical and chemical kinetics in hydrodynamic processes

1. *Dynamics of a nonequilibrium gas*

§1. The gasdynamic equations in the absence of thermodynamic equilibrium

In the preceding chapter we have studied the structure of a shock front in a gas with slow excitation of some of the degrees of freedom and have become acquainted with one of the simplest problems of nonequilibrium gasdynamics. The variables behind the shock wave front, in the region where complete thermodynamic equilibrium is established, are independent of the mechanism and the rates of the nonequilibrium processes. The rates of these processes, however, have an appreciable effect on the distribution of the hydrodynamic variables in the nonequilibrium region and on the thickness of this region. Distortions of gasdynamic flows caused by the nonequilibrium processes are attributable mainly to changes in the specific heats and in the effective specific heat ratio of the nonequilibrium gas on which the progress of the gasdynamic process depends. The effect of the specific heat ratio on gasdynamic solutions may be seen from the examples of those problems which were treated in Chapter I. Thus, in the unsteady expansion of a gas initially at rest from a tube into vacuum, the exhaust velocity is equal to $u = 2c_0/(\gamma - 1)$ where $c_0 = (\gamma p_0/\rho_0)^{1/2}$ is the speed of sound in the initial state. Let us assume that a diatomic gas, contained by a diaphragm in a tube, is initially at equilibrium and is then heated to a temperature at which the vibrational modes are "classically" excited. After the diaphragm is broken it is assumed that the gas expands so rapidly that the vibrational modes remain frozen, and that in the expansion the vibrational energy does not have sufficient time to be converted into the kinetic energy of the expansion*. This would mean that the exhaust velocity does not correspond to the equilibrium value of the specific heat ratio $\gamma = 9/7$ but to $\gamma' = 7/5$, and thus is smaller roughly by a factor of $7/5 = 1.4$.

* During the expansion the density decreases, the rates of various processes are decreased, and the conversion of vibrational energy into the translational energy of the molecules, which is necessary for the subsequent conversion into the energy of directed, hydrodynamic motion, takes a long time.

This simple example shows the appreciable effect that nonequilibrium in a gas can exert on the dynamics of the process. The need to consider the rate of establishment of equilibrium arises whenever we are dealing with rapidly changing processes, or with processes whose characteristic scales are comparable with the relaxation "lengths". One of the more important practical problems of this type deals with the problem of a very rarefied gas flowing past a body, in which the relaxation times are comparable with the flow time about the body, in which the relaxation "length" is comparable with the characteristic dimensions of the body. The reentry of ballistic missiles into the atmosphere at hypersonic speeds is accompanied by the formation of a detached shock wave ahead of the body, as shown in Fig. 8.1. The distance

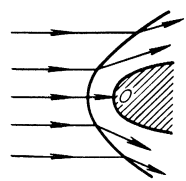

Fig. 8.1. Detached shock wave for supersonic flow past a body.

between the shock and the nose of the body is usually of the order of one-tenth the radius of curvature of the nose. If the gas is sufficiently rarefied that there are not a sufficiently large number of gaskinetic mean free paths over the stand-off distance between the shock and the body, then the slowly relaxing degrees of freedom in the gas particles behind the shock front do not have time to become excited, or in other words, not enough time is available to establish chemical equilibrium. As a result, the temperature of the gas compressed by a shock wave is found to be higher than under conditions of thermodynamic equilibrium, and this changes the manner in which the body is heated. In fact, we are dealing here with a case in which the character of the distribution of the flow variables in the nonequilibrium region which forms behind the compression shock is rather important.

In a number of cases it is possible to approximately describe the dynamics of a nonequilibrium gas by using some effective value of the specific heat ratio, corresponding to some degree of freezing of part of the specific heat, as for example when the energy change in some degrees of freedom can be neglected over the characteristic hydrodynamic flow time. In general, however, one must consider the gasdynamic process simultaneously with the kinetics of the nonequilibrium processes, which complicates the system of equations describing the phenomenon.

The dynamics of a nonviscous and nonheat-conducting gas at thermodynamic equilibrium is described by the equations of continuity, momentum,

and entropy:

$$\frac{D\rho}{Dt} + \rho \nabla \cdot \mathbf{u} = 0, \tag{8.1}$$

$$\rho \frac{D\mathbf{u}}{Dt} + \nabla p = 0, \tag{8.2}$$

$$\frac{DS}{Dt} = 0, \tag{8.3}$$

to which we add the thermodynamic relationship for entropy as a function of pressure and density, $S(p, \rho)$ (for example, in a gas with constant specific heats $S = c_v \ln(p\rho^{-\gamma}) + const$).

We shall now consider the motion of a gas whose state departs from thermodynamic equilibrium. Here again we shall neglect viscosity and heat conduction and assume that the nonequilibrium state is entirely connected with the delayed progress of internal processes which take place only within a given parcel of the fluid, such as, for example, the delayed excitation of molecular vibrations.

In the case of nonequilibrium we replace the entropy equation (8.3), which no longer applies, by the more general equation of conservation of energy, which is always valid. Assuming the absence of any external energy sources*, we can write in place of (8.3)

$$\frac{D\varepsilon}{Dt} + p \frac{DV}{Dt} = 0. \tag{8.4}$$

By virtue of the thermodynamic identity

$$T\, dS = d\varepsilon + p\, dV \tag{8.5}$$

(8.4) and (8.3) are equivalent under conditions of thermodynamic equilibrium. While in the equilibrium case the internal energy ε is determined by the pressure and density only, $\varepsilon = \varepsilon(p, \rho)$, in the absence of equilibrium it also depends on other variables characterizing the state of the system which are not in equilbrium (for example, on the degree of dissociation). Without specifying these parameters, we shall term them λ. To close the system of gasdynamic equations, we must add to (8.1), (8.2), and (8.4) an equation

* The thermal effect of a reversible chemical reaction is not an external energy source; it is taken into account by introducing an appropriate term into the expression for the internal energy of the gas.

connecting the internal energy with the pressure, density, and the state variables λ,

$$\varepsilon = \varepsilon(p, \rho, \lambda),$$

and also rate equations which describe the changes in the variables λ in the gas with time,

$$\frac{D\lambda}{Dt} = f(\lambda, p, \rho).$$

Usually, the functions $\varepsilon(p, \rho, \lambda)$ and $f(\lambda, p, \rho)$ are not expressed explicitly in terms of density and pressure, but instead in terms of temperature

$$\varepsilon = \varepsilon(\rho, T, \lambda), \qquad \frac{D\lambda}{Dt} = f(\lambda, \rho, T).$$

In this case, we must also add the equation of state

$$p = p(T, \rho, \lambda).$$

The temperature T, unless otherwise noted, will always denote the temperature corresponding to the translational degrees of freedom of the molecules (atoms, ions). These are usually in equilibrium even in the most rapid gasdynamic processes, since the Maxwell distribution of molecular velocities is established extremely rapidly.

As an example of a nonequilibrium system let us consider a diatomic gas without dissociation but with slow excitation of the vibrational modes of the molecule (we consider only not too high temperatures, for which the degree of dissociation is still negligibly small). The role of the variable λ is played here by the nonequilibrium vibrational energy ε_{vib} (per unit mass of the gas). For the given case, the equations which must be added to the system, (8.1), (8.2), and (8.4), may be written in the form

$$\varepsilon = \varepsilon_1 + \varepsilon_{\text{vib}} = \tfrac{5}{2}RT + \varepsilon_{\text{vib}}, \tag{8.6}$$

$$p = R\rho T, \tag{8.7}$$

$$\frac{D\varepsilon_{\text{vib}}}{Dt} = \frac{\varepsilon_{\text{vib}}(T) - \varepsilon_{\text{vib}}}{\tau(T, \rho)}. \tag{8.8}$$

Here ε_1 is the sum of the energies of the translational and rotational degrees of freedom of the molecules. (It is assumed that the rotational energy has its equilibrium value, and corresponds to the translational temperature T.) The quantity $\varepsilon_{\text{vib}}(T)$ is the vibrational energy which the gas would have in thermodynamic equilibrium with the translational degrees of freedom, and $\tau(T, \rho)$ is the relaxation time for establishing vibrational equilibrium.

Similar equations which are, however, of a more complex form, can also be written for all the other cases, where there is nonequilibrium dissociation, chemical reactions, ionization, or where the translational temperatures of the electron and atom (ion) gases differ. All these cases were examined in the preceding chapter when we considered the structure of the nonequilibrium layer in a shock front.

§2. Entropy increase

An extremely important property of nonequilibrium gasdynamic processes is the increase in the entropy of the gas and the dissipation of mechanical energy. As with the internal energy ε, the entropy of a nonequilibrium gas is no longer determined by only the two variables pressure and density or temperature and density, but depends on the other variables which characterize the nonequilibrium state; thus $S = S(p, \rho, \lambda)$ or $S(T, \rho, \lambda)$. The increase in entropy dS is no longer equal to the heat supplied by the external sources divided by temperature, as was true for the equilibrium case, so $dS \neq dQ/T$. The entropy increases with time even without a supply of heat (when $dQ = 0$) as a result of the nonequilibrium internal processes only.

We shall clarify our preceding remarks with the aid of the example of nonequilibrium vibrational excitation. The total specific entropy of a gas S is composed of the entropies corresponding to the translational and rotational degrees of freedom, which because of their equilibrium character can be combined, plus the vibrational entropy*. We denote these two parts of the entropy by S_1 and S_{vib}, respectively, with

$$S = S_1 + S_{vib}. \tag{8.9}$$

For the entropy of the translational and rotational degrees of freedom we can write the thermodynamic relation

$$T\,dS_1 = d\varepsilon_1 + p\,dV. \tag{8.10}$$

Usually, the exchange of vibrational energy by molecules takes place much faster than the exchange between the vibrational and translational energies. Thus a Boltzmann distribution with respect to the vibrational excitations of the molecules is established quite rapidly, and we can assign a definite temperature T_{vib} to the vibrations. This temperature corresponds to the actual supply of vibrational energy $\varepsilon_{vib} = \varepsilon_{vib}(T_{vib})$. If we denote the vibrational specific heat by c_{vib}, then $d\varepsilon_{vib} = c_{vib}\,dT_{vib}$. Here, of course, the

* For nonequilibrium dissociation or ionization an expression for the entropy is written in terms of the number of different species of particles (molecules and atoms, for example) which are assumed to be out of equilibrium.

vibrational temperature T_{vib} can be appreciably different from the translational temperature of the molecules T; this difference is the manifestation of the nonequilibrium state of the gas*. If we can assign the specific temperature T_{vib} to the vibrational modes, then for the vibrational contribution to the entropy we can also write the thermodynamic relation

$$T_{vib}\, dS_{vib} = d\varepsilon_{vib}. \tag{8.11}$$

The vibrational energy and entropy are independent of the gas volume.

It is easy to see that the entropy of a nonequilibrium system only increases with time, independent of the transformations the gas undergoes. Indeed, by virtue of (8.9), (8.10), (8.4), and (8.6), we have

$$\frac{DS}{Dt} = \frac{DS_1}{Dt} + \frac{DS_{vib}}{Dt} = \frac{1}{T}\left(\frac{D\varepsilon_1}{Dt} + p\frac{DV}{Dt}\right) + \frac{1}{T_{vib}}\frac{D\varepsilon_{vib}}{Dt} = \frac{D\varepsilon_{vib}}{Dt}\left(\frac{1}{T_{vib}} - \frac{1}{T}\right). \tag{8.12}$$

Taking into account the rate equation (8.8) in which

$$\varepsilon_{vib} = \int_0^{T_{vib}} c_{vib}(T')\, dT' \qquad \text{and} \qquad \varepsilon_{vib}(T) = \int_0^{T} c_{vib}(T')\, dT',$$

we see that for $T_{vib} < T$ the vibrational modes take away energy from the translational and rotational degrees of freedom, $D\varepsilon_{vib}/Dt > 0$, and $DS/Dt > 0$. For $T_{vib} > T$ the vibrations give up their energy $D\varepsilon_{vib}/Dt < 0$, but again $DS/Dt > 0$. The above example illustrates the second law of thermodynamics according to which, without the participation of external factors, heat is always transferred from the hotter to the cooler object, and as a result of which the entropy of the entire system increases. In our case the "objects" are not bodies touching one another, but different degrees of freedom of the same body.

If at a given time the gas is in a state of thermodynamic equilibrium, and it then takes part in a rapidly progressing process during which the equilibrium is disturbed and subsequently the state of the gas changes slowly in order to return to equilibrium, then the entropy of the gas will increase. This increase in entropy is accompanied by the dissipation of mechanical energy, namely by its irreversible conversion into heat. If the process proceeds without the participation of external energy sources, satisfying the energy equation (8.4), then the dissipated energy cannot under any conditions be again converted into mechanical energy. We shall study the phenomenon

* We recall that a similar situation occurs in the case of a plasma. The Maxwell distributions and the temperatures in the electron and ion gases are established very rapidly. The electron and ion temperatures, however, differ from each other as a result of the slow exchange of energy between the electron and ion gases.

of dissipation in more detail in the next section, in which we shall consider the absorption of sound in a relaxing medium. Absorption of sound waves is a characteristic example of the dissipation of mechanical energy.

An example of the incomplete utilization of available energy as a consequence of "irreversibility" is provided by the idealized case of expansion of a gas into vacuum with completely frozen vibrational modes. Only the reversible part of the internal energy, i.e., the energy of the translational and rotational degrees of freedom, is converted into the kinetic energy of the sudden expansion; the vibrational energy remains in the molecules, as a result of which the exhaust velocity of the gas is lower. Such irreversible effects in the presence of nonequilibrium processes can result in additional losses in high-speed turbines at high temperatures, in rocket engine nozzles, etc. The effect of the increase in entropy with time served as the basis for an independent method of measuring the vibrational relaxation time τ by Kantrowitz [1] in investigating relaxation in CO_2.

There is an extensive literature devoted to gasdynamic calculations which take nonequilibrium processes into account, relating primarily to flow problems and to the aerodynamic heating of bodies reentering the atmosphere (satellites, ballistic missiles). For examples, see [2, 2a], which also contain references to many other papers. We shall not consider here problems of the effects of physical and chemical kinetics on gasdynamic motions. In this chapter we shall be interested in another problem, that of the kinetics of nonequilibrium processes not from the point of view of its effect on the motion of a gas, but from the point of view of determining the concentration of the various components under conditions significantly out of equilibrium in chemical reactions, ionization, and vapor condensation in various hydrodynamic phenomena. As a rule, the hydrodynamics will be considered only approximately, by means of effective values of the specific heat ratio, and the kinetics of the processes of interest will be "imposed" on the already known hydrodynamic solution. Exceptions to this plan are the following two sections, in which we shall consider the phenomena of the absorption and dispersion of sound in a relaxing medium. Thus we shall be considering the effect of nonequilibrium processes on a gasdynamic process—the propagation of sound waves.

§3. Anomalous dispersion and absorption of ultrasound

Dispersion and absorption of sound in gases, which are connected with viscosity and heat conduction, ordinarily are appreciable only at very short wavelengths of the sound waves, those comparable with the mean free path of the gas particles, and thus at frequencies comparable with the frequency of gaskinetic collisions (see §22 of Chapter I). Propagation of ultrasonic

waves in molecular gases is, however, sometimes accompanied by an anomalously strong dispersion and absorption in a region of much greater wavelengths and lower frequencies. These phenomena are related to the relaxation processes for the establishment of equilibrium in slowly excited degrees of freedom of the gas.

In the limiting case of low frequencies, the relaxation times for establishing equilibrium in those degrees of freedom which make an appreciable contribution to the specific heat are small in comparison with the period of sound vibrations. Under these conditions a gas particle is in a state of thermodynamic equilibrium at any instant of time, and "follows" the changes in pressure and density in the sound wave. The speed of sound, defined as the square root of the isentropic derivative of the pressure with respect to density, corresponds to its own thermodynamic equilibrium value

$$a^2 = \left(\frac{\partial p}{\partial \rho}\right)_s = \gamma \frac{p_0}{\rho_0}, \qquad \gamma = \frac{c_p}{c_v} = 1 + \frac{R}{c_v}. \tag{8.13}$$

*

On the other hand, in the limiting case of very high frequencies, the slowly relaxing degrees of freedom in the sound wave do not have time to become excited, and their energy simply corresponds to the temperature of the undisturbed state T_0. These degrees of freedom do not participate in the periodic changes in the state of the gas; they are "frozen", and do not affect the isentropic relationship between the changes in pressure and density. The active part of the specific heat is now less than at equilibrium, and the specific heat ratio and the speed of sound are greater than at low frequencies.

A gradual change of the speed of sound from the equilibrium value a_0 to the value a_∞ corresponding to the frozen part of the specific heat takes place in the intermediate frequency region; thus, there is dispersion of sound. For example, measurements of Kneser [3, 4] show the speed of sound in carbon dioxide at room temperature to vary between $a_0 = 260$ m/sec at a frequency ν of the order of 10^4 sec^{-1} (10 kc) to $a_\infty = 270$ m/sec at $\nu \sim 10^6$ sec^{-1} (1 Mc). The lower speed of sound corresponds to the equilibrium value of the specific heat

$$c_v = c_{\text{trans}} + c_{\text{rot}} + c_{\text{vib}} = \tfrac{3}{2}R + R + 0.8R = 3.3R.$$

The CO_2 molecule is linear, so that $c_{\text{rot}} = R$; only the low-frequency molecular vibrations with $h\nu/k = 954°$K are excited at room temperature, and for these the vibrational specific heat is even smaller than its classical value R. The higher speed of sound corresponds to frozen vibrations, with a specific heat $c_v = c_{\text{trans}} + c_{\text{rot}} = 2.5R$. It follows from these data that the relaxation time for vibrational excitation in a CO_2 molecule (at atmospheric pressure)

* We are here using specific heat capacities; R is the gas constant per unit mass. To avoid confusion, we denote the speed of sound here by a instead of c.

corresponds to some intermediate sound frequency, so that roughly $\tau_{vib} \sim 1/\nu \sim 10^{-5}$ sec. Molecular rotations at room temperature are excited very rapidly and dispersion related to slow rotational excitation can be observed at atmospheric pressure only at extremely high frequencies $\nu \sim 1/\tau_{rot} \sim 10^9$–$10^{10}$ sec^{-1} (the only exception is hydrogen; see §2, Chapter VI).

Dispersion of sound is also observed in gases in which slow chemical reactions take place as a result of the temperature (and density) changes in a sound wave. An example is the polymerization of nitrogen dioxide $2NO_2 \rightleftarrows N_2O_4$, which takes place easily at room temperature since its heat of activation in both directions is very low. It was in connection with systems of this type that the theory of sound dispersion was first developed by Einstein in 1920 [5]. Apparently, analogous phenomena also occur in the propagation of ultrasound in some liquids.

Measurements of ultrasonic dispersion and absorption provide one of the most important methods of studying relaxational processes and of experimentally determining relaxation times. There is an extensive literature devoted to this subject* but we shall not consider it in detail here. We shall examine only the basic physical properties and laws governing this phenomenon.

Dispersion of sound in a relaxing fluid is always accompanied by increased absorption, which considerably exceeds the natural absorption due to ordinary viscosity and heat conduction. A fluid parcel in a sound wave performs successive cyclical transformations, returning to its initial state upon the completion of each cycle. If internal nonequilibrium processes take place in the parcel, they inevitably lead to an increase in entropy and to a dissipation of mechanical energy, and thereby to the absorption of sound. It is to be emphasized that in the presence of dissipation the state of a parcel upon completion of a cycle differs somewhat from its initial state (since its entropy increases). However, this difference, let us say the temperature increase, is proportional to the entropy increase, and is a second-order quantity in comparison with the small amplitude of the sound wave Δp or ΔT. This follows from the fact that the entropy increase ΔS is proportional to the sound energy which, in turn, is proportional to $(\Delta p)^2$ (see §3, Chapter I). Therefore, in first approximation the motion in a sound wave even in the presence of absorption is isentropic and we can regard the cycles to be closed.

The mechanism of dissipation of mechanical energy and of sound absorption can be made clearer by considering the cycle in the gas on a p, V diagram. Figure 8.2 shows two families of isentropes, one of which (I) corresponds to equilibrium changes of state, and the other (II) to the frozen part of the specific heat. The isentropes were drawn near the undisturbed region, denoted

* A survey of the literature and references may be found, for example, in [6].

by the point O. For very slow sound vibrations the point describing the state of the gas, p, V, oscillates about the center O along the equilibrium isentrope, denoted in Fig. 8.2 by I′. In the limiting case of very high frequency, the

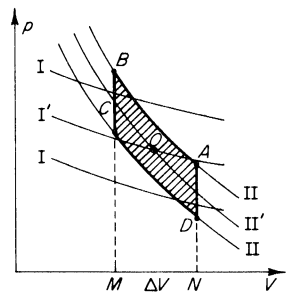

Fig. 8.2. p,V diagram for a cycle in a sound wave with a rectangular profile.

point oscillates about the center along the "frozen" isentrope denoted by II′. In both cases nonequilibrium processes are absent, the entropy of the gas does not change, and there is no sound absorption. The work done on the gas per cycle, which is numerically equal to the area of the figure described by the point on the p, V diagram, is equal to zero, which shows that absorption is absent. Using the example of vibrational relaxation it is easy to see that the entropy of the gas does not change in the second case, as well as in the first case of thermodynamic equilibrium. It is evident from (8.12) that the rate of change of the entropy in a nonequilibrium process is proportional to the rate of change of the vibrational energy. But, for strictly frozen vibrational modes this energy does not change, $\varepsilon_{\text{vib}} = const$, and $DS/Dt = 0$.

Let us now consider sound waves of intermediate frequencies, where relaxation processes are important (for definiteness we again consider vibrational relaxation). For simplicity we imagine that the density profile in the sound wave has the square wave shape shown in Fig. 8.3a*. This plot can be considered either as a density distribution with respect to the position coordinate at a given instant of time, or as the relation governing the change in density in a given gas particle with time. The same applied to Fig. 8.3b, which illustrates the corresponding temperature (or pressure) profiles (the temperature and pressure profiles are in this case similar).

We shall follow the change of state of a gas particle in a wave on the p, V diagram of Fig. 8.2, as well as on Figs. 8.3a and b. When the gas is very rapidly compressed from point A to point B, its state changes along a frozen isentrope II. In this case the entropy does not change, and positive work, numerically equal to the area $NABM$, is done on the gas. The gas temperature and pressure increase sharply while the vibrational energy remains unchanged

* This example, which is distinguished by its clarity, has been considered before, for example in the book by Gorelik [7].

and corresponds to the old, low temperature. Then, for a certain period of time, the gas density remains unchanged (the transition $B \to C$). The vibrational modes are excited, part of the energy is transferred from the transla-

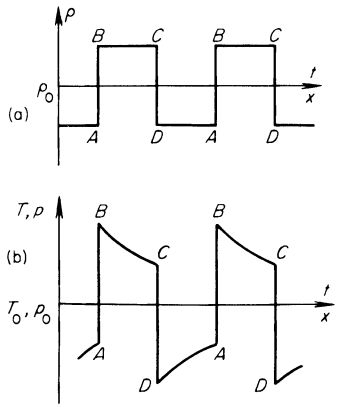

Fig. 8.3. An acoustic wave in a relaxing gas with a square wave density profile: (a) density profile; (b) temperature or pressure profile.

tional and rotational degrees of freedom, the temperature and pressure decrease, and the entropy increases (see (8.12): $T_{\text{vib}} < T$, $D\varepsilon_{\text{vib}}/Dt > 0$, and $DS/DT > 0$). Since the volume does not change, no work is performed during the transition $B \to C$.

Following this the gas then expands very rapidly (the transition $C \to D$) along a frozen isentrope II. The temperature and pressure fall, the entropy remains unchanged, and the vibrational energy also remains unchanged at the value it had at point C. The work done by the gas is numerically equal to the area $MCDN$ (negative work is done on the gas). And, finally, during the slow transition at constant volume $D \to A$, the vibrational modes are partially deexcited since their energy exceeds the value corresponding to the decreased temperature; the vibrational energy is partially transformed into translational and rotational energy, the temperature and pressure increase, and the entropy also increases ($T_{\text{vib}} > T$, $D\varepsilon_{\text{vib}}/Dt < 0$, $DS/Dt > 0$). No work is done in this case.

Thus, during the expansion stage $C \to D$ the gas particle does less work on the surrounding gas than done by the gas on the particle during the compression stage $A \to B$. The particle does not fully "give back" the work. Part of the energy expended during the compression period remains "forever" in the particle. This energy, numerically equal to the difference in work, to the area of the figure $ABCD$, is the mechanical energy which has been irreversibly converted into heat. As a result of the dissipation of mechanical energy the sound wave is also attenuated (absorbed); the absorption of

sound energy per period (or per wavelength) is exactly equal to the area $ABCD$.

On the other hand, irreversible generation of heat is related to the entropy increase per cycle, and is equal to $T_0\Delta S$. This quantity, as is evident from Fig. 8.2, is proportional to $\Delta V \cdot \Delta p \sim (\Delta p)^2$. It follows therefore that the displacement of the final state point A' relative to the initial state point A, $\delta p = (\partial p/\partial S)_V \cdot \Delta S \sim (\Delta p)^2$, is a second-order quantity with respect to the amplitude Δp. Since $(\partial p/\partial S)_V > 0$, $\delta p > 0$, that is, the pressure upon completion of the cycle is slightly higher than the initial pressure. Similarly, the temperature is also slightly higher, $\delta T = (\partial T/\partial S)_V \Delta S = T\Delta S/c_v \approx T_0 \Delta S/c_v$. The temperature increase is equal to the energy dissipated per cycle, divided by the specific heat at constant volume.

In a sinusoidal (harmonic) sound wave a point on the p, V diagram describes a smooth curve. All the state variables, density, pressure, and temperature vary harmonically with time. However, due to the slow excitation and deexcitation of molecular vibrations, the temperature or pressure changes cannot follow the density changes and the sinusoidal pressure variation undergoes a phase shift with respect to the sinusoidal variation in density (volume). It can be shown that a point on the p, V diagram describes, in this case, an elliptical trajectory, with the axes of the ellipse inclined with respect to the p, V coordinate axes.

At low frequencies ν (or angular frequencies $\omega = 2\pi\nu$) the ellipse is stretched out along an equilibrium isentrope (see curve 1 in Fig. 8.4). The thickness of

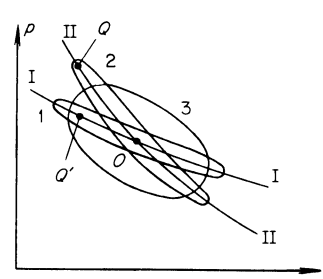

Fig. 8.4. p, V diagram for the cycles in harmonic sound waves of different frequencies.

the ellipse in the limit of small frequencies is proportional to the frequency (to the first term of an expansion in the small quantity ω). The sound energy absorbed per period is proportional to ω and that absorbed per unit time is proportional to the number of cycles, that is, to ω^2. At high frequencies the ellipse is stretched out along a frozen isentrope (curve 2). The thickness of the ellipse is proportional to $1/\omega$ (as can also be seen from an expansion), and the absorption per unit time is proportional to $\omega \cdot 1/\omega$, that is, it is

independent of the frequency. The strongest absorption per period occurs in the intermediate case, when the frequency is of the order of the reciprocal of the relaxation time. In this case the thickness of the ellipse is maximum (curve 3); it is of the order of the vertical distance between the equilibrium and frozen isentropes at the maximum pressure change equal to the amplitude of the wave (the distance between the points Q and Q' in Fig. 8.4). If the relative difference between the equilibrium and frozen adiabatic exponents is large (it is precisely this difference which characterizes the angle between the isentropes I and II, and thus the distance QQ'), then the thickness of the ellipse may even become of the order of its length. This corresponds to a phase shift between the pressure and density of the order of $\pi/2$ (when the ellipse degenerates into a circle the phase shift becomes exactly $\pi/2$).

§4. The dispersion law and the absorption coefficient for ultrasound

The qualitative considerations on the dispersion and absorption of sound in the presence of relaxation processes in a fluid presented in the preceding section can be put into an elegant mathematical form. This was done in a general form by Mandel'shtam and Leontovich* [8]; dispersion and absorption relations, in which the relaxation time τ appears, usually serve to determine that time from the experimentally measured dispersion or absorption curves as a function of the ultrasonic frequency.

Let us show how we may derive the dispersion relation and the expression for the absorption coefficient in a relaxing medium. For simplicity and clarity we shall carry out the calculation using the specific example of a gas with nonequilibrium vibrational modes, for which the complete system of gas-dynamic equations (8.1), (8.2), (8.4), (8.6), (8.7), and (8.8) has been formulated in §1. All the variables in the sound wave, pressure, density, etc., will be written in the form $f = f_0 + f'$, where f_0 is the average value corresponding to the undisturbed gas and f' is a variable part or perturbation, which will be considered a small quantity (the velocity $u = u_0 + u' = u'$, since the undisturbed gas is at rest and $u_0 = 0$). The true vibrational energy can also be expressed as $\varepsilon_{\text{vib}} = \varepsilon_{\text{vib}_0} + \varepsilon'_{\text{vib}}$, where $\varepsilon_{\text{vib}_0}$ is the vibrational energy in the undisturbed gas at equilibrium. The perturbation of the equilibrium vibrational energy we shall write in the form $\varepsilon'_{\text{vib}}(T) = c_{\text{vib}}T'$, where c_{vib} is the vibrational specific heat corresponding to the average temperature T_0 (if at T_0 the vibrational modes have their classical value, then $c_{\text{vib}} = R$, while if this is not the case, c_{vib} is expressed by a quantum-mechanical relation; see §2, Chapter III).

* A presentation of this theory may be found in the book by Landau and Lifshitz [9].

Let us substitute into the equations all of the quantities in the form indicated above and neglect second-order terms, thus linearizing the equations as is usual in acoustics (see §3 of Chapter I). We then obtain for the one-dimensional plane case the following system of equations for the perturbations

$$\begin{aligned} &\frac{\partial \rho'}{\partial t} + \rho_0 \frac{\partial u'}{\partial x} = 0, && \varepsilon' = \tfrac{5}{2} RT' + \varepsilon'_{\text{vib}}, \\ &\frac{\partial u'}{\partial t} + \frac{1}{\rho_0} \frac{\partial p'}{\partial x} = 0, && \frac{p'}{p_0} = \frac{T'}{T_0} + \frac{\rho'}{\rho_0}, \\ &\frac{\partial \varepsilon'}{\partial t} - \frac{p_0}{\rho_0^2} \frac{\partial \rho'}{\partial t} = 0, && \frac{\partial \varepsilon'_{\text{vib}}}{\partial t} = \frac{c_{\text{vib}} T' - \varepsilon'_{\text{vib}}}{\tau}. \end{aligned} \tag{8.14}$$

Here the specific volume in the energy equation (8.4) has been replaced by the density, and both sides of the equation of state have been divided by $p_0 = R\rho_0 T_0$. The relaxation time τ is taken to be constant and given by $\tau = \tau(T_0, \rho_0)$.

A solution of the system (8.14) will be sought in the form of a harmonic plane wave, with all the primed quantities expressed in the form

$$f' = f'^* e^{-i(\omega t - kx)}. \tag{8.15}$$

The wave number k is in general complex: $k = k_1 + ik_2$. The real part k_1 is proportional to the reciprocal of the wavelength $k_1 = 2\pi/\lambda$ and determines the actual speed of sound—the phase velocity of wave propagation $a_1 = \omega/k_1$; the imaginary part k_2 gives the sound absorption coefficient

$$f' = f'^* e^{-i\omega(t - x/a_1)} e^{-k_2 x}. \tag{8.16}$$

The quantity $a = \omega/k$ may be called the complex speed of sound. The amplitudes f'^* are in general also complex, with $f'^* = |f'^*| e^{i\varphi}$. The complex character of the amplitudes testifies to the phase shifts of some of the quantities with respect to the others (through the differences of the angles φ).

Substituting into (8.14) all of the quantities in the form defined by (8.15) and noting that $\partial f'/\partial t = -i\omega f'$, $\partial f'/\partial x = ikf'$ we obtain a system of algebraic equations for the primed quantities (or for the amplitudes, if we cancel out the exponential factor)

$$\begin{aligned} &-i\omega\rho' + \rho_0 iku' = 0, && \varepsilon' = \tfrac{5}{2} RT' + \varepsilon'_{\text{vib}}, \\ &-i\omega u' + \frac{1}{\rho_0} ikp' = 0, && \frac{p'}{p_0} = \frac{T'}{T_0} + \frac{\rho'}{\rho_0}, \\ &-i\omega\varepsilon' + \frac{p_0}{\rho_0^2} i\omega\rho' = 0, && -i\omega\varepsilon'_{\text{vib}} = \frac{c_{\text{vib}} T' - \varepsilon'_{\text{vib}}}{\tau}. \end{aligned} \tag{8.17}$$

Solving the last equation for $\varepsilon'_{\text{vib}}$ we obtain

$$\varepsilon'_{\text{vib}} = \frac{c_{\text{vib}} T'}{1 - i\omega\tau}. \tag{8.18}$$

It is precisely this complex relation between the perturbations of the true vibrational energy and of the temperature that causes dispersion and absorption to arise. It can already be seen from this relation that in the limiting cases $\omega\tau \to 0$ and $\omega\tau \to \infty$, for which $\varepsilon'_{\text{vib}} = c_{\text{vib}} T'$ and $\varepsilon'_{\text{vib}} = 0$, the imaginary unit i drops out completely from the system of equations (8.17) and all the quantities are real (if p', ρ', etc., are understood to denote the amplitudes p'^*, ρ'^*, etc.). Neither absorptions nor phase shifts occur in this case.

The first two equations of the system (8.17), which were obtained from the equations of continuity and motion by eliminating the velocity, yield the usual relationship

$$p' = \frac{\omega^2}{k^2} \rho' = a^2 \rho', \tag{8.19}$$

where a is now the complex speed of sound. Eliminating ε', $\varepsilon'_{\text{vib}}$, and T' from the remaining four equations, we obtain still another relationship between p' and ρ',

$$p' = \gamma \frac{p_0}{\rho_0} \rho', \qquad \gamma = \frac{\frac{7}{2}R + c_{\text{vib}}/(1 - i\omega\tau)}{\frac{5}{2}R + c_{\text{vib}}/(1 - i\omega\tau)}. \tag{8.20}$$

The quantity γ may be termed the complex specific heat ratio. Introducing the notation where $c_{v_0} = \frac{5}{2}R + c_{\text{vib}}$ and $c_{p_0} = \frac{7}{2}R + c_{\text{vib}}$ are the equilibrium specific heats at constant volume and pressure, respectively, and $c_{v_\infty} = \frac{5}{2}R$ and $c_{p_\infty} = \frac{7}{2}R$ are the specific heats with the vibrational modes completely frozen, we can write the complex specific heat ratio and the expression for the complex speed of sound, from (8.19) and (8.20), as

$$a^2 = \gamma \frac{p_0}{\rho_0}, \qquad \gamma = \frac{c_{p_0} - i\omega\tau c_{p_\infty}}{c_{v_0} - i\omega\tau c_{v_\infty}}. \tag{8.21}$$

* Landau and Lifshitz derive a slightly different equation in their book [9] (Chapter VIII, §78, equations (78.3)),

$$\gamma = \frac{1}{1 - i\omega\tau} \left[\frac{c_{p_0}}{c_{v_0}} - i\omega\tau \frac{c_{p_\infty}}{c_{v_\infty}} \right].$$

This difference arises from a difference in the definitions of the relaxation time τ which enters in the rate equation. The quantity $\varepsilon_{\text{vib}}(T)$ in our equation (8.8) represents the equilibrium vibrational energy which corresponds to the translational temperature T. Let us denote the relaxation time in our rate equation by the subscript "T". If the gas volume is constant, and the translational temperature is also maintained constant: $T = const$, then

In the limiting case of very low frequencies $\omega\tau \ll 1$, $\gamma = c_{p_0}/c_{v_0} = \gamma_0$, $a^2 = \gamma_0 p_0/\rho_0 = a_0^2$, we obtain the equilibrium specific heat ratio and speed of sound. In the limit of high frequencies $\omega\tau \gg 1$,

$$\gamma = \frac{c_{p_\infty}}{c_{v_\infty}} = \gamma_\infty\,, \qquad a^2 = \gamma_\infty \frac{p_0}{\rho_0} = a_\infty^2\,,$$

we obtain a specific heat ratio and a speed of sound corresponding to frozen vibrational modes. In both limiting cases the speed of sound and consequently the wave number, $k = \omega/a$, are real, and there is no absorption.

(8.8) gives an exponential relationship with a characteristic time τ_T for the approach to equilibrium

$$\varepsilon_{\text{vib}} = \varepsilon_{\text{vib}}(T) + [(\varepsilon_{\text{vib}})_{t=0} - \varepsilon_{\text{vib}}(T)]\, e^{-t/\tau_T}$$

The energy of the gas $\varepsilon = c_{v_\infty} T + \varepsilon_{\text{vib}}$ is not constant in this case. However, if we assume that the total energy (and, of course, the volume) is constant and use (8.8), then instead of a simple exponential law we obtain a more complex law governing the approach to equilibrium.

Landau and Lifshitz [9] write a rate equation of the type (8.8), but defined so that the equilibrium energy term denotes the vibrational energy at an equilibrium temperature T_{eq} which corresponds to both the translational and vibrational degrees of freedom, and which thus depends on the given volume V and total energy ε of the gas. Let us denote the relaxation time which enters in this rate equation (according to [9]) by τ_S. The equation yields the exponential relationship for the approach to equilibrium

$$\varepsilon_{\text{vib}} = \varepsilon_{\text{vib}}(T_{\text{eq}}) + [(\varepsilon_{\text{vib}})_{t=0} - \varepsilon_{\text{vib}}(T_{\text{eq}})]\, e^{-t/\tau_S}$$

if the gas volume, the energy (i.e., the equilibrium temperature T_{eq}), and the time τ_S are constant. Actually, τ_S depends on the translational temperature, but it is assumed that the departure from equilibrium is slight, so that at $T_{\text{eq}} = const$ the translational temperature changes only very little. For a slight departure from equilibrium, we can consider the condition $V = const$, $\varepsilon = const$ as a condition of approximate constancy of the entropy, $S \approx const$.

Let us consider small changes of all quantities in a sound wave about their average values. Using the definition

$$\varepsilon' = c_{v_\infty} T' + \varepsilon'_{\text{vib}} = c_{v_\infty} T'_{\text{eq}} + \varepsilon'_{\text{vib}}(T_{\text{eq}}) = c_{v_0} T'_{\text{eq}}\,,$$

we can transform one rate equation to the other. In so doing, we find that $\tau_S = (c_{v_\infty}/c_{v_0})\tau_T$. In the equation for γ given at the beginning of this footnote, τ should be understood to denote τ_S, and in our equation (8.21) it should denote τ_T. By using the relationship between τ_S and τ_T we can easily verify that these equations are identical.

The "τ_S" method, used by Mandel'shtam and Leontovich [8], makes it possible to obtain the general equation for γ given above, independently of the actual relaxation mechanism. When considering the particular case of vibrational relaxation it is more convenient to use the "τ_T" method, as was done in this text. Let us note that this is the same manner in which vibrational relaxation in ultrasound was considered in older works (Kneser [3], Landau and Teller [10]).

In the intermediate frequency region, the sound speed a and the wave number $k = \omega/a$ are complex. If we set up an equation for $k = \omega/a$ using (8.21) and separate the real and imaginary parts, we obtain the dispersion relation $a_1(\omega) = \omega/k_1(\omega)$ and the absorption coefficient $k_2(\omega)$*. In general, this leads to rather cumbersome expressions. In the limit of low frequencies $\omega\tau \ll 1$, we obtain approximately

$$k = k_1 + ik_2 = \frac{\omega}{a_0} + i\frac{\omega^2\tau}{2a_0}\frac{c_{v_\infty}}{c_{v_0}}\left(\frac{\gamma_\infty}{\gamma_0} - 1\right). \tag{8.22}$$

The absorption coefficient is of the order $k_2 \sim \omega^2$; the absorption over a distance of one wavelength is of the order $k_2\lambda \sim \omega$. In the limit of high frequencies $\omega\tau \gg 1$, we have

$$k = k_1 + ik_2 = \frac{\omega}{a_\infty} + i\frac{1}{2a_\infty\tau}\frac{c_{p_0}}{c_{p_\infty}}\left(\frac{\gamma_\infty}{\gamma_0} - 1\right). \tag{8.23}$$

The absorption coefficient $k_2 \approx const$ is independent of the frequency, and the absorption over a wavelength is of the order $k_2\lambda \sim 1/\omega$. The dispersion curve $a_1(\omega)$ and the frequency dependence of the absorption over a wavelength $k_2\lambda = k_2 a_1 2\pi/\omega = 2\pi k_2/k_1$ are shown schematically in Fig. 8.5. It is

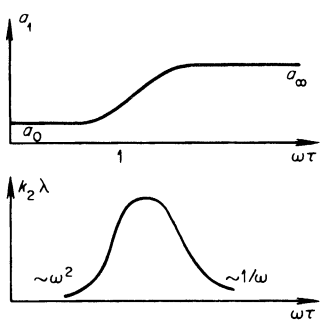

Fig. 8.5. Dependence of the propagation speed a_1 and absorption coefficient $k_2\lambda$ on the ultrasonic frequency in the relaxation region.

not difficult to show that the quantity k_2/k_1 has a maximum at $\omega\tau = (c_{v_0}c_{p_0}/c_{v_\infty}c_{p_\infty})^{1/2} \sim 1$. For a value of $\omega\tau$ which is close to but different from the above value, the dispersion curve has an inflection point.

It follows from (8.19) that the pressure in the sound wave is shifted in phase relative to the density. In fact, if the speed of sound is a complex quantity, then $p' = a^2\rho' = |a^2|e^{i\varphi}\rho'$. In the limiting cases $\omega\tau \ll 1$ and $\omega\tau \gg 1$, where the imaginary part of the speed of sound tends to zero, the

* Let us note that between the functions $k_1(\omega)$ and $k_2(\omega)$ there exists a perfectly general relationship, independent of the dispersion and absorption mechanism. This relationship was first derived by Ginzburg [11].

phase shift φ vanishes. For $\omega\tau \sim 1$, for which the real and imaginary parts are comparable, the phase shift φ is appreciable.

If several nonequilibrium processes with appreciably different relaxation times take place in the fluid, strong absorption and dispersion occurs whenever $\omega\tau \sim 1$ and these frequency regions are clearly separated. However, in the case of relaxation times that are only slightly different from each other the regions merge, and it is difficult to separate them experimentally to obtain the relaxation times from experimental data.

Dispersion and absorption of sound related to nonequilibrium processes are determined by fluctuations in the fluid density, and by virtue of the continuity equation $D\rho/Dt + \rho\nabla \cdot \mathbf{u} = 0$ are related to the divergence of the velocity. They can be formally described by the second coefficient of viscosity μ', which characterizes the dissipation term in the equation of motion which is proportional to the divergence of the velocity (see §§20 and 21 of Chapter I). The second coefficient of viscosity can be formally related to the quantity τ and to the limiting speeds of sound a_0 and a_∞ (see, for example, [9]). The use of the second coefficient of viscosity in describing anomalous absorption is only possible at not too high frequencies ($\omega\tau \ll 1$). Due to viscosity the absorption coefficient increases in proportion to $k_2 \sim \omega^2$ (see §22, Chapter I). Therefore, as $\omega \to \infty$ viscous absorption increases without limit, while actually the coefficient of anomalous absorption as $\omega \to \infty$ tends to a constant value $k_2 = const$ (see equation (8.23)).

Some experimental data on the relaxation times for the excitation of molecular vibrational and rotational modes obtained by means of ultrasonic dispersion and absorption have already been presented in §§2 and 4 of Chapter VI.

2. *Chemical reactions*

§5. Oxidation of nitrogen in strong explosions in air

Atmospheric air consists of nitrogen and oxygen molecules; chemically it is in equilibrium and very stable. Dissociation of the molecules into atoms or their partial transformation into molecules of nitric oxide NO requires heating of the air to temperatures of several thousand degrees. The reaction of nitrogen oxidation requires a large activation energy. The activation energy required for breaking up the oxide molecules into oxygen and nitrogen is somewhat lower, but it is still large. Therefore, despite the ease from the point of view of energy considerations of transforming nitric oxide into oxygen and nitrogen at low temperatures, NO molecules are extremely stable.

It was shown in §8 of Chapter VI that if the time required for establishing the equilibrium concentration of nitric oxide in air of standard density at 4000°K is $\sim 10^{-6}$ sec, then at 2000°K it is approximately equal to 1 sec, and at 1000°K it has the colossal value of the order of 10^{12} sec, approximately 30 thousand years! Once the nitric oxide has been formed and cooled to normal temperature it remains in air for an indefinitely long time. Actually, the oxidized nitrogen remains in the form of the dioxide NO_2 (or of N_2O_4 complexes, the preferred form for NO_2 molecules), since nitric oxide reacts rapidly with atmospheric oxygen and is oxidized to form the dioxide. This exothermic reaction requires a very small activation energy and takes place easily even at room temperature (see §9, Chapter VI). Thus, the chemical processes in heated and subsequently cooled air lead to a state substantially out of equilibrium. This result is in sharp contradiction with the laws of chemical equilibrium, according to which the oxides of nitrogen at low temperatures should be completely transformed into nitrogen and oxygen. This effect, well known in laboratory practice, is called the effect of "freezing" of the oxides of nitrogen.

A large amount of nitrogen oxides is formed in a strong explosion in air. The atmospheric nitrogen is oxidized at that stage of the process when the air in the explosion wave is heated to a temperature of several thousand degrees, at which stage a few percent of the nitrogen is oxidized. As the explosion wave is propagated, the air initially heated by the shock front is cooled very rapidly. The nitric oxide which was formed does not have sufficient time to decompose on cooling, and remains in the air "forever". The total weight of oxides of nitrogen which is formed in air during an explosion with an energy of 10^{21} erg, equivalent to approximately 20,000 tons of TNT, is 100 tons. Several tens of seconds or a minute after the detonation all of the oxide has been transformed into the dioxide.

In its ordinary state nitrogen dioxide is a strongly colored brownish-red gas; this is caused by the preferential absorption of green and blue light by the NO_2 molecules. It imparts the reddish hue to the cloud which rises after the explosion*. This effect has been observed experimentally and is described in [12]; see also §5 of Chapter IX. The presence of the oxides and in particular of small amounts of nitrogen dioxide in the high-temperature air encompassed by an explosion wave has a strong effect on the optical properties of the air behind the wave, since, unlike oxygen and nitrogen molecules, the molecules of the dioxide intensely absorb and emit light in the visible part of the spectrum (the NO molecule also does not absorb visible light).

The specific features of the chemical kinetics for the formation and decom-

* The molecular complexes N_2O_4 do not absorb visible light, so that the N_2O_4 gas is colorless. However, the dioxide disappears only after the explosion cloud dissipates in the atmosphere, since the reaction $2NO_2 \rightarrow N_2O_4$ does not proceed too rapidly.

position of nitrogen oxides in an explosion wave give rise to interesting optical phenomena observed in a strong explosion, a description of which may also be found in [12]. These phenomena are: luminosity of the shock wave at comparatively low temperatures, of the order of 4000—2000°K behind the front, at which the gas, consisting of oxygen and nitrogen atoms only, should not be incandescent; a rather sudden cut-off of the shock wave luminosity at a temperature of about 2000°K, and the separation of the shock wave from the boundary of a glowing body, the so-called "fireball"; the distinctive effect of a minimum in the brightness of the fireball at the instant of separation, when the glow starts to die down and after which the ball again flares up. These effects will be considered in §§5–7 of Chapter IX. Here, we shall consider in more detail the kinetics of the nitrogen oxidation reaction in an explosion wave; these considerations are necessary to explain the above optical phenomena. This problem was considered by one of the present authors [13]. It should be pointed out that the study of the kinetics is in itself very interesting, since it provides a characteristic example of a chemical process substantially out of equilibrium within the gasdynamic phemomenon of a strong explosion.

The gasdynamics of a strong explosion was described in §25 of Chapter I. The process is self-similar, the shock front is propagated from the explosion center as $R_f \sim t^{2/5}$. The distributions of all the flow variables with respect to radius are given in Fig. 1.50. These distributions do not change with time, because the process is self-similar; only the scales are time dependent.

Of interest to us here is the course of the chemical reaction in specific parcels of air. For this it is first necessary to know how the thermodynamic state of a given parcel changes with time. The r, t diagram of Fig. 8.6 shows

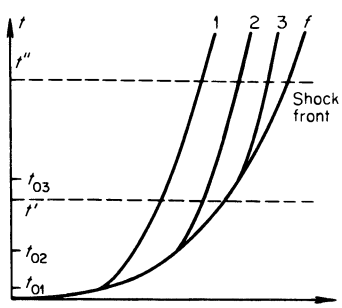

Fig. 8.6. An r, t diagram for a strong explosion in air. f is the trace of the shock front; 1, 2, and 3 are the traces of three parcels over which the front passes at the times t_{01}, t_{02}, and t_{03}.

schematically the trace of the shock front path, and of several of the particle paths behind the front, denoted by the numbers 1, 2, and 3. The parcels which are heated and compressed at the times t_{01}, t_{02}, and t_{03} when the wave front passes them are carried away suddenly by the explosion wave from the center and in the process are isentropically expanded and cooled until the

pressure decreases to atmospheric and the parcels stop moving. The expansion and cooling curves for the air parcels as a function of time are shown schematically in Figs. 8.7 and 8.8.

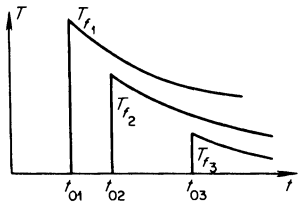

Fig. 8.7. Schematic time dependence of the temperature in three parcels heated by an explosion wave.

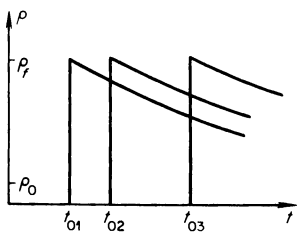

Fig. 8.8. Schematic time dependence of the density in three parcels compressed by an explosion wave.

Calculations carried out with the formulas of §25 of Chapter I show that in an explosion with an energy $E = 10^{21}$ erg, (this value will be used in all our numerical examples), the temperature at the shock front decreases to $T_f = 2000°K$ in a time of the order of 10^{-2} sec from the moment of energy release. The times for cooling the air parcels from a temperature of, let us say, 5000°K to 2000–1500°K are of the same order. The time $t \sim 10^{-2}$ sec is thus a time scale for the gasdynamic process in an explosion with an energy $E = 10^{21}$ erg, to which the characteristic times for the chemical reactions should be compared.

Let us first follow the reaction kinetics in a particular parcel of air. Let, for example, parcel 1 be heated by the shock front to a temperature $T_{f_1} = 3000°K$. The rate of nitrogen oxidation at this temperature is very high and the equilibrium concentration is reached in a time of the order of 10^{-6} sec. Approximately 5% of the nitrogen in the parcel of air is oxidized "instantaneously", after which the concentration of the oxide slowly changes (decreases) in accordance with the laws of chemical equilibrium, following the cooling and expansion. The decomposition of the oxide molecules begins to lag behind the cooling only when the parcel is cooled down to a temperature of the order of 2300°K, at which the relaxation time τ has increased from the initially small value of $\sim 10^{-6}$ sec to a value comparable to the gasdynamic time scale for cooling, i.e., 10^{-2} sec. On further cooling the decomposition stops abruptly, since the decomposition rate drops very

rapidly with decreasing temperature. Thus, already at a temperature of 2000°K the decomposition rate is characterized by a relaxation time $\tau \sim 1$ sec. The residual frozen amount of the oxide in the given parcel corresponds approximately to that concentration which existed at the time when the relaxation time τ was comparable with the characteristic cooling time $\tau \sim 10^{-2}$ sec, when the temperature in the parcel was of the order of 2300°K. However, slightly earlier the concentration was in equilibrium, and the equilibrium concentration changes only very weakly when the temperature is decreased by several hundred degrees; such a drop in temperature, however, appreciably changes the decomposition rate (see §4, Chapter III, and §8, Chapter VI). Hence, the residual concentration of the oxide in the air parcel is simply equal to the equilibrium concentration at a temperature of about 2300°K, and this is a quantity of the order of 1%. The time dependence of the oxide concentration in the parcel is shown schematically in Fig. 8.9. Of

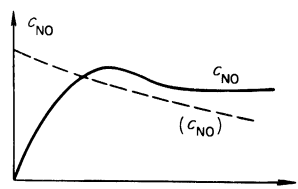

Fig. 8.9. Schematic dependence on time of the equilibrium (c_{NO}) and actual c_{NO} concentrations of nitric oxide in a given air parcel in an explosion wave.

course, the exact value of the residual concentration depends on the particular parcel, in particular on the density with which it arrived at the critical reaction temperature (for this reaction $\approx$2300°K) at which $\tau \sim t$, as well as on the cooling time. These details, however, do not affect the order of magnitude of the residual concentration. The oxidation of the oxide to the dioxide at temperatures of $\sim$2000°K proceeds quite rapidly (see §9, Chapter VI). Therefore, the concentration of the dioxide corresponds to equilibrium, but the dioxide is in this case in equilibrium with the actual frozen amount of the oxide and not with the equilibrium amount of the oxide. At temperatures of the order of 2000°K the concentration of the dioxide is approximately 0.01% (see Table 5.9 in §21 of Chapter V). Subsequently, the entire oxide is gradually oxidized to the dioxide; here the process at first follows the cooling, and then, at temperatures of $\sim$1500°K and below, it lags behind the cooling. Total oxidation of the oxide is completed when the parcel is quite cold, some tens of seconds after the explosion.

In air parcels which were heated by the shock front to temperatures below $\sim$2200–2000°K, in general, no nitric oxide is formed at all, since the oxidation rate at such temperatures is very low, and the parcel quickly passes through the temperature region of approximately 2000°K in which the reac-

tion rate is still appreciable. Thus, a spherical air layer, heated by a shock front to a temperature of ~2200–2000°K, limits, in general, the mass of air in which the oxide and then the dioxide have appeared (the motion of this layer is described on the r, t diagram of Fig. 8.6, say, by the trace 3). From this, we also get the estimate of the total amount of oxides of nitrogen formed in a strong explosion. This amount is determined by the mass of air heated by the shock front to a temperature above ~2200–2000°K, and by the equilibrium concentration of the oxide at this temperature (actually, at a slightly higher temperature—2300°K), since the freezing takes place particularly at these temperatures*. In an explosion with an energy of 10^{21} erg the radius of the shock front at a front temperature $T_f = 2000°K$ is approximately 100 m. The mass of air in a spherical volume of this radius is approximately 5000 tons, and at a concentration of ~1% the mass of the oxide is ~50 tons. The mass of the dioxide, upon addition of still another oxygen atom to each NO molecule, is ~75 tons, that is, about 100 tons as was stated previously.

Let us now consider the distribution of the concentration of oxides with respect to the radius at a given instant of time. Two typical cases are possible. If at the time t' (Fig. 8.10) the temperature at the wave front is above

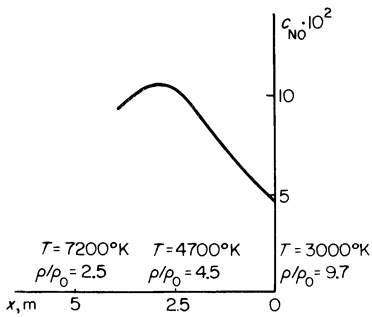

Fig. 8.10. Distribution of nitric oxide concentration behind a shock front in an explosion with an energy $E = 10^{21}$ erg. The temperature at the front $T_f = 3000°K$. The concentration is at equilibrium almost everywhere. Values of temperatures and densities are given at several points. x is the distance behind the shock.

~2300°K, then for practically all the parcels behind the front the concentrations of the oxide and dioxide are equal to their equilibrium values and the distributions of the concentrations are simply determined by the temperature and density distributions behind the front. The only exception is a very thin layer of air immediately behind the front, in which the oxides at this time have not yet formed (Fig. 8.10).

If we consider now the time t'', when the temperature behind the front is less than ~2000°K, for example 1600°K, then we find in the vicinity of the front parcels which have been heated by the front to temperatures below

* We recall that the equilibrium concentration of nitric oxide in air depends only on the temperature, and not on the density (see §4, Chapter III, and §8, Chapter VI).

2000°K; in general, this gas does not contain any oxide. Far from the front, at temperatures above ~2500°K, the concentration is at its equilibrium value, while in an intermediate layer the oxide is present, but not in its equilibrium concentration. Closer to the front it is lower than its equilibrium value, and slightly farther away, in those parcels in which freezing has already begun, it is higher than at equilibrium (Fig. 8.11).

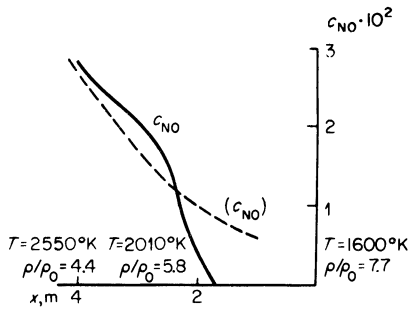

Fig. 8.11. Distribution of the nitric oxide concentration behind a shock wave front in an explosion with $E = 10^{21}$ erg. The temperature at the front $T_f = 1600°K$. The solid curve is the actual concentration, the dashed curve the equilibrium concentration. For $x > 4$ m, $c_{NO} \approx (c_{NO})$. Values of temperatures and densities are given at several points.

In order to calculate the concentration of the oxide in the nonequilibrium region, and also to determine more precisely the amount of frozen oxide, we must solve the rate equation (6.45) for the oxidation of nitrogen in the given parcel of air, taking into account the relationships governing the cooling and expansion behind the explosion wave. The relationships governing the expansion and cooling of air, which follow from the solution of the problem of a strong explosion (§25, Chapter I), can be well approximated by the following equations, which are convenient for use in rate calculations

$$\rho = \rho_0 \left(\frac{t_0}{t}\right)^{2b},$$

$$\frac{1}{T} = \frac{1}{T_0} + \frac{a}{T_0} \ln \frac{t}{t_0}.$$

Here T_0 and ρ_0 are the temperature and density in the parcel at the initial time t_0, when the shock front passed through it, and a and b are numerical constants, depending only on the effective specific heat ratio in the gas-dynamic solution. For $\gamma = 1.30$, $a = 0.44$ and $b = 0.75$.

It has been shown (see [13]) that by an appropriate choice of new variables in the rate equation (6.45) this equation, together with the known relations

for the cooling and expansion, can be reduced to the universal dimensionless form

$$\frac{dy}{dx} = x^{3-\delta}(y^2 - x^2). \tag{8.24}$$

Here the quantity x is related to the time variable, y is proportional to the oxide concentration, and δ is a numerical constant less than unity. The initial condition corresponding to the absence of oxide at the initial time $t = t_0$ reduces to the condition $y = 0$, with x equal to some value x_0 which depends only on the time t_0, the initial values of the state variables, and on the constants entering the rate equation (6.45). Zel'dovich, Sadovnikov, and Frank-Kamenetskii [14] have studied the kinetics of the nitrogen oxidation reaction under laboratory conditions with a cooling law of the type $1/T = (1/T_0) + (a'/T_0)t$, at constant density. With new variables introduced, the rate equation (6.45) was also reduced to an equation of the type (8.24) with the initial condition $y = 0$ when $x = x_0$. Reference [14] gives a tabulation of the solution of the equation $y = y(x, x_0)$*.

Knowing the initial state variables for an air parcel from the gasdynamic solution of the problem of a strong explosion, we can thus obtain a complete solution of the dependence of the oxide concentration c_{NO} on time. This solution is in complete agreement with the qualitative considerations presented above. The curve presented in Fig. 8.11 was calculated in this manner.

3. *Disturbance of thermodynamic equilibrium in the sudden expansion of a gas into vacuum*

§6. Sudden expansion of a gas cloud

The phenomenon of sudden expansion of a gas cloud into vacuum is encountered in various natural, laboratory, and industrial processes. Meteorite impacts on planet surfaces result in the sudden braking of the meteorites and the conversion of their kinetic energy into heat. If the impact velocity is high, of the order of several tens of kilometers per second, very high temperatures result, of the order of tens or hundreds of thousands of degrees. The meteorite and a part of the planet soil are vaporized during the impact. This phenomenon resembles a strong explosion on the planet's surface†. If the

* As was noted by Kompaneets, the equation (8.24) with $\delta = 0$ can be solved exactly in terms of Bessel functions.

† The hydrodynamics of this process will be considered in Chapter XII.

planet is without an atmosphere (as for example in the case of the moon) the vapor cloud generated, with tremendous expansion velocities, overcomes the force of gravity and freely expands into vacuum. A hypothesis has been advanced that the lunar craters were formed as a result of such "explosions" from the impacts of extremely large meteorites. Similar phenomena also take place in the much more frequent collisions between small bodies in the solar system—the asteroids.

Sudden expansion into vacuum of tremendously large gas clouds is observed during nova outbursts, in which a disturbance in the energy balance of the star leads to the release of a large amount of energy and a shock wave is propagated from the central layers to the periphery. This shock wave separates from the surface of the star and emits a gas cloud into space. To some extent, similar phenomena (but on very much smaller scale) are also encountered under laboratory conditions. An example is the vaporization of the anode needle of a pulsed x-ray tube caused by a strong electron discharge (Tsukerman and Manakova [15]); another is the explosion of wires by electric currents in vacuum systems. Of course, the expansion under laboratory conditions is not unbounded since it is bounded by the walls of the vacuum chamber; however, at the stage when the gas has not yet reached the walls, the expansion into the vacuum takes place in the same manner as if the vacuum were "infinite".

Experiments in which a gas cloud suddenly expands into a vacuum were also carried out in connection with rocket probe studies of the upper layers of the atmosphere when sodium vapor and nitric oxide were released into space. The same phenomenon also occurred when an artificial comet was created during the moon flight of the Soviet cosmic rocket.

The dynamics of the sudden expansion of a gas cloud into vacuum is very simple; an idealized problem of the sudden isentropic expansion of a gas sphere into vacuum, for a gas with constant specific heats, was considered in §§28 and 29 of Chapter I. Here we shall be interested in certain fine points concerning the state of the gas during the later stage of the expansion to infinity, when the expansion can be treated on the basis of a very simple scheme. In this scheme we shall consider the behavior of only the mass-averaged flow variables. It is clear that the variables describing any particular gas particle change with time in exactly the same manner as do the averaged quantities and differ from the average values only by numerical factors which are of the order of unity and which are not of great importance for our purpose.

Let us consider a gas sphere of mass M and energy E^*. Almost the entire initial energy has been transformed into kinetic energy during the earlier

* For convenience, we shall repeat here some of the results of §28, Chapter I.

phase of the expansion, and the fluid expands by inertia with the average velocity

$$u = \left(\frac{2E}{M}\right)^{1/2}.$$

The sphere radius is of the order of $R = ut$ and the gas density decreases with time according to the relation

$$\rho = \frac{M}{4\pi R^3/3} = \rho_0\left(\frac{t_0}{t}\right)^3, \tag{8.25}$$

where the characteristic time scale is approximately expressed in terms of the initial radius of the sphere R_0 and the initial fluid density ρ_0 by

$$t_0 = \left(\frac{M}{\rho_0 4\pi u^3/3}\right)^{1/3} = \frac{R_0}{u}. \tag{8.26}$$

If we are interested in the gas temperature during the later stage of the expansion, we must consider the small amount of internal energy that still remains in the gas, which we neglected in calculating the expansion velocity. We take into account the fact that the specific entropy of the gas S remains constant during the expansion. Assuming for simplicity that the fluid behaves as a gas with some constant effective value of the specific heat ratio we obtain for the cooling of the gas the relation

$$T = A(S)\rho^{\gamma-1} \sim t^{-3(\gamma-1)}, \tag{8.27}$$

where $A(S)$ is a constant which depends on the entropy and which can be calculated from the well-known formulas of statistical mechanics and thermodynamics. If we consider relatively high temperatures then, taking into account the processes of ionization, dissociation, etc., we can take as an approximate value for the specific heat ratio $\gamma \approx 1.2$–1.3. In any case, the ratio is not greater than $5/3 = 1.66$, which corresponds to a complete freezing of all the internal degrees of freedom in the gas.

§7. Freezing effect

Let us consider the physical and chemical processes taking place in a gas expanding according to the cubic relation $\rho \sim t^{-3}$ and cooling as $T \sim t^{-3(\gamma-1)}$. We assume that the initial temperature was high, so that the molecules were dissociated and the atoms strongly ionized. We further assume that the initial density of the gas was also high, as is usually the case when a gas cloud is formed by the rapid release of energy in an initially solid substance. Then, during the early stage of the sudden expansion, at high density and temperature, all relaxation processes proceed very rapidly and the gas remains in

thermodynamic equilibrium; the characteristic state variables of the gas, as for example the degrees of ionization or dissociation, follow the expansion and cooling. If during the entire expansion the gas were to remain in thermodynamic equilibrium, then in the process of expansion and cooling all the electrons would rather quickly combine with the ions into neutral atoms, and all the atoms with a chemical affinity would combine into molecules.

Actually, the equilibrium degrees of ionization and dissociation have an exponential dependence on temperature but only a power-law dependence on the density: $\alpha \sim \rho^{-1/2} \exp(-I/2kT)$, where I is the ionization potential or dissociation energy. For an expansion with cooling to low temperatures, the equilibrium degrees of ionization and dissociation rapidly approach zero, since as $T \sim \rho^{\gamma-1} \to 0$ the exponential term decreases extremely rapidly, much more rapidly than the preexponential factor increases. It can be easily seen, however, that no matter how high the initial rate of establishment of thermodynamic equilibrium in comparison with the cooling and expansion rates, there is a time at which the ratio of these rates will be reversed, thermodynamic equilibrium will no longer be established, and the degrees of ionization and dissociation will begin to depart increasingly from their equilibrium values.

In fact, the equilibrium degrees of ionization and dissociation are established as a result of the mutual compensation of the direct and reverse processes. But at low temperatures the ionization and dissociation, which require large expenditures of energy, drop very sharply. The rates of these processes depend on temperature as $\exp(-I/kT)$, and for $kT \ll I$ they depend extremely strongly on temperature, and thus on time. On the other hand the rates of the reverse recombination processes have only a power-law dependence on density and temperature and consequently on time. Thus, ionization and dissociation will essentially stop at a certain instant, after which the degrees of ionization and dissociation will decrease with time following a power law, while the equilibrium values drop exponentially.

The rates of recombination processes decrease as a result of an expansion, and recombination may cease entirely. We can convince ourselves of this by taking as an example the recombination of atoms into molecules (recombination of electrons with ions will be considered in the following sections). Recombination at high densities takes place by three-body collisions, while two-body collisions are responsible for recombination at low densities, so that it is sufficient to consider the latter in the later stage of the expansion. Let N be the number density, $\bar{v} \sim \sqrt{T}$ the thermal speed, and σ the recombination cross section, which is no larger than the gaskinetic cross section. The recombination rate $dN/dt = -N\bar{v}\sigma$ and the characteristic time during which appreciable changes take place in the degree of dissociation is $\tau \approx 1/N\bar{v}\sigma$. Even if we do not take into account the decrease in the number of atoms as a

result of recombination, the atom number density N will decrease in proportion to $1/t^3$ as a result of the expansion of the gas, $\bar{v} \sim \sqrt{T} \sim t^{-\frac{3}{2}(\gamma-1)}$ so that $\tau \sim t^{3+\frac{3}{2}(\gamma-1)} = t^{\frac{3}{2}(\gamma+1)}$, and the characteristic time τ increases faster than t; consequently, at some instant of time it will become greater than t. On the other hand, the time scale characterizing the changes in density and temperature is the time t itself, measured from the beginning of the sudden expansion, since $dT/dt \sim -T/t$ and $d\rho/dt \sim -\rho/t$. Thus, at some time recombination begins to lag ever increasingly behind the cooling. Moreover, beginning approximately at this time, the probability of recombination of the given atom with all other atoms during the remaining expansion to infinity is less than unity; in other words, the recombination does not proceed to completion. In fact, this probability is equal to

$$w = \int_{t_1}^{\infty} N\bar{v}\sigma \, dt = \int_{t_1}^{\infty} \frac{dt}{\tau} \lesssim \frac{1}{\tau_1} \int_{t_1}^{\infty} \left(\frac{t_1}{t}\right)^{\frac{3}{2}(\gamma+1)} dt \approx \frac{t_1}{\tau_1} = const. \quad (8.28)$$

Starting at the time t_1 at which $\tau_1 > t_1$, the recombination probability of a given atom $w < 1$. Thus, the gas expands to infinity in the dissociated state. This phenomenon is called "freezing" of the atoms.

Starting at some time, the gaskinetic collisions in the gas also cease almost entirely. Deexcitation of the vibrational and rotational modes of molecular excitation by particle collisions stops. This follows from the convergence of the same collision integral (8.28). However, freezing of the molecular vibrational and rotational modes does not take place; the vibrational and rotational energies of the molecules are carried away by the spontaneous emission of photons. The vibrational transitions produce radiation in the infrared region of the spectrum and the rotational transitions result in the emission of radio frequencies.

Owing to the convergence of the collision integral when the gaskinetic cross section (for the neutral atoms) is substituted, the exchange of energy of the random translational motion of the atoms also ceases after a certain time in a spherical sudden expansion. The remainder of the expansion then continues without collisions*. All of the particles move by inertia with the velocity which they have acquired in their last collision. In this case the particles, in general, have a nonradial ("random") velocity component. It would seem that "freezing" of the random velocity, that is, "temperature", should take place. Actually, as was noted by Belokon' [16], this does not happen for purely geometrical reasons. The problem consists in the definition of the concepts of hydrodynamic and internal energy when particle collisions are

* It is interesting to note that for a sudden expansion with $\gamma = 5/3$ the frequency of Coulomb collisions of charged particles does not decrease, since $\sigma \sim T^{-2}$ and $N\bar{v}\sigma \sim NT^{-3/2} \sim N^{5/2-3\gamma/2} = const.$

absent. The internal energy of a unit volume of gas is equal to the difference between the total kinetic energy $\frac{1}{2}Nm\overline{v^2}$ (N is the number of particles per unit volume, m their mass, and $\overline{v^2}$ the mean square velocity) and the kinetic energy of "hydrodynamic" motion $\frac{1}{2}Nm(\bar{v})^2$, where $(\bar{v})^2$ is the square of the mean velocity:

$$E_{\text{int}} = E_{\text{total}} - E_{\text{hydrod}} = \tfrac{1}{2}Nm(\overline{v^2} - (\bar{v})^2).$$

Let us suppose that the collisions stop at a time t_1, when the gas occupies a sphere of radius r_1 (Fig. 8.12). Particles leaving the sphere arrive at points A and B at times t' and t'' with velocities whose directions are included within the cones shown in Fig. 8.12. It is clear that the greater is the distance from

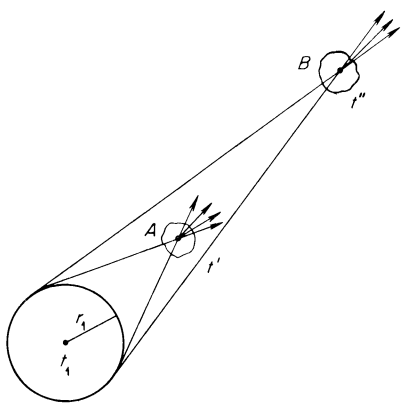

Fig. 8.12. The problem of expansion of a gas into vacuum without collisions.

the center, the narrower is the cone and the closer $\overline{v^2}$ is to $(\bar{v})^2$, the smaller is the difference $\overline{v^2} - (\bar{v})^2$. In the limit $t \to \infty$, $r \to \infty$ all particles move in an exactly radial direction. In this limit $\overline{v^2} = (\bar{v})^2$, and the entire translational internal energy has been transformed into hydrodynamic energy*.

In cylindrical and planar sudden expansions, thermodynamic equilibrium is also definitely disturbed, but of course the changes with time in the degrees of dissociation and ionization follow different laws. It should be noted that, if the mass of the gas is finite, then, when the gas has undergone a sufficiently

* *Editors' note.* Besides the geometrical effect, another effect must be invoked for this conclusion. The particle velocities at the point A are not uniform in magnitude, but lie between $(r' - r_1)/(t' - t_1)$ and $(r' + r_1)/(t' - t_1)$. With t' very large the variation in particle velocity is of the order of r_1/t'. In the limit $t \to \infty$, $r \to \infty$ this variation approaches zero, so that the particle velocities approach uniformity in magnitude as well as in direction. In this limit, then, $\overline{v^2} = (\bar{v})^2$.

large expansion, cases which are initially planar or cylindrical must become spherical cases.

We note a number of other papers [15a, 24–26] devoted to various problems of the free molecular sudden expansion of a gas into a vacuum without collisions (these articles also contain references to other papers). Reference [27] considers the sudden expansion of an ionized gas into a vacuum in which there is a magnetic field.

§8. Disturbance of ionization equilibrium

We now consider in more detail the problem of the disturbance of ionization equilibrium resulting from the expansion of a gas, and show how we can establish approximately the time at which the equilibrium is disturbed (the method presented below was suggested by one of the authors [17]). We assume that initially the gas temperature was high and the atoms were multiply ionized. As the expanding gas cools, electrons are reseated at the appropriate levels in the atoms, and the degree of ionization decreases. Let the ionization equilibrium be disturbed only during the later stage of a sufficiently strong expansion and cooling, when it is the last electrons which are reseated in the atoms, i.e., when the process taking place is the reverse of single ionization of the atoms. The gas at this time is essentially expanding by inertia, with the speed constant and the density changing as $1/t^3$.

The mechanism of recombination of ions and electrons was considered in detail in Chapter VI. The electrons are captured by ions in three-body collisions with an electron acting as the third body; at temperatures which are not too high the electrons, as a rule, are captured into the upper levels of the atoms. Captures by two-body collisions with the emission of a photon are also possible (in this case the electrons are primarily captured into the ground level). Such photorecombination is of importance only at very low electron densities N_e cm^{-3}. The lower the temperature the lower must be the electron density for photorecombination to be important. According to (6.107) this process predominates only under the condition that $N_e < 3.1 \cdot 10^{13} T_{ev}^{3.75} = 3.2 \cdot 10^9 T_{\text{thous. deg}}^{3.75}$. However, in the majority of cases of sudden expansion which are of interest, at the stage when equilibrium is disturbed at temperatures of several thousand degrees, the electron density is much higher and photorecombination plays no role, neither at the time when the equilibrium is disturbed nor later.

If when the gas is still close to equilibrium the main role is played by recombination from three-body collisions, then ionization takes place as a result of the reverse process, that of the removal of electrons primarily from excited atoms by free electron impact. According to the detailed balancing principle, the ionization rate can be expressed in terms of the recombination

coefficient and the equilibrium constant or the equilibrium degree of ionization. In this case the rate equation for the degree of ionization $x = N_e/N$ (N is the number of nuclei, atoms plus ions per unit volume) is expressed in the form

$$\frac{dx}{dt} = bN(x_{eq}^2 - x^2). \tag{8.29}$$

Here b is the recombination coefficient which, at not too high temperatures, not above several thousand degrees, is given by (6.106)

$$b = \frac{ANx}{T^{9/2}}, \tag{8.30}$$

$A = 8.75 \cdot 10^{-27}$ cm$^6 \cdot$ ev$^{9/2}$/sec $= 5.2 \cdot 10^{-23}$ cm$^6 \cdot$ (thousand deg)$^{9/2}$/sec.

Here x_{eq} is the equilibrium degree of ionization given by the Saha equation. For values of x_{eq} not large in comparison with one we have, approximately,

$$x_{eq} \approx 7 \cdot 10^7 \left(\frac{g_+}{g_a} \frac{T^{\circ\, 3/2}}{N}\right)^{1/2} e^{-I/2kT}. \tag{8.31}$$

When the expansion and cooling are governed by the known relations in which $N(t)$ and $T(t)$ are given by (8.25) and (8.27), then (8.29) becomes an ordinary differential equation for the desired function $x(t)$. Since we are primarily interested in the qualitative features of the problem, we shall solve this equation only approximately. The initial ionization and recombination rates, which are proportional to the terms on the right-hand side of (8.29), are large in comparison with the expansion and cooling rates. (For the purpose of comparing rates of the different processes we shall use relative rates expressed in reciprocal seconds, for example, $T^{-1}dT/dt$ and $N^{-1}dN/dt$). Ionization and recombination almost completely cancel each other; the degree of ionization follows the expansion and cooling and remains close to its equilibrium value. Approximately, $x(t) \approx x_{eq}(t) \equiv x_{eq}[T(t), N(t)]$ and the difference $|x_{eq}^2 - x^2| \ll x_{eq}^2$.

The small departure of the degree of ionization from its equilibrium value which inevitably exists (since the temperature and density change with time) can be approximately estimated by setting $dx/dt \approx dx_{eq}/dt$ on the left-hand side of (8.29), replacing x in the expression for the recombination coefficient by x_{eq}, and setting $x_{eq}^2 - x^2 \approx 2x_{eq}(x_{eq} - x)$. It can be easily checked that the relative departure $|x_{eq} - x|/x_{eq}$ increases with time (since the rate of the relaxation process becomes increasingly lower in comparison with the rate of change of the macroscopic parameters temperature and density).

Ionization equilibrium is appreciably disturbed when the difference between the ionization and recombination rates increases to a value of the order of

the rates themselves, that is, when the quantity $|x_{eq}^2 - x^2|$ becomes of the order of x_{eq}^2. To estimate the time t_1 when the equilibrium is disturbed and the values of T_1, N_1, and x_1 at this time, we can again set $dx/dt \approx dx_{eq}/dt$ and $x \approx x_{eq}$ in the recombination coefficient, and equate the difference $x^2 - x_{eq}^2$ to the value of x_{eq}^2. Differentiating with respect to time the equilibrium degree of ionization given by (8.31), taking into account the fact that the most rapidly changing factor is the exponential Boltzmann factor, and then using the cooling relation (8.27) (which yields $dT/dt = -3(\gamma - 1)T/t$), we find an equation which determines the time when the equilibrium is disturbed;

$$b_1 N_1 x_{eq_1} t_1 = \tfrac{3}{2}(\gamma - 1)\frac{I}{kT_1}. \tag{8.32}$$

Here $b_1 = b(T_1, N_1, x_{eq_1})$. This equation, together with the expansion and cooling expressions (8.25), (8.27), and the Saha equation (8.31) referred to the time t_1, reduce to a transcendental equation for the temperature T_1. Having found T_1, it is easy to calculate the remaining quantities t_1, N_1, and x_{eq_1}. (Within the approximation used we can take the actual degree of ionization x_1 equal to the equilibrium value x_{eq_1}.)

§9. The kinetics of recombination and cooling of the gas following the disturbance of ionization equilibrium*

After the equilibrium is disturbed the ionization rate, which is proportional to x_{eq}^2, continues to decrease rapidly with time according to the exponential relation $e^{-I/kT(t)}$. The recombination rate, which is proportional to the square of the actual degree of ionization, decreases much more slowly and soon becomes appreciably larger than the ionization rate: $x(t) \gg x_{eq}(t)$. Under these conditions it is possible to neglect ionization and to assume that only recombination takes place. The rate equation (8.29) will then be approximately written as

$$\frac{dx}{dt} = -bNx^2 \qquad \text{for} \quad t > t_1. \tag{8.33}$$

If the recombination coefficient b were entirely independent or only weakly dependent on the temperature, then, as a result of the rapid decrease in density, the recombination rate would have dropped and recombination would soon have stopped entirely. This is precisely the situation that takes place with the recombination of atoms into a molecule (see §7). On the other hand, in our case the recombination coefficient (8.30) is very temperature sensitive ($b \sim T^{-9/2}$), and the decrease in the recombination rate due

* This section is based on a paper by Kuznetsov and one of the authors [28].

to the drop in density in the expanding gas is compensated to an appreciable extent by the increase in the recombination rate coefficient due to cooling. For this reason particular importance is attached to the question of the relation governing the temperature decrease with time. In fact, let us write the formal solution of the differential equation (8.33) using the recombination coefficient (8.30),

$$x = \frac{x_1'}{\left[1 + 2Ax_1'^2 \int_{t_1'}^{t} N^2 T^{-9/2}\, dt\right]^{1/2}}. \tag{8.34}$$

Here the values of t_1' and x_1' are determined from initial conditions (to the order of this approximation we may require that the integral curve $x(t)$ pass through the point where the equilibrium is disturbed, so that $t_1' = t_1$ and $x_1' = x_1$). We shall, as previously, characterize the temperature drop with time by the power-law behavior $T \sim t^{-m}$; the quantity $N \sim t^{-3}$.

According to (8.34) the asymptotic behavior of the degree of ionization depends to a large extent on the cooling rate, that is, on the value of the exponent m. If the gas is cooled "slowly" and $m < 10/9$ (which corresponds to a specific heat ratio $\gamma = 1 + m/3 < 1.37$) the integral in (8.34) converges for $t \to \infty$ and the degree of ionization approaches a constant value different from zero, so that recombination does not go to completion. However, if the gas is cooled "rapidly" and $m > 10/9$, the integral diverges for $t \to \infty$ and the degree of ionization tends to zero, following $x \sim t^{-(9/4)(m-10/9)}$. For $m = 10/9$ it also goes to zero, but logarithmically, following $x \sim (\ln t)^{-1/2}$. Thus for $m \geqslant 10/9$ the electrons and ions must eventually recombine.

But the rate of cooling of the gas itself depends on the mode of recombination, since the recombination releases the potential energy of the free electrons previously removed from the atoms, and this energy is partially transformed into heat. Consequently, in order to solve for the behavior of the degree of ionization with time we must consider together the kinetics of the recombination and the balance of thermal energy in the gas.

In the recombination of an electron in a three-body collision the electron is first captured by the ion into one of the upper levels of the atom with a binding energy E of the order of kT (see Chapter VI). Then, under the action of electron collisions of the second kind but also as a result of spontaneous radiative transitions, the bound electron descends down the energy levels of the atom to the ground level. The process of deexcitation of an excited atom usually takes place rapidly in comparison with the rates of electron capture by ions and of the change in gas temperature. For this reason we may assume approximately that the excited atom which is formed is deexcited immediately following capture, and the potential energy I from the recombination is immediately transformed into other forms of energy. A part E^* of it is transferred directly to the free electrons by the electron collisions of the second

kind (and then is distributed over the entire gas as a result of energy transfer between the electrons and ions). The other part of the binding energy $I - E^*$ that is released as a result of radiative transitions is first transformed into line radiation. This radiation in part leaves the gas volume and in part is absorbed by atoms, where the absorption is principally that of the resonance radiation corresponding to the transition of the excited atom directly to the ground state. Through absorption of a resonant photon the atom becomes excited; then it re-emits, the new photon is absorbed by other atoms, etc., this process repeating itself until the photon leaves the gas volume. A so-called diffusion of resonance radiation takes place. During the diffusion of the photon the excited atom can be subjected to a collision of the second kind and give off excitation energy in the form of heat. As a result, some portion of the binding energy $I - E^*$ which was first converted into radiation will with time also be transformed into heat. This part will be less the more transparent is the gas, that is, the shorter the duration of the diffusion of resonance radiation.

We assume for simplicity that the energy $I - E^*$ is completely lost by the gas (corresponding to a transparent gas volume). This assumption underestimates the heat release in the gas and tends to underestimate the temperature; the calculation of the recombination kinetics for this condition will lead to an underestimate of the degree of ionization, and thus yields a lower limit. The above assumption is more justified the more transparent is the gas, and thus the later is the stage of the expansion which we consider. Hence the assumption is valid asymptotically.

In setting up the equation of the energy balance for the gas we shall assume for simplicity that the electron and ion (atom) temperatures are the same. Estimates indicate that in the majority of cases, even after a considerable length of time has passed since the ionization equilibrium was first disturbed, the energy transfer between the electron and ion gases takes place rapidly and the temperatures of these gases are close to each other*. Let us write the energy equation for the gas per heavy particle (per original atom). The thermal energy is $\varepsilon = \frac{3}{2}(1 + x)kT$, the specific volume $V = 1/N$, and the gas pressure $p = N(1 + x)kT$. Then

$$\frac{d\varepsilon}{dt} + p\frac{dV}{dt} = E^*\left(-\frac{dx}{dt}\right). \tag{8.35}$$

From this, using the relation for the expansion $N \sim t^{-3}$, we obtain the equation for the temperature

$$\frac{dT}{dt} + 2\frac{T}{t} = \frac{\frac{2}{3}E^*/k + T}{1 + x}\left(-\frac{dx}{dt}\right). \tag{8.36}$$

* In [28] the equations were set up taking differences between the electron and ion temperatures into account.

To calculate the heat release per recombination E^* we consider the process of the deexcitation of the excited atom which is formed as the result of the capture of an electron by an ion. As noted above, in three-body collisions the electron is, as a rule, captured into one of the very high atomic levels with a binding energy $E \sim kT$. The distances between levels in this region are much less than kT. In collisions with free electrons the bound electron in the excited atom moves to neighboring levels with transitions "upward" and "downward" almost equally probable, so that the change in the energy of an excited atom under the action of electron impacts has the character of a diffusion along the energy axis; on recombination the diffusive flux is directed downward, in the direction of the ground state of the atom (see §18 of Chapter VI). The deexcitation rate, that is the rate of increase in the binding energy of the bound electron dE/dt, can be calculated by multiplying the unsteady diffusion equation (6.109) by the energy E and integrating over the entire spectrum. Since we are considering an unsteady case of the motion of an electron along the energy axis E from a source located in the region of low binding energies, it follows that in the region of high energies we should specify the boundary condition that the distribution function and the diffusive flux are zero. The above procedure gives an approximate expression for the rate of change of the electron binding energy

$$\frac{dE}{dt} \approx \frac{D}{kT},$$

where D is the diffusion coefficient given in §18 of Chapter VI. This equation loses its validity in the region where the distance between the levels is greater than kT, since in this region transitions to the lower levels are significantly more probable than transitions to the upper levels, and the motion has a unidirectional character. In this region

$$\frac{dE}{dt} \approx \beta_{n,n-1} N_e \, \Delta E_{n,n-1},$$

where $\beta_{n,n-1} N_e$ is the transition probability from level n to level $n-1$ (in $\sec^{-1}$), and $\Delta E_{n,n-1}$ is the energy distance between the levels. (The expression for the rate constant of the deexcitation transition $\beta_{n,n-1}$ is given in §15, Chapter VI.)

The transition from a diffusion to a unidirectional motion of the bound electron along the energy axis takes place at a binding energy E' for which the distance between levels $\Delta E_{n,n-1}$ is equal to kT. This energy is (for a hydrogen atom)

$$E' = \frac{1}{2} kT \left(\frac{2I}{kT}\right)^{1/3} = 2.1 \cdot 10^{-4} T^{\circ 2/3}.$$

As is known (see §13, Chapter V), the rate of radiative deexcitation, which is very low for low binding energies, increases rapidly as the degree of excitation decreases. After collisional deexcitation of the atom to some level radiative transitions begin to predominate. The radiation rate corresponding to the radiative transitions to neighboring levels, which determines the rate of radiative deexcitation $(dE/dt)_{\text{rad}}$, is given in §13 of Chapter V. The change from impact to radiative deexcitation takes place at a binding energy for which the rates $(dE/dt)_{\text{impact}}$ and $(dE/dt)_{\text{rad}}$ become equal. This binding energy, obviously, is the energy release E^* to be determined. It should be noted that radiative deexcitation is also promoted by radiative transitions in the atom from the upper levels directly to the ground state, after which the atom no longer interacts (see §13, Chapter V). Calculations [28] show that the contribution of this process is comparable with the contribution made by the gradual radiation which takes place with transitions to the neighboring levels.

Calculation of the heat release E^* carried out in [28] gives approximately*

$$E^* = I \times \begin{cases} 4.3 \cdot 10^{-4} N_e^{1/3} T^{\circ\,-1/2}, & \text{if } kT < E^* < E', \\ 3.1 \cdot 10^{-4} N_e^{1/6} T^{\circ\,1/12}, & \text{if } E^* > E'. \end{cases} \tag{8.37}$$

After having determined the heat release E^* we can integrate the system of equations (8.33) and (8.36). As was shown in [28], the order of the system can be reduced, leading to one nonlinear differential equation of first order. Qualitative analysis of the resulting equation and of the numerical solution shows that, depending on the initial conditions, one or the other regime of the recombination process is established.

If the gas cloud expands rapidly (low cloud mass, high speed of the sudden expansion) and the ionization equilibrium is disturbed early, at a high degree of ionization with the store of potential energy of ionization in the gas greater than the thermal energy, then a large amount of heat is generated during recombination. This prevents rapid cooling of the gas and retards the recombination. Under these conditions the recombination soon ceases and the degree of ionization tends to a constant value different from zero. The electrons and ions become frozen. Practically, this happens if at the time the ionization equilibrium is disturbed all the atoms of the gas are at least singly ionized ($x_1 \gtrsim 1$). However, if the gas cloud expands relatively slowly

* If for any value of T and N_e we have $E^* < kT$, this means that radiative deexcitation must start at the beginning of electron capture. This situation is usually not achieved, since in this case photorecombination dominates recombination in three-body collisions, and in photorecombination the electron is ordinarily captured into the lower, rather than into the upper atomic levels. If E^* calculated from (8.37) is found to be larger by an order of magnitude than the ionization potential I, this means that the entire binding energy I is converted into heat, equation (8.37) is inapplicable, and $E^* = I$.

(large mass, low speed of the sudden expansion) and the ionization equilibrium is disturbed late, at a low degree of ionization with the store of potential energy less than the thermal energy, the small amount of heat which is released on recombination is not capable of retarding the rapid cooling of the gas due to expansion, and the recombination rate stays sufficiently high. In this case the recombination proceeds all of the time and the degree of ionization decreases continuously, going to zero. This continues until the energy exchange between the electron and ion gases is disturbed. This happens when the characteristic exchange time τ_{ei} (see §21, Chapter VI) becomes greater than the time t measured from the beginning of the expansion; this time characterizes the relative rates of expansion and cooling $V^{-1}dV/dt$ and $T^{-1}dT/dt$. After the exchange is disturbed, the heat which is released on recombination is no longer distributed uniformly among all the gas particles, but remains only in the electron gas. (The ions and atoms are cooled faster than are the electrons and their temperature decreases relative to the electron temperature.) Under these conditions the energy release in the electron gas is increased comparatively, since the recombination energy is now transferred to only a small number of electrons. As a result the drop in electron temperature takes place more slowly, and the recombination is also retarded. Under these new heat transfer conditions the degree of ionization ceases to approach zero and a residual ionization is retained in the gas (freezing takes place). However, unlike the preceding case, the residual ionization is now very low, since before the time the energy exchange between the electrons and ions is disturbed an appreciable number of the free electrons succeed in recombining.

Figure 8.13 presents curves of $x(t)$ calculated in [28] for two typical cases

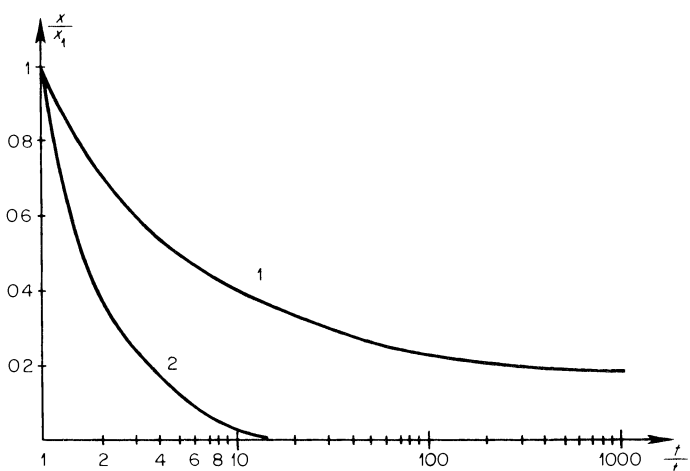

Fig. 8.13. Change in degree of ionization with time for expansion of a gas into vacuum (for explanation see text).

of the sudden expansion of a gas cloud. In the calculations the ionization potential for the atoms was taken to be 13.5 ev and their atomic weight taken to be 14. Curve 1 pertains to the case when the degree of ionization at the time when the ionization equilibrium is disturbed is $x_1 = 0.58$ and the gas temperature and density are $T_1 = 12{,}000°\text{K}$ and $N_1 = 1.7 \cdot 10^{16}\ \text{cm}^{-3}$, respectively. The time when the equilibrium is disturbed is $t_1 = 2 \cdot 10^{-6}$ sec. The radius of the gas cloud at this time is $R_1 = 4.9$ cm, and the expansion velocity $u = 24$ km/sec. The same flow variables given for the time when equilibrium is disturbed can be obtained with different initial conditions. In particular these results can correspond, for example, to an initial temperature, density, and cloud radius $T_0 = 50{,}000°\text{K}$, $N_0 = 2 \cdot 10^{18}\ \text{cm}^{-3}$, and $R_0 = 1$ cm, respectively. As can be seen from the figure, for these conditions the degree of ionization of the gas tends to the rather appreciable constant value of $\approx 0.2x_1 \approx 0.12$, and appreciable freezing takes place. Curve 2 relates to the following values of the parameters at the time when the equilibrium is disturbed: $t_1 = 2.1 \cdot 10^{-6}$ sec, $T_1 = 11{,}700°\text{K}$, $N_1 = 4 \cdot 10^{16}\ \text{cm}^{-3}$, $x_1 = 0.34$, $R_1 = 5$ cm, $u = 24$ km/sec. This case can correspond, for example, to the initial conditions: $T_0 = 50{,}000°\text{K}$, $N_0 = 5 \cdot 10^{18}\ \text{cm}^{-3}$, and $R_0 = 1$ cm. As can be seen, in this case the degree of ionization tends to zero, and it appears that no freezing takes place. Actually, as was noted above, the recombination will also cease at some stage (when the energy transfer from the electrons to the heavy particles slows down), but only when the degree of ionization is very low.

In concluding this section we wish to emphasize again that the diffusion of resonance radiation, which has not been taken into account here, aids in increasing the heat release in the gas, in decreasing the rate of recombination, and in increasing the residual ionization. This process should be considered in relation to the specific problem at hand, since the diffusion of resonance radiation depends on the dimensions and degree of transparency of the gas cloud, the character of the broadening of the spectral lines, the gas composition, etc.

4. Vapor condensation in an isentropic expansion

§10. Saturated vapor and the origin of condensation centers

If the vapor of any substance is isentropically expanded and cooled, there is some time t at which the vapor becomes saturated; then it becomes supersaturated, after which condensation begins. It is well known that condensation is greatly facilitated by the presence of ions, dust, and other foreign particles which become condensation centers, about which liquid drops form.

Ions and dust particles only create favorable conditions for the more rapid formation of condensation centers, but their presence is not at all necessary. In a pure supersaturated vapor condensation centers appear as the result of the agglomeration of molecules into molecular complexes. After reaching the so-called critical size the complexes become stable and do not break up, and exhibit a tendency for further growth and transformation into droplets of liquid.

The phenomenon of vapor condensation in an isentropic expansion is met in industry, in the laboratory, and in nature. It serves as the basis of operation of the Wilson cloud chamber, which is widely used in nuclear physics for recording the motion of high-speed charged particles. The Wilson cloud chamber consists of a vessel filled with vapor of water, alcohol, or other liquid. The required supersaturation is created by an isentropic expansion of the vapor by means of a rapidly receding piston. The vapor condenses on the ions which are formed along the trajectory of the rapidly moving particle, and the drops of liquid are recorded by optical means. The condensation of the water vapor in air is frequently observed in the expansion of air in wind tunnels.

The fact that condensation must start at some time during an isentropic expansion of vapor can be easily explained with the aid of a temperature-specific volume diagram. As is known from thermodynamics, the pressure of a saturated vapor which is in equilibrium with the liquid is governed by the Clapeyron–Clausius equation (see, for example, [18]). If the vapor is considered as a perfect gas, then this equation leads to the following relationship between the specific volume of the saturated vapor V_{vap} and the temperature*

$$V_{\text{vap}} = BTe^{U/RT}, \qquad T = \frac{U}{R}\left(\ln\frac{V_{\text{vap}}}{BT}\right)^{-1}, \tag{8.38}$$

where U is the heat of vaporization, R is the gas constant, and B is a coefficient, which can be taken approximately constant. It is evident from this equation that the saturation temperature has only a weak logarithmic dependence on the vapor volume. On the other hand, the isentrope for the vapor is a power-law type curve of the form $T \sim V^{-(\gamma-1)}$, which must intersect the saturation curve (Fig. 8.14). At the point of intersection O the previously unsaturated expanding vapor becomes saturated.

Let us follow the process in time. If the vapor expands continuously, then the specific volume increases monotonically with time. Instead of considering the temperature change with time $T(t)$, we can consider the temperature

* This follows from the relations $p = const\ e^{-U/RT}$, $pV = RT$, where p is the saturated vapor pressure. *Editors' note.* U is assumed constant, and the specific volume of the liquid is assumed negligible.

change with increasing volume $T(V) = T[V(t)]$, using a T, V diagram (see Fig. 8.14). After passing the saturation state, the vapor continues to expand following the vapor isentrope, and becomes supersaturated (supercooled). The rate of formation of condensation centers has an extremely strong dependence on the degree of supersaturation. Therefore a further increase in

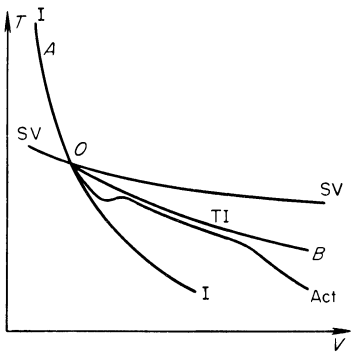

Fig. 8.14. T,V diagram for condensation in an isentropic vapor expansion. I is the isentrope for the vapor, SV is the saturated vapor curve, O is the saturation point, TI is the isentrope for the equilibrium two-phase vapor-liquid system, Act is the actual curve for the vapor-liquid drop systems taking into account the kinetics of condensation.

the degree of saturation results in a rapid increase in the number of nuclei in the liquid phase. Soon after the saturation state is passed, the rate of condensation reaches a value such that the release of the latent heat prevents any further increase in the supersaturation (if, of course, the expansion is not too rapid). The condensation accelerates even if the number of centers remains constant, because of an increase in the surface area of the drops to which the vapor molecules attach. The acceleration of the condensation not only stops the increase in supersaturation, but even leads to a decrease in the degree of supersaturation. The formation of new nuclei, which is highly sensitive to the value of supersaturation, ceases immediately and further condensation proceeds by means of the attachment of molecules to the previously formed drops. Thus all condensation centers, as a rule, are born at the very beginning of the condensation process, as soon as a sufficiently high degree of supersaturation is reached.

In the Wilson cloud chamber the vapor is rapidly expanded to a definite volume, so that a known initial supersaturation is established in the vapor. This supersaturation is chosen to be large enough that all the ions become condensation centers, thus making it possible to determine the number of ions by counting the number of drops*. Therefore, no problem arises as to the number of condensation centers.

It is another matter in gasdynamic processes such as the expansion of gases in wind tunnels, the exhaust from nozzles, or the sudden expansion of a gas cloud which forms as a result of the heating and vaporization of an

* At the same time, practically speaking, nuclei not containing ions do not form.

initially solid substance such as a metal. Here the rate of expansion is determined by the general dynamics of the process, and the number of condensation centers is unknown and depends on the expansion rate. Even if ions are present in the gas (which, of course, does not always happen) by far not all of them become condensation centers if the expansion rate is sufficiently low. As a result of the factors already mentioned, the supersaturation of a system can decrease due to very rapid condensation after only a few of the ions are converted into condensation centers. Even more unknown is the number of pure vapor centers in the absence of foreign particles. The number of condensation centers depends on the maximum attainable supersaturation (supercooling) and is determined by the interplay of opposing effects: cooling of the vapor corresponding to the work of expansion and heating of it as a result of the release of latent heat in condensation. We shall show in §12 how one may calculate the number of condensation centers, knowing the rate of expansion and cooling of the vapor.

§11. The thermodynamics and kinetics of the condensation process

Let us consider the process of condensation in an isentropically expanding fluid from a purely thermodynamic point of view, by assuming that thermodynamic equilibrium exists at any given time. Up to the time of saturation the gas expands along an isentrope. After the saturation state has been reached and condensation begins, the fluid becomes a two-phase vapor-liquid system. The adiabatic equation is complicated because of the conversion of a part of the gas phase into a liquid of different thermodynamic properties and because of the release of the latent heat. The isentrope for this two-phase system satisfies the adiabatic equation

$$[c_1(1-x)+c_2x]\,dT + RT(1-x)\frac{dV}{V} - [U-(c_2-c_1)T]\,dx = 0. \quad (8.39)$$

Here c_1 is the specific heat of the vapor at constant volume; c_2 is the specific heat of the liquid; x is the degree of condensation, defined as the ratio of the number of molecules in the liquid phase to the total number of molecules in the given mass of fluid; V is the specific volume of the fluid, which is less by a factor of $(1-x)$ than the specific volume of the vapor: $V = V_{\text{vap}}(1-x)$*. In this equation we have neglected the surface energy of the liquid drops, which is very small in comparison with the latent heat if the drops contain

* The specific volume of the two phase system is $V = V_{\text{liq}}x + V_{\text{vap}}(1-x)$, where V_{liq} is the specific volume of the liquid phase. Since the density of the liquid is much higher than the density of the vapor, for a degree of condensation which is not too close to unity, the first term can be neglected and $V \approx V_{\text{vap}}(1-x)$. The specific heats of the liquid and the vapor c_2 and c_1 in (8.39) are assumed to be constant.

large numbers of molecules. The adiabatic equation (8.39) is also valid in the absence of thermodynamic equilibrium. In the case of nonequilibrium, the degree of condensation x is determined by the condensation kinetics. Under conditions of thermodynamic equilibrium, for an infinitely slow expansion, the vapor is in equilibrium with the liquid at any instant of time, and is always saturated. The state of the fluid changes in this case along the saturation curve (8.38), which, if we replace the specific volume of the vapor by the specific volume of the fluid, takes the form

$$\frac{V}{1-x} = BTe^{U/RT}. \tag{8.40}$$

If we eliminate the degree of condensation x from (8.39) and (8.40), we obtain a differential equation describing the isentropic process in the two-phase system in terms of the variables T and V. The solution of this equation yields the isentrope $T(V)$. The constant of integration in the general solution is determined by the entropy of the fluid. The constant can be expressed in terms of the temperature and volume at the saturation point O, since it is obvious that the isentrope passes through this point. We shall not write out the solution here, but shall instead illustrate the isentrope in Fig. 8.14. The solution lies somewhat below the saturation curve, which can be seen by comparing (8.38) and (8.40) and taking into account the fact that $x > 0$, $1 - x < 1$. For a small degree of condensation, when $x \ll 1$, the isentrope of the two-phase system almost coincides with the saturation curve. The divergence of the two curves determines the degree of condensation x:

$$1 - x = \frac{V(T)}{V_{\text{vap}}(T)}.$$

The degree of condensation increases monotonically along the isentrope with increasing volume.

It is interesting to note that in an infinite isentropic expansion of a fluid, with $V \to \infty$ (and cooling to zero temperature $T \to 0$), the degree of condensation along the isentrope for thermodynamic equilibrium tends to unity, $x \to 1$. In other words, according to the laws of thermodynamics, in the unlimited expansion of a fluid, the vapor should be completely condensed. In an isentropic expansion to a finite volume only a finite amount of vapor is condensed. In reality, of course, the state of the fluid in the condensation process can never follow the equilibrium isentrope exactly, it only more or less approaches the equilibrium state; it is closer to equilibrium, the slower is the change of the external conditions, i.e., the slower is the expansion.

It was already noted above that condensation centers are born primarily

immediately after passing the saturation state, at the time when maximum supersaturation is reached. Thereafter, if the expansion does not proceed too rapidly, the accelerating condensation stops the supersaturation process and no new nuclei are formed. The state of the fluid after passing through a point of maximum deviation from the equilibrium isentrope (TI) (Fig. 8.14, maximum supercooling) approaches the equilibrium state. The degree of supercooling, however, does not drop to zero and the curve (Act) never reaches the thermodynamic equilibrium curve (TI), always passing below the latter. Condensation now proceeds by the size of the droplets increasing. Two processes take place simultaneously: the forward process, attachment of vapor molecules to the drops, and the reverse process, evaporation of the drops. The rate of growth of the drops (that is, the condensation rate) is determined by the difference between the rates of the forward and reverse processes and is higher, the higher the degree of supersaturation. In the saturated vapor, for a state on the equilibrium isentrope, the adhesion and evaporation rates are exactly equal and the drops do not increase in size*.

In condensation the degree of supersaturation adjusts to the balance between attachment and evaporation, automatically conforming to the process in such a manner that the attachment exceeds the evaporation and that the condensation rate follows the expansion of the fluid. The system is always in a state close to equilibrium, i.e., close to saturation.

An appreciable departure from thermodynamic equilibrium can take place only in a very strong expansion, when the attachments of vapor molecules become exceedingly rare. Thus, in the sudden expansion of vapor into vacuum the attachment rate, which is proportional to the vapor density and thus to t^{-3}, starting at a certain time is no longer capable of following the expansion; condensation ceases and the remaining vapor expands to infinity, again following the gas isentrope (Fig. 8.14). Freezing takes place, and the fluid expanding to infinity is not completely condensed, as would be required by the equilibrium laws of thermodynamics, but is partially in the form of a gas and partially in the form of condensate drops (for more details, see the following section). For a rapid expansion of a fluid, the condensation cannot "follow" the expansion and the state departs substantially from thermodynamic equilibrium from the very beginning. In a very rapid expansion to a given volume, as takes place in the Wilson cloud chamber, condensation does not take place during the expansion and begins only after the expansion has ceased. For a very rapid expansion into vacuum condensation generally does not occur at all and the fluid flows out to infinity in the gas phase. This corresponds to the maximum departure from thermodynamic equilibrium and to maximum freezing.

* The thermodynamic equilibrium isentrope, strictly speaking, corresponds to a saturated state with respect to a plane surface of the liquid, with respect to drops of infinite radius.

§12. Condensation in a cloud of evaporated fluid suddenly expanding into vacuum

In this section we consider in more detail the condensation process in the expansion of a vapor, setting out the basic scheme for quantitative calculations and presenting some numerical results. We shall examine condensation as it occurs in a cloud of evaporated fluid expanding into vacuum. Here, we have in mind the phenomenon of the explosion of large meteorites on impact with planet surfaces (devoid of atmosphere) or asteroid collisions, which were mentioned at the beginning of §6. We are interested in what the form is of the vaporized material of the planet soil and of the meteorite which expands into interplanetary space: Is the material in the form of a pure gas or in the form of minute particles, and if the latter what are the particle dimensions? A solution to this problem was obtained by one of the present authors [19]*.

All the numerical results will pertain to the condensation of iron vapor as applied to the case of vaporization of iron meteorites. Let us consider when saturation is reached in the expansion of iron vapor. In Table 8.1 we give the calculated vapor temperature T_1 and atom number density n_1 at the time of saturation for several values of vapor entropy S. Assuming that the expansion is isentropic, we can say that the "solid" iron at the time of heating had the same entropy S. The table gives the values of the initial energy of

Table 8.1

PROPERTIES OF IRON VAPOR AT SATURATION

ε_0, ev/atom	T_0, ev	S, $\frac{\text{cal}}{\text{mole} \cdot \text{deg}}$	T_1, °K	n_1, cm^{-3}	u, km/sec
25.6	5	48.3	3100	$8.01 \cdot 10^{19}$	9.2
71.9	10	60.8	2130	$7.15 \cdot 10^{16}$	15.5
138	15	71.5	1700	$2.86 \cdot 10^{14}$	21.4
222	20	81.3	1430	$1.43 \cdot 10^{12}$	27.2

heating ε_0 and temperature T_0 of standard density solid iron, corresponding to these values of the entropy. These quantities were calculated by the method described in §14, Chapter III (both the nuclear and the electronic contributions to the specific heat are taken into account). The last column gives the average velocities of sudden expansion of a gas sphere of iron atoms estimated from the equation $u = (2\varepsilon_0)^{1/2}$ (see §6), that is, by assuming that the vapor is already strongly cooled before the time of condensation and that all the

* Some qualitative remarks on the phenomenon of condensation of vaporized matter were made by the present authors in [20].

initial heating energy has been converted into kinetic energy of the expansion.

Let us now estimate the number of condensation centers, that is, the number of condensate particles in the final state. The theory of the formation of nuclei of the liquid phase in pure supersatured vapor has been developed by a number of authors, M. Volmer, R. Becker and W. Döring, L. Farkas, and Zel'dovich and Frenkel. A detailed presentation of the theory with references to original works may be found in the book by Frenkel [21] (see also [22]). We shall recount here only main the ideas of the theory.

In the vapor phase there occur from time to time fluctations during which the vapor molecules join together forming molecular complexes, nuclei of the liquid phase. In unsaturated vapor, when the gas phase is stable, the complexes are unstable and soon break up (evaporate). In supersaturated vapor only complexes of very small dimensions are unstable. The increase in size of the smallest complexes by the attachment of new molecules is energetically unfavorable, because of the increase in surface energy at the interface between the liquid and the gas phases. On the other hand, the increase in size of sufficiently large complexes is energetically favorable, since the favorable volume energy effect (release of latent heat) becomes greater than the unfavorable surface effect with sufficiently large dimensions. For each degree of supersaturation there is a definite critical complex dimension. Supercritical nuclei (with a radius larger than critical) are stable or "viable", and exhibit a tendency for further growth and transformation into liquid droplets. The rate of formation of these viable nuclei of condensation centers is proportional to the probability of appearance of critical size complexes. The formation of these complexes requires the expenditure of a certain energy $\Delta\Phi_{max}$ necessary to overcome the potential barrier, and hence, according to the Boltzmann relation, the probability of such fluctuations is proportional to $\exp(-\Delta\Phi_{max}/kT)$. The potential barrier $\Delta\Phi_{max}$ or activation energy depends on the critical radius of the complex and is uniquely related to the degree of supersaturation. This degree can be characterized, for example, by the supercooling

$$\theta = \frac{T_{sat} - T}{T_{sat}}.$$

Here T_{sat} is the temperature of saturated vapor at the given density and T is the actual vapor temperature.

The rate of formation of viable nuclei, that is, the number of condensation centers per single vapor molecule which appear per unit time under steady-state conditions, assuming that constant supersaturation (supercooling) is maintained in the system and the supercritical nuclei are removed

from the system as formed and replaced by an equivalent amount of vapor, is

$$I = Ce^{-b/\theta^2}, \tag{8.41}$$

where

$$C = n\bar{v}2\omega\left(\frac{\sigma}{kT}\right)^{1/2},$$

$$b = \frac{16\pi\sigma^3\omega^2}{3k^3q^2T}.$$

Here n is the number of vapor molecules per unit volume, $\bar{v}$ their thermal speed, σ the surface tension, ω the volume of liquid per molecule, and $q = U/R$ is the heat of vaporization expressed in degrees. The critical nucleus radius r^* is related to the degree of supersaturation by

$$\theta = \frac{2\sigma\omega}{kqr^*}.$$

The theory can also be generalized to the case of electrically charged nuclei containing an ion (see [19]). The rate of formation of nuclei is again given by (8.41), except that the constant b is now smaller.

Let us set up the rate equation for condensation. We make the basic assumption that the expansion of the vapor proceeds sufficiently slowly that the process of formation of nuclei can be considered as quasi-steady. In this case, the rate of formation always coincides with the steady-state rate (8.41) corresponding to the actual supercooling θ of the system at the given time. If $I(t')$ is the number of condensation centers formed per unit time at the time t' (per vapor molecule), and $g(t, t')$ is the number of molecules at the time t in a liquid drop born from a nucleus which appeared at the time t', then the degree of condensation at the time t, $x(t)$, can be written as

$$x(t) = \int_{t_1}^{t} I(t')g(t, t')\,dt'. \tag{8.42}$$

The integration with respect to time is carried out from the time of saturation, that is, from the time when the nuclei begin to appear.

The rate of increase of a drop of supercritical size is equal to the difference between the rate of attachment of vapor molecules to the drop surface and the rate of evaporation from the drop. It can be written approximately as (see [19, 21])

$$\frac{dg}{dt} = 4\pi r^2 n\bar{v}(1 - e^{-q\theta/T}), \tag{8.43}$$

where $4\pi r^2$ is the surface area of the drop and $n\bar{v}$ is the flux of vapor molecules. The factor in parentheses is proportional to the difference between the attachment and evaporation rates. In the state of saturation, when $\theta = 0$, attachment and evaporation cancel each other and the rate of growth is equal to zero*. In supersaturated vapor $\theta > 0$ and the size of a drop increases on the average, with $dg/dt > 0$; in unsaturated vapor $\theta < 0$ and, on the average, the drop is evaporated, with $dg/dt < 0$.

Equations (8.42), (8.43), and (8.41), together with the adiabatic equation for a two-phase system (8.39), the formula for a saturated vapor (8.38), and the relation for the expansion of the fluid, which in the case of sudden expansion into vacuum is given by (8.25), form a complete system of equations for calculating the condensation kinetics.

In accordance with the qualitative picture presented in the preceding sections, we can break up the solution of this system into two independent stages. The first stage is the analysis of a small time interval immediately after the saturated state has been reached, during which the supercooling first increases, passes through a maximum, and then decreases because of the onset of condensation. The nuclei appear during this short stage. Calculating the number of the nuclei

$$v = \int_{t_1}^{\infty} I(t')\, dt',$$

we get the total number of condensate particles (per initial molecule). Actually, the integration with respect to time extends here not to $t = \infty$, but is carried over a rather small time interval, since by virtue of (8.41), the rate I drops very sharply as soon as the supercooling, having passed through the maximum, begins to decrease. The second stage is the analysis of growth of the already known number of drops during all the ensuing states, up to $t \to \infty$.

A rigorous solution of the system of equations is, of course, very difficult. An approximate solution has been given in [19]. The approximate analysis of the first stage is based on the nature of the extremely sharp dependence $I(\theta)$, by virtue of which we can assume that practically all nuclei are formed in a very short time interval close to the time at which the supercooling is maximum (the solution actually gives an extremum for $\theta(t)$).

Referring for details of the solution to [19], we present here the results of calculations of a specific example. We consider a sphere of iron atoms with a mass of 33,000 tons, which is heated and converted into a dense gas, say, as the result of the impact of a very large iron meteorite on the surface of the moon. Let the impact velocity be such that the initial heating of the iron at standard density is $\varepsilon_0 = 72$ ev/atom. The initial temperature in this case is

* The effect of the curvature of the drop is neglected here.

$T_0 = 10$ ev $= 116{,}000°$K. In the stage of strong cooling at the time of vapor saturation the expansion is taking place practically by inertia, with an average velocity of $u = 15.5$ km/sec. The vapor becomes saturated at $t_1 = 6.8 \cdot 10^{-2}$ sec from the start of the expansion, with the corresponding radius of the cloud equal to 1050 m. In this case $T_1 = 2130°$K and $n_1 = 7.15 \cdot 10^{16}$ cm^{-3}.

For the sudden expansion of an initially highly ionized gas into vacuum, even in the stage of strong cooling some residual ionization is retained which is far above the value for thermodynamic equilibrium. The condensation centers in this case will contain ions. As shown by calculations, the number of condensation centers depends very weakly on whether or not they are charged, since the assumption that the condensation takes place on ions does not appear to be important.

The maximum possible supercooling in our example is found to be $\theta_{max} = 0.0765$ ($b/\theta_{max} = 43.1$). A nucleus of critical size for this supercooling contains 46 atoms. The number of condensation centers is $\nu = 4 \cdot 10^{-11}$ per atom, which is much smaller than the number of ions per atom, in contrast to the process in the Wilson cloud chamber, where all the ions become condensation centers.

Analysis of the second stage, during which the size of the drops increases, shows that during a long period of time the condensation follows the expansion of the fluid and a state close to equilibrium is maintained in the system. Only at the time $t_2 \sim 2.5$ sec, when the sphere has expanded to 40 km, does the density of the fluid become so small that further growth of drops ceases and freezing begins. Up to this time (and thus over the entire process) approximately one half of the iron vapor is condensed. Knowing the degree of condensation x_∞, and the number of condensate particles, we can also find their size (the number of atoms per particle is equal to $x_\infty \nu^{-1}$). In our example the iron particles suddenly expanding to infinity have a radius of $3.1 \cdot 10^{-5}$cm; their total number is $3 \cdot 10^{21}$. Approximately half of the fluid goes out to infinity in gaseous form.

We can establish theoretically approximate similarity relations for transforming to other initial conditions. It appears that for sufficiently slow expansions, when the initial assumptions are valid, the degree of condensation of the given fluid for a sudden expansion to infinity is independent of the initial conditions, and that the size of the condensate particles is proportional to the initial linear dimensions of the vaporizing body (to the cube root of the mass), and decreases rapidly with an increase in initial heating.

§13. On the problem of the mechanism of formation of cosmic dust. Remarks on laboratory investigations of condensation

There are some reasons to believe that the process of condensation of a vaporized substance suddenly expanding into vacuum, which was considered

in the preceding section, is one of the mechanisms of formation of cosmic dust in the solar system (this hypothesis was proposed in [19]). Interplanetary space contains small particles of various sizes, which are called cosmic dust. Sometimes these particles fall on the earth in the form of meteor showers. In their motion about the sun the particles experience some slowing down from the aberration component of the light pressure (Poynting–Robertson effect, *eds.*)*. The very small particles with sizes of the order of 10^{-6}–10^{-5} cm fall into the sun and disappear (for further details see [23]). Consequently, the solar system must have a source for replenishing the store of these very small particles of cosmic dust. It was noted (in particular by Stanyukovich), that this source may be the mechanical disintegration of matter in the collisions of small bodies of the solar system (asteroids), or in meteorite impacts on the surfaces of planets devoid of atmosphere. The particles produced have acquired considerable velocity, overcome the gravity field, and, not being slowed down by an atmosphere, fly out into space.

It is reasonable to assume that the phenomenon we have discussed of condensation of vaporized matter of planet soil, meteorites, or asteroids is also a source of these very small particles. In energetic collisions of asteroids, when the kinetic energy of impact is sufficient for complete vaporization of both colliding bodies, mechanical disintegration of the solid is, in general, not present, since the entire mass is completely vaporized. In this case the condensation mechanism is the only one capable of forming the small particles. The liquid droplets, which have grown in the process of condensation, gradually cool down and solidify due to the energy losses from thermal radiation. It can be shown that the process of radiation cooling proceeds much more quickly than the evaporation of the heated particles, which slows down very rapidly as the vapor is cooled. Thus, the condensate particles which were already created will continue to exist in the form of solid dust particles. Since bodies colliding in space have very different sizes and velocities, the condensate particles which are formed are also of various sizes.

The phenomenon of the condensation of a vaporized substance in a gasdynamic expansion can be also used for laboratory investigation of the condensation of vapors of metals and other solids (and liquids) and for the study of optical properties of very small particles. The dimensions of the condensate particles depend on the initial conditions; hence by properly choosing these conditions it is possible to obtain particles of the desired size

* The light pressure acts basically in the radial direction. The force due to this pressure is inversely proportional to the square of the distance between the particle and the sun, and its effect is equivalent to only a small decrease in the gravitational force; the radial component of the light pressure affects only the radius of the orbit. The slowing down, however, is due to the component of the light pressure which is tangent to the orbit and which arises from the aberration of light. For additional details see the book by Fesenkov [23].

in the laboratory. We present here the results of some rough estimates for conditions close to those encountered in the laboratory. If we rapidly vaporize 1 g of iron by transferring to it in some manner an initial energy of $\varepsilon_0 = 13$ ev/atom, corresponding to the initial temperature (at the density of the solid metal) of $T_0 = 35{,}000°\text{K}$, then the condensation of the vapor in a sudden expansion into vacuum (in an evacuated vessel) ends at the time $t = 5 \cdot 10^{-5}$ sec, when the cloud has expanded to 30 cm. The dimensions of the condensate particles in this case will be of the order of 10^{-4} cm.

The calculations of condensation kinetics can be easily carried over to other relationships governing the expansion of a fluid which takes place, say, in a wind tunnel or in a nozzle exhaust. These calculations do not involve anything basically new in comparison with the case of sudden expansion into vacuum, and we shall not consider them. We note that if the degree of condensation is not too high, or if the total energy of the vapor is much greater than the heat of vaporization, then the effect of the condensation on the gasdynamics of the process is very small. The kinetics of condensation can then be calculated on the basis of the known gasdynamic solution, found in first approximation without taking condensation into account. This is exactly the procedure which we followed in the preceding section.

IX. Radiative phenomena in shock waves and in strong explosions in air

1. Luminosity of strong shock fronts in gases

§1. Qualitative dependence of the brightness temperature on the true temperature behind the front

Optical measurements are of great importance for determining the temperature of highly heated bodies and for studying high-temperature processes in general. The usual methods are to measure by one or another means the luminosity or brightness of the surface of a luminescent body (by photographic means, with the aid of photoelectric elements, or with electron-optical multipliers [image converters, *eds.*]). The radiation brightness temperature, which is by definition the same as the temperature of a perfect black radiator emitting from its surface exactly the same luminous flux as the object under investigation, can then be found from the luminosity (see §8, Chapter II). Particularly widely used are photographic methods for determining the luminosity and brightness temperature, basically by comparing the degree of darkening on a photographic film produced by the light emitted by the body and that from a calibrated source with a known temperature and spectrum, say, from the sun. For greater accuracy the photographs are ordinarily taken in a narrow region of the spectrum, since the emitting object and the calibrated source have different temperatures and therefore emit different radiation spectra; in addition, the sensitivity of the photographic film depends on the wavelength of the light, which creates some difficulties in converting the degree of darkening into temperature.

Optical (in particular, photographic) methods are also widely used in the study of shock waves. A gas heated to a high temperature by a strong shock wave radiates and the surface of the shock front glows. The luminosity of the emission depends on the strength of the shock and the dimensions of the heated region behind the front. In order to obtain the true temperature of the fluid behind the front from the experimentally measured brightness temperature, we must be sure that the glowing mass radiates as a perfect black body.

If the shock front is a "classical" discontinuity behind which there is a sufficiently extensive, optically thick region with a more or less constant

temperature behind the front, then the heated fluid bounded by the front surface radiates from the surface as a perfect black body*. By measuring the luminosity of the front surface we can in this case directly determine the temperature behind the shock front, and hence the wave strength, which not only is important for experimental investigations but also is of great practical significance. It has been shown experimentally that in a certain range of shock strengths (and, of course, for a sufficiently thick heated region behind the front) the shock front actually does radiate as a black body. This is confirmed by the fact that the brightness temperature agrees with the temperature behind the front calculated on the basis of the shock relations and the equation of state, using one of the other experimentally determined front parameters such as the velocity of propagation of the shock wave. We know from experiments and theoretical considerations, however, that this agreement cannot be observed for all wave strengths. The brightness temperature of a sufficiently strong shock becomes lower than the true temperature behind the front and, past a certain strength, it decreases rapidly with increasing strength, reaching a limiting and comparatively low value. Thereafter, the brightness temperature remains almost constant regardless of the strength. A typical dependence of the brightness temperature of a shock front on the true temperature behind the front is shown in Fig. 9.1, which gives a curve of

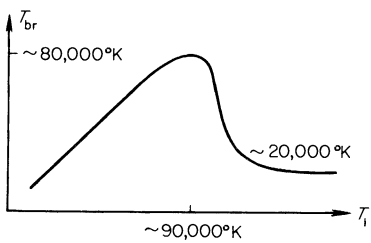

Fig. 9.1. Dependence of the brightness temperature of the surface of a shock front in air on the true temperature behind the front (for red light).

the brightness temperature of red light for a shock wave in standard density air, obtained on the basis of theoretical estimates (carried out in the following sections). Figure 9.1 shows the existence of the luminosity "saturation"

* If the region of heated gas behind the "classical" discontinuity is optically thin (for example, if the shock wave had moved only a small distance from the piston which was pushed into the gas and generated the wave), then the gas radiates as a volume radiator. The spectral flux coming out from the surface of an optically thin plane layer in a direction normal to the surface is equal to $S_\nu = S_{\nu p}[1 - \exp(-\kappa'_\nu d)]$, as was shown in §7, Chapter II, where $S_{\nu p}$ is the flux corresponding to a perfect black body at the same temperature, κ'_ν is the absorption coefficient, and d is the thickness of the layer heated by the shock wave. In the case of small optical thickness $\kappa'_\nu d \ll 1$, $S_\nu = S_{\nu p}\kappa'_\nu d \ll S_{\nu p}$. In the limit $\kappa'_\nu d \gg 1$ the flux approaches the Planck value $S_\nu = S_{\nu p}$. As noted in §21, Chapter V, by studying the increase in luminosity S_ν with time $t = d/D$ (D is the wave velocity), Model' [1] measured the absorption coefficient of red light in a shock wave.

effect. No matter how strongly the gas is heated by the shock wave, even to millions of degrees, it is still not possible "to see" temperatures higher than tens of thousands of degrees; there is an upper limit to the temperature behind a shock wave front which can be "seen". This effect can be easily explained on the basis of the structure of a shock front taking radiation into account, as in Part 3 of Chapter VII. The problem of the luminosity of strong shock fronts was considered in [2–4].

We assume that behind the front of a plane shock wave there exists a sufficiently extensive, optically thick region of constant high temperature, and we consider the flux of visible radiation coming out from the front surface and recorded by an instrument situated far from the front, at infinity. We first consider a shock wave which is not too strong, in which the role of radiation is negligible and the gas ahead of the front is not preheated. If we disregard the temperature change in the front related to the relaxation processes in the gas, then the temperature distribution across the shock wave is the classical jump, shown in Fig. 9.2a. The thickness of the jump together

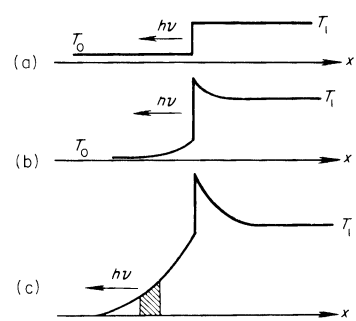

Fig. 9.2. On the problem of the luminosity of a shock wave.

with the relaxation layer is usually much smaller than the radiation mean free path. Therefore we have here a typical example of a perfect black radiator; an optically thick layer of fluid heated to a constant temperature T_1 is bounded by a surface with a very sharp temperature jump. If the cold gas ahead of the front, as is usually the case, is transparent in the visible part of the spectrum (colorless), then the instrument will record a luminous flux corresponding to Planck radiation at the temperature T_1; the radiation brightness temperature will be equal to the true gas temperature behind the front.

Let us now consider a strong shock wave with a temperature of, say, $T_1 = 65{,}000°\mathrm{K}$ behind the front. Photons radiated from the surface of the shock discontinuity are for the most part those with energies of the order of ten to thirty ev. (The maximum of the Planck spectrum at $T = 65{,}000°\mathrm{K}$ is at $h\nu = 2.8kT = 16$ ev.) These photons exceed the ionization potentials of the atoms and molecules, and are strongly absorbed in the cold gas ahead

of the shock discontinuity and preheat it. A heated layer is formed ahead of the shock discontinuity, and the temperature distribution across the shock takes on the form shown in Fig. 9.2b (in air, for example, at $T_1 = 65{,}000°K$ the maximum preheating temperature just ahead of the discontinuity is $T_- = 9000°K$).

Unlike a cold gas, the heated gas always absorbs the low energy visible photons ($h\nu \sim 2$–3 ev). In monatomic gases photons with energies less than the ionization potentials of the atoms I are absorbed by excited atoms, whose excitation energy exceeds $I - h\nu$; in accordance with the Boltzmann relation, the concentration of excited atoms is proportional to $\exp[-(I - h\nu)/kT]$, so that the absorption coefficient also increases sharply with temperature following the Boltzmann relation $\kappa_\nu \sim \exp[-(I - h\nu)/kT]$. In molecular gases, such as air, a number of other mechanisms for absorption of visible light exist, but in any case the absorption coefficient for visible light is always very sensitive to temperature and increases rapidly with heating.

Now the photons of visible light, which are radiated from the surface of the shock discontinuity and whose flux at the discontinuity corresponds, roughly, to the temperature T_1*, must penetrate the preheating layer before arriving at the recording instrument located at infinity. The photons are partially absorbed in this layer. Therefore the brightness temperature of visible radiation from the shock front will be less than the true temperature behind the front. The preheating layer "screens" the highly heated gas behind the shock front. The screening and, consequently, the deviation of T_{br} from T_1 is more pronounced, the greater is the optical thickness of the preheating layer to visible light τ_ν†, that is, the higher is the preheating temperature and the greater is the wave strength. As long as the optical thickness $\tau_\nu \ll 1$, the screening is negligible and the deviation of T_{br} from T_1 is very small; the front glows as a black body at the temperature T_1. By virtue of the fact that the absorption of visible light is strongly temperature dependent, and in turn because the preheating temperature rather strongly depends on the wave strength (see §16, Chapter VII), the onset of strong screening, corresponding to reaching an optical thickness τ_ν of the order of unity, very clearly appears as the wave strength increases. In air, strong screening begins at temperatures behind the front of approximately $T_1 = 90{,}000°K$ (see §3).

* Actually the photon flux is somewhat greater, since the temperature directly behind the discontinuity is higher than the temperature behind the front (see Fig. 9.2b).

† We emphasize that the optical thickness of the preheating layer for visible radiation τ_ν has nothing in common with the optical thickness of the layer averaged over the spectrum, which corresponds to the high energy photons which "lead" the preheating. As was shown in §16 of Chapter VII, the temperature in the preheating layer decreases approximately exponentially with respect to the averaged optical thickness $T - T_-\exp(-\sqrt{3}|\tau|)$ (for $T_- < T_1$), so that the averaged layer thickness is of the order of unity.

In an even stronger shock wave the optical thickness to visible light of the preheating layer is greater than unity and the layer is almost completely opaque to visible light radiated by the highly heated gas behind the wave front; the screening in this region is almost total. Thus, as the wave strength increases, the brightness temperature of the visible light first coincides with the temperature behind the front, then begins to lag behind it, passes through a clearly defined maximum (luminosity "saturation"), and then falls off rapidly. The pronounced screening by the preheating layer does not mean, however, that the luminosity of the front of a very strong shock falls off to zero and that the wave ceases to be luminous. The heated gas ahead of the shock discontinuity not only absorbs, but also radiates visible light. As long as the preheating temperature is not too high and the layer is transparent, this radiation is lost in the background of the passing visible radiation which is emitted by the much more strongly heated gas behind the front. However, when the preheating layer completely stops transmitting the high-temperature light, then its own radiation begins to predominate.

In order to get some idea about the brightness of this natural luminescence of the preheating layer, we note that its temperature increases monotonically, starting from zero, or more exactly, from the temperature of the cold gas ahead of the front. As a result of the sharp temperature dependence of the absorption of visible light, the light is neither absorbed nor radiated in the most forward layers of the preheating region where the temperature is low. In the deeper layers with higher temperature there is a strong emission of photons in the visible region, but they are again absorbed, since they are unable to get through the opaque gas in front. The photons going out from the front surface to infinity are born in some intermediate radiating layer of the preheating region, removed from infinity by an optical distance (corresponding to the frequencies of visible light) of the order of unity. In Fig. 9.2c the radiating layer is shown cross-hatched. Obviously, the radiation brightness temperature agrees with the average temperature of the radiating layer. The position of the layer is determined only by the gas temperature profile $T(x)$ and the temperature dependence of the absorption $\kappa_\nu(T)$ assuming that the layer is located away from the cold gas by an optical distance of the order of unity. As shown in §17 of Chapter VII, the temperature distribution at the leading edge of the preheating region in strong shocks is almost independent of the wave strength. Consequently, the natural luminescence of the preheating layer and the brightness temperature of a very strong shock are also independent of the strength. In air at standard density this limiting brightness temperature for red light is approximately equal to 20,000°K (see §4).

The effect of the screening and the sharp decrease in brightness temperature of the shock front in comparison with the true temperature behind the front

were observed experimentally by Model' [1]. He employed photographic means for measuring the brightness temperature of shock fronts in heavy inert gases, xenon, krypton, and argon, in which high temperatures can be produced by shock waves. The front velocity in these experiments was 17 km/sec. The optical thickness of the heated region behind the shock front was known to be large, so that in the absence of screening the front should have radiated as a black body. However, the brightness temperatures observed in the experiments were 30,000–35,000°K, which is several times lower than the temperatures behind the front T_1, calculated on the basis of the front velocity and shock relations (in Xe, $T_1 \approx 110{,}000$°K, in Kr, $T_1 \approx 90{,}000$°K, and in Ar, $T_1 \approx 60{,}000$°K). If we consider the fact that the accuracy with which the brightness temperature of the visible (red) light was determined in this experiment was not worse than $\pm 20\%$, then this disagreement must be attributed to screening by the preheating layer. Unfortunately, only one point with respect to the wave strength was recorded in the experiments of Model', which precludes the possibility of analyzing the character of the entire curve of dependence of the brightness temperature on the true temperature behind the front.

It should be noted that the luminosity "saturation" phenomenon at high temperatures has been observed by many authors in spark discharges*. It is known that starting with a certain rate any further increase in the rate at which energy is delivered into a spark discharge tube does not result in an increase in the brightness temperature above $\sim 45{,}000$°K in air. The brightness temperature is also similarly limited in discharges in argon and xenon (a higher temperature of approximately 90,000°K in air is observed in discharges in capillaries). The saturation effect may be related to the screening of high temperatures in the tube, which is somewhat similar to the screening in a shock wave, although it is possible that the true temperature in the tube is limited by radiation losses, etc.

§2. Photon absorption in cold air

Of great practical interest is the problem, which we shall consider in more detail, of the luminosity of strong shocks in air at standard density. We must determine the upper limit of the shock strength for which the shock front radiates visible light as a perfect black body, and estimate the maximum and limiting brightness temperatures. The problem, obviously, reduces to estimating the optical thickness of the preheating layer to visible radiation, which determines the degree of screening by the highly heated region behind the front, and also to finding the natural luminosity of the preheating layer.

* A bibliography may be found in the review by Vanyukov and Mak [5] on pulsed sources of light of high luminosity as well as in Model's article [1].

In order to do this we must first determine more precisely the geometric thickness of the preheating layer and its temperature distribution with respect to the geometric coordinate. This, in turn, depends on the absorption mechanism in air of the relatively high energy photons with energies of the order of 10–100 ev, which are responsible for preheating the gas ahead of the shock discontinuity. We shall summarize the published data on the absorption of such photons in cold air.

We have already mentioned several times the generally known fact that cold air is completely transparent to visible light. Noticeable absorption begins in the ultraviolet region of the spectrum at a wavelength $\lambda = 1860$ Å ($h\nu = 6.7$ ev)*. The absorption takes place in the Schumann–Runge band system of an oxygen molecule, which at $\lambda = 1760$ Å ($h\nu = 7.05$ ev) becomes a continuum associated with the dissociation of the molecule with the absorption of light. The absorption rapidly increases with increasing photon energy (for $\lambda = 1860$ Å, $\kappa_\nu = 0.0044$ cm^{-1}, and for $h\nu \approx 8$ ev, $\kappa_\nu \approx 100$ cm^{-1}). The experimental curve showing the dependence of the absorption coefficient on wavelength in this region of the spectrum is shown in Fig. 9.3†. Photons with

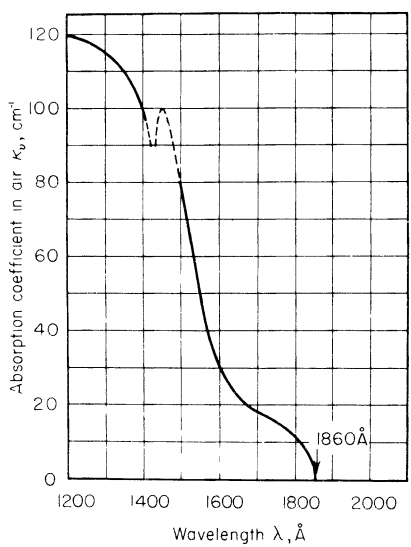

Fig. 9.3. Absorption coefficient for ultraviolet radiation in cold air.

* Strong absorption of the radiation from the sun in the near-ultraviolet region ($\lambda \sim 2000$ –3000 Å) is connected with the existence of an ozone layer at an altitude of about 25 km. Oxygen and nitrogen do not absorb in this part of the spectrum; therefore, when speaking about shock waves in air close to the surface of the earth we should take $\lambda \sim 1860$ Å as an upper limit for the transparency of air.

† The curve was taken from the article of Schneider [6].

energies exceeding the ionization potentials of oxygen and nitrogen molecules ($I_{O_2} = 12.1$ ev and $I_{N_2} = 15.6$ ev) experience strong photoelectric absorption. The absorption cross sections from the ground level of the molecules depend only weakly on frequency in the energy range from $h\nu = I$ to $h\nu \sim 25$ ev and are approximately equal to $\sigma_{O_2} = 3 \cdot 10^{-18}$ cm^2 and $\sigma_{N_2} = 5 \cdot 10^{-18}$ cm^2, which gives an absorption coefficient $\kappa_\nu \approx 120$ cm^{-1}. As the frequency increases further, the absorption coefficient should show jumps due to the successive participation in the absorption process of the various electrons filling the L shells in the nitrogen and oxygen atoms. The energy levels in the L shells are, evidently, not spaced very far apart so that the jumps probably lie in the energy region $h\nu$ from 13 to 30–40 ev (as far as we know, there is no experimental evidence on these jumps). Thereafter, the absorption coefficient falls off monotonically with increasing frequency up to an energy $h\nu_K = 410$ ev, equal to the binding energy of a K electron in a nitrogen atom; the K absorption boundary in oxygen is $h\nu'_K = 530$ ev. At an energy $h\nu_K = 410$ ev the absorption coefficient increases sharply, since photons greater than $h\nu_K$ are capable of knocking out K electrons from nitrogen atoms, and then decreases monotonically up to $h\nu'_K = 530$ ev, when the K electrons of oxygen are included in the absorption process. The absorption coefficients for photons $h\nu_K = 410$ ev before and after the K absorption jump in nitrogen, calculated from the data of [7, 8], are 1.6 cm^{-1} and 35 cm^{-1}, respectively. The experimental data with respect to light absorption in air in the intermediate frequency range from tens to hundreds of ev are rather meager; as far as the authors know, measurements have been carried out only for two lines, at $h\nu = 182$ ev [9] and at $h\nu = 280$ ev [10].

On the basis of the available fragmentary data we have compiled a table which gives a picture of the absorption coefficients and mean free paths for

Table 9.1

ABSORPTION COEFFICIENTS AND MEAN FREE PATHS IN COLD AIR AT STANDARD DENSITY FOR DIFFERENT PHOTON ENERGIES

$h\nu$, ev	κ_ν, cm^{-1}	l_ν, cm
8	100	0.01
13–25	~ 120	0.0083
182	12	0.083
280	5.3	0.19
410 (before the jump)	1.6	0.63
410 (after the jump)	35	0.029

photons with energies in the range of ten to several hundred ev in cold air at standard density.

§3. Maximum brightness temperature for air

It was shown in §16 of Chapter VII that if the shock strength is less than critical (in standard density air the temperature behind the front corresponding to the critical strength is $T_1 \approx 285{,}000°\mathrm{K}$), the radiative transfer from the highly heated region behind the front to the layers ahead of the shock discontinuity does not have a diffusive character. The air in these layers is heated to temperatures much lower than those behind the front and the emission of radiation in the preheating region makes practically no contribution to the radiation flux created behind the discontinuity. The air is heated simply by the absorption of photons passing at distances of the order of the absorption mean free path and the thickness of the preheating region Δx is of the order of the mean free path l of those photons that carry the principal energy of the spectrum. This is expressed mathematically by (7.55), which shows the exponential decrease in preheating with respect to the averaged optical thickness τ corresponding to some frequency averaged absorption coefficient $\kappa = 1/l$:

$$\varepsilon = \varepsilon_- e^{-\sqrt{3}|\tau|}, \qquad \tau = \int_0^x \kappa \, dx. * \tag{9.1}$$

This equation shows that the effective optical thickness of the preheating layer is of the order of unity, that is, that the geometrical thickness is of the order of $\Delta x \sim 1/\kappa = l$.

It follows from Table 9.1 in the preceding section that the mean free paths for photons with energies of the order of 10–100 ev in cold air vary between 10^{-2} and 10^{-1} cm. It is evident that the mean free paths of these photons are approximately the same in the not too high temperature air of the preheating region.

Let us, for example, consider a shock wave with a temperature behind the front $T_1 = 65{,}000°\mathrm{K}$. The maximum of the Planck spectrum occurs for photons of energy $h\nu = 16$ ev, so that a considerable part of the energy of the spectrum is concentrated in the energy region of photons exceeding the ionization potentials of the atoms and molecules $h\nu > I \approx 13$ ev. The highest preheating temperature, as is shown in Table 7.4, is $T_- = 9000°\mathrm{K}$. At this temperature the degree of ionization and excitation of the atoms is small, and photons of energy $h\nu \geqslant I$ are absorbed in practically the same manner as in cold air. If we take a stronger shock wave, say with a temperature

* Equation (7.55) is not written for the specific internal energy, but for the temperature. Equation (9.1) is more general; it is valid also in those cases when the specific heats are temperature dependent, which is the case with air.

behind the front $T_1 = 100{,}000°K$, then photons of energy $h\nu = 24$ ev will correspond to the maximum of the spectrum and the principal energy of the spectrum will be concentrated in a region of higher photon energies of the order of several tens of electron volts. For a preheating temperature $T_- = 25{,}000°K$, single ionization of the atoms is appreciable, although there is practically no double ionization. Photons with energies of several tens of electron volts knock out from the atoms primarily not the external, optical, but the deeper lying electrons, which at a temperature $\sim 25{,}000°K$ do not yet undergo thermal ionization and excitation. Thus, in this case also the photons responsible for the preheating are absorbed in approximately the same manner as in cold air.

We can now conclude that the thickness of the preheating region ahead of the shock discontinuity in subcritical strength waves ($T_1 < 285{,}000°K$) is of the order of the mean free path of photons with energies of 10–100 electron volts in cold air, with $\Delta x \sim 10^{-2}$–10^{-1} cm. In this case, Δx increases within the stated limits for even stronger waves, with temperatures behind the front varying from several tens of thousands of degrees to $T_1 \sim 200{,}000°K$, and with a corresponding shift in the characteristic photon energies from $h\nu \sim 10$–30 to $h\nu \sim 30$–100 ev.

Let us now consider the extent to which the preheating region screens out the visible light. Table 9.2 gives absorption coefficients and absorption mean free paths for red light $\lambda = 6500$ Å in standard density air at different temperatures. Appreciable screening begins when the mean free path l_ν, which

Table 9.2

ABSORPTION COEFFICIENTS AND MEAN FREE PATHS FOR RED LIGHT $\lambda = 6500$Å IN STANDARD DENSITY AIR AT DIFFERENT TEMPERATURES

$T \cdot 10^{-3}$, °K	κ_ν, cm^{-1}	l_ν, cm
15	4.1	$2.5 \cdot 10^{-1}$
17	13.5	$7.4 \cdot 10^{-2}$
20	60	$1.66 \cdot 10^{-2}$
30	290	$3.45 \cdot 10^{-3}$
50	350	$2.85 \cdot 10^{-3}$
100	2000	$5 \cdot 10^{-4}$

decreases rapidly with increasing temperature, becomes comparable with the thickness of the preheating layer, that is, with the preheating radiation mean free path l (averaged over the spectrum). For convenience, we introduce the concept of a "transparency temperature" T^*, defined by the condition

$$l_\nu(T^*) = l. \tag{9.2}$$

The meaning of this concept is self-evident: the transparency temperature serves as the boundary between two temperature regions in the shock. When $T < T^*$, $l_\nu > \Delta x$ and the air in the preheating region is transparent to visible light. When $T > T^*$, $l_\nu < \Delta x$ and the air is opaque.

Since the absorption of visible light is very strongly temperature dependent, and the mean free path changes comparatively little (no more than by an order of magnitude), the transparency temperature defined by the equality (9.2) lies within quite narrow limits, namely: $T^* \approx 17{,}000$–$20{,}000°\mathrm{K}$. We can estimate the optical thickness of the preheating region for visible light by assuming that the temperature dependence of the absorption coefficient for visible light can be described by the Boltzmann relation $\kappa_\nu = const \cdot \exp[-(I - h\nu)/kT]$, and that the mean absorption coefficient κ is constant. We recall that the internal energy of air at standard density and at temperatures of the order of tens of thousands of degrees is, roughly speaking, proportional to $\varepsilon \sim T^{1.4}$. We can then, using (9.1), find the approximate optical thickness in the preheating region from infinity (that is, from the cold air region) to a point at a temperature T. This quantity, $\tau_\nu(T)$ (the total optical thickness of the preheating region is $\tau_\nu(T_-)$), is given by

$$\tau_\nu(T) = \int_{-\infty}^{x} \kappa_\nu \, dx = \int_0^T \kappa_\nu \frac{dx}{dT} \, dT = \int_0^T \frac{const}{\kappa} \frac{1.4}{\sqrt{3}} e^{-(I-h\nu)/kT} \frac{dT}{T}$$

$$\approx \frac{1}{\kappa} \frac{1.4}{\sqrt{3}} \frac{kT}{I - h\nu} \cdot const \cdot e^{-(I-h\nu)/kT} = \frac{1.4}{\sqrt{3}} \frac{kT}{I - h\nu} \frac{\kappa_\nu(T)}{\kappa}. \qquad (9.3)$$

In a shock wave with $T_1 = 90{,}000°\mathrm{K}$, where the temperature ahead of the discontinuity is equal to the transparency temperature $T_- = T^* = 20{,}000°\mathrm{K}$, the optical thickness of the preheating region, in accordance with the definition of the transparency temperature (9.2), is $\tau_\nu = 0.81kT^*/(I - h\nu) \approx 0.12$ ($I \approx 14$ ev, $h\nu \approx 2$ ev). Consequently, if we look at the surface of a shock front in a direction normal to the surface, then the flux of visible radiation coming out from the surface of the shock discontinuity will be attentuated by the preheating layer by approximately 12%, and the brightness temperature will be approximately 80,000°K instead of 90,000°K (at these temperatures low energy visible photons lie in the Rayleigh–Jeans region of the spectrum and their intensity is proportional to the first power of the temperature; hence the brightness temperature is simply proportional to the luminosity).

As the wave strength increases further, the optical thickness of the layer increases and the luminosity decreases; for example, when the temperature behind the front is increased by only 10,000°K, that is, when $T_1 = 100{,}000°\mathrm{K}$ $T_- = 25{,}000°\mathrm{K}$, $\tau_\nu(T_-) \approx 0.37$, $T_{\mathrm{br}} \approx T_1 e^{-0.37} \approx 67{,}000°\mathrm{K}$, so that the brightness temperature is already less than 80,000°K. The maximum lumin-

osity corresponds to a temperature behind the front of approximately $T_1 = 90{,}000°\text{K}$, and the corresponding maximum brightness temperature is approximately $T_{\text{br max}} = 80{,}000°\text{K}$*. For a temperature behind the front $T_1 = 140{,}000°\text{K}$, $T_- \approx 50{,}000°\text{K}$, $\tau_\nu(T_-) \approx 1.5$ and the screening is almost total.

§4. Limiting luminosity of very strong waves in air

Let us estimate the natural luminescence of the preheating layer in a strong shock wave, which determines the limiting luminosity of the shock front. We consider a shock wave of supercritical strength with a temperature behind the front much higher than the critical temperature of 285,000 °K. It was shown in §17 of Chapter VII that in a wave front the temperature distribution with respect to the average optical thickness τ has the shape shown in Fig. 9.4. The preheating temperature just ahead of the shock discontinuity coincides with the temperature behind the front T_1. The temperature in the preheating layer falls off monotonically until it reaches the

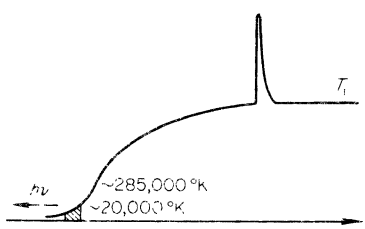

Fig. 9.4. Position of the radiating layer (shaded) in a very strong shock wave.

temperature of the cold air in front. The average optical thickness of the entire preheating region can be very large, and it increases with wave strength. The principal part of the preheating region consists of a region with the temperature ranging from $T_- = T_1$ to a temperature of the order of the critical temperature $T_c \approx 300{,}000°\text{K}$. This part of the region, of course, also expands with increasing wave strength (see Fig. 9.4).

At the leading edge of the region, where the temperatures are below 300,000°K, the temperature distribution (as is the case in the subcritical wave) has an exponential character and is almost independent of the strength

$$\varepsilon = \varepsilon_c e^{-\sqrt{3}|\tau-\tau_c|}, \qquad T = T_c e^{-\frac{\sqrt{3}}{1.4}|\tau-\tau_c|}. \tag{9.4}$$

* We emphasize that all these values are only estimates, since the absorption coefficients for visible light in high-temperature air calculated by Kramers' formula cannot be taken as completely reliable.

(See §17, Chapter VII, equation (7.64), and also Fig. 9.4; the optical coordinate τ_c pertains to the point where the temperature is approximately $T \approx T_c \approx 300{,}000°\text{K}$.)

It has already been noted at the end of §1 how a body with such a temperature distribution radiates visible light. The air is transparent at low temperatures and does not radiate; at high temperatures the gas is completely opaque and does "not let out" the visible photons. The radiating layer, which basically sends out a flux of visible light to infinity in the cold air, lies somewhere between the transparent and opaque regions (shown shaded in Fig. 9.4). The temperature in the radiating layer is obviously close to the transparency temperature for air defined by the equality (9.2), where l is the frequency averaged mean free path in the region containing the radiating layer. The brightness temperature of the visible radiation also approximately agrees with the transparency temperature. If the mean free path again lies in the range of 10^{-2}–10^{-1} cm, then the limiting brightness temperature should be equal to 17,000–20,000°K (see Table 9.2).

Let us satisfy ourselves that this estimate is valid, that the preheating at the leading edge of the preheating layer in a very strong shock wave is caused by photons which have precisely this mean free path. In this regard, we note that at temperatures above the critical, local equilibrium (radiative) exists in the preheating region, while for temperatures below the critical temperature the radiation is out of equilibrium, as is the case in the preheating layer of a subcritical shock wave.

We can assume approximately that from a surface where the temperature $T_c \approx 300{,}000°\text{K}$ a Planck radiation spectrum is emitted to the left (see Fig. 9.4) at this temperature, regardless of how high the value of the temperature is behind this surface. The general behavior of the absorption of high energy photons corresponding to a spectrum with a temperature of 300,000°K (the maximum of the spectrum occurs for photons with $h\nu \approx 70$ ev) is such that the absorption coefficient κ_ν decreases with increasing frequency. As may be seen from Table 9.1, in the region of photon energies of a hundred electron volts, κ_ν decreases monotonically with increasing frequency. Hence, when we move in the direction of decreasing temperatures away from the surface at which $T = 300{,}000°\text{K}$, the low energy photons are absorbed first and then the more energetic photons. As we move into the region of low temperatures the spectrum becomes increasingly heavily weighted in the high energies. Calculations presented in [4] show that only very highly energetic photons, with energies $h\nu \approx 200$ ev, can penetrate the region where the temperature is of the order of the transparency temperature, where, as we expect, the radiating layer is located. Table 9.3 gives the energy of the photons carrying out the preheating in the low-temperature region at the leading edge of the preheating region. The table also gives the corresponding mean free paths for these photons, which are approximately equal to the frequency-averaged mean free

paths. We see that in the region of temperatures $T \sim 20{,}000°K$ the mean free path $l \sim 10^{-1}$ cm, so that (cf. Table 9.2) the transparency temperature is probably closer to 17,000°K.

Table 9.3

ENERGIES AND CORRESPONDING MEAN FREE PATHS OF PHOTONS WHICH PREHEAT LEADING EDGE OF PREHEATING REGION

T, °K	$h\nu$, ev	l, cm	κ, cm^{-1}
50,000	140		
20,000	200	$0.95 \cdot 10^{-1}$	10.5
15,000	212	$1.02 \cdot 10^{-1}$	9.8
10,000	225	$1.16 \cdot 10^{-1}$	8.6

Thus, the limiting brightness temperature of a very strong shock wave is approximately 17,000°K, regardless of the strength. The general dependence of the brightness temperature (in red light) on the temperature behind the front is shown in Fig. 9.1. We note that the absorption coefficients in the visible region of the spectrum depend only weakly on frequency, and hence the values of brightness temperatures estimated above are approximately applicable not only to the red but in general to the entire visible region of the spectrum.

2. *Optical phenomena observed in strong explosions and the cooling of the air by radiation*

§5. General description of luminous phenomena

An atomic explosion in air produces a very strong shock wave and very high temperatures. The temperature behind the wave front takes on a continuous series of values over a wide range, from hundreds of thousands of degrees down to atmospheric. A number of interesting and rather peculiar optical phenomena are observed in such an explosion. Below we present a general description of the development of an explosion in air near the surface of the earth (that is, in air of standard density). This description is taken entirely from the book "The Effects of Atomic Weapons" [11], published in 1950*.

* We are excerpting paragraphs 2.1, 2.6–2.16, 2.22, 6.2, 6.19, 6.20, 6.22, and 6.23 of the second and sixth chapters of the book and we also present Figs. 2.10, 6.6, 6.18, and 6.20. A second edition of this book [12] appeared in 1957. The second edition has been extensively rewritten. It contains expanded chapters pertaining to the harmful effects of the explosion,

"The fission of the uranium or plutonium in an atomic bomb leads to the liberation of a large amount of energy in a very small period of time within a limited space. In the treatment which follows it will be assumed that the energy released in the atomic bomb is roughly equivalent to that produced by the explosion of 20,000 tons of TNT, namely, about 10^{21} erg (more precisely $8.4 \cdot 10^{20}$ erg). Such a bomb will be referred to as a *nominal atomic bomb*. The resulting extremely high energy density causes the fission products to be raised to a temperature of more than a million degrees. Since this material, at the instant of explosion, is restricted to the region occupied by the original constituents of the bomb, the pressure will also be very considerable, of the order of hundreds of thousands of atmospheres*.

"Because of the extremely high temperature, there is an emission of energy by electromagnetic radiations, covering a wide range of wavelengths, from infrared (thermal) through the visible to the ultraviolet and beyond. Much of this radiation is absorbed by the air immediately surrounding the bomb, with the result that the air itself becomes heated to incandescence. In this condition the detonated bomb begins to appear, after a few millionths of a second, as a luminous sphere called the *fireball* (*ball of fire* in [11], *eds.*). As the energy is radiated into a greater region, raising the temperature of the air through which it passes, the fireball increases in size, but the temperature pressure, and luminosity decrease correspondingly. After about 0.1 msec has elapsed, the radius of the fireball is some 14 m, and the temperature is then in the vicinity of 300,000°K. At this instant, the luminosity (illumination, *eds.*). as observed at a distance of 10,000 m, is approximately 100 times that of the sun as seen at the earth's surface.

"Under the conditions just described, the temperature throughout the fireball is almost uniform; since energy, as radiation, can travel rapidly between any two points within the sphere, there are no appreciable temperature gradients. Because of the uniform temperature the system is referred to as an *isothermal sphere* which, at this stage, is identical with the fireball.

"As the fireball grows, a shock wave develops in the air, and at first the shock front coincides with the surface of the isothermal sphere and of the fireball. Below a temperature of about 300,000°K however, the shock wave advances more rapidly than does the isothermal sphere. In other words, transport of energy by the shock wave is faster than by radiation. Nevertheless, the luminous fireball still grows in size because the great compression

---

but chapters devoted to the description of physical phenomena in the fireball have been abridged. Since we are here interested in precisely the latter problems, we are taking the description of the physics of the explosion from the first edition. All lengths measured in feet, yards, and miles have been converted into meters. *Editors' note.* The paragraphs excerpted are not necessarily complete; phrases in parentheses have been added by the authors.

* *Editors' note.* This paragraph has been combined from paragraphs 2.1 and 2.6 of [11].

of the air due to the passing of the shock wave results in an increase of temperature sufficient to render it incandescent. The isothermal sphere is now a high-temperature region lying inside the larger fireball; and the shock front is coincident with the surface of the latter, which consequently becomes sharply defined. The surface of separation between the very hot inner core and the somewhat cooler shock-heated air is called the *radiation front*.

"The phenomena described above are represented schematically in Fig. 9.5; qualitative temperature gradients are shown at the left, and pressure gradients at the right, of a series of photographs of the fireball taken at various intervals after detonation of an atomic bomb. It can be seen that at first the temperature is uniform throughout the fireball, which is then an isothermal sphere. Later, two distinct temperature levels are apparent, where the fireball has moved ahead of the isothermal sphere in the interior. It may be noted that the luminosity of the outer region of the fireball (brightness of the encompassing shock front) prevents the isothermal sphere from being visible on the photograph. At this time, the rise of the pressure to a peak, followed by a sharp drop at the surface of the fireball, indicates that the latter is identical with the shock wave front.

"The fireball continues to grow rapidly in size for about 15 msec, by which time its radius has increased to approximately 90 m; the surface temperature has then dropped to around 5000°K, although the interior is very much hotter. The temperature and pressure of the shock wave have also decreased to such an extent that the air through which it travels is no longer rendered luminous. The faintly seen shock wave front moves ahead of the fireball, and the onset of this condition is referred to as the *breakaway* (of the shock wave from the luminous sphere). The rate of propagation of the shock wave is then in the vicinity of 4500 m/sec.

"Although the rate of advance of the shock front decreases with time, it continues to move forward more rapidly than the fireball. After the lapse of one second, the fireball has essentially attained its maximum radius of 140 m, and the shock front is then some 180 m further ahead. After 10 sec the fireball has risen about 450 m, the shock wave has traveled about 3700 m and has passed the region of maximum damage.

"An important feature of an atomic explosion in air occurs at about the time of the breakaway of the shock front (from the luminous sphere). The surface temperature (of the luminous region) falls to about 2000°K and then commences to rise again to a second maximum around 7000°K. The minimum is reached approximately 15 msec after the explosion, while the maximum is attained about 0.3 sec later. Subsequently, the temperature of the fireball drops steadily due to expansion and loss of energy.

"It is of interest to note that most of the energy radiated in an atomic explosion appears after the point of minimum luminosity of the fireball.

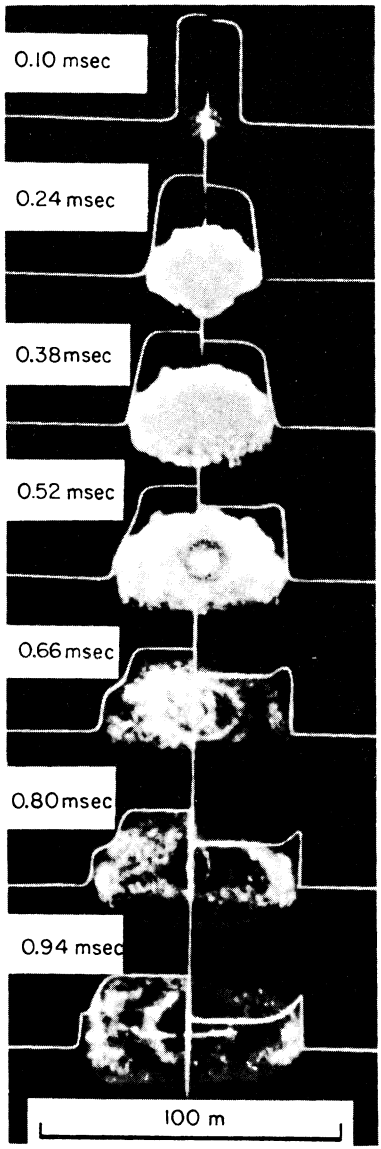

Fig. 9.5. Qualitative representation of the temperature and pressure variations in a fireball. The explosion energy is about 10^{21} erg $\approx$ 16 kg of uranium $\approx$ 20,000 tons of TNT.

Only about 1% of the total is lost before this time, in spite of the much higher surface temperature. The explanation of this result lies, of course, in the fact that the duration of the latter period, i.e., about 15 msec, is very short compared with the several seconds during which radiation takes place after the minimum has been passed.

"As stated above, the fireball expands very rapidly to its maximum radius of 140 m, within less than a second from the explosion. Consequently, if the bomb is detonated at a height of less than 140 m, the fireball can actually touch the earth's surface, as it did in the historic "Trinity" test at Alamogordo, New Mexico. Because of its low density, the fireball rises, like a gas balloon, starting at rest and accelerating within a few seconds to its maximum rate of ascent of 90 m/sec.

"After about 10 sec from detonation, when the luminosity of the fireball has almost died out and the excess pressure of the shock wave has decreased to virtually harmless proportions, the immediate effects of the bomb may be regarded as over.

"Because of its high temperature, and consequent low density, the fireball rises, as stated above, and as it rises it is cooled. At temperatures down to about 1800°K the cooling is mainly due to loss of energy by thermal radiation; subsequently, the temperature is lowered as a result of adiabatic expansion of the gases and by mixing with the surrounding air through turbulent convection. When the fireball is no longer luminous, it may be regarded as a large bubble of hot gases rising in the atmosphere, its temperature falling as it ascends.

"An important difference between an atomic and a conventional explosion is that the energy liberated per unit mass is much greater in the former case. As a consequence, the temperature attained is much higher, with the result that a larger proportion of the energy is emitted as thermal radiation at the time of the explosion. An atomic bomb, for example, releases roughly one-third of its total energy in the form of this radiation. For the nominal atomic bomb discussed, the energy emitted in this manner would be about $6.7 \cdot 10^{12}$ cal, which is equivalent to about $2.8 \cdot 10^{20}$ erg.

"The rate at which energy passes through the whole of the spherical surface of the fireball, that is, over a solid angle of 4π, is $\sigma T^4 \cdot 4\pi R^2$, where R is the radius of the ball (and T is the surface temperature; the dependence of R and T on time is shown in Fig. 9.6). Since only the fraction f_0 of this* penetrates the air, the rate at which the radiant energy reaches all points on a spherical area at a moderate distance from the point of detonation is $f_0 \sigma T^4 \cdot 4\pi R^2$.

* It is assumed that the air transmits only those wavelengths exceeding $\lambda_0 = 1680$ Å, so that f_0 is that part of the energy of the Planck spectrum of temperature T, which is included in the interval from $\lambda_0 = 1860$ Å to $\lambda = \infty$. The function f_0 is shown in Fig. 9.7.

The radiant energy flux φ per unit area at a distance D is then obtained upon dividing by the total spherical area $4\pi D^2$, so that

$$\varphi = f_0 \sigma T^4 \left(\frac{R}{D}\right)^2.$$

"From this equation the (radiant energy) flux at a given point, distant D, can be computed for various times after an atomic explosion, using the values of R and T from Fig. 9.6 and of f_0 from Fig. 9.7. In order to avoid plotting values for individual distances, the quantity φD^2, which is equal to $f_0 \sigma T^4 R^2$, is given in Fig. 9.8 as a function of the time; the energy flux is in

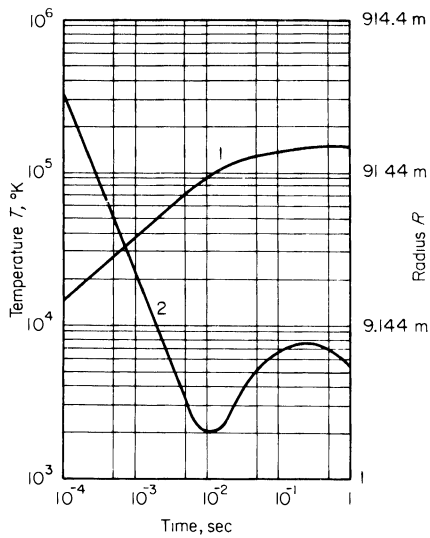

Fig. 9.6. Radius (curve 1) and temperature (curve 2) of fireball as a function of time after explosion.

cal/cm^2 · sec, and the distance is in m. From the curve, the energy flux at any given moderate distance at a specific time can be readily determined.

"In order to obtain some indication of the magnitude of the illumination, it is convenient to introduce a unit called a *sun*; this is defined as a flux of 0.032 cal/cm^2 · sec, and is supposed to be equivalent to the energy received from the sun at the top of the atmosphere. The ordinates at the right of Fig. 9.8 give the value of φD^2, with φ in suns and D in m.

"At the luminosity minimum, the value of φD^2 is about $6.8 \cdot 10^6$ sun-m^2, so that at this point the fireball, as seen at a distance of about 2600 m, should appear about as bright as the sun. Actually, it will be somewhat

less bright, to an extent depending on the clearness of the air, because of atmospheric attenuation."

At this point we end the description taken from [11].

As long as the shock wave front has not broken away from the boundary of the luminous body and the latter simply coincides with the shock wave front, the propagation of the fireball is well described by the relation $R \sim t^{2/5}$, which follows from the solution of the strong explosion problem considered

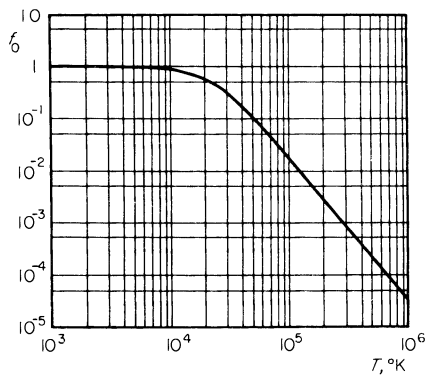

Fig. 9.7. Fraction of equilibrium radiation included in the wavelength interval from $\lambda = 1860$ Å to $\lambda = \infty$ as a function of temperature.

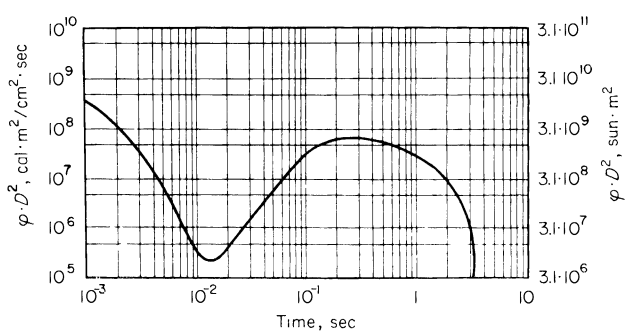

Fig. 9.8. Energy flux emitted by fireball as a function of time after explosion.

in §25 of Chapter I. At the instant of breakaway the temperature at the shock front is approximately equal to 2000°K, which corresponds to a pressure $p_f \approx 50$ atm. This pressure is much higher than atmospheric, and thus the assumptions on which the solution is based ($p_f \gg p_0$) are satisfied.

A comparison of the theoretical relation $R \sim t^{2/5}$ with experiment was presented in the book of Sedov [13]. In the book is given a graph of the

straight line $\frac{5}{2}\log R$ as a function of $\log t$, on which were plotted the experimental points pertaining to the 1945 New Mexico atom bomb explosion*. The experimental points fit the theoretical curve very well. According to (1.110), the slope of the straight line is related to the explosion energy E by

$$R = \left[\alpha(\gamma)\frac{E}{\rho_0}\right]^{1/5} t^{2/5}; \qquad \frac{5}{2}\log R = \frac{1}{2}\log\left(\alpha\frac{E}{\rho_0}\right) + \log t.$$

Here $\alpha = \xi_0^5$, where ξ_0 is the coefficient in (1.110). For an air density $\rho_0 = 1.25 \cdot 10^{-3}$ g/cm^3 the value obtained for αE is $8.45 \cdot 10^{20}$ erg. The dependence of the coefficient α on the specific heat ratio γ is given in Sedov's book [13]. If we assume $\gamma = 1.4$, as was done by Sedov, we get $\alpha = 1.175$ and $E = 7.19 \cdot 10^{20}$ erg. Actually, the effective specific heat ratio is slightly lower, since at high temperatures the air is strongly dissociated and ionized. Therefore the coefficient α is smaller and the explosion energy is greater. Thus, for example, if we take $\gamma = 1.32$, we find $\alpha = 0.88$ and $E = 9.6 \cdot 10^{20}$ erg.

§6. Breakaway of the shock front from the boundary of the fireball

Let us examine the nature of the luminescence of a fireball for temperatures behind the shock front of the order of several thousand degrees and clarify the causes for the phenomenon of breakaway of the shock front from the boundary of the luminous mass and for the minimum in the luminosity of the fireball. These problems were treated by one of the present authors [14, 15].

Many mechanisms participate in the absorption (and emission) of visible light in high-temperature air. These include photoionization of strongly excited atoms and molecules of oxygen and nitrogen and of nitric oxide molecules, knocking out the additional weakly bound electron from negative oxygen ions, molecular absorption (without the removal of electrons) by excited O_2, N_2, and NO molecules, and, finally, molecular absorption by NO_2 molecules, present in small amounts in high-temperature air. The absorption coefficients for all these mechanisms were estimated in Chapter V. The relative role of the various absorption mechanisms and the absolute values of the coefficients depend very strongly on the temperature and density of the air. The dominant process at temperatures above $\sim$12,000–15,000°K is the photoionization of the molecules and atoms of oxygen and nitrogen. The mean free path for visible photons in air at the density of 10 times higher than atmospheric that exists behind the shock front and at temperatures $\sim$12,000–15,000°K is found to be of the order of millimeters. The mean free path decreases sharply as the temperature increases.

* *Editors' note.* This plot was taken from the paper by Taylor [27] on this subject.

In the lower temperature range of ~6000–8000°K the dominant processes are the photoionization of NO molecules, absorption by negative oxygen ions, and molecular absorption by O_2, N_2, and NO molecules. The mean free paths for visible light in this temperature range are also strongly temperature dependent and are of the order of 10–100 cm (for a density ratio of 10 across the shock wave). At the still lower temperatures below ~5000°K all these mechanisms produce a very weak absorption, which, in addition, decreases rapidly with decreasing temperature. Practically the only absorption mechanism of visible light in air at $T < 5000$°K is absorption by nitrogen dioxide molecules NO_2. Despite its small concentration, nitrogen dioxide absorbs visible light very strongly, leading to mean free paths measured in meters. Thus, the nitrogen dioxide concentration at $T = 3000$°K and at a density five times atmospheric is $c_{NO_2} = 1.6 \cdot 10^{-4}$*, and the mean free path for red light, calculated using an absorption cross section $\sigma_{NO_2} = 2.15 \cdot 10^{-19}$ cm^2, is $l_\nu = 220$ cm.

It is known that the temperature behind the shock front produced by a strong explosion increases from the front to the center (see §25, Chapter I). If we consider that stage of the explosion at which the temperature at the front is equal to several thousand degrees, then for the nominal explosion energy $E = 10^{21}$ erg (corresponding to approximately 20,000 tons of TNT) the explosion wave encompasses a sphere with a radius of the order of hundreds of meters and the temperature behind the front increases appreciably for a distance away from the front toward the center of the order of meters. At this stage the radiant preheating of the air ahead of the shock discontinuity and the screening of the front surface, considered in §§1 and 3, are negligibly small. The thickness of the relaxation layer in the shock front, in which the equilibrium values of dissociation and ionization are established, is much smaller than a photon mean free path. Hence we can state that, as long as the photon mean free path is less than the order of a meter, the shock front is followed by an optically thick region with an almost constant temperature and the front radiates as a perfect black body. The brightness temperature of the fireball as measured by the visible radiation does not in this case differ from the temperature of the shock front. The situation is different when the shock strength falls to a point where the absorption behind the front becomes weak and the photon mean free path becomes comparable to the characteristic distance over which there is an appreciable change of temperature behind the front, that is, where it becomes of the order of a meter or more.

However, before we consider the deviation of the brightness temperature from the temperature of the front, which will be done in the following section, let us determine the point at which the shocked air ceases to be incandescent.

* The concentration c_i is defined as the ratio of the number of ith particles to the original number of molecules in the cold air.

We have noted above that at temperatures below $\sim 5000°K$ the nitrogen dioxide molecules are responsible for the absorption and emission of the visible light. But, because of the nature of the kinetics of the oxidation of nitrogen in an explosion wave (see §5, Chapter VIII) the nitric oxide molecules, from which the dioxide molecules are subsequently formed, practically do not form in air heated by a shock wave to temperatures below about 2000°K. The reason is the large activation energy of the nitrogen oxidation reaction, which results in the extremely pronounced temperature dependence of the reaction rate. At temperatures below about 2000°K the time required for the formation of any appreciable amount of oxide is extremely large in comparison with the lifetime of the particles in the shock wave, so that the reaction does not take place. Thus nitrogen dioxide, the only absorption agent in the air layers heated by the shock front to temperatures below $\sim 2000°K$, is not formed in these layers; they are completely transparent to visible light and are not incandescent.

At the time when the front temperature T_f is below 2000°K, say when $T_f = 1000°K$, a luminous disk with a radius smaller than the radius of the shock front becomes visible from afar. The horizontal cross section of an explosion wave is shown in Fig. 9.9. Rays such as B intersect the air layers

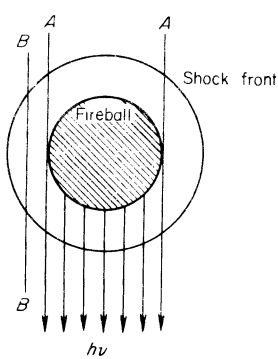

Fig. 9.9. Schematic representation of the luminescence of a fireball after breakaway. The inner circle is the boundary of the luminous mass, the fireball; the outer circle is the shock front.

heated by the shock to a temperature below about 2000°K and therefore are not luminous. The fireball is bounded by the rays A, which are displaced from the center O exactly the distance R_{fb}. This distance is the radius at the given time of those air layers which were previously heated by the front to a temperature of about 2000°K and which still contain a sufficient amount of nitrogen dioxide to produce perceptible luminescence. Since the air particles in the explosion wave expand rapidly away from the center (although slower than the shock wave front), the radius of the fireball R_{fb} increases. The fireball expands until the pressure in the explosion wave drops to atmospheric

and the motion ceases*. The nonluminous shock front, after breaking away from the fireball at the time when its temperature was $\sim 2000°K$, moves far ahead of it. (The traces of the front and of the fireball are shown schematically in Fig. 9.10.)

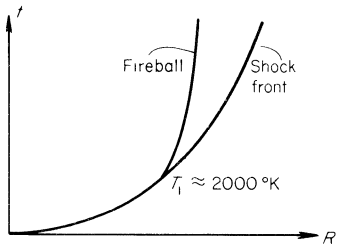

Fig. 9.10. Trace of the shock front and the fireball boundary on an R, t diagram.

§7. Minimum luminosity effect of the fireball

Let us consider how the luminosity and brightness temperature of the fireball surface change with time during the process of the breakaway of the shock wave from the boundary of the luminous mass. When the temperature of the front drops below $\sim 5000°K$, the mean free path for visible light increases to a value of the order of a meter and the fireball ceases to radiate as a perfect black body. Under these conditions the brightness temperature should be calculated from the general formula (2.52) in accordance with the distribution of temperature and absorption coefficient with respect to the distance behind the shock front†.

Let us consider as an example the time $t = 1.5 \cdot 10^{-2}$ sec, when the radius of the front $R = 107$ m and the temperature at the front $T_f = 3000°K$ (all

* Air particles initially at the temperature $T_f \approx 2000°K$, corresponding to a pressure at the front $p_f \approx 50$ atm, cool to $T \sim 800°K$ in an adiabatic expansion to atmospheric pressure. Probably, as time increases the boundary of the luminous region is displaced deeper, into those layers with temperatures closer to 2000°K. The reason is that the emission coefficient, which is proportional to $\exp(-h\nu/kT)$, decreases very rapidly with a decrease in temperature even if the absorption coefficient is unchanged ($h\nu \gg kT$ for $h\nu \approx 2$ ev, $T \sim 2000$–$1000°K$). To be more precise, the boundary of the fireball is determined by the sensitivity of the recording instrument.

† The radiating layer has a thickness of the order of ten meters, which is considerably less than the sphere radius $R_{fb} \sim 100$ m. Therefore, we can neglect the curvature of the layer and consider it to be planar, and thus we may use equation (2.52). We note that (2.52), in which an exponential-integral enters because the oblique rays are taken into account, gives a brightness temperature averaged over the disk. If we are interested in the luminosity at the center of the disk, then the exponential-integral $E_2(\tau_\nu)$ should be replaced by the ordinary exponential $\exp(-\tau_\nu)$, where τ_ν is the optical thickness measured with respect to the radius from the front surface toward the center of the sphere. We can then calculate the average brightness temperature.

calculations pertain to an explosion with an energy of $E = 10^{21}$ erg). Figure 9.11 shows the distribution of the absorption coefficient for red light $\lambda =$ 6500 Å with respect to distance behind the shock front (the x coordinate is measured from the front into the fireball). Also given on the figure are the

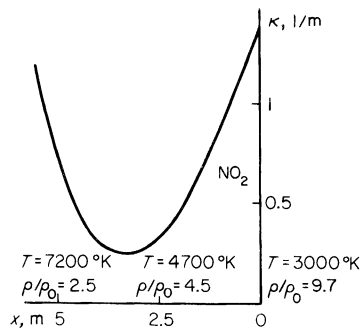

Fig. 9.11. Distribution of the absorption coefficient of red light behind a shock front at a temperature $T_f =$ 3000°K for an explosion with $E = 10^{21}$ erg. Values of the temperature and density are shown at several points. The specific heat ratio $\gamma = 1.23$.

temperature and the density ratio ρ/ρ_0 for air at several points. The temperature and density distributions behind the front are taken from the solution of the strong explosion problem; the nitrogen dioxide concentration was calculated by the method of §5, Chapter VIII. Since the exact values of the cross sections for the absorption of red light by excited NO_2 molecules are not known, we have taken for calculational estimates the reasonable values given in Table 9.4 (see §21, Chapter V).

Table 9.4

ESTIMATED CROSS SECTIONS FOR ABSORPTION OF RED LIGHT BY EXCITED NO_2 MOLECULES

T, °K	4000	3000	2600	2000
$\sigma_{NO_2} \cdot 10^{19}$, cm²	3.0	2.15	1.8	0.84

It is evident from Fig. 9.11, that at temperatures above 6000–7000°K, the absorption, due to the many mechanisms listed above, is very strong and that it increases rapidly as we move away from the front where the temperature goes up. In the region of $T \sim 6000$°K the absorption decreases and passes through a minimum, since at this temperature the absorption coefficient for all the other mechanisms is very small and the concentration of the dioxide is still too low (equilibrium for the reaction $NO + \frac{1}{2}O_2 \rightleftarrows NO_2$ at such high temperatures is displaced in the direction of dissociation of the dioxide). The concentration of the dioxide increases at still lower temperatures ~4000–3000°K, which then leads to an increase in the absorption near the wave front.

The air layers at temperatures above ~6000–7000°K are essentially

found to be completely opaque, and a Planck radiation flux is emitted through the surface from the internal "hot" sphere at this temperature. The external air layer containing the dioxide plays a dual role. On the one hand, it absorbs this high-temperature radiation emerging from the surface of the "hot" sphere, and on the other hand, it radiates itself. This situation can be described formally by breaking up the integral with respect to τ_ν in (2.51) into two parts: one with respect to the external layer containing the dioxide and with an optical thickness τ_ν^*, and the other with respect to the internal hot region $\tau_\nu^* < \tau_\nu < \infty$:

$$S_\nu(T_{\text{br}}) = 2\int_0^\infty S_{\nu p}E_2(\tau_\nu)\,d\tau_\nu = 2\int_0^{\tau_\nu^*} S_{\nu p}E_2(\tau_\nu)\,d\tau_\nu + 2\int_{\tau_\nu^*}^\infty S_{\nu p}E_2(\tau_\nu)\,d\tau_\nu.$$

Here we have replaced the radiation density in (2.51) by the equivalent flux. In the second integral we can factor out some average value of $S_{\nu p}^*$, corresponding to the brightness temperature of the hot sphere T^* ($T^* \sim 7000°\text{K}$), and, using the properties of the exponential-integral functions, we can write

$$S_\nu(T_{\text{br}}) = 2\int_0^{\tau_\nu^*} S_{\nu p}E_2(\tau_\nu)\,d\tau_\nu + S_{\nu p}(T^*)E_3(\tau_\nu^*).$$

The first term gives the natural radiation of the dioxide layer and the factor $E_3(\tau_\nu^*)$ in the second term takes into account the screening by this layer of the high-temperature radiation from the hot sphere. Calculations show that the relative importance of the second term increases with time, and that the natural luminescence of the dioxide becomes small, that is, the role of the dioxide reduces basically to that of screening the high-temperature radiation. In our example $T_f = 3000°\text{K}$, the optical thickness of the dioxide layer $\tau_\nu^* = 2.42$, and the brightness temperature of the fireball is found to be $T_{\text{br}} = 4110°\text{K}$.

Another typical distribution of the absorption coefficient with respect to the radius is obtained when the temperature at the shock front drops below 2000°K. In this case, the absorption does not begin immediately behind the front, but slightly deeper, since the layers close to the front have been heated only to temperatures below 2000°K and contain no dioxide. These layers do not absorb any light. This situation is shown in Fig. 9.12 ($t = 2.64 \cdot 10^{-2}$ sec, $R = 138$ m, $T_f = 1600°\text{K}$).

Let us follow how the radiation brightness temperature changes with time. As long as the temperature at the shock front is higher than $\sim 2000°\text{K}$, dioxide is formed in the air layers through which the front passes; the total

optical thickness of the dioxide layer increases and the luminosity decreases. The brightness temperature for $T_f \lesssim 5000°K$ exceeds the temperature of the front, since the dioxide layer does not completely screen the high-temperature radiation (with $T^* \sim 7000°K$) arriving from inside the sphere. When the

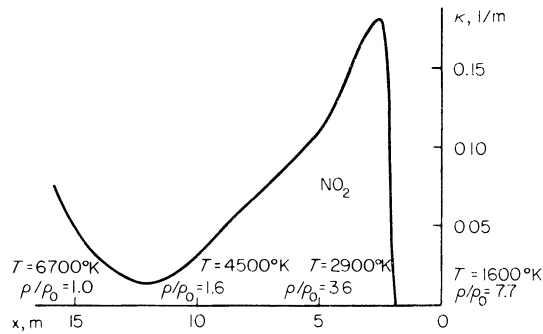

Fig. 9.12. Distribution of the absorption of red light behind a shock front at a front temperature $T_f = 1600°K$, for an explosion of $E = 10^{21}$ erg. Values of the temperature and density are shown at several points. The specific heat ratio $\gamma = 1.30$.

temperature of the front decreases below 2000°K, the dioxide no longer forms in the newer layers over which the front passes. Even if the total number of NO_2 molecules that are present in the air at this time were to remain unchanged, the optical thickness of the screening dioxide layer would still decrease with time, since the expansion of the air would result in a distribution of the same number of NO_2 molecules over a spherical layer of larger and larger radius. It is easy to see that the optical thickness of the dioxide layer

$$\tau_\nu^* = \int_0^R n_{NO_2} \sigma_{NO_2}\, dr,$$

where n_{NO_2} is the number of NO_2 molecules per unit volume, decreases roughly as $R^{-2} \sim t^{-4/5}$ if the total number of NO_2 molecules

$$N_{NO_2} = \int_0^R 4\pi r^2 n_{NO_2}\, dr \approx 4\pi R^2 \int_0^R n_{NO_2}\, dr$$

remains constant. However, the total amount of dioxide, after its formation has stopped, falls off slightly due to the decomposition of the NO_2 molecules (see §5, Chapter VIII). This leads to an even more rapid decrease of the optical thickness τ_ν^*.

Thus, starting at the time when the temperature at the front falls below ~2000°K, the screening of the dioxide layer decreases and the internal hot

region is gradually "revealed". The brightness temperature of the fireball after having passed through a minimum again increases; the fireball thus appears to flare up again—a fact which has been observed experimentally. The above description of the nature of the luminosity minimum is illustrated in Table 9.5, in which are presented the results of calculations of the brightness temperature for an explosion with an energy of $E = 10^{21}$ erg. T_{br} passes through a minimum at 3600°K and τ_ν^* goes through a maximum when the front temperature $T_f = 2600$°K is close to the breakaway temperature $T_f = 2000$°K.

Table 9.5

BRIGHTNESS TEMPERATURE OF A FIREBALL IN RED LIGHT $\lambda = 6500$Å IN THE REGION OF MINIMUM LUMINOSITY, AS CALCULATED IN [15]

$t \cdot 10^2$, sec	R, m	T_f, °K	T_{br}, °K	τ_ν^*
		$E = 10^{21}$ erg		
0.75	82	5000	5930	1.06
1.05	93	4000	4810	1.96
1.50	107	3000	4110	2.42
1.81	109	2600	3600	3.23
1.95	112	2300	4150	2.16
2.25	128	2000	4520	1.80
2.39	132	1800	4810	1.61
2.64	138	1600	5400	1.15
2.94	143	1400	5600	1.11
		$E = 10^{20}$ erg		
0.43	49	5000	6380	0.61
0.61	53	4000	5560	1.16
0.72	58	3000	5060	1.42
0.82	60	2600	4800	1.77
0.95	65	2300	5380	1.18
1.01	66	2000	5850	0.96
1.16	70	1800	6050	0.88
1.38	73	1600	6510	0.71
1.41	75	1400	6980	0.54

It is interesting to observe what happens to the luminosity minimum for different explosion energies. All times and lengths in a strong explosion change in a similar manner, proportionally to $E^{1/3}$ (from the fact that the self-similar solution of the strong explosion problem is approximately valid). Roughly speaking, the optical thicknesses at corresponding times (at the

same front temperature), also vary as $E^{1/3}$ (since the dioxide concentration over the main area is in equilibrium and depends primarily on the particle temperature and density, and not on the time it is in the heated state). It follows, therefore, that the screening by the dioxide layer decreases with decreasing explosion energy, and the difference between T_{br} and T_f becomes greater; also, the minimum becomes shallower. As an example, in Table 9.5 are presented the results of calculations of $T_{br}(T_f)$ for an explosion energy $E = 10^{20}$ erg. The position of the minimum remains the same, but the minimum luminosity increases: $T_{br\,min} \approx 4800°K$.

In the limit of very low explosion energies the minimum should disappear entirely. Conversely, in the limit of very high explosion energies all lengths and optical thicknesses become large, the radiation of the fireball approaches closer and closer to black body radiation, and T_{br} approaches T_f up to the time when T_f becomes equal to approximately 2000°K, that is, the minimum becomes lower than $T_{br\,min} \approx 2000°K$. The brightness temperature cannot drop below 2000°K, since even for very high explosion energies and large lifetimes the dioxide does not form for $T < 2000°K$ and the air heated by the shock wave to temperatures $T_f < 2000°K$ is transparent and does not radiate.

§8. Radiation cooling of air

We consider that the gasdynamic process in a strong explosion in air with an energy $E \sim 10^{21}$ erg takes place adiabatically, as described in §25, Chapter I. The expansion of the air encompassed by the shock wave is strongly decelerated up to the time its pressure drops to a value of the order of atmospheric. Thereafter, the shock wave gradually weakens and becomes an acoustic wave which moves far out, carrying with it a large part of the explosion energy. The central regions, however, after atmospheric pressure has been reached and the motion has ceased, contain a large mass of air irreversibly heated by the shock wave. This mass of air contains the "residual" explosion energy, which also constitutes an appreciable fraction (of the order of tens of percent) of the total explosion energy. The air mass is heated to very high temperatures. Thus, for example, the air layers heated to a temperature $T_f = 11{,}000°K$ by the passage of a shock front with a strength such that $p_f = 750$ atm will be at a temperature of the order of 2000°K* after expanding to atmospheric pressure. Layers closer to the center, which were initially heated by the shock front to several hundreds of thousands of degrees (with the pressure at the front of the order of a hundred thousand atmospheres), remain heated to about ten thousand degrees, etc. Thus, the explosion leaves behind a tremendous volume of air with a radius of the

* The residual temperature, roughly speaking, is $T_{res} \approx T_f(1\text{ atm}/p_f\text{ atm})^{(\gamma-1)/\gamma}$. For an estimate we may take an effective value of the specific heat ratio $\gamma \approx 1.3$.

order of hundreds of meters, heated to high temperatures. The temperature in the central regions reaches hundreds of thousands of degrees, while at the periphery it gradually decreases to a thousand degrees and lower, down to standard atmospheric temperature.

We ask the question, what subsequently happens to the residual energy of the air irreversibly heated by the explosion wave, and how does this air cool down? This problem was considered in papers by Kompaneets and the present authors [16, 17]. It is clear that the dissipation of energy by molecular heat conduction plays no role. For a thermal diffusivity coefficient (thermal conductivity) for air of the order of 1 cm^2/sec, a volume with a radius $\sim 10^4$ cm would take about a year to cool down. Convective ascent of the heated sphere due to the difference in density of the hot and cold air at the same atmospheric pressure and the resulting mixing of the hot air with the surrounding mass of cold gas is a more substantial effect. However, the ascent during the first 2–3 seconds after the explosion is not great. It cannot exceed $gt^2/2$ (where g is the acceleration due to gravity), which is 5 m for the first second, 20 m in two seconds, and 45 m during the third second. Hence, convection is also eliminated as a factor in the first few seconds after the explosion.

The basic process which leads to the cooling of the air and to the dissipation of the irreversible thermal energy is the radiation of light. Radiative cooling is made possible by the fact that cold air is transparent in a certain spectral window, in the visible region of the spectrum and in the neighboring ultraviolet and infrared regions. Because of this transparent window, the corresponding photons, radiated by the heated gas, can move away freely to large distances, carrying with them the energy of the heated mass.

A characteristic feature of the process of energy emission from the heated air is the fact that it is unsteady. In this respect it is basically different from the process of stellar radiation (in particular the radiation from the sun, which supplies our planet with energy), which at first glance appears similar. The energy lost by radiation from the surface of a star is compensated for by a flow of energy from within, which is released as the result of nuclear reactions taking place in the central regions (see Chapter II, §14). In the state which results, each volume element receives an amount of radiant energy equal to that it emits, and the temperature distribution with respect to the radius of the star has a steady character (over observable time periods). In our case there are not internal energy sources; the initial temperature distribution is determined by the previous history of the phenomenon, by the gasdynamics of the propagation of the explosion wave, and the air cools gradually by the transfer of energy away by radiation.

Our problem is to clarify how the cooling process proceeds, to determine how the temperature changes at different points of the heated volume, and

finally, which is most important, to determine what is the rate of radiative cooling and what is the radiant flux from the surface of the heated mass.

§9. Origin of the temperature drop—the cooling wave

The basic factor which determines the features of this process is the extremely pronounced temperature dependence of the transparency of air, which has already been discussed several times. If we consider the temperature dependence of the mean free path of radiation suitably averaged over a spectrum which is characteristic for a given temperature, say, the mean free path of photons $h\nu$ with energies of 3–5 times kT*, and keep in mind that at a constant pressure close to atmospheric the density of air decreases with increasing temperature, we arrive at the following conclusions: The mean free path of photons changes from kilometers at temperatures of the order of 6000°K to hundreds of meters at $T \sim 8000$°K, tens of meters at $T \sim 10{,}000$°K, and to tens of centimeters at $T \sim 15{,}000$°K.

Obviously, the radiant flux emerging from a heated volume with a smooth temperature distribution is determined by the temperature of that (radiating) layer in which the mean free path is of the order of the characteristic dimension of the problem, that is, of the order of tens of meters. The external, less heated, layers are transparent and practically do not radiate. The deeper layers are opaque and the photons born there cannot move too far away. We have already encountered a similar situation in considering the radiation of the preheating zone of air ahead of the discontinuity in a very strong shock. By analogy, one can also introduce in this problem the concept of a transparency temperature T_2, defined as the temperature at which the mean free path for light is of the order of the characteristic distance over which the temperature changes appreciably. In contrast to the problem of the luminescence of the preheating layer, where the dimensions were 10^{-2}–10^{-1} cm and the transparency temperature was ~20,000°K, the scale here is of the order of 10 m and the transparency temperature $T_2 \sim 10{,}000$°K.

Let us now imagine a spherical volume of stationary air with an initially smooth temperature distribution which varies with radius from ~100,000°K at the center to several thousand degrees at the periphery, and let us consider how this distribution changes with time (here we shall neglect the motion of the air resulting from pressure gradients). In accordance with what was said above, we may expect that radiation and cooling will begin in a layer whose temperature is of the order of the transparency temperature ($T_2 \sim$ 10,000°K); at the following moment we should observe a "depression" in the

* We recall that the maximum of the Planck frequency spectrum occurs for photon energies $h\nu = 2.8kT$; the maximum of the weighting function appearing in the Rosseland method for averaging the mean free path lies in the region $h\nu \approx 4kT$.

initially smooth temperature distribution, as shown in Fig. 9.13. Subsequently this "depression" acquires the form of a temperature drop which is propagated toward the center of the heated sphere. The air layers are successively

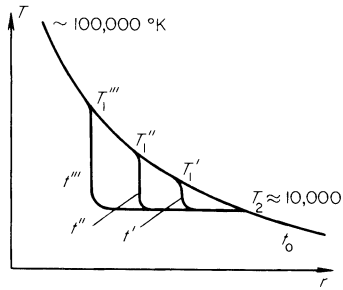

Fig. 9.13. Origin of a temperature drop (cooling wave) in an originally continuous temperature distribution, and its propagation in stationary air; $t_0 < t' < t'' < t'''$.

cooled from the initial temperature to a temperature of the order of 10,000°K, after which they become transparent and practically stop radiating. The internal layers essentially retain their temperature until reached by the drop, since the mean free path for light in these layers is very small and emitted photons are immediately absorbed.

Thus, the air cools as a result of the propagation through it of a certain narrow temperature drop, which can be called a "cooling wave". The temperature in the cooling wave drops sharply (in comparison with the initial smooth distribution) from the initial value T_1, equal to the temperature at the point reached at the given instant by the upper boundary of the wave, to a lower value, the transparency temperature T_2 at which the air practically stops radiating.

In describing the successive changes in the temperature distribution in Fig. 9.13, we have digressed from the consideration of temperature changes due to the gasdynamic motion by taking the air to be stationary. Actually, however, the temperature drop is formed even prior to the time when the air pressure falls to atmospheric and the motion ceases, namely, when the rate of radiative cooling of a layer with temperature ~10,000°K becomes comparable to the rate of adiabatic cooling connected with the expansion of the air in the explosion wave. The adiabatic cooling rate at the earlier stage of the explosion is high and the air has no time to emit its energy, since the temperature region around 10,000°K at which the drop could form is "passed by" very rapidly, and the air becomes transparent without having had a chance to lose any appreciable amount of energy by radiation. Subsequently, however, when the adiabatic cooling slows down as the pressure falls and the expansion becomes slower, the radiant cooling becomes dominant. Estimates show that the drop behind the shock wave front in an explosion with $E = 10^{21}$ erg begins to appear in a layer with $T \sim 10{,}000$°K at $t \sim 10^{-2}$ sec, when the temperature at the front is of the order of 2000°K and the pressure is of the

order of 50 atm (the pressure in an explosion wave changes by only a small amount from the front to the center; see §25, Chapter I).

The temperature distributions in air through which a cooling wave propagates, including the effect of the adiabatic cooling, are given in Fig. 9.14. The

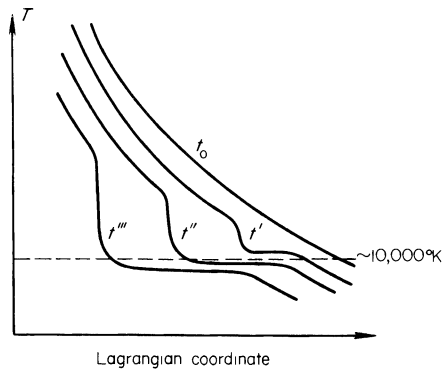

Fig. 9.14. Origin and propagation of a cooling wave in air undergoing an explosion and adiabatic cooling; $t_0 < t' < t'' < t'''$.

abscissa is expressed in terms of a Lagrangian rather than an Eulerian coordinate, and Fig. 9.14 shows the temperature changes of given air particles and the propagation of the cooling wave not through space but with respect to mass in the gas.

§10. Energy balance and propagation velocity of the cooling wave

The cooling wave travels through air that is practically undisturbed by radiative losses. The gas temperature at the time when it is reached by the upper boundary of the temperature drop is determined solely by the previous history of the process and by the hydrodynamic motion (if such exists). This is a result of the fact that at temperatures of the order of tens of thousands of degrees and with temperature gradients of the order of thousands of degrees per meter, which exist initially, the radiative heat transfer is too small to give any appreciable flow of energy in the opaque region that has not yet been reached by the cooling wave. The radiation heat conduction coefficient, which is proportional to the Rosseland mean free path $l(T)$ and to the cube of the temperature*, increases rapidly with increasing temperature and becomes appreciable only in the region of temperatures of the order of hundreds of thousands of degrees, near the center of the explosion. It limits the tem-

* We recall that the energy flux transported by radiation heat conduction is $S = -\kappa\, \partial T/\partial r$, where the radiation heat conduction coefficient is $\kappa = 16\sigma l(T)T^3/3$ (see §12, Chapter II).

perature rise at the center to this order of magnitude and equalizes the temperature near the center.

The radiation conduction coefficient becomes large again in the temperature region below 10,000°K, where the mean free path, increasing sharply with decreasing temperature, becomes very large*. This does not mean, however, that the radiation heat conduction equalizes the temperature also at the low temperatures, since the heated air becomes transparent in this region and the concept of radiation heat conduction, in general, loses its meaning; the character of the radiative transfer changes and, in particular, it leads to the formation of the cooling wave.

Thus, because of the small heat conduction at the upper edge of the cooling wave, the radiant energy flux flowing into the wave from within is close to zero and cannot affect the properties of the wave. The entire radiant flux, carrying away the energy of the air particles being cooled in the wave, is generated within the wave itself. The determination of this flux, which we shall denote by S_2, is a basic theoretical problem (Part 3 of this chapter is devoted to its solution). This problem is nontrivial, since a very steep temperature distribution exists within the wave. It is clear only that the flux is bounded within the limits $\sigma T_1^4 > S_2 > \sigma T_2^4$, since the radiating layer in the wave is at a temperature below the upper temperature T_1 (at which the air is completely opaque) but above the lower temperature T_2 (below which the air is transparent, does not radiate, and is not cooled by energy emission). If the flux S_2 is known, then the velocity u at which the cooling wave propagates through the gas, which in the end determines the cooling time of the heated volume, can be found from an energy balance. According to estimates the cooling wave propagates through air undisturbed by radiative losses with a velocity less than the speed of sound. In this case the pressure along a thin layer—the wave "front"—becomes equalized and practically constant. The gas density automatically adjusts itself to the temperature change, so that an air particle passing through the wave and being cooled is compressed proportionally to $1/T$ (if we assume that the pressure $p \sim \rho T$). This is shown in Fig. 9.15†.

The air is cooled by the wave at a constant pressure. If ρ_1 is the initial density of the air at the time of the wave's approach, then the mass of air per unit area of front surface per unit time is equal to $\rho_1 u$. The change in

* $l(T)$ passes through a minimum at $T \sim 50{,}000$°K, and the coefficient of radiation thermal conductivity, which is proportional to $l(T)T^3$, has a minimum at $T \sim 10{,}000$°K.

† *Editors' note.* The idealized cooling wave described by the authors is an endothermic gasdynamic discontinuity of the detonation type. The Hugoniot curve is simply an isotherm at the transparency temperature. The cooling wave may be considered as the inverse of a weak deflagration. As with most ordinary weak deflagrations (idealized flames), the pressure jump is not strictly zero but is small enough to be negligible.

enthalpy in cooling from T_1 to T_2 is (for constant specific heats) $\rho_1 u c_p(T_1 - T_2)$. This change is, clearly, equal to the energy carried away from the wave front surface by radiation, to the flux S_2. In this manner we obtain the basic

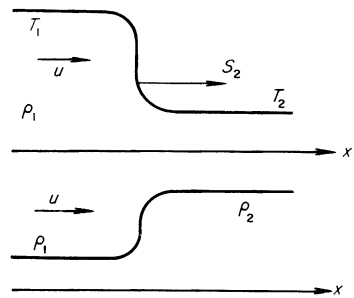

Fig. 9.15. Schematic representation of the gas temperature and density distributions in a cooling wave front. The arrow on u shows the direction of air velocity into the wave.

energy balance equation for the cooling wave, which is here considered as a discontinuity,

$$S_2 = \rho_1 u c_p(T_1 - T_2). \tag{9.5}$$

If we take into account that the specific heat c_p is not constant, then we obtain the more general expression

$$S_2 = \rho_1 u(h_1 - h_2), \tag{9.6}$$

where h is the specific enthalpy of the air.

If γ is the effective adiabatic exponent in front of the wave, then $h_1 = [\gamma/(\gamma - 1)]p/\rho_1$ (see (3.67)) and the wave velocity is

$$u = S_2 \frac{\gamma - 1}{\gamma} \frac{1}{p}\left(1 - \frac{h_2}{h_1}\right)^{-1}. \tag{9.7}$$

It will be shown in the third part of this chapter that the radiation emerging from the surface of the cooling wave is always generated at the lower edge of the temperature drop (at the rear of the wave front), independent of the wave strength characterized by the ratio T_1/T_2 or h_1/h_2; hence, no matter how high the temperature of the hot gas T_1, the temperature of the emerging radiation will be close to T_2.

The flux S_2 is determined basically by the transparency temperature and is approximately equal to

$$S_2 = 2\sigma T_2^4. \tag{9.8}$$

The transparency temperature is not an exactly defined quantity. As was pointed out previously, it serves as a specification of the boundary between the transparent and opaque temperature regions and is found from the condition that the frequency-averaged radiation mean free path at a tempera-

ture equal to the transparency temperature is of the order of the characteristic scale d of the problem. This distance is, for example, the distance over which the air temperature drops from T_2 to a sufficiently small value, say, to 2000°K. When the wave travels through expanding air this scale is determined by the hydrodynamics of the process as a whole; it is smaller, the higher is the

Table 9.6

u, KM/SEC AT $p = 1$ ATM

T_1, °K	T_2, °K		
	10,700	9,700	9,300
20,000	2.7	2.1	1.7
50,000	1.8	1.4	1.1
100,000	1.6	1.2	1.0

adiabatic cooling rate. If we describe the absorption coefficient for air approximately by the Boltzmann relation $\kappa \sim \exp(-I/kT)$ with some effective value of the "ionization potential"*, then the transparency temperature is found to have only a weak logarithmic dependence on the scale d, and also on the air density, which is contained only in the preexponential factor;

$$l(T_2) = const\, e^{I/kT_2} = d; \qquad T_2 = \frac{I}{k}\left(\ln \frac{d}{const}\right)^{-1}. \tag{9.9}$$

We have already said that $T_2 \sim 10{,}000$°K for $d \sim 10$ m and atmospheric pressure (when $d \sim 100$ m, $T_2 \sim 8000$°K; when $d \sim 1$ m, $T_2 \sim 12{,}000$°K). Thus, the value of flux $S_2 = 2\sigma T_2^4$ changes within rather narrow limits and, if we consider strong cooling waves with a large temperature drop ($T_1 \gg T_2$, $h_1 \gg h_2$), it will be found that the velocity with which the wave travels through the air in the initial state depends basically only on the gas pressure p and is independent of the upper temperature T_1

$$u \approx S_2 \frac{\gamma - 1}{\gamma} \frac{1}{p} \qquad \text{when} \quad h_1 \gg h_2 .$$

To illustrate the numerical values, Table 9.6 lists the velocity u for atmospheric

* Actually, κ is the sum of terms of the type $e^{-I/kT}$, where I is the ionization potential for the components corresponding to photoelectric absorption and the excitation energy for the components of molecular absorption. All values of I are of the order of 5–10 ev; if we consider a small temperature interval, then we can always interpolate $\kappa(T)$ by a relation of the type $\exp(-I/kT)$.

pressure and several values of T_1 and T_2. It is evident from the table that the velocity of the cooling wave is of the order of 1 km/sec.

§11. Contraction of the cooling wave toward the center

The character of the cooling and the dependence of the cooling time on the dimensions of the heated volume in our problem differ appreciably from the values that would have resulted if the heat were dissipated by the mechanism of ordinary heat conduction. The temperature of a body cooled by ordinary heat conduction decreases gradually and uniformly and the cooling time for a body with a radius R is proportional to the square of the radius $t \sim R^2 c_p \rho/\kappa$, where κ is the coefficient of thermal conductivity. In the case of radiative cooling, a wave travels through the gas and the cooling time is proportional to the first power of the radius, $t \sim R/u$.

If the dimensions of the heated body are of the order of $R \sim 100$ m and the pressure is of the order of atmospheric, then a cooling wave traveling at $u \sim 1$ km/sec passes from the periphery to the center in a time $t \sim 0.1$ sec. During this time the air cools from high temperatures of the order of tens and hundreds of thousands of degrees to the transparency temperature $T_2 \sim$ 10,000°K. The trace of the path of the cooling wave, together with traces of the paths of the shock front and of the fireball boundary, are shown schematically on the radius-time diagram of Fig. 9.16.

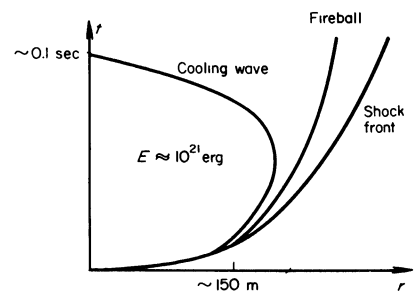

Fig. 9.16. Traces of the paths of the shock front, of the fireball boundary, and of the cooling wave front on an r, t diagram. The scales in this example correspond to an explosion energy $E \approx 10^{21}$ erg.

The wave originates at a time when the temperature at the front is of the order of 2000°K *. The drop forms in a layer with $T \sim$ 10,000°K, which is approximately 10 m away from the surface of the front. At the beginning,

* Despite the fact that the formation of the cooling wave and the breakaway of the shock front from the boundary of the fireball occur almost simultaneously, no direct physical relationship exists between these two essentially different phenomena.

when the pressure is still high ($p \sim 50$ atm at the time when the drop forms), the wave travels through the gas at a moderate velocity. Thus, despite the fact that with respect to the gas the wave travels toward the center, it actually moves outward in space, being carried away by the rapidly expanding air. Gradually the wave slows down (in space), then changes its direction and "collapses" to the center. The turning point, determining the maximum radius of the cooling wave front, corresponds to zero wave velocity in space, that is, to the point at which the gasdynamic velocity of the expanding air particles and the velocity with which the wave travels with respect to the mass of gas become equal.

After the cooling wave passes through the air heated by the explosion, the air temperature is everywhere below $\sim$10,000°K and the entire volume becomes more or less transparent. The subsequent radiative cooling proceeds much more slowly and has a volume character; each particle emits light corresponding to its emission coefficient, and this light travels almost without absorption far from the point of explosion. Of course, the volume is not completely transparent and some part of the radiation is held back in the outer layers, so that some energy is transferred from the central regions to the periphery. In particular, this process is promoted by the nitrogen dioxide contained in the outer layers at temperatures $\sim$3000–1000°K (which were previously heated by the shock wave to a temperature higher than 2000°K).

A similar energy transport also takes place at the time of passage of the cooling wave, since the radiation flux emerging from the wave surface is partially absorbed in the "transparent" (and actually not completely transparent) peripheral layers. In general, absorption in the ultraviolet region of the spectrum is strong and the ultraviolet photons are absorbed in the neighborhood of the wave front. This, however, does not introduce any substantial changes in the qualitative description of cooling of the air by a wave as presented above. This picture was based on the assumption that a high degree of transparency exists at temperatures lower than T_2, since the strong absorption region with wavelengths $\lambda < 2000$ Å contains less than 4% of the energy of the spectrum corresponding to a temperature of 10,000°K.

It should not be assumed that the cooled air ceases to be luminescent after the cooling wave "collapses" to the center and that the surface of the cooling wave at the stage when it still exists is also the boundary of the fireball. The air that has passed through the cooling wave emits enough radiation to glow brilliantly even when the energy effects of the emission have become small and further cooling ceases. The wave is within the fireball and collapses toward the center, leaving behind it still strongly heated and brightly glowing air. The boundary of the fireball (that is, the incandescent boundary) during the later stage of the explosion is made up of layers with temperatures of the order of 2000–3000°K, which are cooled extremely slowly by radiation. After

the pressure becomes equal to atmospheric and the motion practically ceases, these layers are found to be practically stationary. The fireball boundary first moves out from the center together with the expanding air, and then slows down and stops, as shown in Fig. 9.16.

The cooling wave in approaching the center establishes a flow of air from the periphery toward the center, since the wave leaves behind highly cooled particles and cooling at constant pressure is accompanied by compression. For example, if the initial temperature at the center was 100,000°K, and after "collapse" of the wave it dropped to 10,000°K, with the pressure remaining constant at the time of collapse (equal to atmospheric pressure), then the air density at the center is increased by a factor of several tens, and accounts for the flow of air into the center. This inflow, however, does not affect layers that are far from the center and have comparatively low temperatures (of the order of 2000–3000°K), so that the position of the fireball boundary remains unchanged.

At this point we conclude our study of the air cooling process as a whole, of the laws governing the propagation of the cooling wave, and of the luminescence of the fireball, in other words, of the consideration of the "macroscopic" picture*. In the next part we shall study the internal structure of the cooling wave, in a manner similar to that in which general gas flows with shock waves are treated in gasdynamics together with the "microscopic" picture of the internal structure of the shock front. The study of the internal structure of the cooling wave will enable us to find the most important characteristic of the wave—the radiation flux from the wave surface.

§12. The spark discharge in air

Hydrodynamic phenomena which have the character of an explosion also arise in air in connection with spark discharges. These phenomena were investigated by Mandel'shtam and his co-workers [19–24]. We present here the general picture of the process. A thin electrically conducting column is formed in the air discharge gap between the electrodes immediately after the discharge. As a result of Joule heating the air in this column is heated to temperatures of the order of several tens of thousands of degrees and is strongly ionized (at least singly). As a result of the increase in pressure, the column expands and acts on the surrounding air like a piston, sending into it a cylindrical shock wave†.

* We note that a cooling wave also arises in supernovae clouds after emergence of the shock wave at the surface. This was shown by Imshennik and Nadezhin [18], who gave a numerical solution for the problem of the explosion of a massive star as a result of an energy release at the center of the star.

† After the shock wave travels a distance exceeding the column length, it gradually becomes spherical.

In the early stage the air density distributions with respect to radius have a character appropriate to a cylindrical explosion. In [22] the density distributions at successive times were measured by an interferometer. A typical development is shown in Fig. 9.17 (the electrical parameters of the circuit in

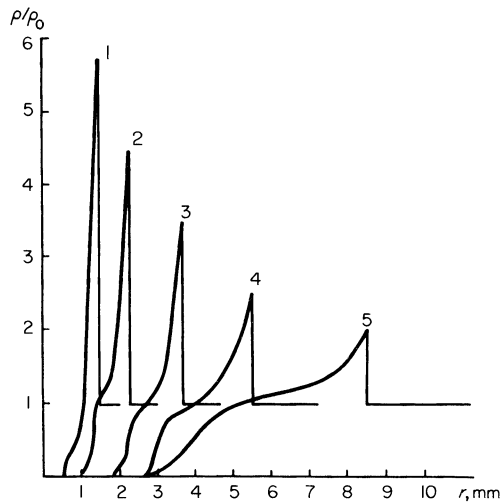

Fig. 9.17. Distribution of air density as a function of spark radius. Curves 1–5 refer to the following times: 1.0, 1.7, 2.9, 5.6, and 9.8 μsec.

this experiment were the following: $C = 0.25$ μf, $L = 2$ μhenries, $V = 10$ kv, and the discharge gap = 5 mm). As can be seen from the figure, at the beginning the shock wave is still rather strong (the velocity is about 2 km/sec) and the density distribution corresponds to that in a strong explosion. At a later stage the wave weakens and the counterpressure of the air ahead of the shock wave begins to have an effect (see §27, Chapter I). In this case the density at the periphery of the blast wave does not differ strongly from standard density, while in the central regions the density is very low. Since the pressure behind the blast wave is equalized spatially, the temperature in the central regions is very high. This central, strongly rarefied and high-temperature region is the electrically conducting column. The average density of air in the column is approximately 10^{-3} of that in the undisturbed air, and the average temperature is approximately 40,000°K. Spectroscopic measurements give consistent results. (Thermodynamic equilibrium in the column is established quite rapidly [23, 24], making it possible to determine the actual gas temperature by spectroscopic means.)

The theory of the explosion wave which results from a spark discharge was developed by Drabkina [20]. It should be noted that the flow differs somewhat from that which takes place with an instantaneous energy release,

since in the given case the time for the generation of the Joule heat in the column, which is determined by the half-period of the discharge, is comparable with the time over which the shock wave is observed. This was taken into account in [20]. The rate of energy generation, which enters into the relation governing the motion of the shock wave, was determined experimentally in this case. Braginskii [25] has considered theoretically not only the motion of the air but also the discharge mechanism, taking into account the conductivity and expansion of the spark column. This makes it possible to relate the shock wave parameters directly with the relation governing the increase in discharge current.

Phenomena which are similar to those investigated in the laboratory, but which take place on a much larger scale, are encountered in a storm. Lightning is simply an electrical discharge and the thunder is produced by the shock wave which is formed and which degenerates into an acoustic wave at large distances. Zhivlyuk and Mandel'shtam [26] measured by spectroscopic means the average temperature in a lightning column, and found it to be approximately equal to 20,000°K. This value is in agreement with calculations based on formulas given in [25], assuming for typical values of the current and time the values 30 kamp and 100–1000 μsec (the radius of the lightning column is $\sim$10 cm). Estimates of the pressure behind the shock front were found to be such that at distances of the order of several meters the thunder can be quite destructive.

3. *Structure of cooling wave fronts*

§13. Statement of the problem

Up to now, when referring to a cooling wave we have considered it as a discontinuity in which the gas temperature experiences a sharp drop. We have also pointed out the energy balance condition, which is equivalent to the relation describing the conservation of total energy flux for a gas flowing through a shock wave. In constrast to shock waves, however, it was sufficient here to formulate only one energy relation, since the motion across the cooling wave is subsonic and the pressure change across the wave front can be neglected (in this respect the cooling wave is similar to a slow flame front). Such macroscopic considerations do not permit us to draw any conclusions on the most important quantity that determines the wave speed, the radiant flux S_2 which goes out from the wave front to "infinity". The flux S_2 can only be found by considering the internal structure of the transition layer through the wave front, by finding the continuous solution of the equations which describe the radiative transfer in the wave. This was done in the previously cited articles [16, 17].

Leaving aside the specific dimensions and shape of the mass of gas being cooled, we shall seek a solution of the unsteady equations of radiative heat transfer in the form $T(x - ut)$, corresponding to a plane wave which travels with a constant velocity u through a gas with given values of the temperature and density T_1, ρ_1. The velocity u should be found from the equations in a manner similar to the way in which the flame speed in a combustible mixture is determined. Actually the equations do not admit of an exact solution of the form $T(x - ut)$. As the wave travels, the thickness of the cooled gas layer, in which the light absorption is small but different from zero, increases; the transparency temperature, defined by the relation $l(T_2) = d$, where d can denote the thickness of the cooled layer, decreases with time.

In an infinite medium, in which the mean free path has an inverse dependence on temperature, the transparency temperature in general becomes equal to zero, since a gas layer of infinite extent cooled to an arbitrarily low temperature is completely opaque even if the radiation mean free path is extremely large. The radiation flux from the wave front is equal to zero in this case and the cooling wave, in the strict sense, does not exist. To some extent, a similar situation occurs in the theory of steady-state flame propagation. If it is not assumed that the rate of chemical reaction in the unburned mixture is identically equal to zero, despite the fact that the actual rate is finite (although vanishingly small), we could obtain the result that the mixture burns prior to being reached by the flame front. This situation, which is fundamental to the case of an infinite medium, does not lead to any difficulties under actual conditions. The fact is that the region which is heated and then cooled by the cooling wave is always bounded, and the transparency temperature has only a logarithmic dependence on the dimensions of the cooled region, and so changes weakly with the distance traveled by the wave, being, for actual cases of interest, bounded within quite narrow limits. The additional very slow dependence of the solution on time $T(x - ut, t)$ arises only at the lowest, most extended edge of the wave, in a region where the gas is already cooled and almost transparent. The presence of the adiabatic cooling occurring when the wave is propagating through an expanding gas makes this additional dependence even less important, since the air which passed through the wave is cooled by the expansion to lower temperatures and rapidly "skips" the temperature region in which it is still not completely transparent. The additional slow variation with time $T(x - ut, t)$ will exist only in the region of pure adiabatic cooling and will have almost no effect on the temperature distribution in the wave.

In order to find the temperature distribution in the cooling wave front, which in turn also determines the flux S_2, one should consider a planar steady process in a coordinate system moving with the front, as is usually done in the theory of wave structure. This was illustrated in Chapter VII using shock waves as an example. To eliminate the difficulty discussed above and to render

the problem steady, that is, to go from the actual solution $T(x - ut, t)$ to an idealized case $T(x - ut)$ (in the laboratory coordinate system), we can use one of two formally artificial methods, which, however, are by virtue of our preceding discussion physically justifiable and correspond to the actual situation. In the first method we can introduce into the energy equation an additional constant term A representing the adiabatic cooling. The quantity A specifies a constant scale d, which determines the transparency temperature T_2 and limits the absorption in the region cooled by radiation, making the optical thickness of this region finite. In the second method, we can disregard the adiabatic cooling, but instead introduce right at the beginning the transparency temperature T_2 obtained from an estimate such as (9.9), and assume formally that for $T < T_2$ the medium is completely transparent (the mean free path $l = \infty$). Then the gas will be cooled only to T_2, after which the emission, which is proportional to $\kappa = 1/l$, and any further cooling will cease.

Since the gas motion across the cooling wave is subsonic (this is shown by estimates), we may neglect the kinetic energy of the gas flow in comparison with the thermal energy. In this case, the energy equation at a point x within the wave is written for the general case by introducing an additional term to describe the adiabatic cooling

$$u\rho_1 c_p \frac{dT}{dx} + \frac{dS}{dx} = -A, \qquad A > 0. \tag{9.10}$$

If the specific heats are not taken constant, it is more convenient to write this equation in terms of the specific enthalpy of the gas

$$u\rho_1 \frac{dh}{dx} + \frac{dS}{dx} = -A. \tag{9.11}$$

Here S is the radiant energy flux at the point x in a wave (from conservation of mass flux $\rho u(x) = \rho_1 u$, where u is the wave speed, equal to the rate at which gas flows into the wave, ρ_1 is the initial density, and ρ and $u(x)$ are quantities at the point x).

The directions of flow, of the x axis, and of the velocity are given in Fig. 9.15, which shows schematically the temperature drop in the wave front. The gas flows into the wave from left to right, while the wave travels through the undisturbed gas from right to left. Ahead of the wave, at $x = -\infty$, the temperature has a known value $T = T_1$ and the flux $S = 0$, in accordance with the remark made in §10 to the effect that the radiative heat transfer in a high-temperature gas is unimportant and that the flux in this region is small. The radiation flux S varies from zero to S_2 as x goes from $-\infty$ to $+\infty$, where S_2 is the flux going out of the wave front to infinity.

If the adiabatic cooling is not taken into account, but it is assumed that the transparency temperature T_2 is given (the second method), then the energy relation (9.11) yields the integral

$$S = u\rho_1(h_1 - h). \tag{9.12}$$

Here the constant of integration is expressed in terms of the enthalpy of the original gas $h_1 = h(T_1)$, in accordance with the boundary condition $x = -\infty$, $T = T_1$, and $S = 0$. If we apply the energy integral (9.12) to the rear of the wave, where $T = T_2$ and the flux is equal to that going out to infinity $S = S_2$, we obtain (as expected) the energy balance equation (9.6), relating the variables on both sides of the wave front if the front is regarded as a discontinuity.

To the energy equation must be added the radiative transfer equation, which determines the flux S. The radiative transfer will be described in the diffusion approximation, as was done when considering the structure of a shock front with radiation taken into account (see Chapter VII, Part 3). In addition, we shall introduce, as before, some frequency-averaged photon mean free path l. The equations for the diffusion approximation are then written as

$$\frac{dS}{dx} = c\frac{U_p - U}{l}, \tag{9.13}$$

$$S = -\frac{lc}{3}\frac{dU}{dx}, \tag{9.14}$$

where U is the true radiation density and U_p is its equilibrium value corresponding to the temperature of the medium at the point x: $U_p = 4\sigma T^4/c$.

As will be shown below, the radiation density in a considerable part of the wave will be close to equilibrium. It is well known (see §12, Chapter II), that under these conditions the spectral mean free path l_ν is to be averaged by the Rosseland method. However, local equilibrium no longer exists in the region of highly cooled air, and the Rosseland method of averaging no longer applies. The averaging method, however, cannot introduce any qualitative changes in the results, since the exponential Boltzmann factor of the form $e^{I/kT}$, which effectively describes the basic temperature dependence of the mean free path, is retained regardless of the averaging method; the preexponential factor, which, of course, changes with the method of averaging, has only a very weak logarithmic influence (just as with the transparency temperature T_2) on the effects in the wave. Therefore, for simplicity, we shall always imply by $l(T)$ the Rosseland mean free path.

It is convenient to rewrite (9.13) and (9.14) in terms of the optical

co-ordinate τ, which we shall measure from $x = +\infty$, where the gas is transparent and $l = \infty$ (the τ axis is directed opposite to the x axis)

$$d\tau = -\frac{dx}{l}, \qquad \tau = -\int_{+\infty}^{x} \frac{dx}{l} = \int_{x}^{+\infty} \frac{dx}{l}.$$

In this case (9.13) and (9.14) take the form

$$\frac{dS}{d\tau} = -c(U_p - U), \tag{9.15}$$

$$S = \frac{c}{3}\frac{dU}{d\tau}. \tag{9.16}$$

To the radiative transfer equations must be added the boundary conditions. At the front edge of the wave where $\tau = \infty$, as already stated, we have

$$\tau = \infty, \qquad S = 0, \qquad T = T_1. \tag{9.17}$$

At the rear edge, which is the boundary between the absorbing and perfectly transparent media (vacuum), the radiation flux and density should satisfy the known diffusion condition at a vacuum interface (see (2.66))

$$\tau = 0, \qquad S_2 = \frac{cU_2}{2}. \tag{9.18}$$

The radiative transfer equation, together with the energy equation and the boundary conditions completely defines the structure of the wave front, the flux S_2, and the speed u.

§14. Radiation flux from the surface of the wave front

Of practical interest are mainly the strong cooling waves in which the gas, being cooled from the initial temperature T_1 to the transparency temperature T_2, emits a considerable part of its energy: $T_1 \gg T_2$. Weak waves, where the difference between T_1 and T_2 is small*, are of interest mainly from the point of view of methodology, since in this case it is possible to obtain an exact analytic solution of the equations. It is clear that in a weak wave the radiation flux from the front S_2 lies in the range $\sigma T_1^4 > S_2 > \sigma T_2^4$; it is defined quite exactly, since T_1 is close to T_2, with the result that the major problem, that of the flux, does not appear: $S_2 \approx \sigma T_2^4 \approx \sigma T_1^4$. An analytic solution for a weak wave can be found in [16]. We do not consider it here but proceed directly with the consideration of a strong cooling wave.

* Despite the fact that T_1 is close to T_2 we assume, however, that the temperature dependence of the mean free path $l(T)$ is sufficiently sharp that $l(T) \ll l(T_2)$. This inequality is a condition for the existence of the cooling wave.

It was pointed out in the preceding section that the steady solution can be found by one of two methods, either by introducing into the energy equation a constant term representing the adiabatic cooling, or by determining at the very beginning the transparency temperature T_2 and assuming that for $T \leqslant T_2$ the gas is perfectly transparent ($l = \infty$), thus excluding from consideration the region already cooled by radiation and which only very weakly absorbs light. The first approach gives a more complete picture of the temperature distribution, since it permits us to investigate the temperature changes in the cooled air and to take into account its weak absorption. It leads, however, to excessive mathematical complications which arise from considering the temperature distribution within the wave itself (for temperatures above the transparency temperature) and in determining the flux which goes out from the wave front to infinity. In addition, the adiabatic cooling within the wave is small in comparison with the radiative cooling, and therefore the second method is preferable for investigating the internal structure of the wave. In §16 we shall point out certain properties of this regime that are related to the adiabatic cooling.

In the absence of adiabatic cooling the integral of the energy equation is given by (9.12); let us rewrite this equation assuming for simplicity that the specific heats are constant

$$S = u\rho_1 c_p(T_1 - T). \tag{9.19}$$

The problem consists in solving the system of equations (9.15), (9.16), (9.19) together with the boundary conditions (9.17) and (9.18). Before investigating this sytem, we shall attempt to estimate the radiation flux S_2 going out from the front on the basis of the most general physical considerations. These considerations will also tell us what approximations can be made in solving the system of equations and in finding the temperature distribution in the wave.

From the statement of the problem we know that the temperature at any point of the wave cannot be lower than the transparency temperature T_2, since on being cooled to T_2 the gas ceases to absorb and emit radiation, and further cooling stops. Consequently, T_2 is the lowest temperature in the wave, and near the rear edge of the wave the temperature increases as we move away from the interface with the "vacuum", the perfectly transparent region where $T = T_2$ and $l = \infty$, Thus, at the rear edge, where $\tau = 0$, $dT/d\tau \geqslant 0$. It follows from the energy equation (9.19) that as we move away from the rear edge into the wave the flux decreases, and for $\tau = 0$, $dS/d\tau \leqslant 0$. The continuity equation for the radiation (9.15) shows that the radiation density at the rear edge of the wave is not higher than its equilibrium value $U_2 \leqslant U_{p2} = 4\sigma T_2^4/c$ (the divergence of the flux dS/dx is not negative; the fluid is not heated by radiation). In the diffusion approximation the flux at the fluid-vacuum interface is related to the radiation density by the condition (9.18): $S_2 = cU_2/2$.

Noting that $U_2 \leqslant U_{p2}$, we find that the upper limit of S_2 is given by $2\sigma T_2^4$,

$$S_2 = \frac{cU_2}{2} \leqslant \frac{cU_{p2}}{2} = 2\sigma T_2^4.$$

On the other hand, the radiation brightness temperature T_{br}, defined by $S_2 = \sigma T_{\text{br}}^4$, coincides with some average temperature of the radiating layer and thus cannot be less than T_2, since the temperature of the fluid in the radiating layer, as at any other point in the wave, is always higher than T_2. It follows therefore that $S_2 > \sigma T_2^4$, and that the flux S_2 which goes out from the wave front to infinity is found to be bounded within rather narrow limits

$$\sigma T_2^4 < S_2 < 2\sigma T_2^4, \tag{9.20}$$

$$T_2 < T_{\text{br}} < \sqrt[4]{2}T_2. \tag{9.21}$$

Thus, regardless of the wave strength, and for arbitrarily high initial temperatures T_1, the radiation always emerges from the rearmost edge of the wave and the radiation flux from the wave front surface corresponds to a temperature close to T_2. Under no circumstances should one think that the use of the diffusion approximation to describe the radiative transfer, which led to the boundary condition (9.18), was of importance in our estimates. Indeed, the diffusion condition (9.18) corresponds to the assumption that the photons emerging from the medium into vacuum have an isotropic angular distribution, and that no photons arrive in the medium from the vacuum (no light sources exist in the vacuum). Even if we had made the different extreme assumption that the radiation at the vacuum interface is highly anisotropic and all the photons leave the medium normal to its surface, the diffusion condition (9.18) would have been replaced by the condition $S_2 = cU_2$, which would have led to the inequalities $\sigma T_2^4 < S_2 < 4\sigma T_2^4$, and $T_2 < T_{\text{br}} < \sqrt[4]{4}T_2$. These differ from (9.20) and (9.21) by only a small numerical factor. Actually the limitation on the flux $S_2 < 2\sigma T_2^4$ is related to the fact that the solution is steady state, as a result of which the temperature distribution, which completely defines the flux, cannot be arbitrary and is determined completely by the steady state equations.

An important corollary follows from the inequality (9.21) which permits us to solve the whole problem of front structure by very simple means despite the fact that it is described by nonlinear equations. The radiation from a heated body which is bounded by a transparent medium (or vacuum) is essentially generated in a layer near the surface of the body which has an optical thickness of the order of unity (photons born in deeper layers cannot leave the surface, are almost completely absorbed in transit). The radiation brightness temperature coincides with some average temperature of this radiating layer. But, by virtue of the inequality (9.21), the brightness temperature is

very close to the temperature of the lower edge of the wave T_2. This means that the temperature of the fluid behind the point $\tau = 0$, where $T = T_2$, changes very little over a distance of the order of several optical thicknesses into the wave. This allows us to draw the following conclusions: In a strong cooling wave, in which $T_1 \gg T_2$, the radiant flux in the radiating layer, at the rear edge of the wave, changes very little and is almost constant. Indeed, when the temperature changes by $\Delta T \lesssim T_2$ the flux changes by

$$|\Delta S| \sim u\rho_1 c_p \Delta T \lesssim u\rho_1 c_p T_2,$$

and for $T_1 \gg T_2$ the flux at the point $\tau = 0$, $T = T_2$ is approximately equal to $S_2 \approx u\rho_1 c_p T_1$ (see (9.19)). As a result

$$\frac{|\Delta S|}{S_2} \approx \frac{T_2}{T_1} \ll 1.$$

Since the flux near the rear edge of a strong wave is almost constant, the situation is completely analogous to that prevailing in the photospheres of stationary stars, where the radiant flux is strictly constant. Thus, the problem of relating the flux S_2 with the transparency temperature T_2 (the temperature at the vacuum interface) in the limit of a strong wave is equivalent to the well-known Milne problem (see §15, Chapter II). Taking into account the angular distribution of radiation rigorously, it has the exact solution

$$S_2 = \frac{4}{\sqrt{3}} \sigma T_2^4, \tag{9.22}$$

which differs only slightly from the solution in the diffusion approximation

$$S_2 = 2\sigma T_2^4. \tag{9.23}$$

It is now evident that the value of the flux S_2, within the framework of the diffusion approximation, coincides with the upper limit of the inequality (9.20) in the limit of a strong wave.

§15. Temperature distribution in the front of a strong wave

The fact that the temperature changes little over the radiating layer with a thickness of the order of several optical units shows that local equilibrium exists between the radiation and the fluid. The relative departure of the radiation density at the rear edge of the wave from its equilibrium value is smaller, the stronger is the wave, the greater is the ratio T_1/T_2. Indeed, it follows from (9.15) that

$$\left(\frac{U_p - U}{U_p}\right)_{\tau=0} = \frac{U_{p2} - U_2}{U_{p2}} = -\frac{1}{cU_{p2}}\left(\frac{dS}{d\tau}\right)_2.$$

But, by virtue of what was said previously

$$\left|\frac{dS}{d\tau}\right|_2 \sim \frac{|\Delta S|}{\Delta\tau} \lesssim S_2 \frac{T_2}{T_1} = 2\sigma T_2^4 \frac{T_2}{T_1},$$

since $|\Delta S| \sim S_2 T_2/T_1$ is the change in flux over an optical distance $\Delta\tau \sim 1$. Consequently, the relative departure of the radiation density from its equilibrium value in a strong wave is

$$\frac{U_{p2} - U_2}{U_{p2}} \sim \frac{S_2}{cU_{p2}} \frac{T_2}{T_1} \sim \frac{T_2}{T_1} \ll 1.$$

We can show that as we move away from the rear edge into the wave the relative departure of the radiation from equilibrium can only decrease, so that if the wave is sufficiently strong and the departure at the rear edge is small, then the condition of local equilibrium is satisfied throughout the wave. Thus, the equations describing the structure of the front of very strong cooling waves can be solved in the radiation heat conduction approximation by setting

$$S \approx \frac{c}{3}\frac{dU_p}{d\tau} = \frac{16\sigma T^3}{3}\frac{dT}{d\tau}.$$

Combining this equation with (9.19), we obtain an equation for the function $T(\tau)$, which can be integrated by quadratures.

At the rear edge of the wave we obtain an approximate form of the solution which naturally agrees with the diffusional solution of the Milne problem, since the flux $S \approx const$ (see §15, Chapter II)

$$T = T_2(1 + \tfrac{3}{2}\tau)^{1/4}. \tag{9.24}$$

The asymptotic temperature distribution at the front edge of a strong wave has the form

$$T = T_1(1 - e^{-\tau/\tau_{ed}}), \qquad \tau \gg \tau_{ed}, \tag{9.25}$$

where the quantity τ_{ed}, which may be regarded as the effective optical thickness of the wave, depends only on the wave strength

$$\tau_{ed} \approx \frac{8}{3}\left(\frac{T_1}{T_2}\right)^4.$$

The optical thickness increases rapidly with the ratio T_1/T_2. We do not give here the general expression for the distribution $T(\tau)$, which at the rear and front edges takes on the simplified forms given by (9.24) and (9.25) (see [17]), and in Fig. 9.18 only present a curve of the temperature distribution for the case $T_1/T_2 = 5$ and $\tau_{ed} = 1670$.

Knowing the distribution $T(\tau)$ and the mean free path as a function of temperature, it is easy to find the temperature distribution with respect to the geometric coordinate by means of the relation $-x = \int_0^{\tau} l(T)\, d\tau$*. On Fig. 9.19 is shown the temperature distribution $T(x)$ at the lower edge of the

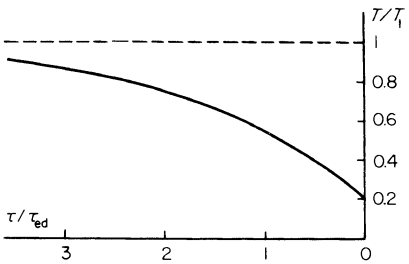

Fig. 9.18. Temperature distribution in a cooling wave as a function of the optical coordinate with $T_2/T_1 = 5$, $\tau_{ed} = 1670$.

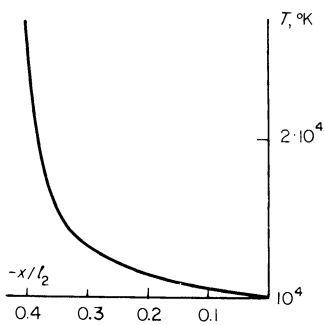

Fig. 9.19. Temperature distribution near the rear edge of a cooling wave as a function of the geometric coordinate; $T_2 = 10{,}000°\text{K}$.

wave for the case of a Boltzmann dependence $l(T) = const \exp(I/kT)$. The length scale is taken to be $l_2 = l(T_2)$. The transparency temperature is taken as $T_2 = 10{,}000°\text{K}$. Figure 9.19 shows that the wave has the form of a step. In fact, the Boltzmann dependence of $l(T)$, which gives rise to the sharp temperature step in the wave, is valid only to temperatures of about 30,000–40,000°K, with no multiple ionization taking place. At higher temperatures the mean free path passes through a minimum and then begins to increase with temperature. Therefore the front edge of a sufficiently strong wave with $T_1 \sim 50{,}000$–$100{,}000°\text{K}$ is highly extended (for $l = const$ the distribution of $T(x)$ at the upper edge would be identical with the distribution of $T(\tau)$) in accordance with (9.25). An approximate temperature distribution in a wave with $T_1 = 40{,}000°\text{K}$ is shown in Fig. 9.20.

If we neglect the extension of the front edge of the wave, which only slightly affects the cooling conditions of the air (since the flux and its divergence, which determines the cooling at the upper edge, are very small), then the

* Actually, since $l(T_2) \neq \infty$, the temperature at the lower edge does not approach T_2 asymptotically, but with a slope different from zero. Therefore the coordinate origin $x = 0$ can be placed at a point where $\tau = 0$ and $T = T_2$.

geometric thickness of the step comprises, as shown in Fig. 9.19, several tenths of the mean free path $l(T_2)$. For $T_2 \sim 10{,}000°\text{K}$ and $l_2 \sim 10$ m, the thickness of the wave is of the order of several meters, that is, a cooling wave

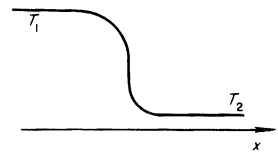

Fig. 9.20. Temperature distribution in a cooling wave.

traveling through a large volume of air with a radius of about a hundred meters is actually narrow and can be regarded as a discontinuity in the temperature and density of the fluid (but not in pressure, which changes very little through the wave).

§16. Consideration of adiabatic cooling

In the preceding sections, by means of artificially cutting off the absorption at the transparency temperature T_2 ($l = \infty$ when $T < T_2$), we eliminated from consideration the region of cooled air whose temperature is below the transparency temperature. Actually, the absorption in this region, although very small, is still finite, and therefore it is natural to inquire how the temperature in the cooled gas behaves under the influence of the radiant flux going out from the wave front. The process in this region is basically unsteady and depends on the particular conditions, on the dimensions, the hydrodynamics of the flow, and the mechanics of light absorption. In this section we shall consider the practically important case in which the cooling wave travels through expanding rather than stationary air, in which the air that is cooled by radiation continues to be cooled adiabatically. The adiabatic cooling rapidly brings the air into the temperature region where it is completely transparent, where it no longer exerts any effect on the behavior of the cooling wave. During the relatively short time interval in which the air undergoing the adiabatic cooling still absorbs an appreciable amount of light, the adiabatic cooling rate changes very little. Hence a process with adiabatic cooling can be approximately regarded as steady and can be described by the energy equation (9.10) with the constant term A. The integral of this equation is

$$u\rho_1 c_p T + S = -Ax + const. \tag{9.26}$$

The constant of integration is here arbitrary, since it is simply determined by the choice of the origin of the x coordinate; it can be set equal to zero.

At the front edge of the wave where $x \to -\infty$, the flux $S \to 0$. It may seem

that this artificially imposed condition contradicts the existence of the temperature gradient related to the presence of adiabatic cooling. However, it is assumed that the mean free path $l(T)$ drops so rapidly with increasing temperature that the product $S \sim -l(T)T^3\, dT/dx$ tends to zero as $T \to \infty$; this is physically justified, since the flux of radiation heat conduction from the outside (from the region of hot air) is very small. At the rear edge of the wave, where $x \to +\infty$, the flux tends to the constant value S_0, i.e., the value of the flux going out to infinity*. Therefore, the temperature in the wave, as $x \to \pm\infty$, asymptotically approaches two straight lines

$$u\rho_1 c_p T = -Ax \qquad \text{for} \quad x \to -\infty,$$

$$u\rho_1 c_p T = -Ax - S_0 \qquad \text{for} \quad x \to +\infty.$$

These straight lines are displaced along the ordinate by an amount S_0 (in Fig. 9.21 they are displaced by $S_0/u\rho_1 c_p$). The problem consists in determining the value of S_0. We do not present here the mathematical solution (see [17]), but limit ourselves to a qualitative discussion of the process.

Let us follow the successive changes of state of a gas particle entering the cooling zone, coming from $-\infty$ in the positive x direction (Fig. 9.21). At the

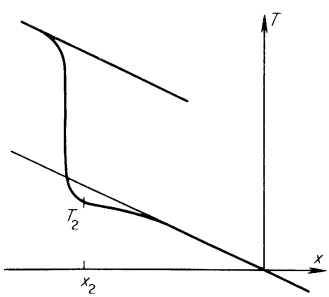

Fig. 9.21. Temperature distribution in a cooling wave taking into account adiabatic cooling.

beginning, when the temperatures are very high, radiation heat conduction is negligible and the particle is cooled entirely adiabatically with its temperature falling off along the upper straight line. Then the particle begins to be increasingly cooled by radiation, and its temperature falls below the upper straight line. The radiation density in the particle in this case is less than its equilibrium value (the particle emits more light than it absorbs), and the radiant flux increases.

The rate of radiative cooling at this stage is considerably higher than the rate of adiabatic cooling and the temperature drops very sharply (the particle passes through the cooling wave). This continues until the time when the

* This flux, as we shall see below, differs slightly from the flux S_2 emerging from an effectively specified surface of the wave front.

particle is cooled to such a low temperature that the rate of radiant heat exchange becomes less than the adiabatic cooling rate. As a result of the extremely sharp decrease in the absorption (and emission) with decreasing temperature, even the small adiabatic cooling that follows makes the particle completely transparent and the radiant heat exchange ceases entirely.

In this case, the radiation density, which is determined by the flux born in hotter layers and passing through the particles, remains almost unchanged. However, the equilibrium radiation density, which is proportional to T^4, rapidly decreases. Therefore the radiation density in the "transparent" region, in contrast to the "opaque" region, is higher than equilibrium, the absorption exceeds emission, and the particle is heated by radiation; the radiant flux decreases as shown in Fig. 9.22*. Consequently, a point $x = x_2$

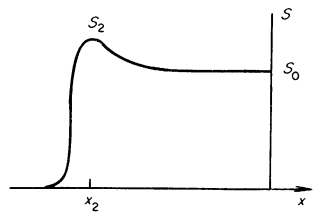

Fig. 9.22. Distribution of radiant flux in a cooling wave taking into account adiabatic cooling.

(the temperature and flux corresponding to this point will be denoted by T_2 and S_2) exists on the x axis which separates the opaque air, intensely cooled by radiation, and the almost transparent air, which is only weakly heated by radiation. At this point the radiation density is exactly equal to its equilibrium value $U_2 = U_{p2}$, the divergence of the flux is zero, and the flux is a maximum $S_{\max} = S_2$.

It is natural to take this point at which the radiative cooling of air ceases as the rear boundary of the cooling wave, to refer to its temperature T_2 as the transparency temperature, and to denote the flux going out from the surface of the wave front as S_2. This flux is only slightly absorbed in the almost transparent region, so that the flux S_0 going out to infinity is only slightly smaller than S_2. The temperature and flux distributions $T(x)$ and $S(x)$ corresponding to the situation described are shown in Figs. 9.21 and 9.22. At low temperatures the curve $T(x)$ goes below the lower asymptote, approaching it from below, since the gas is heated by radiation: the maximum flux lies at the point where the temperature has its maximum downward displacement from the asymptote (this follows from (9.26)).

We can show that the flux S_2 is related to the transparency temperature by

* This situation recalls to a certain extent the situation in a shock wave front with radiation: the radiation density behind the shock discontinuity is below equilibrium, the gas is cooled by radiation and emits a flux in the region ahead of the discontinuity, where it is absorbed; the radiation density is higher than at equilibrium and the gas heats up.

the same relation as in a wave without adiabatic cooling, with $S_2 = 2\sigma T_2^4$. The transparency temperature can be estimated from the condition that the rate of radiative cooling at a temperature close to T_2 becomes equal to the adiabatic cooling rate A, which then approximately determines the rear edge of the wave. The temperature T_2 has only a logarithmic dependence on the arbitrarily specified quantity A, because of the exponential dependence of $l(T)$, similar to its earlier logarithmic dependence on the arbitrarily specified characteristic length scale d (based on the condition $l(T_2) = d$). In our case the characteristic scale is the distance over which the temperature drops, as a result of adiabatic cooling, from T_2 to zero. This distance, incidentally, also determines the position of the rear edge of the wave, the coordinate x_2. Actually, the transparency temperature is still determined from the condition $l(T_2) \approx d$, except that now the prescribed quantity is no longer d itself, but the quantity A which defines the scale d.

X. Thermal waves

§1. The thermal conductivity of a fluid

If a fluid body is heated nonuniformly or if energy is released within the body, a thermal flux transported by heat conduction appears. Heat conduction promotes energy diffusion and temperature equalization. In general, with temperature gradients also arise pressure gradients, which set the fluid into motion. In many cases hydrodynamic energy transport dominates over that associated with heat conduction. However, often the motion and hydrodynamic energy transfer are unimportant and heat from any source present is transported by means of thermal conduction alone. For temperatures which are not too high it is ordinary heat conduction which serves as the mechanism of heat transfer.

Ordinary heat conduction transports thermal disturbances comparatively slowly through a medium (we shall prove this subsequently using a gas as our example). Small pressure disturbances propagate with the speed of sound, leaving certain redistributions of density, and the pressure equalizes more rapidly than the temperature. If the temperature changes in the medium are not large, the fluid moves at a speed much less than the speed of sound, and the motion of the fluid can often be neglected when considering heat propagation by thermal conduction, treating the process as one at constant pressure.

The energy balance equation takes the form

$$\rho c_p \frac{\partial T}{\partial t} = -\nabla \cdot \mathbf{S} + W, \tag{10.1}$$

where ρ is the density, which can approximately be taken as constant, c_p is the specific heat at constant pressure, $\mathbf{S}$ is the heat flux vector, and W is the energy release per unit volume per unit time from external sources. The conductive heat flux is in first approximation proportional to the temperature gradient,

$$\mathbf{S} = -\kappa \nabla T, \tag{10.2}$$

where κ is the coefficient of thermal conductivity, which depends on the properties and state of the fluid. Substituting (10.2) into (10.1), we obtain the general heat conduction equation, which describes the temperature of

the medium as a function of the coordinates and time

$$\rho c_p \frac{\partial T}{\partial t} = \nabla \cdot (\kappa \nabla T) + W. \tag{10.3}$$

The coefficient of thermal conductivity and specific heat change very little over a moderate range of temperatures and may be considered as practically constant. The heat conduction equation (10.3) then becomes linear (with the exception of those cases where the energy release W is a nonlinear function of the temperature). With $\kappa = const$ we have

$$\rho c_p \frac{\partial T}{\partial t} = \kappa \nabla^2 T + W. \tag{10.4}$$

Dividing the heat conduction equation (10.4) by ρc_p it assumes a form in which the fluid properties are characterized by only one parameter, the coefficient of thermal diffusivity $\chi = \kappa/\rho c_p$:

$$\frac{\partial T}{\partial t} = \chi \nabla^2 T + q, \qquad q = \frac{W}{\rho c_p}. \tag{10.5}$$

The coefficient of thermal diffusivity in gases is approximately equal to the molecular diffusion coefficient,

$$\chi = \frac{l_a \bar{v}}{3},$$

where l_a is the molecular mean free path and $\bar{v}$ is the mean thermal speed of the molecules; for example, in air at standard conditions $\chi = 0.205$ cm^2/sec. The heat conduction mechanism in liquids and solids is more complex and will not be discussed here. We only note that in water at room temperature $\chi = 1.5 \cdot 10^{-3}$ cm^2/sec.

To the heat conduction equation must be added initial and boundary conditions. The initial temperature distribution in the medium is given as

$$T(x, y, z, 0) = T_0(x, y, z). \tag{10.6}$$

The heat flux at the interface between two media 1 and 2 with different properties is continuous,

$$\mathbf{n} \cdot (\kappa \nabla T)_1 = \mathbf{n} \cdot (\kappa \nabla T)_2, \tag{10.7}$$

where $\mathbf{n}$ is the unit vector normal to the interface. The temperature itself is continuous. The temperature or heat flux is given on the boundaries of a body as a function of time or, more generally, a relation between the two.

The mathematical theory of linear heat conduction, which is concerned with the solution of (10.5) in various specific applications is well developed and is extensively used in various fields of physics and engineering.

§2. Nonlinear (radiation) heat conduction

A new heat transfer mechanism comes into play at temperatures of the order of tens and hundreds of thousands of degrees, that of radiation heat conduction. The radiation heat conduction process was discussed in detail in Chapter II, and also in Chapters VII and IX, where we considered the front structure of a very strong shock and the radiative cooling of air. The essential difference between radiation and ordinary heat conduction processes lies in the fact that the coefficient of radiation thermal conductivity is highly temperature dependent, as a result of which the heat conduction equation becomes nonlinear.

The heat flux transported by radiation heat conduction is (see (2.76))

$$\mathbf{S} = -\frac{lc}{3}\nabla U_p = -\frac{lc}{3}\nabla\frac{4\sigma T^4}{c}, \tag{10.8}$$

where $U_p = 4\sigma T^4/c$ is the equilibrium radiation energy density and l is the Rosseland radiation mean free path*. The energy flux (10.8) can be written in terms of the gradient of temperature in the form (10.2), if the coefficient of radiation thermal conductivity is defined as

$$\kappa = \frac{lc}{3}\frac{dU_p}{dT} = \frac{16\sigma T^3 l}{3}. \tag{10.9}$$

The coefficient of radiation thermal conductivity is temperature dependent because the radiation specific heat $c_{\text{rad}} = dU_p/dT \sim T^3$, and because the radiation mean free path l depends on temperature.

The radiation heat conduction mechanism can transfer energy at a speed much faster than the speed of sound in the medium. This is so because the speed of light at nonrelativistic temperatures is very much greater than the speed of sound. If energy is released in a body of fluid and it is heated to a sufficiently high temperature, then this energy will initially be rapidly dissipated by radiation heat conduction. As long as the thermal propagation speed is much higher than the speed of sound, the fluid does not have sufficient time to be set into motion, the pressure does not equalize, and the heat flows through a stationary medium. Later on we shall present an estimate of the conditions under which motion arises. Here, we shall consider the propagation of heat by radiation heat conduction in a stationary medium only, one whose density does not change with time.

* We recall that for radiative transfer to have the character of heat conduction, the radiation energy density at each point of the medium must be close to equilibrium. For this it is necessary that the dimensions of the heated region be appreciably greater than the radiation mean free path. *Editors' note.* This condition is also a sufficient one only within the diffusion approximation. A sufficient condition in general requires that the gradients must be small (see §12, Chapter II).

The energy balance is again given by (10.1) or (10.3) (but not by (10.4) since $\kappa \neq const$), with the only difference that the specific heat at constant pressure c_p is replaced in all the equations by the specific heat at constant volume c_v. It is also assumed that the radiation energy density U_p can be neglected in comparison with the energy density of the medium $\rho\varepsilon(T)$.

If c_v is regarded approximately as being temperature independent, and the heat conduction equation is divided by ρc_v, we get the equation

$$\frac{\partial T}{\partial t} = \nabla \cdot (\chi \nabla T) + q, \tag{10.10}$$

which corresponds to (10.5). The coefficient of radiation thermal diffusivity χ is

$$\chi = \frac{\kappa}{\rho c_v} = \frac{lc}{3} \frac{c_{\text{rad}}}{\rho c_v}. \tag{10.11}$$

There is a close parallel between this quantity and the ordinary coefficient of thermal diffusivity for a gas $\chi = l_a \bar{v}/3$. The latter coincides with the diffusion coefficient of the molecules which transfer the heat. In the case of radiation heat conduction the fluid is heated and cooled and energy is transferred by the radiation, which acts as an "intermediary". For this reason the coefficient of radiation thermal diffusivity is not simply equal to the radiation diffusion coefficient $lc/3$, but is also proportional to the ratio of the specific heats of the radiation and the medium.

In many cases it is possible to consider the radiation mean free path l as proportional to some power of the temperature (it is assumed that the density of the medium is constant)

$$l = AT^m, \qquad m > 0. \tag{10.12}$$

In a fully ionized gas, where the radiation and absorption of light proceeds entirely by bremsstrahlung, $m = 7/2$. In the region of multiply ionized gases $m \sim 1.5$–2.5. For the power law (10.12) the coefficient of radiation thermal conductivity is also proportional to a power of the temperature

$$\kappa = \frac{16\sigma A}{3} T^n = BT^n, \qquad n = m + 3, \tag{10.13}$$

where the exponent $n \sim 4.5$–5.5 in the multiply ionized region. In the approximation in which the specific heat of the gas is assumed constant, we arrive at (10.10) with the radiation thermal diffusivity coefficient equal to

$$\chi = \frac{\kappa}{\rho c_v} = \frac{B}{\rho c_v} T^n = aT^n. \tag{10.14}$$

The nonlinear heat conduction equation then takes the form

$$\frac{\partial T}{\partial t} = a\,\nabla\cdot(T^n\,\nabla T) + q. \tag{10.15}$$

Usually the specific heats and internal energy of a gas at high temperatures in the multiply ionized region can be approximated by power-law functions of temperature

$$\varepsilon = \alpha T^{k+1}, \qquad c_v = \frac{\partial \varepsilon}{\partial T} = (k+1)\alpha T^k,$$

where α is a constant and k is a quantity approximately equal to 0.5 (see §8 of Chapter III). When the specific heat varies as a power of the temperature, the heat conduction equation can also be reduced to the form of (10.15). Let us introduce in place of the temperature another unknown function, namely the internal energy per unit volume

$$E = \rho\alpha T^{k+1}, \qquad T = \left(\frac{E}{\rho\alpha}\right)^{1/(k+1)}.$$

We get

$$\frac{\partial E}{\partial t} = a'\,\nabla\cdot(E^{n'}\,\nabla E) + q', \tag{10.16}$$

where

$$n' = \frac{n-k}{k+1}, \qquad a' = \frac{B}{(k+1)(\rho\alpha)^{(n+1)/(k+1)}}, \qquad q' = W. \tag{10.17}$$

Equation (10.16) is identical with (10.15) and their solutions are the same. The transformation of the solution of (10.15), $T = T(x, y, z, t)$, for any specific problem to the solution of (10.16), $E = E(x, y, z, t)$, for the same problem can be simply carried out by replacing the constants a and n by a' and n', and also by replacing the source function q by $q' = W = q\rho c_v$. We note that when $n = 5$ and $k = 0.5$, $n' = 3$. In what follows, for convenience in comparing the results of the nonlinear and linear heat conduction theories, we shall use the temperature equation (10.15). In so doing, we should bear in mind that the solution which is found for any particular problem can be immediately written also for the case when the specific heat is proportional to some power of the temperature.

In addition to radiation heat conduction, which is of the greatest interest, still another example of nonlinear heat conduction can be given. This is electron heat conduction in a plasma, which was discussed in §12 of Chapter VII. (Ion heat conduction in a plasma is also strongly temperature dependent, but it is considerably less important than electron heat conduction.) The coefficient of electron thermal diffusivity is $\chi_e \sim T_e^{5/2}$.

It is interesting to note that the nonlinear heat conduction equation of the form (10.15) also describes an entirely different process, namely, the motion of a polytropic gas (the pressure and density of which are connected by the equation $p = const\ \rho^n$) in a porous medium. The gas density ρ satisfies the equation

$$\frac{\partial \rho}{\partial t} = b\,\nabla \cdot (\rho^n \nabla \rho),$$

where n is the polytropic exponent and b is a constant that is determined by the porosity and permeability of the medium and by the properties of the gas. Problems in filtration theory are also similar to certain problems in nonlinear heat conduction.

Nonlinear heat conduction processes were first considered by Zel'dovich and Kompaneets [1], who, in particular, found an exact solution to the problem of heat propagation from an instantaneous plane source. Analogous problems in filtration theory were studied independently by Barenblatt [2]. He obtained the same solution for the case of an instantaneous concentrated source, and also solved a number of other specific problems.

§3. Characteristic features of heat propagation by linear and nonlinear heat conduction

The basic features of the nonlinear heat conduction process and the characteristic properties distinguishing it from linear heat conduction are best explained by the example of the propagation of heat from an instantaneous plane source in an infinite initially cold medium. Let the energy $\mathscr{E}$ per unit area of surface be the energy released at the initial time $t = 0$ in the plane $x = 0$ ($\mathscr{E}$ is in erg/cm^2). For $t > 0$ the heat propagates in both directions away from the plane $x = 0$.

The heat conduction equation (10.10) for the problem considered takes the form

$$\frac{\partial T}{\partial t} = \frac{\partial}{\partial x} \chi \frac{\partial T}{\partial x}, \tag{10.18}$$

with the spatial temperature distribution satisfying the condition of energy conservation

$$\int_{-\infty}^{\infty} T\,dx = Q. \tag{10.19}$$

The quantity Q is equal to $\mathscr{E}/\rho c_p$ if the process takes place at constant pressure, and to $\mathscr{E}/\rho c_v$, if the specific volume is constant.

In the given case the two equations (10.18) and (10.19) are equivalent to the single heat conduction equation (10.10) with a delta function source (with respect to time as well as with respect to position)

$$q(x, t) = Q\delta(x)\delta(t).$$

Initially at $t = 0$ the temperature of the medium is assumed to be identically equal to zero everywhere, with the exception of the point where the energy release takes place

$$T(x, 0) = Q\delta(x).$$

The solution to the problem posed for the case of linear heat conduction with $\chi = const$ is well known. It is given by the expression

$$T = \frac{Q}{(4\pi\chi t)^{1/2}} e^{-x^2/4\chi t}. \tag{10.20}$$

The characteristic property of linear heat conduction lies in the fact that the heat is concentrated at the point of energy release only at the initial time $t = 0$ (for $x = 0$, $T \to \infty$ as $t^{-1/2}$). For $t > 0$ the heat instantaneously propagates throughout all of space and the temperature tends to zero at infinity, as $x \to \pm\infty$, only asymptotically. The major part of the energy is concentrated in a region whose dimensions are of the order of $x \sim (4\chi t)^{1/2}$, which increases with time proportionally to $\sqrt{t}$. Accordingly, the temperature also decreases as $1/\sqrt{t}$, so that the total amount of heat, which is proportional to $\int T\,dx \sim Tx \sim (1/\sqrt{t})\sqrt{t} \sim 1$, remains constant. The temperature distribution at successive instants of time is shown in Fig. 10.1.

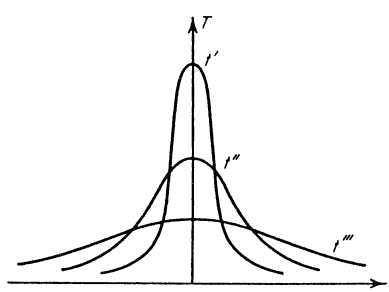

Fig. 10.1. Propagation of heat from an instantaneous plane source by linear heat conduction.

The asymptotic character of the decrease in temperature at infinity and the instantaneous propagation of heat to infinite distance can be explained within the framework of the theory of heat conduction by the fact that the coefficient of thermal conductivity is finite at zero temperature. In practice, of course, only a negligibly small amount of heat reaches a very distant point at a given

time; the temperature decrease at infinity is very sharp, following a Gaussian behavior. In principle, however, at any arbitrarily large but finite distance from the source the temperature is finite immediately following the release of energy. It should be noted that the Gaussian law governing the behavior of the temperature at infinity is related to the approximate description of the heat propagation within the framework of the heat conduction theory. Actually the temperature at large distances is not determined by the diffusion of "hot" molecules from the heated region (in a gas), but rather by the direct "unimpeded" molecules that arrive at points distant from the heated region without experiencing any collisions. Therefore, the drop-off in temperature toward infinity is actually not governed by the Gaussian relationship (10.20) but by the exponential relation $T \sim e^{-x/l_a}$, where l_a is the molecular mean free path. It is clear that no matter what the preexponential factor, for a given time the simple exponential $\exp(-x/l_a)$ will eventually become greater than the Gaussian exponential $\exp(-x^2/4\chi t)$, $(\chi = l_a \bar{v}/3)$. However, this region at large distances contains such a negligible amount of heat, that consideration of it is of no interest.

Let us now verify the assumption that the motion of the fluid can be neglected. If we are dealing with a gaseous medium then a compression wave (or shock wave) is propagated from the point of energy release (in our case, from the plane $x = 0$). The shock propagates through the undisturbed medium with a speed of the order of the speed of sound in the heated region, and thus of the order of the thermal speed of the heated molecules $\bar{v}$. The rate of propagation of heat by thermal conduction is

$$\frac{dx}{dt} \sim \frac{d}{dt}(\chi t)^{1/2} \sim \left(\frac{\chi}{t}\right)^{1/2} \sim \frac{\chi}{x} \sim \frac{l_a}{x}\bar{v}.$$

Hence, as soon as the heat propagates a distance greater than the molecular mean free path, the rate of propagation of heat by thermal conduction becomes less than the hydrodynamic speed. Since, in general, there is no reason to consider distances smaller than a molecular mean free path, we can assume that the heat always travels with subsonic speed. If the amount of the energy released is not large, the compression wave is weak and the fluid velocity is small in comparison with the speed of sound. We can assume, as noted at the very beginning, that the role of the hydrodynamics is simply to equalize the pressure, and that the process of heat propagation proceeds at constant pressure. If the amount of energy released is large and the compression wave at a large distance from the energy source is a shock wave, then we are dealing with the purely hydrodynamic process of a strong explosion, considered in §25 of Chapter I. In this case the role of the thermal conductivity of the fluid in the propagation of energy is insignificant.

Let us now assume that the coefficient of thermal conductivity depends on

the temperature and, furthermore, let it decrease with decreasing temperature and vanish at zero temperature, as in the case of radiation heat conduction. In this case the heat cannot instantaneously penetrate over an arbitrarily large distance, but propagates from the source with a finite velocity in such a manner that a sharply defined boundary exists between the heated region and the cold region which has not yet been reached by the thermal disturbance. The heat propagates from the source in the form of a wave, with the above boundary surface serving as the wave front. This wave is called a thermal wave. The temperature distribution in a thermal wave at successive times is shown schematically in Fig. 10.2.

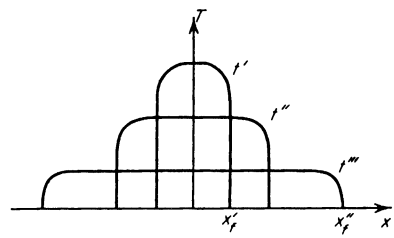

Fig. 10.2. Propagation of a thermal wave from an instantaneous plane source.

The temperature and the heat flux in the cold undisturbed medium are zero, since the coefficient of thermal conductivity goes to zero. From continuity, the flux at the wave front also goes to zero. In the case of linear heat conduction, with $\kappa = const$, the vanishing of the heat flux can be attributed only to the vanishing of the temperature gradient. In the case of nonlinear heat conduction, with the coefficient decreasing to zero as $T \to 0$, the flux can vanish if the temperature gradient is nonzero because the coefficient of thermal conductivity goes to zero. This condition, in particular, is responsible for the generation of a sharp thermal wave front.

To clarify what has been said, let us consider a layer near the wave front. If we restrict ourselves to small enough time intervals that the wave travels through distances which are small in comparison with the dimensions of the region encompassed by the wave, in comparison with the coordinate of the front x_f (see Fig. 10.2), then the front velocity during this time can be taken to be approximately constant.

The temperature distribution near the front can be sought in the form of a standing wave $T = T(x - vt)$, where v is the front velocity. The temperature distribution near the front is quasi-steady in a coordinate system moving with the front. Substituting a solution in the form $T = T(x - vt)$ into (10.18), we obtain the following equation for the temperature distribution near the front

$$-v\frac{\partial T}{\partial x} = \frac{\partial}{\partial x}\chi\frac{\partial T}{\partial x}. \tag{10.21}$$

Assuming that $\chi = aT^n$ $(n > 0)$ and integrating this equation twice with the boundary condition $T = 0$ at $x = x_f$, we get for the temperature distribution

$$T = \left[\frac{nv}{a}|x_f - x|\right]^{1/n}. \tag{10.22}$$

This distribution is shown schematically in Fig. 10.2. The front coordinate x_f and its velocity $v = dx_f/dt$ in this equation represent undetermined functions of time. They are found from the complete spatial solution.

The fact that the temperature vanishes in the manner described by (10.22) also justifies the assumption of the existence of a sharp boundary for the heated region, i.e., a thermal wave front. If the exponent $n \leqslant 0$, the coefficient of thermal diffusivity χ does not go to zero for $T = 0$ and (10.21) has no solutions which vanish at a finite distance, and this case corresponds to the instantaneous propagation of heat to arbitrarily large distances. It follows from (10.22) that the temperature gradient near the thermal wave front satisfies the proportionality $dT/dx \sim |x_f - x|^{(1/n)-1}$. If $n > 1$, then the temperature gradient at the front (at $x = x_f$) becomes infinite, i.e., the front is steep. If $n < 1$, $(dT/dx)_{x_f} = 0$. The flux, however, is always zero at $x = x_f$: $S \sim T^n dT/dx \sim |x_f - x|^{1/n} \to 0$ for $n > 0$.

In examining the structure of a shock front (§§12 and 17 of Chapter VII) in which electron and radiation heat conduction were considered, it was shown how thermal conductivity produces a preheating "tongue" which travels through the gas ahead of the compression shock. The temperature profile ahead of the discontinuity is given by (10.22) (if the motion of the gas ahead of the discontinuity may be neglected), with the velocity v representing the speed of the shock front. The form of the profile is shown in Fig. 10.3a. The "tongue" lies ahead of the shock by the definite finite distance $\Delta x = x_f - x_1$ (Fig. 10.3a), which depends on the shock front temperature T_1

$$T_1 = \left(\frac{nv}{a}\Delta x\right)^{1/n}, \qquad \Delta x = \frac{aT_1^n}{nv} = \frac{\chi(T_1)}{nv} = \frac{\chi_1}{nv}.$$

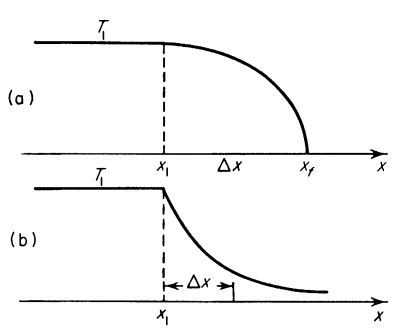

Fig. 10.3. Preheating by heat conduction ahead of a compression shock: (a) for nonlinear heat conduction; (b) for linear heat conduction.

In the case of linear heat conduction $\chi = const$ and the preheating "tongue" extends to infinity, although its effective thickness is finite and constant (for a shock wave moving with a constant velocity). The solution of (10.21) with $\chi = const$ in this case has the form

$$T = T_1 e^{-(x-x_1)/\Delta x'}, \qquad \Delta x' = \frac{\chi}{v}.$$

The temperature profile in the preheating layer is shown in Fig. 10.3b. As previously noted, the temperature vanishes only at infinity.

The relation governing the temperature decrease at infinity due to the "unimpeded" molecules in the case of molecular heat conduction differs from that dictated by the heat conduction theory, which does not consider the motion of individual molecules. Similarly, the thermal wave profile near the boundary, in the case of radiative heat transfer, is given by (10.22) only within the framework of the radiation heat conduction approximation. If we also take into account the presence of "unimpeded" photons, i.e., the fact that the radiation at the leading edge of the wave is out of equilibrium, we find that the temperature at the leading edge of the thermal wave decreases exponentially as $T \sim e^{-x/l}$, where l is the radiation mean free path. This effect was studied in detail in Part 3 of Chapter VII, where we considered the structure of shock fronts including the effect of radiative transfer.

Up to now we have considered the propagation of heat in a medium with zero initial temperature. If $T_0 \neq 0$, then the nonlinear coefficient of thermal conductivity in the undisturbed medium is finite and the relation for the temperature decrease is no longer given by (10.22); however, if T_0 is not too large, the coefficient of radiation thermal conductivity is sufficiently small that this effect can be neglected. Of greater importance is the effect mentioned above of nonequilibrium radiation at the leading edge of the thermal wave, which leads to an exponential temperature drop $T \sim e^{-x/l}$ instead of the power-law relation (10.22).

Let us note one more important difference between nonlinear and linear heat conduction. In the linear case the superposition principle is valid. Therefore, if there are a number of energy sources the heat propagates from each of them completely independently of the others. The solution of the heat conduction equation for distributed sources can be represented as an integral "over the sources" of the solutions corresponding to point sources. The superposition principle does not hold for nonlinear heat conduction. The propagation of heat from a single source depends on the temperature to which the medium is heated by a thermal disturbance coming from another source. In the general case of distributed sources the solution cannot be represented in the form of an integral over the sources.

§4. The law of propagation of thermal waves from an instantaneous plane source

The law of propagation of heat from a source can be easily obtained even without an exact solution by estimating the order of magnitude of the characteristic dimension of the heated region, or from dimensional considerations. Problems on the propagation of heat from an instantaneous concentrated source (plane, point, line) can be solved exactly (see below). However, the semiqualitative estimates describe rather clearly the physical meaning of the governing laws and, in addition, are frequently useful when considering more complex problems for which no exact solutions can be found.

Let us consider the propagation of heat from an instantaneous plane source. The results for the case of linear heat conduction were already presented in the preceding section, where the exact solution to the problem was given. We shall restate these results in order to demonstrate the general procedure for our semiqualitative approach. Let the coefficient of thermal conductivity be constant. Equation (10.18) contains only a single parameter—the coefficient of thermal diffusivity χ measured in cm^2/sec. The other dimensional parameter is the energy per unit area: $\mathscr{E}$ in erg/cm^2 or the quantity Q in deg · cm. If x is the width of the region in which most of the heat is concentrated at the time t, then it is evident from dimensional considerations that $x^2 \sim \chi t$, $x \sim (\chi t)^{1/2}$. The rate of propagation of heat is $dx/dt \sim (\chi/t)^{1/2} \sim \chi/x \sim x/t$. The average temperature in the heated region is of the order of $T \sim Q/x \sim Q/(\chi t)^{1/2}$. These simple results, which agree in order of magnitude with those given by the exact solution (10.20), can be obtained directly from (10.18) by replacing the derivatives $\partial T/\partial t$ and $\partial T/\partial x$ by T/t and T/x, $\partial(\chi\, \partial T/\partial x)/\partial x$ by $\chi T/x^2$. This leads immediately to the same relationships.

We now turn to the case of propagation of a nonlinear thermal wave. We assume that the coefficient of thermal diffusivity has the power-law form $\chi = aT^n$, for which the equation of heat conduction becomes

$$\frac{\partial T}{\partial t} = a \frac{\partial}{\partial x} T^n \frac{\partial T}{\partial x}. \tag{10.23}$$

This equation contains only the single parameter a, in $cm^2/sec \cdot deg^n$. The other dimensional parameter is Q, in deg · cm. We can combine them into a single (independent) dimensional combination containing only the units of length and time, aQ^n in $cm^{n+2} \cdot sec^{-1}$. From this the law governing the motion of the thermal wave front follows

$$x_f \sim (aQ^n t)^{1/(n+2)} = (aQ^n)^{1/(n+2)} t^{1/(n+2)}.$$

The speed of propagation of the thermal wave is of the order of

$$\frac{dx_f}{dt} \sim (aQ^n)^{1/(n+2)} t^{1/(n+2)-1} \sim \frac{x_f}{t} \sim \frac{aQ^n}{x_f^{n+1}}.$$

It is evident that when the exponent n is large, the thermal wave is slowed down very rapidly. This is so because, as a result of the thermal propagation, the temperature drops and the coefficient of thermal diffusivity decreases sharply. Recalling that the average temperature in the thermal wave is of the order of Q/x_f and the average coefficient of thermal diffusivity $\chi = aT^n \sim aQ^n/x_f^n$, we can write the law for the propagation of a thermal wave in a form corresponding to the linear theory: $x_f \sim (\chi t)^{1/2}$. It should be noted that the average coefficient of thermal diffusivity in this equation depends on time according to the relation

$$\chi \sim \frac{aQ^n}{x_f^n} \sim \frac{aQ^n}{(aQ^n)^{n/(n+2)} t^{n/(n+2)}} = (aQ^n)^{2/(n+2)} t^{-n/(n+2)}.$$

The law governing the propagation of a thermal wave can be also obtained from the heat conduction equation by replacing approximately the derivatives of all quantities by their values: $\partial T/\partial t \to T/t$; $\partial T/\partial x \to T/x_f$; $\partial(T^n \partial T/\partial x)/\partial x \to T^{n+1}/x_f^2$. We thus obtain $x_f^2 \sim aT^n t \sim \chi t$; using the fact that $T \sim Q/x_f$, we arrive at the relationships previously found.

§5. Self-similar thermal waves from an instantaneous plane source

Let us find the exact solution for the planar problem of a thermal wave propagating in an infinite medium as the result of the instantaneous release of energy at the time $t = 0$ in the plane $x = 0$. The process is described by the nonlinear heat conduction equation (10.23), with the solution satisfying the law of conservation of energy (10.19). It is evident from the dimensional considerations presented in the previous section that the solution to this problem is self-similar*. In fact, the only dimensionless combination that can be obtained from the coordinate x, the time t, and the parameters a and Q of this problem is

$$\xi = \frac{x}{(aQ^n t)^{1/(n+2)}}. \tag{10.24}$$

The quantity $Q/(aQ^n t)^{1/(n+2)} = (Q^2/at)^{1/(n+2)}$ has the dimensions of tem-

* The concept of self-similarity is discussed in §§11 and 25, Chapter I. See also Chapter XII.

perature. Therefore a solution for $T(x, t)$ should be sought in the form

$$T = \left(\frac{Q^2}{at}\right)^{1/(n+2)} f(\xi), \tag{10.25}$$

where $f(\xi)$ is a new unknown function.

Substituting (10.25) into (10.23) and transforming to the similarity variable ξ by means of the relations

$$\frac{\partial f}{\partial t} = -\frac{1}{n+2}\frac{df}{d\xi}\frac{\xi}{t}, \qquad \frac{\partial f}{\partial x} = \frac{1}{(aQ^n t)^{1/(n+2)}}\frac{df}{d\xi},$$

we obtain an ordinary differential equation for the function f

$$(n+2)\frac{d}{d\xi}\left(f^n \frac{df}{d\xi}\right) + \xi\frac{df}{d\xi} + f = 0. \tag{10.26}$$

The solution of this equation must satisfy the following conditions, which follow from the physical conditions of the problem: $T = 0$ at $x = \pm\infty$; or $T = 0$ at $x = +\infty$ and $\partial T/\partial x = 0$ at $x = 0$ (by virtue of the symmetry with respect to the plane $x = 0$). It follows that

$$f(\xi) = 0 \quad \text{for} \quad \xi = \infty; \qquad \frac{df}{d\xi} = 0 \quad \text{for} \quad \xi = 0. \tag{10.27}$$

A solution of (10.25) satisfying the boundary conditions (10.27) was given in [1, 2]. It has the form

$$\begin{aligned} f(\xi) &= \left[\frac{n}{2(n+2)}(\xi_0^2 - \xi^2)\right]^{1/n} \\ &= \left[\frac{n}{2(n+2)}\xi_0^2\right]^{1/n}\left[1 - \left(\frac{\xi}{\xi_0}\right)^2\right]^{1/n} \quad \text{for} \quad \xi < \xi_0, \\ f(\xi) &= 0 \quad \text{for} \quad \xi > \xi_0, \end{aligned} \tag{10.28}$$

where ξ_0 is a constant of integration. This constant is to be found from the equation of conservation of energy (10.19), which takes the form

$$\int_{-\infty}^{+\infty} f(\xi)\, d\xi = \int_{-\xi_0}^{+\xi_0} f(\xi)\, d\xi = 1. \tag{10.29}$$

Calculation gives

$$\xi_0 = \left[\frac{(n+2)^{1+n}2^{1-n}}{n\pi^{n/2}}\right]^{1/(n+2)}\left[\frac{\Gamma(1/2 + 1/n)}{\Gamma(1/n)}\right]^{n/(n+2)}, \tag{10.30}$$

where Γ is the Gamma function. The law for the motion of the thermal wave front $\xi = \xi_0$ is

$$x_f = \xi_0 (aQ^n t)^{1/(n+2)}. \tag{10.31}$$

As expected, this relation agrees to within the numerical coefficient ξ_0 with the one obtained by semiqualitative considerations in the preceding section.

It is convenient to write the temperature in a plane thermal wave in the form

$$T = T_c \left(1 - \frac{x^2}{x_f^2}\right)^{1/n}, \tag{10.32}$$

where $x_f(t)$ is the front coordinate, whose dependence on time is given by (10.31) and (10.30), and T_c is the temperature in the central plane $x = 0$. This temperature can be expressed in terms of the average temperature in the wave (averaged over the heated volume)

$$T_c = \frac{\overline{T}}{J}, \tag{10.33}$$

where

$$\overline{T} = \frac{Q}{2x_f}; \qquad J = \int_0^1 (1 - z^2)^{1/n}\, dz = \frac{\sqrt{\pi}}{n+2} \frac{\Gamma(1/n)}{\Gamma(1/n + 1/2)}.$$

For example, for $n = 5$, $\xi_0 = 0.77$ and $T_c = 1.12\overline{T}$.

When the specific heat is taken to be variable, the temperature distribution differs very little from (10.32). Indeed, the energy distribution is

$$E = E_c \left(1 - \frac{x^2}{x_f^2}\right)^{1/n'}.$$

But $E \sim T^{1+k}$ and $n' = (n - k)/(k + 1)$, from which

$$T = T_c \left(1 - \frac{x^2}{x_f^2}\right)^{1/(n-k)}.$$

Since $n \sim 5$ and $k \sim 0.5$, this expression differs very little from (10.32) (in the first case the exponent $1/n = 1/5$; in the second it is $1/(n - k) = 1/4.5$). The new constant $\xi_0(n')$ in the relation for the propagation equation itself changes more appreciably. For $n = 5$ and $k = 0$ (constant specific heats) $x_f \sim t^{1/7}$, $dx_f/dt \sim x_f^{-6}$; for $n = 5$ and $k = 0.5$ (that is, $c_v \sim T^{0.5}$), $x_f \sim 1/t^{n'+2} \sim t^{1/5}$, $dx_f/dt \sim x_f^{-4}$.

The temperature distribution T/T_c as a function of x/x_f is given in Fig. 10.4a for the case $n = 5$. A thermal wave with a strongly temperature-dependent coefficient of thermal conductivity has a characteristic temperature

"plateau". The temperature is almost constant, being equalized by heat conduction within the entire heated region, with the exception of a relatively thin layer near the front where it rapidly drops to zero. This tendency is

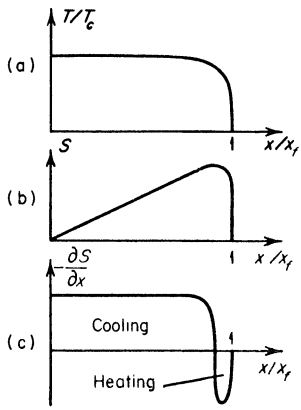

Fig. 10.4. Distributions of temperature, flux, and divergence of flux in a thermal wave.

exhibited more strongly, the larger is the nonlinear exponent n. The distribution of flux with respect to the position coordinate is given by

$$S \sim -T^n \frac{\partial T}{\partial x} \sim \left(1 - \frac{x^2}{x_f^2}\right)^{1/n} x.$$

The flux increases almost linearly from the origin $x = 0$ to the very edge of the wave and drops very rapidly to zero only near the edge, as shown in Fig. 10.4b. The divergence of the flux $\partial S/\partial x$ is almost constant in the entire region of the plateau. The main region of hot gas is cooled almost uniformly, and only near the edge of the wave is the gas heated by energy removed from the main mass of gas (see Fig. 10.4c). The heat propagates in such a manner that the volume of gas is cooled almost uniformly and the energy lost by the gas is absorbed near the wave front, which is the manner by which the wave continually encompasses the new layers of cold gas. The temperature distribution near the front can be approximately given as

$$T \sim \left(1 - \frac{x^2}{x_f^2}\right)^{1/n} \sim \left[\frac{2}{x_f}(x_f - x)\right]^{1/n} \sim (x_f - x)^{1/n},$$

which was already given earlier (see (10.22)).

Let the exponent n in the solution of (10.25), (10.28), and (10.30) go to the limit $n \to 0$, which corresponds to the transition to linear heat conduction (the constant a in (10.23) in the limit $n = 0$ plays the role of a constant coefficient

of thermal diffusivity $\chi = const$). For $n \to 0$, $\xi_0 \to 2/\sqrt{n}$

$$T = \frac{Q}{(at)^{1/2}}[f(\xi)]_{n\to 0} = \frac{Q}{(at)^{1/2}} \frac{1}{(4\pi)^{1/2}} \left[\left(1 - \frac{nx^2}{4at}\right)^{1/n}\right]_{n\to 0}$$

$$= \frac{Q}{(4\pi at)^{1/2}} e^{-x^2/4at}, \qquad a = \chi,$$

and we arrive at the well-known solution (10.20) of the linear heat conduction equation.

In concluding this section, let us note that the second-order nonlinear equation (10.26) may be subjected to a group of transformations which leave the equation invariant. Indeed, it can be easily checked by direct substitution, that if ξ and f are replaced by a new independent variable ξ' and function f' given by

$$\xi' = C^n \xi, \qquad f' = C^2 f, \qquad C = const,$$

then in terms of the new variables the equation has the same form as (10.26). According to the theory of Lie groups, the order of an ordinary differential equation which admits a one-parameter group of transformations can be decreased by one. For this purpose it is convenient to introduce the new variables

$$y = \xi^{-2/n} f, \qquad z = \ln \xi.$$

In terms of these variables the new equation contains z only in terms of the differential dz. Therefore, a new variable $p = dy/dz$ can be introduced and z eliminated, yielding a first-order equation in the variables p and y

$$y^n p \frac{dp}{dy} + np^2 y^{n-1} + \frac{4+3n}{n} p y^n + \frac{1}{n+2} p + \frac{4+2n}{n^2} y^{n+1} + \frac{y}{n} = 0.$$

Thus, the solution of the second-order equation (10.26) reduces to solving a first-order equation and to quadratures. This situation is characteristic of many self-similar problems of nonlinear heat conduction theory*.

§6. Propagation of heat from an instantaneous point source

Let us consider the spherically symmetric case. Suppose that at the time $t = 0$ an energy of $\mathscr{E}$ erg is released at the point $r = 0$. The heat conduction equation in this case takes the form

$$\frac{\partial T}{\partial t} = \frac{1}{r^2} \frac{\partial}{\partial r}\left(r^2 \chi \frac{\partial T}{\partial r}\right). \tag{10.34}$$

* And also of self-similar problems in gasdynamics. For details, see Chapter XII. *Editors' note*. The Blasius equation of boundary layer theory may be reduced to first order with the help of the same approach.

The law of conservation of energy gives

$$\int_0^\infty T 4\pi r^2 \, dr = \frac{\mathscr{E}}{\rho c_v} = Q \quad \text{deg} \cdot \text{cm}^3.$$

The solution of the problem for linear heat conduction $\chi = const$ is well known

$$T = \frac{Q}{(4\pi\chi t)^{3/2}} e^{-r^2/4\chi t}. \tag{10.35}$$

The heat flows in such a manner that the main part of the energy is concentrated in a sphere whose radius is of the order of

$$r \sim (4\chi t)^{1/2},$$

in close analogy with the plane case, where we had $x \sim (4\chi t)^{1/2}$. The temperature at the center falls off as $T_c \sim Q/r^3 \sim Q/(\chi t)^{3/2}$. These relationships follow directly from dimensional considerations; they can also be obtained from estimates based on (10.34) and (10.35), by replacing the derivatives by their corresponding values (see §4).

Let us now consider the case of nonlinear heat conduction with $\chi = aT^n$ and $n > 0$. The equation takes the form

$$\frac{\partial T}{\partial t} = \frac{a}{r^2} \frac{\partial}{\partial r} \left(r^2 T^n \frac{\partial T}{\partial r} \right). \tag{10.36}$$

Let us find the equation of motion for the thermal wave front, as was done in the plane case. We have

$$r_f^2 \sim \chi t,$$

where χ is the coefficient of thermal diffusivity, corresponding to the average temperature of the heated region at time t. But

$$T \sim \frac{Q}{r_f^3}, \tag{10.37}$$

so that $r_f^2 \sim aT^n t \sim aQ^n r_f^{-3n} t$, whence

$$r_f \sim (aQ^n)^{1/(3n+2)} t^{1/(3n+2)}. \tag{10.38}$$

The velocity of the thermal wave front is expressed by the proportionality

$$\frac{dr_f}{dt} \sim \frac{r_f}{t} \sim \frac{(aQ^n)^{1/(3n+2)}}{t^{(3n+1)/(3n+2)}} \sim \frac{aQ^n}{r_f^{3n+1}}. \tag{10.39}$$

This velocity decreases extremely rapidly as the wave propagates. For example, with $n = 5$, $dr_f/dt \sim 1/r^{16}$.

We seek an exact solution of the heat conduction equation in the self-similar form

$$T = \left(\frac{Q^{2/3}}{at}\right)^{3/(3n+2)} \varphi(\xi), \tag{10.40}$$

where the similarity variable ξ is defined as

$$\xi = \frac{r}{(aQ^n t)^{1/(3n+2)}}. \tag{10.41}$$

Substituting (10.40) into (10.36) we obtain an ordinary differential equation for the function $\varphi(\xi)$, which differs only slightly from the equation (10.26) for the plane case. This equation was solved by the late S. Z. Belen'kii, and independently by Barenblatt [2]*.

The final solution can be written in a form similar to (10.32)

$$T = T_c\left(1 - \frac{r^2}{r_f^2}\right)^{1/n}, \tag{10.42}$$

where the radius of the front is

$$r_f = \xi_1 (aQ^n t)^{1/(3n+2)}. \tag{10.43}$$

The constant ξ_1 is given by

$$\xi_1 = \left[\frac{3n+2}{2^{n-1} n\pi^n}\right]^{1/(3n+2)} \left[\frac{\Gamma(5/2 + 1/n)}{\Gamma(1 + 1/n)\Gamma(3/2)}\right]^{n/(3n+2)}.$$

The temperature at the center T_c is

$$T_c = \frac{4\pi}{3} \xi_1^3 \left[\frac{n\xi_1^2}{2(3n+2)}\right]^{1/n} \overline{T}, \tag{10.44}$$

where

$$\overline{T} = Q\sqrt{\frac{4\pi}{3} r_f^3}$$

is the temperature averaged over the volume at the time when the radius of the wave front is r_f.

For example, for $n = 5$, $\xi_1 = 0.79$ and $T_c = 1.28\overline{T}$. When the specific heat is variable, with $c_v \sim T^k$,

$$E = E_c\left(1 - \frac{r^2}{r_f^2}\right)^{1/n'}, \qquad T = T_c\left(1 - \frac{r^2}{r_f^2}\right)^{1/(n-k)}, \qquad n' = \frac{n-k}{1+k},$$

* The propagation of an almost-spherical thermal wave was considered by Andriankin and Ryzhov [3]. Andriankin [4] has also considered a spherical thermal wave with radiant energy taken into account.

as in the plane case. The thermal wave radius, instead of $r_f \sim t^{1/(3n+2)}$, is now given by $r_f \sim t^{1/(3n'+2)}$. For $n = 5$ and $k = 0$, $r_f \sim t^{1/17}$, $dr_f/dt \sim r_f^{-16}$; for $n = 5$ and $k = 0.5$, $n' = 3.0$, $r_f \sim t^{1/11}$, and $dr_f/dt \sim r_f^{-10}$.

The temperature distribution with respect to radius in the spherical case is exactly the same as in the plane case. The flux increases linearly with respect to the radius in almost the entire region from the center to the front and only drops to zero near the front:

$$S \sim -T^n \frac{\partial T}{\partial r} \sim \left(1 - \frac{r^2}{r_f^2}\right)^{1/n} r.$$

The divergence of the flux is almost constant over the entire sphere with the exception of a thin layer near the front. The gas is cooled comparatively uniformly, releasing energy which is absorbed near the front, and in this manner heating new layers of fluid.

Let us imagine a small volume of a gas in which a large amount of energy was rapidly released with the result that the fluid was heated to a very high temperature. A thermal wave will then travel from the place where the energy is released through the surrounding gas. The speed of propagation of a thermal wave, according to (10.39), decreases as the wave propagates and as the temperature of the heated spherical region decreases; the speed is given by $dr_f/dt \sim aQ^n/r_f^{3n+1}$. But $r_f \sim (Q/T)^{1/3}$, so that $dr_f/dt \sim aT^{n+\frac{1}{3}}Q^{-\frac{1}{3}}$. In the case of radiation heat conduction $n = 5$ and $dr_f/dt \sim T^{5.3}$. The speed of sound in a high-temperature gas, roughly speaking, is proportional to $\sqrt{T}$. Consequently, if the initial temperature is very high, the speed of propagation of the thermal wave is necessarily much greater than the speed of sound. When a wave travels through a stationary cold gas of constant density, the pressure of the gas increases. Roughly speaking, the pressure behind the front of a thermal wave is proportional to the temperature $p \sim \rho T$, so that the pressure distribution approximately follows the temperature distribution. The existence of the pressure gradient in the wave results in the acceleration of the gas; it then suddenly expands from the center, and redistributes its mass so that it tends to concentrate at the periphery, near the thermal wave front. The disturbances travel through the gas with the speed of sound. For this reason, when initially the thermal wave travels much faster than the speed of sound, the fluid behind it cannot acquire any appreciable motion. As we have seen, the propagating thermal wave is very rapidly decelerated. After a certain time its speed drops off to a value of the order of the speed of sound and then becomes less than the latter. Starting at this time, the heat conduction wave no longer travels ahead of the sonic disturbances, the fluid is set into motion, and a shock wave is formed which then moves ahead of the thermal wave, traveling with a speed which is of the order of magnitude of the speed of sound in the heated gas behind it. The process gradually comes to resemble that which is

described by the solution of the problem of a strong explosion (see §25, Chapter I). The time of formation of a shock wave and of its overtaking of the thermal wave thus approximately coincides with the time at which the speed of the thermal wave drops to the speed of sound in the heated gas.

It has been estimated that for air at standard density this takes place when the temperature in the heated spherical region drops to a value of the order of 300,000°K. If the initial temperature of the air at the time of energy release is much higher than this value, then there is a sharply defined stage at which the energy travels through the stationary air by radiation heat conduction in the form of a thermal wave. When the temperature of the expanding heated spherical region drops to ~300,000°K, a shock wave is formed which then moves ahead, and the role of the radiation heat conduction is reduced exclusively to that of equalizing the temperature in the central region. If, however, the initial energy concentration is such that the air temperature is below 300,000°K, then in general no thermal wave is formed, and the energy from the very beginning is transported by hydrodynamic means, carried by the shock wave.

It was noted at the end of §3 that the temperature profile at the lower edge of a thermal wave is the same as the temperature profile in the preheating zone of a very strong shock wave (in a very strong shock wave a "tongue" preheated by radiation heat conduction moves ahead of the shock front). In particular, the radiation at the very leading edge of the thermal wave is out of equilibrium, due to the presence of "unimpeded" photons, and the temperature drops to zero exponentially in the optical coordinate. This means that the visible luminosity of the surface of a thermal wave front is the same as the luminosity of the surface of a very strong shock front. It was shown in §4 of Chapter IX that this limiting luminosity, in air at standard density, corresponds to a brightness temperature in the visible region of the spectrum of approximately 17,000°K. The brightness temperature at the surface of the front of a thermal wave is also the same. Thus, observing from afar the thermal wave propagating through air, we shall "see" a temperature of the order of 17,000°K, despite the fact that the temperature in the central regions of the wave can be as high as many hundreds of thousands of degrees.

§7. Some self-similar plane problems

Let us consider several self-similar problems. Two of them will be treated by the semiqualitative method presented in §4. We shall obtain an exact solution for one of them.

Constant temperature on the boundary. Let a constant temperature T_0 be maintained at the boundary of the plane half space ($x = 0$) with zero initial temperature. A thermal wave travels from the boundary into the medium, as

shown in Fig. 10.5. Since there exists a characteristic temperature T_0, the coefficient of thermal diffusivity is of the order of $\chi \sim aT_0^n$, and the thermal wave front propagates according to the relation

$$x_f \sim (\chi t)^{1/2} \sim (aT_0^n t)^{1/2}.$$

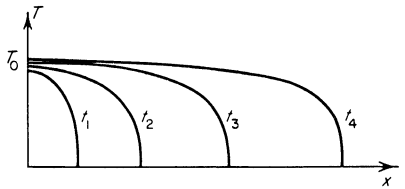

Fig. 10.5. Propagation of a thermal wave for a given temperature on the boundary.

The value of the numerical coefficient in this equation and the temperature distribution (obviously self-similar) can be found by numerical integration of an ordinary differential equation for the dimensionless function $f(\xi)$, where

$$T = T_0 f(\xi), \qquad \xi = \frac{x}{(aT_0^n t)^{1/2}},$$

subject to the boundary conditions $f(0) = 1$ and $f(\infty) = 0$.

The heat flux through the boundary decreases with time as

$$S \sim aT_0^n \frac{\partial T}{\partial x} \sim \frac{aT_0^{n+1}}{x_f} \sim \frac{aT_0^{n+1}}{(aT_0^n t)^{1/2}} \sim \frac{a^{1/2} T_0^{(n+2)/2}}{t^{1/2}}.$$

The change of energy in the thermal wave with time can be estimated by either of two means,

$$\mathscr{E} \sim \int_0^{x_f} T\, dx \sim T_0 x_f \sim t^{1/2}, \qquad \text{or} \qquad \mathscr{E} \sim \int_0^t S\, dt \sim \int_0^t \frac{dt}{t^{1/2}} \sim t^{1/2}.$$

Constant flux at the boundary. Let us assume that a constant heat flux S_0, externally supplied to the fluid, is specified at the boundary

$$S_0 = -\kappa \left(\frac{\partial T}{\partial x}\right)_0 = -c_v \rho a T^n \left(\frac{\partial T}{\partial x}\right)_0 = const \qquad \text{for} \quad x = 0.$$

The laws of propagation of the thermal wave and of the temperature change in the wave with time may be found by replacing all derivatives by their corresponding ratios. The flux across the thermal wave changes from S_0 to zero. The order of magnitude of the average temperature in the wave is given by

$$S_0 \sim c_v \rho \frac{aT^{n+1}}{x_f}.$$

From the heat conduction equation it follows, however, that in order of magnitude

$$\frac{T}{t} \sim \frac{S_0}{x_f}.$$

From these two approximate relations we find the equation of propagation of the thermal wave and the change of temperature with time:

$$x_f \sim (c_v \rho a S_0^n)^{1/(n+2)} t^{(n+1)/(n+2)}, \qquad T \sim \left(\frac{S_0^2}{c_v \rho a}\right)^{1/(n+2)} t^{1/(n+2)}.$$

For $n = 5$, $x_f \sim t^{6/7}$, $T \sim t^{1/7} \sim x_f^{1/6}$, $dx_f/dt \sim t^{-1/7}$.

The speed of the thermal wave decreases very slowly, and the average temperature slowly increases. The temperature increase appears because as the wave propagates the temperature gradient becomes smaller, and in order to maintain a constant flux the coefficient of thermal conductivity must increase. The propagation of the wave is shown in Fig. 10.6.

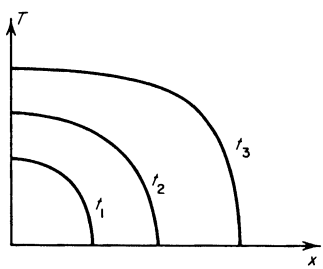

Fig. 10.6. Propagation of a thermal wave for a given flux at the boundary.

The dipole-type solution. Let the energy be released instantaneously in some layer near the plane boundary of the half space. Let us assume that immediately after the energy release the temperature at the boundary is made to fall very rapidly to a small value, practically to zero, and is maintained there. Despite the fact that the temperature at the boundary is very low, the heat flux through the boundary remains finite (correspondingly, the temperature gradient is very large), so that the energy flows out from the fluid. This problem does not admit an energy integral.

Let us idealize the problem in order to eliminate dimensional length parameters (for example, the thickness of the layer where the energy is released, or its distance from the boundary). We shall assume that the energy is released instantaneously in an infinitesimally thin layer at the surface of the body $x = 0$, in such a way that in the limit, when the thickness of the layer in which the energy release took place tends to zero and the layer itself

approaches the surface $x = 0$, the first moment of the temperature remains finite

$$\int_0^\infty xT(x, 0)\, dx < \infty.$$

It can be easily shown that in this case, under the condition that the temperature at the boundary is zero, the energy integral in the problem of an instantaneous plane source is replaced by a moment integral, and the first moment of the temperature is conserved in time. This proposition was proved by Barenblatt [5].

Let us multiply the heat conduction equation (10.23) by x and integrate it from 0 to ∞, noting that the flux at infinity vanishes. Integrating by parts, we get

$$\frac{d}{dt}\int_0^\infty xT(x, t)\, dx = +\frac{a}{n+1}\, T^{n+1}(0, t).$$

If $T(0, t) = 0$ at the boundary, then the first or dipole moment of the temperature is conserved in time,

$$\int_0^\infty xT(x, t)\, dx = P = const. \tag{10.45}$$

This problem is self-similar, since it contains only two dimensional parameters, P in deg · cm^2 and a in cm^2 · sec^{-1} · deg^{-n}. It was solved by Barenblatt and Zel'dovich [6], with reference to the process of gas filtration. The thermal wave front propagates as

$$x_f = \xi_0(\alpha P^n t)^{1/2(n+1)}.$$

The temperature can be expressed in the form

$$T = \left(\frac{P}{at}\right)^{1/(n+1)} M\left(\frac{x}{x_f}\right)^{1/(n+1)}\left[1 - \left(\frac{x}{x_f}\right)^{(n+2)/(n+1)}\right]^{1/n}, \tag{10.46}$$

where the numerical constants ξ_0 and M are given by

$$\xi_0 = (n+2)^{1/2}(n+1)^{-n/2(n+1)} n^{-1/2(n+1)} 2^{1/2(n+1)} \times \left[B\left(1 + \frac{1}{n}, \frac{n+1}{n+2} + 1\right)\right]^{-n/2(n+1)},$$

$$M = \left[\frac{n}{2(n+2)}\right]^{1/n} \xi_0^{2/n}.$$

Here $B(p, q)$ is the Beta function, which may be found tabulated.

For $n = 5$, the temperature function is

$$T \sim \frac{1}{t^{1/6}} \left(\frac{x}{x_f}\right)^{1/6} \left[1 - \left(\frac{x}{x_f}\right)^{7/6}\right]^{1/5},$$

and the front travels as

$$x_f \sim t^{1/12}, \qquad \frac{dx_f}{dt} \sim \frac{1}{t^{11/12}} \sim \frac{1}{x_f^{11}}.$$

The propagation of the thermal wave is shown in Fig. 10.7.

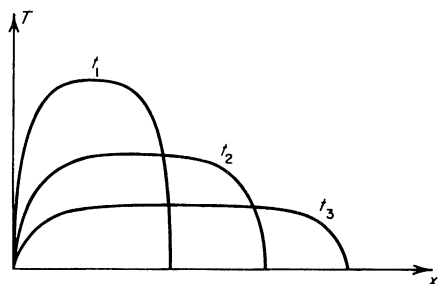

Fig. 10.7. The dipole-type solution.

It is evident that the flux through the boundary $x = 0$ is different from zero, and that energy flows out from the medium. Indeed, for $x/x_f \ll 1$,

$$T \sim \left(\frac{x}{x_f}\right)^{1/(n+1)},$$
$$S \sim T^n \frac{\partial T}{\partial x} \sim \frac{\partial T^{n+1}}{\partial x} \sim \frac{\partial}{\partial x}\left(\frac{x}{x_f}\right) \neq 0. \tag{10.47}$$

(The total energy $\mathscr{E} \sim x_f^{-1} \sim t^{-1/2(n+1)}$, *eds.*)

Barenblatt [2] investigated an entire class of self-similar solutions of plane problems subject to the very general conditions at the half-space boundary

$$T = const\ t^q, \qquad q \geqslant 0,$$

or

$$S = const\ t^q, \qquad q \geqslant 0$$

(the temperature or flux at the boundary increases with time following a power law). He also considered problems with cylindrical and spherical symmetry.

§8. Remarks on the penetration of heat into moving media

It was noted above that it is possible to neglect the motion of the medium when considering thermal waves because in the early stage of propagation of

the thermal wave from the source, when the temperature is very high, the propagation speed is much higher than the speed of sound and the fluid is simply unable "to get moving". In some cases, however, the motion of the medium is appreciable from the very beginning.

Let us assume that the temperature at the boundary of the medium increases with time according to the power law $T_0 = const\, t^q$ $(q > 0)$. The distance through which the heat is carried into the medium by the radiation heat conduction mechanism is given by the proportionality

$$x_f \sim (\chi t)^{1/2} \sim T^{n/2} t^{1/2} \sim t^{(nq+1)/2} \qquad (\chi \sim T^n). \tag{10.48}$$

The speed of the thermal wave is expressed by the proportionality

$$\frac{dx_f}{dt} \sim \frac{x_f}{t} \sim t^{(nq-1)/2}.$$

The shock wave travels from the energy source at the boundary of the medium into the medium with a speed of the order of the speed of sound in the heated fluid:

$$D \sim \sqrt{T} \sim t^{q/2}.$$

Let us compare the speeds of the thermal and shock waves, dx_f/dt and D. If $(nq-1)/2 < q/2$, $q < 1/(n-1)$, then at the beginning of the process as $t \to 0$ the speed of the thermal wave is always higher than that of the shock wave and the thermal wave outruns the shock. The motion of the medium at this stage can be neglected, as was done above. It is only starting at a certain time t', when D becomes greater than dx_f/dt, that the shock wave will move in front of the thermal wave and the fluid in the neighborhood of the thermal wave will be set into motion (obviously, there is no clearly defined time t' and the fluid is accelerated gradually; t' represents an effective boundary between these two stages).

If $(nq-1)/2 > q/2$, $q > 1/(n-1)$, the situation is reversed. As $t \to 0$, $D > dx_f/dt$, the shock wave outruns the thermal wave, and the thermal wave from the very beginning travels through a moving medium. Starting at a certain effective time t'', the thermal wave moves in front of the shock wave and then travels through a stationary medium. The mass of the moving fluid, which is proportional to $Dt \sim t^{(q/2)+1}$ (per unit area of surface), then makes up an increasingly smaller fraction of the mass heated by the thermal wave, which is proportional to $x_f \sim t^{(nq+1)/2}$.

In the intermediate case, $(nq-1)/2 = q/2$, $q = 1/(n-1)$, the speeds of the thermal and shock wave increase at the same rate with time. In this case, in general, the stages when the energy penetrates the medium by one method only (either by hydrodynamic means or by heat conduction) are not separable, as they are asymptotically in the cases $q \lesssim 1/(n-1)$. The fluid is heated by heat conduction and is set into motion almost simultaneously.

It is remarkable that in the particular case $n = 6$ (when the radiation mean free path $l \sim T^3$) the hydrodynamic equations with radiation heat conduction (but not radiation energy and pressure) taken into account admit a self-similar solution. This solution corresponds to the case when the temperature at the boundary of the medium increases as $T_0 \sim t^{1/5}$ (the existence of such a self-similar solution was pointed out by Marshak [7]). The reference density in this case is constant and equal to the initial density of the medium ρ_0, the pressure $p \sim \rho T \sim t^{1/5}$, and the fluid velocity $u \sim (p/\rho)^{1/2} \sim t^{1/10}$. The coordinate of the boundary of the disturbed region (the front of the thermal or shock wave) increases with time according to the relation

$$x \sim ut \sim (\chi t)^{1/2} \sim (T^6 t)^{1/2} \sim t^{11/10}. \tag{10.49}$$

The similarity variable in this case is $\xi = const\, xt^{-11/10}$, so that the solution of the equations is expressed in the form

$$T = const\, t^{1/5} f_1(\xi), \qquad u = const\, t^{1/10} f_2(\xi), \quad \text{etc.}$$

It is significant that a self-similar solution is possible when the thermal conductivity (radiation mean free path) is an arbitrary function of the density, $\chi = f(\rho)T^6$ (since the density scale is not time dependent). That the gasdynamic equations including radiation heat conduction actually admit the above self-similar solution can be easily verified from a direct examination of these equations*.

The character of the self-similar region for the case considered depends on which is larger, the speed of sound $c \sim \sqrt{T}$, or the speed with which the disturbances travel by heat conduction $x/t \sim (\chi/t)^{1/2}$. Both quantities increase with time as $t^{1/10}$, so that the relation between them is determined by the proportionality coefficients. For this reason the character of the process depends on the numerical value of the coefficient in the relation $T_0 \sim t^{1/5}$, determining the temperature increase with time at the boundary of the medium. A state is possible in which a shock wave travels ahead through the undisturbed fluid with a thermal wave following it through the heated and compressed fluid. Another state is possible in which the front of the thermal wave behind which the fluid is set into motion is the boundary between the disturbed and undisturbed regions.

In concluding we note the article by Nemchinov [8], in which some problems of radiative heat transfer including the motion of the medium are considered.

* We recall that the equations of continuity and of motion do not change when radiation heat conduction is included, but that an additional energy flux (10.8) is introduced into the energy equation (see §9, Chapter II).

§9. Self-similar solutions as limiting solutions of nonself-similar problems

Self-similar solutions are of interest not so much as particular solutions of a specific narrow class of problems, but mainly as limits which are asymptotically approached by solutions of more general problems that are not self-similar. This problem was investigated by Zel'dovich and Barenblatt [9], as applied to an initial value problem for the nonlinear heat conduction equation in the one-dimensional planar case (10.23).

The basic physical features of the asymptotic behavior of a solution can best be clarified by using an example of linear heat conduction for which the solution is particularly simple. Let the temperature distribution $T(x, 0) = T_0(x)$ along the x axis at the time $t = 0$ be given, with the temperature differing from zero only on a finite part of the x axis*. As is well known, the solution of the heat conduction equation (10.18) in this case is ($\chi = const$).

$$T(x, t) = \frac{1}{(4\pi\chi t)^{1/2}} \int_{-\infty}^{\infty} T_0(y) e^{-(x-y)^2/4\chi t}\, dy. \tag{10.50}$$

This is a generalization of the solution (10.20) to the case of a distributed source.

Let us consider the behavior of the temperature as $t \to \infty$ at large distances from the place where the heat was initially concentrated, for $x \gg y$. Expanding the integrand in a power series in the small quantity y/x we obtain

$$T(x, t) = \frac{1}{(4\pi\chi t)^{1/2}} e^{-\xi^2}\left[\int_{-\infty}^{\infty} T_0(y)\, dy + \frac{\xi}{(\chi t)^{1/2}} \int_{-\infty}^{\infty} T_0(y) y\, dy + \frac{2\xi^2 - 1}{4\chi t} \int_{-\infty}^{\infty} T_0(y) y^2\, dy + \cdots\right], \tag{10.51}$$

where

$$\xi = \frac{x}{(4\chi t)^{1/2}}.$$

The solution is seen to be a sum of self-similar terms, in which the powers of inverse time increase by 1/2 with each successive term, and the coefficients are expressed in terms of successive moments of the initial temperature distribution. In the limit $t \to \infty$ we are left with the first term in the brackets, corresponding to the solution of (10.18) for a concentrated source. The next term

* This initial condition is one applicable for the problem of nonlinear heat conduction. In the linear case the more general condition of a sufficiently rapid temperature decrease at infinity is permissible.

in the expansion, which characterizes the difference between the actual and the limiting solution, is of the order of $1/t^{1/2}$ with respect to the leading term,

$$T = T_{\text{lim}}\left[1 + \frac{\varphi(\xi)}{t^{1/2}} + \cdots\right]. \tag{10.51'}$$

Since the coordinate origin, the time origin, and the temperature scale in (10.18) can be chosen arbitrarily (that is, the group of transformations $x' = x - x_0$, $t' = t + \tau$, $T' = kT$ are admissible), this equation admits of a more general self-similar solution than (10.20), given by

$$T_{\text{sim}}(x - x_0, t + \tau, Q) = \frac{Q}{[4\pi\chi(t+\tau)]^{1/2}}\, e^{-(x-x_0)^2/4\chi(t+\tau)}. \tag{10.52}$$

This solution corresponds to the instantaneous release of a definite amount of heat $E = c_v \rho Q$ at the point $x = x_0$ and at the time $t = -\tau$.

It can be easily proved that by a proper choice of the parameters x_0, τ, and Q we can obtain a self-similar solution of the type (10.52) which describes the exact solution (10.51) better than does the self-similar solution (10.20), in which $x_0 = 0$ and $\tau = 0$. Indeed, let us expand the function (10.52) in a power series in the small parameters x_0/x and τ/t (in the limit $t \to \infty$, $x \to \infty$). Comparing the expansion with the exact solution (10.51), we see that by choosing the values of Q, x_0, and τ so that

$$\begin{aligned} Q &= \int_{-\infty}^{\infty} T_0(y)\, dy, \\ x_0 &= \frac{\int_{-\infty}^{\infty} T_0(y) y\, dy}{\int_{-\infty}^{\infty} T_0(y)\, dy}, \\ \tau &= \frac{\int_{-\infty}^{\infty} T_0(y) y^2\, dy}{2\chi \int_{-\infty}^{\infty} T_0(y)\, dy} - \frac{x_0^2}{2\chi}, \end{aligned} \tag{10.53}$$

terms of the order of $t^{-1/2}$ and t^{-1} in the expansion disappear, so that

$$T(x, t) = T_{\text{sim}}(x - x_0, t + \tau, Q)\left[1 + \frac{\psi}{t^{3/2}} + \cdots\right]. \tag{10.54}$$

The second term in the brackets in (10.54) is a higher order quantity as $t \to \infty$, than is the second term in (10.51').

The physical reason for the better agreement of the similar solution (10.52)

with the exact solution lies in the fact that (10.52) corresponds to an instantaneous release of the same amount of heat at the point x_0, which is the center of gravity $\bar{x}$ of the initial temperature distribution $T_0(x)$. The instant of energy release corresponds to the time required for the heat to acquire the same lateral dispersion (measured by the second moment) relative to the center of gravity as has the initial temperature distribution. The "effective" amount of heat $E = c_v \rho Q$ in the improved similar solution (10.52) is found to be exactly equal to the actual amount of heat $c_v \rho \int_{-\infty}^{\infty} T_0(x)\, dx$. In a similar manner it is possible to find a self-similar solution which best approximates the exact solution with distributed heat sources in the case of nonlinear heat conduction.

The self-similar solution of (10.23) corresponding to an instantaneous heat release at the point $x = 0$ at the time $t = 0$ was given in §5 (equations (10.32), (10.33), (10.31), and (10.30)). It was shown in [9], which also discusses the mathematical features of this problem, that by an appropriate shift in position and time, that is, by properly selecting x_0 and τ, it is possible to obtain a self-similar solution $T(x - x_0,\ t + \tau,\ Q)$, which differs from the exact solution $T(x, t, Q)$ by terms of order higher than $t^{-(2n+3)/(n+2)}$*.

§10. Heat transfer by nonequilibrium radiation

Let us imagine that a spherical region of radius R_0 has been formed in low density air at a temperature T high enough that the heated sphere is completely transparent to its own thermal radiation and radiates as a volume radiator. If the radiation mean free path which characterizes the emission

* *Editors' note.* Since the energy and first moment integrals are both conserved in the nonlinear case also, Q and x_0 are still given by the expressions of (10.53). The second moment obeys the law

$$\frac{d}{dt}\int_{-\infty}^{\infty} Tx^2\, dx = \frac{2a}{n+1}\int_{-\infty}^{\infty} T^{n+1}\, dx,$$

and when taken about the center of gravity must approach $(t+\tau)^{2/(n+2)}$ asymptotically. Let us define $\tau'(t)$ by

$$t + \tau'(t) = \frac{\int_{-\infty}^{\infty} Tx^2\, dx - x_0^2 Q}{\frac{(n+2)a}{n+1}\int_{-\infty}^{\infty} T^{n+1}\, dx},$$

and note that $\tau'(0)$ is given by an analogue of the formula for τ in (10.53). The quantity $\tau' \to \tau$ as $t \to \infty$. We can show (with $n > 0$) that $d\tau'/dt \geqslant 0$, so that τ' approaches its limit τ monotonically from below. Thus $\tau'(0)$, although useless in general as an estimate for τ, does serve as a lower bound.

coefficient of the air is $l_1(T)$, then the condition for transparency is $l_1(T) \gg R_0$. (We recall that the radiation mean free path, as a rule, increases rapidly with increasing temperature.) Photons born in the highly heated region leave almost unimpeded and are absorbed in the surrounding layers of cold air. The air in the central sphere is thus cooled by light emission and the peripheral layers are heated by light absorption. The heated region expands and the temperature in it drops. The process is quite similar to that of propagation of a thermal wave, with the difference, however, that the radiation that transfers the energy is here substantially out of equilibrium. This process of the transfer of heat by nonequilibrium radiation was treated by Kompaneets and Lantsburg [10, 11].

The radiation, having been absorbed first in the opaque peripheral layers of the sphere, heats them to a temperature T^* at which the air becomes transparent. Let the mean free path of photons which carry the major part of the energy of the radiation spectrum of the central sphere with temperature T be l_T in the peripheral region. It depends both on the characteristic frequencies (on T) and on the temperature of the air in which the absorption takes place. It is clear that the approximate condition which defines the transparency temperature T^* is

$$l_T(T^*) = R, \tag{10.55}$$

where R is the radius of the heated sphere, which increases with time in comparison with the initial radius R_0. The temperature distribution is illustrated in Fig. 10.8.

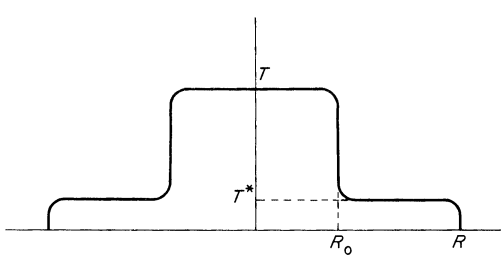

Fig. 10.8. Nonequilibrium radiation from a very hot central region.

If the temperature T in the central sphere is initially very high and the air in it is highly transparent to radiation, then the transparency temperature T^* is found to be appreciably lower than T, and the radiation born in the peripheral layers with temperatures of the order of T^* can be neglected. In this case the rate of expansion of the heated region is determined simply by an energy balance equation. The amount of energy radiated during the time

interval dt at a time t in the highly heated central region is of the order of

$$\frac{cU_p(T)}{l_1(T)}\frac{4\pi R_0^3}{3}\,dt,$$

where $U_p = 4\sigma T^4/c$. This energy is absorbed in a peripheral layer of thickness dR and radius R and the air in this layer is heated to a temperature which is of the order of the transparency temperature T^*. It follows that

$$\frac{cU_p(T)}{l_1(T)}\frac{4\pi R_0^3}{3}\,dt = 4\pi R^2\,dR\,\rho\varepsilon(T^*),$$

where ρ is the density and ε is the specific internal energy of the air. From this we obtain the rate of expansion of the sphere

$$v = \frac{dR}{dt} = \frac{cU_p(T)}{\rho\varepsilon(T^*)}\frac{R_0}{3l_1(T)}\left(\frac{R_0}{R}\right)^2. \tag{10.56}$$

Here T, the temperature in the radiating central region, drops in accordance with the cooling equation

$$\rho\frac{d\varepsilon(T)}{dt} = -\frac{cU_p(T)}{l_1(T)}. \tag{10.57}$$

From (10.56) it might appear that the velocity of the sphere boundary v can be as large as we wish, even larger than the speed of light (if the radiation energy density U, which is of the order of $U_p R/l_1$ is higher than the energy density of the medium $\rho\varepsilon$). In fact, however, this is not so for the reason that (10.56) is valid only for the case when $v \ll c$. If the rate of expansion of the sphere is comparable with the speed of light, then this means that the radiated energy is used up not only in heating the medium, but also in "filling" the expanding sphere with radiation. Mathematically this is expressed by the fact that the velocity v is proportional not to $U/\rho\varepsilon$ but to $U/(U + \rho\varepsilon)$, and this automatically sets an upper limit for the velocity v which is less than c.

As the heated sphere expands and the air in the central region is cooled, the latter becomes less and less transparent and the temperatures T and T^* approach each other. When they become equal opaqueness sets in. At the same time the radiation from the peripheral layers, which sends photons not only outward, as from the central region, but also back into the interior of the sphere, becomes appreciable. The radiation density in the sphere then approximates the equilibrium density at the given temperature, and gradually the process takes on the character of the thermal wave considered in the preceding sections.

In order to indicate better how the transition takes place from one regime

to the other at the transparency condition for the entire sphere, $T \approx T^*$, $l_1 \approx R$, let us estimate the speed of propagation of the boundary of the heated sphere in this limiting case from the formulas for nonequilibrium and thermal waves, respectively.

In the nonequilibrium regime, in the limit R tending to l_1 (from the side $R \ll l_1$) and T tending to T^*, the radiation comes not only from the central sphere but from the entire heated region, so that in the energy balance equation as expressed by formula (10.56) we should substitute R for R_0. Then, to the right order of magnitude with $T \sim T^*$ and $R \sim l_1$,

$$v \sim c \frac{U_p}{\rho\varepsilon} \frac{R}{l_1} \sim c \frac{U_p}{\rho\varepsilon}. \tag{10.58}$$

On the other hand, in the equilibrium regime the speed of the thermal wave is given approximately by

$$v = \frac{dR}{dt} \sim \frac{\chi}{R} \qquad [R \sim (\chi t)^{1/2}],$$

where the coefficient of radiation thermal conductivity χ, according to the definition (10.11), can be written in the form $\chi \sim lc\, U_p/\rho\varepsilon$. It follows that in order of magnitude the speed of the thermal wave is

$$v \sim c \frac{U_p}{\rho\varepsilon} \frac{l}{R},$$

where in the equilibrium case $R \gg l$. If we now let R tend to l, we obtain at the transparency condition, $R \sim l \sim l_1$, the same value as (10.58), $v \sim c\, U_p/\rho\varepsilon$.

XI. Shock waves in solids

§1. Introduction

The study of the laws governing the propagation of shock waves through condensed media, such as metals, water, etc., is of great theoretical and practical importance. In particular, such studies are necessary for the understanding and calculation of explosion phenomena. The theoretical analysis of data obtained from such studies yields information on the equation of state of solids and liquids subjected to high pressures, which is very important in the solution of a large number of problems in geophysics, astrophysics, and other branches of science.

A knowledge of the thermodynamic properties of the medium is necessary for describing the hydrodynamic processes which take place within it. While no appreciable difficulties are encountered in calculating the thermodynamic properties of gases, a theoretical description of the thermodynamic properties of solids and liquids at the high pressures generated by very strong shocks presents a very complex problem, which at the present time is still very far from understood. Therefore, experimental methods play a major role in the study of condensed media in a compressed state.

Until recently, the physics of high pressures was limited to the study of media compressed under static conditions in piezometers of various design. However, the pressures obtainable by this means can not exceed a hundred thousand atmospheres without the construction of extremely large facilities. Also, and more important, it is impossible to provide conditions for reliable measurements, since under higher pressures the piezometer bomb deforms, preventing the measurement of physical properties to the accuracy desired. Nevertheless, many problems in modern science and engineering are concerned with pressures of hundreds of thousands and millions of atmospheres.

In the postwar years, both in the USSR and in other countries, it was suggested that dynamic methods, based on the utilization of strong shock waves, be used for obtaining high pressures and compressions. Shock waves in metals and other condensed media with pressures of hundreds of thousands and millions of atmospheres were obtained and investigated. In the USSR these new methods were developed in works by Al'tshuler, Kormer, Krupnikov, Ledenev, Bakanova, Sinitsyn, Funtikov, Zhuchikhin, and others [1–5], and in the USA by Walsh, Christian, Mallory, Goranson, Bancroft, McQueen, Marsh, and others [22–26].

Soviet scientists were particularly successful in this direction, having succeeded in obtaining record pressures of five million atmospheres (the American authors investigated weaker shock waves; papers reporting the attainment of pressures of two million atmospheres, which were the highest achieved by them, were published later than those of the Soviet authors*). For the first time in the history of mankind a solid body was compressed by a factor of 2 or more; until then such a dense medium could be "encountered" only in the central regions of the earth and of other cosmic bodies. These outstanding achievements in obtaining high pressures and densities in solids have made it possible to draw a large number of interesting conclusions on the thermodynamic behavior of media under such extraordinary conditions and to determine by semi-empirical means important thermodynamic characteristics of highly compressed metals. The extremely short duration of the impact loads required seeking new measurement techniques that would permit the determination of physical properties under conditions of high-rate processes, and required the design of appropriate instrumentation. A large contribution in this direction was made by the Soviet investigators Tsukerman, Shnirman, Dubovik, Kevlishvili, Zavoiskii, and others [6–12].

The basic feature distinguishing the condensed from the gaseous state and determining the behavior of solids and liquids compressed by shock waves is the strong interaction between the atoms (or molecules) of the medium. The range of interatomic forces is very limited. It is of the order of the dimensions of the atoms and molecules, of the order of 10^{-8} cm. In a sufficiently rarefied gas, where the average distances between particles are very much greater than the particle dimensions, the interaction takes place mainly through collisions, during which the atoms or molecules approach each other closely.

The pressure in a gas is of thermal origin; it is related to the transfer of momentum by particles participating in the thermal motion, and is always proportional to the temperature: $p = nkT$. Relatively small pressures are required to compress a gas strongly. The limiting compression of atmospheric gas across a shock wave, as dictated by the conservation laws, is reached for pressures behind the front of several tens or a hundred atmospheres, so that a shock wave of this strength may be regarded as strong.

The behavior of a condensed medium with respect to a compression is different. The atoms or molecules of solids and liquids are close to each other and interact strongly. This interaction, in particular, is responsible for holding the atoms within the body. The interaction forces have a dual character. On the one hand, particles separated by sufficiently large distances are attracted to each other; on the other hand, when brought close together they

* This refers to the earliest publications (Soviet and American). In subsequent years papers have appeared describing investigations at still higher pressures. See the review [55].

repel each other as a result of the interpenetration of the electronic shells of the atoms. Equilibrium distances of atoms in a solid body in the absence of external pressure correspond to a mutual compensation between the attractive and repulsive forces, to a minimum in the interaction potential energy. In order to separate the atoms by a large distance, it is necessary to overcome the binding forces and to supply energy equal to the binding energy, which for metals is of the order of several tens or hundreds of kcal/mole (of the order of several ev/atom)*. In order to compress a material it is necessary to overcome the repulsive forces, which increase very rapidly as the atoms are brought together. The compressibility of metals is, by definition, $\kappa_0 = -(1/V) \cdot \partial V/\partial p$, and at standard conditions is of the order of 10^{-12} cm^2/dyne $\approx 10^{-6}$ atm^{-1}. In order to compress a cold metal by 10% an external pressure of 10^5 atm must be applied; the compressibility usually decreases with increasing pressure. Compression of metals by a factor of 2 requires pressures of the order of several million atmospheres.

Thus, a strong compression of a condensed medium generates a colossal internal pressure, even in the absence of heating, due only to the repulsive forces between the atoms. The existence of this nonthermal pressure, which is not a property of gases, determines the basic features of the behavior of solids and liquids compressed by shock waves. As we shall see below, the material is also very strongly heated by strong shock waves, and this results in the appearance of a pressure associated with the thermal motion of the atoms (and electrons). This pressure is referred to as "thermal" pressure, in contrast to the elastic or "cold" pressure caused by the repulsive forces. In principle, as the shock strength tends to infinity, the relative importance of the thermal pressure increases and, in the limit, the elastic pressure becomes small in comparison with the thermal pressure; under the action of extremely strong waves the initially solid medium behaves as a gas. However, for shock waves with pressures of the order of millions of atmospheres, as obtained in the laboratory, these two pressures are of comparable magnitude. The elastic pressure is dominant in weaker shock waves, with pressures of the order of hundreds of thousands of atmospheres and below. The thermal energy of the material compressed by the shock wave is also small in this case. Essentially all of the internal energy acquired by the medium from the wave is expended in overcoming the repulsive forces due to the compression and is concentrated in the form of potential elastic energy. The speed of propaga-

* The binding forces in solids are of various types. In accordance with their nature, solids are usually subdivided into five groups: (1) ionic crystals—for example, NaCl, with a binding energy $U = 180$ kcal/mole; (2) crystals with a covalent bond—for example, diamond, $U = 170$ kcal/mole; (3) metals, $U \sim 30$–200 kcal/mole; (4) molecular crystals, bound by van der Waals forces, with a weak bond—for example, for CH_4, $U = 2.4$ kcal/mole; (5) crystals with hydrogen bonds—for example, ice, $U = 12$ kcal/mole. Here we shall be mainly interested in metals.

tion of small disturbances in a condensed medium is, in contrast to gases, not temperature dependent. It is determined by the elastic compressibility of the medium.

The numerical characterization of the "strength" of a shock wave is also different in solids. The strength of a wave in gases is measured by the pressure ratio across the wave front. The limiting density ratio of about 4 to 10 is obtained when this ratio is equal to several tens or a hundred. In this case the shock wave velocity is considerably greater than the speed of sound in the initial gas, and the gas behind the front is accelerated to velocities close to that of the shock wave. If the gas was initially at atmospheric pressure, then a shock wave with a strength of even a hundred atmospheres is regarded as strong. In a solid or liquid, a shock wave with a strength of even a hundred thousand atmospheres is regarded as weak. Such a wave differs little from an acoustic wave: it travels with a speed close to the speed of sound, compresses the material by only a few percent or perhaps of the order of ten percent, and imparts a velocity to the material behind the front which is of the order of a tenth the velocity of the wave itself. If we characterize the strength of the shock wave by the ratio of its speed to the speed of sound in the undisturbed medium or by the closeness of the density ratio to its limiting value, then a strong wave for condensed media is one whose pressure is not less than tens or hundreds of millions of atmospheres.

In this chapter we shall consider in detail the physical behavior of solids at high pressures and densities, we shall familiarize ourselves with the properties of shock compression, we shall describe experimental methods for studying shock waves moving through solids, and we shall discuss the results obtained by these methods. We shall also consider some physical phenomena observed in the passage of shock waves through metals and other media and on unloading of the substance, when a shock wave reaches a free surface.

A great deal of valuable information about these problems may be found in the recently published review by Al'tshuler [55], in which a large amount of experimental data are brought together and analyzed.

1. Thermodynamic properties of solids at high pressures and temperatures

§2. Compression of a cold material

The pressure p and the specific internal energy ε of a solid material can be divided into two parts. The first part, the elastic component p_c or ε_c, is related exclusively to the forces of interaction between the atoms of the

medium* and is entirely independent of the temperature. The other part, the thermal component, is related to the heating of the body, that is, with the temperature. The elastic components p_c and ε_c depend only on the density of the material ρ or the specific volume $V = 1/\rho$ and are equal to the total pressure and specific internal energy at absolute zero temperature; that is why they are sometimes called the "cold" pressure and energy. In this section we shall consider only the elastic components of the pressure and energy. Therefore we shall assume that the body is at absolute zero.

The state of mechanical equilibrium of a solid at zero temperature and pressure† is characterized by the mutual compensation of the interatomic forces of attraction and repulsion and by a minimum in the elastic potential energy; this minimum can be taken as the origin for the energy $\varepsilon_c = 0$‡. Let us denote the specific volume of a body in this state ($p = 0$, $T = 0$) by V_{0c}. This volume is slightly smaller than the volume V_0 of the body under standard conditions ($p = 0$ or 1 atm, which are equivalent, and $T_0 \approx 300°\text{K}$), since heating the material from absolute zero to room temperature T_0 results in a thermal expansion, discussed in the following section. The standard volume of metals V_0 is usually 1–2% larger than V_{0c}, which we shall call the zero volume. In many cases the small difference in volume between V_0 and V_{0c} can be neglected. In considering the behavior of a solid whose volume is being changed, we shall be referring to the compression (and expansion) of the body isotropically in all directions, without discussing the effects connected with the anisotropy of the elastic properties, shearing strain, strength, etc., which are present at comparatively low pressures and compressions.

The potential energy curve for a body as a function of its specific volume V has the same qualitative character as the potential energy curve for the interaction of two atoms of a molecule as a function of the internuclear distance. This curve is shown schematically in Fig. 11.1. If the volume V is greater than the zero volume V_{0c}, then the attractive forces predominate. The interaction forces fall off rapidly as the distance between the atoms increases. Hence when the volume increases, when the atoms move farther apart, the potential energy increases asymptotically to a constant value U equal to the binding energy of the atoms in the body. The energy which must be expended to

* We shall be dealing primarily with metals, which are composed of atoms rather than molecules.

† Atmospheric pressure is negligibly small in comparison with the pressures which arise even for very small changes in the volume of the body. Therefore it makes no difference whether the body is in vacuum ($p_c = 0$) or at atmospheric pressure ($p_c = 1$ atm).

‡ At absolute zero the atoms perform so-called zero-point oscillations, with an energy $h\nu/2$ per normal vibration mode of frequency ν. This energy can be accounted for in the potential energy $\varepsilon_c(V)$ in such a way that ε_c is measured from the zero-point vibrational level in the equilibrium state of the body at $p_c = 0$.

remove all atoms of a unit mass of a material to infinity is given by U; it is approximately equal to the heat of vaporization of the body (strictly speaking, it is equal to the heat of vaporization at absolute zero). Heats of vaporization for metals are usually of the order of several tens or hundreds of kcal/mole,

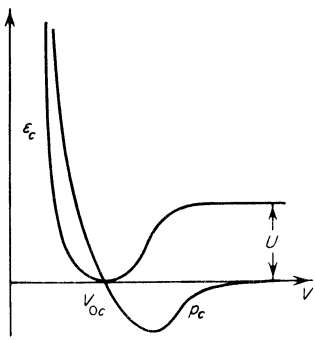

Fig. 11.1. Potential energy and elastic pressure curves of a body as a function of the specific volume.

of several electron volts per atom*. The binding forces weaken at distances of the order of the dimensions of an atomic cell, so that the curve of $\varepsilon_c(V)$ approaches its asymptote $\varepsilon_c(V) = U$ when the body expands by an order of magnitude (say when the distance between the atoms doubles).

The repulsive forces, which increase sharply with decreasing interatomic distance, dominate when a body is compressed, and thus the potential energy $\varepsilon_c(V)$ increases rapidly when the volume is less than its zero value. In order to have some idea of the rate of increase and of the order of magnitude of the energy, we note that according to [1] the energy needed for the cold compression of iron by 7% is $\varepsilon_c = 5.25 \cdot 10^8$ erg/g $= 0.03$ ev/atom, and for compression by a factor of 1.5 is $\varepsilon_c = 2.42 \cdot 10^{10}$ erg/g $= 1.4$ ev/atom (here the pressures are equal to $p_c = 1.31 \cdot 10^5$ atm and $p_c = 1.36 \cdot 10^6$ atm, respectively).

The elastic pressure is related to the potential energy by

$$p_c = -\frac{d\varepsilon_c}{dV}, \tag{11.1}$$

which formula has a natural mechanical meaning (increase of energy is equal to the work of compression) and can be regarded as the equation for the isotherm or isentrope of cold compression. Indeed, (11.1) follows from the general thermodynamic relation $T\,dS = d\varepsilon + p\,dV$, in which we set T equal to zero. But if $T = 0$ then the entropy S, according to Nernst's theorem, is

* For example, for iron—94 kcal/mole $= 4.1$ ev/atom $= 6.96 \cdot 10^{10}$ erg/g; for aluminum —55 kcal/mole $= 2.4$ ev/atom $= 8.45 \cdot 10^{10}$ erg/g.

also equal to zero, and hence remains constant. Therefore, the isotherm $T = 0$ is also the isentrope $S = 0$.

The pressure curve $p_c(V)$ is also shown schematically in Fig. 11.1. The elastic pressure at the point $V = V_{0c}$ is zero; the pressure increases rapidly with compression, and, at least formally, becomes negative with expansion. The negative sign on the pressure describes the physical fact that in order to expand the body from the zero volume corresponding to mechanical equilibrium at $T = 0$ and $p = 0$, a tensile force must be applied to the body. This force must overcome the binding forces tending to return the body to the equilibrium volume V_{0c}.

The process of cold expansion $p_c(V)$ for $V > V_{0c}$ cannot be directly followed experimentally, since it is not possible in practice to achieve a strong extension of a metal in all directions. The magnitude of the negative pressures can be estimated from the heat of vaporization of the material. By definition, the area under the curve for cold expansion from zero volume to infinity is

$$\int_{V_{0c}}^{\infty} p_c(V)\, dV = -U. \tag{11.2}$$

If the binding forces weaken considerably when the body expands by a factor of approximately 10 (the interatomic distance is about doubled), then the maximum negative pressure is of the order $p_{\max} \sim U/10V_{0c}$, which for iron, for example, is $p_{\max} \sim 6 \cdot 10^{10}$ bar $= 6 \cdot 10^4$ atm*.

The slope of the elastic pressure curve at the point of zero pressure corresponds to the definition of the compressibility of the material under ordinary conditions (the isentropic compressibility differs only slightly from the isothermal compressibility; at $T = 0$ they are identical). The compressibility of iron is

$$\kappa_0 = -\frac{1}{V_0}\left(\frac{\partial V}{\partial p}\right)_{T_0} = 5.9 \cdot 10^{-13} \quad \text{bar}^{-1},$$

from which

$$-V_{0c}\left(\frac{dp_c}{dV}\right)_{V=V_{0c}} \approx 1.7 \cdot 10^{12} \quad \text{bar}.$$

The slope of the cold compression curve determines the speed of propagation of elastic waves in the body, the speed of sound. It will be shown later that in a solid there exist several "speeds of sound". For the time being we note that the speed of sound defined in the ordinary manner in terms of the

* This value is appreciably greater than the ultimate tensile strength of iron, which is usually of the order of 10^9 bar $= 10^3$ atm. The low value of the tensile strength is related to the one-sided character of the extension, to the cracks which are present in actual metals, to the polycrystalline structure, etc. We note that the ultimate strength of some types of iron can reach 1 to $2 \cdot 10^4$ atm.

compressibility $c_0 = V|\partial p/\partial V|_S^{1/2}$, is equal to 5.85 km/sec for iron at standard conditions.

Theoretical calculations of cold compression curves $p_c(V)$ or $\varepsilon_c(V)$ in the range of compressions and pressures attainable in practice are based on a quantum-mechanical consideration of the interatomic interaction. In a number of cases it is possible to obtain satisfactory agreement with experimental compressibility data, in particular for alkaline and alkaline-earth metals at low pressures. A detailed presentation of these calculations and a comparison with the experimental data of Bridgman on the static compression of materials up to several tens of thousands of atmospheres can be found in the book of Gombàs [13], in which may also be found references to the literature. Detailed data on cold compression curves for a number of metals (and also for sodium chloride) up to pressures of several million atmospheres and densities approximately twice standard were obtained by Al'tshuler, Krupnikov, Kormer, Bakanova, Trunin, Pavlovskii, Kuleshova, and Urlin [1–5, 14, 15], from theoretical analysis of experimental shock compression results (see [55]). We shall say more about these experiments later on; here for illustration we present the $p_c(V)$ and $\varepsilon_c(V)$ curves for iron (Fig. 11.2).

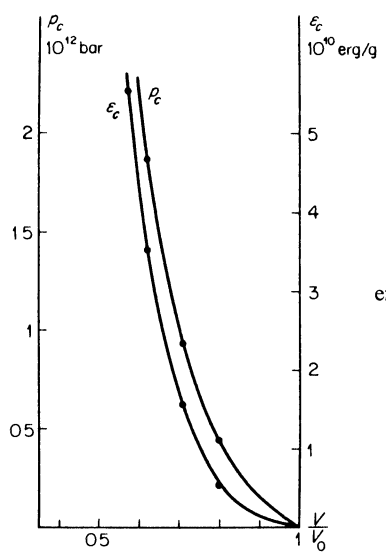

Fig. 11.2. Elastic pressure p_c and energy ε_c of iron (from the data of [1]).

Theoretically it is possible to establish a limiting law for the cold compression of a material at very high pressures and densities. Under conditions of very strong compression the electronic shells of atoms, to some extent, lose their individual structure. The state of the material in this case can be approximately described by the Thomas–Fermi statistical model of an atom,

or, somewhat more exactly, by the Thomas–Fermi–Dirac model (the latter model takes exchange energy into account)*. The equation of state for a material in the Thomas–Fermi model was discussed in §13 of Chapter III. In the limit of very high pressures and densities the cold compression pressure is

$$p_c \sim \rho^{5/3} \sim V^{-5/3}. \tag{11.3}$$

This is also only a limiting law for this statistical model of the atom, since for compressions which are not too large the model gives another dependence for $p_c(V)$. In order to compare the actual elastic pressure curves with those obtained from the statistical model, we present a logarithmic plot from [1] which gives the experimental curve for iron and the curves calculated by the Thomas–Fermi and Thomas–Fermi–Dirac methods (Fig. 11.3). It is evident

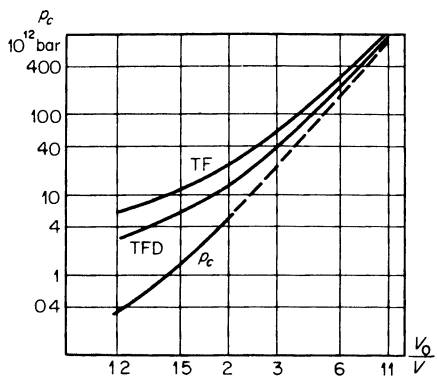

Fig. 11.3. Elastic pressure p_c for iron. p_c is the experimental curve; TF is the calculated Thomas–Fermi curve, and TFD is the calculated Thomas–Fermi–Dirac curve. The dashed line is an extrapolation of the p_c curve.

from the plot that for compressions of 1.2–1.8 (which have been obtained experimentally) the statistical models greatly overestimate the pressure. Gandel'man [37] has carried out quantum-mechanical calculations of the cold compression curve of iron over a wide range of pressures.

§3. Thermal motion of atoms

The atoms of a material are set into motion by heating. A definite energy and pressure are connected with the thermal motion of the atoms. At temperatures of the order of tens of thousands of degrees and above the thermal excitation of the electrons plays an important role. As noted in the preceding

* Calculations by the Thomas–Fermi–Dirac method have a real meaning only in those cases when the exchange correction is small. They essentially indicate the limits of applicability of the Thomas–Fermi method. If the exchange correction is found to be large, it shows that the Thomas–Fermi–Dirac method is no longer valid.

section, the total energy and pressure can be represented as a sum of their elastic and thermal contributions. The thermal contributions, in turn, can be broken up into two parts, one part corresponding to the thermal motion of the atoms (or rather their nuclei) ε_T, p_T, and another part corresponding to the thermal excitation of the electrons ε_e, p_e. The specific internal energy and pressure of a solid can then be written as

$$\varepsilon = \varepsilon_c + \varepsilon_T + \varepsilon_e, \tag{11.4}$$

$$p = p_c + p_T + p_e. \tag{11.5}$$

The electronic terms will be discussed later. At temperatures below approximately ten thousand degrees, these terms are small and can be neglected in (11.4) and (11.5).

Let us consider the thermal motion of the atoms, without making a distinction between a solid and a liquid and without discussing the effect of melting. Thermal motion of the atoms in a liquid differs very little from that in a solid. From an energy point of view melting has a very small effect on the thermodynamic properties of a substance at high temperatures of the order of ten thousand degrees and above, since the heat of fusion is comparatively small. For example, for lead at standard pressure the melting point is $T_{\text{melt}} = 600°\text{K}$, and the heat of fusion $U_f = 1.3$ kcal/mole, which corresponds to 650°K if we divide this quantity by the gas constant $\mathscr{R} = 2$ cal/deg · mole; for iron $T_{\text{melt}} = 1808°\text{K}$, $U_f = 3.86$ kcal/mole, and $U_f/\mathscr{R} = 1940°\text{K}$.

If the temperature is not too high, the atoms of a solid (and of a liquid) undergo small vibrations about their equilibrium positions (the crystal lattice sites in a solid). These vibrations are harmonic as long as their amplitude is much smaller than the interatomic distance, in other words, as long as the vibrational energy (of the order of kT per atom) is appreciably less than the height of the potential barrier which prevents the atoms from jumping from the lattice sites into the interstitial space or into other vacant sites. The height of the barrier in a solid at standard density is of the order of one or several electron volts*, so that the value of kT is comparable with the height of the potential barrier at temperatures of the order of ten or several tens of thousands of degrees. At higher temperatures the atoms are almost completely free to move within the body, and the thermal motion loses its oscillatory character and becomes closer to a random motion, akin to that in a gas. Thus the substance is transformed into a dense gas of strongly interacting atoms.

The situation becomes different, however, when the heating is accompanied

* This quantity is approximately equal to the activation energy for self-diffusion of atoms in the body ΔU. It is usually somewhat less than the binding energy, but of the same order of magnitude, $\Delta U \approx (0.5\text{–}0.7)U$.

by compression. The compression very sharply increases the repulsive forces between neighboring atoms, with the result that the height of the potential barrier which must be overcome by the atom in order to move out of its cell (from its site in the crystal lattice) sharply increases. Free displacement of the atoms in the body becomes very difficult and the motion of the atom remains limited to the space of its cell. This is illustrated in Fig. 11.4.

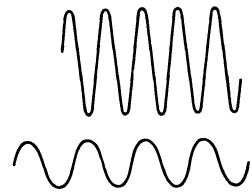

Fig. 11.4. Schematic diagram illustrating the change in height of the potential barrier for atoms in a compressed solid.

Within some rough approximation we can regard the thermal motion of the atoms in a compressed material as small vibrations about their equilibrium positions even at the maximum temperatures of 20,000–30,000°K attainable in the strongest shock waves which have been studied experimentally.

At temperatures above several hundreds of degrees Kelvin quantum effects play no role in the vibrations and the specific heat of a body whose atoms vibrate harmonically is equal to its classical value of $3k$ per atom or $c_v = 3Nk$ per unit mass, where N is the number of atoms per unit mass. To take into account the difference of the specific heat from its value at low temperatures where quantum effects are important, let us express the thermal energy connected with vibrations of the atoms in the form

$$\varepsilon_T = c_v(T - T_0) + \varepsilon_0, \qquad c_v = 3Nk, \tag{11.6}$$

where $\varepsilon_0 = \int_0^{T_0} c_v(T)\, dT$ is the thermal energy at room temperature, obtainable from appropriate tables. For temperatures T much higher than T_0 we can neglect the difference between $c_v T_0$ and ε_0, since both quantities are small in comparison with $c_v T$. In this case

$$\varepsilon_T = c_v T, \qquad c_v = 3Nk. \tag{11.7}$$

The specific heat is equal to $3k$ per atom only when the thermal motion of the atoms has an oscillatory character. At sufficiently high temperatures the atoms move freely through the body; the specific heat then corresponds only to the translational degrees of freedom of the atoms and is equal to $\frac{3}{2}k$ per atom, as in a monatomic gas. The transition from vibrational to translational motion of the atoms and the corresponding decrease in the specific heat occur gradually, in the range of temperatures for which the kinetic energy of

an atom $\frac{3}{2}kT$ is of the order of the potential barrier against the motion of the atoms through the body $\Delta U/N$. An effective boundary dividing the regions with the limiting values of specific heat of $3k$ and of $\frac{3}{2}k$ may be defined by the threshold temperature

$$T_k = \frac{2}{3}\frac{\Delta U}{kN}. \tag{11.8}$$

At high temperatures $T \gg T_k$ we can represent the thermal energy per atom as the sum of the kinetic energy of translational motion $\frac{3}{2}kT$ and the average value of the potential energy, which in the case of small vibrations was also equal to $\frac{3}{2}kT$ but which is now of the order of $\Delta U/k$. This corresponds to an effective definition of the specific heat by the discontinuous relation

$$c_v = 3Nk \quad \text{when} \quad T < T_k; \qquad c_v = \tfrac{3}{2}Nk \quad \text{when} \quad T > T_k.$$

For $T > T_k$, the energy is then equal to

$$\varepsilon_T = \int_0^T c_v\, dT = \int_0^{T_k} 3Nk\, dT + \int_{T_k}^T \tfrac{3}{2}Nk\, dT = \tfrac{3}{2}NkT + \Delta U. \tag{11.9}$$

As an example, we note that for iron at standard density

$$\frac{\Delta U}{k} \approx 2.5 \text{ ev} \qquad \text{and} \qquad T_k \approx 20{,}000^\circ\text{K}.$$

As the body is compressed the height of the potential barrier increases and the threshold temperature T_k rises, so that the curves giving the temperature

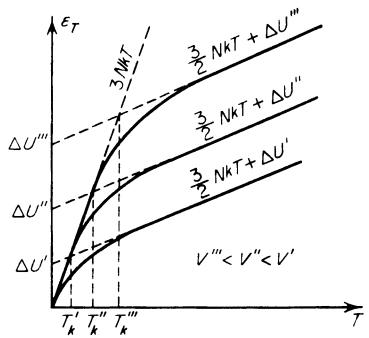

Fig. 11.5. Dependence of thermal energy on temperature for different densities (volumes).

dependence of the thermal energy for different densities (volumes) have the form shown schematically in Fig. 11.5.

In the limiting case $T \gg T_k$, when the thermal motion of the atoms (more precisely, of the nuclei) does not differ from that of a gas, the thermal pressure

related to this motion is, as usual,

$$p_T = nkT = \frac{NkT}{V} = \frac{2}{3}\frac{\varepsilon_T}{V}.$$

§4. Equation of state for a material whose atoms undergo small vibrations

We shall assume that the atoms of the body undergo small vibrations about their equilibrium positions, and we shall find the value of the thermal pressure $p_T(V, T)$ corresponding to these vibrations. If the temperature is not too high and we can neglect the electronic excitation, then the equation of state and the internal energy of the body can be expressed in the form

$$p = p_c(V) + p_T(V, T), \tag{11.10}$$

$$\varepsilon = \varepsilon_c(V) + 3NkT. \tag{11.11}$$

The temperature dependence of the thermal pressure can be obtained immediately from the general thermodynamic identity

$$\left(\frac{\partial \varepsilon}{\partial V}\right)_T = T\left(\frac{\partial p}{\partial T}\right)_V - p. \tag{11.12}$$

The elastic terms, in accordance with (11.1), satisfy this equation automatically. Noting that the specific heat $c_v = 3Nk$ is independent of volume, we obtain from (11.12) the result that the thermal pressure is proportional to the temperature: $p_T = \varphi(V)T$, where $\varphi(V)$ is some function of the volume.

Let us rewrite this equation in the form

$$p_T = \Gamma(V)\frac{c_v T}{V} = \Gamma(V)\frac{\varepsilon_T}{V}. \tag{11.13}$$

The quantity Γ characterizing the ratio of the thermal pressure to the thermal energy of the lattice is called the Grüneisen coefficient. The Grüneisen coefficient for a body at standard volume $\Gamma_0 = \Gamma(V_0)$ is related to the other properties of the material through the well-known thermodynamic relation (see, for example, [16])

$$\left(\frac{\partial p}{\partial T}\right)_V \left(\frac{\partial T}{\partial V}\right)_p \left(\frac{\partial V}{\partial p}\right)_T = -1. \tag{11.14}$$

Setting $-(1/V_0)(\partial V/\partial p)_T = \kappa_0$ for the isothermal compressibility of the material at standard conditions, and $(1/V_0)(\partial V/\partial T)_p = \alpha$ for the coefficient of thermal expansion at constant pressure, we obtain

$$\Gamma_0 = \frac{V_0 \alpha}{c_v \kappa_0} = \frac{\alpha}{\rho_0 c_v \kappa_0} = \frac{\alpha c_0^2}{c_v} \tag{11.15}$$

(c_0 is the speed of sound determined by the isothermal compressibility). The properties of several metals at standard conditions are given in Table 11.1, taken from [3]*. The Grüneisen coefficient Γ corresponds to the specific heat ratio for a calorically perfect gas (with constant specific heats) decreased by unity (we recall the equation of state for such a gas is $p = (\gamma - 1)\,\varepsilon/V$).

Table 11.1

SOME CHARACTERISTICS OF METALS AT STANDARD CONDITIONS

	Al	Cu	Pb
ρ_0, g/cm^3	2.71	8.93	11.34
$c_v \cdot 10^{-6}$, erg/g · deg	8.96	3.82	1.29
$\kappa_0 \cdot 10^{12}$, cm^2/dyne	1.37	0.73	2.42
$\alpha \cdot 10^5$, deg^{-1}	2.31	1.65	2.9
Γ_0	2.09	1.98	2.46
c_0, km/sec	5.2	3.95	1.91
$\varepsilon_0 \cdot 10^{-8}$, erg/g	16.1	7.71	3.23
β_0, erg/g·deg^2	500	110	144

By virtue of the condition used in deriving (11.13), that the specific heat c_v is independent of volume, it was found that the Grüneisen coefficient is independent of temperature. However, in reality, in the limit of very high temperatures for which the thermal motion of the atoms (nuclei) becomes random, (11.13) should become the equation of state for a monatomic gas, and $\Gamma \to \frac{2}{3}$ as $T \to \infty$. If we imagine that the atoms are separated and removed to large distances by an external force (the volume increases), then the material becomes a gas even at low temperatures, so that formally, as $V \to \infty$, $\Gamma \to \frac{2}{3}$. As may be seen from Table 11.1, the Grüneisen coefficient for metals at standard conditions is close to 2.

In order to clarify the physical meaning of the Grüneisen coefficient $\Gamma(V)$, which arose formally as an arbitrary function from the integration of (11.12), we turn to a well-known expression from statistical physics for the free energy of a body whose atoms vibrate harmonically. At high temperatures, when kT is much larger than the energy of vibrational quanta $h\nu$, the specific free energy is (see [16])

$$F = \varepsilon_c(V) + 3NkT \ln \frac{h\bar{\nu}}{kT}, \tag{11.16}$$

where $\bar{\nu}$ is a certain average vibrational frequency which is related to the

* The meaning of β_0 will be given in the next section.

Debye temperature θ by $h\bar{\nu} = e^{-1/3}k\theta = 0.715k\theta$ (for example, for iron $\theta = 420°\text{K}$). The first term in (11.16) represents the potential energy of interaction of the atoms and is the same as the energy of the cold body. The second term describes the thermal part of the free energy. From (11.16), using general thermodynamic relationships, we can easily find the specific internal energy and pressure of the body

$$\varepsilon = F - T\frac{\partial F}{\partial T} = \varepsilon_c(V) + 3NkT = \varepsilon_c + \varepsilon_T$$

(we naturally arrived at (11.11)) and

$$p = -\frac{\partial F}{\partial V} = -\frac{d\varepsilon_c}{dV} - 3NkT\frac{\partial \ln \bar{\nu}}{\partial V}.$$

The first term gives the elastic pressure (which we already know), and the second the thermal pressure. Using (11.13), which defines the Grüneisen coefficient, we find

$$\Gamma(V) = -\frac{\partial \ln \bar{\nu}}{\partial \ln V}. \tag{11.17}$$

The Grüneisen coefficient can be related to the function of cold compression by the following simple considerations. The average frequency of the spectrum of elastic vibrations of the lattice $\bar{\nu}$ is, obviously, close to the maximum frequency. The order of magnitude of the maximum frequency is equal to the ratio of the speed of propagation of elastic compression waves c_0 to the minimum wavelength which, in turn, is of the order of the interatomic distance r_0, so that $\bar{\nu} \sim c_0/r_0$. However, the speed of sound is $c_0 = (-V^2\, dp_c/dV)^{1/2}$, and $r_0 \sim V^{1/3}$, whence

$$\bar{\nu} \sim V^{2/3}\left(-\frac{dp_c}{dV}\right)^{1/2}.$$

Taking the logarithmic derivative of this expression, we obtain

$$\Gamma(V) = -\frac{\partial \ln \bar{\nu}}{\partial \ln V} = -\frac{2}{3} - \frac{V}{2}\frac{(d^2p_c/dV^2)}{(dp_c/dV)}. \tag{11.18}$$

This equation was obtained by Slater [17] and by Landau and Stanyukovich [18]. It has been shown experimentally that the Grüneisen coefficient decreases slightly on compression (for a decrease in the specific volume V).

In order to get some idea of the order of magnitude of the thermal pressure (11.13), we note that if, for example, aluminum is heated at constant (standard) volume to a temperature of 1000°K, the pressure will rise to $p_T = 51{,}000$ atm. A solid expands when heated at standard conditions, at constant

atmospheric pressure. The reason for this thermal expansion is perfectly clear and may be seen from an examination of equation (11.10) for the pressure. The positive thermal pressure p_T increases on heating. The total pressure can thus remain constant only if the elastic pressure p_c becomes negative, and the body must expand up to that point when the binding forces holding the atoms in the lattice, or the negative pressure, will no longer counterbalance the repulsive effect of the positive thermal pressure. This clarifies the relationship expressed by (11.15) between the Grüneisen coefficient, the coefficient of thermal expansion, and the compressibility. Actually, a small expansion at constant pressure is related to a small amount of heating by the condition

$$dp = dp_c + dp_T \approx \frac{dp_c}{dV}\,dV + \frac{\partial p_T}{\partial T}\,dT = \frac{dp_c}{dV}\,dV + \Gamma_0 \frac{c_v}{V_0}\,dT = 0,$$

from which (11.14) and (11.15) follow*.

As an example let us estimate the expansion of aluminum heated at constant pressure (zero or atmospheric, which is equivalent) from absolute zero to room temperature $T = 300°\text{K}$. Using the constants given in Table 11.1, we find $\Delta V/V \approx \Gamma_0(c_v/V_0)\kappa_0\,\Delta T \approx 2\%$ ($\Delta T = 300°\text{K}$). Moreover, the thermal pressure at $T_0 = 300°\text{K}$ is the same as the absolute value of the elastic pressure, equal to $p_{T_0} = 17{,}000$ atm. It is thus evident that it is always possible to consider atmospheric pressure as being equal to zero, since it is negligibly small in comparison with both pressure components even at room temperature.

If the function $\Gamma(V)$ is known, the entropy of the material is easily found. Considering states with densities differing little from standard, we can regard Γ as constant and equal to its standard value Γ_0. We then get for the entropy the relation

$$dS = \frac{d\varepsilon + p\,dV}{T} = \frac{d\varepsilon_T + p_T\,dV}{T} = c_v \frac{dT}{T} + \Gamma_0 c_v \frac{dV}{V},$$

from which the specific entropy is

$$S = c_v \ln \frac{T}{T_0}\left(\frac{V}{V_0}\right)^{\Gamma_0} + S_0, \tag{11.19}$$

where S_0 is the entropy at standard conditions T_0, V_0, and can usually be found tabulated. The isentropic relation between the temperature and volume is given by†

$$\frac{T}{T_0} = \left(\frac{V_0}{V}\right)^{\Gamma_0}. \tag{11.20}$$

* We only consider materials with normal properties, which expand on heating.

† Compare with the isentropic relation between T and V in a gas with constant specific heats $T \sim V^{-(\gamma-1)}$; Γ corresponds to $\gamma - 1$.

Expressing the temperature in terms of pressure by means of the equation of state

$$p = p_c(V) + \Gamma_0 \frac{c_v T}{V}, \tag{11.21}$$

we find the isentropic relation between the pressure and volume

$$\frac{p - p_c(V)}{p_{T_0}} = \left(\frac{V_0}{V}\right)^{\Gamma_0 + 1}, \tag{11.22}$$

where $p_{T_0} = \Gamma_0 c_v T_0 / V_0$ is the thermal component of the pressure at standard conditions*. In the case of small compressions, which nevertheless are accompanied by a sharp increase in pressure (in comparison with atmospheric pressure, but not with p_{T_0}), the isentrope $p(V)$ passes at an almost constant distance from the cold compression curve $p_c(V)$. For relatively large compressions (by a factor of 1.5 to 2) $p \gg p_{T_0}$ and the relative deviation of the isentrope from the cold compression curve $[p - p_c(V)]/p_c(V)$ becomes small.

§5. Thermal excitation of electrons

In the simplest model of a metal the outer valence electrons of the metal atoms are removed from their places in the atom and, together, form a free electron gas, completely filling the crystalline body whose sites are now filled by ions or atomic remainders†. The electron gas is governed by Fermi–Dirac quantum statistics, the elements of which were presented in §12 of Chapter III.

At absolute zero the electron gas is completely degenerate; in accordance with the Pauli principle the electrons occupy the lowest energy states and their kinetic energy does not exceed the Fermi limiting energy (3.88)

$$E_0 = \frac{h^2}{8\pi^2 m_e} (3\pi^2 n_e)^{2/3}$$

(n_e is the number density of free electrons and m_e is the electron mass). The energy E_0 in metals is usually of the order of several electron volts, and the degeneracy temperature corresponding to it $T^* = E_0/k$ is of the order of several tens of thousands of degrees‡.

The kinetic energy of a completely degenerate electron gas, which is of the order of E_0 per electron, is included in the elastic energy of the body and is not related to the thermal energy. In exactly the same manner, the "kinetic"

* The isotherm is $[p - p_c(V)]/p_{T_0} = V_0/V$. When the volume changes are small the isotherm almost coincides with the isentrope (the pressure change in this case is large).

† We restrict ourselves here to elementary considerations and shall not be concerned with the modern electron theory of metals.

‡ For example, for Na, $T^* = 37{,}000°\mathrm{K}$; for K it is 24,000°K, for Ag it is 64,000°K, and for Cu it is 82,000°K.

pressure corresponding to it is included in the elastic pressure, together with the "potential" pressure which arises from the electrostatic interaction between the electrons and ions. The sum of the total pressure of nonthermal origin is equal to zero if the body is in a vacuum at absolute zero.

If the temperature increases, the electrons partially move over to higher energy states, exceeding the Fermi limiting energy, and the energy of the electron gas increases. If the temperature T is much lower than the Fermi temperature T^*, then, roughly speaking, electrons escape from the initial Fermi sphere in momentum space with an energy increase of the order of kT from the Fermi limit. The number of excited electrons is a fraction of the order of kT/E_0 of the total number of electrons. Each of these electrons acquires an additional energy of the order of kT. The order of magnitude of the thermal energy per electron is thus $(kT/E_0)kT$ and is proportional to $V^{2/3}T^2$ (since $E_0 \sim n_e^{2/3} \sim V^{-2/3}$). With the inclusion of a numerical coefficient, the thermal energy of the electrons per unit mass of metal for $T \ll T^*$ is found to be (see, for example, [16])

$$\varepsilon_e = \tfrac{1}{2}\beta T^2, \tag{11.23}$$

where the coefficient β depends on the density of the material and is given by

$$\beta = \beta_0\left(\frac{V}{V_0}\right)^{2/3}, \qquad \beta_0 = \frac{4\pi^4}{(3\pi^2)^{2/3}}\frac{k^2 m_e}{h^2} N_e^{1/3} V_0^{2/3} \tag{11.24}$$

(N_e is the number of free electrons per unit mass of metal and V_0 is the standard specific volume of the metal). The specific heat at constant volume is proportional to the temperature and is equal to

$$c_{v_e} = \beta T. \tag{11.25}$$

Knowing the number of free electrons per atom of metal, we can use (11.24) to calculate the coefficient β_0 and to find the electronic specific heat at a given temperature. Experimentally, the electronic specific heat is determined at very low temperatures, where the specific heat of the lattice is governed by quantum laws and is proportional to T^3. At sufficiently low temperatures the electronic specific heat, which is proportional only to the first power of T, dominates, and thus can be measured. At room temperature, however, the electronic specific heat is usually smaller by a factor of tens and even a hundred than the specific heat of the lattice, which under these conditions is constant and equal to its classical value $c_v = 3Nk$.

Experimental values of the electronic specific heat coefficients β_0 for several metals are given in Table 11.1*. In comparing the values of the electronic and lattice specific heats at different temperatures it becomes apparent that even at temperatures as low as 10,000°K the electronic specific

* They agree in order of magnitude with the values calculated from (11.24).

heat is quite appreciable, and, say, at 50,000°K it becomes even larger than the specific heat of the lattice. It should be noted, however, that (11.25) is valid only as long as the temperature is below the Fermi temperature.

For $T \gg T^*$ a free electron gas with a constant number of electrons is not degenerate, and its specific heat is given by the classical value $c_{v_e} = \frac{3}{2}N_e k$. In reality, however, the actual number of "free" electrons increases at high temperatures and the electronic specific heat of the material can no longer be described by simple equations. The problem of the electronic specific heat of a dense gas at high temperatures was considered in detail in §14 of Chapter III. At temperatures of the order of 10,000–20,000°K, which have been attained in experiments on shock compression of metals, this situation is still far from being reached, and the electronic specific heat can be taken approximately as being proportional to the temperature, as follows from (11.25). We should mention that the degeneracy temperature T^* increases as the metal is compressed ($T^* \sim V^{-2/3}$), so that the temperature range in which the approximation $\varepsilon_e \sim T^2$, $c_{v_e} \sim T$ holds is greater in a compressed material than at standard density.

According to the equation of state for a free electron gas (degenerate, as well as nondegenerate), the thermal part of the electron pressure is

$$p_e = \frac{2}{3}\frac{\varepsilon_e}{V} = \tfrac{1}{3}\beta\frac{T^2}{V} \sim V^{1/3}T^2. \tag{11.26}$$

If we define the "electronic Grüneisen coefficient" Γ_e by a relationship similar to (11.13),

$$p_e = \Gamma_e \frac{\varepsilon_e}{V}, \tag{11.27}$$

then we find that for a free electron gas it is equal to 2/3.

Kormer (see [3]) carried out a detailed analysis of the thermal behavior of electrons on the basis of the Thomas–Fermi and Thomas–Fermi–Dirac statistical models of an atomic cell (see §§12–14, Chapter III). He used the approximate calculations of Gilvarry [19], who considered the temperature terms as a correction to the Thomas–Fermi model of a cold atom, Latter's calculations [20], which were discussed in §14 of Chapter III, and experimental data. This analysis showed that the electronic specific heat to temperatures of the order of 30,000–50,000°K, as in the free electron model, is proportional to the temperature, with $c_{v_e} \sim T$, $\varepsilon_e \sim T^2$, where with increasing density this relationship remains valid to increasingly higher temperatures.

With respect to thermal pressure, the coefficient Γ_e is equal to 2/3 only in the limiting cases of very high temperatures or very large densities, for which the kinetic energy of the electrons is much greater than the Coulomb energy. The value of Γ_e in the temperature and density ranges obtained in shock

compression experiments is slightly lower; it is approximately equal to 0.5–0.6. It was found that it is sufficiently accurate to take $\Gamma_e = const = \frac{1}{2}$. However, for consistency with the thermodynamic identity (11.12), it is necessary to change together with the coefficient Γ_e the exponent related to this coefficient in the relation between energy and volume, in particular to replace $\varepsilon_e \sim V^{2/3}T^2$ by $\varepsilon_e \sim V^{1/2}T^2$ *. Assuming that the coefficient of electronic specific heat at standard volume is equal to its experimental value, we can, according to Kormer, write approximately for $T < 30{,}000$–$50{,}000°\mathrm{K}$,

$$\varepsilon_e = \tfrac{1}{2}\beta T^2, \qquad \beta = \beta_0\left(\frac{V}{V_0}\right)^{1/2}, \tag{11.28}$$

$$p_e = \frac{1}{2}\frac{\varepsilon_e}{V}. \tag{11.29}$$

§6. A three-term equation of state

Let us briefly summarize the results of §§2–5. The specific internal energy and pressure of a solid or a liquid can be represented as a sum of three components, which describe the elastic properties of the cold body, the thermal motion of the atoms (nuclei), and the thermal excitation of the electrons. For temperatures which are not too high, not above several tens of thousands of degrees (and large compressions), we can assume approximately that the atoms undergo small vibrations and that their specific heat is $c_v = 3Nk$. The electronic terms at these temperatures are described by the approximate equations (11.28) and (11.29). Thus, the energy and pressure are

$$\varepsilon = \varepsilon_c(V) + \varepsilon_T + \varepsilon_e, \qquad p = p_c(V) + p_T + p_e,$$

where

$$\begin{aligned} \varepsilon_c(V) &= \int_V^{V_{0c}} p_c(V)\,dV, \\ \varepsilon_T &= 3Nk(T - T_0) + \varepsilon_0, \\ \varepsilon_e &= \tfrac{1}{2}\beta_0\left(\frac{V}{V_0}\right)^{1/2} T^2, \\ p_T &= \Gamma(V)\frac{\varepsilon_T}{V}, \qquad p_e = \frac{1}{2}\frac{\varepsilon_e}{V}. \end{aligned} \tag{11.30}$$

T_0 is room temperature, and ε_0 is the thermal energy of the atomic lattice at room temperature and is tabulated. The electronic specific heat coefficient at

* For a dependence $\varepsilon_e \sim V^k T^2$ with an equation of state $p = \Gamma_e \varepsilon_e / V$ with $\Gamma_e = const$, it is easy to check that the thermodynamic identity is satisfied only for $k = \Gamma_e$.

standard volume β_0 is obtained from experiments which measure the specific heat at very low temperatures.

The Grüneisen coefficient $\Gamma(V)$ is related to the function $p_c(V)$ by the differential relation (11.18). Only one unknown quantity remains, the elastic pressure as a function of volume $p_c(V)$, and this must be determined experimentally.

2. *The Hugoniot curve*

§7. Hugoniot curve for a condensed substance

The laws of conservation of mass, momentum, and energy across a shock wave (1.61)–(1.63) are entirely general, regardless of the aggregate state of the medium through which the wave propagates. Since the pressures behind even very weak waves are measured in thousands of atmospheres, one may always neglect the initial atmospheric pressure, setting it equal to zero. As usually, we denote by D the propagation speed of the shock wave through the undisturbed medium, and by u the jump in particle velocity across the front, equal to the velocity of the material behind the front (in laboratory coordinates) if the material ahead of the front is at rest. With unsubscripted quantities denoting conditions behind the front, we may write the laws of conservation of mass and momentum in the form

$$\frac{V_0}{V} = \frac{D}{(D-u)}, \tag{11.31}$$

$$p = \frac{Du}{V_0}. \tag{11.32}$$

Eliminating the velocity u from these equations, we get

$$p = \frac{D^2}{V_0}\left(1 - \frac{V}{V_0}\right). \tag{11.33}$$

As the third relation (energy equation) we take the Hugoniot equation (1.71) with $p_0 = 0$

$$\varepsilon - \varepsilon_0 = \tfrac{1}{2}p(V_0 - V). \tag{11.34}$$

The total energy acquired by a unit mass of the substance as a result of shock compression $p(V_0 - V)$ is divided equally between the kinetic energy $u^2/2$ and the internal energy $\varepsilon - \varepsilon_0$ (in a coordinate system in which the undisturbed medium is at rest). The change in the internal energy, in turn, is composed of the changes in the elastic and thermal energies.

Let us first consider a shock wave traveling through a body at zero temperature: $T_0 = 0$, $\varepsilon_0 = 0$, and $V_0 = V_{0c}$. On a p, V diagram (Fig. 11.6) we draw the cold compression curve $p_c(V)$ (which is an isentrope) and the Hugoniot curve $p_H(V)$; the Hugoniot naturally lies above the cold compression curve

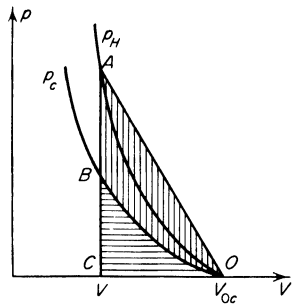

Fig. 11.6. p, V diagram for shock compression of a cold material. p_H is the Hugoniot curve; p_c is the cold compression curve.

since the total pressure behind the front is composed of the elastic and thermal pressure contributions. The elastic energy ε_c acquired by the material is numerically equal to the area of the curved triangle OBC, which is shaded horizontally ($\varepsilon_c = \int_V^{V_{0c}} p_c\, dV$). The total internal energy ε, according to (11.34), is equal to the area of the triangle OAC; the difference between these areas is shaded vertically and comprises the thermal energy of the material subjected to shock compression. As is evident from Fig. 11.6 the area OAC is always greater than the area OBC, as long as the cold compression curve is convex with respect to the volume axis $d^2p_c/dV^2 > 0$, as is ordinarily always the case. Therefore, the material is always heated by a shock wave and its entropy increases. This completely general statement, which was illustrated in Chapter I using as an example a perfect gas with constant specific heats, follows just as obviously in the case of a solid from the elastic properties of the material.

Let us now consider a shock compression of a body initially at standard conditions V_0, T_0. In this case the initial elastic pressure is negative, and the curve of $p_c(V)$ is located as shown in Fig. 11.7. The ordinary isentrope

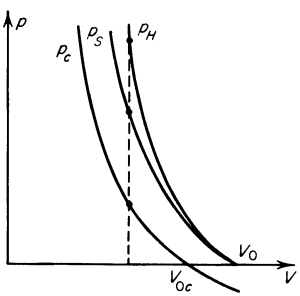

Fig. 11.7. p, V diagram for shock compression of a solid heated to room temperature. p_H is the Hugoniot curve; p_S is the isentrope; p_c is the cold compression curve.

$p_S(V, S_0)$ passing through the initial state lies above the cold compression curve by an amount which increases somewhat with decreasing volume. For small compressions the electron pressure is negligibly small; the Grüneisen coefficient may be taken to be constant and the isentrope $p_S(V, S_0)$ is given by (11.22).

As we know (Chapter I, §18), the Hugoniot curve $p_H(V)$ has a second-order tangency with the isentrope $p_S(V)$ at the initial point, so that the Hugoniot curve is located as shown in Fig. 11.7. Figure 11.7 has been drawn to a scale which makes clear the mutual position of all three curves p_c, p_S, and p_H in a range from relatively small pressures up to values of the order of a hundred thousand atmospheres. If we consider a wider range of pressures, up to millions of atmospheres, then the difference between V_0 and V_{0c} and the difference between the isentrope and the cold compression curve are almost imperceptible, while the deviation of the Hugoniot curve from the isentrope p_S or from the curve p_c becomes appreciable because of the increased effect of the thermal components of energy and pressure, or equivalently, as a result of the significant increase in the entropy. The picture in this case is the same as in Fig. 11.6, where we can assume that $V_{0c} = V_0$ and that the isentrope p_{S_0} coincides with the cold compression curve.

In shock waves with pressures of the order of a million atmospheres the thermal energy which is associated with the increase in the entropy of the material is comparable with the total energy. In exactly the same manner, the thermal pressure is comparable with the total pressure. This is illustrated by Fig. 11.8 taken from [3], on which are shown experimental Hugoniot

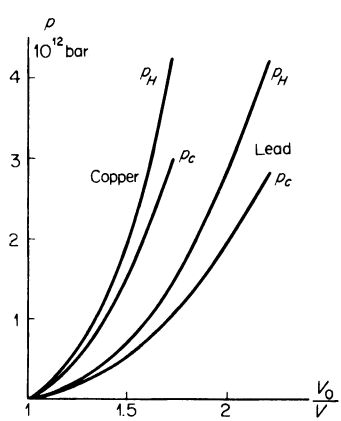

Fig. 11.8. Hugoniot and cold compression curves for copper and lead.

curves for copper and lead up to pressures of the order of $4 \cdot 10^6$ atm, and cold compression curves calculated on the basis of experimental data (the density

ratio $\rho/\rho_0 = V_0/V$, rather than the specific volume, is used as the abscissa)*.

Table 11.2 provides an idea of the relative role of the various pressure and energy components for different shock pressures†.

Table 11.2

PARAMETERS BEHIND A SHOCK WAVE IN LEAD

$\frac{\rho}{\rho_0}$	p	p_c	p_T	p_e	$\varepsilon - \varepsilon_0$	ε_c	$c_v(T - T_0)$	ε_e	Γ	T,°K
	in 10^{10} dyne/cm^2 = 10^4 atm				in 10^8 erg/g					
1.3	25.0	21.6	3.35	0.051	25.4	15.3	9.6	0.69	1.9	1,045
1.5	65.5	51.0	13.9	0.63	96.3	46.7	42.3	7.4	1.77	3,580
1.7	133.0	95.3	34.0	3.8	242.0	95.8	107.0	39.4	1.60	8,600
1.9	225.5	156.0	56.0	12.7	471.0	163.2	191.0	118.0	1.35	15,100
2.1	335.5	233.0	73.0	29.0	775.0	248.0	284.0	243.0	1.07	22,300
2.2	401.0	277.0	93.0	41.5	965.0	297.0	337.0	332.0	0.98	26,400

It follows from the table that for the shock compression of lead by a factor of 2.2, the material behind the front is heated to a temperature of 26,400°K; in this case the thermal pressure is 32% of the total pressure and the thermal energy is 69% of the total energy, with half of the thermal energy ascribable to the electrons and the other half to the atomic vibrations. The thermal pressure of the electrons is 34% of the total thermal pressure. Qualitatively the behavior with increasing wave strength is the same for all other metals studied. Quantitative data can be found in [3] and the review by Al'tshuler [55] but will not be given here.

The greater the shock strength, the greater the role of the thermal components of pressure and energy. At very high pressures, of the order of hundreds of millions of atmospheres and above, the role of the elastic components becomes small and the material behaves practically as a perfect gas (perfect in the sense that interactions between particles are absent). Accordingly, a Hugoniot curve under these conditions in principle does not differ from the Hugoniot curve for a perfect gas (when ionization processes are taken into account; see Chapter III), and a limiting density ratio across a shock wave exists also for a solid body. In the limit $p \to \infty$ the temperature also tends to infinity, the atoms are fully ionized, and the material becomes a perfect,

* The experiments and methods for obtaining the experimental cold compression curves are described in §§12 and 13.

† The table is taken from [3]. It has been supplemented with some additional properties for the sake of completeness. These properties were calculated using the constants given in [3].

classical electron-nuclear gas with a specific heat ratio $\gamma = 5/3$, which corresponds to a limiting density ratio of 4 (if effects connected with radiation are disregarded; see Chapter III).

§8. Analytical representation of Hugoniot curves

From the thermodynamic functions $p(V, T)$ and $\varepsilon(T, V)$ it is possible in principle to find an explicit equation for the Hugoniot curve $p_H(V, V_0)$. Practically this cannot be done, since the theoretical dependence of the elastic pressure on the volume $p_c(V)$ is unknown. However, it is useful to write down the equation for the Hugoniot curve in terms of the unknown function $p_c(V)$. We shall consider shock waves that are not too strong, in which the electronic components of pressure and energy can be neglected and the Grüneisen coefficient Γ can be taken to be constant and equal to its value at standard conditions Γ_0. At the same time we assume that the wave is not too weak either, so that the initial energy of the undisturbed medium ε_0 can be neglected. Physically this means that we consider the initial temperature to be equal to zero and make no distinction between the standard volume V_0 and the zero volume V_{0c}.

Let us substitute into the Hugoniot equation (11.34) the energy $\varepsilon = \varepsilon_c + \varepsilon_T$, expressing the thermal energy contribution ε_T in terms of pressure by means of (11.21)

$$p - p_c = p_T = \Gamma_0 \frac{\varepsilon_T}{V}; \qquad \varepsilon = \varepsilon_c + \frac{V(p - p_c)}{\Gamma_0}.$$

Solving the resulting equation for p, we obtain the equation for the Hugoniot curve in the form

$$p_H = \frac{(K-1)p_c(V) - 2\varepsilon_c(V)/V}{K - V_0/V}, \qquad \varepsilon_c = \int_V^{V_{0c}} p_c(V)\, dV, \qquad (11.35)$$

where $K = 2/\Gamma_0 + 1$.

If we formally apply (11.35) to very strong shocks, we find that in the limit $p_H \to \infty$, $V_0/V = K$, so that formally K represents the limiting density ratio across the shock wave. The situation here is completely analogous to that for a perfect gas with constant specific heats. We recall that the Grüneisen exponent Γ corresponds to the specific heat ratio γ minus one. From this, the limiting density ratio K corresponds to the quantity $(\gamma + 1)/(\gamma - 1)$, which is the limiting density ratio for gases. The formal analogy with gases is connected with the fact that in the limit $p_H \to \infty$ the major role is played by the thermal pressure ($p_T = p_H - p_c \to \infty$, while $p_c(V) \to const$), and the equation of state in this case is the same as that for a gas.

It is sometimes convenient to express the Hugoniot curve analytically by

means of an interpolation formula. It has been shown experimentally that the relationship between the front velocity and the velocity of the material (relative to the undisturbed medium) behind the front is linear over a wide range of shock strengths:

$$D = A + Bu. \tag{11.36}$$

Thus, for example, for iron $A = 3.8$ km/sec, $B = 1.58$*. Using (11.36) we can easily obtain the equation of the Hugoniot curve from (11.34) and (11.32)

$$p_H = \frac{A^2(V_0 - V)}{(B-1)^2 V^2 \left[\frac{B}{B-1} - \frac{V_0}{V}\right]^2}. \tag{11.37}$$

The Hugoniot curve $p_H(V, V_0)$ can be interpolated by polynomials of the type

$$p_H = \sum_{k=1}^{m} a_k \left(\frac{V_0}{V} - 1\right)^k,$$

where the constant coefficients are determined partially on the basis of experimental shock compression data and partially from the properties of the material in the standard state.

§9. Weak shock waves

The pressure range of the order of several tens and hundreds of thousands of atmospheres is of great practical importance. These pressures are typical of those generated in detonating explosives, in explosions in water, on the impact of detonation products on metallic obstacles, etc. The following empirical equation of state for a condensed material is frequently used in the isentropic flow region:

$$p = A(S)\left[\left(\frac{V_0}{V}\right)^n - 1\right], \tag{11.38}$$

where the exponent n is assumed to be constant, and where the coefficient A depends on the entropy and in fact is also always taken to be constant. The constants A and n are related by an equation which depends on the compressibility of the material at standard conditions (the speed of sound)

$$c_0^2 = -V_0^2\left(\frac{\partial p}{\partial V}\right)_S = V_0 An. \tag{11.39}$$

* Equation (11.36) cannot be extrapolated to small strengths $p \to 0$ and $u \to 0$, so that the constant A is not the speed of sound in the standard state.

In accord with Jensen's data, Baum, Stanyukovich, and Shekhter [21] took $n = 4$ for metals and calculated the constant A for a number of metals using (11.39) and the experimentally measured values of the compressibility. In a number of cases they obtained good agreement with values of A which they determined experimentally. Thus, for example, for iron, $A_{\text{calc}} = 5 \cdot 10^5$ atm, which is 11% larger than the experimental value; for copper $A_{\text{calc}} = 2.5 \cdot 10^5$ atm, 6% larger than the experimental value; for duraluminum $A_{\text{calc}} = 2.03 \cdot 10^5$ atm, practically the same as the experimental value. For water it is usually assumed that $n \approx 7$–8 and $A \approx 3000$ atm.

In calculating flows with shock waves in the above pressure range we can, to first approximation, neglect the entropy change across the shock wave and use the isentropic equation of state (11.38) with $A = const$ to relate the pressure and the density across the wave front. Here the velocities D and u are found either from (11.30) and (11.32) or from (11.31) and (11.33). The energy equation (11.34) can be used in this case in the next approximation to estimate the increase in internal energy connected with the irreversibility of the shock compression. Indeed, if we consider (11.38) to be the equation of the isentrope, then the internal energy can be determined as a function of V by using the equation $T\,dS = d\varepsilon + p\,dV = 0$,

$$\varepsilon(V) - \varepsilon_0 = -\int_{V_0}^{V} p\,dV = AV_0\left\{\frac{1}{n-1}\left[\left(\frac{V_0}{V}\right)^{n-1} - 1\right] - \left[1 - \frac{V}{V_0}\right]\right\}.$$

This value of the energy and the pressure obtained from (11.38) naturally do not satisfy the energy equation across the shock front (11.34). By definition, the difference

$$\Delta\varepsilon = \tfrac{1}{2}p(V_0 - V) - \int_{V}^{V_0} (p\,dV)_{S=const}$$

is equal to the increase in internal energy caused by the increase in entropy across the shock wave. The smallness of this quantity in comparison with the total increase in energy across the shock wave $\varepsilon - \varepsilon_0$ is a condition for the validity of the isentropic approximation for the shock compression.

Calculating the ratio $\Delta\varepsilon/(\varepsilon - \varepsilon_0)$ with $n = 4$ we find that for $V_0/V = 1.1$ the ratio is equal to 4.5%, and for $V_0/V = 1.2$ it is 17.5% (this ratio is independent of A). A density ratio of 1.1 corresponds to a pressure of the order of 100,000 atm (90,000 atm for aluminum and 210,000 atm for iron). Thus, for pressures of $\sim 10^5$ atm the isentropic approximation for the shock compression yields an error in the energy of not more than 5% (the error in pressure is even less). We can, therefore, consider the shock wave as an acoustic wave in many practical calculations.

§10. Shock compression of porous materials

The process of shock compression of porous bodies exhibits some distinctive features. Experimental studies of the shock compression of the same material at different initial densities make it possible to obtain more complete information on the thermodynamic properties of the material at high pressures and temperatures. Porous media can have quite different forms and structures (powders, bodies with internal voids, fibrous bodies, etc.). All of them are characterized by the presence of more or less large particles or segments of a solid (continuous) material with standard density $\rho_0 = 1/V_0$ and void segments, as a result of which the average specific volume V_{00} is greater than the standard volume V_0 (and the average density ρ_{00} is less than the standard density ρ_0).

Let us imagine that a porous body is subjected to a slow compression on all sides. Initially the work of the external pressure forces is used in closing up the voids, in packing the material and reducing it to standard volume. This work involves overcoming the friction forces between the particles, pulverizing the particles, crumpling the fibers, etc. The completion of this work requires a relatively small pressure, the scale of which is the ultimate strength of the material. For metals this pressure is of the order of a thousand atmospheres, and much less than this for many other materials. If we consider compressions in the range of pressure of hundreds of thousands of atmospheres, then the pressure on the portion of the p, V curve where the material is reduced to standard volume can for practical purposes be taken equal to zero, and the p, V curve starting from the point V_{00} can be taken as a straight line on the axis of V from V_{00} to V_0 ($p = 0$). For compression above standard density the curve can be taken to be an isentrope for the continuous material (Fig. 11.9).

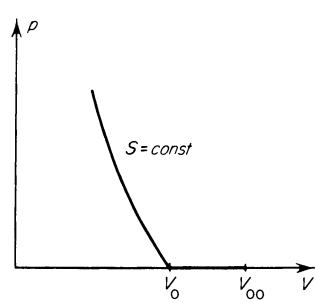

Fig. 11.9. Isentrope for the compression of a porous material.

Let us now consider the shock compression of a porous body. For simplicity we consider shock compression to high pressures, of the order of hundreds of thousands and millions of atmospheres, so that the ordinary isentrope for

the continuous material is the same as the cold compression curve. We neglect the effects related to the strength of the material, and the fact that the initial temperature $T_0 \approx 300°K$ is different from zero. We also assume that in the final state behind the front the material is both continuous and homogeneous.

It follows from the conservation laws across the shock wave and from the equation of state of the medium that the Hugoniot curve has the form shown in Fig. 11.10 (this will be clarified below). The point corresponding to the standard volume V_0 and zero pressure $p = 0$ lies on the Hugoniot curve. The internal energy acquired by the medium in the shock wave $\varepsilon = \frac{1}{2}p(V_{00} - V)$ is equal to the area of the horizontally shaded triangle. The elastic part of the internal energy is equal to the area of the curvilinear triangle bounded by the curve $p_c(V)$ and densely cross-hatched in Fig. 11.10. The larger the initial

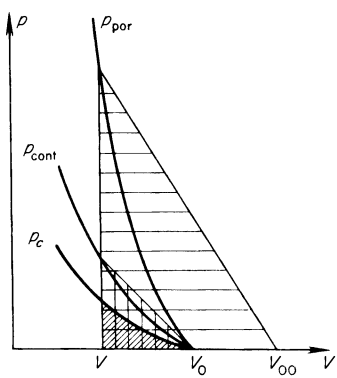

Fig. 11.10. p, V diagram for shock compression of a porous material. p_{por} is the Hugoniot curve for a porous medium; p_{cont} is the Hugoniot curve for a continuous material; p_c is the cold compression curve for a continuous material.

volume V_{00}, i.e., the greater the porosity of the material, for compression of the porous material to the same final volume the greater is the difference between these areas; this difference corresponds to the thermal part of the energy (the elastic energy is the same for a given volume, while the total energy increases). However, the greater the thermal energy, the larger is the thermal pressure. Therefore, the higher the porosity, the steeper is the Hugoniot curve. In particular, the Hugoniot curve for a porous material lies above the Hugoniot curve for a continuous material, as shown in Fig. 11.10. A higher pressure is required to compress a porous material to a given volume than a continuous material. This pressure is higher, the higher is the porosity. The qualitative nature of the picture given will not be altered if we consider the initial temperature (and entropy) to be different from zero.

In order to get some idea of how sharply the thermal components of pressure and energy increase for shock compression of a porous body as compared to the compression of a continuous one, we present experimental Hugoniot

curves for iron of standard density and for porous iron with a density lower by a factor of 1.4 ($V_{00} = 1.412V_0$). These curves (Fig. 11.11) were taken from [1] (the density ratio V_0/V with respect to standard density rather than

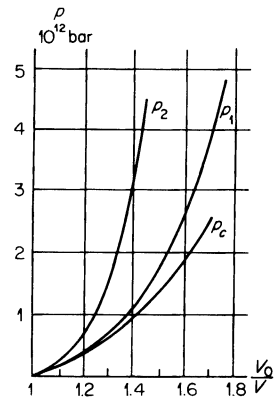

Fig. 11.11. Hugoniot curves for continuous (p_1) and porous (p_2) iron. p_c is the cold compression curve.

the specific volume alone is plotted on the abscissa). For example, for a density ratio of $V_0/V = 1.22$, which corresponds to decreasing the volume of the porous iron by a factor of 1.74 ($V_{00}/V = 1.74$), the pressure for porous iron is found to be greater by a factor of 2.63 than the pressure for continuous iron, while the energy is 8.64 times larger.

The strong heating caused by shock compression of porous bodies can lead to sharp anomalies in the Hugoniot curves. In particular, the relative role of the thermal pressure in compressing a highly porous material to a given pressure can turn out to be so great that the density in the final state at high pressure is below standard density ($V > V_0$). In this case, the volume does not decrease with increasing pressure, as is usually the case, but increases, and the Hugoniot curve has the anomalous shape shown in Fig. 11.12.

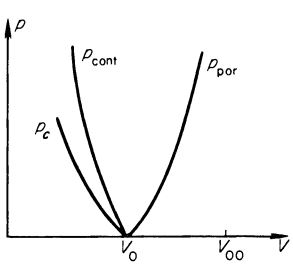

Fig. 11.12. Anomalous Hugoniot curve for a highly porous material.

In order to make clear the origin of this curious effect, we shall use the Hugoniot equation derived under the assumptions that the electron pressure and energy are small, the Grüneisen coefficient is constant, and the initial

energy of the medium can be neglected. This is equation (11.35), in which the initial volume V_0 is understood to denote the initial volume of the porous material V_{00} (equation (11.35) was derived without assuming that the material is continuous in its initial state):

$$p_H(V, V_{00}) = \frac{(K-1)p_c(V) - 2\varepsilon_c(V)/V}{K - V_{00}/V}, \qquad K = \frac{2}{\Gamma_0} + 1. \quad (11.40)$$

Equation (11.40) describes a family of Hugoniot curves corresponding to different initial volumes V_{00}, that is, to different degrees of porosity which may be characterized by the coefficient $k = V_{00}/V_0 \geqslant 1$. When $k = 1$, and $V_{00} = V_0$, we have the Hugoniot curve for a continuous material. The point $V = V_0$, $p_H = 0$ satisfies (11.40) for any initial volume V_{00} (since $p_c(V_0) = 0$ and $\varepsilon_c(V_0) = 0$), so that the family of Hugoniot curves represents a bundle of curves emanating from this point. According to (11.40), as $p_H \to \infty$, $V_{00}/V \to K$, and the limiting volume $V_{\text{lim}} = V_{00}/K$. If this value is smaller than V_0, as is the case for small porosity $k < K$, the Hugoniot curves have their normal shape and are higher the larger is the initial volume. If, however, $V_{\text{lim}} > V_0$ (which happens for the case of high porosity, with $k > K$), then the Hugoniot curves are anomalous: the final volume increases with increasing pressure. A family of Hugoniot curves corresponding to different porosities is shown in Fig. 11.13.

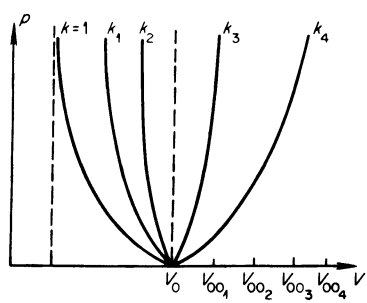

Fig. 11.13. Hugoniot curves for different porosities: $k_4 > k_3 > K > k_2 > k_1 > 1$.

We emphasize again that (11.40) describes only the initial behavior of the Hugoniot curve for low pressures. Actually at large pressures the role of the electronic terms becomes important and the Grüneisen coefficient is not constant. This fact, however, does not invalidate the qualitative conclusion regarding the possibility of having an anomalous Hugoniot curve for a highly porous material.

In the paper by Kormer, Funtikov, Urlin, and Kolesnikova [56] are presented results of studies of the shock compression of porous metals at

pressures from 0.7 to 9 million atmospheres. They also give a number of theoretical derivations of an equation of state for porous materials and determine the parameters which enter into the equation of state on the basis of experimental data.

§11. Emergence of weak shock waves from the free surface of a solid

Experimental methods for determining Hugoniot curves for a solid, which will be considered in the following section, make extensive use of the so-called velocity doubling rule in an unloading wave. When a shock wave which propagates through a solid emerges from the free surface, the compressed material expands, or "unloads" practically to zero pressure. The unloading (rarefaction) wave travels backwards into the material with the speed of sound that corresponds to the state behind the shock front, and the material being unloaded acquires an additional velocity in the direction of the initial motion of the shock*.

In this section we shall consider only weak shock waves, which impart to the solid an energy which is not sufficient to melt it and even less so to vaporize it†, so that the final state of the material after unloading may be assumed to be solid. In this case, the final volume of the unloaded material V_1 differs but little from the standard volume of the solid V_0. At the same time we shall also assume that the shock wave is not too weak, so that we can neglect effects associated with the strength of the solid. It is assumed that the pressure in the solid compressed by a shock is isotropic, as in a gas or liquid. This assumption is valid when the pressure is large in comparison with the ultimate strength, the critical shear stress, etc. The speed of sound is then determined by the compressibility of the material, by the bulk compression modulus, just as in the case of a gas or liquid. When this is not so the unloading is described by formulas from the theory of elasticity, which we shall discuss later.

Let a plane shock wave of constant strength (pressure p, particle velocity u, and volume V which is only slightly smaller than the standard volume V_0)

* If the body borders on air rather than on a vacuum, the moving boundary of the unloaded material acts as a piston with respect to the air and pushes ahead an air shock. Therefore, strictly speaking, the material is not unloaded to zero pressure, but to the pressure behind the air shock. However, this pressure, even though it may be large in comparison with atmospheric pressure, is so small in comparison with the initial pressure in the shock-compressed solid that it can always be neglected, and we may consider that unloading into air does not differ from unloading into vacuum. The strength of the shock wave in the air is determined in this case by the equivalent piston velocity, the velocity of the solid after unloading.

† The vaporization of a solid initially compressed by a very strong shock wave will be discussed in §§21 and 22.

propagate through a solid. At a specified time the wave emerges from the free surface, which is assumed to be parallel to the surface of the shock front. A weak shock wave, across which the compression is small, $V_0 - V \ll V_0$, does not differ from an acoustic compression wave and can be described by acoustic equations. The shock travels through the body with the speed of sound c_0. The pressure behind the shock is related to the particle velocity through the relation $p = \rho_0 c_0 u$ ($\rho_0 = 1/V_0$). Starting from the time $t = 0$ at which the shock wave emerges from the free surface, an unloading wave, also an acoustic wave, propagates back into the body. The unloading wave travels through the material with the speed of sound (differing but little from the speed of sound c_0 under standard conditions). The pressure across the wave drops from the initial pressure p to zero and the material acquires a velocity u', related to the pressure change $\Delta p = -p$ by the acoustic formula $u' = -\Delta p/\rho_0 c_0 = p/\rho_0 c_0$ (see Fig. 11.14; the density decreases only slightly, and the final density ρ_1 differs but little from the standard density of the solid: $V_1 - V_0 \ll V_0$). It is evident from comparison of the equations $p = \rho_0 c_0 u$ and $u' = p/\rho_0 c_0$ that u', the additional velocity acquired by the

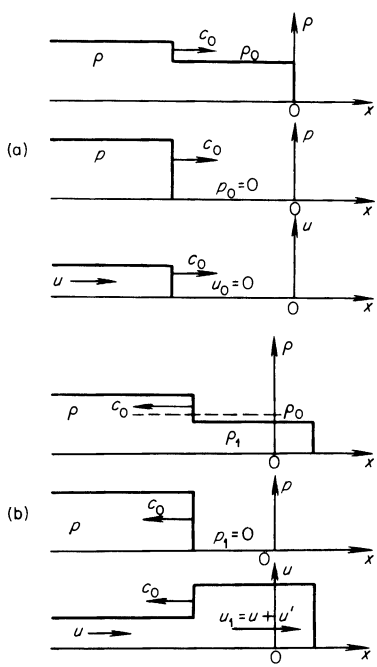

Fig. 11.14. Density, pressure, and velocity distributions for a weak shock wave emerging from a free surface. (a) Prior to the time of emergence, $t < 0$; (b) after emergence, $t > 0$.

material on unloading, is equal to u, the particle velocity behind the original shock. This means that, when a weak shock wave emerges from the free surface, the velocity of the material doubles: $u_1 = u + u' \approx 2u$.

The velocity doubling rule can also be obtained from the general shock and rarefaction wave equations in the limiting case of weak waves. We know from gasdynamics (see §10, Chapter I) that the additional velocity acquired by a material unloaded from an initial pressure p to a final pressure $p_1 = 0$, is

$$u' = \int_0^p \frac{dp}{\rho c} = \int_0^p \left(-\frac{\partial V}{\partial p}\right)_S^{1/2} dp = \int_V^{V_1} \left(-\frac{\partial p}{\partial V}\right)_S^{1/2} dV,$$

where the derivatives, by virtue of the fact that the unloading process is isentropic, are taken at a constant entropy equal to the entropy behind the shock front. The initial particle velocity of the material behind a shock wave, by virtue of the conservation laws (11.31) and (11.32), is

$$u = [p(V_0 - V)]^{1/2}.$$

In a weak shock, where the entropy change is small, the compression is also not large. To first approximation we can express the volume increase in the form

$$V - V_0 = \left(\frac{\partial V}{\partial p}\right)_S p,$$

where S denotes the entropy of the original state of the material prior to the shock compression. Then the particle velocity behind the shock is

$$u \approx \left(-\frac{\partial V}{\partial p}\right)_S^{1/2} p \approx \frac{p}{\rho_0 c_0}.$$

To the same approximation we can neglect the change in the isentropic compressibility in the pressure range from 0 to p and take the derivative constant in the equation for u'. We obtain

$$u' = \int_0^p \left(-\frac{\partial V}{\partial p}\right)_S^{1/2} dp \approx \left(-\frac{\partial V}{\partial p}\right)_S^{1/2} p \approx \frac{p}{\rho_0 c_0} \approx u.$$

Walsh and Christian [22] established from rather general considerations the upper and lower limits for possible variations of the additional velocity u' and have found that for pressures $p \sim 4 \cdot 10^5$ atm for a large number of metals the velocity doubling rule is accurate to within 2%. It has been experimentally verified [3] that the velocity doubling rule for iron is approximately satisfied up to quite high pressures of $\sim 1.5 \cdot 10^6$ atm. In general, the departure from the velocity doubling rule is greater the stronger is the shock.

Let us now consider the fact that even a weak shock wave is not acoustic and that the entropy across it does increase. Here we assume that to first

approximation the additional velocity acquired after unloading u' is, as before, equal to u. The density and temperature in the final state will be considered to satisfy the following approximation. When a body is unloaded isentropically to the initial, zero pressure, it is found to be heated and expanded in comparison with the initial state prior to shock compression. The energy of irreversible heating and the final temperature of the unloaded material T_1 can be easily found if the thermodynamic properties and initial state ahead of the shock wave are known. For this we use the equation for isentropic unloading $d\varepsilon + p\,dV = 0$, according to which the final energy ε_1 is equal to

$$\varepsilon_1 = \varepsilon - \int_V^{V_1} (p\,dV)_S. \tag{11.41}$$

Since the energy behind a shock wave is $\varepsilon = \varepsilon_0 + \frac{1}{2}p(V_0 - V)$, the irreversible energy increase after unloading is

$$\varepsilon_1 - \varepsilon_0 = \tfrac{1}{2}p(V_0 - V) - \int_V^{V_1} (p\,dV)_S. \tag{11.42}$$

The magnitude of this energy is given by the difference in the areas of the curvilinear triangle $DBCS$ and the triangle ABC in Fig. 11.15, in which the

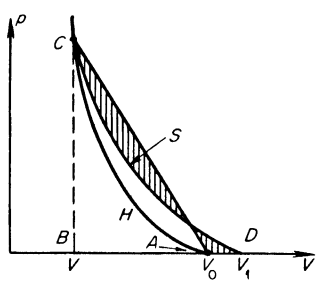

Fig. 11.15. p, V diagram for shock compression and unloading of a solid.

curve H is a Hugoniot curve and the curve S is the unloading isentrope. Numerically this energy is equal to the difference between the upper and lower shaded areas.

Let us assume that the shock wave is weak, so that all three volumes V, V_0, and V_1 differ little from each other and that the Grüneisen coefficient can be assumed to be constant and equal to its standard value Γ_0. In this case the isentropic relation between temperature and volume is given by (11.20), so that the final temperature T_1 is related to the temperature behind the shock wave T by

$$\frac{T_1}{T} = \left(\frac{V}{V_1}\right)^{\Gamma_0}. \tag{11.43}$$

On the other hand, considering the process of thermal expansion of the body at constant, zero pressure from the initial volume V_0 to V_1, we can write

$$V_1 - V_0 = V_0 \alpha (T_1 - T_0), \tag{11.44}$$

where α is the coefficient of thermal expansion at constant pressure. The irreversible increase of energy (11.42) is expressed in terms of the temperature increase by

$$\varepsilon_1 - \varepsilon_0 = c_p (T_1 - T_0),$$

where c_p is the specific heat at constant pressure* of the body. If V and T, the volume and temperature behind the shock, are known, then the volume and temperature in the final state may be calculated from the system of two equations (11.43) and (11.44).

As an example, we present the results for aluminum obtained in [23]. When aluminum is compressed by a shock wave to a pressure $p = 2.5 \cdot 10^5$ atm, the volume decreases to $V = 0.82 V_0$, and the temperature increases by $T - T_0 = 331°\text{K}$ (the initial temperature T_0 was 300°K). After unloading, the residual increase in temperature was $T_1 - T_0 = 134°\text{K}$†. When $p = 3.5 \cdot 10^5$ atm, $V = 0.78 V_0$, $T - T_0 = 522°\text{K}$, then $T_1 - T_0 = 216°\text{K}$. Naturally, the stronger the shock wave, the greater is the entropy increase imparted to the material and the higher is the residual heating.

If a shock wave with decreasing rather than constant pressure and velocity behind the front (for example, the triangular compression pulse of Fig. 11.16)

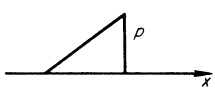

Fig. 11.16. Triangular compression pulse.

travels through a flat plate, then after such a wave emerges at the free surface "scabbing"‡ can occur. The phenomenon of scabbing consists of the following: After the compression wave is reflected from the free surface, the pressure distribution in the body results from the superposition of two waves, the incident compression wave and the reflected unloading wave. In the acoustic approximation (see §3, Chapter I)

$$p = \rho c [f_1(x - ct) + f_2(x + ct)],$$

* In solids over small ranges of temperature changes, it is practically the same as the specific heat at constant volume c_v.

† The residual temperature was calculated in [23] with greater accuracy than that given by (11.43), taking into account the small change in the Grüneisen coefficient with the change in volume; the more exact isentropic relation with a variable $\Gamma(V)$ was integrated for this purpose.

‡ *Editors' note.* Also commonly termed spalling. The authors' term is "break-away", or more literally, "split-off".

where the function f_1 describes the incident wave propagating to the right with the speed of sound, and f_2 describes the reflected wave propagating to the left. In this case the function f_1 corresponds to the triangular pressure distribution shown in Fig. 11.16. The function f_2 can be determined starting from the boundary condition that the pressure at the free surface is zero.

The functions f_1 and f_2 and the resulting pressure distribution in the body at the time of emergence of the shock at the free surface and at two subsequent instants of time are shown in Fig. 11.17. If x_1 is the coordinate of the free surface (Fig. 11.17), then the region $x > x_1$ corresponds to vacuum and the determination of the functions f_1 and f_2 in this region is purely formal and without physical significance. The only physically real values of f_1 and f_2 and of pressure are those for $x < x_1$, within the body. To emphasize this point, the functions f_1 and f_2 for $x > x_1$ in Fig. 11.17 are shown dashed.

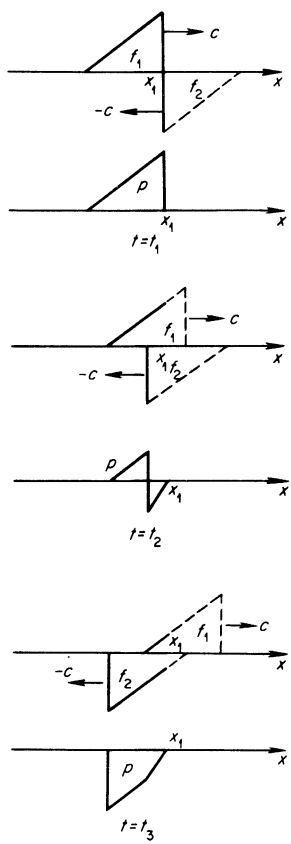

Fig. 11.17. Reflection of an acoustic triangular compression wave from a free surface. (a) $t = t_1$ refers to the time at which the leading edge of the wave emerges at the free surface; (b) $t = t_2$ and (c) $t = t_3$ refer to subsequent instants of time.

It is evident from Fig. 11.17 that after the compression wave is reflected from the free surface, negative pressures arise in the body, i.e., the material experiences a tensile stress. If the tensile stress exceeds the ultimate tensile strength of the material, then a fracture or "scabbing" occurs at this point of the body, and a layer of material (the scab) is split away from the surface and separates from the remaining material, moving away from the surface with a definite speed. Thus, for example, steel breaks down under impulsive loadings when the stresses become of the order of 30,000 kg/cm^2 *.

§12. Experimental methods of determining Hugoniot curves for solids

The conservation laws of mass and momentum (11.31) and (11.32) connect four shock front variables: the propagation speed of the shock wave through the undisturbed material D, the jump in the particle velocity u, equal to the velocity of the compressed material with respect to that of the undisturbed material, the pressure p, and the specific volume V (or density $\rho = 1/V$). If D and u are measured experimentally, then we may use (11.31) and (11.32) to find the pressure and the volume, and then, using the energy equation (11.34), we can calculate the specific internal energy ε. Thus, the problem of determining all of the flow variables of a shock front reduces to an experimental determination of any two of them, in particular, of the two kinematic parameters D and u, the ones which can be most easily measured.

The front speed D can be measured comparatively simply by recording the time of passage of the shock front at fixed points separated by a known distance. The use of such a direct method for determining the jump in particle velocity u is more difficult experimentally. Therefore, the second variable is determined by various indirect methods, utilizing certain mechanical considerations.

The experimental methods described below for studying the compressibility of solids by means of very strong shock waves and for measuring the shock front variables were proposed and developed by Al'tshuler, Krupnikov, Ledenev, and Bakanova [1–5], and also by the American authors Walsh and Christian, as well as others [22–26] (the latter did not use the "collision" method; see below). However, Soviet scientists have investigated a much wider range of pressures, up to 4 million atmospheres. The idea of measuring the kinematic variables for the study of Hugoniot curves was also developed independently by Baum, Stanyukovich, and Shekhter [21], who carried out their experiments with relatively weak shock waves.

References [1–3] describe three methods for measuring the shock wave variables, the principal features of which are presented here (see also [55]).

* *Editors' note.* If the pulse is strong enough, the process may be repeated, producing a second or more additional scabs.

1. *The "free surface" method**. This method is based on measuring the velocity of the free surface of a body which is unloaded after a shock wave emerges from its surface, and on applying the velocity doubling rule, according to which the particle velocity u is approximately equal to one half of the free surface velocity u_1. The applicability of this method is limited, since the departures from the doubling rule begin to be appreciable at very high pressures, resulting in experimental errors in the determination of u. The basic experimental setup consists in the following: A flat plate of the test material is placed against an explosive charge, as shown in Fig. 11.18 (the corresponding diagram of motion in the x, t plane is given in Fig. 11.19).

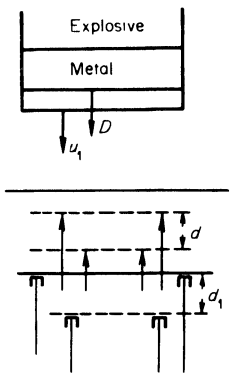

Fig. 11.18. Experimental arrangement for the "free surface" method.

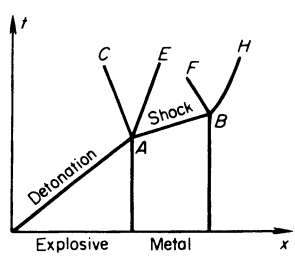

Fig. 11.19. x, t diagram for the "free surface" method.

When the detonation wave emerges from the explosive at the boundary with the metal, the discontinuity breaks up; a shock wave (line AB) travels through the metal with velocity D, the velocity of the contact surface between the explosive and the metal (line AE) is equal to the particle velocity of the metal u (a reflected wave AC propagates through the explosive). When the shock emerges at the free surface (point B) the discontinuity breaks up again, an unloading wave BF travels back into the specimen, and the boundary of

* *Editors' note.* Called the "break-away" or "split-off" method by the authors, which is the term they use for the scabbing phenomenon. The velocity doubling approximation is sometimes referred to as the free surface approximation (see, e.g., [60]).

the metal acquires the doubled velocity $u_1 \approx 2u$ (line BH). The front speed D was measured in experiments described in [1–5] by placing electrical contact pickups at known distances inside the specimen, as shown in Fig. 11.18, which closed at the time the wave passed and sent a pulse which was recorded by means of a special circuit and an oscilloscope.

Dividing the distance d by time the average wave speed across the measuring "base" d could be found (the bases d were of the order of 5–8 mm, the speeds $D \sim 5$–10 km/sec, and the time $\sim 10^{-6}$ sec; this required the development of special methods for recording such short time intervals). By the use of the pickups the time at which the free boundary of the unloaded material passed through fixed points was similarly measured* (see Fig. 11.18). The electrical contact method for measuring velocities was proposed by Tsukerman and Krupnikov. This method was used to measure the Hugoniot curve for iron up to pressures of $p \sim 1.5 \cdot 10^6$ atm ($D \sim 7.5$ km/sec, $u \sim 2.4$ km/sec).

The free surface method is not suitable for studying porous materials, since in this case the additional velocity u' upon unloading is appreciably less than the velocity u, and the doubling rule does not apply.

2. *The "collision" method*†. For the study of stronger shock waves, for which the velocity doubling rule introduces an appreciable error, the authors of [1] used another method, which is termed the "collision" method. This method is perfectly exact in principle and is suitable for the study of all materials, including porous ones.

An explosive charge is used to accelerate a plate made of the test material to a velocity w. The plate (striker) strikes another plate (target), which is at

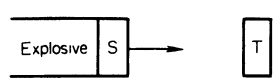

Fig. 11.20. Sketch of the experimental setup in the "collision" method.

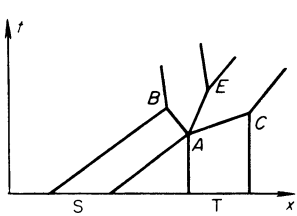

Fig. 11.21. x, t diagram for the "collision" method.

rest and made of the same material. The experimental setup is shown in Fig. 11.20, and an x, t diagram of the process is given in Fig. 11.21. Two shock waves originate at the time of impact and propagate through both bodies

* The pickups were equipped with protective caps to prevent their being closed by the air shock which the metal boundary pushes.

† *Editors' note.* The authors of [1] and the authors used the term "braking" method. The method is sometimes called the "momentum transfer" method (see [60]).

(AB and AC on the x, t diagram). The pressures p and particle velocities u on both sides of the contact surface between the bodies are the same and equal to the values of these quantities behind the shock waves up to the time the shocks reach the opposite boundaries of the specimens*. This velocity u is also the velocity of the contact surface (the line AE). Pressure and velocity distributions after impact are shown in Fig. 11.22.

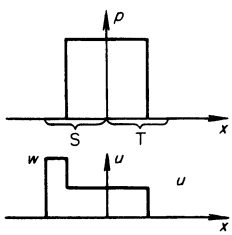

Fig. 11.22. Pressure and velocity distributions after impact in the "collision" method.

Since the materials are identical, the two shock waves are also identical, and the jumps in particle velocity are the same for both waves. The velocity jump for the target is the same as the velocity of the compressed material u, since the target was initially at rest. With respect to the striker, however, the material ahead of the shock moves with the striker velocity w, and behind the wave with the velocity u, so that the absolute value of the velocity jump is equal to $w - u$. Consequently, $w - u = u$ and $u = w/2$. Thus, the problem reduces to measuring the wave velocity D in the target and the striker velocity w. This is carried out experimentally in the same manner as in the free surface method, by using a system of electrical contact pickups.

Using the collision method Hugoniot curves for iron were obtained up to pressures of $p \sim 5 \cdot 10^6$ atm ($D \sim 12$ km/sec, $u \sim 5$ km/sec, and $V_0/V \sim 1.75$) in [1]. Porous iron with a density 1.4 times less than standard was also studied.

The collision method can also be extended to the case when the test target and striker are made from different materials. In this case, however, the striker must be made of a material for which the Hugoniot curve is known. In a number of cases this turns out to be more expedient than making the striker from the test material, since by an appropriate choice of the striker material it is possible from the same explosive charge to obtain a more powerful shock in the test material.

If the striker and target materials are different, then, in spite of the fact that the pressure behind both shock waves is the same, the velocity jumps are no longer the same, and $w - u \neq u$. However, if the Hugoniot curve for the striker is known, then we also know the dependence of the pressure on the particle velocity jump, that is, the function $p = f(w - u)$. On the other hand, the pressure p is related to the jump of the particle velocity in the

*See §24, Chapter I.

target, equal to the velocity of the contact surface u, by (11.32): $p = Du/V_0$. Measuring as before the shock velocity in the target and the striker velocity w, we can find u from

$$f(w-u) = \frac{Du}{V_0}. \tag{11.45}$$

A graphical method, based on the use of a pressure-velocity diagram (see §24, Chapter I), is very convenient for this purpose. These diagrams are widely used when considering various processes involving shock waves in which two contiguous media are involved, since the velocity and pressure at the contact surface between the two media are the same.

Let us consider the collision between the striker and target on a p, u diagram, where u is the particle velocity of the material in the laboratory coordinate system, in this case in that system in which the target is initially at rest. The initial states of the target ($p = 0$, $u = 0$) and of the moving striker $p = 0$, $u = w$, are represented by the points O and A in Fig. 11.23. If the shock

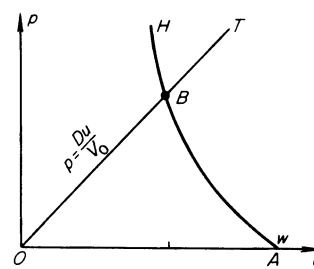

Fig. 11.23. p, u diagram for the "collision" method. *HBA* is the Hugoniot curve for the striker. *OBT* is the locus of target states after impact.

velocity measured at the target is D, then the locus of states of the target material behind the shock wave is the straight line $p = Du/V_0$, with the known slope D/V_0. Let us depict the Hugoniot curve for the striker material, considering the dependence of the pressure on the velocity jump instead of on the volume. In this case the velocity jump is equal to $w - u$, so that $p = f(w-u)$. The point of intersection B of the two lines, according to (11.45), determines the state (pressure and particle velocity) behind the two shock waves. If the striker and target are made from the same material, then (as we already know) the point of intersection lies exactly half-way between points O and A ($u = w/2$).

3. *The "calibrated reflection" method**. In this method use is made of the relationships governing the breakup of an arbitrary discontinuity resulting from the reflection of a shock wave from the contact surface between two

* *Editors' note.* Termed "reflection" method by the authors and sometimes referred to as the "impedance match" method (see, e.g., [60]).

media (see §24 of Chapter I). The advantage of this method in comparison with the preceding one is that it does not require the measurement of particle velocities, which are more difficult to measure than the shock front velocity. However, the method requires the use of a calibrated material with a known equation of state. This method was worked out by the authors of [2] together with G. M. Gandel'man.

Let us consider the passage of a strong shock from material A to material B. The wave traveling through material B is always a shock wave, while the wave reflected in A is either a shock wave, in case material B is "harder" than A, or a rarefaction wave, in case B is "softer" than A (this is most easily visualized by considering the two limiting cases, where A is a gas and B is a solid, and where A is a solid and B is a gas). The velocity and pressure distributions in the two cases are given in Fig. 11.24. The corresponding x, t diagrams are also shown there.

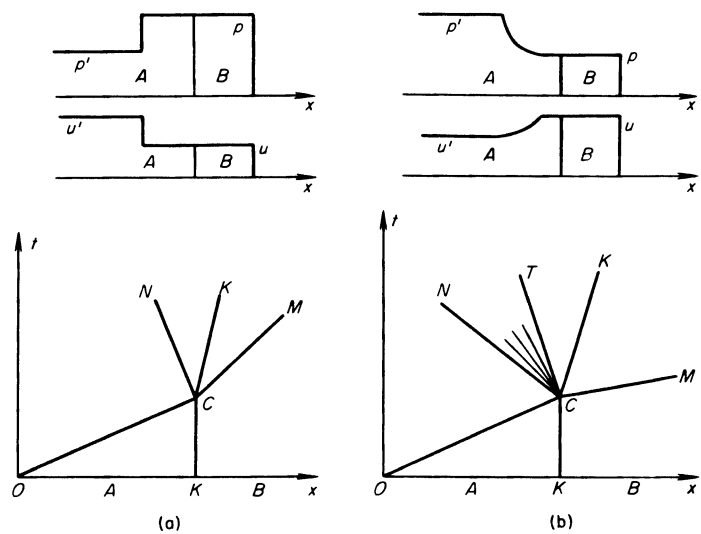

Fig. 11.24. Pressure and velocity distributions and x, t diagrams for the "calibrated reflection" method. (a) Case when the reflected wave is a shock wave. OC is the shock wave in A, CM is the shock wave in B, CN is the reflected shock wave in A, and KCK is the contact surface between A and B. (b) Case when the reflected wave is a rarefaction wave. OC is the shock wave in A, CM is the shock wave in B, CN is the head of the rarefaction wave, CT is the tail of the rarefaction wave, and KCK is the contact surface between A and B.

Let us consider this process on a pressure-velocity diagram (in the initial state both A and B are at rest in the laboratory system of coordinates). We assume that the equation of state of the material A is known. We draw on the

p, u diagram (Fig. 11.25) the Hugoniot curve for the material A, $p_A(u)$ for the first shock wave traveling through the undisturbed material. If we measure experimentally the front velocity of the initial shock D_1, then we can find the state behind it, represented by the point of intersection of the straight line $p = D_1 u / V_{0A}$ with the Hugoniot curve $p_A(u)$ (the point $a(p_a, u_a)$).

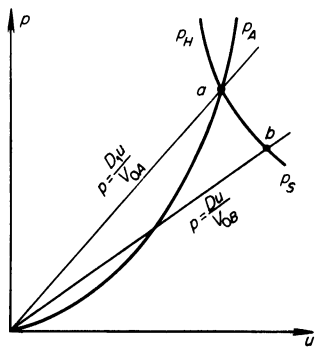

Fig. 11.25. p, u diagram for the "calibrated reflection" method.

After this shock wave is reflected from the contact surface between A and B, a new state is established in the material A. If the reflected wave is a shock wave, then the state lies on a Hugoniot curve of a second compression whose initial state is $a(p_a, V_a, u_a)$; this Hugoniot curve is depicted by the curve p_H going upward from the point a. However, if the reflected wave is an isentropic expansion wave, then the new state lies on the rarefaction isentrope, going downward from the point a (the curve p_S). Since the equation of state for the material A is assumed known, then both the Hugoniot curve of the second compression $p_H(V, V_a, p_a)$ and the expansion isentrope with the entropy equal to $S_a = S(p_a, V_a)$ can be transformed so as to replace the volume by the velocity as the argument. In the first case this is done by using the relations across a shock front, and in the other case by using the relation for an expansion wave (see §10, Chapter I).

If the shock wave velocity D in the material B is also measured experimentally, then the straight line $p = Du/V_{0B}$ which is the locus of states behind this wave can be drawn. The point of intersection b of this line with curve $p_H a p_S$, which is the locus of possible states in the material A after reflection of the shock wave, determines the pressure and velocity behind the shock wave in the material B, equal to the pressure and velocity at the contact surface between A and B (see Fig. 11.24). The p, u diagram of Fig. 11.25 illustrates the second case, in which the reflected wave is a rarefaction wave. In the first case the line $p = Du/V_{0B}$ passes above the line $p = D_1 u / V_{0A}$ and the point

of intersection b lies above point a on the Hugoniot curve for the second compression of the material A, described by the curve ap_H*.

Summing up, the calibrated reflection method consists in the following: A shock wave is generated in the plate made of material A with a known equation of state, either directly by an explosive charge, or by impact with another plate previously accelerated by an explosive to a high velocity. This wave passes into specimens of the test material B, with which is also included a sample of material A (a diagram of the experiment is shown in Fig. 11.26).

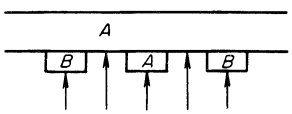

Fig. 11.26. Sketch of the experimental setup in the "calibrated reflection" method.

By recording the closing times of the electrical contact pickups located at the points denoted by arrows in Fig. 11.26, the front velocities D_1 and D are determined. Having constructed the Hugoniot curve $p_A(u)$ on a p, u diagram and having drawn the line $p = D_1 u/V_{0A}$, the point a giving the state behind the shock wave in a material A can be found. Then the Hugoniot curve for the second compression is drawn upward through point a, and the isentrope is drawn downward through point a; the line $p = Du/V_{0B}$ is also drawn. Thereby the sought state point $b(p, u)$ behind the shock wave is determined for the test specimen.

Actually (in the experiments), the pressure changes between states a and b were always small. Under these conditions, as shown by calculations, the curve $p_H ap_S$ can to a high degree of accuracy be represented as a mirror image of the Hugoniot curve of the primary compression at the point a. We note that the slope of the line $p_H ap_S$ at point a is determined by the speed of sound behind the front of the primary shock wave in A. Actually, for either a rarefaction wave or a weak compression wave, $dp = \pm \rho c du$ (see (1.59)); thus the slope of $p_H ap_S$ at point a is $|dp/du| = \rho c = c/V$, where c and V are the speed of sound and the volume in the material A after compression by the first shock wave. Experimental methods for determining the speed of sound behind the shock wave will be considered below.

Al'tshuler, Krupnikov, and Brazhnik have used the calibrated reflection method for obtaining Hugoniot curves for a large number of metals (Cu, Zn,

* In addition, we see here what characterizes the "hardness" of a material. Let us assume that the shock waves are weak and that their speeds are close to the speeds of sound: $D \approx c_B$ and $D_1 \approx c_A$. Material B is harder than A and the reflected wave will be a shock wave if $c_B/V_B > c_A/V_A$ or $\rho_B c_B > \rho_A c_A$. The quantity ρc is sometimes called the acoustic impedance. It determines the relation between pressure and velocity in an acoustic or weak shock wave, with $p = \rho c u$.

Pb, etc.) [2]. This method was used for studying the compressibility of sodium chloride (reference [5]), and was also used in the majority of works of non-Soviet scientists. Iron, aluminum, or brass were most frequently used as the material A.

§13. Determination of cold compression curves from the results of shock compression experiments

One of the most valuable results of experiments on shock compression of solids is the determination for a material of its cold compression curve $p_c(V)$, which characterizes the repulsive forces between the atoms. The functions $p_c(V)$ and $\varepsilon_c(V)$ are determined from a theoretical treatment of experimental data on the Hugoniot curves for the material. In [3] the cold compression curves were determined over a wide range of compressions and pressures by expressing the thermodynamic functions $p(V, T)$ and $\varepsilon(V, T)$ as the sum of three terms in the form of (11.30). The electronic terms p_e and ε_e were written on the basis of purely theoretical considerations (see §§5 and 6), with known experimental values used for the electronic specific heat coefficient β_0.

Using the experimental functional dependences for $p(V)$ and $\varepsilon(V)$ given by the Hugoniot curve, we can regard equations (11.30) as two equations with three unknown functions $p_c(V)$, $\Gamma(V)$, and $T(V)$, where $T(V)$ corresponds to the dependence of the temperature on the volume along the Hugoniot curve. For the third equation we may use the relation between the Grüneisen coefficient $\Gamma(V)$ and the cold compression curve $p_c(V)$, given by the Slater–Landau formula (11.18)*. A numerical solution of this system of equations gives the cold compression curve $p_c(V)$, the function $\Gamma(V)$, and the temperature behind the shock wave T. The data in Table 11.2 and the curves of Fig. 11.8 (§7) were obtained in this manner. Specific results for other metals tested can be found in the tables in [3].

If the Hugoniot curves for both porous and continuous forms of a material are known from experiment, then the relation between the functions $\Gamma(V)$ and $p_c(V)$ is not required. If we consider temperatures that are not too high and neglect the electronic terms p_e and ε_e, we can write

$$\frac{1}{\Gamma} = \frac{\Delta\varepsilon_T}{V\,\Delta p_T} = \frac{1}{V}\,\frac{\varepsilon_{\text{por}}(V) - \varepsilon_{\text{cont}}(V)}{p_{\text{por}}(V) - p_{\text{cont}}(V)},$$

where the quantities on the right-hand side are the experimental values on

* In a number of cases a slightly different relation between the functions $\Gamma(V)$ and $p_c(V)$ was used, one given by the Dugdale–McDonald formula [27].

the Hugoniot curves for the continuous and porous forms of the same material compressed to the same volume. The elastic components of pressure and energy are identical in both cases, so that the differences in ε and p are equal to the excess of the purely thermal energy and pressure in the compressed porous material over those of the compressed continuous material. This was the method used in [1] to obtain the cold compression curve for iron (Fig. 11.2).

The cold compression curve for sodium chloride was reported in [5]. Comparison with expressions for the repulsive forces in ionic crystals permitted the determination of the parameters characterizing the interaction forces which enter these equations. The method for calculating the temperature on the Hugoniot curve for comparatively weak waves, when the thermal terms are small in comparison with the elastic terms and the Hugoniot curve follows the cold compression curve closely, is described in [22] (in this case, obviously, the electronic terms were not taken into account).

Frequently, various interpolation equations are employed to characterize the Hugoniot and cold compression curves $p_c(V)$ analytically. This is done by specifying state functions of given forms containing several parameters, which are then determined from experimental data. As an example, we can take the widely used equation $p_c = A[(V_0/V)^n - 1]$, containing the two parameters A and n. In investigating sodium chloride [5] the $p_c(V)$ curve was obtained in analytic form by using a power-law or exponential representation for the repulsive forces in ionic crystals. The constants which enter the equation were determined from data on dynamic compressibility.

Kormer and Urlin [14] constructed an interpolation formula for the cold compression curve of the form

$$p_c = \sum_{n=1}^{6} a_n \left(\frac{V_{0c}}{V}\right)^{\frac{1}{3}n+1}.$$

The coefficients a_n were determined without using experimental data on shock compression, only using the relations between the coefficients and the known parameters of the standard state (the compressibility, the Grüneisen coefficient, etc.) and also the condition that at high pressures the curve should agree with the relation derived from the Thomas–Fermi–Dirac model. Good agreement was obtained with the experimentally determined curves for $p_c(V)$*.

* Subsequently Kormer, Urlin, and Popova [15] refined this method, adding one more term to the series and using one experimental point on the Hugoniot diagram. Very good agreement with the experimental curves was obtained.

3. *Acoustic waves and splitting of waves*

§14. Static deformation of a solid

In the study of shock compression of solids, we have assumed up till now that the pressure in the compressed material is isotropic, that it has a hydrostatic character as in a liquid or gas. The increase in density was then considered as a result of an isotropic compression. Correspondingly, the elastic properties of the material were characterized by a single quantity, the isentropic compressibility $\kappa = -(1/V)(\partial V/\partial p)_S$, which determined the speed of propagation of acoustic compression (and rarefaction) waves, the speed of "sound"

$$c_0 = \left[-V^2\left(\frac{\partial p}{\partial V}\right)_S\right]^{1/2} = \left(\frac{V}{\kappa}\right)^{1/2}.$$

This can be done only in the case when the pressures are sufficiently high and the effects connected with the strength of solids and the existence of shear strains and stresses are not important. If the loads are small, then it becomes necessary to take into account the elastic properties of the solid which distinguish it from a liquid. This has an appreciable effect on the character of the dynamic processes and, in particular, on the propagation of elastic compression and rarefaction waves. Thus, it is found that acoustic waves can propagate in a solid with different speeds, depending on the particular conditions. Before considering these dynamic phenomena, let us examine the behavior of a solid under static loads. Here we assume that the deformations and loads are small, so that linear elasticity theory is applicable.

The state of a deformed body is described by two tensors, the strain tensor and the stress tensor. In what follows we shall consider only a few simple cases of homogeneous deformations (where each element of the body is deformed in the same manner), which are characterized by simple and obvious quantities. For this reason we shall not introduce the strain tensor in general form*.

The stress tensor component σ_{ik}, where the subscripts i and k denote the x, y, and z coordinate directions, represents the ith component of a force acting on a unit area of the body whose normal is in the k direction. The components σ_{xx}, σ_{yy}, and σ_{zz} represent normal stresses and the components σ_{xy}, σ_{xz}, and σ_{yz} are tangential or shear stresses (Fig. 11.27). The tensor σ_{ik} is symmetric, so that $\sigma_{xz} = \sigma_{zx}$, $\sigma_{yz} = \sigma_{zy}$, $\sigma_{xy} = \sigma_{yx}$.

Let us consider some examples of deformations.

1. Imagine a cylindrical rod of length L and diameter d, with a compressive

* See, for example, Landau and Lifshitz [28].

force or a pressure p applied to its ends. The z axis is directed along the axis of the rod, as shown in Fig. 11.28. The lateral surface of the rod we assume to be free. Under the action of the load the rod is contracted by a length ΔL

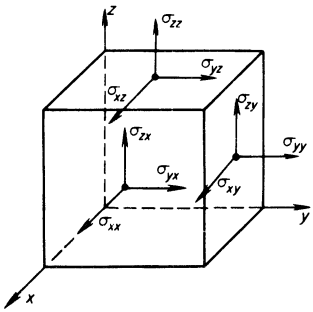

Fig. 11.27. Diagram illustrating the stress tensor components.

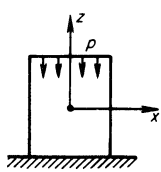

Fig. 11.28. Diagram of a rod in compression.

and it is thickened (the diameter increases by Δd). In this case only the normal stress in the axial direction σ_{zz}, which is minus* the external pressure $\sigma_{zz} = -p$, is different from zero. The normal stresses in the transverse directions, σ_{xx} and σ_{yy}, are absent, since the lateral surface of the rod is free and nothing prevents the rod from expanding in this direction. It is obvious that the tangential or shearing stresses σ_{xy}, σ_{xz}, and σ_{yz} are also equal to zero in the coordinate system chosen.

According to Hooke's law for small deformations the relative contraction of the rod is proportional to the applied force:

$$\frac{\Delta L}{L} = -\frac{p}{E} = \frac{\sigma_{zz}}{E}, \tag{11.46}$$

where E is Young's modulus (this is the definition of Young's modulus). The relative thickening of the rod is proportional to the relative contraction

$$\frac{\Delta d}{d} = -\sigma \frac{\Delta L}{L}, \tag{11.47}$$

* *Editors' note.* It is customary to define the normal stresses as positive when tensile, and we have changed some of the equations for consistency with this practice. Under compression σ_{zz} and $\Delta L/L$ are negative.

where σ is Poisson's ratio. Poisson's ratio is always positive and smaller than $\frac{1}{2}$. This follows from the observations that a compressed rod becomes thicker and that its volume can only be reduced (for constant volume $d^2L = const$, and $\Delta d/d = -\frac{1}{2}\Delta L/L$, $\sigma = 1/2$).

2. Let the lateral surface of the rod be constrained in a manner such that for an axial compression the rod cannot deform in the transverse direction (the rod is placed in a shell with rigid walls). This will give rise to normal stresses in the transverse directions $\sigma_{xx} = \sigma_{yy}$ which exactly balance the external lateral forces acting on the shell walls. The normal axial stress σ_{zz} is as before minus the external compressive pressure p. From the theory of elasticity the relative contraction of the rod in the unidirectional axial deformation of this case is related to the external pressure by an equation analogous to (11.46):

$$\frac{\Delta L}{L} = -\frac{p}{E'} = \frac{\sigma_{zz}}{E'}, \tag{11.48}$$

where

$$E' = \frac{E(1-\sigma)}{(1+\sigma)(1-2\sigma)}. \tag{11.49}$$

The quantity E' is always greater than Young's modulus E. In order to decrease the length of a laterally constrained rod by the same amount as that of a free rod it is necessary to apply a larger compressive force. The normal stresses in the transverse directions are

$$\sigma_{xx} = \sigma_{yy} = \frac{\sigma}{1-\sigma}\sigma_{zz} = -\frac{\sigma}{1-\sigma}p. \tag{11.50}$$

Tangential stresses are absent in the coordinate system chosen. All the relationships in the above two examples are equally valid in the case when the rod is extended, is in tension.

3. A body subjected to an isotropic compression (or expansion) changes its volume while retaining its shape, i.e., while remaining similar to itself in shape. An isotropic compression is obtained by applying a constant pressure to the surface of the body. The stress tensor for such a compression is diagonal ($\sigma_{xy} = \sigma_{xz} = \sigma_{yz} = 0$); all three normal components are the same and equal to minus the pressure. This remains true in any coordinate system. The "pressure" in the body is isotropic in this case and is hydrostatic in character, as in a liquid. For small deformations, the relative change in volume* is proportional

* The sum of the diagonal strain tensor components is $u_{xx} + u_{yy} + u_{zz} = \Delta V/V$ and is termed the dilatation. For an isotropic compression $u_{xy} = u_{yz} = u_{xz} = 0$ and $u_{xx} = u_{yy} = u_{zz}$.

to the pressure:

$$\frac{\Delta V}{V} = -\kappa p = -\frac{p}{K}, \tag{11.51}$$

where κ is the compressibility, and its reciprocal $K = 1/\kappa$ is the bulk modulus.

4. Finally, let us consider a pure shear deformation in one direction, as shown in Fig. 11.29. In pure shear the body only changes its shape but not its volume. In the example shown in Fig. 11.29 only the tangential stress

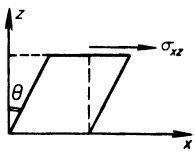

Fig. 11.29. Pure shear strain in one direction.

σ_{xz} is different from zero. All the other components of the stress tensor are equal to zero. According to Hooke's law, the shear strain angle is proportional to the shearing force τ (per unit area), which is equal to the stress σ_{xz}

$$\theta \approx \tan\theta = \frac{\tau}{G} = \frac{\sigma_{xz}}{G}, \tag{11.52}$$

where G is the shear modulus.

As is well known (see [28]), we can represent an arbitrary deformation as the sum of pure shear strains and an isotropic compression (or extension). Because of this interrelationship between the strains in axial compression of a rod and the elementary strains of isotropic compression and shear, the four characteristics of the material E, σ, K, and G are not independent, but are connected by two relations. One can show (see [28], for example) that

$$E = \frac{9KG}{3K+G}, \qquad \sigma = \frac{1}{2}\frac{3K-2G}{3K+G}, \tag{11.53}$$

and, conversely, that

$$G = \frac{E}{2(1+\sigma)}, \qquad K = \frac{E}{3(1-2\sigma)}.^{*} \tag{11.54}$$

Thus, we can rewrite Hooke's law for the axial deformation of a laterally constrained rod (11.48) in terms of the moduli K and G in the form

$$\frac{\Delta L}{L} = -\frac{p}{E'}, \qquad E' = K + \tfrac{4}{3}G. \tag{11.55}$$

* It is evident from this equation that $\sigma \leqslant 1/2$, since $K > 0$ and $E \geqslant 0$.

In order to give some idea of the numerical values of the parameters we note that for iron (with a 1% carbon content)

$$E \approx 2.1 \cdot 10^6 \text{ kg/cm}^2, \qquad G \approx 0.82 \cdot 10^6 \text{ kg/cm}^2,$$

$$K \approx 1.61 \cdot 10^6 \text{ kg/cm}^2, \qquad \sigma \approx 0.28.$$

For a body subjected to an isotropic compression or extension the stress tensor is diagonal in any coordinate system, and all three of its components are the same. For other deformations the stress tensor is diagonal and the tangential stresses vanish only in certain specially selected coordinate systems. The deformations of a rod in compression examined above, either free or constrained laterally, can serve as an example. The inequality of the diagonal elements of the stress tensor is connected with the fact that in reality the deformation is not a pure isotropic compression (or extension) and does contain an element of shear. This is manifested explicitly if we change to another coordinate system, or, equivalently, if we consider forces acting on areas which are inclined with respect to the rod axis. In this case it becomes immediately clear that the inclined areas experience tangential stresses, which shows that shear strains are present.

Let us calculate the tangential stress acting on an area inclined at 45° to the direction of the external pressure (Fig. 11.30). For simplicity we shall not

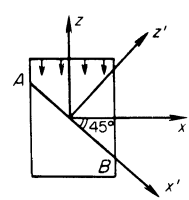

Fig. 11.30. The question of non-diagonality of the stress tensor.

consider a cylindrical rod, but rather a plane layer infinite in the y direction and constrained laterally so that there are no displacements in the x direction. In the x, y, z coordinate system we have stresses σ_{zz} and $\sigma_{xx} = \sigma_{yy}$. In order to find the tangential stress acting on the plane AB, we introduce a new coordinate system, x', y', z', rotated with respect to the old system about the y axis (the axes y and y' coincide). According to the rule for transformation of a tensor on rotating the coordinate system, we find

$$\sigma_{x'z'} = -\sigma_{zz} \cos^2 45^\circ + \sigma_{xx} \cos^2 45^\circ = -\tfrac{1}{2}(\sigma_{zz} - \sigma_{xx}).$$

This is a tangential stress acting in the x' direction on the area AB, whose normal is in the direction of the z' axis.

§15. Transition of a solid medium into the plastic state

One of the characteristic properties of a solid that distinguishes it from a fluid is the stability of its shape, its resistance to shear. A fluid has no resistance to shear and readily assumes any shape as long as this does not require any change in its volume (density). Tangential shear stresses are absent in a fluid in a static state*. A fluid is characterized by the fact that its shear modulus $G = 0$. Formally, for $G = 0$ Poisson's ratio σ is, according to (11.53), equal to $\frac{1}{2}$. The stress tensor in this case is diagonal in any coordinate system, with all its three normal components identical and equal to minus the "hydrostatic" pressure, which is isotropic. The elastic properties of a fluid are characterized only by its compressibility or bulk modulus.

It is well known that, for sufficiently high loads that do not reduce to an isotropic compression, a solid changes its elastic properties and becomes plastic, or flowing, similar in some respects to a fluid. The plastic state of a solid is not characterized by the total absence of tangential stresses, as in the case of a fluid, but by the absence of an increase in the tangential stresses with an increase in shear strains. Starting at certain critical shear strains and stresses, a solid no longer resists any further increase in shear.

Above we have defined the shear modulus G as a coefficient of proportionality between the tangential stress in pure shear and the shearing strain (see (11.52)). As a result of the linearity of the relation between stress and strain, the increments in strain and stress are also proportional

$$\sigma_{xz} = G\theta, \qquad d\sigma_{xz} = G\, d\theta$$

(in pure shear through the angle θ, as shown in Fig. 11.29). When a solid medium is in the plastic state, after the values of the shear strain angle θ and stress σ_{xz} become equal to critical values θ_{cr} and σ_{cr}, there is no longer an increase in stress with increasing strain (or its rate of increase drops sharply). This is illustrated by the $\sigma_{xz}(\theta)$ diagram in Fig. 11.31. If we formally define the shear modulus in this state as the coefficient of proportionality between the increments $d\sigma_{xz}$ and $d\theta$, rather than between the quantities σ_{xz} and θ themselves, then the shear modulus should be set equal to zero.

Let us consider an axial compression of a nonplastic and of a plastic body. Let a cylindrical solid body be placed in a cylindrical container with rigid walls and be compressed by a piston along its axis (Fig. 11.32). A schematic representation of the changes in the positions of the atoms in the body is given in Fig. 11.33. For simplicity we assume a cubic lattice. If the body is nonplastic, then the interatomic distances in the direction of the axis decrease,

* They arise only at the time when the shape changes and do not depend on the strains themselves but on their rate of change.

while they remain unchanged in the transverse directions. In this case the atoms remain "in their places". This is shown in Fig. 11.33b. If, however, the body is plastic, then all interatomic distances are decreased, the lattice is rearranged, and the atoms are redistributed in such a manner that the lattice remains cubic even in the compressed state (Fig. 11.33c). For clarity, the atoms in Fig. 11.33c have been renumbered, without any implication that the atoms in question have been redistributed in the particular manner shown.

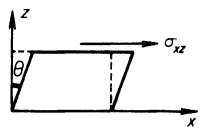

Fig. 11.31. Tangential stress-shear strain angle diagram.

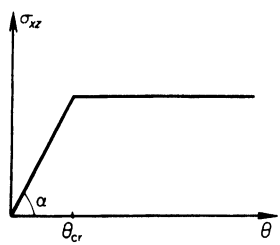

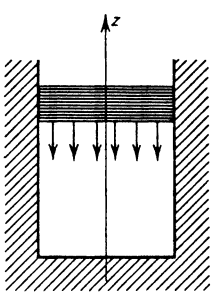

Fig. 11.32. Diagram showing axial compression (constrained) of a rod.

The first case (Fig. 11.33b) contains within it an element of shear. Thus, in the undeformed state (Fig. 11.33a) the projection of atom 2 on the inclined plane AB passing through atoms 1–6 of two neighboring horizontal rows falls at point C situated at the midpoint of the segment AB. In the deformation of a nonplastic body (Fig. 11.33b) point C moves closer to point B. The inclined rows of atoms are displaced with respect to each other: the upper row 2–7–12 is displaced to the right and downward with respect to the lower row 1–6–11.

However, in the deformation of a plastic body the lattice remains cubic, the projection of atom 5 on the inclined plane AB passing through atoms 1–13, labeled point C as in the undeformed state, lies at the midpoint of

segment AB. The inclined rows of atoms 5–10 and 1-13 are not displaced with respect to each other, as also in the undeformed state.

During deformation a body acquires elastic energy resulting from the work of the external forces producing the deformation. If the body is nonplastic, then this energy is related to the change in volume as well as to the shear. For a given volume the elastic energy is a minimum if the compression is

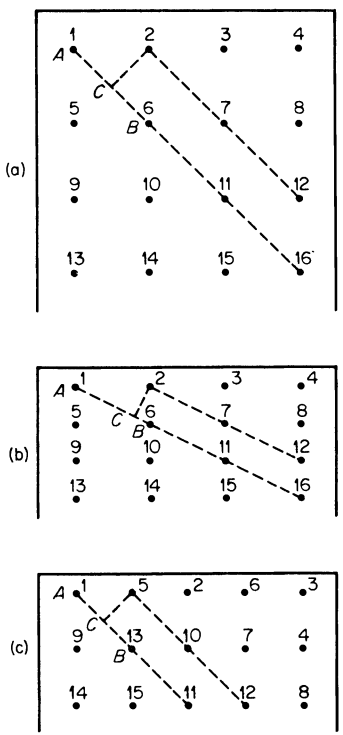

Fig. 11.33. Diagram illustrating the deformation of nonplastic (b) and plastic (c) bodies; (a) shows the undeformed state.

isotropic and there are no shearing strains. Therefore, a nonplastic body subjected to an axial compression to a given volume is in a nonequilibrium state. The equilibrium state for the given volume would correspond to an isotropic compression, that is, to one with a rearranged crystal lattice. The rearrangement of the lattice requires an activation energy, as the atoms must overcome potential barriers*. At small loads rearrangement does not take place and the solid exhibits nonplastic behavior with respect to deformation.

However, when the loads are sufficiently great, the solid loses its firmness or nonplasticity and becomes similar to a fluid, in the sense that it becomes

* It is possible that rearrangement involves a macroscopic breaking up of the particles of the body.

capable of rearranging itself in such a manner that its energy at a given volume is a minimum. In particular, this occurs for axial compression of a body when the tangential stress in a plane inclined at 45° to the direction of the compressive force $\sigma_{x'z'}$ (see the end of the preceding section) exceeds the critical shear stress σ_{cr}. Noting that

$$\sigma_{x'z'} = -\tfrac{1}{2}(\sigma_{zz} - \sigma_{xx}) = -\frac{1}{2}\frac{1-2\sigma}{1-\sigma}\sigma_{zz} = \frac{1}{2}\frac{1-2\sigma}{1-\sigma}p,$$

we find for the critical compressive load p_{cr} above which the solid becomes plastic

$$p_{cr} = \frac{1-\sigma}{1-2\sigma}2\sigma_{cr}. \tag{11.56}$$

In contrast to the thermodynamic constants of the material (Young's modulus or the compressibility), the critical shear stress, as a quantity characterizing the strength, depends strongly on the processing of the metal, impurities, etc. For iron, approximately, $\sigma_{cr} = 600$ kg/cm^2, and $p_{cr} = 1900$ kg/cm^2.

Let us consider an axial compression of a body in the z direction by a compressive load p. No deformations occur in the transverse directions x and y (the rod is laterally constrained). We shall formally describe the transition from the nonplastic to the plastic state by setting the shear modulus in the proportionality relation between the stress and strain increments equal to zero for loads exceeding the critical value. According to (11.48) and (11.55), for $p = -\sigma_{zz} < p_{cr}$,

$$\sigma_{zz} = (K + \tfrac{4}{3}G)\frac{\Delta L}{L}, \qquad \frac{d\sigma_{zz}}{d(\Delta L/L)} = K + \tfrac{4}{3}G.$$

Then from (11.50) and (11.53)

$$\sigma_{xx} = \sigma_{yy} = (K - \tfrac{2}{3}G)\frac{\Delta L}{L}, \qquad \frac{d\sigma_{xx}}{d(\Delta L/L)} = K - \tfrac{2}{3}G;$$

$$\sigma_{x'z'} = -\tfrac{1}{2}(\sigma_{zz} - \sigma_{xx}) = -G\frac{\Delta L}{L}, \qquad \frac{d\sigma_{x'z'}}{d(\Delta L/L)} = -G.$$

After the load reaches its critical value, in the equations for the derivatives of the stresses (but not in the relations for the stresses themselves) we set $G = 0$. For $p > p_{cr}$ we obtain

$$\frac{d\sigma_{zz}}{d(\Delta L/L)} = \frac{d\sigma_{xx}}{d(\Delta L/L)} = K, \qquad \frac{d\sigma_{x'z'}}{d(\Delta L/L)} = 0. \tag{11.57}$$

The normal stresses $-\sigma_{zz}$, $-\sigma_{xx}$, and $-\sigma_{yy}$ now increase uniformly in correspondence with the bulk modulus (in axial compression $\Delta L/L = \Delta V/V$). The

tangential stress in the inclined plane remains constant and given by $\sigma_{x'z'} = \sigma_{cr}$ (the critical strain is $(\Delta L/L)_{cr} = \sigma_{cr}/G$). The stress-strain diagram is shown in Fig. 11.34.

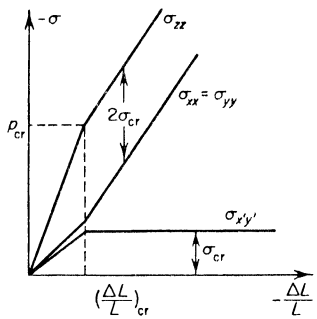

Fig. 11.34. Stress-strain diagram for axial compression of a solid.

For loads less than or of the order of the critical load, σ_{zz} is very different from σ_{xx} and the "pressure" is substantially nonhydrostatic in character. In the limit when the loads are sufficiently large, with $p \gg p_{cr}$, the relative difference $(\sigma_{zz} - \sigma_{xx})/\sigma_{zz} = -2\sigma_{cr}/\sigma_{zz} \to 0$, and all the three normal stresses become almost identical. The tangential stress $\sigma_{x'z'} = \sigma_{cr}$ becomes small in comparison with the normal stresses. It remains constant or increases slowly, much more slowly than before.

§16. Propagation speed of acoustic waves

Let us extend the results of the preceding sections to the case of dynamic loads and find the propagation speeds of acoustic compression (and rarefaction) waves under different conditions. Let a constant compressive force with pressure p be applied at an initial time to the end of a thin rod with a free lateral surface*. A compression wave will travel through the body, with a propagation speed which we denote by c_1. The material between the wave front and the end of the rod deforms as in example 1 of §14, and acquires a constant velocity u in the direction of the axial force. As may be seen from Fig. 11.35 the relative contraction of the rod in the compression region is

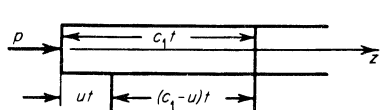

Fig. 11.35. Diagram illustrating the propagation of an acoustic compression wave.

* This statement of the problem is analogous to the piston problem treated in gasdynamics (see Chapter I).

$[c_1 t - (c_1 - u)t]/c_1 t = u/c_1$. If we consider small loads and deformations, then, according to Hooke's law (11.46),

$$\frac{u}{c_1} = \frac{p}{E}. \quad * \tag{11.58}$$

In a time t the mass of material encompassed by the wave $\rho c_1 t$ (per unit cross sectional area of the rod) acquires a momentum $\rho c_1 t u$. According to Newton's law this momentum is equal to pt, so that

$$p = \rho u c_1. \tag{11.59}$$

This equation is completely analogous to the corresponding gasdynamic equation. From (11.58) and (11.59) the expression for the propagation speed of a compression wave through the rod (the speed of "sound") is

$$c_1 = \left(\frac{E}{\rho}\right)^{1/2}. \quad \dagger \tag{11.60}$$

When the compressive load is removed, a tensile or unloading wave is propagated at the same speed.

Let us now imagine a laterally constrained rod, as in example 2 of §14, such that the body is not deformed by the compression wave in the plane perpendicular to the direction of wave propagation‡. Repeating the preceding considerations and using (11.55), we find the speed of "sound" in this case to be

$$c_l = \left(\frac{E'}{\rho}\right)^{1/2} = \left(\frac{K + \frac{4}{3}G}{\rho}\right)^{1/2}. \tag{11.61}$$

The speed c_l is nothing else but the "longitudinal" speed of sound, that is,

* In a dynamic process that takes place adiabatically (isentropically), Young's modulus differs somewhat from that used in statics corresponding to isothermal conditions. This difference is usually negligibly small (see [28]). The same is true of Poisson's ratio and the bulk modulus. The isentropic and isothermal shear moduli do not differ from each other, since shear is not accompanied by a change in volume of the body.

† *Editors' note.* This speed is termed the thin rod wave speed. Wave propagation in a rod of finite width is dispersive, and this wave speed is a limiting speed for large values of the ratio of wavelength to rod width. Analogous is the thin plate wave speed $(E''/\rho)^{1/2}$, where $E'' = E/(1 - \sigma^2) = 4G(3K + G)/(3K + 4G)$. This speed applies when a rectangular bar is free in one lateral direction and constrained in the other, and is a limiting speed in the same sense as c_1.

‡ We can also treat the rod as free, but consider times during which the compression wave travels through distances which are appreciably smaller than the diameter. An unloading wave from the lateral surface propagates to the axis with a finite speed, so that over the time considered it encompasses only the outer layers. However, in the central regions close to the axis no transverse displacements have as yet taken place, and the deformation of these layers will be purely axial.

the propagation speed of longitudinal waves in an infinite elastic medium*. Actually, when a compression wave propagates through an infinite medium no displacements take place in the plane perpendicular to the direction of propagation, and the phenomenon takes place in the same manner as for a laterally constrained rod. The speed c_l is always greater than the wave speed in the unconstrained rod, since $E' > E$ (see §14).

The speed c_l is the propagation speed only for sufficiently weak compression (and rarefaction) waves, in which the "pressure" or (more precisely) normal stress perpendicular to the direction of propagation is sufficiently small, less than the critical stress defined by (11.56). If a rarefaction wave propagates through a material previously stressed in compression (let us say an unloading wave), the absolute value of the drop in stress must be less than critical for c_l to be the propagation speed (for more detail on this see §17). However, if the dynamic load is great, greater than critical, then the compressed solid, as shown in the preceding section, goes over to a plastic state, similar to that of a fluid. The wave propagation speed, as we know, is determined by the derivative of the "pressure" with respect to volume, in this case of the normal stress with respect to volume. In the plastic state this derivative is proportional to the bulk modulus, as if the shear modulus were equal to zero. Therefore, the propagation speed of sufficiently strong acoustic compression and rarefaction waves is determined only by the compressibility of the material, and is

$$c_0 = \left(\frac{K}{\rho}\right)^{1/2} = \left(\frac{V}{\kappa}\right)^{1/2}. \tag{11.62}$$

The speed c_l is sometimes called the elastic wave speed, and the speed c_0 the plastic wave speed. The quantity c_0 is always less than c_l; for example, for iron $c_l = 6.8$ km/sec and $c_0 = 5.7$ km/sec. The propagation speed of strong compression waves (shock waves) depends on the wave strength. It is always greater than c_0 or close to this value. The propagation speed of weak disturbances is always equal to c_l, independent of the strength.

* The speed of propagation of transverse waves, in which the particles are displaced perpendicular to the direction of propagation of the wave and in which only shearing strain, without compression and rarefaction takes place, is $c_t = (G/\rho)^{1/2}$; $c_t < c_l$. *Editors' note.* The speed c_l is termed the "dilatation" wave speed, as the dilatation (see (11.51)) obeys a wave equation for which this speed is characteristic. It has also been termed the "irrotational" wave speed, as it is characteristic of any motion which is irrotational, for which the displacement has a scalar potential. The speed c_t is termed the "rotation" (sometimes "distortion" or "shear") wave speed, as the rotation vector (curl of the displacement) obeys a wave equation for which this speed is characteristic. It has also been termed the "equivoluminal" wave speed, as it is characteristic of any motion in which there is no density change. Both c_l and c_t are elastic wave speeds, but only c_l is of importance in the wave propagation treated in this chapter.

Problems of the propagation of rarefaction and compression waves in an elastic-plastic medium with a nonlinear relation between stress and strain, one similar to the dependence $\sigma_{zz}(\Delta L/L)$ shown in Fig. 11.34, were investigated in detail by Rakhmatulin. References to original articles in this field may be found in the review by Rakhmatulin and Shapiro [29]. In the next section we shall consider the simplest case of wave propagation in a material having the properties discussed.

§17. Splitting of compression and unloading waves

Let us see what actually happens when a constant pressure p is applied at an initial time to the surface of a flat body. The pressure is assumed to be sufficiently small that the deformation depends linearly on the pressure, that it follows Hooke's law. Let us draw a p, V diagram for the state of the compressed material behind the wave front. Because of the "anisotropy" of the pressure in the case of small deformations we shall, in place of the pressure, use the normal stress component σ_{zz} acting on an area parallel to the surface of the wave front with the wave taken to propagate in the z direction. The abscissa is taken to be the specific volume of the material. For small deformations and pressures the state is described by Hooke's law in the form (11.55), which, according to (11.61), may be rewritten in the form

$$\sigma_{zz} = \frac{\Delta V}{V}\rho c_l^2, \qquad -\sigma_{zz} < p_{cr}.$$

When the pressure exceeds the critical value p_{cr} and the change in volume exceeds $\Delta V_{cr}/V = p_{cr}/\rho c_l^2$ the body becomes plastic and the slope of the line $\sigma_{zz}(\Delta V)$ changes. According to (11.57) and (11.62), we have in this region

$$\sigma_{zz} = \frac{\Delta V}{V}\rho c_0^2 + const, \qquad -\sigma_{zz} > p_{cr}.$$

The σ_{zz}, V diagram is shown in Fig. 11.36.

If the external pressure $p < p_{cr}$ then one elastic compression wave will

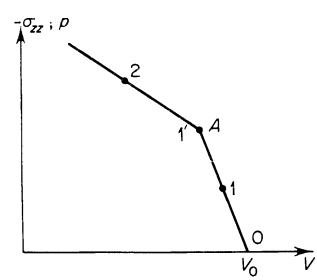

Fig. 11.36. Stress (or pressure)-volume diagram.

propagate through the body with the speed c_l (Fig. 11.37a; state 1 on the σ_{zz}, V diagram of Fig. 11.36). If, however, the applied pressure $p > p_{cr}$, then in the body the final state 2 shown in the σ_{zz}, V diagram is reached. In this case not one but two waves travel through the body: One is an elastic wave

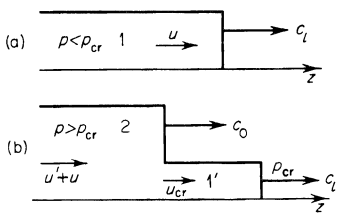

Fig. 11.37. Two cases of propagation of an acoustic compression wave: (a) one elastic wave; (b) a system consisting of a plastic and an elastic wave.

with a strength p_{cr} and with the state 1′ behind the front; this is followed by a plastic wave with the state 2 behind the front (see Fig. 11.37b). Since $c_0 < c_l$, the plastic wave cannot overtake the elastic wave, and the combination of the two waves is stable*. The plastic wave propagates through a slightly compressed medium moving with the velocity $u_{cr} = p_{cr}/\rho c_l$. This velocity is very low; for example, in iron the critical compression by the elastic wave is equal to $\Delta V_{cr}/V = 5 \cdot 10^{-4}$, and the particle velocity $u_{cr} = 3.6$ m/sec. The particle velocity behind the plastic wave is $u' = (p - p_{cr})/\rho c_0$ relative to the moving medium behind the elastic wave, and $u' + u_{cr}$ relative to the undisturbed medium.

If we consider strong compression waves, and even more so shock waves with pressures of hundreds of thousands of atmospheres and higher, then the effects of preliminary compression of the medium by the elastic wave to one or two thousand atmospheres and its acceleration to velocities of the order of several meters per second can be neglected and the plastic wave taken to propagate with respect to the undisturbed medium at rest with the speed c_0 corresponding to the compressibility. Sufficiently strong shock waves propagate at a velocity which appreciably exceeds c_0. If the shock velocity $D > c_l$, then in general no splitting of the wave occurs. The shock wave (plastic) propagates faster than the elastic wave from the very beginning and merges with it into a single wave.

Sufficiently strong unloading waves in an initially compressed medium also split into elastic and plastic waves. Let the medium be unloaded from a pressure p_0 to a pressure p (for example, first a compression wave with a pressure p_0 behind it is generated in the body by compressing it with a piston,

* The existence of the combination of elastic and plastic compression waves was noted by Bancroft *et al.* [30], in a study devoted to phase transitions in iron (for a discussion of this see §19). *Editors' note.* It was also noted by Donnell [61]. The elastic wave is sometimes referred to as a "precursor", particularly when it is much weaker than the plastic wave.

and then after a certain time the pressure at the piston drops to the value p). If $p_0 - p < p_{cr}$, then one elastic unloading wave travels through the compressed medium with the speed c_l. However, if $p_0 - p > p_{cr}$ an elastic unloading wave, in which the pressure drops from p_0 to $p_0 - p_{cr}$, moves ahead followed by a plastic unloading wave propagating at a lower speed. In the plastic wave the pressure drops to the value p, equal to the pressure at the "piston" (in particular, if the piston is retracted p can be equal to zero). These two cases are shown in Fig. 11.38. The phenomenon of splitting the

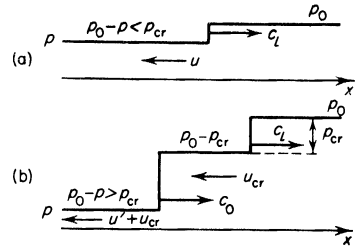

Fig. 11.38. Two cases of propagation of an acoustic unloading wave: (a) elastic wave only; (b) a system consisting of a plastic and an elastic wave.

unloading wave into two waves was observed experimentally by the authors of [4] and will be described in the following section. These authors explained the observed phenomena in the manner discussed above.

§18. Measurement of the speed of sound in a material compressed by a shock wave

The experimental determination of the speed of sound behind a shock front is of great interest. This is the speed of propagation of disturbances which overtake the shock wave and affect its strength*. The speed of sound (or the isentropic compressibility) determines the slope of the isentrope on a p, V diagram that passes through the point representing the state behind the shock front; thus it determines the initial behavior of the compressed material on unloading and its behavior behind the weak secondary shock. A knowledge of the speed of sound is important for establishing the equation of state for the material and for the correct design of shock compression experiments. Finally, values of the speed of sound in a solid at high pressures are also of interest in a number of geophysical problems.

Methods for measuring the speed of sound behind a shock front have been developed by Al'tshuler and Kormer, together with Speranskaya, Vladimirov, Funtikov, and Brazhnik [4]. One of the methods (method of lateral unloading) consists in the following. A cylindrical flanged specimen (Fig. 11.39) is sub-

* We recall that a shock propagates through the medium with the velocity behind the shock subsonic.

jected to a shock compression. Lateral unloading starts after the wave front passes the corner O. Disturbances from the unloading overtake the front and weaken the shock. The front velocity in the weakened outer section of the front surface decreases and the shock curves, as shown in Fig. 11.39, while

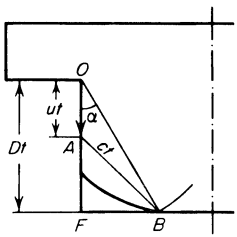

Fig. 11.39. Geometric construction for the lateral unloading experiment.

the central part of the surface not yet reached by the disturbances remains planar and the shock velocity there remains the same as before.

The point at which the weakening of the shock wave begins may be easily found from simple geometric considerations. In the time t which elapses from the time at which the shock passes the corner O, the shock moves through a distance Dt. The material previously situated near the corner is carried ahead through a distance ut to the point A. The earliest disturbances generated at the time the shock passed the corner, which travel through the medium with the speed of sound c, at this time reach a sphere of radius ct about the point A, and the weakening of the shock begins at the point B (see Fig. 11.39). Considering the triangles OBF and ABF, we can relate the speed of sound with the velocities D and u and with the tangent of the unloading angle α:

$$c = D\left[\tan^2\alpha + \left(\frac{D-u}{D}\right)^2\right]^{1/2}.$$

The problem is reduced to that of the determination of the front velocity D and the angle α (it is assumed that the Hugoniot curve for the medium is known, so that the particle velocity u can be calculated).

The problem is solved experimentally as follows. The shock wave emerges at the free surface with a defined velocity. On the central (unweakened) part of the front surface this velocity is everywhere uniform while on the outer (weakened) part the velocity is less, as shown by the arrows in Fig. 11.40. In the experiment the time at which the free surface reaches a Plexiglas plate P is recorded (this is done by streak or sweeping image photography). The picture obtained on the film is depicted in Fig. 11.40 (the curve on the film results from the luminescence produced when the medium strikes the Plexiglas). Point B is determined from the film and, with the geometry of the

experimental setup known, it is then possible to determine the unloading angle α.

It was found that in the case of water the boundary between the weakened and undisturbed regions of the shock surface is very sharp and that the bulk

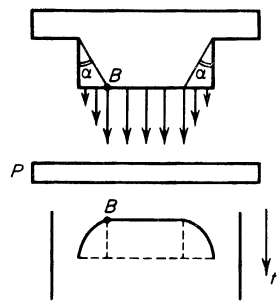

Fig. 11.40. Diagram for the experiment with lateral unloading.

modulus $\rho_0 c^2$ calculated from the speed of sound c is smaller than the slope of the Hugoniot curve (in the variables p, ρ/ρ_0) $\rho_0 dp/d\rho$ at the point corresponding to the state behind the front. This is in complete agreement with the respective locations of the Hugoniot curve and the isentrope as shown in Fig. 11.41.

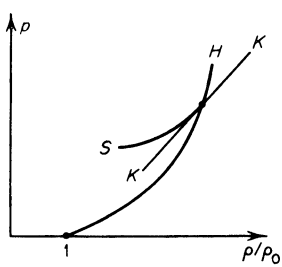

Fig. 11.41. Pressure-density diagram. H is the Hugoniot curve; S is the unloading isentrope; KK is the tangent to the isentrope at a point corresponding to the state behind the shock.

In the case of a metal (iron, copper), however, the shape of the curve on the film is rounded without a sharply defined boundary, as if the outer parts of the front surface were strongly unloaded and those closer to the center (to the axis of the specimen) were unloaded only very weakly. The bulk modulus $\rho_0 c^2$ as calculated using the point where a weak curving of the front surface began was found to be greater than the corresponding slope of the Hugoniot curve $\rho_0 dp/d\rho$ by a factor of approximately 1.5. The experimental data taken from [4] are given in Table 11.3.

This phenomenon was explained by the authors of [4] on the basis of the existence of two speeds of sound in a solid, which we discussed in §§15 and 16. Weak rarefaction disturbances are propagated through the compressed

medium with the elastic wave speed c_l (the "pressure" in the medium compressed by the strong shock wave is isotropic). This increased elastic speed of sound corresponds to the beginning of the weak distortion of the front surface; the corresponding modulus $\rho_0 c_l^2$ is found to be too large, larger than the slope of the Hugoniot curve $\rho_0 dp/d\rho$, because the shock velocity corresponds to the smaller, plastic sound speed. A plastic wave with the decreased plastic sound speed moves through the partially unloaded material. Disturbances of significant strength travel with this speed and appreciably weaken the shock front. The speed of the plastic wave is determined only by the compressibility and it is this speed which must be compared with the slope of the Hugoniot curve. The bulk modulus $\rho_0 c_0^2$, calculated with the plastic sound speed c_0, is found in the case of metals, just as in the case of water, to be smaller than the slope $\rho_0 dp/d\rho$, in complete agreement with the Hugoniot theory (water, being a fluid, has only one, plastic speed of sound c_0). The existence of two speeds of sound makes extremely difficult the exact determination of the boundary of plastic unloading, which is of major interest because it determines the compressibility of the medium.

In order to eliminate this effect, the authors of [4] developed another method (the "overtaking" unloading method, which in its initial form was proposed by E. I. Zababakhin). This method considers the collision between an accelerated plate and a test sample, made from the same material with a known Hugoniot curve. The x, t diagram for this process is shown in Fig. 11.42. Shock waves OA and OB propagate from the point of collision O

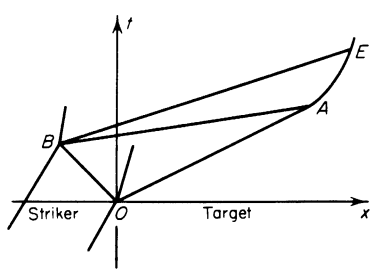

Fig. 11.42. x, t diagram for the "overtaking" unloading method.

through both bodies. After the shock wave in the striker reaches the free surface B, the unloading begins there and a rarefaction wave travels through the medium, overtaking the shock front in the test sample at the point A. From this time onward the shock is attenuated and the trajectory of the front curves upward, as shown in Fig. 11.42. By experimentally determining the trajectory of the shock front AE during the stage of appreciable attenuation,

Table 11.3

DATA FROM LATERAL UNLOADING EXPERIMENT [4]

Material	α, deg	D, km/sec	u, km/sec	Elastic c_l, km/sec	Elastic $\rho_0 c_l^2$, 10^{10} bar	$\rho_0 \frac{dp}{d\rho}$, 10^{10} bar	Plastic $\rho_0 c_0^2$, 10^{10} bar
Water	47.5	4.42	1.52	5.6	31.4	34.2	
Copper	41.0	5.24	0.87	6.33	357.8	288.8	240
Iron	46.5	5.34	0.98	7.15	401.3	298.2	240

with a consideration of the process of propagation of the rarefaction disturbances, we can find the speed of sound in the compressed medium behind the front. We are considering a stage of strong attenuation of the shock wave, which can result only from the plastic wave and not from the weak elastic wave. Hence the speed of sound determined in this experiment is the plastic speed related to the compressibility of the medium (for details of this method see [4]). To illustrate the numerical values we show in Table 11.4 some experimental results. For comparison, the speeds of sound (plastic) c_0 at standard conditions are also given.

Table 11.4

EXPERIMENTALLY DETERMINED SPEEDS OF SOUND AT HIGH PRESSURES

Metal	p, 10^{10} bar	V_0/V	c_0, km/sec	c_0, km/sec (at standard conditions)
Al	195.5	1.76	11.74	5.2
	160.0	1.701	11.23	
Cu	379.6	1.694	9.48	3.9
	311.7	1.638	8.93	
Fe	347.8	1.650	9.48	5.7
	284.9	1.600	9.53	

§19. Phase transitions and splitting of shock waves

Many solids can have different crystalline forms under different conditions. At certain temperatures and pressures, which are related in a defined manner, transitions from one form to another are possible. These transitions, accompanied by changes in volume and the release (or absorption) of latent heat,

are called phase transitions of the first kind. Such transitions are often referred to as polymorphic transformations*.

An example of a material capable of undergoing a polymorphic transformation is iron. At atmospheric pressure and a temperature of 910°C iron is transformed from the α phase to the γ phase; the change is accompanied by a 2.5% decrease in volume and the absorption of 203 cal/mole of latent heat. Polymorphic transformations frequently occur at high pressures. In particular, at a pressure of 130,000 atm the above transition in iron takes place at a temperature slightly above standard temperature.

Distinctive phenomena can appear during shock compression of a material capable of undergoing polymorphic transformations at high pressures. These phenomena were treated theoretically (mainly qualitatively) in papers by Bancroft, Peterson, and Minshall [30], Duff and Minshall [31], and Drummond [32]. Experimentally, shock waves in the presence of polymorphic transformations were reported in the first two papers (in the first in iron and in the second in bismuth) and in papers by Dremin and Adadurov [33] (in marble), and Dremin and Karpukhin [34] (in paraffin)†. In a certain range of pressures not one, but two shock waves following one another travel through a material capable of undergoing a polymorphic transformation. This splitting of a shock wave is related to the anomalous behavior of the Hugoniot curve for the material in the region of phase transition. For pressures behind the shock which are not too large the entropy increases only very slightly across the shock wave; hence the Hugoniot curve is close to the isentrope and in examining the above phenomenon we may use the ordinary isentrope.

The isentrope for a material undergoing a polymorphic transformation is depicted schematically in Fig. 11.43. When the material is compressed from its original volume to beyond that of a certain state A, a transition from phase I to phase II begins. The crystal lattice then begins to rearrange itself in such a manner that the new equilibrium positions of the atoms correspond to smaller interatomic distances. Therefore decreasing the volume in the phase transition region requires a much smaller increase in pressure than in the initial phase I. (At absolute zero the phase transition I–II takes place at constant pressure, and the portion AB of the isentrope $S = 0$ is a horizontal line, as shown in Fig. 11.43b.) If there were no rearrangement, the pressure curve would have extended upward from the point A as shown by the dashed lines in Fig. 11.43. In the region AB the material is in a two-phase state. Complete

* For sufficiently strong shock waves the solid will melt, which is also a phase transition of the first kind.

† *Editors' note.* Bethe [62] noted that when isentropic expansion leads to a phase transition from a two-phase state to a one-phase state, compression shocks in general are split and expansion shocks exist.

rearrangement of the lattice and complete transformation of the material from phase I to phase II end at the point B, after which the isentrope of the second phase again goes upward steeply. The compressibility of the material is different in different phases, so that the slopes of the curves corresponding to the single-phase states at points A and B are different in general.

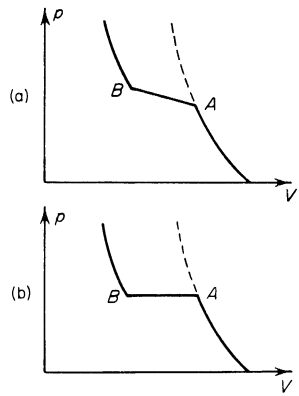

Fig. 11.43. An isentrope for a material undergoing a polymorphic transformation: (a) at a temperature different from zero $T > 0$; (b) at absolute zero.

Let us now consider a solid possessing a Hugoniot curve of the type described above, and assume that at an initial time a constant pressure p is applied at the surface (we shall consider a one-dimensional plane case). We take the pressure to be sufficiently high that we may neglect effects associated with the strength of the material and consider the pressure to be hydrostatic; in other words, we shall disregard the possible existence of an elastic wave (see §17) and consider the shock wave to be plastic.

If the pressure p is lower than the pressure p_A at which the phase transition begins, then an ordinary shock wave propagates through the material, and the state behind the shock corresponds to a point on the Hugoniot curve (say, to point C on Fig. 11.44). The propagation velocity of the shock wave D is determined by the slope of the straight line drawn from the initial state point O to the final state point on the Hugoniot curve

$$D = V_0\left(\frac{p - p_0}{V_0 - V}\right)^{1/2}.$$

If the pressure p is greater than p_E (which corresponds to the intersection with the Hugoniot curve of the line OAE that touches the Hugoniot curve at the point A), say it is equal to p_F, then again only one shock wave will propagate through the body, with the state behind the shock that of point F. However, in this case the material behind the front is in another phase—phase II. The transition from phase I to phase II takes place across the shock front.

Usually the time required for a polymorphic transformation is much larger than that required to establish thermodynamic equilibrium in an ordinary, single-phase material. The situation in this case is quite similar to that which

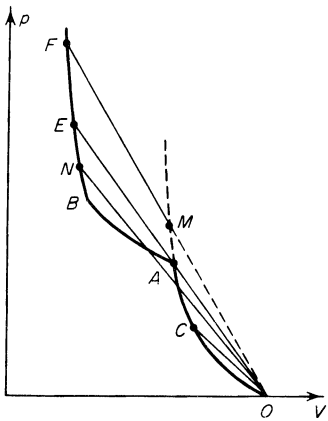

Fig. 11.44. p,V diagram illustrating various cases of shock wave propagation with polymorphic transformation of a material (explanation in text).

takes place in a shock wave propagating through a gas with retarded excitation of some of the degrees of freedom (for example, through a dissociating gas). The direct shock compression leads to the intermediate state M that lies on the extrapolated Hugoniot curve for phase I, corresponding to the absence of a phase transition (this corresponds to the viscous shock in a gas). After that the phase transition begins and the thickness of the front is determined by the relaxation time of the transition, in a manner similar to that in which the shock front thickness in a gas is determined by the dissociation time. The pressure distribution in the shock wave has the form shown in Fig. 11.45, one

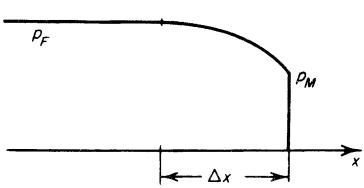

Fig. 11.45. Pressure distribution in a shock wave with phase transition relaxation.

which is completely analogous to the pressure distribution in a shock wave in a dissociating gas. The point characterizing the state in the thickened region of the wave front moves along the straight line segment MF in Fig. 11.44.

Let us now consider the intermediate case in which the pressure applied to the body lies between p_A and p_E, equal to p_N (point N on the Hugoniot

curve of Fig. 11.44). The velocity of the shock wave determined by the slope of the line ON is now less than the velocity of the shock with the lower pressure p_A corresponding to the point A. This latter velocity is determined by the slope of the steeper line OA. Therefore, the wave with the pressure p_A moves faster than the shock wave with the pressure p_N. (We note that the line ON intersects the Hugoniot curve three times, that is, for the same wave speed there are three possible pressure-volume values. Obviously, this non-uniqueness is physically meaningless.

At such an intermediate value of the pressure $p_E > p > p_A$ the shock wave is split into two independent waves moving at different speeds (this case is shown separately in Fig. 11.46). In the first shock wave the material is compressed from the initial state O to state A corresponding to the beginning of

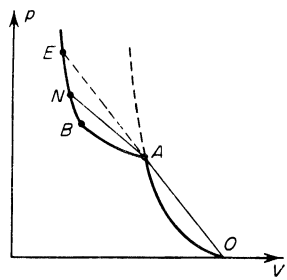

Fig. 11.46. p,V diagram illustrating the splitting of a shock wave.

the phase transition, with the propagation velocity of the first shock through the undisturbed material determined by the slope of the line OA, by

$$D_1 = V_0\left(\frac{p_A - p_0}{V_0 - V_A}\right)^{1/2}.$$

The first wave is followed by another shock in which the material is compressed from state A to the final state N. The propagation velocity of this second wave through the compressed and moving material which is in the state A is determined by the slope of the line AN and is

$$D_2 = V_A\left(\frac{p_N - p_A}{V_A - V_N}\right)^{1/2}.$$

The propagation velocity of the second shock wave relative to the original stationary material is equal to the sum of the velocity D_2 and of the particle velocity of the material behind the first shock u_A

$$D_2' = D_2 + u_A.$$

It is apparent that the second wave does not overtake the first one, so that the combination of the two separate shocks is stable. Indeed, the propagation

velocity of the first wave relative to the material behind it is

$$D_1'' = V_A\left(\frac{p_A - p_0}{V_0 - V_A}\right)^{1/2}.$$

Since the slope of the line OA is by definition ($p_N < p_E$) greater than the slope of the line AN, we have $(p_A - p_0)/(V_0 - V_A) > (p_N - p_A)/(V_A - V_N)$ and $D_1'' > D_2$, so that the first wave travels through the material faster than the second one.

A phase transition takes place in the front of the second shock wave. In the initial state A the material is in the first phase, and in the final state N it is either in the second phase (if $p_N > p_B$) or in a two-phase state (if $p_N < p_B$); the transformation in the latter case is incomplete. Since the process of phase transition is retarded, the front of the second shock is found to be greatly thickened, in contrast with the thin front of the first wave. The pressure distribution in the case of the system of two waves is shown schematically in Fig. 11.47. With increasing time the distance between the two wave fronts increases, since their velocities are different, but the pressure profile in the second wave is stationary and propagates unchanged.

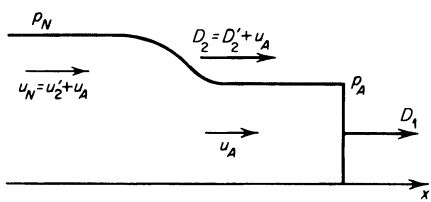

Fig. 11.47. Pressure distribution in the case of splitting of a shock wave into two waves.

The combination of two shock waves in the presence of a phase transition is in many respects analogous to the combination of an elastic and a plastic compression wave considered in §17. The cause for the appearance of the two waves in both cases is the anomalous behavior of the isentrope and of the Hugoniot curve, where by anomalous behavior we mean that there is a region of the p, V curve where it is convex. It was shown in Chapter I that the increase or decrease of entropy across a shock wave depends on the sign of $\partial^2 p/\partial V^2$; this sign determines purely thermodynamic consequences. From this we can conclude that an anomalous Hugoniot curve leads to anomalous kinematic results, in this case to the splitting of a shock wave into two waves. The limiting condition $p > p_E$ for the recombination of the two waves into one corresponds to the situation in the case of the combination of elastic and plastic waves when the plastic wave speed (because of the departure of the Hugoniot curve from Hooke's law) becomes greater than the elastic wave

speed, when the second wave overtakes the first one and coalesces with it.

As we pointed out above, the phenomenon of splitting of a shock wave in materials which undergo polymorphic transformations has been observed experimentally. For illustration, we present in Fig. 11.48 the experimental

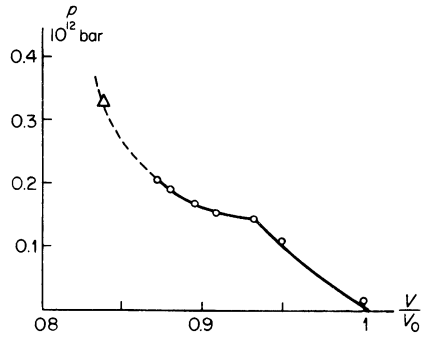

Fig. 11.48. Hugoniot curve for iron in the region of phase transition. △— data from [24], ○— data from [30].

Hugoniot curve for iron in the region of phase transition reported in [30]. We note that a phase transition in bismuth takes place at a pressure of ~28,500 atm, with the relaxation time for the transition at 42°C found to be less than 1 msec.

Alder and Christian [35] found a phase transition of the first kind in iodine I_2 (iodine crystals are molecular) at a pressure $p \approx 7 \cdot 10^5$ atm and a relative volume $V/V_0 \approx 0.53$. The transition was fixed by determining the point at which there was a change in slope in the relation between shock and particle velocities. Calculations show that the temperature behind the wave at the phase transition point is about 1 ev. It is comparable with the dissociation energy of 1.53 ev for iodine molecules. It is assumed that the phase transition is connected with the transformation of a diatomic molecular crystal into a monatomic metallic state.

It is interesting that anomalies in the cold compression curves for metals (and hence also in the Hugoniot curves) similar to those which appear in the presence of polymorphic transformations can also arise even if the atomic lattice is not rearranged. Such anomalies are a result of changes in the structure of electron zones, from overlapping of individual zones under compression. The possibility that metal properties can change with changes in the zone structure has been noted by Lifshitz [36]. The effect of these changes on the cold compression curves for metals and on the appearance of anomalously shaped parts of the curve, with $\partial^2 p/\partial V^2 < 0$, was studied by Gandel'man [37].

For a sufficiently strong shock wave melting of the solid takes place, and this leads to a discontinuous change in slope of the Hugoniot curve. Problems of shock wave melting have been treated in a number of papers [44, 57–59].

§20. Rarefaction shock waves in a medium undergoing a phase transition

According to the general theory presented in §§17, 18, and 19 of Chapter I, an anomalous behavior of an isentrope, one with a segment of the curve which is convex ($\partial^2 p/\partial V^2 < 0$), leads to the possibility of rarefaction shocks. Isentropes for solids undergoing a phase transition represent exactly such a possibility. This was noted in [32]*. Regimes with rarefaction shocks in a metal in the presence of phase transitions were studied by Ivanov and Novikov (and Tarasov) [38], who were the first to give clear experimental evidence of the existence of rarefaction shocks in iron (and steel).

The isentrope of a material undergoing a polymorphic transformation has an anomalous shape in the region of the point of inflection A (Fig. 11.43). Although the second derivative $\partial^2 p/\partial V^2$ at all points where the isentrope behaves normally is positive, nevertheless there exists a segment in the neighborhood of the point A where a chord connecting any two points 1 and 2 lies entirely below the isentrope (Fig. 11.49). This is related to the fact that the mean value of the second derivative on the segment 1–2 is negative†,

$$\left\langle \frac{\partial^2 p}{\partial V^2} \right\rangle_{1\text{-}2} = \frac{(\partial p/\partial V)_2 - (\partial p/\partial V)_1}{V_2 - V_1} < 0.$$

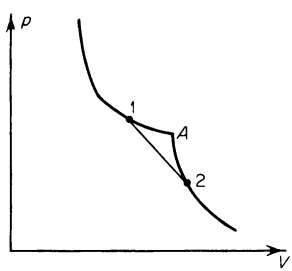

Fig. 11.49. Anomalous segment of an isentrope.

As is known from the general theory, this is the situation which leads to anomalies in the hydrodynamic relationships. The propagation of compression shocks in such a material was considered in the preceding section.

Let us now consider the unloading of a material that has been compressed by a shock wave. We assume that at the time $t = 0$, in a body previously compressed by a shock wave to the state 1 (p_1, V_1), there is a rarefaction wave in which the pressure and volume change smoothly to the values p_2, V_2 (state 2; $p_2 < p_1$, $V_2 > V_1$). The initial pressure distribution as a function of position is shown in Fig. 11.50. We assume that the points of the initial and

* See *Editors' note*, p. 751.

† At all points of the segment 1–2, with the exception of the point of inflection A, $\partial^2 p/\partial V^2 > 0$, but at the point A itself $\partial^2 p/\partial V^2 = -\infty$, so that the mean value on the segment 1–2 is nevertheless negative.

final state, 1 and 2, as well as all of the intermediate points of the smooth distribution lie on the isentrope and that the subsequent process is adiabatic*. Corresponding points in Fig. 11.50 are indicated on the isentrope of Fig. 11.51 by the same letters and numbers.

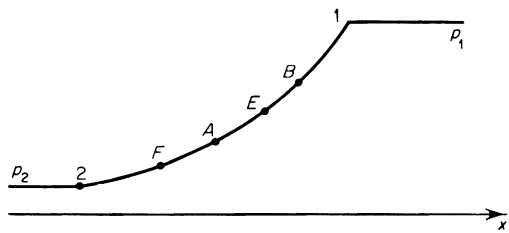

Fig. 11.50. Problem of the evolution of a rarefaction wave; the initial pressure distribution.

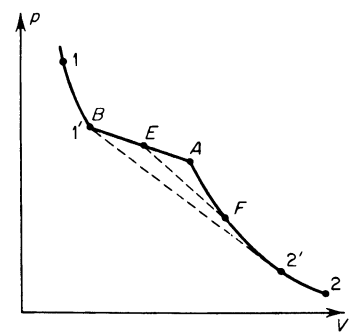

Fig. 11.51. Problem of the evolution of a rarefaction wave; states on the p, V diagram correspond to the distribution shown in Fig. 11.50.

We shall assume that the rarefaction wave is a simple wave (see §8, Chapter I), propagating to the right through the compressed medium. In order for the wave to be simple it is necessary that the initial pressure and velocity distributions with respect to position $p(x, 0)$ and $u(x, 0)$ satisfy the condition that the Riemann invariant $J_-(x, 0)$ be constant. It follows that $J_-(x, t) = const$ at later times. Let us assume that this condition is satisfied. As is known (see §8, Chapter I), the C_+ characteristics in a simple wave propagating to the right are straight lines in the x, t plane; along these lines the pressure and other flow variables are constant.

Let us consider what happens to our initial pressure distribution at later times. To do this we draw on the x, t plane of Fig. 11.52 the C_+ characteristics, which are straight lines of slope $dx/dt = u + c$. The speeds of propa-

* We are considering only low pressures, for which thermal effects are small and the Hugoniot curve practically coincides with the isentrope. In addition, we assume that the phase transitions take place sufficiently rapidly, "instantaneously", so that the states of the material never depart from the thermodynamic equilibrium isentrope.

gation of disturbances (sound speeds) at different points of the initial distribution are determined by the slopes of the tangents to the isentrope at the corresponding points. At the two break points A and B the speed of sound undergoes a jump (the dependence of the speed of sound on volume is shown in Fig. 11.53). The velocity of the material, by virtue of the condition $J_- = const$, is given by $u = -\int c\, d\rho/\rho + const$ and is continuous at the points A and B. Hence the slopes of the characteristics change discontinuously with the jumps in speed of sound.

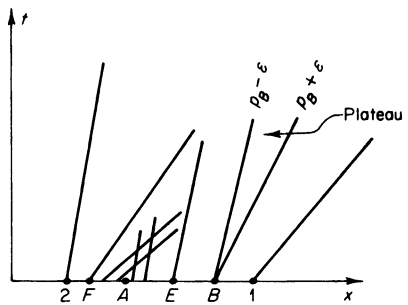

Fig. 11.52. x, t diagram illustrating the evolution of an initial rarefaction wave in a material with an anomalous isentrope.

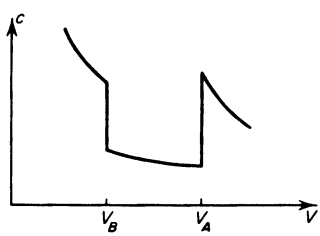

Fig. 11.53. Dependence of the speed of sound on volume, corresponding to the isentrope shown in Fig. 11.51.

Two C_+ characteristics with different slopes, along which the pressure is the same but the speed of sound is different, emanate from the "normal" break point B. These sound speeds correspond to the values immediately before and after the point where the slope of the isentrope changes discontinuously. The propagation speed of the characteristic with the value of the pressure $p_B + \varepsilon$ (ε is infinitesimally small) is greater than that of the characteristic with the slightly lower value $p_B - \varepsilon$. The situation at the "anomalous" break point A is different. Point A also serves as the origin of two characteristics but the characteristic with the higher pressure $p_A + \varepsilon$ propagates slower than the one with lower pressure $p_A - \varepsilon$. Characteristics drawn from points neighboring A tend to intersect (see Fig. 11.52), and the limiting characteristics originating from A behave as if they had intersected at the outset. This means that in the initial pressure distribution a small discontinuity is

formed at point A from the very beginning (in the limit $t \to 0$ the discontinuity is infinitesimal) and it grows with time*.

The propagation of the rarefaction wave and the pressure distributions at successive instants of time are shown schematically in Fig. 11.54. The pressure plateau p_B is bounded by the characteristics emanating from the point B and shown in Fig. 11.52. The rarefaction shock wave which originated at point A grows in accordance with its intersection with the characteristics. The jump

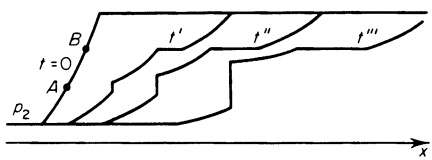

Fig. 11.54. Evolution of the pressure distribution in a rarefaction wave; formation of a rarefaction shock wave. $t = 0$, t', t'', and t''' are successive instants of time.

increases, the upper initial pressure increases, and the lower final pressure decreases, as long as the upper point of the shock moves supersonically with respect to the material ahead of the shock and the lower point moves subsonically with respect to the material behind the shock. In this case the upper boundary of the shock "eats up" portions of the smoothly increasing pressure distribution in front, while the rarefaction disturbances behind the shock overtake it and thereby strengthen it (are "eaten up" by the shock). The jump ceases to grow when the upper pressure reaches the pressure of the plateau and the propagation speed of the lower boundary with respect to the material behind the shock becomes sonic†.

The steady-state position of the discontinuity (the points 1′–2′ on the isentrope of Fig. 11.51) and the pressure distribution in the rarefaction wave are shown in Fig. 11.55. As we know (see §14, Chapter I), the propagation velocities of the discontinuity 1′–2′, u_1 with respect to the material ahead of it and

* The situation for an initially smooth compression wave in a material with normal properties is somewhat different. The characteristics in this case do not immediately intersect (see §12, Chapter I), the pressure distribution steepens gradually, and the compression shock wave does not form immediately. However, for the rarefaction shock the discontinuity is generated at the very beginning and its strength increases proportionally with time. *Editor's note.* With an initially smooth compression wave in the material of Fig. 11.51, a compression shock is generated at the very beginning at point B.

† *Editors' note.* Point 2′ in the final asymptotic profile is a Chapman–Jouguet point (see p. 346). Thus the determining asymptotic conditions here are analogous to the usual ones in detonations. However, it is possible in principle for $p_2 > p_{2'}$. In this case the Chapman–Jouguet point is never reached and the relative velocity behind the wave remains subsonic in the final profile.

u_2 with respect to the material behind it, are determined by the slope of the line 1′–2′ on the isentrope (actually on the Hugoniot curve)*

$$u_1^2 = V_{1'}^2 \frac{p_{1'} - p_{2'}}{V_{2'} - V_{1'}}, \qquad u_2^2 = V_{2'}^2 \frac{p_{1'} - p_{2'}}{V_{2'} - V_{1'}}.$$

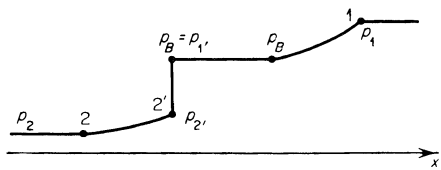

Fig. 11.55. Character of the final pressure distribution in a rarefaction wave. The distribution expands with time, without changing its shape.

It is clear from Fig. 11.51 that the point 2′ is determined by the point of tangency to the isentrope of the line 1′–2′, since at that point $u_2 = c_{2'}$. The propagation velocity of the discontinuity with respect to the material ahead of it u_1 is less than the larger speed of sound at the break point B, but greater than the lower speed of sound at that point; the line 1′–2′ has a slope intermediate between the slopes of the two tangents to the isentrope at the point B.

In practice a rarefaction wave ordinarily arises when a shock wave emerges at the free surface of a solid. The regime in this case is self-similar; all the C_+ characteristics in the x, t plane originate from a single point and the entire steady-state pressure distribution shown in Fig. 11.55 is formed at the outset, as in an ordinary self-similar rarefaction wave (see §11, Chapter I). Thus, the rarefaction wave has a complex profile consisting of two parts where the pressure decreases smoothly, a pressure plateau (all of these three parts expand with time in accordance with the self-similarity of the regime), and a rarefaction shock wave (if the surface of the solid is a free surface, point 2 of the final state corresponds to zero pressure). An x, t diagram for a centered rarefaction wave is shown in Fig. 11.56.

In the experiments described in [38] unusual scabbing phenomena were observed when explosive charges were detonated on the surfaces of iron and steel specimens. The split-off surface was extremely smooth. This phenomenon has been interpreted as resulting from the collision of two rarefaction shock waves, when the pressure on some surface changes in a discontinuous manner from a positive to a negative value. Usually during smooth unloading, the zone of tensile stresses giving rise to the scabbing phenomenon is not

* These equations follow from the conservation laws of mass and momentum across the discontinuity and are equally valid for compression and rarefaction shocks.

sharply defined and the split-off surface is rough, due to the micro-inhomogeneity of the material over the extensive zone of tensile stresses. From an analysis of the complex picture of the motion which takes place under the

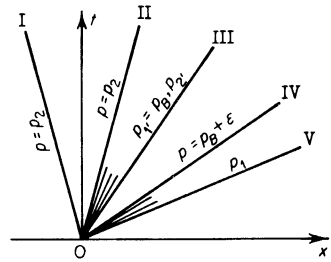

Fig. 11.56. x, t diagram for a self-similar rarefaction wave, formed when a shock wave emerges at a surface. I is the line of the free surface, II is the tail of the rarefaction wave, III is the line of the rarefaction shock, IV is the head of the pressure plateau, and V is the head of the rarefaction wave.

experimental conditions, the authors of [38] were able to conclude that the observed phenomena are attributable to the existence of rarefaction shock waves. This is also substantiated by the fact that in other materials (not iron or steel), in which no phase transitions take place in the pressure range under consideration, no unusual scabbing was observed.

4. *Phenomena associated with the emergence of a very strong shock wave at the free surface of a body*

§21. Limiting cases of the solid and gaseous states of an unloaded material

In §11 we considered the process of unloading of a solid initially compressed by a shock wave, after the shock emerges at the free surface. It was assumed that the shock was not too strong, that the temperature behind the front was relatively low, and that the material when unloaded to zero pressure remained solid. It is clear that if the shock wave is very strong and the internal energy of the heated material ε_1 exceeds by many times the binding energy of the atoms U (equal to the heat of vaporization at zero temperature), then, when the material expands to a low (zero) pressure after the shock wave has emerged from the free surface, the material is completely vaporized and behaves like a gas during the unloading*. In particular, for unloading into a vacuum to

* Sometimes reference is made to the "vaporization" of the material inside the shock wave itself. This statement is incorrect if "vaporization" is understood to denote a phase transition in the ordinary thermodynamic sense. A dense medium can be called a "liquid" or a "gas" only in a conditional sense, depending on the relationship between the kinetic energy of thermal motion of the atoms and the potential energy of their interaction. The transition from a "liquid" to a "gas" in a material heated at constant volume takes place in a continuous manner. In general, we should recall that at pressures and temperatures

strictly zero pressure, the density and temperature at the leading edge of the material are also equal to zero. The density, velocity, and pressure distributions in the unloading wave have the same qualitative character as in a rarefaction wave in a gas (see §§10 and 11 of Chapter I). They are represented in Fig. 11.57.

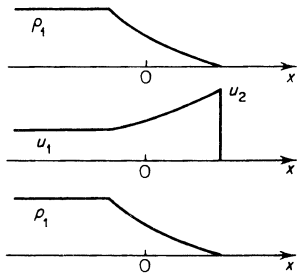

Fig. 11.57. Density, velocity, and pressure distributions after the emergence of a very strong shock wave at a free surface.

The hydrodynamic solution for a self-similar unloading wave can be written in a general form, independent of the thermodynamic properties of the medium. It is given by the equations

$$\frac{x}{t} = u - c, \tag{11.63}$$

$$u + \int \frac{dp}{\rho c} = const \tag{11.64}$$

for a wave moving to the left, and is shown schematically in Fig. 11.57. The integration is carried out at constant entropy S, since the unloading process is isentropic. In this case the entropy is equal to the entropy of the material behind the shock front. The constant can be expressed in terms of the properties of the material behind the shock (which are denoted by the subscript "1"). Then (11.64) becomes

$$u = u_1 + \int_p^{p_1} \frac{dp}{\rho c}. \tag{11.65}$$

The velocity of the leading edge of the unloaded material (the velocity of the free surface) is

$$u_2 = u_1 + \int_0^{p_1} \frac{dp}{\rho c}. \tag{11.66}$$

---

above critical the entire material is homogeneous and no phase separation takes place. It should be noted that a statement to the effect that a material in a sufficiently strong shock wave ceases to be solid has a completely physical meaning (the solid material melts).

We have already used (11.66) in §11 in order to obtain the law of velocity doubling. The distribution of hydrodynamic variables in the unloading wave can be found if the thermodynamic properties of the material are known (i.e., the functions $\rho(p, S)$ and $c(p, S)$, with which the integral in (11.65) can be evaluated). The corresponding formulas for a gas with constant specific heats were given in §10 of Chapter I. In the case of interest to us of unloading of a solid this cannot be done as yet, since no satisfactory theory exists for calculating the thermodynamic functions of materials for densities somewhat less than the standard density of the solid (we refer here to intermediate temperatures, for which the material cannot be considered as either a solid or a perfect gas). For this reason we shall limit ourselves here to rough estimates and to a qualitative description of the process.

For simplicity we shall assume that prior to compression by the shock wave the solid was at zero temperature and zero volume V_{0c}, and also that the unloading takes place into a vacuum, to zero pressure. In addition, we shall not make any distinction between the solid and liquid states. The heat of fusion is usually much smaller than the heat of vaporization* (the volume change on melting is also small), and hence when considering phenomena with energies for which the material is completely vaporized we can neglect the effect of melting.

Let us follow the unloading of a given particle of the material on a p, V diagram. Figure 11.58 shows the elastic pressure curve p_c extended into the region of negative pressures, the Hugoniot curve p_H, and the curve OKA separating the single- and two-phase regions. The branch OK up to the critical point K represents the boiling curve (beginning of vaporization), while the branch KA is the saturated vapor curve (beginning of condensation). In addition, the figure also shows several isentropes S, which pass through different possible states behind the shock wave.

Let us consider the simplest limiting cases. Let the shock wave be weak (state 1 on the Hugoniot curve). The compressed material is unloaded along the isentrope S_1, the pressure drops to the point B_1 where the isentrope intersects the boiling curve, after which the solid (or liquid) should, in principle, begin to boil. However, to form nuclei of the new phase, i.e., vapor bubbles, requires a rather large activation energy to destroy the continuity of the material and to form the bubble surfaces. The rate of this process (for metals) at the low temperatures of the order of hundreds and even thousands of degrees is so negligibly small that actually the solid continues to expand and cool down to zero pressure along the "superheated liquid" isentrope shown in Fig. 11.58 by the dashed curve from the point B_1. In its final state

* For example, for lead the heat of fusion is 1/46 times as large, and for aluminum 1/22 times as large as the heat of vaporization.

the volume of the material is V_2*, which somewhat exceeds the zero volume V_{0c}, and is heated to a temperature T_2, which is related to the volume difference $V_2 - V_{0c}$ by the thermal expansion relation (see §11). Even if

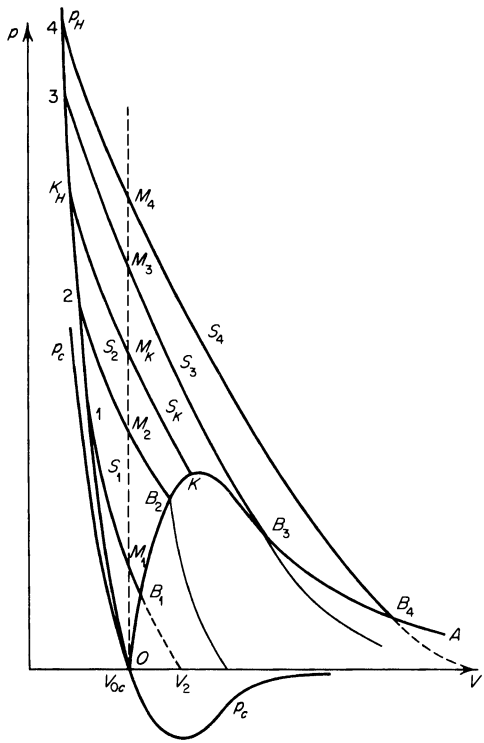

Fig. 11.58. Unloading isentropes on a p,V diagram.

problems concerning the kinetics of the volume vaporization could be disregarded, the vaporized fraction of the material could not exceed a value of the order of $c_v T_{B_1}/U$ (U is the heat of vaporization or the binding energy). This quantity is very small at temperatures T_{B_1} of the order of hundreds of degrees (for metals $U/c_v \sim 10^4$°K). This case of unloading was considered in §11.

In the other limiting case, when the shock wave is very strong (state 4), the unloading isentrope S_4 passes in the purely gaseous region far above the

* In contrast to the notation used in §11, all the quantities in the final unloaded state will be denoted here by the subscript "2", with the subscript "1" referring to quantities behind the shock front.

critical point K, and the material expands as a gas to infinite volume. In general, the isentrope will at some time intersect the saturated vapor curve (the point B_4), after which condensation should begin*. However, if the time for the expansion of the vapor is limited, which is usually the case under laboratory conditions, there is insufficient time for condensation to take place and the material continues to expand along the supercooled vapor isentrope (the dashed line from the point B_4 in Fig. 11.58).

§22. Criterion for complete vaporization of a material on unloading

Let us establish a quantitative criterion for the complete vaporization of a material on unloading, one which is more specific than the obvious condition that the energy of the shock wave should be appreciably greater than the heat of vaporization, $\varepsilon_1 \gg U$. We shall speak of complete vaporization if the material being unloaded, following the laws of thermodynamics, passes through the stage of a purely gaseous state (we do not claim that the final state in this case is also purely gaseous, since in principle condensation must set in when expanding to infinite volume). We shall consider a range of shock strengths intermediate between the two limiting cases when the wave is weak and it is known that the material will remain solid on unloading and when the wave is very strong and it is known that the material will behave as a gas on unloading.

The internal energy of the material compressed by a shock wave is made up of the elastic ε_{c1} and thermal ε_{T1} energy (where in the thermal energy we do not make any distinction between the atomic and electronic contributions). When a compressed material expands to the zero volume V_{0c}, the elastic energy acquired on compression is completely returned, and is transformed into kinetic energy of the material that is accelerated on unloading†. A part of the initial thermal energy ε_T, expended in performing the work of expansion and equal to $\int_{V_1}^{V_{0c}} p_T \, dV$, is also transformed into kinetic energy. Let us denote the thermal energy remaining in the material at the time it reaches the zero volume V_{0c} by ε'_T. This energy is the same as the total internal energy at this instant. It is quite clear that in order to achieve complete vaporization during the subsequent expansion the energy ε'_T must exceed the binding energy U,

$$\varepsilon'_T > U.$$

The question here is what the magnitude of this excess energy should be. In expanding to volumes greater than the zero volume, the excess energy ε'_T

* Condensation in the expansion of vapor into vacuum was considered in detail in Chapter VIII.

† In this case, however, it does not remain concentrated in the same parcel, as for a flow for which Bernoulli's law is applicable; see §11, Chapter I.

is partially expended in performing the work of expansion (this part of the energy is transformed into the kinetic energy of the hydrodynamic motion), and partially into overcoming the binding forces characterized by the negative p_c (this part of the energy is transformed into potential energy).

Let us assume that the energy ε'_T is sufficient to completely vaporize the material, that is, it is sufficient to prevent the pressure $p = p_T + p_c = p_T - |p_c|$ from dropping to zero before the material expands to infinite volume. From the adiabatic relation $d\varepsilon + p\,dV = 0$, it follows from the fact that $d\varepsilon_c + p_c\,dV = 0$ that $d\varepsilon_T + p_T\,dV = 0$. Integrating this equation from the zero volume V_{0c} to infinity, where the thermal energy vanishes, we obtain

$$\varepsilon'_T = \int_{V_{0c}}^{\infty} p\,dV + \int_{V_{0c}}^{\infty} |p_c|\,dV = \int_{V_{0c}}^{\infty} p\,dV + U.$$

The first term represents that part of the excess energy which is expended in the work of expansion, and the second represents the energy expended in breaking the atomic bonds.

Let us represent the pressures p, p_T, p_c on a p, V diagram (Fig. 11.59).

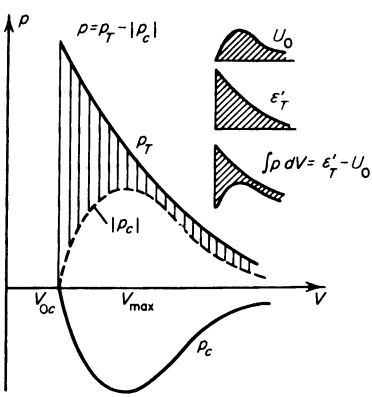

Fig. 11.59. The problem of vaporization of a condensed material on expansion (for explanation see text).

Also shown on the figure are the values of the various energies as represented by the areas defined by the appropriate curves. In the limit of complete vaporization, at that stage of expansion where the binding forces are weakened ($V > V_{\max}$), the pressure is close to zero and the thermal pressure is sufficient to overcome the binding forces ($p_T \approx |p_c|$). However, at an earlier stage, when $V_{0c} < V < V_{\max}$, the pressure p is high and the thermal pressure is appreciably larger than the elastic pressure, $p_T > |p_c|$. This is clear from the fact that in the state where $V = V_{0c}$, $p' = p'_T = \Gamma\varepsilon'_T/V_{0c} > \Gamma\,U/V_{0c}$, where Γ is the effective Grüneisen coefficient, which is of the order of unity ($|p_c|_{\max} \sim U/V_{0c}$). The decrease in thermal pressure on expansion is more or less monotonic (the energy ε_T decreases and the volume V increases). Therefore

the curve $p_T(V)$ has the shape shown in Fig. 11.59. From Fig. 11.59 it is clear that the vertically shaded area, equal to the work of expansion $\int_{V_{0c}}^{\infty} p\, dV$, is of the same order of magnitude as the area corresponding to the potential energy U, and that in the limit of complete vaporization the excess energy ε'_T should be roughly twice the binding energy U.

In order to express these rather qualitative considerations quantitatively, the thermodynamic properties of the material must be known in the range of volumes greater than the standard volume of the condensed state, in a range where the binding forces are of importance. Unfortunately, this range of volumes with $V_{0c} < V \lesssim 5V_{0c}$ has been the least investigated, either theoretically or experimentally.

We can approach the evaluation of the shock strength which separates the regions of complete and incomplete vaporization under unloading in a somewhat different manner, by characterizing the vaporization boundary not in terms of the energy ε'_T but in terms of the entropy. It is clear from Fig. 11.58 that the effective boundary between complete and incomplete vaporization on isentropic unloading is defined by a state K_H behind the shock such that the entropy is equal to the entropy S_{cr} of the critical point, the entropy corresponding to the expanding material passing through the critical point K. The fact that for an entropy greater than S_{cr} the material at some instant of time begins to condense (state 3, isentrope S_3, condensation point B_3) means that all the atomic bonds had been broken earlier, that the material had become a gas. Conversely, if the entropy is less than S_{cr} (state 2, isentrope S_2, boiling point B_2), the thermal energy is not sufficient to bring about complete vaporization. For entropies close to critical (from either side) the material is in a two-phase state during unloading, and both vapor and liquid drops are present. An important role is played here by the kinetics of the phase transitions. These very interesting problems have not as yet been studied either theoretically or experimentally.

The entropy criterion, despite its limitations, has an advantage over the energy criterion in that it allows us to approach the estimate of the limiting critical entropy S_{cr} from the "gas side", omitting the poorly investigated range of volumes two to three times greater than the standard volume of the solid. Here, of course, there is also the uncertainty coming from the fact that the critical parameters of liquid metals are unknown as a rule.

Let us illustrate the above qualitative considerations by carrying out an estimate for lead. The entropy of lead at the critical point is calculated by means of the entropy equation (3.18) for a perfect gas which is monatomic, as is lead vapor. We take for the critical temperature $T_{cr} = 4200°K$ and for the volume $V_{cr} = 3V_{0c}$* (ordinarily the critical volume is about three times

* The quantity T_{cr} was estimated in [39]; according to van der Waals equation, $p_{cr} = (3/8)n_{cr}kT_{cr} \approx 2400$ atm.

greater than the standard volume of the liquid). The statistical weight of lead atoms is $g_0 = 9$. Using these parameters gives $S_{cr} = 42.8$ cal/mole · deg*.

The entropy behind the shock can be calculated from the functions $\varepsilon(T, V)$ and $p(T, V)$ described in §6. The simplest procedure is to find the entropy in the state T, V by integrating the equation

$$dS = \frac{d\varepsilon + p\,dV}{T} = \frac{d\varepsilon_T + p_T\,dV}{T}$$

first at constant temperature equal to the standard temperature T_0, from the volume V_0 to V, and then with respect to temperature at $V = const$, from T_0 to T. In the first integration we can neglect the electronic terms, which are negligible at $T_0 \approx 300°K$. For purposes of estimation we take the Grüneisen coefficient to obey $\Gamma(V) \approx \Gamma_0(V/V_0)^m$, where the exponent m for lead, according to the data of Table 11.2, is approximately 1. After integration we obtain

$$S(T, V) = S_0 + c_v \ln\frac{T}{T_0} + \beta_0\left(\frac{V}{V_0}\right)^{1/2}(T - T_0) - \frac{\varepsilon_0}{mT_0}[\Gamma_0 - \Gamma(V)].\dagger \tag{11.67}$$

Here S_0 is the entropy of metallic lead under standard conditions T_0, V_0, and ε_0, which, according to data quoted in [40], is $S_0 = 15.5$ cal/mole · deg. Substituting the shock parameters from Table 11.2 into (11.67), we can find the entropy behind the wave. An entropy close to the critical value S_{cr} is obtained with the following shock wave parameters: $V_0/V_1 = 1.9$, $p_1 = 2.25 \cdot 10^6$ atm, $T_1 = 15{,}000°K$, $\varepsilon_1 = 4.71 \cdot 10^{10}$ erg/g‡ (more exactly, for these parameters $S_1 = 44.5$ cal/mole · deg). The energy ε'_T upon isentropic expansion to the zero volume V_{0c} is found to be equal to $1.9 \cdot 10^{10}$ erg/g, and thus twice the binding energy $U = 0.94 \cdot 10^{10}$ erg/g, in complete agreement with the expected value mentioned above ($T' = 9500°K$, $p'_T = p' \approx 5 \cdot 10^5$ atm). Thus, it is to be expected that for stronger shock waves complete vaporization of lead will occur on unloading. As another example, we present calculations for the strongest shock waves observed experimentally in lead. Namely, for $p_1 = 4 \cdot 10^6$ atm and $V_0/V_1 = 2.2$ the entropy $S_1 = 51.7$ cal/mole · deg, and the energy at the time of expansion to standard volume $\varepsilon'_T = 3.57 \cdot 10^{10}$ erg/g and thus is 3.6 times greater than the binding energy U ($T' = 15{,}000°K$). In

* The use of van der Waals equation to take into account the departure from the perfect gas law leads to a very small correction in the entropy; this correction is $\Delta S_{nonideal} = \mathscr{R} \ln(2/3) = -0.8$ cal/mole · deg (for the same volume at which the ideal S is calculated). This correction was included in the calculated value of S_{cr}.

† The last term, which depends on Γ, is of little importance, so that the error resulting from the approximation of $\Gamma(V)$ by a power law relation is negligible.

‡ It is interesting to note that the energy behind a shock wave for which complete vaporization just begins is five times greater than the binding energy.

this case, complete vaporization on unloading has apparently already taken place.

In conclusion we wish to emphasize that an unloading wave propagating through a body after a shock wave has emerged at the free surface contains from the outset particles of the material in widely differing states, from those with the pressure p_1 (at the head of the rarefaction wave) down to those with zero pressure (at the free surface). All states through which the given particle passes when going from the pressure p_1 to zero are present in the wave. We also note that the pressure of the particles close to the free surface drops to zero so rapidly that in the case of complete vaporization the vapor in this region is strongly supersaturated, although for thermodynamic equilibrium the medium should be in a two-phase state.

§23. Experimental determination of temperature and entropy behind a very strong shock by investigating the unloaded material in the gas phase

A number of sections in this chapter have been devoted to the study of the thermodynamic properties of solids at high pressures and temperatures and to the description of experimental methods for studying these properties by the measurement of the state and flow variables in the material behind the compression shock. A general feature of these methods is that they allow only the determination of the mechanical state variables of the material, in particular of the pressure, the density, and the total internal energy. Measurement of the kinematic variables of the shock wave, the front velocity and the particle velocity, together with the use of relationships across the shock front, does not make it possible to determine directly such important thermodynamic variables as the temperature and entropy. In order to find the temperature and entropy from mechanical measurements we must adopt some theoretical scheme for characterizing the thermodynamic functions. Earlier we made use of a three-term representation of the pressure and energy in which certain parameters, such as the specific heat of the atomic lattice, the electronic specific heats, and the electron pressure, had to be determined theoretically.

On the other hand, it would be very interesting and important to find some means for the direct experimental determination of the temperature or entropy behind a shock wave to reduce as far as is possible the number of theoretical parameters. Unfortunately, such a procedure is extremely difficult, both in principle and experimentally. Optical methods, one of the major means of measuring high temperatures, can be used only when the body is transparent, while the overwhelming majority of solids are opaque; this particularly includes metals, the solids of greatest interest to us.

The temperature behind the front of a shock wave in Plexiglas was meas-

ured optically by Zel'dovich, Kormer, Sinitsyn, and Kuryapin [41]. In these experiments the surface brightness was measured from the front of a very strong shock wave propagating through a transparent material, in this case Plexiglas. The surface brightness was converted to temperature under the assumption that the heated region bounded by the front surface radiates as a perfect black body. The surface brightness was measured in the red and blue regions of the spectrum, and not only the brightness temperature but also the color temperature was determined (see §8, Chapter II). The temperature behind a shock wave with a pressure $p \approx 2 \cdot 10^6$ atm and a density ratio $\rho/\rho_0 \approx 2.7$ was found to be $T \approx 10{,}000$–$11{,}000°$K. The temperature estimated from the internal energy (known from mechanical measurements) and by making suitable assumptions on the energy balance (the dissociation of Plexiglas molecules is important) shows the measured value of the temperature to be reasonable.

It might have been possible to try to measure the temperature optically at the time when the shock emerges from the free surface. However, in order for the measured temperature to agree with the actual temperature behind the shock, the experiment would have to satisfy almost impossible requirements. Metals are opaque to visible light even in very thin layers $\sim 10^{-5}$ cm. A shock with a velocity of 10 km/sec would travel through such a layer in $\sim 10^{-11}$ sec. Even if it were possible to build a light recording instrument with a resolution time of $\sim 10^{-12}$–10^{-13} sec, in order to record just before the instant at which the wave emerges from the surface, when the wave is separated from the surface by a transparent layer of $\sim 10^{-6}$–10^{-7} cm, it would still be impossible to ensure the simultaneous emergence of the shock at different points of the free surface with the requisite accuracy. In other words, it is impossible to ensure that the front surface is parallel to the free surface to within $\sim 10^{-6}$ cm. If, however, we measure the surface luminosity in the practically measurable time of $\sim 10^{-8}$ sec after the emergence of the wave, then we will record the luminosity not behind the wave front, but behind the unloading wave, since in a time of $\sim 10^{-8}$ sec the unloading wave traverses a layer which is optically very thick, of the order of 10^6 cm/sec $\times$ 10^{-8} sec $= 10^{-2}$ cm; such a layer is completely opaque to the light produced in the unloaded region whose temperature we want to determine. (The problem of the luminosity from the surface of an unloading wave will be considered in detail in the next section.)

The possibilities for determining the temperature (and entropy) behind a shock wave experimentally were given in a paper by one of the authors [42]. Let the shock wave be so strong that after it emerges from the free surface the material completely vaporizes on unloading. Then the material at the leading edge of the expanding medium is in the gas phase. If we could somehow measure in the gas phase the mechanical quantities density and pressure,

or the temperature, then the entropy could be calculated theoretically, since the thermodynamic properties of gases can be calculated relatively simply (see Chapter III). However, since the unloading process is isentropic the entropy of the material behind the shock wave is the same as the entropy in the gas phase on unloading. Thus, knowing the entropy in the gas phase, we would also know the entropy behind the shock wave.

A method was given in [42] for calculating the temperature along the entire unloading isentrope if the specific internal energy ε is known as a function of pressure and density along the isentrope and if one value of the temperature is known at any point on the isentrope. In this regard, it follows from the thermodynamic identity

$$dS = \frac{d\varepsilon + p\,dV}{T} = \frac{1}{T}\frac{\partial \varepsilon}{\partial p}\,dp + \frac{1}{T}\left(\frac{\partial \varepsilon}{\partial V} + p\right)dV$$

and from the condition that the entropy is a state function and dS a total differential, that

$$\frac{\partial}{\partial V}\left(\frac{1}{T}\frac{\partial \varepsilon}{\partial p}\right) = \frac{\partial}{\partial p}\left[\frac{1}{T}\left(\frac{\partial \varepsilon}{\partial V} + p\right)\right].$$

Differentiating and simplifying we obtain a partial differential equation for the function $T(p, V)$

$$\left(\frac{\partial \varepsilon}{\partial V} + p\right)\frac{\partial T}{\partial p} - \frac{\partial \varepsilon}{\partial p}\frac{\partial T}{\partial V} = T. \tag{11.68}$$

The characteristics of this equation are lines along which

$$\frac{dp}{dV} = -\frac{\partial \varepsilon/\partial V + p}{\partial \varepsilon/\partial p}.$$

But this is the equation for an isentrope. Along the characteristics, then, along an isentrope, according to (11.68)

$$\left(\frac{dT}{dV}\right)_S = -\frac{T}{\partial \varepsilon/\partial p}.$$

From this we obtain

$$T = T_0 \exp\left(-\int_{V_0}^{V} \frac{dV}{\partial \varepsilon/\partial p}\right) = T_0 \exp\left(\int_{p_0}^{p} \frac{dp}{\partial \varepsilon/\partial V + p}\right),$$

where the integrals are taken along the isentrope. The method is simply the application of this formula.

We note that knowing the entropy behind two shock waves whose strengths are close to each other (not necessarily the absolute values of the entropy, but

only their difference), we can easily calculate the temperature behind the shock wave from the thermodynamic relation

$$T = \frac{\Delta\varepsilon + p\,\Delta V}{\Delta S},$$

since $\Delta\varepsilon$, p, and ΔV are taken to be known from mechanical measurements. In addition, knowing the temperatures along the Hugoniot curve we can also find the absolute values of the entropy by integrating the thermodynamic relation

$$dS = \frac{d\varepsilon + p\,dV}{T}$$

along the Hugoniot curve, having set the constant of integration equal to the tabulated value of the entropy of the material at standard conditions.

§24. Luminosity of metallic vapors in unloading

It was noted in the preceding section that any attempt to "see" the high-temperature luminosity from the front of a very strong shock propagating through a solid at the time it emerges from the free surface is doomed to failure. Let us consider in more detail what should be observed in this case, what luminosity will be recorded by an instrument directed at the free surface, and how the surface brightness will vary with time. The theory of the phenomenon was given in a paper by the authors [43], and the corresponding experiments were carried out by Kormer, Sinitsyn, and Kuryapin.

Let a very strong shock wave with a front temperature T_1 of the order of several tens of thousands of degrees emerge at the time $t = 0$ from a plane free surface of a metal bounded by a vacuum (the wave front surface is assumed to be strictly parallel to the free surface of the body). The body must be in a vacuum, as otherwise the material which is being unloaded will generate a shock wave ahead of itself in the air; the air temperature can be very high and we would observe the luminosity of the highly heated air instead of the luminosity of the metal, the quantity of interest to us. We consider the shock wave to be so strong that the metal is completely vaporized on unloading and expands in the gas phase. The temperature distributions at $t = 0$ and at a later time are shown in Fig. 11.60. In the time t the rarefaction wave encompasses a layer of the material of thickness $c_1 t$, where c_1 is the speed of sound in the compressed material behind the shock front. Since the material moves with the velocity u_1 in the laboratory system of coordinates, then at the time t the head of the rarefaction wave is at the position $x = (u_1 - c_1)t$ (the initial location of the free surface is taken to be at $x = 0$). The leading edge of the expanding metallic vapor moves ahead with a velocity

u_2 given by (11.66). Since the material in the unloading wave is in the gas phase, the temperature at the vacuum interface is zero, as are the density and pressure.

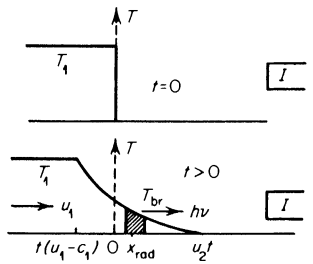

Fig. 11.60. Temperature distributions at the time of emergence of a shock wave from a free surface, at $t = 0$ and at a later time $t > 0$. The radiating layer is shaded. I is a light-recording instrument.

It was stated in the preceding section that metals are opaque in very thin layers of $\sim 10^{-6}$ cm. This means that even as early as $t \sim 10^{-11}$ sec (for a speed $c_1 \sim D \sim 10^6$ cm/sec) the layer of unloaded metal almost completely shields the high-temperature radiation at the temperature T_1, and the metal which was originally heated by the shock wave becomes invisible. Let us examine the nature of the surface luminosity of the material in the continuous spectrum and the type of radiation recorded by an instrument directed toward the planar free surface. The metallic vapor constitutes a monatomic gas, whose radiative properties in the continuous spectrum were studied in detail in Chapter V. The absorption coefficient for visible light is extremely temperature dependent, increasing rapidly with an increase in temperature, with the cold vapor completely transparent in the continuous spectrum. The luminosity of a layer with a temperature distribution similar to that shown in Fig. 11.60 has already been considered in Chapter IX. The phenomenon is completely analogous to that with the luminosity of air in the preheating layer which forms ahead of the compression shock in a strong (supercritical) shock wave. At low temperatures at the vacuum interface the vapor is transparent and radiates only very weakly. On the other hand, in the deeper layers where the temperature is high, the vapor is completely opaque to visible light and does not "release" the photons born in these layers. The photons escaping to infinity from the surface of the material are born in some intermediate radiating layer, removed from the vacuum interface by an optical distance τ_ν of the order of unity (the radiating layer is shown shaded in Fig. 11.60).

Knowing the temperature and density distributions as a function of position and the light absorption coefficient κ_ν for a given frequency ν as a function of temperature and density, we can calculate the brightness temperature for radiation of this frequency using the general relation (2.52). However, we can proceed in a simpler manner by noting that the brightness temperature

is the same as the temperature of the radiating layer (the geometric thickness of the radiating layer is small and the temperature in it changes little); we can set up an expression for the optical thickness measured from the vacuum interface and set it equal to unity

$$\tau_\nu = -\int_{u_2 t}^{x(T_{br})} \kappa_\nu(x)\, dx = 1. \tag{11.69}$$

With temperature as the variable of integration in place of x, we write

$$-\int_0^{T_{br}} \kappa_\nu(T) \frac{dx}{dT}\, dT = 1. \tag{11.70}$$

This equation determines the brightness temperature. The derivative of the temperature distribution is calculated using the general solution for a rarefaction wave (11.63) and (11.64).

Since the material at the leading edge, close to the vacuum interface and precisely in that region which contains the radiating layer, is in the gas phase, then by specifying an effective adiabatic exponent γ for the gas we can find the approximate distribution of all quantities in this region in explicit form. To do this (11.64) should be integrated not from the undisturbed compressed material, as was done in deriving (11.65), but from the vacuum interface,

$$u = u_2 - \int_0^p \frac{dp}{\rho c} = u_2 - \int_0^\rho c \frac{d\rho}{\rho}, \tag{11.71}$$

using the isentropic relation $c(\rho, S)$.

The solution will contain the velocity of the interface u_2 and the entropy S as parameters. We shall not write out this solution, but shall find the derivative directly from (11.63) and the differential relation $du = -c\, d\rho/\rho$,

$$\frac{1}{t}\frac{dx}{dT} = \frac{\partial u}{\partial T} - \left(\frac{\partial c}{\partial T}\right)_S = -c\left(\frac{\partial \ln \rho}{\partial T}\right)_S - \left(\frac{\partial c}{\partial T}\right)_S,$$

or

$$\frac{dx}{dT} = -\frac{ct}{T}\left\{\left(\frac{\partial \ln \rho}{\partial \ln T}\right)_S - \left(\frac{\partial \ln c}{\partial \ln T}\right)_S\right\} \approx -\frac{\gamma+1}{2(\gamma-1)}\frac{ct}{T}.$$

Here we have used the relation $c \sim \sqrt{T}$, and also the isentropic relation $T \sim \rho^{\gamma-1}$. Equation (11.70) now takes the form

$$\frac{\gamma+1}{2(\gamma-1)}\, t \int_0^{T_{br}} \kappa_\nu(T) \frac{c(T)}{T}\, dT = 1. \tag{11.72}$$

It is evident that the integral and, consequently, the brightness temperature

decrease with time. The physical reason for this result is that as the unloading wave encompasses a larger and larger mass of the material with time, the geometric and optical thicknesses of the layer between the vacuum interface and the point with the given temperature increase continuously. Therefore the radiating layer, which is separated from the interface by the specified optical distance of the order of unity, moves into a region of increasingly lower temperatures (Fig. 11.61).

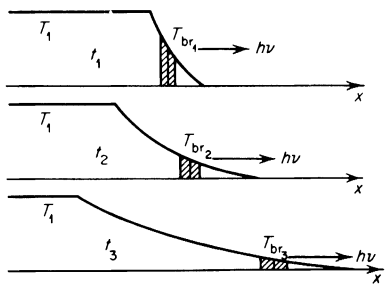

Fig. 11.61. Displacement of the radiating layer (shaded) with time in an unloading wave.

It is remarkable that the interface velocity u_2 has dropped out of the equation (11.72) for $T_{br}(t)$*. The interface velocity is an unknown because it is determined by the thermodynamic properties of the material along the entire unloading isentrope, including the unexplored region where the density is somewhat less than the standard density of the solid. The only parameter contained in (11.72) is the entropy S, which appears because of the dependence of the absorption coefficient κ_ν on the density (the atom number density n), which is related to the temperature by the adiabatic relation

$$n = B(S)T^{1/(\gamma-1)}, \tag{11.73}$$

where $B(S)$ is the entropy constant.

If the basic mechanism of absorption of visible light in metallic vapors is photoelectric absorption by highly excited atoms (and also bremsstrahlung absorption in the fields of the ions), then the absorption coefficient κ_ν can be calculated approximately from (5.44)

$$\kappa_\nu = \frac{a_\nu n}{T^2} e^{-(I-h\nu)/kT}, \tag{11.74}$$

where a_ν is a constant depending on frequency ($a_\nu \sim \nu^{-3}$), and I is the ionization potential.

In dense vapors with very weak ionization an important role may be played by bremsstrahlung absorption in the fields of neutral atoms (see

* Since (11.70) does not explicitly contain the coordinate x but only the derivative dx/dT.

Chapter V). In this case the absorption coefficient κ_ν is proportional to the number of free electrons n_e, that is, to the degree of ionization, and the basic temperature dependence of the absorption coefficient is Boltzmann-like but with a different exponent

$$\kappa_\nu \sim n n_e = b_\nu e^{-I/2kT} n^{3/2}, \tag{11.75}$$

where b_ν depends only weakly on temperature. The general character of the temperature dependence of κ_ν is the same in both cases: $\kappa_\nu \sim e^{-E/kT}$, where $E = I - h\nu$ in the first case and $E = I/2$ in the second case. It should be noted that numerically the two values of E do not differ much for metals (where $I \approx 6$–8 ev and $h\nu \approx 2$–3 ev).

Let us evaluate approximately the integral of (11.72), taking the basic temperature dependence of the integrand to be contained in the exponential factor. Setting all the slowly varying functions which are powers of the temperature constant, we find $te^{-E/kT_{br}} = const$ and obtain a logarithmic decrease of the radiation brightness temperature with time (Fig. 11.62)

$$T_{br} = \frac{const}{\ln t + const'}.$$

Detailed calculations show that the brightness temperature for metals is of the order of 7000–4000°K* at times $t \sim 10^{-7}$–10^{-6} sec, irrespective of the assumed absorption mechanism. In these times the free surface moves away approximately 10^{-1}–1 cm at speeds of $\sim$ 10km/sec.

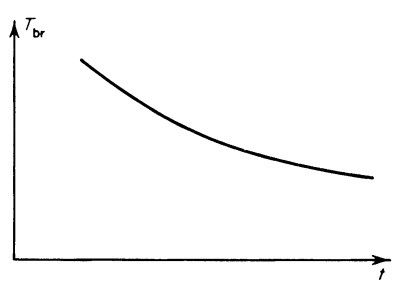

Fig. 11.62. Time dependence of the brightness temperature of the surface of an unloading wave.

§25. Remarks on the basic possibility of measuring the entropy behind a shock wave from the luminosity during unloading

Equation (11.72) contains only one parameter characterizing the shock wave—the entropy S. If the radiative properties of the material, i.e., the function $\kappa_\nu(T, \rho)$, are known, then by plotting the experimental luminosity

* While behind the shock wave the temperature T_1 can reach tens of thousands of degrees.

curve $T_{br}(t)$ we can find the absolute value of the entropy behind a shock wave. On the other hand, by specifying the entropy on the basis of other considerations (calculating it using thermodynamic properties of the compressed solid and measured shock wave parameters), we can extract from the experiment on the luminosity of an unloaded surface data on the radiative properties of metallic vapors, namely to determine the preexponential factor in the expression for the absorption coefficient. It is interesting to note that assuming that only one absorption mechanism exists and that κ_ν is expressed either by (11.74) or (11.75), the final equation for the function $T_{br}(t)$ (11.72) contains only the product of the unknown parameters $a_\nu B(S)$ for the case of (11.74) and $b_\nu B^{3/2}(S)$ for the case of (11.75) (since in (11.74) $\kappa_\nu \sim a_\nu n \sim a_\nu B$, while in (11.75) $\kappa_\nu \sim b_\nu n^{3/2} \sim b_\nu B^{3/2}$). The entropy constant B in the adiabatic equation (11.73) depends on the absolute value of the entropy S as $B \sim e^{-S/\mathscr{R}}$ ($\mathscr{R}$ is the gas constant per mole). This means that by taking the luminosity curves from two experiments with slightly differing shock strengths and determining the parameters, say, the product $a_\nu B$, we find the difference of entropies behind the shock waves even if the optical constant a_ν is not known, from

$$\frac{a_\nu B'}{a_\nu B''} = \exp\left[-\frac{S' - S''}{\mathscr{R}}\right].$$

Here the single and double prime refer to the first and second experiments. As noted in the preceding section, we can also find the temperature behind the shock wave by knowing the entropy difference.

The experiment described above can serve as a specific application of the considerations given in the preceding section on the use of measurements in the gas phase in an unloading wave for an experimental determination of the entropy and temperature behind a shock wave.

5. *Some other phenomena*

§26. Electrical conductivity of nonmetals behind shock waves

Under normal conditions gases are good insulators. Behind sufficiently strong shock waves they become conductors. A similar situation also occurs with solid dielectrics, which conduct electric currents behind strong shock waves. However, while the appearance of conductivity in gases involves simply the thermal ionization that takes place at high temperatures of the order of ten thousand degrees and above, attainable in shock waves, the physical cause of the transformation of solid dielectrics into conductors by shock waves is considerably more complex. It is more likely connected with

the compression than with the temperature increase, though in many respects this is still not clear.

The electrical conductivity of condensed materials behind shock waves has been studied by several authors. Brish, Tarasov, and Tsukerman developed a method for the measurement of conductivity and have measured the conductivity of the detonation products of condensed explosives [45], and also of water, Plexiglas, paraffin, and air [46] behind strong shock waves with pressures of up to a million atmospheres. The conductivity of an ionic crystal of sodium chloride at pressures up to a million atmospheres was studied in the previously cited reference [5]. Alder and Christian [47], who measured the electrical conductivity of ionic and molecular crystals of CsI, I_2, CsBr, $LiAlH_4$, and others worked with weaker shock waves (up to 250,000 atm).

The essence of the basic electrical contact method described in [45], used for the measurements of conductivity reported in [45, 46, 5], consists of the following: Electrodes (contacts) E are connected by a shunt resistance R_{sh} and are placed in the body through which the shock wave propagates (Fig. 11.63). As long as the shock wave does not reach the contacts, the resistance of the dielectric is practically infinite. After the shock wave reaches the contacts the dielectric becomes a conductor and the desired resistance R_x is connected in parallel with the resistance R_{sh}.

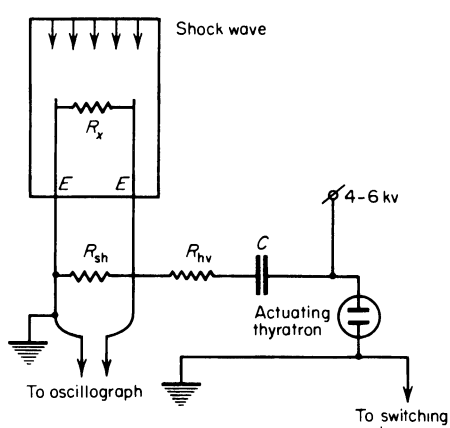

Fig. 11.63. Diagram of the experimental setup for the measurement of electrical conductivity behind a shock wave.

Shortly before the shock wave reaches the contacts the capacitor C, which was previously charged to a voltage of several kilovolts with the help of the actuating thyratron, is discharged through the high-voltage resistance R_{hv}

and the contacts. The resistance $R_{hv} \gg R_{sh}$, so that the current in the circuit is determined only by R_{hv}. The potential difference at the contacts is proportional to the resistance between the contacts. This resistance is equal to R_{sh} before the arrival of the shock wave and $R = R_{sh} R_x/(R_{sh} + R_x)$ after the shock wave reaches the contacts (the resistance R_{sh} is chosen so that it is of the order of R_x). If U_{sh} and U_x correspond to the potential difference at the contacts, then $U_{sh}/U_x = R_{sh}/R = (R_{sh} + R_x)/R_x$. The voltages U_{sh} and U_x are measured by an oscillograph, R_{sh} is known, and the unknown resistance R_x is found from the equation given.

The measured resistance R_x is converted to the specific electrical conductivity of the material by electrolytic simulation. For this purpose the electrodes are immersed into an electrolyte bath maintaining the same geometry as in the experiment. By changing the electrolyte density, a resistance equal to that measured in the experiment is obtained. The unknown conductivity is then equal to the known conductivity of the electrolyte (for other methods of measuring the conductivity of materials behind a shock wave see [45, 5]).

Experiments [46] have shown that the electrical conductivity of dielectrics is increased behind a shock wave by many orders of magnitude. The initial conductivity of distilled water was $\sigma \sim 10^{-5}$ ohm^{-1}cm^{-1}, while at a pressure $p = 10^5$ atm it became $\sigma = 0.2$ ohm^{-1}cm^{-1}. The conductivity behind the shock was completely independent of the initial conductivity of the water, which depends on the purity of the water. The same value of σ behind a shock wave was also obtained for ordinary water with an initial conductivity $\sigma \sim 10^{-3}$ ohm^{-1}cm^{-1}.

Perfect dielectrics such as paraffin ($\sigma \sim 10^{-16}$ ohm^{-1}cm^{-1}) and Plexiglas ($\sigma \sim 10^{-15}$ ohm^{-1}cm^{-1}) were, at pressures of the order of 10^6 atm, converted into fair conductors with conductivities $\sigma \sim 1\text{–}2 \cdot 10^2$ ohm^{-1}cm^{-1}*. In paraffin a significant increase in the conductivity is observed at a pressure of $\sim 6\text{–}7 \cdot 10^5$ atm, and as the pressure is increased further, σ increases rapidly. An extremely sharp increase in the conductivity of Plexiglas takes place at a pressure of $8 \cdot 10^5$ atm.

The change in the electrical conductivity of Plexiglas and paraffin behind a shock wave by 15–20 orders of magnitude attests to the "metallization" of these dielectrics when compressed to pressures of the order of a million atmospheres†. This phenomenon cannot be explained by thermal ionization. It is related to the change in structure of the electron zones of a solid on compression. The zones are brought closer on compression, the distances between

* For comparison with the conductivity of metals we note that for copper $\sigma \sim 10^6$ ohm^{-1}cm^{-1}, for iron $\sigma \sim 10^5$ ohm^{-1}cm^{-1}, and for mercury $\sigma \sim 10^4$ ohm^{-1}cm^{-1}.

† Alder and Christian [47] measured considerably lower electrical conductivities. The "metallization" phenomenon in the comparatively weak waves with which these authors worked manifested itself much more weakly.

them decrease, and this facilitates electron transitions leading to the appearance of free electrons and metallic conductivity in a material which was previously a dielectric*. Qualitative ideas concerning the metallization of any material under sufficiently strong compression were discussed in a paper by Zel'dovich and Landau [48], in which they considered the transformation of metals from the solid to gaseous state. The metallization of hydrogen at high densities was studied by Abrikosov [49].

It must be said that the details of the mechanism of metallization of dielectrics by a shock wave are still not entirely clear, and this phenomenon requires further theoretical and experimental study. In particular, it would be interesting to clarify the separate roles of temperature and compression in increasing the conductivity.

Experiments [5] with sodium chloride, which under normal conditions has a small ionic electrical conductivity, make it possible to assume that the basic role there in the increase of electrical conductivity with increasing shock strength is played by temperature, in contrast to our previous considerations. The curve of $\sigma(T)$ is Boltzmann-like, $\sigma \sim e^{-E/kT}$ with an activation energy $E \approx 1.2$ ev, and this apparently attests to the ionic nature of the conductivity of NaCl behind a shock wave. The limits for the range of shock strengths studied were $p = 10^5$ atm, which gave $T = 440°\text{K}$, $V_0/V = 1.26$, $\sigma = 2 \cdot 10^{-5}$ $\text{ohm}^{-1}\text{cm}^{-1}$, and $p = 7.9 \cdot 10^5$ atm, which gave $T = 6150°\text{K}$, $V_0/V = 1.85$, $\sigma = 3.26$ $\text{ohm}^{-1}\text{cm}^{-1}$.

§27. Measuring the index of refraction of a material compressed by a shock wave

The thickness of a shock front in solids and liquids is comparable with interatomic distances and much less than the wavelengths of visible light $\lambda \sim 4000$–7300 Å. Therefore light passing through a transparent undisturbed material incident on the surface of a shock front separating the undisturbed from the compressed material is reflected in the same manner as from an ordinary boundary between two different media. The reflection of light from the surface of a shock front in transparent materials, water and Plexiglas, was investigated experimentally by Zel'dovich, Kormer, Sinitsyn, and Yushko [51]. Knowing the index of refraction of the undisturbed material, knowing the angle of incidence, and measuring the reflectivity, it is then possible to

* The effect of pressure on the electrical conductivity of dielectrics had been studied previously (in a region of comparatively low pressures). Thus, Bridgman [50] established that yellow phosphorus, which is a dielectric, is transformed at pressures of 1.2–$1.3 \cdot 10^4$ atm and a temperature of 200°C into a new form, black phosphorus, which has a metallic conductivity. The density of black phosphorus is 1.4 times greater than that of yellow phosphorus.

use the known Fresnel formulas (see [52] for example) to calculate the index of refraction n of a material compressed by a shock wave*. This method is, in general, also applicable to those cases when the material compressed by the shock is opaque. If the absorption mean free path is comparable with the wavelength of light, then, in principle, it is possible to measure both the real and the imaginary parts of the refractive index. To do this it is necessary to determine the degree of polarization of the reflected light and the dependence of the reflectivity on the angle of incidence [54]. A material which is transparent in the undisturbed state becomes opaque behind a sufficiently strong shock wave. The loss of transparency at high pressures can occur for various reasons, from cracking of the material, from phase transitions, or from rearrangement of the electronic levels (in particular, in the "metallization" of dielectrics, mentioned in the preceding section).

The basic experimental arrangement for the study [51] of the reflection of light from a shock front in water is shown in Fig. 11.64. A layer of water is

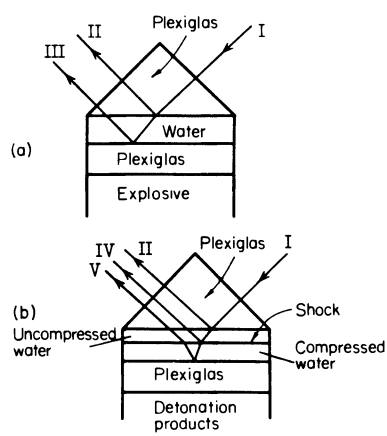

Fig. 11.64. Experimental arrangement for measuring the reflection of light from a shock front: (a) before detonation; (b) during the propagation of the shock through water.

located on top of a Plexiglas plate, which is placed on the flat surface of an explosive charge. A Plexiglas prism is placed on top of the water. The paths of the light rays before the detonation are shown in Fig. 11.64a. Ray I from a light source is incident on the prism, from which emerge rays II and III reflected from the two water surfaces. The paths of the rays after the detonation during the passage of the shock wave through the water are shown in

* The thickness of a shock front in a gas, the thickness of the transition layer between the undisturbed and compressed media, is of the order of a wavelength of light; therefore, the Fresnel formulas are not applicable. However, in gases the index of refraction at different densities is known. A study of the reflection of light under these conditions makes it possible to determine the front thickness. Such measurements were carried out by Cowan and Hornig [53] for weak shock waves (see Chapters IV and VI).

Fig. 11.64b. Ray IV is produced by reflection from the surface of the shock front, while ray V is produced by reflection from the now moving boundary between the compressed Plexiglas plate and the compressed water. Ray V replaces ray III.

The reflected rays are recorded by streak photography. A schematic diagram of a photographic record is shown in Fig. 11.65. Prior to detonation

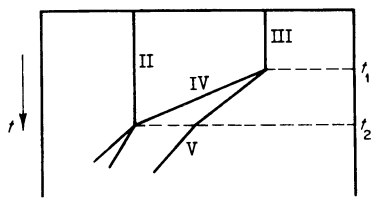

Fig. 11.65. Diagram of a photochronogram.

rays II and III give straight lines on the moving film. At the time t_1 at which the shock wave passes into the water, the two lines produced by rays IV and V appear, with line V now replacing the terminated line III. Line II continues, remaining undisturbed up to the time the shock wave emerges at the upper surface of the water (the time t_2). It is evident from Fig. 11.64b that as the wave front approaches the upper boundary of the water the distance between rays IV and II decreases. At the time of emergence t_2 the rays IV and II come together, and the line IV in Fig. 11.65 reaches the line II. In practice the distance between rays II and III was approximately 20 mm, and the difference in time $t_2 - t_1$ approximately $4 \cdot 10^{-6}$ sec.

The shock front velocity in water was measured by the slope of the line IV. Knowing the Hugoniot curve for water, the density and other parameters behind the front could be determined. The reflectivity was calculated from the ratio of the intensities of the incident and reflected rays; the intensities were determined by photometric methods. The refractive index of compressed water was determined by two methods, one geometric (from the distance between the reflected rays), and the other using the reflectivity. Average values from several experiments, calculated by both methods, were found to be close to each other. As the water density changes from $\rho/\rho_0 = 1.47$ to $\rho/\rho_0 = 1.81$, which corresponds to pressures from 50 to 150 thousand atmospheres, the index of refraction remains almost constant and equal to $n = 1.49 \pm 0.03$ (from the geometric method) or $n = 1.46 \pm 0.03$ (from the reflectivity method). In standard density air $n = n_0 = 1.333$.

Experimental results obtained by other authors on the measurement of the refractive index of water at relatively low pressures are quite well described by the linear relation $n = 1 + 0.334\rho$*, where ρ is the density in g/cm^3.

* The Lorenz-Lorentz formula gives much worse agreement with the experimental data.

This formula also agrees with experimental values for water vapor and with the experimental value of the refractive index for ice at 0°C and $\rho = 0.92$ g/cm^3 equal to 1.311.

The values of the refractive index obtained for water compressed by a shock wave are much lower than the values derived from the above equation. In all probability the difference can be ascribed to a temperature effect (water compressed by a shock wave to a density $\rho = 1.8\rho_0$ was heated to 1100°C). The mechanism of such a temperature effect (the higher the temperature, the lower the index of refraction) has not yet been clarified.

Investigation of the reflection of light from shock fronts shows that the front surface is smooth. Otherwise the reflection would be diffuse rather than specular.

XII. Some self-similar processes in gasdynamics

1. *Introduction*

§1. Transformation groups admissible by the gasdynamic equations

In Chapter I we have already become familiar with several examples of self-similar motions (the self-similar rarefaction wave, the problem of a strong explosion). In Chapter X we considered self-similar problems in the theory of heat propagation in a stationary medium by thermal conduction. In this chapter we shall consider in detail self-similar motions of one of two basic types. We shall show in the introductory part of the chapter how the gasdynamic equations admit the existence of self-similar solutions and shall present the general characteristics of self-similar motions. It would appear worthwhile at first to become familiar with the general group properties of the gasdynamic equations.

We shall consider one-dimensional adiabatic flows of a perfect gas with constant specific heats, with either planar, cylindrical, or spherical symmetry. Let us write the system of equations for flows of this type. In the continuity equation (1.2) we expand the divergence term and write the equation in a form appropriate to all three types of symmetry. In addition, we divide the equation through by the density ρ. The entropy in the entropy equation (1.13) is expressed by (1.14) (with the density in place of specific volume). The equation of motion (1.6) we leave unchanged. We then obtain the following system of equations for the density, pressure, and velocity as functions of position and time:

$$\begin{aligned} &\frac{\partial \ln \rho}{\partial t} + u\frac{\partial \ln \rho}{\partial r} + \frac{\partial u}{\partial r} + (\nu - 1)\frac{u}{r} = 0, \\ &\frac{\partial u}{\partial t} + u\frac{\partial u}{\partial r} + \frac{1}{\rho}\frac{\partial p}{\partial r} = 0, \\ &\frac{\partial}{\partial t}\ln p\rho^{-\gamma} + u\frac{\partial}{\partial r}\ln p\rho^{-\gamma} = 0. \end{aligned} \tag{12.1}$$

In the continuity equation $\nu = 1$, 2, and 3, for the plane, cylindrical, and

spherical cases, respectively. The variable r represents the x coordinate in the plane case and the radius in the cylindrical and spherical cases.

Equations (12.1) admit several transformation groups, which we shall presently enumerate. It is assumed that analogous transformations are made at the same time in the initial and boundary conditions of the problem.

(a) The time t enters the equations only in terms of time derivatives. Therefore, a shift in time, carried out by introducing the new variable $t' = t + t_0$, does not alter the equations. The fact that a time shift is possible is related to the arbitrariness in the selection of the initial time.

(b) In the plane case ($\nu = 1$) the coordinate also enters the equations only in terms of distance derivatives. Therefore, a shift in position, related to the arbitrariness in the selection of the coordinate origin, is also possible in the plane case. The introduction of the new variable $x' = x + x_0$ does not alter the equations. This is not possible in the spherical and cylindrical cases, since the radius enters the continuity equation directly and not just in terms of its differential.

The gasdynamic equations contain five dimensional quantities ρ, p, u, r, and t, the dimensions of three of which are independent. For example, if we choose the density, distance, and time as the basic dimensional quantities, then the dimensions of the velocity and pressure are represented in the form $[u] = [r]/[t]$ and $[p] = [\rho][r^2]/[t^2]$. As a result of the existence of three independent dimensional quantities the equations admit three independent similarity transformation groups which are related to the arbitrariness in choice of the units of the basic dimensional quantities.

(1) Let the functions $\rho = f_1(r, t)$, $p = f_2(r, t)$, and $u = f_3(r, t)$ represent solutions of the equations for some specified motion. Let us change the scale of the density without changing the coordinate and time scales by introducing the new variables $\rho' = k\rho$ and $p' = kp$, leaving the remaining variables unchanged. This transformation does not change the equations. If at the same time we similarly transform the boundary and initial conditions by multiplying the density and pressure by k, then the new motion will be described by the functions

$$\rho' = kf_1(r, t), \qquad p' = kf_2(r, t), \qquad u = f_3(r, t).$$

The new motion is similar to the old one, differing only in the density and pressure scales.

(2) Let us change the length scale without changing the density and time scales. The equations are not changed if we transform to the new variables $r' = mr$, $u' = mu$, and $p' = m^2p$, with the remaining variables ρ and t left unchanged, $\rho' = \rho$ and $t' = t$. This means that if some motion is described by the functions $\rho = f_1(r, t)$, $p = f_2(r, t)$, and $u = f_3(r, t)$, then by a simple change of scales it is possible to describe a new motion in which the distances and velocities are multiplied by a factor of m and the pressure is multiplied

by a factor of m^2 (the density remains the same). The solution for the new motion is expressed by the functions

$$\rho' = f_1(r', t), \qquad p' = m^2 f_2(r', t), \qquad u' = m f_3(r', t).$$

(3) Finally, let us change the time scale, leaving the length and density scales unchanged. The equations admit the following transformation

$$t' = nt, \qquad u' = \frac{u}{n}, \qquad p' = \frac{p}{n^2}, \qquad \rho' = \rho, \qquad r' = r.$$

This means that if in the boundary and initial conditions the velocity is multiplied by the factor n^{-1}, the pressure is multiplied by the factor n^{-2}, and the density is left unchanged, then the new process will be similar to the old one, except that its rate will be multiplied by a factor of n^{-1}.

By the successive application of these three groups of similarity transformations we can obtain solutions for an infinite number of new motions with altered density, length, and time scales. In particular, if the length and time scales are simultaneously increased by the same factor $r' = lr$ and $t' = lt$, then the solution will remain unaltered. Such a transformation is equivalent to the successive application of transformations (2) and (3) with $m = n = l$. In symbolic form this can be expressed

$$u(r, t) \to lu(lr, t) \to \frac{1}{l} \cdot lu(lr, lt) = u(lr, lt)$$

with similar rules for the other functions ρ and p*.

§2. Self-similar motions

It was shown in the preceding sections that the gasdynamic equations admit similarity transformations, that there are possible different flows similar to each other which are derivable from each other by changing the basic scales of length, time, and density. The motion itself may be described by the most general functions of the two variables r and t, $\rho(r, t)$, $p(r, t)$, and $u(r, t)$. These functions also contain the parameters entering the initial and boundary conditions of the problem (and the specific heat ratio γ).

* *Editors' note.* The equations of state of the fluid must also follow the transformation. With a general equation of state (an imperfect gas, say) and with the identity of the fluid unchanged under the transformation, the equations admit the time shift and coordinate translation transformations mentioned earlier (also rotation and Galilean transformations), plus the scale transformation $r' = lr$ and $t' = lt$ discussed above. Transformations (1), (2), and (3) separately are not admitted. A perfect gas with γ not constant also admits transformation (1), but not (2) and (3) separately. A free Fermi–Dirac gas (see p. 220) admits transformations for which $m = nk^{1/3}$, and gives an example of a fluid which is not a perfect gas but which admits transformations besides the scale transformation.

However, there exist motions whose distinguishing property is the similarity in the motion itself. These motions are called self-similar. The distribution as a function of position of any of the flow variables, such as the pressure p, evolves with time in a self-similar motion in such a manner that only the scale of the pressure $\Pi(t)$ and the length scale $R(t)$ of the region included in the motion change, but the shape of the pressure distribution remains unaltered. The $p(r)$ curves corresponding to different times t can be made the same by either expanding or contracting the Π and R scales. The function $p(r, t)$ can be written in the form $p(r, t) = \Pi(t)\pi(r/R)$, where the dimensional scales Π and R depend on time in some manner, and the dimensionless ratio $p/\Pi = \pi(r/R)$ is a "universal" (in the sense that it is independent of time) function of the new dimensionless coordinate $\xi = r/R$. Multiplying the variables π and ξ by the scale functions $\Pi(t)$ and $R(t)$, we can obtain from the universal function $\pi(\xi)$ the true pressure distribution curve $p(r)$ as a function of position for any time t. The other flow variables, density and velocity, are expressed similarly.

For self-similar motions the system of partial differential equations of gasdynamics reduces to a system of ordinary differential equations in new unknown functions of the similarity variable $\xi = r/R$. Let us derive these equations. To do this we represent the solution of the partial differential equations (12.1) in terms of products of scale functions and new unknown functions of the similarity variable ξ,

$$\xi = \frac{r}{R}, \qquad R = R(t). \tag{12.2}$$

The pressure, density, velocity, and length scales are not all independent of each other. If we choose R and ρ_0 as the basic scales, then the quantity $dR/dt \equiv \dot{R}$ can serve as the velocity scale and $\rho_0\dot{R}^2$ as the pressure scale. This does not limit the generality of the solution, as the scale is only defined to within a numerical coefficient which can always be included in the new unknown function. We seek a solution of the form

$$p = \rho_0\dot{R}^2\pi(\xi), \qquad \rho = \rho_0 g(\xi), \qquad u = \dot{R}v(\xi), \tag{12.3}$$

where π, g, and v are new dimensionless functions of the similarity variable ξ, in terms of which the differential equations are to be formulated. These functions are here termed the reduced pressure, density, and velocity, respectively, or simply the reduced functions*. The scales R, ρ_0, and $\dot{R}$ are time dependent in some as yet unknown manner.

* *Editors' note.* These functions are termed by the authors the "representatives" of the pressure, density, and velocity, respectively. They are sometimes referred to as the dimensionless pressure, density, and velocity. The similarity variable ξ may be termed the dimensionless or reduced distance.

We now substitute the relations (12.3) into equations (12.1), taking account of the definition of the similarity variable (12.2), and applying relations of the type

$$\frac{\partial \rho}{\partial t} = \frac{d\rho_0}{dt} \cdot g - \rho_0 \frac{dg}{d\xi} \frac{r}{R^2} \frac{dR}{dt} = \dot{\rho}_0 g - \rho_0 g' \xi \frac{\dot{R}}{R},$$

$$\frac{\partial \rho}{\partial r} = \frac{\rho_0 g'}{R},$$

to transform the derivatives. The differentiation of scales with respect to time is denoted by a dot and differentiation of the reduced functions with respect to the similarity variable is denoted by a prime. After some rearrangement we obtain the equations

$$\frac{\dot{\rho}_0}{\rho_0} + \frac{\dot{R}}{R}\left[v' + (v - \xi)(\ln g)' + (v - 1)\frac{v}{\xi}\right] = 0,$$

$$\frac{R\ddot{R}}{\dot{R}^2} v + (v - \xi)v' + \frac{\pi'}{g} = 0, \tag{12.4}$$

$$\frac{R}{\dot{R}} \frac{d}{dt} (\ln \rho_0^{1-\gamma} \dot{R}^2) + (v - \xi)(\ln \pi g^{-\gamma})' = 0.$$

In order that the solution form (12.3) have meaning, so that it is possible to write ordinary differential equations for the new unknown functions $\pi(\xi)$, $g(\xi)$, and $v(\xi)$, it is necessary that the variables t and ξ in equations (12.4) be separated. To do this, in the second equation we must set $R\ddot{R}/\dot{R}^2 = const$, from which (with $const \neq 1$)

$$R = At^{\alpha}. \tag{12.5}$$

Here A and α are constants (A is dimensional and α is a pure number). In the first equation of (12.4) we must set $\dot{\rho}_0/\rho_0 = const\ \dot{R}/R$, which yields

$$\rho_0 = Bt^{\beta}, \tag{12.6}$$

where B and β are also constants. The first term in the third equation of (12.4) then automatically becomes a constant. Thus all the scales in the self-similar motion have a power-law dependence on time, and the similarity variable has the form*

$$\xi = \frac{r}{R} = \frac{r}{At^{\alpha}}. \tag{12.7}$$

* As was noted by Stanyukovich [1], in addition to power-law self-similarity it is also possible to have exponential self-similarity, in which $R = A'e^{mt}$, $\rho_0 = B'e^{nt}$, $\xi = re^{-mt}/A'$, where A', B', m, and n are constants. The exponential solution satisfies the equation $R\ddot{R}/\dot{R}^2 = const$ for $const = 1$. The majority of problems of practical interest have a power-law character.

Equations (12.4) are thus transformed into a system of three ordinary differential equations for the three unknown functions $\pi(\xi)$, $g(\xi)$, and $v(\xi)$. The system contains the constant exponents α and β. In a similar manner, the boundary and initial conditions of the problem are made dimensionless and in turn transformed into conditions on the functions π, g, and v. We shall not write out here the system of equations in general form. Instead, the equations will be presented later in context with their application to specific problems.

In many flows the density scale ρ_0 is constant ($\beta = 0$). This is true, for example, in all cases when a shock (or rarefaction) wave propagates through a gas of uniform density. The exponent β is usually different from zero for those problems in which the spatial distribution of the initial gas density is given by a power law of the type $\rho_{00} = const\, r^{\delta}$. In these cases the exponent β is defined in terms of the known exponents δ and α (if $\delta = 0$, $\beta = 0$). Thus, the system of equations for the functions π, g, and v (and the boundary conditions) will contain only one new parameter, the similarity exponent α.

The exponents in the scale functions are uniquely related to the exponents α and β (i.e., α and δ). For example, in the case when the density scale is constant ($\beta = 0$, $\rho_0 = const$), $R \sim t^{\alpha}$, $\dot{R} \sim t^{\alpha-1}$, $\Pi = \rho_0 \dot{R}^2 \sim t^{2(\alpha-1)}$. Since the length scale R is uniquely related to time, we can consider the velocity, density, and pressure scales to be functions of the length scale R, rather than of time. Using the relation $R \sim t^{\alpha}$, we find

$$\dot{R} \sim t^{\alpha-1} \sim R^{(\alpha-1)/\alpha}, \qquad \rho_0 \sim t^{\beta} \sim R^{\beta/\alpha},$$
$$\Pi \sim \rho_0 \dot{R}^2 \sim t^{\beta+2(\alpha-1)} \sim R^{[\beta+2(\alpha-1)]/\alpha}.$$

It is evident from the expression for the density scale $\rho_0 \sim t^{\beta} \sim R^{\beta/\alpha}$ and from the spatial distribution of the initial density $\rho_{00} = const\, r^{\delta}$, that ρ_0 must have the form $\rho_0 = \rho_{00}(R)$. For example, the initial gas density at the point where the shock wave is located at a time t can serve as the density scale ρ_0 (R is then the coordinate of the shock front). The relationship between the exponents β and δ indicated above then follows: $\beta = \alpha\delta$.

For $\beta = 0$ and $\rho_0 = const$, the functions p, ρ, and u given by (12.3) can be expressed in any of the equivalent forms:

$$\begin{aligned} p &= const\, t^{2(\alpha-1)}\pi(\xi) = const\, R^{2(\alpha-1)/\alpha}\pi(\xi), \\ u &= const\, t^{\alpha-1}v(\xi) = const\, R^{(\alpha-1)/\alpha}v(\xi), \\ \rho &= const\, g(\xi). \end{aligned} \tag{12.8}$$

§3. Conditions for self-similar motion

It is natural to pose the following question: what requirements must be satisfied by the conditions of a problem in order that the motion be self-

similar? To answer this question we shall resort to dimensional considerations.

The gasdynamic equations (12.1) do not contain any dimensional parameters other than the dependent variables p, ρ, and u and the independent variables r and t (the only parameter γ is dimensionless). The boundary and initial conditions of the problem do contain dimensional parameters. It is this circumstance which makes it possible to construct the functions $p(r, t)$ and $\rho(r, t)$, since all the five variables p, ρ, u, r, and t have different dimensions, with three of the variables independent. Since the dimensions of pressure and density contain the unit of mass, at least one of the parameters in the problem must also contain a unit of mass. In many cases this is the constant initial density of the gas ρ_0, which has the dimensions* of ML^{-3}. In a number of problems the initial spatial distribution of the density is governed by the power law $p_{00} = br^{\delta}$. In this case it is the parameter b whose dimensions are $[b] = ML^{-3-\delta}$.

Let us denote the parameter containing the unit of mass by a. In the most general case it has the dimensions $[a] = ML^kT^s$. Bearing in mind the dimensions of the functions, $[p] = ML^{-1}T^{-2}$, $[\rho] = ML^{-3}$, and $[u] = LT^{-1}$, we can, without any loss in generality, represent them in the form suggested by Sedov [2]

$$p = \frac{a}{r^{k+1}t^{s+2}}P, \qquad \rho = \frac{a}{r^{k+3}t^{s}}G, \qquad u = \frac{r}{t}V, \tag{12.9}$$

where P, G, and V are dimensionless functions that depend on dimensionless groups containing r, t, and the parameters of the problem. In general there are two dimensionless variables: r/r_0 and t/t_0, where r_0 and t_0 are parameters with dimensions of length and time, which either enter directly in the conditions of the problem, or can be constructed by combining parameters with other dimensions. In this case, the functions P, G, and V will then depend separately on r and t and the problem is not a self-similar one.

We can give a large number of examples of families of similar flows. Let us cite one: the problem of a rarefaction wave generated by withdrawing a piston from a gas with the variable speed $u_1 = U(1 - e^{-t/\tau})$ (see §10, Chapter I). In this example the role of the parameter is played by the constant initial density of the gas ρ_0. In addition, the problem also contains the dimensional parameters $[\tau] = T$, $[U] = LT^{-1}$, and the initial speed of sound $[c_0] = LT^{-1}$ (or the initial pressure p_0, with $c_0^2 = \gamma p_0/\rho_0$). The ratios t/τ and $r/c_0\tau$ or $r/U\tau$ ($r_0 = c_0\tau$ or $U\tau$) can, for example, serve as the dimensionless variables. If length and time scales cannot be constructed from the parameters of the problem, then the variables r and t cannot enter the functions P, G, and V separately; the functions can depend only on a dimensionless combination of

* *Editors' note.* The symbols M, L, and T are introduced to denote mass, length, and time, respectively.

r and t, $\xi = r/At^{\alpha}$, where A is a parameter with the dimensions $[A] = LT^{-\alpha}$. Equations (12.9) then take the form

$$p = \frac{a}{r^{k+1}t^{s+2}}P(\xi), \qquad \rho = \frac{a}{r^{k+3}t^{s}}G(\xi), \qquad u = \frac{r}{t}V(\xi). \tag{12.10}$$

In this case the problem is self-similar and the expressions (12.10) are equivalent to (12.3), differing from them only in the form of the reduced functions. Let us demonstrate this using as an example self-similar motions with a constant density scale. In this case, $a = \rho_0$, $k = -3$, and $s = 0$, so that the expressions of (12.10) take the form

$$p = \rho_0 \frac{r^2}{t^2}P(\xi), \qquad \rho = \rho_0 G(\xi), \qquad u = \frac{r}{t}V(\xi). \tag{12.11}$$

Substituting $r = \xi R$ and noting that $\dot{R} = \alpha R/t$, we find that (12.11) and (12.3) are equivalent if

$$P(\xi) = \alpha^2 \frac{\pi(\xi)}{\xi^2}, \qquad G(\xi) = g(\xi), \qquad V(\xi) = \alpha \frac{v(\xi)}{\xi}. \tag{12.12}$$

The study of self-similar motions is of great interest. The fact that it is possible to reduce a system of partial differential equations to a system of ordinary differential equations for new reduced functions simplifies the problem greatly from the mathematical standpoint and in a number of cases makes it possible to find exact analytic solutions. In addition, the self-similar solutions frequently represent the limits which are approached asymptotically by the solutions of nonself-similar problems. This statement will be clarified later when we consider specific problems.

§4. Two types of self-similar solutions

There exist two rather different types of self-similar solutions. Solutions of the first type possess the property that the similarity exponent α and the exponents of t and R in all scales are determined either by dimensional considerations or from the conservation laws. In this case the exponents are simple rational fractions with integral numerators and denominators. Problems of this type always contain two parameters with independent dimensions*. These parameters are used to construct one parameter whose dimensions contain the unit of mass a (see (12.10)) and another parameter A

* *Editors' note.* There is a type of self-similar solution in which the exponents are determined by the boundary conditions and may be set arbitrarily within certain limits. Although the exponents in such solutions are not simple rational fractions in general, the solutions are to be considered as of the authors' first type, because the two independent parameters exist and the exponents are determinable in advance. See, for example, the solutions of [18] and [19].

that contains only the units of length and time. With the second parameter A it is possible to construct a dimensionless combination, the similarity variable $\xi = r/At^{\alpha}$. The dimensions of the parameter A, $LT^{-\alpha}$, are determined by the similarity exponent α. Two motions of this type were considered in Chapter I, the problem of a self-similar rarefaction wave (§11) and the problem of a strong explosion (§25). In the first case the two independent dimensional parameters are the initial density and pressure of the gas ρ_0 and p_0. They can be combined into a dimensional parameter which does not contain the unit of mass, the initial speed of sound $c_0 = (\gamma p_0/\rho_0)^{1/2}$. The role of the parameter A is played by the speed of sound c_0. Correspondingly

$$\xi = \frac{r}{c_0 t}, \qquad \alpha = 1.$$

The parameters in the problem of a strong explosion are the initial density of the gas $\rho_0 \sim ML^{-3}$ and the explosion energy $E \sim ML^2T^{-2}$. The energy E is always equal to the total energy of the moving gas, and as a result an energy integral appears in the problem. (We recall that the initial pressure and speed of sound p_0 and c_0 in the problem of a strong explosion are assumed to be equal to zero, and hence that these quantities are not parameters of the problem.) The parameters ρ_0 and E are used to construct a parameter which does not contain mass, $A = (E/\rho_0)^{1/5} \sim LT^{-2/5}$, so that the similarity variable is $\xi = r/(E/\rho_0)^{1/5}t^{2/5}$, and $\alpha = \frac{2}{5}$.

For a strong explosion in a medium with variable initial density $\rho_{00} = br^{\delta}$, the explosion energy $E \sim ML^2T^{-2}$ and the coefficient $b \sim ML^{-3-\delta}$ serve as the parameters. They can be used to construct a parameter A not containing the unit of mass

$$A = \left(\frac{E}{b}\right)^{1/(5+\delta)} \sim LT^{-2/(5+\delta)}.$$

The similarity variable has the form

$$\xi = \frac{r}{(E/b)^{1/(5+\delta)}t^{2/(5+\delta)}}, \qquad \alpha = \frac{2}{5+\delta}.$$

(The self-similar problem of an explosion in a medium with variable density was considered by Sedov [2].) The self-similar problem of the propagation of a thermal wave from the point of release of a specified amount of energy is also of this general type (see Chapter X).

As shown in §2, the similarity exponent enters as a parameter in the system of differential equations for the reduced functions. Since in self-similar problems of this type the number α is found immediately from dimensional considerations (or from the conservation laws), the problem is thus reduced to the integration of a system of equations with known boundary conditions and parameters.

In self-similar problems of the second type, the exponent α cannot be found from dimensional considerations or from the conservation laws without solving the equations. In this case the determination of the similarity exponent requires that the ordinary differential equations for the reduced functions be integrated. It turns out that the exponent is found from the condition that the integral curve must pass through a singular point, as otherwise the boundary conditions cannot be satisfied. Examples of self-similar motions of the second type are the problems of an imploding shock wave and of an impulsive load, both of which will be discussed later.

Examination of solutions to specific problems of the second type shows that in all these cases the initial conditions of the problem contain only one dimensional parameter with the unit of mass but lack another parameter which could be used to form the parameter A. This circumstance eliminates the possibility of determining the number α from the dimensions of A. Actually, of course, the problem does have a dimensional parameter $A \sim LT^{-\alpha}$ relevant to it; otherwise it would not be possible to construct the dimensionless combination $\xi = r/At^{\alpha}$. However, the dimensions of this parameter (i.e., the number α) are not dictated by the inital conditions of the problem, but rather are found from the solution of the equations. The numerical value of A cannot be found from self-similar equations alone. It can be determined only by knowing how the given motion arose. Thus, for example, if the self-similar motion originated as a result of some nonself-similar flow that approaches a self-similar regime asymptotically, then the value of A can only be found by a numerical solution of the complete nonself-similar problem in which it is possible to follow the transition of the nonself-similar motion into the self-similar one. These statements will be explained in more detail when we consider specific problems.

Self-similar motions of the first type, in which the similarity exponent is determined by dimensional considerations, were investigated in detail by Sedov. Since Sedov's book [2], which gives an exhaustive treatment of these motions and the solution to a number of specific problems, is available, we shall in this chapter not dwell on self-similar motions of the first type, and shall devote our attention to motions of the second type only.

2. *Implosion of a spherical shock wave and the collapse of bubbles in a liquid*

§5. Statement of the problem of an imploding shock wave

Let us imagine a spherically symmetric flow in which a strong shock wave travels to the center of symmetry through a gas of uniform initial density ρ_0

and zero pressure. We shall not discuss the origin of the wave. The wave could have been generated, for example, by a "spherical piston" which pushed the gas inward, imparting to it a certain amount of energy. As the wave converges to the center the energy becomes concentrated at the front (cumulation), and the wave is strengthened. We shall be interested in the motion of the gas at small distances from the center (say, small in comparison with the initial radius of the "piston"). It is reasonable to assume that at times close to the instant of collapse and at small radii, the motion "forgets" to a considerable extent (which will be defined below) about the initial conditions and reaches some limiting regime which must be determined.

The problem does not contain characteristic parameters of either length or time. The initial radius of the "piston" cannot serve as the scale for the limiting motion in a region whose dimensions are very small in comparison with it. The only length scale is the radius of the shock front R, which itself varies with time. The velocity scale is the time-dependent velocity of the front $dR/dt \equiv \dot{R} \equiv D$. Therefore, it is natural to assume that the limiting motion will be self-similar. We have here no basis for determining in advance the similarity exponent α. Apart from the initial density ρ_0 there are no other evident parameters which could be used for constructing the similarity variable. Of course, the energy of the entire gas, equal to the energy imparted to the gas by the piston, has a definite magnitude. However, in the self-similar region, the dimensions of which are small (of the order of R) and decrease with time as the wave converges to the center, only a small part of the total energy is concentrated and it also decreases with time*. As will be shown below, the energy in the self-similar region, the radius of which is of the order of R and the mass within which is of the order of $\rho_0 R^3$, decreases with time following a power law. However, as $R \to 0$, it decreases slower than R^3 as a result of the strengthening of the shock wave and of the increase in the energy density (pressure). It is evident from what was said that this self-similar motion must be of the second type. The solution will contain some parameter A, whose dimensions are not known in advance, related to the similarity exponent α ($[A] = LT^{-\alpha}$; see §2). If the similarity exponent (or the dimensions of A) is found from the limiting solution, then the numerical value of A remains undetermined. It depends on the initial conditions of the problem, on the motion of the gas as a whole.

As was already stated, the limiting self-similar solution holds only in a region of small dimensions of the order of the radius of the front, and then only close to the instant of collapse of the shock wave, when this radius is small. If we solve numerically the problem of the motion of the gas as a whole

* The assumption that the initial pressure is equal to zero, that we are dealing with a strong wave, also eliminates from the problem the velocity parameter given by the initial speed of sound c_0. This quantity, along with the initial pressure, is equal to zero.

with some initial conditions that ensure that an imploding shock wave will be generated (the problem with a "spherical piston" pushing inward), we shall find that the true solution in a region with a radius which decreases in proportion to the radius of the front will approach the limiting self-similar solution closer and closer with time. The form of the limiting solution does not depend on the initial conditions or on the character of the gas motion at large distances, and in particular does not depend on the manner in which the piston moves. However, the limiting solution does not entirely "forget" the initial conditions. It "forgets" the form of the initial motion, but selects from the entire set of information provided by the initial conditions the single number A which characterizes the intensity of the initial push (a "stronger" push corresponds to a greater value of A).

If the form of the limiting solution does not depend on the initial conditions and on the motion of the gas at a large distance from the center, then the manner in which the true solution approximates the limiting solution will obviously depend on the initial conditions. The closer the initial motion corresponds to the limiting motion, the earlier will the true motion near the front reach the self-similar regime. However, it will reach it sooner or later, regardless of the initial conditions and of the type of motion at large distances. Therefore, we shall seek a self-similar solution to the problem of the implosion of a shock wave. This interesting and important problem was solved independently by Landau and Stanyukovich [1] and by Guderley [3].

§6. Basic equations

The origin for time $t = 0$ is taken to be at the instant of collapse, when $R = 0$. Thus, the time up to the instant of collapse is negative. In this regard, we modify slightly the definition of the similarity variable, setting

$$R = A(-t)^{\alpha}, \qquad \xi = \frac{r}{R} = \frac{r}{A(-t)^{\alpha}}. \tag{12.13}$$

Formally, the solution which we seek includes all of space up to infinity, so that the intervals for the variables are

$$-\infty < t \leqslant 0, \qquad R \leqslant r < \infty, \qquad 1 \leqslant \xi < \infty$$

(actually the self-similar solution holds only in a region with a radius of the order of R, and at large distances it is connected with the solution of the complete nonself-similar problem in some manner). At the shock front $\xi = 1$. The front velocity is directed toward the center and is negative, with $D \equiv \dot{R} = \alpha R/t = -\alpha R/|t| < 0$.

Let us substitute into the gasdynamic equations (12.1) a solution of the self-

similar form (12.3). The system reduces to the equations (12.4) in which $\nu = 3$, in accordance with the spherical symmetry of the motion. The problem has a constant density scale $\rho_0 = const$ (we shall satisfy ourselves that this quite obvious statement is valid when we consider the boundary conditions at the shock front). Therefore, the term $\dot{\rho}_0/\rho_0$ in the first equation of (12.4) vanishes and the bracketed terms are equal to zero. The factors, which depend on the scale in (12.4), reduce to the following constants:

$$\frac{R\ddot{R}}{\dot{R}^2} = \frac{\alpha - 1}{\alpha}, \qquad \frac{R}{\dot{R}}\frac{d}{dt}(\ln \rho_0^{1-\gamma}\dot{R}^2) = \frac{2(\alpha - 1)}{\alpha}.$$

We thus obtain the following system of equations for the reduced functions:

$$\begin{aligned} (v - \xi)(\ln g)' + v' + \frac{2v}{\xi} &= 0, \\ (\alpha - 1)\alpha^{-1}v + (v - \xi)v' + g^{-1}\pi' &= 0, \\ (v - \xi)(\ln \pi g^{-\gamma})' + 2(\alpha - 1)\alpha^{-1} &= 0. \end{aligned} \tag{12.14}$$

To simplify the system we make a number of transformations. We use (12.12) to replace the functions π, g, and v by the new reduced functions P, G, and V (of course, it is possible to seek the solution of (12.1) in the form of (12.11) from the very beginning). Further, we also replace the pressure by a new unknown function, the square of the speed of sound*, and correspondingly introduce a new reduced function for the square of the speed of sound. In dimensional variables $c^2 = \gamma p/\rho$. In the form of (12.3) $c^2 = \gamma \dot{R}^2 \pi/g = \dot{R}^2 z$, where the reduced function is $z = \gamma\pi/g$. In the new form (12.11), to which we have changed, $c^2 = \gamma(r^2/t^2)P/G = (r^2/t^2)Z$, where the reduced function is $Z = \gamma P/G$. The formulas (12.12) relate the reduced functions z and Z through

$$Z = \alpha^2 \frac{z}{\xi^2}.$$

* The system of gasdynamic equations (12.1) can be also written in terms of the functions ρ, u, and c^2 instead of ρ, u, and p:

$$\begin{aligned} \frac{\partial \ln \rho}{\partial t} + u\frac{\partial \ln \rho}{\partial r} + \frac{\partial u}{\partial r} + (\nu - 1)\frac{u}{r} &= 0, \\ \frac{\partial u}{\partial t} + u\frac{\partial u}{\partial r} + \frac{c^2}{\gamma}\frac{\partial \ln \rho}{\partial r} + \frac{1}{\gamma}\frac{\partial c^2}{\partial r} &= 0, \\ \frac{\partial}{\partial t}\ln c^2\rho^{1-\gamma} + u\frac{\partial}{\partial r}\ln c^2\rho^{1-\gamma} &= 0. \end{aligned} \tag{12.1'}$$

After the introduction of the new variables the system (12.14) takes the form

$$\frac{dV}{d\ln\xi} + (V-\alpha)\frac{d\ln G}{d\ln\xi} = -3V,$$

$$(V-\alpha)\frac{dV}{d\ln\xi} + \frac{Z}{\gamma}\frac{d\ln G}{d\ln\xi} + \frac{1}{\gamma}\frac{dZ}{d\ln\xi} = -\frac{2}{\gamma}Z - V(V-1), \quad (12.15)$$

$$(\gamma-1)Z\frac{d\ln G}{d\ln\xi} - \frac{dZ}{d\ln\xi} = 2\left[\frac{\alpha-1}{\alpha(V-\alpha)} + 1\right]Z.$$

This is a system of three first-order ordinary differential equations in the three unknown functions V, G, and Z of the independent variable ξ.

Let us consider the boundary conditions. At the shock front the conservation laws give the well-known relations between the flow variables behind the front and the speed of the front (see (1.111))

$$\rho_1 = \rho_0\frac{\gamma+1}{\gamma-1}, \qquad p_1 = \frac{2}{\gamma+1}\rho_0 D^2, \qquad u_1 = \frac{2}{\gamma+1}D, \qquad c_1^2 = \frac{2\gamma(\gamma-1)}{(\gamma+1)^2}D^2. \quad (12.16)$$

Substituting the expressions (12.11) for the dimensional quantities in terms of the reduced functions, noting that at the shock front $r = R$ and $\xi = 1$, and also noting that $D \equiv \dot{R} = \alpha R/t$, we obtain the boundary conditions for the reduced functions at $\xi = 1$,

$$V(1) = \frac{2}{\gamma+1}\alpha, \qquad G(1) = \frac{\gamma+1}{\gamma-1}, \qquad Z(1) = \frac{2\gamma(\gamma-1)}{(\gamma+1)^2}\alpha^2. \quad (12.17)$$

Here one should note that it is clear that the density scale depends neither on the time nor on the front radius. Otherwise it would have been impossible to satisfy the condition $\rho_1 = [(\gamma+1)/(\gamma-1)]\rho_0 = const$ at the shock front.

The reduced functions also satisfy boundary conditions at infinity. At the instant of collapse $t = 0$, the velocity, pressure, and speed of sound at any finite radius r are bounded. But with $t = 0$ and finite r, $\xi = \infty$. In order for the quantities $u = (r/t)V$ and $c^2 = (r^2/t^2)Z$ to be bounded when $t = 0$ and r is finite, V and Z must vanish. We thus obtain still another condition which must be satisfied by the solution,

$$V(\infty) = 0, \quad Z(\infty) = 0 \qquad \text{at} \quad \xi = \infty. \quad (12.18)$$

In general, the boundary conditions (12.17) are sufficient to start the integration of equations (12.15) from the point $\xi = 1$ in the direction of increasing ξ, after some value of α has been assigned. However, analysis of these equations, with which we shall be concerned in the following section, show

that with an arbitrary value of α it is not possible to obtain a single-valued solution which satisfies (12.17) and arrives at the point (12.18). This is possible only for a certain particular value of α, which is then the desired choice of the similarity exponent.

§7. Analysis of the equations

In this section we shall show how to determine the similarity exponent in the solution of the equations (12.15). In order to do this it is first necessary to analyze the equations. We shall not, however, attempt to present rigorous mathematical proofs or carry out detailed calculations. We shall only consider the most important aspects and present the basic methods for solving the problem. In so doing we shall attempt to emphasize certain features of the problem which are common either to all self-similar solutions, or to solutions of the second type. We shall follow the system of presentation suggested by N. A. Popov, to whom we are thankful for valuable advice.

It becomes immediately evident on inspection of (12.15) that the variable $\ln \xi$, which can be regarded as a new independent variable in place of ξ, enters in the system only as the differential $d \ln \xi$. Similarly, one of the unknown functions, G, appears only as the differential $d \ln G$. This property of equations (12.15), which is characteristic of all self-similar motions, permits the reduction of the system of three differential equations to a single differential equation in V and Z and two quadratures*.

Let us solve the system (12.15) for the derivatives $dV/d \ln \xi$, $d \ln G/d \ln \xi$, $dZ/d \ln \xi$. Instead of writing down the rather lengthy expressions which result, we write the solution of the algebraic system in symbolic form using determinants,

$$\frac{dV}{d \ln \xi} = \frac{\Delta_1}{\Delta}, \qquad \frac{d \ln G}{d \ln \xi} = \frac{\Delta_2}{\Delta}, \qquad \frac{dZ}{d \ln \xi} = \frac{\Delta_3}{\Delta}, \tag{12.19}$$

* This property is not accidental but is a result of the dimensional structure of the gas-dynamic equations, which do not contain any dimensional quantities besides the variables themselves. The fact that a quantity is a logarithmic derivative shows that the choice of units for this quantity is arbitrary. In the case of the density $\rho = \rho_0 G$, this can be seen directly from equations (12.1′) for the quantities ρ, u, and c^2 (see footnote in paragraph following (12.14)). If in the general nonself-similar equations we transform to the new independent variables $\xi = r/At^\alpha$ and $\eta = r/r_0$, where A and r_0 are dimensional parameters introduced arbitrarily, then, since no limitations were imposed on the choice of these parameters, they should drop out from the equations. Indeed, the transformation shows that the new variables are contained in the equations only in the form $d \ln \xi$, and $d \ln \eta$ (in the case of self-similar motions all functions depend only on ξ and are independent of η, so that the terms in $d \ln \eta$ vanish).

The dimensionless quantities V and Z are formed from dimensional variables, $V = tu/r$ and $Z = t^2c^2/r^2 = \gamma pt^2/\rho r^2$, without the appearance of any arbitrary parameters; hence, they enter the equations in a free form and not as logarithmic differentials.

where the determinant of the system Δ is given by

$$\Delta = \begin{vmatrix} 1 & V-\alpha & 0 \\ V-\alpha & \dfrac{Z}{\gamma} & \dfrac{1}{\gamma} \\ 0 & (\gamma-1)Z & -1 \end{vmatrix} = -Z + (V-\alpha)^2. \tag{12.20}$$

The determinants Δ_1, Δ_2, and Δ_3 are obtained by replacing the corresponding columns in (12.20) by the right-hand sides of (12.15).

The coefficients of the derivatives and the right-hand sides in equations (12.15) depend only on V and Z and do not depend on G and ξ, so that all the determinants Δ, Δ_1, Δ_2, and Δ_3 are functions of V and Z only. Dividing the third equation of (12.19) by the first, we obtain the first-order ordinary differential equation

$$\frac{dZ}{dV} = \frac{\Delta_3(Z, V)}{\Delta_1(Z, V)}. \tag{12.21}$$

After the solution $Z(V)$ of this equation is found, it can be substituted into the first equation in (12.19) and the function $V(\xi)$ obtained by quadratures. Then, substituting $V(\xi)$ and $Z[V(\xi)]$ into the second equation, the function $G(\xi)$ may be obtained by quadratures.

Actually, only one quadrature is necessary, since the system (12.15) possesses a first integral which has the form of an algebraic relation connecting all the variables. The existence of this integral, termed the adiabatic integral, is related to the law of conservation of entropy on a gas particle path*. In general, the satisfaction of the conservation laws is always accompanied by the existence of corresponding integrals of the self-similar equations. Thus, in the problem of a strong explosion (see §25, Chapter I), the equations admit an energy integral. The main problem, therefore, reduces to

* To derive the adiabatic integral we use the first and third equations of (12.15). The first (continuity) equation is divided by $(V-\alpha)$ and written in the form

$$d\ln G + d\ln(V-\alpha) = -3\,d\ln\xi - \frac{3\alpha\,d\ln\xi}{V-\alpha}.$$

The third (entropy) equation is divided by Z and written in the form

$$d\ln G^{\gamma-1}Z^{-1} = \frac{2(\alpha-1)\alpha^{-1}d\ln\xi}{V-\alpha} + 2\,d\ln\xi.$$

Eliminating from these two equations the differential $d\ln\xi/(V-\alpha)$ and collecting all terms on one side, we obtain an equation of the form $d\ln F\{\xi, G, V, Z\} = 0$. This leads to the integral $F\{\xi, G, V, Z\} = const$, with the constant to be determined from the boundary conditions (12.17).

the solution of (12.21) subject to the boundary conditions (12.17) and (12.18).

Let us consider the behavior of the desired integral curve on the V, Z plane. At the shock front where $\xi = 1$, $V = V(1)$ and $Z = Z(1)$ (see (12.17)). Let us plot this point on the plane, denoting it by the letter A. At infinity, where $\xi = \infty$, $V(\infty) = 0$ and $Z(\infty) = 0$, so that the integral curve $Z(V)$ moves from the point A to the coordinate origin O (Fig. 12.1).

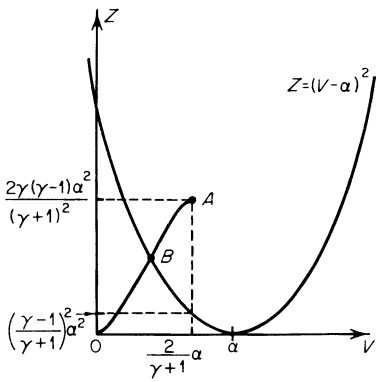

Fig. 12.1. Behavior of the integral curve on the V, Z plane.

In order for the solution of the gasdynamic equations to be physically meaningful, it must be single valued. To each value of the independent variable ξ should correspond unique values of V and Z. This means that ξ as a function of V and ξ as a function of Z or, equivalently, $\ln \xi(V)$ and $\ln \xi(Z)$, should not have extrema. The derivatives $d \ln \xi/dV = \Delta/\Delta_1$ and $d \ln \xi/dZ = \Delta/\Delta_3$ in the correct solution must not become zero in the domain of interest $1 < \xi < \infty$, $0 < \ln \xi < \infty$. But the determinant $\Delta = -Z + (V - \alpha)^2$ is equal to zero on the parabola $Z = (V - \alpha)^2$ in the V, Z plane (Fig. 12.1). It can be easily checked by direct calculation that the point A lies above the parabola, so that the desired integral curve must intersect the parabola on its path from point A to point O. At the point of intersection, in order that the derivatives $d \ln \xi/dV$ and $d \ln \xi/dZ$ not vanish, it is necessary that the determinants Δ_1 and Δ_3 also vanish (it can be checked that if $\Delta = 0$, both Δ_1 and Δ_3 must vanish simultaneously). Thus, the point of intersection of the correct integral curve $Z(V)$ and the parabola is the singular point of (12.21) ($\Delta_1 = 0$, $\Delta_3 = 0$, $dZ/dV = 0/0$).

If we specify some arbitrary value of the similarity exponent α and start the integration of (12.21) from point A, the integral curve will in general have no point of intersection with the parabola or else will intersect it at some ordinary point, and the curve will not correspond to the correct solution. Only for a particular value of α will the integral curve intersect the parabola and pass through the required singular point of (12.21), then moving on to its final

point O. This requirement that the correct integral curve must pass through a specific singular point of (12.21) determines the exponent α. The singular point B and a diagram of the correct integral curve are shown in Fig. 12.1 (it can be shown that point B lies on the left branch of the parabola).

At the singular point B, through which the correct integral curve $Z(V)$ passes, the quantities Z and V take on specific values, which also satisfy the equation of the parabola $Z = (V - \alpha)^2$. Since V and Z are functions of ξ, the singular point corresponds to a specific value of $\xi = \xi_0$. In turn, there is a line on the r,t plane, the ξ_0-line, which corresponds to the value $\xi = \xi_0$. The equation of this line is $r = R(t)\xi_0 = A(-t)^\alpha \xi_0$, or in differential form is $dr/dt = \dot{R}\xi_0$. The shock front line is $\xi = 1$, $r = R(t)$, $dr/dt = \dot{R}$. Both lines are shown in Fig. 12.2 (note that the r axis is the line $\xi = \infty$).

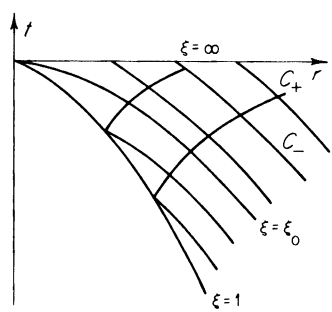

Fig. 12.2. r,t diagram for the implosion of a shock wave. $\xi = 1$ is the shock front line, $\xi = \xi_0$ is the ξ_0-line. Several characteristics of the C_+ and C_- families are also indicated.

The ξ_0-line has the important property that it is one of the C_- characteristics. In order to satisfy ourselves that this is so, we shall transform the dimensional equation for the C_- characteristics $dr/dt = u - c$ to similarity variables. It should be noted here that the speed of sound c is always a positive quantity. The assumed scale for it, $\dot{R}$ or r/t, is negative. Consequently, in taking the root of the expression $c^2 = r^2/t^2 Z$ it is necessary to set $c = -r/t|\sqrt{Z}|$. Thus,

$$\frac{dr}{dt} = u - c = \frac{r}{t} V + \frac{r}{t}|\sqrt{Z}| = \frac{R}{t}\xi(V + |\sqrt{Z}|) = \frac{\dot{R}\xi}{\alpha}(V + |\sqrt{Z}|).$$

We shall consider the C_- characteristics which pass through the ξ_0-line on the r, t plane. To do this, we set $\xi = \xi_0$ in the equation for the characteristics. But for $\xi = \xi_0$

$$Z(\xi_0) = [V(\xi_0) - \alpha]^2, \qquad |\sqrt{Z(\xi_0)}| = \alpha - V(\xi_0)$$

since $V < \alpha$. (We note that for $\xi = 1$, $V(1) = [2/(\gamma + 1)]\alpha < \alpha$, while for $\xi = \infty$, $V = 0$ and the function $V(\xi)$ is monotonic). Therefore, the slope of the C_- characteristics at any point on the ξ_0-line is $dr/dt = (\dot{R}\xi_0/\alpha)[V(\xi_0) +$

$|\sqrt{Z(\xi_0)}| = \dot{R}\xi_0$, which is the same as the slope of the ξ_0-line itself. This means that the ξ_0-line is either the envelope of a family of C_- characteristics, or simply coincides with one of them. It turns out that the second statement is the correct one; the ξ_0-line coincides with a C_- characteristic, and is thus itself a C_- characteristic.

From this result follows an important conclusion on the causality of the phenomena. As we know, the characteristics of the same family never intersect in a continuous flow region. This means that all the C_- characteristics which pass above the ξ_0-line (see Fig. 12.2) never overtake the shock front prior to the instant of collapse. The C_- characteristics passing below the ξ_0-line do overtake the front (the C_+ characteristics originate from the front line). Thus, the ξ_0-line bounds the region of influence. The state of the motion at a given time for points which lie to the right of the ξ_0-line, at distances r greater than $r_0 = R(t)\xi_0$, can in no way affect the motion of the shock wave.

The two special properties of the solution noted above, the passing of the correct integral curve through a singular point, which is possible only for a specific value of the similarity exponent α (determined by this property), and the existence of a ξ_0-line on the r,t plane which corresponds to the singular point and is itself a characteristic bounding the region of influence, are properties peculiar to all self-similar solutions of the second type.

§8. Numerical results for the solutions

In practice the solution and the similarity exponent are found by trial and error. A value of α is assumed, (12.21) is integrated numerically from the initial point A ($\xi = 1$), and the behavior of the integral curve is determined. The value of α is corrected by successive approximations in order to obtain an integral curve which intersects the parabola at the required singular point and then goes to the final point O. Landau and Stanyukovich [1] have given an approximate method which yields a value of α quite close to the correct value. This value was used for the initial guess and then refined. After the exponent α and the function $Z(V)$ are found it is not difficult to determine the functions $V(\xi)$, $Z(\xi)$, and $G(\xi)$.

By such a method [1, 3] the similarity exponent α was found equal to 0.717 for a specific heat ratio $\gamma = 7/5$. In [1] it was also found that $\alpha = 0.638$ for $\gamma = 3$, and it was established that in the limit $\gamma \to 1$, $\alpha \to 1$. The relations governing the radius and velocity of the shock front and the pressure behind the front for $\gamma = 7/5$ are given by

$$R \sim |t|^{\alpha} \sim |t|^{0.717},$$

$$|\dot{R}| \sim |t|^{\alpha-1} \sim R^{(\alpha-1)/\alpha} \sim |t|^{-0.283} \sim R^{-0.395},$$

$$p_1 \sim |t|^{2(\alpha-1)} \sim R^{2(\alpha-1)/\alpha} \sim |t|^{-0.566} \sim R^{-0.79}.$$

The velocity and pressure distributions u and p as functions of the radius at different times for the case $\gamma = 7/5$ are given in Fig. 12.3, taken from the book of Stanyukovich [1]. The velocity behind the front decreases monotonically with increasing radius, while the pressure first increases slightly and then also drops*. The density behind the front increases monotonically.

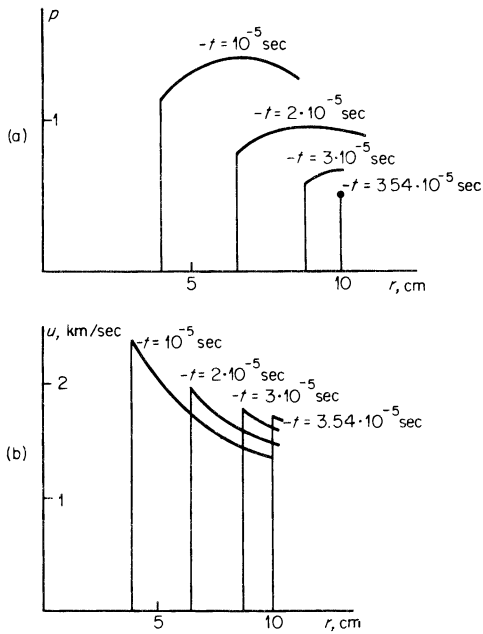

Fig. 12.3. (a) Pressure (in arbitrary units) and (b) velocity distributions at different times during the implosion of a shock wave with $\gamma = 7/5$. The curves are taken from [1].

The shock wave accelerates continuously and is strengthened as it converges to the center. As $t \to 0$ and $R \to 0$ the pressure and temperature behind the front tend to infinity; the density of the gas remains finite, and behind the wave front it is constant and equal to $[(\gamma + 1)/(\gamma - 1)]\rho_0$.

As the shock wave converges, energy becomes concentrated near the shock front as the temperature and pressure there increase without limit. However, the dimensions of the self-similar region decrease with time, and the total energy concentrated within this region also decreases. We consider now a self-similar solution only within some sphere whose radius decreases in proportion to the radius of the front R. The effective boundary of this self-similar region is then considered to be at some constant value of $r/R = \xi = \xi_1$.

* Such behavior of the pressure is not general; for example, when $\gamma = 3$ the pressure as well as the velocity behind the shock front decreases monotonically.

The energy contained in this region, i.e., in a sphere with the variable radius $r_1 = \xi_1 R$, is equal to

$$E_{\text{sim}} = \int_R^{r_1} 4\pi r^2 \, dr \, \rho\left(\frac{1}{\gamma - 1}\frac{p}{\rho} + \frac{u^2}{2}\right)$$

$$= 4\pi R^3 \rho_0 \dot{R}^2 \int_1^{\xi_1} g\left(\frac{1}{\gamma - 1}\frac{\pi}{g} + \frac{v^2}{2}\right)\xi^2 \, d\xi.$$

The integral with respect to ξ from 1 to ξ_1 is a constant, so that the energy $E_{\text{sim}} \sim R^3\dot{R}^2 \sim R^{5-(2/\alpha)}$. The exponent on R is positive for all real values of the specific heat ratio γ. For example, for $\gamma = 7/5$, $\alpha = 0.717$,

$$E_{\text{sim}} \sim R^{2.21} \to 0 \qquad \text{as} \quad R \to 0.$$

With the integration with respect to ξ extended to infinity ($\xi_1 = \infty$) the integral diverges (this is explained in the following footnote on limiting relationships). Thus, the total energy in all space is infinite within the framework of the self-similar solution. In particular, this conclusion also shows that the self-similar solution cannot be applied to indefinitely large radii r. The energy contained in a sphere of constant radius r can increase (but not indefinitely) with time. If the true solution coincides with (or is a very close approximation to) the self-similar solution at a given time from $r = R$ to $r = r_1 > R\xi_0$, the true solution will continue to agree with (or be very close to) the self-similar solution within a sphere of at least some finite radius smaller than r_1 all the way to and through the instant of collapse. Note that the C_- characteristics to the right of the ξ_0-line in Fig. 12.2 intersect the $t = 0$ axis at finite values of r, and signals from the nonself-similar part of the true solution can only be propagated inward on these characteristics.

The form of the limiting distributions of the flow variables with respect to the radius at the instant of collapse $t = 0$ can be established by using dimensional considerations. We have at our disposal one and only one parameter $A(LT^{-\alpha})$ which can be used to relate the velocity u and the speed of sound c with the radius r. This gives the limiting relationship at $t = 0$

$$u \sim c \sim A^{1/\alpha} r^{1-1/\alpha} = A^{1/\alpha} r^{-(1-\alpha)/\alpha}.$$

Since $\xi = \infty$ at $t = 0$ and $r \neq 0$, the limiting density $\rho_{\text{lim}} = \rho_0 G(\infty)$ is constant with respect to the radius. Consequently, the limiting pressure distribution is given by

$$p = \frac{1}{\gamma}\rho c^2 \sim \rho_0 A^{2/\alpha} r^{-2(1-\alpha)/\alpha}.$$

The limiting relationships $u(r)$, $c(r)$, and $p(r)$ naturally have the same behavior

as the relationships at the front during the process $u_1(R)$, $c_1(R)$, and $p_1(R)$ (except for numerical coefficients)*.

The numerical coefficients in the limiting relations for $u(r)$, $c(r)$, and $p(r)$, as well as the limiting value of the density $\rho_{\lim} = \rho_0 G(\infty)$, can only be found by solving the equations of self-similar motion. For $\gamma = 7/5$ the limiting density is $\rho_{\lim} = 21.6\rho_0$ (behind the shock front $\rho_1 = 6\rho_0$). The density at large distances from the front $r \to \infty$ before the instant of collapse is also $\rho = 21.6\rho_0$, since for $R \neq 0$ and $r \to \infty$, $\xi = r/R \to \infty$ and $\rho/\rho_0 = G(\xi) \to G(\infty)$.

The energy concentrated in a sphere of radius r at the instant of collapse is

$$\int_0^r 4\pi r^2 \, dr \, \rho\left(\frac{1}{\gamma - 1}\frac{p}{\rho} + \frac{u^2}{2}\right) \sim r^{5-2/\alpha}$$

(just as $E_{\text{sim}} \sim R^{5-2/\alpha}$; see above). The energy concentrated in a sphere with a finite radius is finite and tends to zero as $r \to 0$. The larger the sphere, the larger is the energy included in it (within the framework of the self-similar regime).

After the instant of collapse, with $t > 0$, the shock wave reflected from the center propagates outward through the gas which is moving inward toward the center. The motion in this stage is also self-similar, and the similarity exponent does not change. For $t > 0$ the reflected wave propagates following the relation $R \sim t^{\alpha}$. Calculations show that for $\gamma = 7/5$ the density of the gas behind the reflected shock front is $\rho_{1\text{ref}} = 137.5\rho_0$, and thus the density is 23 times greater than the density behind the front of the incident wave $\rho_1 = 6\rho_0$. The velocity behind the front is positive and the gas is expanding from the center, with the expansion velocity decreasing with time as $\dot{R} \sim t^{-(1-\alpha)}$ starting from infinity†.

* The limiting relationships can also be established analytically starting from the equations for the reduced functions by finding the asymptotic solution in the neighborhood of the point $\xi = \infty$, $V = 0$, and $Z = 0$. We get $V \sim \xi^{-1/\alpha}$, $Z \sim \xi^{2-2/\alpha}$, which, upon transforming to dimensional variables, yields the limiting relationships given in the text. The quantities v^2 and $z = \gamma\pi/g$ are, according to (12.12), proportional to $\xi^2 V^2 \sim \xi^{2-2/\alpha}$ as $\xi \to \infty$; $g(\infty) = G(\infty) = const$. It is evident from this result that the energy integral diverges as $\xi_1 \to \infty$, since

$$\int_1^{\xi_1} g\left(\frac{1}{\gamma - 1}\frac{\pi}{g} + \frac{v^2}{2}\right)\xi^2 \, d\xi \sim \int_1^{\xi_1} \xi^{4-2/\alpha} \, d\xi \sim \xi_1^{5-2/\alpha} \to \infty,$$

and the total energy in all space within the framework of the self-similar solution is infinite at any instant of time.

† In a paper by one of the authors [26] a family of self-similar solutions for cylindrical motion is constructed within the acoustic approximation. This family is obtained by means of the superposition of plane waves. The similarity exponent is arbitrary and is chosen in accordance with the initial conditions. For a converging cylindrical shock wave (in the acoustic approximation) the pressure behind the front $p \sim |t|^{-1/2}$, where the front radius $R = c|t|$.

It is interesting that the pressure behind the front of the reflected shock wave is infinite

§9. Collapse of bubbles. The Rayleigh problem

A process which has much in common with the implosion of a shock wave is the collapse of bubbles in a liquid (water). Small bubbles filled with the vapor of the liquid and undissolved gases are frequently formed in a real liquid. The phenomenon of bubble formation is called cavitation. Under steady state conditions the bubble is stable and the internal gas pressure balances the pressure in the liquid. When the liquid moves and goes from a low to a high pressure region, the internal pressure in the bubble (previously formed at the lower pressure) is lower than the new, higher pressure of the liquid. This causes the liquid to move to the center, collapsing the bubble. As in the implosion of a shock wave, the energy of the bubble becomes concentrated as the bubble collapses. As the bubble radius decreases the rate of collapse and the pressure increase and attain very large values. After collapse, a pressure peak is formed in the central region and a shock wave travels away from the center. When such a process takes place near a solid surface, the shock wave can damage the surface material. This is considered to be one of the causes of rapid wear of screw propellers and turbines.

An idealized problem of the liquid motion during the collapse of a bubble was solved by Rayleigh [4]. The liquid was assumed to be ideal (inviscid) and incompressible. The spherically symmetric cavity was regarded as a void, with the pressure within and at the surface of the cavity assumed equal to zero*.

At an initial time let there be a spherical cavity of radius R_0 in the liquid. The pressure in the surrounding liquid is p_0 and the liquid is at rest. After the motion starts the velocity distribution as a function of the radius r is found from the continuity equation with $\rho = const$

$$u = \dot{R}\frac{R^2}{r^2} = \dot{R}\frac{1}{\xi^2}, \qquad \xi = \frac{r}{R}, \tag{12.22}$$

where $R(t)$ is the radius of the cavity and $\dot{R}$ is the velocity of the boundary. Substituting the expression for the velocity into the equation of motion and

---

for $R \neq 0$. The results for the shock wave were obtained earlier by Zababakhin and Nechaev [27]. The pressure behind the front becomes infinite only within the framework of the acoustic approximation, as is explained in [26, 27].

* Apparently the internal vapor pressure in the actual process increases during the last stage of the collapse to such an extent that it withstands the motion thrust of the liquid and forces it to turn back. As a result of the very rapid compression the vapor does not succeed in condensing and its compression at the end is isentropic. However, if we consider the process of collapse of the bubble only up to a radius which is not too small the vapor pressure can be neglected. We may also neglect the surface tension at the boundary with the liquid.

integrating with respect to r from r to ∞ we obtain the pressure distribution

$$p = p_0 + \rho \frac{\ddot{R}R + 2\dot{R}^2}{\xi} - \rho \frac{\dot{R}^2}{2\xi^4}. \tag{12.23}$$

If we apply this equation at the boundary of the cavity $\xi = 1$, where $p = 0$, we obtain an equation for $R(t)$

$$0 = p_0 + \rho(\ddot{R}R + \tfrac{3}{2}\dot{R}^2). \tag{12.24}$$

Integrating this equation once under the initial condition $\dot{R} = 0$ when $R = R_0$, we obtain the law for the increase in velocity during collapse

$$\dot{R}^2 = \frac{2p_0}{3\rho}\left(\frac{R_0^3}{R^3} - 1\right). * \tag{12.25}$$

This equation can also be obtained directly from energy considerations. Let us take the energy of the liquid without the bubble to be zero. The potential energy of the liquid with a bubble of radius R is equal to the work done in overcoming the external pressure forces in the formation of a cavity of volume $4\pi R^3/3$. This work is equal to $p_0 4\pi R^3/3$, independent of the distribution of pressure in the region of the bubble†. The kinetic energy of the liquid is equal to

$$\int_R^\infty 4\pi r^2 \frac{\rho u^2}{2}\, dr = \int_R^\infty 4\pi r^2 \rho \frac{\dot{R}^2 R^4}{2r^4}\, dr = 2\pi\rho\dot{R}^2 R^3.$$

The total energy, equal to the sum of the kinetic and potential energies, is conserved, so that

$$2\pi\rho\dot{R}^2 R^3 + \frac{p_0 4\pi R^3}{3} = E = \frac{p_0 4\pi R_0^3}{3}. \tag{12.26}$$

Equation (12.25) follows directly from this relation.

Using (12.24) we can express the pressure distribution (12.23) in the form

$$p = p_0\left(1 - \frac{1}{\xi}\right) + \frac{\rho\dot{R}^2}{2}\left(\frac{1}{\xi} - \frac{1}{\xi^4}\right), \qquad \xi = \frac{r}{R}.$$

* Integration of (12.25) gives the time of collapse of the bubble as $\tau = 0.915\, R_0(\rho/p_0)^{1/2}$. For example, in water with $\rho = 1$ g/cm^3, $p_0 = 1$ atm and $R_0 = 1$ mm, $\tau = 0.915 \cdot 10^{-4}$ sec.

† This statement can be explained as follows. Let us imagine a vessel containing a liquid at a pressure p_0, closed by a movable piston with a surface area S. If a cavity with volume Ω is formed inside, the liquid, due to its incompressibility, will displace the piston through a distance l such that $lS = \Omega$. In doing this the cavity does an amount of work $p_0 Sl = p_0\Omega$ on the piston. This work is determined only by the pressure p_0 far from the bubble and is independent of the pressure distribution near the bubble.

(The velocity and pressure distributions are illustrated schematically in Fig. 12.4.)

It is clear from the formula for the pressure that the problem is not self-similar (despite the apparent self-similar form of the velocity (12.22)). This

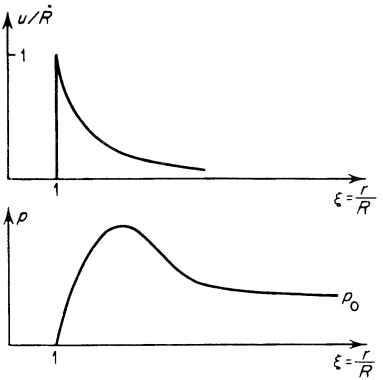

Fig. 12.4. Velocity and pressure distributions in Rayleigh's problem.

is evident from the fact that the problem contains a characteristic length scale R_0 and velocity scale $(p_0/\rho)^{1/2}$. However, in the limit, when the radius of the cavity tends to zero, $R \to 0$, the velocity and pressure increase, tending to infinity, and the solution asymptotically takes on a self-similar character, and

$$p \approx \frac{\rho \dot{R}^2}{2}\left(\frac{1}{\xi} - \frac{1}{\xi^4}\right), \qquad \dot{R}^2 \approx \frac{2p_0}{3\rho}\frac{R_0^3}{R^3}. \tag{12.27}$$

The length scale, the initial radius, becomes too large and the pressure scale p_0 becomes too small to characterize the actual process, whose scales are now the time-dependent cavity radius R and boundary velocity $\dot{R}(R \ll R_0;$ $\dot{R} \gg (p_0/\rho)^{1/2};\ p \sim \rho\dot{R}^2 \gg p_0)$. The motion appears as though it "forgets" the initial conditions. This is demonstrated in particular by the fact that the parameters p_0 and R_0 do not appear separately in the equation of motion of the boundary as before (see (12.25)), but only in the combination $p_0 R_0^3$, proportional to the total energy of the liquid $E = 4\pi R_0^3 p_0/3$ (see (12.27)).

It can be seen that this is a self-similarity of the first type, appearing because the energy is conserved. The dimensional parameters in the self-similar flow are the same as in the problem of a strong explosion, i.e., energy and density. The motion of the boundary is described by (12.27), $\dot{R}^2 \sim E/\rho R^3$ and the pressure by $p \sim E/R^3$. Hence we immediately obtain $R \sim (E/\rho)^{1/5}(-t)^{2/5}$, $\dot{R} \sim (E/\rho)^{1/5}(-t)^{-3/5}$, as in the problem of a strong explosion (the instant of collapse is taken to be zero). The similarity exponent $\alpha = 2/5$.

In the limit $R \to 0$, we obtain from (12.22) and (12.27)

$$u \sim \dot{R}\frac{R^2}{r^2} \sim \frac{R^{1/2}}{r^2}, \qquad p \sim \frac{1}{R^3}\left(\frac{R}{r} - \frac{R^4}{r^4}\right) \sim \frac{1}{R^2 r} - \frac{R}{r^4}.$$

The velocity of the boundary tends to infinity as $\dot{R} \sim R^{-3/2}$, but the velocity at a finite radius $r \neq 0$ tends to zero. In the limit $R \to 0$ the potential energy $4\pi p_0 R^3/3$ tends to zero and the total energy E, which is now all kinetic, is concentrated at the coordinate origin. The energy density at this point is infinite. Unlike the velocity, the pressure at the time of collapse is also infinite at any finite radius $r \neq 0$ (energy is not related to the pressure in an incompressible liquid model). This shows that the model of an incompressible liquid is imperfect. As will be shown in the following section, if we take compressibility into account, we find that the pressure at finite distances from the center is bounded.

§10. Collapse of bubbles. Effect of compressibility and viscosity

The collapse of an empty cavity in water, taking into account compressibility (but not viscosity) was considered by Hunter [5]. The equation of state was assumed to be of the form

$$p = B\left[\left(\frac{\rho}{\rho_0}\right)^{\gamma} - 1\right]$$

with $\gamma = 7$. Actually, however, in the limit of high pressures the term 1 was dropped, so that the equation of state had a form analogous to that for a perfect gas, $p = B(\rho/\rho_0)^{\gamma}$. It was assumed that B is a constant independent of the entropy (the flow was assumed isentropic). The value of B was taken equal to 3000 atm.

Numerical solution of the hydrodynamic equations (in terms of the variables u and c) with properly selected initial and boundary conditions showed that, in the limit when the radius of the cavity becomes very small and the velocity of the boundary very large, the solution becomes self-similar. Accordingly, a solution of the equations was sought in the self-similar form $u = \dot{R}v(r/R)$ and $c^2 = \dot{R}^2 z(r/R)$, where the radius of the cavity is $R = A(-t)^{\alpha}$.* The general properties and behavior of the equations in similarity variables or reduced functions are in many respects analogous to the problem of the imploding shock wave. Numerical integration yielded the value $\alpha = 0.555$ for the similarity exponent (for $\gamma = 7$).

The energy of the entire flow, as in the problem of the implosion of a shock

* For analysis and solution of the equations it was found more convenient to choose $\xi' = -(R/r)^{1/\alpha} = A^{1/\alpha} t r^{-1/\alpha}$ rather than $\xi = r/R = r/A(-t)^{\alpha}$ as the similarity variable (at the boundary of the cavity $r = R$, $\xi' = -1$; at infinity $r = \infty$, $\xi' = 0$).

wave, is infinite. (The energy contained in a sphere of radius r at the instant of collapse $t = 0$, $R = 0$, is proportional to $r^{1.13}$.) It is the absence of an energy integral which leads to a self-similar problem of the second type. The distributions of velocity, of the square of the speed of sound, and of the density with respect to the radius at the instant of collapse of the cavity, when $R = 0$, are of the form

$$u \sim r^{-(1-\alpha)/\alpha}, \qquad c^2 \sim r^{-2(1-\alpha)/\alpha},$$

$$\rho \sim r^{-2(1-\alpha)/\alpha(\gamma-1)}, \qquad p \sim r^{-2(1-\alpha)\gamma/\alpha(\gamma-1)}.$$

In contrast to the implosion of a shock wave, where the distributions of u and c^2 ($c^2 \sim p/\rho$) have the same form as above, the limiting density is variable in this case. This is a result of the fact that the problem was initially assumed to be isentropic. The sharp increase in c^2 and p is not connected with an increase in entropy, as in a shock wave, but with the increase in density.

To some extent the self-similar solution describes the actual process only in regions of very small radii, when the initial conditions have effectively been "forgotten". A comparison of the self-similar solution with the results of numerical integration of the partial differential equations for initial conditions corresponding to atmospheric pressure in water and to an initial radius of $R_0 = 0.5$ cm showed the following: At the instant of complete collapse $t = 0$, $R = 0$, the self-similar solution is valid in a region whose radius is of the order of 10^{-2} cm. Such a sphere contains about 10–20% of the energy of the liquid, and the pressure at its boundary is of the order of several tens of thousands of atmospheres. Hunter [5] also found the self-similar solution for the shock wave propagating outward from the center after the collapse of the bubble.

The inclusion of the viscosity of the liquid in the calculation leads to interesting laws for the behavior of the flow. The problem of collapse of an empty spherical cavity in an incompressible viscous liquid was solved by Zababakhin [6]. Analysis of the governing equations shows that the character of the flow depends on the Reynolds number $\mathrm{Re} = (R_0/\nu)(p_0/\rho)^{1/2}$, where $\nu = \mu/\rho$ is the kinematic viscosity. When $\mathrm{Re} > \mathrm{Re}^*$ (low viscosity) where Re^* is some critical Reynolds number, the velocity of the cavity boundary $\dot{R}$ becomes infinite as $R \to 0$ in the same manner as in the Rayleigh problem, with $\dot{R} \sim R^{-3/2}$ but with a smaller proportionality coefficient (part of the energy is converted into heat by dissipation). When $\mathrm{Re} < \mathrm{Re}^*$ (high viscosity) viscosity strongly interferes with the acceleration of the liquid and the bubble collapse takes place slowly, taking an infinite time. The cumulation of energy, characteristic of the Rayleigh problem, is absent here. In the intermediate case, when $\mathrm{Re} = \mathrm{Re}^*$, the bubble does collapse in a finite time. The velocity $\dot{R}$ becomes infinite as $R \to 0$, but less rapidly than R^{-1}.

Numerical integration of the equations gives $\mathrm{Re}^* = 8.4$ for the critical Reynolds number. For a given liquid under a given pressure, i.e., for given ρ, ν, and p_0, we can define a critical bubble radius R_0^*. For $R_0 < R_0^*$ the cumulation is completely eliminated by the viscosity. Actually, the critical radius is exceedingly small; for example, in water ($\rho = 1$ g/cm^3, $p_0 = 1$ atm, $\nu = 0.01$ cm^2/sec) $R_0^* = 0.8 \cdot 10^{-4}$ cm. Consequently, viscosity has only a weak effect on the collapse of bubbles whose radius exceeds $0.8 \cdot 10^{-4}$ cm.

3. *The emergence of a shock wave at the surface of a star*

§11. Propagation of a shock wave for a power-law decrease in density

It is well known (see [7], for example) that near the surface of a star the density decreases to zero approximately according to the power law

$$\rho_{00} = bx^{\delta}, \tag{12.28}$$

where x is a coordinate measured from the surface into the star and b and δ are constants. This density distribution is a result of the combined action of gravity and thermal pressure. In the establishment of the distribution of temperature, which is proportional to the gas pressure, radiation heat conduction plays an important role (cf. §14, Chapter II). The exponent δ in the density distribution (12.28) is related to the constants appearing in the equation of radiation heat conduction. It is usually of the order of 3.

When internal disturbances accompanied by an increase in pressure take place in the central regions of a star, a shock wave is formed, which travels from the central regions to the periphery and emerges at the surface. The propagation of a shock wave through a gas whose density is decreasing to zero, as occurs near the surface of a star, is accompanied by the concentration (cumulation) of energy. This process is of great interest in astrophysics and relevant to the problem of the origin of cosmic rays (see following section).

There is a certain physical similarity between the cumulation processes in the propagation of a shock wave through a gas whose density decreases to zero, and in the implosion of a shock wave. In both cases energy is imparted to a mass of material that is ever decreasing without limit, in such a manner that the specific energy (per unit mass) increases indefinitely. The difference between the two cases lies in the cause of the decrease in the mass to which the energy is imparted. In the first case the mass decreases as a result of a decrease of gas density, and in the second case as a result of decrease of volume.

We shall be interested in the limiting form of the motion when the shock

front is close to the star surface. Under these conditions we can neglect the curvature of the star surface and of the wave front and we can treat the motion as plane. Since the shock is strong, we may neglect gravitational forces. Radiation heat conduction plays an important role in the establishment of the steady-state distributions of gas temperature and density. Over the short period of passage of the very strong shock wave, it does not introduce appreciable changes as a result of the redistribution of heat, so that we may regard the process as approximately adiabatic. Within this formulation the problem of the limiting form of the motion was first solved by Gandel'man and Frank-Kamenetskii [8]. The same problem was later treated by Sakurai [9], who found exactly the same solution, but for other numerical values of the exponent δ in (12.28) and of the specific heat ratio γ. A schematic representation of the shock wave propagation is given in Fig. 12.5.

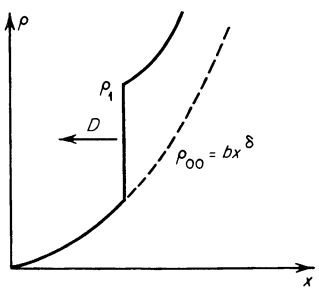

Fig. 12.5. Schematic representation of the emergence of a shock wave at the surface of a star. The density distribution.

The only dimensional parameter for the given conditions of the problem is the constant b, which contains the symbol of mass. There are no other dimensional parameters. It is therefore natural to seek a self-similar solution of the second type. We represent the solution in the form (12.3), (12.5)–(12.7). In accordance with the planar symmetry we denote the coordinate of the wave measured from the star surface $x = 0$ by $X(t)$. As the density scale ρ_0 we take the value of the density of the undisturbed gas ahead of the shock front. Since the wave travels through a gas of variable density, this scale depends on time or, equivalently, on the coordinate of the front X (see the end of §2). The scale ρ_0 is given by

$$\rho_0 = \rho_{00}(X) = bX^{\delta}. \tag{12.29}$$

As in the problem of the imploding shock wave, we take $t = 0$ to be the instant at which the shock wave emerges at the surface, in accordance with which we change the sign of t in the similarity relation

$$X = At^{\alpha} \to X = A(-t)^{\alpha}.$$

Thus, we seek a solution of the form

$$\rho = \rho_0 g(\xi), \qquad p = \rho_0 \dot{X}^2 \pi(\xi), \qquad u = \dot{X} v(\xi),$$
$$\xi = \frac{x}{X}, \qquad \rho_0 = bX^\delta, \qquad X = A(-t)^\alpha. \tag{12.30}$$

Equations (12.4) in this case ($\nu = 1$) become

$$\begin{gathered} \delta + (v - \xi)(\ln g)' + v' = 0, \\ (\alpha - 1)\alpha^{-1} v + (v - \xi)v' + \frac{\pi'}{g} = 0, \\ (v - \xi)(\ln \pi g^{-\gamma})' + \lambda = 0, \\ \lambda = 2(\alpha - 1)\alpha^{-1} - (\gamma - 1)\delta. \end{gathered} \tag{12.31}$$

The boundary conditions at the shock front, which we take to be strong, are given by (12.16). From these we obtain the boundary conditions analogous to (12.17) for the reduced functions at $\xi = 1$

$$g(1) = \frac{\gamma + 1}{\gamma - 1}, \qquad v(1) = \frac{2}{\gamma + 1}, \qquad \pi(1) = \frac{2}{\gamma + 1}. \tag{12.32}$$

At the time the shock wave emerges at the surface, at $X = 0$, the similarity coordinate $\xi = \infty$ for any nonzero value of x. The flow variables for any finite value of x must be bounded at the time of emergence. This imposes an additional boundary condition on the reduced functions at $\xi = \infty$.

The solution is found in a manner which is completely analogous to the solution of the problem of the implosion of a shock wave. We introduce new reduced functions V, G, and Z, and obtain a system corresponding to (12.15). The system reduces to a single first-order ordinary differential equation in V and Z and to two quadratures. Actually, instead of the two quadratures we have one quadrature and one algebraic relation between the variables, i.e., that from the adiabatic integral. The eigenvalue of the system of equations, the exponent α, is found by a trial and error method in which we numerically integrate the equation for $Z(V)$, and must satisfy the condition that the integral curve pass through the correct singular point. As before, the singular point has a corresponding ξ_0-line on the x, t plane, which is a C_- characteristic and which bounds the region of influence for the motion of the shock front.

In [8] the similarity exponent for $\delta = 13/4 = 3.25$ and $\gamma = 5/3$ was found to be $\alpha = 0.590$. In [9] the exponents α were determined for a number of other values of δ and γ. These results are given in Table 12.1.

The fact that α is always less than one shows that the shock wave is continuously accelerated

$$X \sim |t|^\alpha, \qquad |\dot{X}| \sim |t|^{-(1-\alpha)} \sim X^{-(1-\alpha)/\alpha}, \qquad |\dot{X}| \to \infty \qquad \text{as} \quad X \to 0.$$

Correspondingly, the temperature behind the front, which is proportional to the square of the front velocity or to the square of the speed of sound, $T \sim |\dot{X}|^2 \sim X^{-2(1-\alpha)/\alpha}$, also increases without limit. The unbounded increase

Table 12.1

SIMILARITY EXPONENT α

γ	δ			
	3.25	2	1	0.5
5/3	0.590	0.696	0.816	0.877
7/5	—	0.718	0.831	0.906
6/5	—	0.752	0.855	0.920

in temperature, as pointed out above, appears because a finite amount of energy is imparted to a mass of gas which decreases to zero. The pressure behind the shock front decreases as the front approaches the surface, despite the increase in the velocity, since the density ahead of the front decreases faster than the temperature (or square of the velocity) increases

$$p_1 \sim \rho_0 \dot{X}^2 \sim X^{\delta-2(1-\alpha)/\alpha}.$$

It can be easily checked from the results of Table 12.1 that the exponent of X in this equation is always positive, that

$$p_1 \to 0 \qquad \text{as} \quad X \to 0.$$

The limiting distributions of the flow variables with respect to the x coordinate at the instant of emergence of the shock wave at the surface $t = 0$, $X = 0$ ($t = 0$, $x \neq 0$ corresponds to $\xi = \infty$), are evidently of exactly the same form as the relations at the shock front. As in the problem of an imploding shock wave, these distributions follow simply from dimensional considerations. At the time $t = 0$ we get

$$u \sim x^{-(1-\alpha)/\alpha}, \qquad T \sim u^2 \sim c^2 \sim x^{-2(1-\alpha)/\alpha},$$

$$\rho \sim x^{\delta}, \qquad p \sim x^{\delta-2(1-\alpha)/\alpha}.$$

Of course, the same relations follow from the equations in the limit $\xi \to \infty$. The final density distribution is increased by a constant factor with respect to the initial density distribution. The distributions of the flow variables with respect to the x coordinate before emergence and at the instant of emergence of the wave at the surface are shown schematically in Fig. 12.6.

The energy of the gas at $t = 0$ contained in a layer between $x = 0$ and x in a column of unit cross-sectional area is proportional to the quantity

$$\int_0^x \rho u^2 \, dx \sim \int_0^x p \, dx \sim x^{\delta+1-2(1-\alpha)/\alpha}.$$

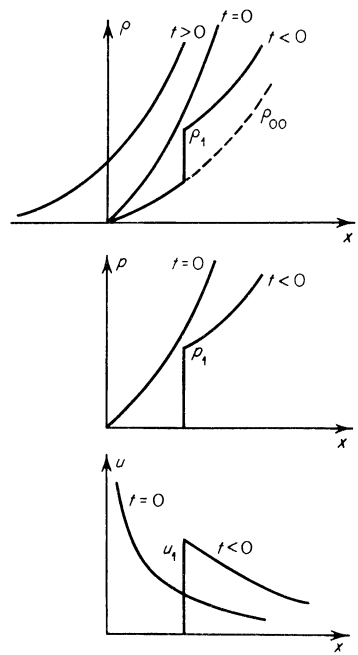

Fig. 12.6. Density, pressure, and velocity distributions for the emergence of a shock wave at the surface of a star. $t < 0$ before emergence, $t = 0$ at the instant of emergence, $t > 0$ after emergence.

As $x \to \infty$ the energy becomes infinite; there is no energy integral. The energy of a layer of finite thickness remains finite and tends to zero, as $x \to 0$. Unlike the case of an imploding shock wave, the energy density, which is proportional to the pressure, also goes to zero at the boundary, as $x \to 0$. Only the temperature or energy per unit mass becomes infinite. An infinite specific energy is imparted to a vanishingly small mass of gas. Of course, the temperature cannot actually become infinite as indicated by the mathematical solution. Thus, for example, when the shock wave comes so close to the surface that the small remaining mass of the layer from $x = 0$ to $x = X$ includes only a small number of gaskinetic mean free paths, gasdynamic considerations are no longer meaningful. The infinite temperature increase can also be limited by physical factors, such as energy lost by radiation from the highly heated gas.

As in the problem of the implosion of a shock wave, the self-similar solution is valid only in a limited region near the boundary $x = 0$. Far from the front

the solution is not self-similar and depends on the conditions under which the shock originated. If at a given time the actual solution is very close to the self-similar solution for $1 < \xi < \xi_1 > \xi_0$, it will remain so within some finite distance of the boundary through the instant of emergence.

After the shock wave emerges at the surface, the gas flows into a vacuum, and the initial density, pressure, and velocity distributions are given by the power laws for $t = 0$. As shown in [9], the solution for the outflow stage is also self-similar, but, of course, has a completely different character (the flow is continuous and there are no shock waves). An approximate density distribution for a time $t > 0$ is shown in Fig. 12.6.

§12. On explosions of supernovae and the origin of cosmic rays

It has been suggested that the origin of cosmic rays, of the protons and nuclei with tremendously high energies that are present throughout the universe and that strike the earth, is connected with explosions of supernovae. Such a theory was developed by Ginzburg and I. S. Shklovskii (see the review [10]). The process of the infinite increase in shock strength and of the cumulation of energy in the emergence of a shock wave at the surface of a star from the interior may be the cause of the acceleration of the particles to their tremendously high energies. This idea was used by Colgate and Johnson [11], who considered such a process in detail. They showed by calculations that some of the material ejected from the surface during the explosion of a supernova acquires relativistic velocities and kinetic energies, corresponding to the energies of cosmic rays. (The highest energies of particles presently observed in the cosmic ray spectrum are of the order of 10^8 Bev $= 10^{17}$ ev.) Below we shall present the results obtained by Colgate and Johnson.

Temperatures at the center of supernovae reach the order of 300–500 kev ($\sim 5 \cdot 10^9$ °K). At these temperatures nuclear fusion proceeds up to the formation of the most stable element, iron. The layers further out consist of the lighter elements, carbon, nitrogen, and oxygen. Still closer to the surface the main element is helium, and, finally, the outermost layers consist of hydrogen. Astronomical data show that in the explosion of a supernova a mass of material is ejected that is of the order of one tenth of the entire mass of the star and of the order of the mass of the sun, equal to $M_\odot = 2 \cdot 10^{33}$ g.

Calculations of the mechanical and radiative equilibrium for a star with a mass of $10M_\odot$ give a behavior for the density and temperature distribution as a function of radius as shown in Fig. 12.7*. The density at the center of the

* Under conditions of radiative equilibrium the density dependence on temperature follows the relation $\rho \sim T^{13/4} = T^{3.25}$. This was the basis for the assumption made in [8] that the density distribution near the surface is given by $\rho \sim x^{3.25}$, although in a layer near the surface the temperature depends only weakly on the coordinate x (the temperature at

star is higher than 10^8 g/cm^3, while at the surface it drops to zero. In any case, propagation of an ordinary shock wave is observable out to layers with $\rho \sim 10^{-5}$ g/cm^3.

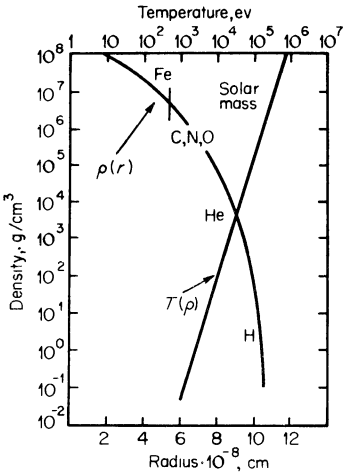

Fig. 12.7. Density and temperature distributions before a star explosion. $\rho \sim T^{3.25}$, corresponding to radiative equilibrium.

It is usually assumed that the energy source for the shock wave is the so-called gravitational instability, which occurs when the isentropic exponent (effective specific heat ratio) in the isentropic equation of state $\gamma < 4/3$. In the central regions of the star, at temperatures ~ 500 kev, the nuclei are highly dissociated. It is well known that the specific heat of a gas markedly increases and the isentropic exponent decreases as a result of dissociation. Small disturbances are amplified as a result of the gravitational instability. The pressure pulse generated grows in strength, and this leads to the formation of a shock wave. The shock moves out from the central region to the surface. The gas behind the shock wave suddenly expands out from the center, and owing to the increase in wave strength the outer layers obtain extremely high velocities.

The material in the peripheral layers, which has acquired the large kinetic energy of the sudden expansion, overcomes the gravitational forces and breaks away from the star after the shock wave emerges at the surface. The star, as it were, sheds a shell. This phenomenon is well known in astrophysics. It is assumed that the Crab nebula was formed in this manner. It has been estimated that an amount of energy of the order of 10^{52} ergs is required to

---

the surface of the star is not equal to zero). On Fig. 12.7 is given the radius of the layer whose mass is equal to the mass of the sun. It must be assumed that this layer is also ejected during explosion. The regions containing the different elements are indicated approximately.

overcome the forces of gravity when a mass equal to the mass of the sun is ejected. Consequently, this is the order of magnitude of the energy which is liberated at the center of the star and goes into the formation of the shock wave.

Hydrodynamic calculations of the propagation of a shock generated by such a source give velocities behind the shock front shown by curve I in Fig. 12.8. The abscissa is the initial density of the material ahead of the front.

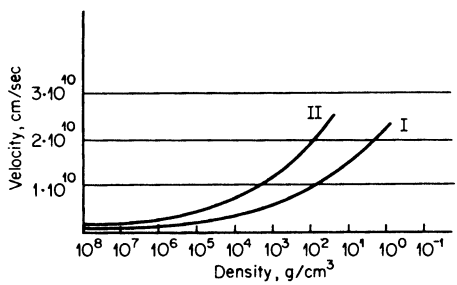

Fig. 12.8. The velocity of the material as a function of its initial density. Curve I is the velocity immediately behind the wave front; curve II is the velocity after expansion.

Curve II indicates the velocity acquired by a layer with the given density after the shock wave emerges at the surface and the material expands. The velocity after expansion is larger approximately by a factor of 2 than the velocity at the time of passage of the shock front. Figure 12.8 shows that the peripheral layers, where the density is less than approximately 30 g/cm^3, acquire velocities behind the strengthened shock wave greater than 10^{10} cm/sec, which is 1/3 the speed of light. Therefore, relativistic effects must be considered in calculating the motion of the shock wave in these peripheral layers. In [11] a numerical calculation was carried out on the basis of relativistic gasdynamics. An approximate analytic solution to the problem was also given, based on the use of characteristic equations and relativistic analogs of the Riemann invariants.

It is interesting to note that the internal energy behind the front of such a powerful shock wave is almost entirely concentrated in equilibrium thermal radiation. An approximate solution shows that the final kinetic energy per unit mass acquired by the material in a layer with an initial density ρ_0 g/cm^3 is of the order of $c^2(30/\rho_0)^{0.64}$ erg/g. If we note that 1 erg/g in hydrogen corresponds to approximately 10^{-12} ev/proton $= 10^{-21}$ Bev/proton, then we find that a kinetic energy of the order of 10^4 Bev is acquired by particles previously contained in a layer with an initial density $\rho_0 \sim 10^{-5}$ g/cm^3. The mass per unit surface area of a layer in a star which surrounds a spherical surface with such an initial density is approximately 1 g/cm^2. Such a thin

layer is no longer capable of holding back or "locking in" the thermal radiation, which is out of equilibrium in the outer layers closer to the surface. Therefore, the shock wave can no longer propagate through these outer layers in the same manner as under equilibrium conditions.

As pointed out in [11], the subsequent propagation of the shock wave through a gas of even lower density is connected with the mechanism of plasma oscillations in an essential manner. The shock wave reaches a surface where the Debye length becomes comparable with the length scale of the outer unshocked layer. Calculations show that this occurs at a radius where the initial density $\rho_0 \sim 10^{-12}$ g/cm^3. Particles at this radius are accelerated by the shock wave to energies of the order of 10^8 Bev, which corresponds to the maximum observed energies of cosmic rays.

It is important to check whether the number of particles accelerated to cosmic ray energies by the explosions of supernovae is sufficient to produce the existing "stockpile" of cosmic rays in the galaxy. The initial density of the material which is accelerated by the passage of a shock wave to an energy of ~ 10 Bev is approximately 1 g/cm^3. The mass of a star in a layer surrounding a spherical surface with $\rho_0 \sim 1$ g/cm^3 is of the order of 10^{26} g or $6 \cdot 10^{49}$ protons. We can say that the energy imparted to $6 \cdot 10^{49}$ protons by an explosion exceeds 10 Bev. The lifetime of a high energy proton in the galaxy, with an average particle density of matter in the galaxy of the order of 0.1 particles/cm^3, is $\tau \sim 5 \cdot 10^8$ years. This means that $\sim 5 \cdot 10^8$ years after the "start" of explosions in the galaxy a steady-state number of protons N will be set up. Supernova explosions occur approximately once every 100 years. Consequently, $6 \cdot 10^{49}/100 = 6 \cdot 10^{47}$ protons are born per year, and N/τ protons "die" per year. It follows from the steady-state condition that $N/\tau = 6 \cdot 10^{47}$ protons/year $= const$, that $N = 3 \cdot 10^{56}$. The volume of our galaxy is $V \sim 5 \cdot 10^{68}$ cm^3. The average density of high energy protons is $N/V \sim 6 \cdot 10^{-13}$ cm^{-3}, and their flux is of the order of $Nc/V \sim 2 \cdot 10^{-2}$ cm$^{-2} \cdot$ sec^{-1}. This value is in agreement with observations. According to the calculations given, of the order of $5 \cdot 10^6$ supernova explosions were required to produce the cosmic rays in our galaxy.

4. Motion of a gas under the action of an impulsive load

§13. Statement of the problem and general character of the motion

Let us imagine a half-space $x > 0$ occupied by a perfect gas with constant specific heats. Initially, at $t = 0$, the density of the gas is everywhere uniform and equal to ρ_0, and the pressure, temperature, and initial speed of sound are zero. The half-space $x < 0$ is empty. The surface $x = 0$ is the boundary between the gas and the vacuum.

Let a pressure pulse of short duration* be applied to the external surface of the gas (the gas surface is subjected to an impulsive load). Various methods are possible for producing an impulsive load in practice.

(1) In a short time interval τ a plane piston is pushed into the gas with a constant velocity U_1, creating a pressure Π_1 in the gas. To within a numerical coefficient of the order of unity (depending on the specific heat ratio γ) $\Pi_1 \approx \rho_0 U_1^2$. The velocity of the shock D that is created by the action of the piston is close to U_1. After a time interval τ the piston is "instantaneously" withdrawn (the pressure pulse is shown in Fig. 12.9a).

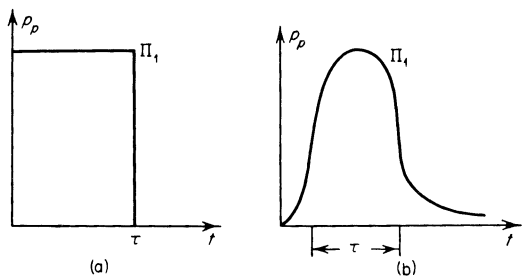

Fig. 12.9. Shapes of initial pressure pulses.

(2) A thin layer of explosive is detonated on the gas surface. If the mass thickness of the layer is m units of mass per unit area and the energy released per unit mass is Q, then the energy released by the explosion per unit area is $E = mQ$. The explosion products suddenly expand with a velocity $U_1 \approx \sqrt{Q}$. Since the products expand suddenly in both directions and since before the detonation the gas was everywhere at rest, the total momentum is equal to zero. However, the momentum of the detonation products moving in one direction is, in order of magnitude, equal to $I \approx mU_1 \approx m\sqrt{Q}$ (per unit surface area). The detonation products generate a shock wave in the gas with a pressure of the order of $\Pi_1 \approx \rho_0 U_1^2$. The time τ over which the pressure acts is determined from the condition that in the time τ the energy and momentum are transferred from the detonation products to the gas,

$$\tau \approx \frac{E}{\Pi_1 U_1} \approx \frac{I}{\Pi_1} \approx \frac{m}{\rho_0 \sqrt{Q}}.$$

During this time the shock wave in the gas will travel through a distance $\sim U_1 \tau \sim (Q\tau)^{1/2}$ and will encompass a mass $\sim \rho_0 (Q\tau)^{1/2} \sim m$, a mass of the order of the mass of the explosive.

* *Editors' note.* The authors' literal term "of short duration" has generally been translated as "impulsive". The term whose literal translation is "blow" is here rendered as "load", or sometimes as "impact". Later in the chapter the term "concentrated" appears, and means concentrated in a spatial sense rather than in a temporal sense.

(3) A thin plate with a small mass m per unit area is made to strike the gas surface with a velocity U_1. The impact of the plate creates a shock wave in the gas, which propagates with the velocity $D \approx U_1$. The pressure in the gas will then be $\Pi_1 \approx \rho_0 U_1^2$. The initial momentum and energy of the plate, $I = mU_1$ and $E = mU_1^2/2$, are transferred to the gas during the time τ in which the plate is decelerated, which is of the order of $\tau \approx E/\Pi_1 U_1 \approx I/\Pi_1 \approx m/\rho_0 U_1$. During this time the shock wave in the gas travels through a distance $U_1\tau$ and encompasses a mass $\rho_0 U_1 \tau \approx m$.

Thus, we shall assume in general that, as shown in Fig. 12.9b, there is a pressure acting on the surface of the gas which drops sufficiently rapidly with time. The pressure can be expressed in the form $p_p = \Pi_1 f(t/\tau)$, where f is a function which characterizes the shape of the pressure pulse. For definiteness and convenience in discussing the initial conditions we shall use the "piston" concept, as in the first example. It should be noted, however, that all the conclusions derived are equally valid regardless of the method by which the impact has been produced.

The problem is to determine the motion of the gas, i.e., the functions $p(x, t)$, $\rho(x, t)$, and $u(x, t)$, after a time which is large in comparison with the impact time τ (to find the asymptotic state for $t/\tau \gg 1$ for a given applied external pressure history). The problem can also be formulated in a slightly different manner. Preserving the shape of the curve $f(t/\tau)$ we let the time τ go to zero, and the pressure Π_1 become infinite, and seek, for finite times, the limiting solutions of the resulting gasdynamic equations. The solution to this problem should, in particular, answer the question of how the pressure Π_1 must increase as $\tau \to 0$, in order to ensure that the pressure in the gas be finite after a finite time t. For example, if the solution contains the combination $\Pi_1 \tau^\beta$, this means that as $\tau \to 0$, Π_1 must increase as $\tau^{-\beta}$

The above problem was formulated and analyzed in a paper by one of the present authors [12] in which the physical features of the resulting motion and of the mathematical solution were explained. The equations were analyzed and integrated numerically by Adamskii [13]; Zhukov and Kazhdan [14], Häfele [15], and von Hoerner [16] found an analytic solution for one particular case ($\gamma = 7/5$). The last two papers are extensions of the work of von Weizsäcker [17], who posed the problem concerning the limits within which the similarity exponent varies for plane motions. It should be noted that in [15–17] the physical meaning was not given for the solution, which was obtained by purely formal means.

The general character of the motion resulting from the action of an impulsive load is illustrated in Fig. 12.10. A shock is propagated through the undisturbed gas with the density ratio across the shock attaining the limiting value $K = (\gamma + 1)/(\gamma - 1)$. Behind the shock the gas expands unhindered into the vacuum; at the vacuum interface the density and pressure drop to zero.

The pressure, density, and velocity decrease with distance behind the shock front. At some point the velocity changes sign, since directly behind the front the gas moves to the right, while at the interface it expands into the vacuum to the left. The strength of the shock decreases with time.

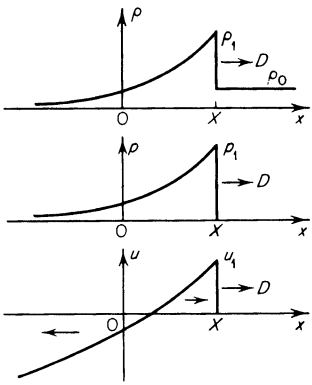

Fig. 12.10. Density, pressure, and velocity distributions for the problem of an impulsive load.

The solution to the problem of an instantaneous pressure pulse should answer the question as to the maximum possible rate of decrease of the strength of a plane shock wave traveling into a gas with a constant initial density. It is clear that if the pressure is applied over a longer time, then the only effect will be to sustain the shock and delay its attenuation. The behavior of the limiting solution is independent of the specific shape of the pressure pulse, i.e., of the form of the function $f(t/\tau)$, as long as it drops sufficiently fast. It was noted above that, under the action of the pressure Π_1, the gas acquires during impact a velocity $U_1 \sim (\Pi_1/\rho_0)^{1/2}$. The gas interface expands into vacuum with a velocity of the same order. In the limit $\tau \to 0$, $\Pi_1 \to \infty$, the velocity of the interface becomes infinite, so that the distributions of p, ρ, and u in the limiting solution, shown in Fig. 12.10, extend to the left to $x = -\infty$.

§14. Self-similar solutions and the energy and momentum conservation laws

The motion which results immediately after applying a pressure pulse is, of course, not self-similar. It is characterized by the time scale τ and the length scale $x_0 = (\Pi_1/\rho_0)^{1/2}\tau$, and depends on the shape of the applied pressure curve $f(t/\tau)$. However, after a sufficiently long time $t \gg \tau$, when the shock front has moved through a distance $X \gg x_0$, the initial scales τ and x_0 are very small in comparison with the natural scales of the motion t and X, and no longer characterize the process. The limiting motion, corresponding to

the stage when $t \gg \tau$ and $X \gg x_0$ or, equivalently, to the limit $\tau \to 0$, will be self-similar. The only length scale in this motion is the shock coordinate X, which is variable, while the velocity scale is the front velocity $\dot{X}$. Therefore, a solution should be sought in the self-similar form

$$\rho = \rho_0 g(\xi), \qquad u = \dot{X} v(\xi), \qquad p = \rho_0 \dot{X}^2 \pi(\xi), \qquad \xi = \frac{x}{X} = \frac{x}{At^\alpha}. \quad (12.33)$$

Before proceeding to the mathematical solution, we should decide to which of the two types the self-similar motion belongs and whether the similarity exponent α can be determined from dimensional considerations or from conservation laws. In contrast to the two problems considered previously, the implosion of a shock wave and the emergence of a shock wave at the surface of a star, here at any given time t a completely known finite mass of gas $\rho_0 X$ (per unit surface area) is involved in the motion.

After the piston which produced the impact at the gas surface is withdrawn, the pressure at the vacuum interface is zero, and the gas is no longer subjected to any external forces. Thenceforth the momentum and energy of the gas must be preserved. The momentum of the gas is equal to the momentum produced by the piston pressure

$$I = \int_0^\infty p_p \, dt = \Pi_1 \tau \int_0^\infty f\left(\frac{t}{\tau}\right) d\left(\frac{t}{\tau}\right).$$

To within a numerical factor, this quantity is equal to $\Pi_1 \tau$. The energy of the gas is equal to the work done by the piston over the time during which the pressure acts. In order to calculate this work exactly we would require the full solution of the gasdynamic equations over the period during which the piston acts, since the work is equal to $\int_0^\infty p_p u_p \, dt$, where $u_p(t)$ is the piston speed. The piston speed is unknown in advance if it is the pressure $p_p(t)$ that has been specified. However, to within a numerical factor that depends on the form of the function $f(t/\tau)$, this work is equal to

$$E \approx \Pi_1 U_1 \tau \approx \Pi_1 \left(\frac{\Pi_1}{\rho_0}\right)^{1/2} \tau = \Pi_1^{3/2} \tau \rho_0^{-1/2}$$

(U_1 is the piston velocity scale).

If we substitute into the integral expressions for the momentum and energy of the entire gas the pressure, velocity, and density in the self-similar form (12.33), and take into account the fact that the integrals must vanish in the cold undisturbed region $X < x < \infty$, then the momentum and energy

conservation laws (per unit surface area) can be written in the forms

$$I = \int_{-\infty}^{\infty} \rho u \, dx = \rho_0 \dot{X} X \int_{-\infty}^{1} g v \, d\xi = const, \tag{12.34}$$

$$E = \int_{-\infty}^{\infty} \left(\rho \frac{u^2}{2} + \frac{1}{\gamma - 1} p \right) dx = \rho_0 \dot{X}^2 X \int_{-\infty}^{1} \left(\frac{g v^2}{2} + \frac{1}{\gamma - 1} \pi \right) d\xi = const. \tag{12.35}$$

It would seem natural to assume that the dimensionless integrals are constants. Then, each of the two conditions taken separately could serve to determine the similarity exponent α. The conservation of momentum condition would give $\dot{X}X = const$, whence $X \sim t^{1/2}$ and $\alpha = \frac{1}{2}$. On the other hand, the conservation of energy condition gives $\dot{X}^2 X = const$, whence $X \sim t^{2/3}$ and $\alpha = 2/3$. Taken together these conditions contradict each other, since they lead to different values of the exponent α. A paradoxical situation arises in which the conservation laws of momentum and energy, which are the basis of the gasdynamic equations, cannot be satisfied simultaneously. This would seem to indicate that the problem does not have a self-similar solution, since the substitution of such a solution into the conservation laws leads to a contradiction. This contradiction has, however, another resolution. The point is that the self-similar solution, which does exist and which will be found below, is of the second type. The similarity exponent α is found neither from the conservation laws nor from dimensional considerations, but by solving the equations for the reduced functions under the condition that the correct solution pass through a singular point, as in the problems considered in preceding sections.

In order to resolve the above paradox, we note that when the specific heat ratio $\gamma = 7/5$, the similarity exponent is found by means of an analytic solution to be $\alpha = 3/5$*. This exponent lies between the values of α dictated by the conditions of conservation of momentum and energy, $1/2 < 3/5 < 2/3$. It will be shown below that for any value of the specific heat ratio $1 < \gamma < \infty$, the similarity exponent α lies between these limits, $1/2 < \alpha < 2/3$.

In the case where the similarity exponent $\alpha = 3/5$ the dimensions of the parameter A in the relation $X = At^{\alpha}$ are $[A] = LT^{-3/5}$. As we have seen already (see §5), the limiting self-similar motion does not completely "forget" the initial conditions, but from the extensive information included in the initial conditions it "selects" and "remembers" one specific constant A,

* In general, for an arbitrary value of γ the exponent α is not expressible as a rational fraction. However, fortunately, for $\gamma = 7/5$ a solution of the self-similar equations can be found in analytic form, and in this case α is equal to 3/5 (see below).

which somehow characterizes the initial "push". In this case, the limiting solution "selects" one parameter A from the information given by the pressure relation at the piston $p_p = \Pi_1 f(t/\tau)$ and the value of the initial density ρ_0. In order of magnitude A is given by the following combination of characteristic scales:

$$A \approx \left(\frac{\Pi_1}{\rho_0}\right)^{1/2} \tau^{1-\alpha} = \left(\frac{\Pi_1}{\rho_0}\right)^{1/2} \tau^{2/5} \quad (LT^{-3/5}). \tag{12.36}$$

The numerical value of the proportionality coefficient is determined by the form of the pressure relation $f(t/\tau)$.

From the above relation it is easy to determine the manner in which the pressure at the piston Π_1 must become infinite as τ tends to zero in order to ensure a finite (not equal to 0 or ∞) pressure at a finite distance in the limiting motion. In order for the limiting solution to exist, the parameter A must have a finite value, and the product $\Pi_1^{1/2}\tau^{1-\alpha}$, equal to $\Pi_1^{1/2}\tau^{2/5}$ in the case $\gamma = 7/5$, must remain finite as $\tau \to 0$. Therefore, as $\tau \to 0$, Π_1 must increase as $\Pi_1 \sim \tau^{-2(1-\alpha)} \sim \tau^{4/5}$.

We can now clarify the question of the satisfaction of the conservation laws. The momentum imparted by the piston to the gas, or the impulse of the load, is in order of magnitude $I \sim \Pi_1 \tau$, or in proportional form $I \sim \Pi_1 \tau \sim \tau^{2\alpha-1} \sim \tau^{1/5}$. As $\tau \to 0$, the momentum $I \to 0$. Therefore, the total momentum in the limiting, self-similar motion is zero (the momentum of the gas which is moving with the shock wave to the right is exactly canceled by the momentum of the gas expanding into vacuum to the left; see Fig. 12.10). The momentum conservation law is written in the form

$$I = \rho_0 \dot{X} X \int_{-\infty}^{1} gv \, d\xi \sim t^{1/5} \int_{-\infty}^{1} gv \, d\xi = 0.$$

The only conclusion which follows is the fact that the reduced functions must satisfy the condition $\int_{-\infty}^{1} gv \, d\xi = 0$. It is obvious that we cannot take $\dot{X}X$ to be constant and determine the similarity exponent α in this way.

The energy imparted by the piston to the gas is in order of magnitude $E \sim \Pi_1^{3/2} \tau \rho_0^{-1/2}$, or in proportional form $E \sim \Pi_1^{3/2} \tau \sim \tau^{3\alpha-2} \sim \tau^{-1/5}$. As $\tau \to 0$, $E \to \infty$. The total energy of the gas in the self-similar motion turns out to be infinite. Conservation of energy

$$E = \rho_0 \dot{X}^2 X \int_{-\infty}^{1} \left(\frac{gv^2}{2} + \frac{1}{\gamma - 1}\pi\right) d\xi \sim t^{-1/5} \int_{-\infty}^{1} \left(\frac{gv^2}{2} + \frac{1}{\gamma - 1}\pi\right) d\xi = \infty$$

shows only that the integral of the dimensionless reduced functions diverges, but says nothing about the value of $\dot{X}^2 X$. The similarity exponent cannot be determined from conservation of energy, either. The fact that the energy is

infinite and that the energy integral diverges is connected with the fact that in the exactly self-similar motion that corresponds to the limit $\tau \to 0$ the velocity at which the gas boundary expands into vacuum is infinite (see end of §13). The kinetic energy at the boundary is also infinite since, as $\xi \to -\infty$, the square of the reduced velocity v^2 tends to infinity faster than the reduced density g decreases.

The physical meaning of an infinite energy in the self-similar motion will be discussed below. Here we note only that the actual energy of the gas is of course finite and equal to the work done by the piston. It is simply that the self-similar solution is not valid for a small amount of mass near the gas boundary, and this leads to the divergence of the energy integral.

§15. Solution of the equations

The general method of finding the self-similar solution for the problem of an impulsive load does not differ in principle from the method of solving the problems of an imploding shock wave or the propagation of a shock through a gas whose density decreases with distance following a power law (see §§2 and 3 of this chapter). As before, we shall seek a solution of the gasdynamic equations (12.1) in the self-similar form (12.33) and obtain a system of ordinary differential equations for the reduced functions π, v, and g. These equations become identical with (12.31) when we set δ equal to zero, corresponding to a constant density scale,

$$\begin{aligned} (v-\xi)(\ln g)' + v' &= 0, \\ (\alpha-1)\alpha^{-1}v + (v-\xi)v' + g^{-1}\pi' &= 0, \\ (v-\xi)(\ln \pi g^{-\gamma})' + 2(\alpha-1)\alpha^{-1} &= 0. \end{aligned} \tag{12.37}$$

The boundary conditions (12.32) at the shock front where $\xi = 1$ were given in §11. At the gas-vacuum interface the pressure and density vanish and minus the velocity becomes infinite, so that for $\xi = -\infty$, $\pi(-\infty) = 0$, $g(-\infty) = 0$, $v(-\infty) = -\infty$.

After a number of transformations, the equations again reduce to one first-order ordinary differential equation, one quadrature, and one algebraic relation between all the variables (the adiabatic integral). The similarity exponent is determined by the condition that the desired solution of the differential equation pass through a singular point.

Actually, in [13, 14] the equations were written and solved in Lagrangian rather than in Eulerian coordinates. In the one-dimensional plane case with constant initial density the Lagrangian form leads to simpler and more convenient relations. Of course, the transition from Eulerian to Lagrangian coordinates introduces nothing new in principle. The Lagrangian coordinate

is defined as the mass of gas per unit surface area, measured from the vacuum interface,

$$m = \int_{-\infty}^{x} \rho \, dx, \qquad dm = \rho \, dx. \tag{12.38}$$

In place of time in the scale functions it is convenient to introduce the Lagrangian coordinate of the shock front $M = \rho_0 X$, equal to the mass of gas per unit surface area that has been encompassed by the motion at the time t. The Lagrangian similarity variable is given by the ratio

$$\eta = \frac{m}{M}, \tag{12.39}$$

which varies from $\eta = 0$ (at the gas-vacuum interface) to $\eta = 1$ (at the shock front).

The solution is then written in the form

$$p = B\rho_0 M^{-n} f(\eta), \qquad u = \sqrt{B} M^{-n/2} w(\eta), \qquad \rho = \rho_0 q(\eta), \tag{12.40}$$

where B is a parameter of the problem that is related to the parameter A in the relation $X = At^{\alpha}$ and that replaces it in the new formulation. The new reduced functions are now f, w, and q. The new similarity exponent n is uniquely related to the old one α. In fact,

$$M = \rho_0 X \sim t^{\alpha}, \qquad u \sim M^{-n/2} \sim t^{-\alpha n/2}, \qquad u \sim \dot{X} \sim t^{\alpha - 1},$$

whence $\alpha n/2 = \alpha - 1$ and

$$n = \frac{2(1-\alpha)}{\alpha}, \qquad \alpha = \frac{1}{1 + n/2}. \tag{12.41}$$

The mathematical features of the problem, the sequence of transformations of the equations, the analysis, and the specific methods of solution may be found in [13, 14]. Here, we shall discuss in more detail the results for the particular case of $\gamma = 7/5$, for which an exact analytic solution of the equations can be obtained. All the main features of the process are clarified by considering this analytic solution.

The exponents α and n for $\gamma = 7/5$ have the values $\alpha = 3/5$ and $n = 4/3$. The solution in Lagrangian coordinates takes the form

$$f = \eta, \qquad w = -\tfrac{1}{2}(\tfrac{5}{6})^{1/2}(\eta^{-2/3} - 3), \qquad q = 6\eta^{5/3}. \tag{12.42}$$

The pressure, density, and velocity distributions as a function of the Lagrangian similarity variable are shown in Fig. 12.11. We note that by definition $f = p/p_1$, $w(6/5)^{1/2} = u/u_1$, $q/6 = \rho/\rho_1$, where the subscript "1" denotes quantities behind the shock front.

From the definition of the Lagrangian coordinate (12.38) and of the

similarity variable (12.39) the solution (12.42) can be easily transformed to the Eulerian variable $\xi = x/X$. In this regard, with the time t and the Lagrangian shock coordinate M fixed,

$$dm = \rho\, dx, \qquad \frac{dm}{M} = \frac{\rho}{\rho_0}\frac{dx}{X}, \qquad \text{and} \qquad d\eta = q\, d\xi.$$

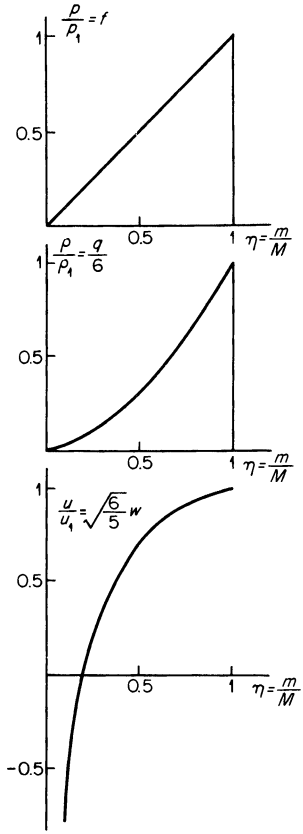

Fig. 12.11. Pressure, density, and velocity distributions in the problem of an impulsive load (in Lagrangian coordinates); $\gamma = 7/5$.

Substituting $q(\eta)$ given by (12.42) into this equation, integrating, and applying the boundary condition $\eta = 1$ at $\xi = 1$ (at the shock front), we obtain

$$\eta = (5 - 4\xi)^{-3/2}, \qquad \xi = \tfrac{1}{4}(5 - \eta^{-2/3}). \tag{12.43}$$

In terms of the Eulerian variable the functions f, w, and q have the form

$$f = (5 - 4\xi)^{-3/2}, \qquad w = -(\tfrac{\xi}{6})^{1/2}(1 - 2\xi), \qquad q = 6(5 - 4\xi)^{-5/2}. \tag{12.44}$$

The reduced functions f, w, and q are related to the original reduced functions π, v, and g by the relations*

$$\pi = \tfrac{5}{6}f, \qquad v = (\tfrac{5}{6})^{1/2}w, \qquad g = q. \tag{12.45}$$

The pressure, density, and velocity distributions as functions of the Eulerian reduced coordinate are shown in Fig. 12.12. It is interesting to note

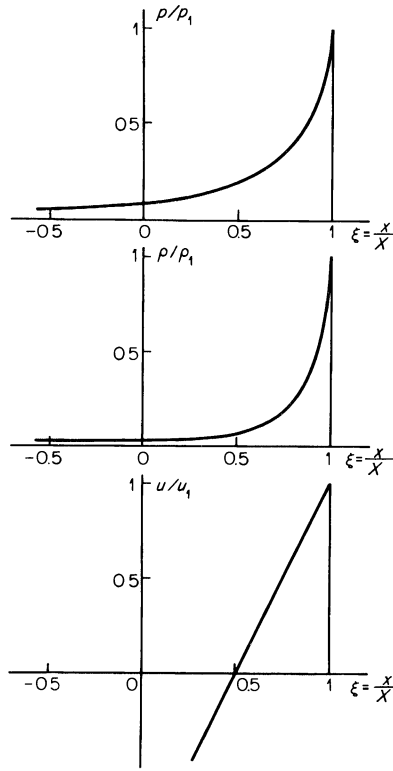

Fig. 12.12. Pressure, density, and velocity distributions in the problem of an impulsive load (in Eulerian coordinates); $\gamma = 7/5$.

that the pressure distribution is linear with respect to the Lagrangian mass coordinate, while the velocity is linear with respect to the spatial coordinate. The velocity becomes zero and changes direction at the point $\xi = \frac{1}{2}$. The mass contained between the initial position of the gas interface $x = 0$ and the wave front at any time constitutes 90 percent of the entire mass set into motion. The remaining 10 percent of the mass is pushed to the left of the initial gas

* We leave it as an exercise for the reader to check, by directly substituting the functions π, v, and g given by (12.45) and (12.44) into (12.37) with $\gamma = 7/5$ and $\alpha = 3/5$, that they indeed satisfy the equations and the boundary conditions (12.32).

interface as a result of the expansion following the shock compression. We note that 78 percent of the mass is moving to the right and 22 percent to the left.

The asymptotic behavior of the solution in the low density region as $\xi \to -\infty$ and $\eta \to 0$ is given by the expressions

$$f \sim (-\xi)^{-3/2}, \qquad w \sim \xi, \qquad q \sim (-\xi)^{-5/2},$$
$$f = \eta, \qquad w \sim \eta^{-2/3}, \qquad q \sim \eta^{5/3}. \tag{12.46}$$

The values of the similarity variables corresponding to the singular point through which the solution of the differential equation passes are $\eta_0 = 7^{-3/2} = 0.054$ and $\xi_0 = -\frac{1}{2}$. As in the problem of the imploding shock wave, the ξ_0-line on the x, t plane (the η_0-line on the m, t or the m, M plane) is the characteristic ($dx/dt = u + c$; $dm/dt = \rho c$) that separates the region of influence of the shock from the rest of the space. On the x, t, and m, M diagrams of Figs. 12.13 and 12.14 we have plotted the shock line $\xi = 1$, $\eta = 1$, the singular line $\xi = \xi_0$, $\eta = \eta_0$, and characteristics of both families*. The

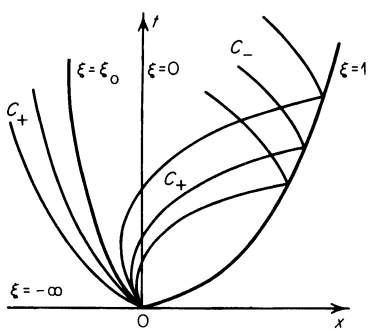

Fig. 12.13. x,t diagram for the problem of an impulsive load. $\xi = 1$ is the shock line, $\xi = \xi_0$ is the singular ξ_0-line. Characteristics of the C_+ and C_- families are shown.

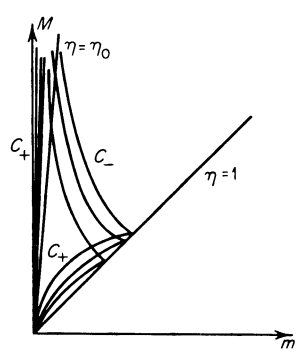

Fig. 12.14. m,M diagram for the problem of an impulsive load. $\eta = 1$ is the shock front line, $\eta = \eta_0$ is the singular η_0-line. Characteristics of the C_+ and C_- families are shown.

* We note that the M axis is the $\eta = 0$ line, and that the t axis on the x, t plane is the $\xi = 0$ line. The negative semiaxis x on the x, t plane is the $\xi = -\infty$ line.

singular line is a C_+ characteristic. All the characteristics of the C_+ family emanate from the origin. Those passing to the right of the singular line overtake the shock front and those passing to the left of it never catch up with it. Thus, the state of the motion in the relatively small mass contained between the vacuum interface and the singular line does not affect the propagation of the shock front*.

In [15] the values of the similarity exponent were obtained by numerical integration for several other values of the specific heat ratio γ. The results are given in Table 12.2†. The pressure, density, and velocity distributions for different values of the specific heat ratio are qualitatively similar to the distributions for the case of $\gamma = 7/5$ (see Figs. 12.11 and 12.12).

Table 12.2

SIMILARITY EXPONENTS IN THE PROBLEM OF AN IMPULSIVE LOAD

γ	1.0	1.1	7/5	5/3	2.8	∞
n	2	1.516	4/3	1.275	1.191	1.117
α	0.5	0.569	3/5	0.611	0.627	0.642

It is clear from the table that the larger the specific heat ratio the more slowly is the shock wave attenuated. However, the attenuation is always faster than in the case when the gas at the interface does not suddenly expand into vacuum but is at rest, as in the problem of a strong plane explosion. If an instantaneous energy release E (per unit area) takes place in the plane $x = 0$ and if the gas in the plane $x = 0$ is always at rest (either the gas occupies the space symmetrically on both sides of the plane or is bounded by a rigid wall), then the energy is conserved and the shock wave is attenuated following the relation

$$p_1 \sim X^{-1} \sim t^{-2/3}; \qquad n = 1, \qquad \alpha = \tfrac{2}{3}.$$

We shall show in the following section how the limitation $n > 1$, $\alpha < 2/3$

* In particular, the gas may border not on a vacuum, but on a "piston", on which the pressure drops following a sufficiently rapid power law. The distortion in the state of the motion in the region between the interface and the ξ_0-line resulting from the presence of the piston affects neither the motion to the right of the ξ_0-line nor the relation governing the shock propagation, as long as the pressure at the piston drops sufficiently rapidly. This was shown in a paper by Adamskii and Popov [18]. This paper and also a paper by Krasheninnikova [19] treated the self-similar problem of the gas motion resulting from the pressure at a piston whose motion follows a power law.

† *Editors' note.* The result for the limit $\gamma \to \infty$ has been added and is from [18]. In the limit $\gamma \to 1$, the solution approaches one with impulse conserved, with $\alpha = 1/2$; this case has been included in the table for completeness.

follows from conservation of energy when the value of γ is arbitrary. We shall also show how conservation of momentum imposes a limitation on the exponents from the other side, $n < 2$, $\alpha > \frac{1}{2}$.

§16. Limitations on the similarity exponent imposed by conservation of momentum and energy

The character of the motion that results from an impulsive load is such that some part of the gas is carried away by the shock wave to the right, while the remaining gas expands to the left into the vacuum. There exists a point which divides these two parts of the gas; we shall denote the coordinate of this point by x^*. The particle velocity of the gas is equal to zero at the point x^*, or $u^* = u(x^*) = 0$. The boundary x^* itself propagates to the right both with respect to the spatial and the mass coordinate. In the self-similar solution the point at which the velocity changes sign corresponds to a specific value of the similarity variable $\xi = \xi^*$; $x^* = \xi^* X$.

Let us consider the volume contained between the shock front surface $x = X$ and the "dividing" surface $x = x^*$. This volume contains a mass (per unit surface area)

$$M^* = \int_{x^*}^{X} \rho \, dx = \rho_0 X \int_{\xi^*}^{1} g \, d\xi = const \cdot \rho_0 X.$$

This mass is a specific fraction of the total mass involved in the motion $M = \rho_0 X$ (for $\gamma = 7/5$, $M^*/M = 0.78$). The remaining mass $M - M^*$ expands to the left. The mass M^* increases with time as $M^* \sim X \sim t^\alpha$, as does the total mass M.

The boundary x^* propagates through the mass to the right, and the gas flows out through the surface x^* to the left. The expressions for the momentum and energy of the gas moving with the shock wave to the right are

$$I^* = \int_{x^*}^{X} \rho u \, dx = \rho_0 \dot{X} X \int_{\xi^*}^{1} g v \, d\xi = const \cdot t^{2\alpha - 1}, \tag{12.47}$$

$$E^* = \int_{x^*}^{X} \left(\frac{\rho u^2}{2} + \frac{p}{\gamma - 1} \right) dx = \rho_0 \dot{X}^2 X \int_{\xi^*}^{1} \left(\frac{g v^2}{2} + \frac{\pi}{\gamma - 1} \right) d\xi = const \cdot t^{3\alpha - 2}. \tag{12.48}$$

Undisturbed gas at zero pressure and temperature flows in from the right, through the surface of the shock front into the volume $x^* < x < X$. The undisturbed gas introduces neither momentum nor energy into the volume. Gas with zero velocity, but with a finite pressure p^*, leaves the volume to the left through the surface x^* (the gas leaves the volume not because of its own

motion, but because of the propagation of the surface bounding the volume). There is no momentum flow through the surface x^*. The change of momentum in the volume is equal to the pressure applied to its boundary

$$\frac{dI^*}{dt} = p^* > 0. \tag{12.49}$$

The momentum within the volume increases with time. It follows from (12.47) that $2\alpha - 1 > 0$, and $\alpha > \frac{1}{2}$, and (12.41) shows that $n < 2$.

The change of energy in the volume is due only to the loss of internal energy through the surface x^* to the left. Kinetic energy is not lost, since the gas velocity u^* and the kinetic energy are both zero at the boundary x^*. The work of the pressure forces $p^*u^*\,dt$ on the surface x^* is also equal to zero. Therefore,

$$\frac{dE^*}{dt} = -\frac{1}{\gamma - 1}\frac{p^*}{\rho^*}\rho^*\frac{dx^*}{dt} = -\frac{1}{\gamma - 1}p^*\xi^*\dot{X} < 0. \tag{12.50}$$

The energy in the volume decreases with time, it is transferred to the left out of the volume, together with the mass of gas whose velocity changes direction and begins to expand to the left into the vacuum. It follows from (12.48) that $3\alpha - 2 < 0$, $\alpha < 2/3$, and (12.41) then gives $n > 1$. We thus arrive at the following ranges for the similarity exponents

$$\frac{1}{2} < \alpha < \frac{2}{3}, \qquad 2 > n > 1. \tag{12.51}$$

The limit $n = 1$, $\alpha = 2/3$ corresponds to constant energy $E^* = const$, while the limit $n = 2$, $\alpha = \frac{1}{2}$ corresponds to constant momentum $I^* = const$.

§17. Passage of the nonself-similar motion into the limiting regime and the "infinite" energy in the self-similar solution

Strictly speaking, the self-similar solution corresponds to idealized initial conditions, in which the duration of the impact τ is infinitesimally small and the pressure at the piston Π_1 during the impact is infinitely great. In this case, the passage to the limit $\tau \to 0$, $\Pi_1 \to \infty$ is carried out in such a manner that the product $\Pi_1^{1/2}\tau^{1-\alpha}$, which is proportional to the parameter A (see (12.36)), remains finite. Corresponding to the limit $\tau \to 0$, $\Pi_1 \to \infty$, the piston imparts an infinite energy to the gas

$$E \approx \rho_0{}^{-1/2}\Pi_1^{3/2}\tau \sim \tau^{-(2-3\alpha)} \to \infty, \qquad \alpha < \frac{2}{3}, \tag{12.52}$$

and zero momentum

$$I \approx \Pi_1 \tau \sim \tau^{2\alpha-1} \to 0, \qquad \alpha > \frac{1}{2}. \tag{12.53}$$

Let us compare the energy E^* and momentum I^* of that part of the gas which moves to the right in the direction of the shock propagation (see equations (12.47) and (12.48)) with the total gas energy E and momentum I. We obtain

$$\frac{E^*}{E} \sim \left(\frac{\tau}{t}\right)^{2-3\alpha}, \qquad \frac{I^*}{I} \sim \left(\frac{t}{\tau}\right)^{2\alpha-1}, \qquad \frac{1}{2} < \alpha < \frac{2}{3}. \tag{12.54}$$

The ratio of the energy E^* of the gas moving to the right with the shock wave at a given time t to the initial energy E is the smaller the shorter is the duration of the impact. It is not surprising that in the limit of a vanishingly short duration of impact $\tau \to 0$ the piston is required to do an infinite amount of work (infinite energy of the gas E) in order for the energy of a specific fraction of the mass to remain finite after being decreased by a ratio which approaches zero. All this infinite energy is now concentrated in that part of the mass which expands into the vacuum, or more exactly, at the very edge of the mass of gas. At the edge the gas possesses infinite expansion velocity and infinite kinetic energy. The shorter the duration of impact the greater is the unidirectional momentum I^* at a given time t in comparison with the momentum I imparted by the piston. In the limit $\tau \to 0$, the unidirectional momenta of the gas particles which move to the right and to the left cancel each other out with an accuracy corresponding to the vanishingly small value of I.

Essentially, the idealized limiting solution does not simply correspond to zero duration of the impact τ, but to an infinitely large ratio t/τ. As $t/\tau \to \infty$, $E^*/E \to 0$ and $I^*/I \to \infty$. In interpreting this condition we have considered finite times t, with vanishingly small durations of impact τ, in which limit the work of the piston E was infinite and the momentum I was zero. Closer to reality is another interpretation of this limit, the interpretation in which the duration of the impact does not go to zero but in which the actual duration and energy of the impact E are finite and we consider times t which are large in comparison with τ ($t/\tau \to \infty$ not because $\tau \to 0$, but because $t \to \infty$).

In considering the limiting regime from this point of view we must determine the manner in which the real motion, nonself-similar because τ is finite, asymptotically approaches the limiting regime. How will the fact that the energy of the limiting motion is infinite be reconciled with the fact that the actual work of the piston is finite? The point is that the real solution does not approach the self-similar one uniformly in time. As the time t and the mass of gas involved in the motion $M = \rho_0 X$ increase, the pressure and all

other quantities approach values corresponding to the self-similar solution. However, this process does not occur everywhere.

The state of a certain mass m_0 near the vacuum interface that was subjected to the direct action of the piston during impact never approaches the one dictated by the self-similar solution. In order of magnitude this mass is equal to the mass of the gas through which the shock wave travels during the impact, or $m_0 \sim \rho_0 U_1 \tau \sim (\Pi_1 \rho_0)^{1/2} \tau$. The velocity with which this mass expands into vacuum always remains finite and equal in order of magnitude to U_1 ($U_1 \sim (\Pi_1/\rho_0)^{1/2}$, whereas the expansion velocity of the gas interface in the self-similar solution is infinite (as $\tau \to 0$, $\Pi_1 \to \infty$, and $U_1 \to \infty$). Because the motion is isentropic, the entropy of the mass m_0, equal to the initial entropy, is also finite. In fact, $S = c_v \ln p\rho^{-\gamma} + const$, and the value of $p\rho^{-\gamma}$ in the mass m_0 is, in order of magnitude, $\Pi_1 \rho_0^{-\gamma}$. Thus the entropy is bounded for finite τ and Π_1. In the self-similar solution for $\gamma = 7/5$ we have from (12.42)

$$p\rho^{-\gamma} \sim fq^{-\gamma} \sim \eta^{-4/3} \sim m^{-4/3} \to \infty \qquad \text{as} \quad m \to 0.$$

Thus, the mass m_0 at the interface always carries the imprint of the initial conditions and its state is not described by the self-similar solution even in the limit $t \to \infty$.

This situation in no way contradicts the general tendency of the actual solution to transform into the self-similar one in the limit $t \to \infty$. The mass m_0 comprises, with time, an increasingly smaller fraction of the entire mass of gas involved in the motion (Fig. 12.15). In the limit $t \to \infty$, this small mass

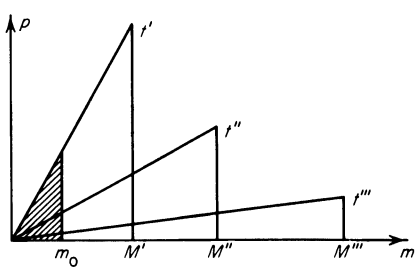

Fig. 12.15. The mass m_0 as a fraction of the total mass M involved in the motion with increasing time ($t''' > t'' > t'$).

need not be considered in the differential equations or in the convergent momentum integral*. However, the replacement, in the small mass m_0, of the actual solution by the self-similar one when evaluating the energy integral

* *Editors' note.* The actual finite momentum I is equal to the difference in the momentum integral over m_0 between the actual solution and the self-similar solution.

causes an essential change in the integral, making it divergent. In the self-similar solution the velocity and kinetic energy become infinite as the vacuum interface is approached ($m \to 0$), whereas actually with a finite pressure at the piston Π_1 and with a finite duration τ, the velocity and kinetic energy of the gas are finite near the interface.

In order to obtain a finite energy of the gas, corresponding to the finite work actually done by the piston, it is necessary when evaluating the energy using the self-similar solution to cut off the integration before the region in which the self-similar solution is inapplicable. We shall evaluate the energy in terms of the Lagrangian coordinate. Then, when integrating the specific energy over the mass of gas encompassed by the motion, we take as the lower limit a mass coordinate equal in order of magnitude to the mass m_0, which is not correctly described by the self-similar solution,

$$E = \int_{m_0}^{M} \left(\frac{u^2}{2} + \frac{1}{\gamma - 1} \frac{p}{\rho} \right) dm = \rho_0 \dot{X}^2 X \int_{m_0/M}^{1} \left(\frac{v^2}{2} + \frac{1}{\gamma - 1} \frac{\pi}{g} \right) d\eta.$$

To this term could be added separately the finite limiting energy of the mass m_0.

Let us carry out the integration in the case $\gamma = 7/5$. The main contribution to the integral is given by the region near the lower limit, where the velocity of the gas and its kinetic energy are very large (in the limit $m_0/M \to 0$, $v \to -\infty$). Therefore, in order to evaluate the integral approximately we use the asymptotic expression for the velocity (12.46) (see also (12.45)). We then obtain

$$E \sim \rho_0 \dot{X}^2 X \int_{m_0/M}^{1} \eta^{-4/3}\, d\eta \sim \rho_0 \dot{X}^2 X \left(\frac{m_0}{M} \right)^{-1/3}.$$

Let us express the variables in this relation in terms of X, using

$$M = \rho_0 X, \qquad \dot{X} = A^{5/3} X^{-2/3} \qquad (\text{since} \quad X = At^{3/5}).$$

Noting the relations $A \approx (\Pi_1/\rho_0)^{1/2} \tau^{2/5}$ (equation (12.36)) and $m_0 \approx (\Pi_1 \rho_0)^{1/2} \tau$, we find that

$$E \sim \rho_0 A^{10/3} X^{-4/3} X m_0^{-1/3} \rho_0^{1/3} X^{1/3} = \rho_0^{4/3} A^{10/3} m_0^{-1/3} \approx \Pi_1^{3/2} \rho_0^{-1/2} \tau.$$

It may be seen that the energy of the entire mass of the gas, with the exclusion of the small mass m_0 to which the self-similar solution does not apply, is constant in time, finite, and equal in order of magnitude to the work done by the piston. The energy contained in the relatively small mass m_0 is of the same order. This mass travels into the vacuum with a velocity of the order of U_1 and with a kinetic energy of the order of $m_0 U_1^2 \approx \rho_0 U_1^3 \tau \approx \rho_0 (\Pi_1/\rho_0)^{3/2} \tau \approx \Pi_1^{3/2} \rho_0^{-1/2} \tau \approx E$. Within the framework of the self-similar solution, however, an infinite amount of energy is concentrated in the mass

m_0, despite the fact that with time it constitutes an ever decreasing fraction of the total mass M of the gas encompassed by the shock.

It is an essential feature that the region of the gas that is not described by the self-similar solution and that produces the divergence in the energy integral if the self-similar solution is extrapolated into it lies beyond the limits of the domain of influence. It is located to the left of the singular line, and thus has no influence on the propagation of the shock wave. Actually, the boundary of the nonsimilar region is described by $m \approx m_0$, and the singular line by $m = \eta_0 M$ ($m = 0.054M$ for $\gamma = 7/5$). As $t \to \infty$ and $M \to \infty$, $m_0 \ll \eta_0 M$.

In order to get some idea how the nonself-similar solution passes to the limiting self-similar regime Zhukov and Kazhdan [14] carried out a numerical integration of the gasdynamic equations with $\gamma = 7/5$ for the rectangular pressure pulse shown in Fig. 12.9a. Figure 12.16 gives the curves of p/p_1,

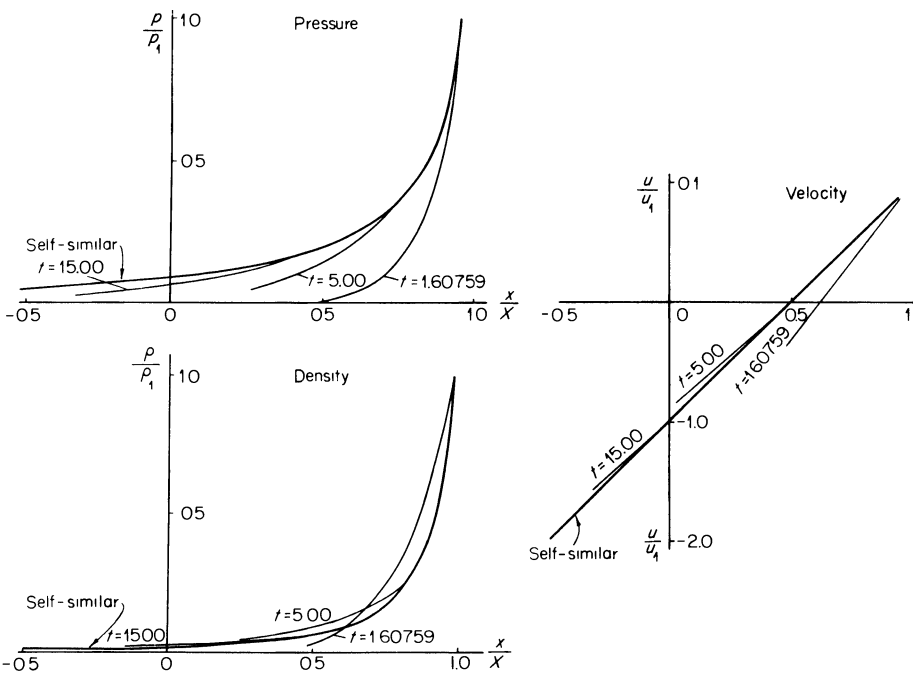

Fig. 12.16. Passage of nonself-similar motion into the self-similar regime. The curves are taken from [14]. The unit of time has been taken as the time of duration of the piston action τ.

u/u_1, and ρ/ρ_1 as functions of the similarity variable x/X for several times (p_1, u_1, and ρ_1 are quantities behind the front). Curves for the exact self-similar solution are also given in this figure. As may be seen from the curves, as early

as $t/\tau = 5$ the actual solution is quite close to the self-similar one, and for $t/\tau = 15$ it is almost identical with it. Thus the motion passes into the self-similar regime quite rapidly. From the solution of the nonself-similar problem we can determine the value of the numerical coefficient in equation (12.36) for the parameter A. It turns out to be equal to 1.715, so that $A = 1.715(\Pi_1/\rho_0)^{1/2}\tau^{2/5}$. The value of the numerical coefficient is a characteristic of the shape of the piston pressure pulse. Therefore the value 1.715 is associated with the rectangular pulse with $\gamma = 7/5$.

§18. Concentrated impact on the surface of a gas (explosion at the surface)

Let us consider a "spherical" analogue of the plane motion of a gas subjected to an impulsive load on its surface. A "cylindrical" analogue will be considered at the same time. This problem was treated by one of the present authors [20].

Let the half-space $z > 0$ be occupied by a perfect gas with a specific heat ratio γ. The density of the gas ρ_0 is constant, and the pressure and temperature are zero. The space $z < 0$ on the other side of the plane $z = 0$ is empty. At the initial time $t = 0$ in a mass of gas m surrounding the point 0 at the interface $z = 0$, an energy E is suddenly released. This can occur as the result of an explosion at the surface, or as a result of the concentrated impact at the surface from a high-velocity projectile if the projectile does not penetrate too deep into the fluid but is sharply decelerated near the surface. In this case its kinetic energy is rapidly converted into heat, and something similar to an explosion takes place. A shock wave travels from the point 0 through the gas, while in the other direction the heated gas expands into the vacuum. The initial velocities both in the direction of propagation of the shock wave and in the direction of the vacuum are of the order of $u_0 \sim (E/m)^{1/2}$*.

The surface of the shock front, which is a surface of revolution about the z axis, forms something like a "bowl", as shown in Fig. 12.17. The gas heated by the shock wave flows from the bowl through the round opening (the section of the bowl in the plane $z = 0$) into the vacuum. The outflow of the gas weakens the shock wave in comparison with what would be the case if the opening were closed by a fixed "cover"; this case would correspond to an explosion in an infinite medium.

The shock wave moves most rapidly in the downward direction and most slowly along the surface $z = 0$, where it is strongly attentuated owing to the expansion of the gas into vacuum. Therefore, the front surface is like a hemisphere but elongated in the downward direction. The gas near the front moves

* If the motion is caused by the impact of a projectile then m is of the order of the mass of the projectile, E is of the order of its kinetic energy, and u_0 is of the order of the impact velocity.

in the direction of propagation of the wave. Somewhere within the bowl there is a surface on which the vertical component of the velocity changes direction. Above this surface, which is shown in Fig. 12.17 by the dashed line, the gas

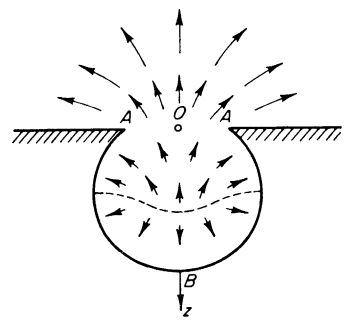

Fig. 12.17. The velocity field for a concentrated impact.

moves in the direction of the vacuum (the approximate directions of the velocity are indicated by the arrows). As the gas moves away from the plane $z = 0$ the expansion velocity in the previously empty space $z < 0$ increases, as shown schematically in the figure by arrows of increasing length*.

It is rather evident that in the limit, when the shock wave encompasses a mass $M \gg m$, the motion is self-similar. In this case the front surface expands in a similar fashion. The coordinate of any point of the front, say point B, increases with time as $z_1 \sim t^{\alpha}$. The pressure behind the front, say at the same point B, decreases with an increase in the mass M as $p_1 \sim M^{-n}$. Here, the constants n and α are related by the simple expression† $n = 2(1 - \alpha)/3\alpha$.

In the case of a concentrated impact, as in the plane case, the exponent n is limited by the inequality

$$1 < n < 2. \tag{12.55}$$

In order to check that this is indeed the case, let us consider the stage when $M \gg m$ and $p \sim M^{-n}$ and set up approximate expressions for the energy and vertical z component of the momentum of the gas in the bowl. Taking the dimensional parameters into account in the coefficient of proportionality between p and M but neglecting the numerical coefficients, the average

* Apparently, the gas flowing out of the opening near the plane interface with the undisturbed medium may move along the plane $z = 0$, and the pressure on the plane itself may be equal to zero. It is possible that a "blowout" may occur for certain values of γ, with a conical cavity formed near the plane $z = 0$ outside the hole. It is possible that for some values of γ much more complicated flow patterns may be formed, with, for example, a shock triple point near the point A.

† $M \sim z_1^3 \sim t^{3\alpha}$. The velocity of the gas behind the front u is proportional to $dz_1/dt \sim t^{\alpha-1} \sim p^{1/2} \sim M^{-n/2} \sim t^{-3\alpha n/2}$. From this $\alpha - 1 = -3\alpha n/2$ or $n = 2(1 - \alpha)/3\alpha$.

pressure over the bowl volume can be written as

$$p \sim \frac{E\rho_0}{m}\left(\frac{m}{M}\right)^n \sim p_0\left(\frac{m}{M}\right)^n. \tag{12.56}$$

Here $p_0 \sim E\rho_0/m$ is the initial pressure at the time of impact or explosion. The average velocity of the gas in the bowl is equal, in order of magnitude, to

$$u \sim \left(\frac{p}{\rho_0}\right)^{1/2} \sim u_0\left(\frac{m}{M}\right)^{n/2} \sim \left[\frac{E}{m}\left(\frac{m}{M}\right)^n\right]^{1/2}. \tag{12.57}$$

The energy in the bowl is of the order of

$$E_1 \sim Mu^2 \sim \frac{Mp}{\rho_0} \sim E\left(\frac{m}{M}\right)^{n-1} \sim E_{10}\left(\frac{m}{M}\right)^{n-1}, \tag{12.58}$$

where E_{10} is the initial energy in the bowl, which obviously is of the order of the total energy E. The momentum in the bowl is of the order of

$$I_1 \sim Mu \sim \left[Em\left(\frac{m}{M}\right)^{n-2}\right]^{1/2} \sim I_{10}\left(\frac{m}{M}\right)^{(n-2)/2}, \tag{12.59}$$

where $I_{10} \sim (Em)^{1/2}$ is the initial momentum*.

The energy flows out from the bowl through the opening, since the velocity of the gas in the opening is directed toward the vacuum. Consequently, the energy E_1 contained in the bowl decreases with time (with an increase in the mass M), and according to (12.58), $n > 1$.

We compare the momentum of the gas in the entire bowl to the momentum of that part of the gas that is contained between the surface of the shock front and the dotted surface across which the vertical component of the velocity changes sign and on which it is zero. No momentum flows out through this surface in the vertical direction and the pressure is positive on the surface. Consequently, the momentum increases with time and, according to (12.59), $n < 2$. The vertical momentum of the gas in the bowl is also balanced by the increasing but oppositely directed momentum of the gas which flows out of the bowl and expands into the vacuum. Thus (12.55) can be considered as proved†. The value $n = 1$ would correspond to conservation of energy in the bowl i.e., to an explosion in an infinite medium. The value $n = 2$ would correspond to conservation of momentum.

The same inequality (12.55) is also valid in the cylindrical case, in the case of

* In the case of impact by a projectile, I_{10} is of the order of the momentum of the impacting body.

† We note that the passage to the limit of the self-similar regime corresponds to $m \to 0$. In order for the pressure to be finite, it is necessary that the energy be infinite, $E \sim m^{-(n-1)} \to \infty$, and that the initial momentum be zero, $I_{10} \sim (Em)^{1/2} \sim m^{1-n/2} \to 0$.

a "line" impact. The picture of the motion in a line impact or explosion is qualitatively similar to that given in Fig. 12.17. In this case, however, the explosion takes place not at a single point O, but along a straight line passing through the point O perpendicular to the plane of the figure. The entire motion is symmetric with respect to the plane passing through this line and the z axis. The surface of the front will not form a bowl but an infinitely long "trough", the cross section of which is depicted by the figure. M is the mass per unit length of the trough encompassed by the shock.

We can establish an even narrower interval for the exponent which appears in the relation governing the attenuation of the shock wave. Physically, it is clear that in the case of a concentrated impact the degree of weakening of the shock wave per unit increase of mass is less than in the plane case for the same value of the specific heat ratio. In fact, the relatively smaller the area through which the gas flows out into the vacuum the less pronounced is the attenuating effect of the outflow of gas from the front. In the "spherical" case the area of the opening is much smaller than the surface area of the shock front (see Fig. 12.17). In the plane case both areas are equal. The "cylindrical" case is intermediate in this respect.

Thus denoting the exponents in the relation for the attenuation of the shock wave $p \sim M^n$ by n_1, n_2, and n_3 for the plane, line, and concentrated impacts, respectively, then for the same specific heat ratio

$$1 < n_3 < n_2 < n_1 < 2. \tag{12.60}$$

For example, for $\gamma = 7/5$, $n_1 = 4/3$ and $1 < n_3 < 4/3$. For $\gamma = 5/3$, $n_1 = 1.275$ and $1 < n_3 < 1.275$. The concentrated impact is thus closer to a point explosion in an infinite medium than the plane impact is to a plane explosion.

§19. Results from simplified considerations of the self-similar motions for concentrated and line impacts

As in the plane case, in order to determine the exponent $n(\gamma)$ in the attenuation relation $p \sim M^{-n}$ for the shock wave, it is necessary to solve the equation for the self-similar motion. However, the "spherical" and "cylindrical" problems are incommensurably more complex than the plane problem, since they are essentially two-dimensional and the self-similar motion is described by partial differential equations rather than by ordinary differential equations. The situation is also complicated by the fact that the shape of the shock front surface at which the boundary conditions are specified is not known beforehand and must itself be found from the solution. For this reason even a numerical integration of the self-similar equations can become very difficult.

Some idea of the numerical values of the exponents and of the general characteristics of the motion can be obtained from the simplified consider-

ations presented in [20]. An exact particular solution of the self-similar differential equations was obtained, which is a generalization of the exact solution for the one-dimensional problem (see §15) and which in some respects correctly indicates the features of the two-dimensional process. The solution contains a number of unknown constants. With this rather arbitrary particular solution it is impossible to satisfy the boundary conditions at the shock front. For this reason, the solution, instead of being required to satisfy boundary conditions at the front, was instead required to satisfy general integral relations expressing balances of mass, energy, and the components of the momentum of the gas contained in the bowl or trough. For this purpose, a very simple shape was chosen for the shape of the front surface. The bowl was replaced by a circular cylinder with a flat bottom and the rounded cross section of the trough was replaced by a rectangular cross section (see Fig. 12.18).

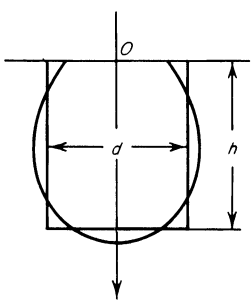

Fig. 12.18. Replacement of the bowl by an equivalent cylinder.

Just as the exact analytic solution in the one-dimensional case exists for only one particular value of the specific heat ratio γ (equal to 7/5), so the approximate solution here, which is a generalization of the exact one-dimensional solution, is applicable with only one particular value of γ. This value, along with the corresponding value of n, is found from the solution.

It was found that in the case of a concentrated impact $n = 1.07$ for $\gamma = 1.205$, the ratio of the height of the cylinder h to its diameter d is equal to 1.05. The density of the gas in the opening $\rho_{\text{open}} = 0.0187\rho_0$, and only 1.6% of the mass encompassed by the shock wave flows out of the opening. The density of the gas at the bottom of the cylinder $\rho_{\text{bot}} = 10.3\rho_0$, which is very close to the actual density behind the shock front $[(\gamma + 1)/(\gamma - 1)]\rho_0 = 10.7\rho_0$. The vertical velocity component changes direction at a depth of $0.846h$ from the opening and at a distance of $0.154h$ from the bottom. In the case of a line impact $n = 1.14$ for $\gamma = 1.266$, $h/d = 1.21$ (h is the height of the trough and d is the width), and 2% of the total mass flows out of the trough.

We see that the exponents n are very close to unity, so that the outflow of gas away from the shock front due to its expansion into vacuum weakens the

shock wave only slightly in comparison with an explosion in an infinite medium. This is clearly a result of the fact that only a small fraction of the entire mass flows out from the boundaries of the bowl or trough. The shape of the bowl is evidently appreciably different from hemispherical, the shape which would have corresponded to an explosion in an infinite medium. The height of the bowl, i.e., the cylinder, is approximately equal to the diameter, whereas if a hemisphere is replaced by an equivalent cylinder the height would be approximately half the diameter. The same is also true for the line impact.

Fortunately, the specific heat ratios $\gamma = 1.205$ and $\gamma = 1.266$ for which the approximate solutions are valid are close to the actual values of the effective specific heat ratios for gases at high temperatures with dissociation and ionization important. We note that in the plane case the exponent n decreases monotonically as γ increases. If the situation in the two-dimensional case is the same, which seems quite likely, then for a concentrated impact $1 < n < 1.07$ for $\gamma > 1.205$, and for a line impact $1 < n < 1.14$ for $\gamma > 1.266$. Values appreciably smaller than 1.205 or 1.266 are hardly likely to be of interest in actual processes. As a consequence, in the majority of actual processes for which the problem of a concentrated (or line) impact could serve as a model, the shock wave is attenuated only slightly more rapidly than in an explosion in an infinite medium.

§20. Impact of a very high-speed meteorite on the surface of a planet

The process which takes place when a meteorite with a velocity of several tens or a hundred km/sec (and higher) strikes a planet can serve as a characteristic example of the phenomenon of a concentrated impact. For this problem it is only meaningful to consider either planets lacking an atmosphere, such as the moon, or sufficiently large meteorites. Small meteorites, or rather meteors, are vaporized, "burned up" by atmospheric friction, and never reach the surface of the planet.

When a meteorite impacts it is sharply decelerated and the initial kinetic energy $E = mv^2/2$ (where m is the mass of the meteorite and v is the impact velocity) is largely converted into internal energy or heat. The depth to which the meteorite penetrates the surface is usually of the order of the dimensions of the meteorite itself, so that at the initial time the energy release takes place in a mass of the order of m. A shock wave travels through the ground from the point of energy release*.

We consider only impacts with very high velocities, where the specific energy $v^2/2$ is many times larger than the binding energy (or heat of vaporiza-

* We do not consider low impact velocities, where the deceleration process and the propagation of the shock wave through the meteorite are important, or in other words, where we cannot assume that the energy release is instantaneous.

tion) of the atoms and molecules of the meteorite and of the ground. In this case a stage exists when the shock wave encompasses a ground mass M that appreciably exceeds the initial mass m, but when the material encompassed by the shock wave can be regarded as a dense gas. The ground and the meteorite are totally vaporized during the expansion and expand from the planet surface in a gaseous state. In the stage when the material has not expanded too much, the gas pressure is considerably higher than atmospheric and the existence of an atmosphere (if there is one) can be neglected. The vapor expands as if into a vacuum. As can be seen, we are dealing here with a typical picture of a concentrated impact on the surface of a "gas", as described in the preceding section.

Let us estimate what the required impact velocities are. The heat of vaporization of iron (both iron and stone meteorites occur) is equal to 94 kcal/mole $= 7 \cdot 10^{10}$ erg/g. The heat of vaporization of stone is of the order of 83 kcal/mole $= 5.8 \cdot 10^{10}$ erg/g. This is the value for silica (SiO_2), which is the main component of various soils and rocks. If in addition we also consider the dissociation of the SiO_2 molecules during vaporization, then the total binding energy comes to 203 kcal/mole $= 1.4 \cdot 10^{11}$ erg/g. As an estimate, let us say that complete vaporization requires that the specific energy exceed the heat of vaporization, for which we take the approximate value $U \approx 10^{11}$ erg/g, by a factor of 10. Then the minimum velocity at which a mass of the order of the mass of a meteorite will vaporize will be $v_{\min} \approx (2 \cdot 10 \cdot 10^{11})^{1/2} =$ 14 km/sec. In exactly the same way we can state that the expansion following the passage of the shock wave vaporizes those ground layers which were reached by the shock wave while the specific internal energy ε_1 behind the front is at least of the order of $\varepsilon_k \sim 10U \sim 10^{12}$ erg/g. The assumption that ε_1 must exceed U by a factor of 10 was based on estimates obtained in §22 of Chapter XI, where it was shown that complete vaporization in the unloading of a solid body compressed by a strong shock wave is obtained if the energy behind the wave front is at least five times greater than the binding energy of the material.

In order to estimate the total mass of ground which vaporizes on the impact of a meteorite we must use the relation governing the attenuation of the shock wave. An estimate of this type was first carried out by Stanyukovich [21], who studied the phenomenon of the "explosion" on impact of a meteorite on the surface of a planet as the cause for the formation of lunar craters. He did not take into account the effect of the expansion of the vapor into the vacuum, assuming that the shock wave propagates in the same manner as it would in a strong explosion in an infinite medium, following the relations $p_1 \sim M^{-1}$, $\varepsilon_1 \sim E/M$. The arguments presented in the preceding section substantiate this assumption. The order of magnitude of the vaporized mass M_k is determined by $\varepsilon_k \sim E/M_k$, from which $M_k \sim E/\varepsilon_k \sim m(v^2/\varepsilon_k) =$

$m(v/v_k)^2$, where $v_k = \varepsilon_k^{1/2} \sim 10$ km/sec. For example, if the impact velocity $v \sim 100$ km/sec the vaporized mass of ground exceeds the mass of the meteorite by a factor of 100.

When the energy behind the shock wave drops below $\sim 10^{12}$ erg/g, the ground encompassed by the shock wave no longer vaporizes on unloading. However, the energy in the wave is still sufficient for the mechanical pulverization of the material. The limiting energy required for pulverization is much less than the heat of vaporization. Therefore, the mass of the pulverized material exceeds the mass of the vaporized substance by a large factor. The pulverized material is ejected upward in the form of solid particles, and this results in the formation of the crater. Questions as to the dimensions of craters produced by meteorite impact, as to the role played by the gravitational force which prevents the material from being thrown to large distances, and other questions were considered by Stanyukovich [21].

The explosion-like effects of high-speed meteorite impacts also take place when a body moves through a rarefied atmosphere at hypersonic velocity. The impacts of air molecules with the surface of the body are similar to meteorite impacts at planet surfaces. A "microexplosion" takes place at each impact, and a certain amount of vaporized material is ejected from the surface of the body. The body receives an additional recoil momentum, which increases the drag coefficient and the rate of deceleration of the body in the atmosphere. This phenomenon was considered in a paper by Stanyukovich [22]. The impact of a high-speed body on the surface of a liquid which is assumed to be incompressible has been considered by Lavrent'ev [23].

§21. Strong explosion in an infinite porous medium

Kompaneets [24] solved the problem of a strong point explosion in a plastic compacting medium with constant compaction behind the shock front*. Here we consider the simplified problem (by neglecting plastic shear stress, *eds.*) of the propagation of a shock wave from a point explosion in a porous medium, with the condition that the continuous medium is incompressible (for example, in a sand consisting of incompressible grains). We neglect the strength of the sand grains, and we assume that the adiabatic compression of the material to the density of the continuous medium (total elimination of voids) does not require any expenditure of energy. In other words, the shock is taken to be strong with respect to the strength of the material, but weak with respect to its elasticity (the compressibility of the continuous medium). The initial pressure p_0 is equal to zero.

The average density of the undisturbed medium will be denoted by ρ_0, and the density of the continuous medium (the "sand grains") by ρ_1, $\rho_0 =$

* In [25] the compaction was assumed to depend on the wave strength.

$\rho_1(1-k)$, where k is the porosity, which can vary from zero to one (not the same k as in §10, Chapter XI, *eds.*).

Let a strong explosion take place at some point. An intense initial push is imparted to the material (as for example, if a spherical "piston" were to rapidly expand and then stop). A shock wave will travel through the material, with the material compressed across the shock to the density of the continuous medium and with the voids completely filled. Thereafter the density of the medium no longer changes but remains equal to ρ_1. The material encompassed by the shock wave moves behind the front. A spherical layer with constant density ρ_1 is formed behind the shock front surface, and behind that a cavity, as shown in Fig. 12.19a.

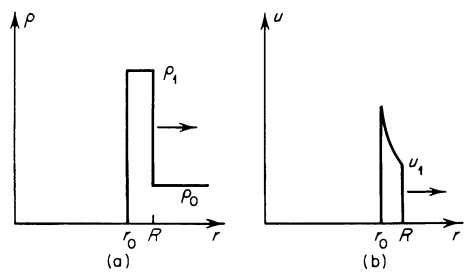

Fig. 12.19. Density (a) and velocity (b) distributions as functions of radius for an explosion in sand with incompressible grains.

If the radius of the wave front is R and the radius of the internal surface of the layer is r_0, then conservation of mass gives

$$M = \frac{4\pi}{3} R^3 \rho_0 = \frac{4\pi}{3} (R^3 - r_0^3)\rho_1$$

or

$$r_0^3 = R^3\left(1 - \frac{\rho_0}{\rho_1}\right) = R^3 k. \tag{12.61}$$

The velocity distribution in the layer is found using the equation of continuity for an incompressible fluid $\nabla \cdot \mathbf{u} = 0$,

$$u = u_1\left(\frac{R}{r}\right)^2, \qquad r_0 < r < R, \tag{12.62}$$

where u_1 is the particle velocity behind the shock front (see Fig. 12.19b). It is related to the front velocity $D = dR/dt$ by

$$u_1 = D\left(1 - \frac{\rho_0}{\rho_1}\right) = Dk.$$

With the assumptions made, the Hugoniot curve for the material has the shape shown in Fig. 12.20*. Let the pressure behind the shock wave be p_1 (point B on the Hugoniot curve). As is known (see §16, Chapter I), a material initially at rest acquires, in a strong shock wave ($p_1 \gg p_0$), the same kinetic and internal energies of $u_1^2/2$ per unit mass. These energies are numerically equal to the area of triangle OAB in Fig. 12.20. Since the solid

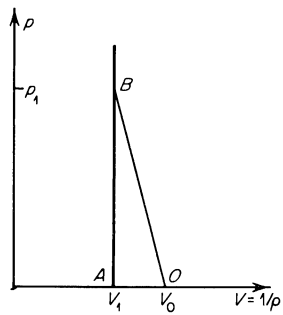

Fig. 12.20. Hugoniot curve for sand with incompressible grains without taking the strength of the material into account.

particles are assumed to be incompressible, we shall not be interested in the fate of the internal energy acquired by the material in the shock wave. This energy is converted into heat and simply represents a loss of the mechanical energy of motion. The decrease in the kinetic energy of the entire mass M in the time dt is thus equal to the increase in the internal energy of a mass dM encompassed by the shock wave in the time dt, and

$$-d\left(\frac{M\overline{u^2}}{2}\right) = -\beta\, d\left(\frac{Mu_1^2}{2}\right) = \frac{u_1^2}{2}\, dM. \tag{12.63}$$

Here $\overline{u^2} = \beta u_1^2$ denotes the mean square of the velocity in the mass M. The coefficient β is readily calculated from (12.62) and (12.61), and is $\beta = 3/(k + k^{2/3} + k^{1/3})$. Integrating (12.63), we find the relation governing the attenuation of the shock wave

$$u_1^2 = const\, M^{-(1+\beta)/\beta} = const\, M^{-n}.$$

In analogy with preceding sections, we have here denoted the exponent of the mass in the expression for the specific energy by n, with $n = (1 + \beta)/\beta$.

The total kinetic energy is proportional to $E_k = M\overline{u^2}/2 \sim M^{-(n-1)}$, and the momentum is proportional to $I \sim Mu_1 \sim M^{1-n/2}$. Since $\beta > 0$, the exponent n is always bounded between the limits $1 < n < 2$ (cf. the results of §18). In the limiting case of a continuous incompressible medium $k \to 0$, $\beta \to \infty$, $n \to 1$, the energy is conserved, and the momentum increases with

* For a discussion of the shock compression of a porous material when compressibility of the continuous medium is taken into account, see §10, Chapter XI.

time. In the limiting case of an extremely porous substance (a highly "compressible" medium) $k \to 1$, $\beta \to 1$, $n \to 2$, the momentum is conserved, and the energy decreases. In the general case $0 < k < 1$, the energy decreases (it is converted into heat), and the momentum increases. As we see, the situation is the same as that which occurs for an impact on the surface of a gas (see §18). As in the limiting case of a concentrated impact the initial energy is infinite (if $k \neq 0$, $n > 1$ and $E_k \sim M^{-(n-1)} \to \infty$ as $M \to 0$). In a manner analogous to what has been done here, one can also consider an imploding shock wave in a porous medium with incompressible grains.

5. *Propagation of shock waves in an inhomogeneous atmosphere with an exponential density distribution*

§22. Strong point explosion

In Part 4 of Chapter I we considered the problem of a strong explosion in an infinite homogeneous medium. As we know, the earth's atmosphere is not homogeneous and the air density decreases with altitude; the dependence of the density ρ_0 on altitude h can be approximated by the barometric formula $\rho_0 = \rho_{00} e^{-h/\Delta}$. Here ρ_{00} is the density at sea level and Δ is the so-called scale height of the standard atmosphere, which at the earth's surface is approximately equal to 8.5 km*.

Let us examine the propagation of a shock wave induced by a strong point explosion in an inhomogeneous atmosphere. Our interest here is in the stage of the wave motion at which the wave has moved away from the source of the explosion through a distance comparable to the scale height Δ; only in this case does the inhomogeneity of the medium appreciably influence the wave. We shall assume that we are dealing with a strong shock wave (with the pressure behind the front much greater than the pressure ahead of the front). The gasdynamic process is not self-similar, since we have the length scale Δ, and, in addition, the flow is now two-dimensional instead of one-dimensional. In cylindrical coordinates with the vertical axis passing through the point of the explosion, the flow is a function of the z coordinate and of the radius r. The complete solution to this problem can be found only by a numerical integration of the flow equations. It is possible, however, to get some idea of the character of the shock propagation and of the shock shape on the basis of some simple considerations given by Kompaneets [28].

* Actually, since the air temperature also varies with altitude, the density of the earth's atmosphere does not strictly follow the exponential law. The scale height Δ, defined as $\Delta = -(d \ln \rho/dh)^{-1}$, is variable between 6 and 15 km for altitudes below 150 km, and becomes still larger above 150 km.

Let us assume that, as with the strong explosion in a homogeneous medium, the pressure is almost constant throughout the entire volume bounded by the explosion wave, and is thus constant along the back of the surface of the front. We assume also that it is proportional to the average pressure in the volume, to the ratio of the explosion energy to the volume bounded by the wave Ω

$$p_1 = (\gamma - 1)\lambda \frac{E}{\Omega}. \tag{12.64}$$

Here $\lambda(\gamma)$ is a numerical coefficient which can be estimated from the solution to the explosion problem in a homogeneous medium (see Chapter I).

Let the equation of the surface of the shock front in cylindrical coordinates be $f(z, r, t) = 0$. Differentiating, we get

$$\frac{\partial f}{\partial z} dz + \frac{\partial f}{\partial r} dr + \frac{\partial f}{\partial t} dt = 0$$

or

$$\frac{\partial f}{\partial z} D_z + \frac{\partial f}{\partial r} D_r = \mathbf{D} \cdot \nabla f = -\frac{\partial f}{\partial t},$$

where D_z and D_r are the components of the velocity vector $\mathbf{D}$. The normal component of the wave front velocity is given by

$$D_n = -\frac{\partial f/\partial t}{|\nabla f|}.$$

We know, however, that at the front of a strong shock wave

$$D_n = \left(\frac{p_1}{\rho_0} \frac{\gamma + 1}{2}\right)^{1/2},$$

where ρ_0 is the density ahead of the front at a given point on the shock surface. From the last two expressions we obtain

$$\left(\frac{p_1}{\rho_0} \frac{\gamma + 1}{2}\right)^{1/2} = -\frac{\partial f/\partial t}{|\nabla f|}.$$

We now substitute the pressure p_1 from (12.64) and, using the equation for the surface, express the volume Ω bounded by the surface of the wave front in the integral form $\Omega = \int d\Omega$. We assume that the equation $f(z, r, t) = 0$ is solved for the radius $r = r(z, t)$ and consider the atmosphere to be exactly exponential. Combining the above results we obtain for the function $r = r(z, t)$ a partial differential equation, one which is solved exactly in [28].

The evolution of the shock front surface is shown in Fig. 12.21, taken from [28]. This figure shows the wave front cut by a vertical plane passing through

the point of explosion (through the z axis), at successive instants of time. The wave is spherical at the beginning, and gradually becomes egg shaped.

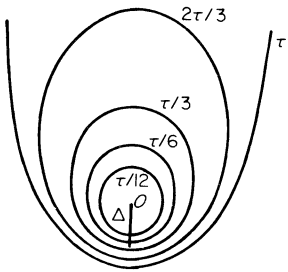

Fig. 12.21. Shock front at successive instants of time for a strong explosion at high altitude. Sections shown are formed by passing a vertical plane through the origin of the explosion. The density of the atmosphere changes by a factor of e over the distance Δ.

The strength of the wave does not change in the same way for its motion in different directions. When moving vertically downward in the direction of the strongest density increase, the shock wave is weakened and decelerates most rapidly. Conversely, when moving vertically upward in the direction of the strongest density decrease, it is even accelerated and, in a finite time τ, it moves to infinity, "breaking through" the atmosphere. The front surface forms something like a "bowl" and, in the huge cavity bounded by this surface, the pressure drops to a very low value (within the framework of the assumptions made, to zero). When moving horizontally the wave is weakened, but more slowly than when moving downward.

The physical reason for the acceleration of the shock wave at large distances when moving upward is easily understood [31]. If R is the distance of the upper point of the shock wave to the explosion center, then the volume of the cavity Ω is proportional to R^3 and the pressure $p_1 \sim E/R^3$. The density ahead of the front is $\rho_0 = \rho_c \exp(-R/\Delta)$, where ρ_c is the density at the level of the explosion. Therefore, as $R \to \infty$ the front velocity

$$D \sim \left(\frac{p_1}{\rho_0}\right)^{1/2} \sim \frac{E^{1/2}}{\rho_c^{1/2} R^{3/2}} e^{R/2\Delta} \tag{12.65}$$

approaches infinity, while the time required by the wave to move upward to infinity,

$$\tau = \int_0^\infty \frac{dR}{D} \sim \frac{\rho_c^{1/2}}{E^{1/2}} \int_0^\infty R^{3/2} e^{-R/2\Delta}\, dR$$

is finite*. It follows from this equation that the time for "breaking through"

* We note that the energy concentrated in a given solid angle whose vertex is located at the point of the explosion does not remain constant as is the case with spherical symmetry. The energy has a tendency to "flow" upward from the bottom and this process also aids in accelerating the shock wave upward. The mass, on the other hand, has a tendency to "flow" downward, and to accumulate near the lower part of the shock.

the atmosphere is $\tau = v(\rho_c \Delta^5/E)^{1/2}$, where v is a numerical constant determined from the complete solution of the problem). It is easy to see that τ is the only quantity with the dimensions of time which can be constructed from the dimensional parameters E, ρ_c, and Δ of the problem.

The relations governing the motion of the shock wave, the shape of the front surface, and the constant v were improved somewhat in comparison with those given in [28] by Andriankin, Kogan, Kompaneets, and Krainov [29]. These authors analyzed the problem as formulated above, but took into account the pressure distribution behind the shock wave along the front surface. In their treatment the motion of each part of the front surface was determined separately. The more accurate value of the constant v was found to be $v \approx 24$ for a specific heat ratio $\gamma = 1.2$. Up to the time of breaking through the atmosphere the shock wave travels a distance of about 2Δ downward and 3.5Δ horizontally (at the level of the point of the explosion). In accordance with the statement of the problem, the solution given in [28, 29] is no longer valid near the time of breaking through the atmosphere, since then the pressure drops to zero and the shock wave stops moving (under the approximations used).

The inhomogeneity of the atmosphere is felt only in those explosions where the shock wave moves through a distance that exceeds the scale height Δ and still remains sufficiently strong. When this is not so the shock wave will be attenuated before the inhomogeneity is felt, and the explosion takes place in the same manner as in a homogeneous atmosphere. An approximate condition for obtaining a shock front evolution as described above can be defined as in [29], that the ratio of pressures behind the front to the air pressure ahead of the front p_1/p_0 for the propagation of the wave over a distance Δ (as calculated from the relations for an explosion in a homogeneous atmosphere) should exceed $(\gamma + 1)/(\gamma - 1)$ by a factor of, say, 10 (see footnote on page 94 in §25, Chapter I). For example, at an altitude of 100 km, $p_0 \approx 10^{-6}$ atm = 1 bar, and this condition ($p_1/p_0 \approx 100$) is satisfied only for explosions with energies $E > 10^{20}$ erg. At low altitudes, an explosion whose strength is not extremely large takes place in practically the same manner as in a homogeneous atmosphere.

§23. Self-similar motion of a shock wave in the direction of increasing density

Let us consider in more detail the nature of the gasdynamic process in the region of the lowest point of the shock wave produced by a strong explosion which moves vertically downward. In an explosion in a homogeneous atmosphere the pressure in the volume is equalized and is only lower than the pressure behind the shock front by a factor of $\frac{1}{2}$ to $\frac{1}{3}$ (see §§25 and 26 of Chapter I). This internal pressure "maintains" the shock wave, and is responsible

for the fact that the wave is attenuated more slowly than it would be in the absence of an internal pressure. The role of the internal pressure becomes particularly understandable if we compare the motion for a plane explosion with the motion for a plane impulsive load (see the preceding part of this chapter). In the latter case, the pressure in the region behind the shock front decreases to zero and there is no internal pressure to maintain the wave. For this reason the shock wave is attenuated faster than in a plane explosion. A similar effect appears in an explosion in an inhomogeneous atmosphere. The pressure in the cavity drops rapidly, owing to the increase in its volume brought about by the upward acceleration of the wave. As a result of this volume increase the internal pressure is no longer large enough to maintain the shock wave which propagates downward, and the gas from the lower layers flows upward away from the front, rushing into the "empty" cavity. The situation to some extent approximates that which takes place in the problem of an impulsive load. Another reason for its similarity to this problem is that, when the shock wave moves away a sufficiently large distance from the point of the explosion, the curvature of the lower part of the front surface becomes small; this part, together with the gas layer behind the front which is adjacent to it, then appears as approximately plane. Thus, to describe the flow of the gas in the lower part of the shock wave approximately it is convenient to consider the idealized problem of the propagation of a plane shock wave in an inhomogeneous atmosphere in the direction of increasing density.

The problem to be considered may be formulated as follows: Let the gas density be distributed in space following the exponential law

$$\rho_0 = \rho^* e^{x/\Delta}, \qquad \Delta = const \tag{12.66}$$

(for convenience the x axis is directed downward). This distribution has the property that the mass of gas concentrated in a column of unit cross-sectional area, from $x = -\infty$, where $\rho_0 = 0$, to $x = X$, is equal to a mass of gas of density $\rho_0(X)$ in a column whose length is Δ,

$$M = \int_{-\infty}^{X} \rho_0(x)\, dx = \rho_0(X)\Delta. \tag{12.67}$$

Let an impulsive load be applied at the initial time $t = 0$, somewhere in the region of very low density, where $x \approx -\infty$. A shock wave will travel through the gas in the direction of increasing density, and the heated gas will expand in the direction of the vacuum.

We shall seek the limiting motion at the stage when the shock wave encompasses a mass of gas M that is much greater than the mass m_0 subjected to the initial impact in the low-density region. The initial pressure and temperature of the gas are taken equal to zero. It is clear that the statement

of the problem is entirely analogous to the statement of the problem of an impulsive load applied to the surface of a constant density gas bordering on a vacuum (see §13). The problem of an impulsive load in the case of an inhomogeneous atmosphere was formulated and solved by one of the present authors [30].

It is clear that the limiting motion ($M \gg m_0$) is self-similar. However, this similarity has an unusual character. Unlike the other self-similar motions which have been considered, the conditions of this problem contain a length scale Δ and do not contain a parameter with the units of mass (usually such a parameter is connected with the given initial density of the gas). The quantity ρ^* in (12.66) cannot serve as a parameter, because the x coordinate origin is chosen arbitrarily and thus the choice of ρ^* is arbitrary*.

The x coordinate is defined only to within an additive constant, as a result of which the motion can depend only on a difference of coordinates, but not on the x coordinate itself. The difference in coordinates is the distance measured from the shock front, the coordinate of which will be denoted by X; the motion must depend on the dimensionless distance

$$\xi = \frac{X - x}{\Delta}. \tag{12.68}$$

This quantity is the similarity variable. Here, in contrast to all the other self-similar motions which have been considered, the similarity variable does not contain the units of time. The motion, of course, possesses a certain parameter A that characterizes the strength of the impact†. However, owing to the absence of another parameter with the units of mass it is impossible to construct from the quantities x, A, and Δ a combination with the dimension of time. Consequently, from the independent variables and the parameters x, t, A, and Δ it is impossible to construct a dimensionless variable which would contain the time t.

From the remarks made concerning the dimensional properties of the problem and the arbitrariness of the x coordinate, it is easy to find the relation governing the motion of the shock wave and to write down the general expressions for the unknown functions, the velocity, pressure, and density. The velocity of the shock front is

$$D = \dot{X} = \alpha \frac{\Delta}{t}, \tag{12.69}$$

where the numerical coefficient α depends only on the specific heat ratio γ.

* ρ^* is the density at the point $x = 0$, but we are justified in placing the coordinate origin $x = 0$ at any point at any density.

† It will be related below to the explosion energy.

The coordinate of the front X increases logarithmically with time as

$$X = \alpha \cdot \Delta \ln t + const. \tag{12.70}$$

The expressions for the velocity, density, and pressure of the gas behind the shock front have the form

$$\begin{aligned} u &= u_f \tilde{u} = \frac{2}{\gamma+1} \alpha \frac{\Delta}{t} \tilde{u}, \\ \rho &= \rho_f \tilde{\rho} = \frac{\gamma+1}{\gamma-1} \rho_0(X) \tilde{\rho}, \\ p &= p_f \tilde{p} = \frac{2}{\gamma+1} \alpha^2 \frac{\Delta^2}{t^2} \rho_0(X) \tilde{p}, \end{aligned} \tag{12.71}$$

where the dimensionless reduced functions $\tilde{u}$, $\tilde{\rho}$, and $\tilde{p}$ depend on γ and on the similarity variable ξ, the dimensionless distance measured from the shock front. The reduced functions are defined so that at the shock front ($\xi = 0$) they all become one,

$$\tilde{u}(0) = \tilde{\rho}(0) = \tilde{p}(0) = 1. \tag{12.72}$$

The other boundary condition is that in the vacuum at $x = -\infty$, $\xi = \infty$, $\tilde{p}(\infty) = 0$.

The density $\rho_0(X)$ of the gas directly ahead of the shock front is given in terms of the mass coordinate of the front M by (12.67). In contrast to the geometric coordinate, the mass of the gas encompassed by the shock wave depends on time as usual, following a power law. We have $\dot{M} = \rho_0(X)\dot{X} = M\dot{X}/\Delta = M\alpha t^{-1}$, from which

$$M = At^{\alpha}. \tag{12.73}$$

Here A is the constant of integration, and is also the parameter characterizing the strength of the impact. Its dimensions are $[A] = ML^{-2}T^{-\alpha}$. We can thus substitute into equations (12.71) the explicit dependence of $\rho_0(X)$ on time,

$$\rho_0(X) = \frac{M}{\Delta} = \frac{At^{\alpha}}{\Delta}. \tag{12.74}$$

As was noted before, the self-similarity of the motion is unusual: the velocity, density, and pressure distributions appear as though "tied" to the shock front and move together with the front, without expanding in time (only the amplitudes of these quantities change). However, in Lagrangian coordinates the motion is self-similar in the usual sense. The Lagrangian coordinate m is

$$m = \int_{-\infty}^{x} \rho(x)\, dx = const \cdot M \int_{\xi}^{\infty} \tilde{\rho}(\xi)\, d\xi.$$

Thus ξ and, consequently, also $\tilde{u}$, $\tilde{\rho}$, and $\tilde{p}$ are functions of the similarity variable $\eta = m/M = m/At^{\alpha}$.

The equations for the self-similar motion are most conveniently solved in terms of Lagrangian coordinates. Substituting (12.71) and (12.74) into the gasdynamic equations

$$\frac{\partial u}{\partial t} + \frac{\partial p}{\partial m} = 0, \qquad \frac{\partial (1/\rho)}{\partial t} - \frac{\partial u}{\partial m} = 0, \qquad p\rho^{-\gamma} = F(m),$$

we obtain equations for the reduced functions $\tilde{u}(\eta)$, $\tilde{\rho}(\eta)$, and $\tilde{p}(\eta)$

$$\begin{aligned} &\tilde{u} + \alpha\eta\tilde{u}' = \alpha\tilde{p}', \\ &\frac{1}{\tilde{\rho}} + \eta\left(\frac{1}{\tilde{\rho}}\right)' = -\frac{2}{\gamma - 1}\tilde{u}', \\ &\tilde{p}\tilde{\rho}^{-\gamma}\eta^{(2/\alpha)+\gamma-1} = 1. \end{aligned} \tag{12.75}$$

Integrating the second of these equations and eliminating $\tilde{\rho}$ and $\tilde{u}$ from the system, we obtain the basic equation for the problem

$$\frac{d\tilde{p}}{d\eta} = \frac{\gamma + 1}{2\alpha} \frac{1 - \dfrac{\gamma - 1}{\gamma + 1}\left(1 - \dfrac{2 - \alpha}{\gamma}\right)\tilde{p}^{-1/\gamma}\eta^{-(2-\alpha)/\alpha\gamma}}{1 - \dfrac{\gamma - 1}{2\gamma}\tilde{p}^{-(1/\gamma)-1}\eta^{1-(2-\alpha)/\alpha\gamma}}. \tag{12.76}$$

The solution $\tilde{p}(\eta)$ must pass through the two points $\tilde{p}(1) = 1$ and $\tilde{p}(0) = 0$, and this condition determines the exponent α.

An exact solution to the problem may be obtained for the particular case $\gamma = 2$. We have*

$$\begin{aligned} &\alpha = \tfrac{3}{2}, \qquad M \sim t^{3/2}, \qquad D = \frac{3}{2}\frac{\Delta}{t}; \\ &u_f \sim \frac{1}{t}, \qquad \rho_f \sim t^{3/2}, \qquad p_f \sim \frac{1}{t^{1/2}}; \\ &\tilde{p} = \eta, \qquad \tilde{\rho} = \eta^{5/3}, \qquad \tilde{u} = \tfrac{3}{2}(1 - \tfrac{1}{3}\eta^{-2/3}). \end{aligned} \tag{12.77}$$

The solution in Eulerian coordinates has the form

$$\tilde{p} = (1 + 2\xi)^{-3/2}, \qquad \tilde{\rho} = (1 + 2\xi)^{-5/2}, \qquad \tilde{u} = 1 - \xi. \tag{12.78}$$

An analytic solution can also be obtained for the case $\gamma = 1 : \alpha = 1$, $\tilde{p} = \eta$, $\tilde{\rho} = \eta^3$, $\tilde{u} = 1$. This case is of interest only from the point of view of furnishing a limit on the similarity exponent α; it corresponds to infinite compression of

* The solution in Lagrangian coordinates is completely analogous to the analytic solution for the problem of an impulsive load in the case $\gamma = 7/5$. (See (12.42).)

the gas across the wave front, with the result that $\tilde{p}$, $\tilde{\rho}$, and $\tilde{u}$ in Eulerian coordinates become δ functions, proportional to $\delta(\xi)$. Since common values of γ are contained in the interval $1 < \gamma < 2$, we may assume that the corresponding values of the similarity exponent lie in the interval $1 < \alpha < 3/2$*.

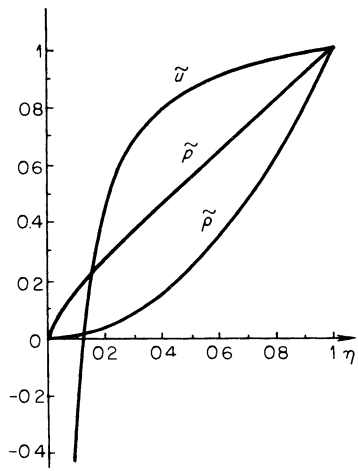

Fig. 12.22. Reduced velocity $\tilde{u}$, pressure $\tilde{p}$, and density $\tilde{\rho}$ as functions of the mass coordinate.

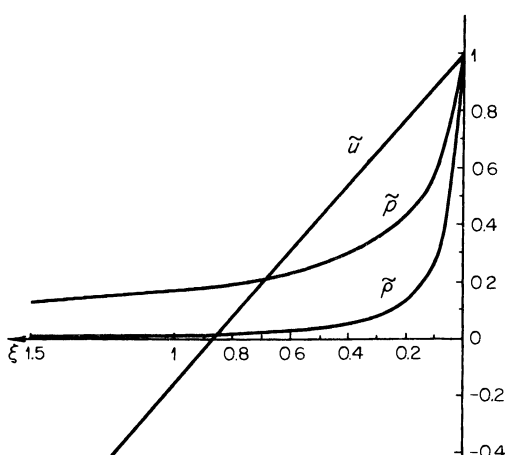

Fig. 12.23. Spatial distributions of reduced velocity $\tilde{u}$, pressure $\tilde{p}$, and density $\tilde{\rho}$ behind the shock wave.

* Consideration of energy and momentum balances, analogous to those given in §16, leads to the general limits $1 < \alpha < 2$.

For arbitrary values of γ the solutions can be found by trial and error, by numerical integration of (12.76). Figures 12.22 and 12.23 present the reduced velocity, density, and pressure distributions as functions of the mass and spatial coordinates which were obtained for $\gamma = 1.25$. In this case the exponent $\alpha = 1.345$*.

§24. Application of the self-similar solution to an explosion

The downward motion of the shock wave produced by a strong point explosion takes on the features of the self-similar motion described in the preceding section after the pressure in the cavity p_c becomes small in comparison with the pressure p_f behind the shock front at the lowest point. Both of these quantities enter into the numerical calculation of the motion of the shock wave carried out in [29], so that we are in a position to "tie-in" the self-similar solution at some particular point in the numerical calculation. It should be noted that at the point when the pressure in the cavity drops sharply the solution of [29] is no longer valid, since the force moving the shock wave vanishes at zero pressure in the cavity according to the approximation made there. Actually, however, the motion of the shock wave continues afterwards for quite a long time, and it has exactly the character of the motion ensuing as a result of an initial "push".

Numerical estimates show that the pressure in the cavity can become much less than the pressure behind the front while the front velocity is still sufficiently large that the counterpressure in the undisturbed air can still be neglected in treating the subsequent motion. Therefore the self-similar solution can describe the downward propagation of the shock wave for some time after the atmospheric break-through.

To be specific let us assume that the transition to the new regime is reached for $p_f/p_c = 10$. According to [29] this value corresponds to a time from the explosion of $t_1 = 19\tau_k$, where $\tau_k = (\rho_c \Delta^5/E)^{1/2}$ is the time scale characteristic of an explosion in an inhomogeneous atmosphere (ρ_c is the air density at the explosion altitude and E is the energy of the explosion). At the time t_1 the shock wave has moved downward from the point of explosion through a distance $z = 1.9\Delta$; at this time the shock front velocity is $D_1 = 2.5 \cdot 10^{-2} \cdot \Delta/\tau_k$.

* *Editors' note.* Calculations of one of the editors give the following values for α in this problem [33]:

γ	α	γ	α
2	1.500	4/3	1.369
5/3	1.450	9/7	1.351
3/2	1.417	5/4	1.338
7/5	1.392	11/9	1.324

Let us extrapolate the limiting shock propagation relations (12.69) and (12.70) to the time of transition to the new regime, with the position and time measured so that the initial condition $D = D_1$ when $X = 0$ is satisfied. Here the process up to the time of transition plays the role of the impulsive load. We obtain the approximate dependence of the front position on its velocity and on time (the coordinate is measured downward from the point of transition to the new regime), with $X = \alpha \cdot \Delta \ln(D_1/D) = \alpha \Delta \ln(t/\theta)$. The parameters D_1 and θ are determined in terms of the parameters of the explosion by the expressions $D_1 = 2.5 \cdot 10^{-2}(\Delta/\tau_k) = 2.5 \cdot 10^{-2}(E/\rho_c \Delta^3)^{1/2}$*, $\theta = 40\alpha\tau_k$, and $\alpha = 1.345$ for $\gamma = 1.25$. The impact parameter A is, to the same approximation, given by $A = e^{1.9}\rho_c \Delta\theta^{-\alpha} = 6.7\rho_c \Delta\theta^{-\alpha}$.

It has been estimated using actual numerical values† of the parameters that the distance through which the shock wave moves downward while decelerating from the transition velocity D_1 to the velocity $D \approx 1$ km/sec, a speed a few times the speed of sound in cold air, is approximately 2 to 3 times the scale height Δ. To this is added the distance of about 2Δ downwards from the explosion center, obtained from the theory given in [28, 29]. Thus a shock wave produced by a strong explosion moves downward from the point of the explosion through a distance of about 4 to 5 times Δ in decelerating to a velocity of the order of 1 km/sec.

§25. Self-similar motion of a shock wave in the direction of decreasing density. Application to an explosion

We now consider the self-similar propagation of a shock wave in the exponential atmosphere of (12.66) in the direction from $+\infty$ to $-\infty$. This problem is analogous to that of the emergence of a shock wave at the surface of a star (see Part 3 of this chapter) with the sole difference that there the atmospheric density did not have an exponential but rather a power-law behavior. However, it is the exponential character of the atmosphere which imparts to the motion its special features. The problem as formulated was solved by one of the present authors [31]. It is clear that this solution can also be used to describe the motion of the upper part of the shock wave

* The numerical values of the parameters D_1 and θ depend only weakly on the choice of the transition value of p_f/p_c. Thus, for example, for the last time calculated in [29], $t = 23.4\tau_k$, which was close to the time of the atmospheric break-through, $z \approx 2\Delta$, $D = 2.12 \cdot 10^{-2}\Delta/\tau_k$, $p_f/p_c = 22$.

† *Editors' note.* This estimate appears to be for a high energy, high altitude explosion, say of the order of 10^{24} erg at 100 km altitude. Only a high energy, high altitude explosion will "break-through" or "vent" in the sense of the Kompaneets model. The reader should be warned that at high altitudes the hydrodynamic model of a strong explosion fails, because of the large values of photon mean free paths at very low densities.

resulting from a strong explosion and those neighboring regions which, some time after the explosion, "break loose" from the sphere of influence of the central regions.

We assume that the shock wave emerges at the "boundary" of the atmosphere $x = -\infty$, where $\rho_0 = 0$, at the time $t = 0$; thus we take the time prior to emergence as negative. All our considerations regarding the dimensional properties of the motion in an exponential atmosphere presented at the beginning of §23 hold here as well. Therefore, all of the equations of §23 are applicable. The only feature which must be taken into account is the change in the sign of the time. The front velocity is as before

$$D = \dot{X} = \alpha \frac{\Delta}{t}, \qquad t < 0, \quad D < 0,$$

and the coordinate of the front is now given by

$$X = \alpha \Delta \ln(-t) + const.$$

The Lagrangian coordinate of the front is

$$M = A(-t)^{\alpha}, \qquad \alpha > 0.$$

As before, the constant A characterizes the strength of the shock wave source*. Equations (12.71), (12.75), and the basic differential equation (12.76) remain unchanged, and only the region of integration changes. Previously $\eta = m/M$ varied from 1 at the wave front to 0 in the low-density regions. In the present case it varies from 1 at the front to ∞ in the high-density regions. The boundary conditions at the front remain the same as before, while the boundary condition for $\eta = \infty$, which corresponds to the time $t = 0$ ($M = 0$), is defined so that in the limit $t \to 0$ time disappears from equations (12.71).

Results of numerical calculations for the two specific heat ratios $\gamma = 1.2$ and $\gamma = 5/3$ are shown in Figs. 12.24 and 12.25. The similarity exponents were found to be $\alpha = 6.48$ and $\alpha = 4.90$†, respectively. For sufficiently large η the equations can be solved by means of an approximate analytic solution

* Of course, the similarity exponent α and constant A are unrelated to the corresponding quantities of §23, since the problem is completely different.

† *Editors' note.* Calculations of one of the editors give the following values for α in this problem [33]:

γ	α	γ	α
2	4.57	4/3	5.68
5/3	4.90	9/7	5.90
3/2	5.18	5/4	6.10
7/5	5.45	11/9	6.29
		6/5	6.47

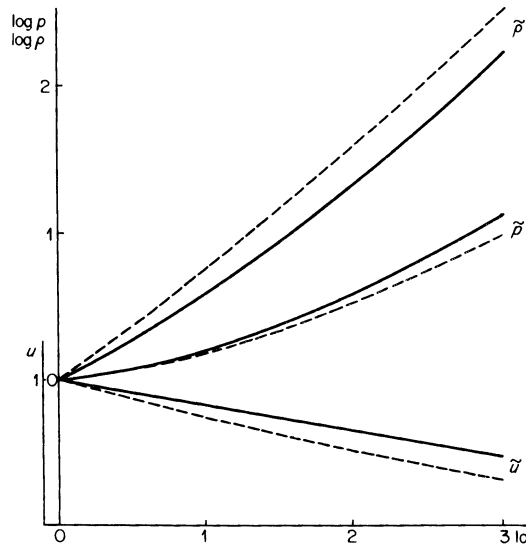

Fig. 12.24. Distributions of reduced pressure $\tilde{p}$, density $\tilde{\rho}$, and velocity $\tilde{u}$ as functions of the mass coordinate for the upward motion of the shock wave. The solid curves are for $\gamma = 1.2$ and the dashed ones for $\gamma = 5/3$.

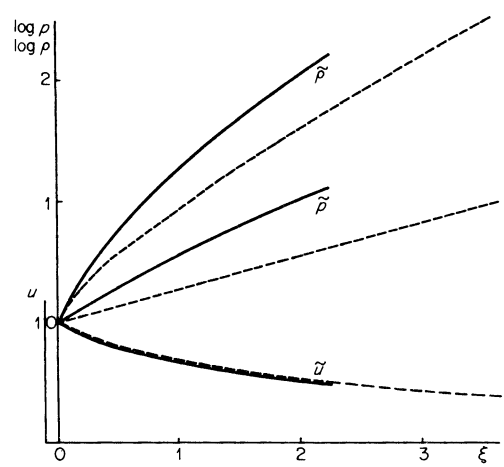

Fig. 12.25. Spatial distributions of reduced pressure $\tilde{p}$, density $\tilde{\rho}$, and velocity $\tilde{u}$ for the upward motion of the shock wave. The solid curves are for $\gamma = 1.2$ and the dashed ones for $\gamma = 5/3$.

from which the velocity, pressure, and density distributions can be determined as functions of the mass at the time of emergence of the shock wave at the "boundary" of the atmosphere. From this solution

$$(u)_{t=0} \sim -m^{-1/2}, \qquad (p)_{t=0} \sim m^{1-2/\alpha}, \qquad (\rho)_{t=0} = \frac{m}{\Delta}^{*}.$$

The third of these equations shows that each gas particle (with Lagrangian coordinate m), compressed by the shock wave by the factor $(\gamma+1)/(\gamma-1)$, at the time $t=0$ has expanded to its initial density $\rho_0 = m/\Delta$. This means that at the time when the shock wave emerges at the "boundary", the initial atmosphere as a whole has been displaced in the direction of motion by a definite distance d. This displacement is found to be equal to $d/\Delta = 7.50$ for $\gamma = 1.2$ and to $d/\Delta = 4.57$ for $\gamma = 5/3$. Each of the particles of the gas at the time $t=0$ has been accelerated to a velocity larger by a known factor than the velocity which it acquired at the time of shock compression. This factor is 1.54 for $\gamma = 1.2$ and 1.85 for $\gamma = 5/3$.

After the shock wave emerges at the "boundary" (after "breaking through" the atmosphere) and $t > 0$, the gas continues to expand in the direction of the vacuum. This outflow remains self-similar, since it is characterized by the same pair of dimensional parameters Δ and A, the similarity exponent α remaining unchanged. It was for this motion that the approximate analytic solution of [31] was obtained. It was shown that after "breaking through" the atmosphere the gas particles fly upward practically without further acceleration, by inertia at constant velocity.

In order to apply the solution obtained to the description of the flow field in the upper region of the atmosphere far above the explosion point, it is necessary to relate the arbitrary parameter A with the quantities which characterize the explosion, with the energy E and the density ρ_c at the level of the explosion. To do this we can use the estimate (12.65) for the velocity of a shock wave propagating upward. We can determine the numerical coefficient in the formula by means of (12.64), which applies to an explosion in a homogeneous atmosphere. As can be seen from (12.65), the wave velocity first decreases as the wave moves away from the point of explosion (the density decrease does not as yet affect the motion), and then begins to increase. It has a minimum at $R = 3\Delta$. It can be assumed approximately that the time at which the wave begins to accelerate is the time when the self-similar relation $|D| = \alpha\Delta/(-t)$ governing the motion becomes applicable†. From this relation

* The proportionality coefficients are given in [31].

† *Editors' note.* The effect of the curvature of the rising shock on its propagation in an exponential atmosphere is not negligible. Approximate calculations of one of the editors for $\gamma = 7/5$ give $\alpha = 7.89$ for a rising curved shock wave in place of the 5.45 valid for the plane shock [34].

the time required by the wave to move to infinity is found to be equal to

$$\tau = \frac{\alpha\Delta}{|D|_{\min}} = const\left(\frac{\Delta^5}{\rho_c E}\right)^{1/2} *.$$

For $\gamma = 1.2$ the constant is equal to 25, which is almost exactly the value found in [29]. Consequently, the same result could have been obtained by "tying" the self-similar solution to the calculations of [29]. Knowing the time $t = -\tau$ when the wave is at a distance $R = 3\Delta$ above the point of explosion, i.e., at a point with a known Lagrangian coordinate, we can also determine A,

$$A = const\, E^{\alpha/2}\Delta^{1-5\alpha/2}\rho_c^{1-\alpha/2}.$$

In conclusion we note that in principle, the air layers accelerated by the shock wave to high velocities, exceeding the earth's escape velocity, should have broken loose from the earth's gravitational field and "spilled out" into space. However, owing to the ionization of the air that has been highly heated by the strong shock wave, its upward expansion is limited by the decelerating effect of the earth's magnetic field. Some problems relating to the expansion of a highly rarefied plasma into a vacuum containing a magnetic field were considered in [32].

* The time for the wave to move from the point of the explosion to the point $R = 3\Delta$ is much smaller than τ.

Cited references

Editors' note:

In the references cited we have used, as far as possible, the abbreviations for journals and reports used by *Chemical Abstracts*. A list of these abbreviations may be found in the List of Periodicals of the Chemical Abstracts Service published by the American Chemical Society.

Transliteration of Russian names has essentially followed the system adopted by the Library of Congress, but with no distinction between e and ё or between и and й, and with yu used for ю and ya for я. In the case of books translated from Russian into English the transliterated author names are those appearing on the translation. Russian titles have been translated into English, but where a translation is indicated the title given is that appearing on the translated version. A source of an English translation for all cited Russian references has been given whenever known to the editors.

Chapter VII

1. Landau, L. D., and Lifshitz, E. M.
   Fluid Mechanics. Addison-Wesley, Reading, Mass., 1959.
2. Becker, R.
   Stosswelle und Detonation, *Z. Physik* **8**, 321–362 (1922).
3. Morduchow, M., and Libby, P. A.
   On a complete solution of the one-dimensional flow equations of a viscous, heat conducting, compressible gas, *J. Aeron. Sci.* **16**, 674–684, 704 (1949).
4. Meyerhoff, L.
   An extension of the theory of the one-dimensional shock-wave structure, *J. Aeron. Sci.* **17**, 775–786 (1950).
5. Thomas, L. H.
   Note on Becker's theory of the shock front, *J. Chem. Phys.* **12**, 449–453 (1944).
6. Herpin, A.
   La théorie cinétique de l'onde de choc, *Rev. Sci.* **86**, 35–37 (1948).
7. Puckett, A. E., and Stewart, H. J.
   The thickness of a shock wave in air, *Quart. Appl. Math.* **7**, 457–463 (1950).
8. von Mises, R.
   On the thickness of a steady shock wave, *J. Aeron. Sci.* **17**, 551–554, 594 (1950).
9. Lieber, P., Romano, F., and Lew, H.
   Approximate solutions for shock waves in a steady, one-dimensional, viscous and compressible gas, *J. Aeron. Sci.* **18**, 55–60 (1951).
10. Gilbarg, D., and Paolucci, D.
    The structure of shock waves in the continuum theory of fluids, *J. Rational Mech. Anal.* **2**, 617–642 (1953).

11. Bernard, J. J.
Thickness of a steady shock wave, *J. Aeron. Sci.* **18**, 210 (1951).
12. Roy, M.
Sur la structure de l'onde de choc, limite d'une quasi-onde de choc dans un fluide compressible et visqueux, *Compt. Rend.* **218**, 813–816 (1944).
13. Libby, P. A.
The effect of Prandtl number on the theoretical shock-wave thickness, *J. Aeron. Sci.* **18**, 286–287 (1951).
14. Zoller, K.
Zur Struktur des Verdichtungsstosses, *Z. Physik* **130**, 1–38 (1951).
15. Cowan, G. R., and Hornig, D. F.
The experimental determination of the thickness of a shock front in a gas, *J. Chem. Phys.* **18**, 1008–1018 (1950).
Greene, E. F., Cowan, G. R., and Hornig, D. F.
The thickness of shock fronts in argon and nitrogen and rotational heat capacity lags, *J. Chem. Phys.* **19**, 427–434 (1951).
Greene, E. F., and Hornig, D. F.
The shape and thickness of shock fronts in argon, hydrogen, nitrogen, and oxygen, *J. Chem. Phys.* **21**, 617–624 (1953).
16. Mott-Smith, H. M.
The solution of the Boltzmann equation for a shock wave, *Phys. Rev.* **82**, 885–892 (1951).
17. Sakurai, A.
A note on Mott-Smith's solution of the Boltzmann equation for a shock wave, *J. Fluid Mech.* **3**, 255–260 (1957).
Note on Mott-Smith's solution of the Boltzmann equation for a shock wave II, *Research Report, Tokyo Electrical Engineering College*, 1958, No. 6, 49–51.
18. Lord Rayleigh
Aerial plane waves of finite amplitude, *Proc. Roy. Soc. (London), Ser. A* **84**, 247–284 (1910).
19. Chapman, S., and Cowling, T. G.
The Mathematical Theory of Non-Uniform Gases, Cambridge Univ. Press, New York, 2nd edition, 1958.
Frank-Kamenetskii, D. A.
Diffusion and Heat Exchange in Chemical Kinetics. Izdat. Akad. Nauk SSSR, Moscow, 1947. English transl. by N. Thon, Princeton Univ. Press, Princeton, 1955.
19a. Zhdanov, V., Kagan, Yu., and Sazykin, A.
Effect of viscous transfer of momentum on diffusion in a gas mixture, *Soviet Phys. JETP (English Transl.)* **15**, 596–602 (1962).
20. D'yakov, S. P.
Shock waves in binary mixtures, *Zh. Eksperim. i Teor. Fiz.* **27**, 283–287 (1954).
21. Sherman, F. S.
Shock-wave structure in binary mixtures of chemically inert perfect gases, *J. Fluid Mech.* **8**, 465–480 (1960).
22. Cowling, T. G.
The influence of diffusion on the propagation of shock waves, *Phil. Mag.* **33** (7th Series), 61–67 (1942).
23. Zel'dovich, Ya. B.
Propagation of shock waves in a gas in the presence of a reversible chemical reaction, *Zh. Eksperim. i Teor. Fiz.* **16**, 365–368 (1946).
24. Zel'dovich, Ya. B.

Theory of Shock Waves and an Introduction to Gasdynamics. Izdat. Akad. Nauk SSSR, Moscow, 1946.

25. Griffith, W., Brickl, D., and Blackman, V.
Structure of shock waves in polyatomic gases, *Phys. Rev.* **102**, 1209–1216 (1956).
26. Blackman, V.
Vibrational relaxation in oxygen and nitrogen, *J. Fluid Mech.* **1**, 61–85 (1956).
27. Matthews, D. L.
Interferometric measurement in the shock tube of the dissociation rate of oxygen *Phys. Fluids* **2**, 170–178 (1959).
28. Losev, S. A.
Investigation of the dissociation process of oxygen behind a strong shock wave, *Dokl. Akad. Nauk SSSR* **120**, 1291–1293 (1958).
29. Generalov, N. A., and Losev, S. A.
On an investigation of nonequilibrium phenomena behind the front of a shock wave in air. Dissociation of oxygen, *Zh. Prikl. Mekhan. i Tekhn. Fiz.*, 1960, No. 2, 64–73.
30. Britton, D., Davidson, N., Gehman, W., and Schott, G.
Shock waves in chemical kinetics: further studies on the rate of dissociation of molecular iodine, *J. Chem. Phys.* **25**, 804–809 (1956).
Britton, D., and Davidson, N.
Shock waves in chemical kinetics. Rate of dissociation of molecular bromine, *J. Chem. Phys.* **25**, 810–813 (1956).
Palmer, H. B., and Hornig, D. F.
Rate of dissociation of bromine in shock waves, *J. Chem. Phys.* **26**, 98–105 (1957).
31. Losev, S. A., and Osipov, A. I.
The study of nonequilibrium phenomena in shock waves, *Soviet Phys.–Usp.* (*English Transl.*) **4**, 525–552 (1962).
32. Duff, R. E., and Davidson, N.
Calculation of reaction profiles behind steady state shock waves. II. The dissociation of air, *J. Chem. Phys.* **31**, 1018–1027 (1959).
33. Losev, S. A., and Generalov, N. A.
On the nonequilibrium state behind a shock wave in air, *Dokl. Akad. Nauk SSSR* **133**, 872–874 (1960).
34. Biberman, L. M., and Veklenko, B. A.
Radiative processes ahead of a shock-wave front, *Soviet Phys. JETP* (*English Transl.*) **10**, 117–120 (1960).
35. Petschek, H., and Byron, S.
Approach to equilibrium ionization behind strong shock waves in argon, *Ann. Phys.* (*N.Y.*) **1**, 270–315 (1957).
36. Bond, J. W., Jr.
Structure of a shock front in argon, *Phys. Rev.* **105**, 1683–1694 (1957).
37. Rostagni, A.
Ricerche sui raggi positivi e neutrali. V. Ionizzazione per urto di ioni e di atomi, *Nuovo Cimento* **13**, 389–406 (1936).
38. Wayland, H.
The ionization of neon, krypton and xenon by bombardment with accelerated neutral argon atoms, *Phys. Rev.* **52**, 31–37 (1937).
39. Weymann, H. D.
Electron diffusion ahead of shock waves in argon, *Phys. Fluids* **3**, 545–548 (1960).
40. Manheimer-Timnat, Y., and Low, W.
Electron density and ionization rate in thermally ionized gases produced by medium strength shock waves, *J. Fluid Mech.* **6**, 449–461 (1959).

Niblett, B., and Blackman, V. H.
An approximate measurement of the ionization time behind shock waves in air, *J. Fluid Mech.* **4**, 191–194 (1958).
41. Hammerling, P., Teare, J. D., and Kivel, B.
Theory of radiation from luminous shock waves in nitrogen, *Phys. Fluids* **2**, 422–426 (1959).
42. Zel'dovich, Ya. B.
Shock waves of large amplitude in air, *Soviet Phys. JETP* (*English Transl.*) **5**, 919–927 (1957).
43. Shafranov, V. D.
The structure of shock waves in a plasma, *Soviet Phys. JETP* (*English Transl.*) **5**, 1183–1188 (1957).
44. Jukes, J. D.
The structure of a shock wave in a fully ionized gas, *J. Fluid Mech.* **3**, 275–285 (1957).
44a. Tidman, D. A.
Structure of a shock wave in fully ionized hydrogen, *Phys. Rev.* **111**, 1439–1446 (1958).
45. Greenberg, O. W., Sen, H. K., and Trève, Y. M.
Hydrodynamic model of diffusion effects on shock structure in a plasma, *Phys. Fluids* **3**, 379–386 (1960).
46. Krook, M.
Structure of shock fronts in ionized gases, *Ann. Phys.* (*N.Y.*) **6**, 188–207 (1959).
Bond, J. W., Jr.
Plasma physics and hypersonic flight, *Jet Propulsion* **28**, 228–235 (1958).
47. Raizer, Yu. P.
On the structure of the front of strong shock waves in gases, *Soviet Phys. JETP* (*English Transl.*) **5**, 1242–1248 (1957).
48. Raizer, Yu. P.
On the brightness of strong shock waves in air, *Soviet Phys. JETP* (*English Transl.*) **6**, 77–84 (1958).
49. Zel'dovich, Ya. B., and Raizer, Yu. P.
Strong shock waves in gases, *Usp. Fiz. Nauk* **63**, 613–641 (1957).
50. Belokon', V. A.
Disappearance of the isothermal jump at large radiation density, *Soviet Phys. JETP* (*English Transl.*) **9**, 235–236 (1959).
51. Imshennik, V. S.
Shock wave structure in a dense high-temperature plasma, *Soviet Phys. JETP* (*English Transl.*) **15**, 167–174 (1962).
Numerical integration of differential equations of the structure of shockwaves in plasma, *U.S.S.R. Comp. Math. Math. Phys.* (*English Transl.*) **2**, 217–229 (1963).
52. Gustafson, W. A.
On the Boltzmann equation and the structure of shock waves, *Phys. Fluids* **3**, 732–734 (1960).
53. Muckenfuss, C.
Bimodal model for shock wave structure, *Phys. Fluids* **3**, 320–321 (1960).
54. Ziering, S., and Ek, F.
Mean-free-path definition in the Mott-Smith shock wave solution, *Phys. Fluids* **4**, 765–766 (1961).
55. Glansdorff, P.
Solution of the Boltzmann equations for strong shock waves by the two-fluid model, *Phys. Fluids* **5**, 371–379 (1962).

56. Hansen, K., and Hornig, D. F.
Thickness of shock fronts in argon, *J. Chem. Phys.* **33**, 913–916 (1960).
57. Blythe, P. A.
Comparison of exact and approximate methods for analysing vibrational relaxation regions, *J. Fluid Mech.* **10**, 33–47 (1961).
58. Anisimov, S. I.
On the attainment of oscillatory equilibrium behind a shock wave, *Soviet Phys.–Tech. Phys.* (*English Transl.*) **6**, 1089–1090 (1962).
59. Generalov, N. A.
Vibrational relaxation in oxygen at high temperatures. I, *Vestn. Mosk. Univ., Ser. III: Fiz., Astron.*, 1962, No. 3, 51–59.
60. Camac, M.
O_2 vibrational relaxation in oxygen-argon mixtures, *J. Chem. Phys.* **34**, 448–459 (1961).
61. Roth, W.
Shock tube study of vibrational relaxation in the $A\ ^2\Sigma^+$ state of NO, *J. Chem. Phys.* **34**, 999–1003 (1961).
62. Matthews, D. L.
Vibrational relaxation of carbon monoxide in the shock tube, *J. Chem. Phys.* **34**, 639–642 (1961).
63. Johannesen, N. H., Zienkiewicz, H. K., Blythe, P. A., and Gerrard, J. H.
Experimental and theoretical analysis of vibrational relaxation regions in carbon dioxide, *J. Fluid Mech.* **13**, 213–224 (1962).
64. Hurle, I. R., and Gaydon, A. G.
Vibrational relaxation and dissociation of carbon dioxide behind shock waves, *Nature* **184**, 1858–1859 (1959).
65. Camac, M., and Vaughan, A.
O_2 dissociation rates in O_2-Ar mixtures, *J. Chem. Phys.* **34**, 460–470 (1961).
66. Rink, J. P., Knight, H. T., and Duff, R. E.
Shock tube determination of dissociation rates of oxygen, *J. Chem. Phys.* **34**, 1942–1947 (1961).
67. Patch, R. W.
Shock-tube measurement of dissociation rates of hydrogen, *J. Chem. Phys.* **36**, 1919–1924 (1962).
68. Allen, R. A., Keck, J. C., and Camm, J. C.
Nonequilibrium radiation and the recombination rate of shock-heated nitrogen, *Phys. Fluids* **5**, 284–291 (1962).
69. Wray, K. L., Teare, J. D., Kivel, B., and Hammerling, P.
Relaxation processes and reaction rates behind shock fronts in air and component gases, *Eighth Symposium* (*International*) *on Combustion*, pp. 328–339. Williams & Wilkins, Baltimore, 1962.
70. Lin, S. C.
Low density shock tube studies of reaction rates related to the high altitude hypersonic flight problem, *Rarefied Gas Dynamics* (L. Talbot, ed.), pp. 623–642. Academic Press, New York, 1961.
71. Sayasov, Yu. S.
On the kinetics of oxidation of nitrogen in a normal shock wave, *Zh. Prikl. Mekhan. i Tekhn. Fiz.*, 1962, No. 1, 61–67.
On the structure of an oblique shock wave in a chemically reacting gas, *Zh. Prikl. Mekhan. i Tekhn. Fiz.*, 1961, No. 6, 172–174.
72. Kuznetsov, N. M.
Shock wave structure in air taking into account the kinetics of chemical reactions, *Inzh. Fiz. Zh. Akad. Nauk Belorussk.* 1960, No. 9, 17–24.

The kinetics of chemical reactions for expanding air, *Inzh.-Fiz. Zh., Akad. Nauk Belorussk.*, 1962, No. 6, 97–101.

73. Bortner, M. H.
The effect of errors in rate constants on non-equilibrium shock layer electron density calculations, *Planetary Space Sci.* **6**, 74–78 (1961).

74. Lun'kin, Yu. P.
Measurement of entropy in the relaxation of a gas mixture behind a shock wave, *Soviet Phys.–Tech. Phys.* (*English Transl.*) **6**, 810–814 (1962).

75. Dorrance, W. H.
On the approach to chemical and vibrational equilibrium behind a strong normal shock wave, *J. Aerospace Sci.* **28**, 43–50 (1961).

76. Wetzel, L.
Precursor effects and electron diffusion from a shock front, *Phys. Fluids* **5**, 824–830 (1962).

77. Pipkin, A. C.
Diffusion from a slightly ionized region in a uniform flow, *Phys. Fluids* **4**, 1298–1302 (1961).

78. Bortner, M. H.
Shock layer electron densities considering the effects of both chemical reactions and flow field variations, *Planetary Space Sci.* **3**, 99–103 (1961).

79. Blackman, V. H., and Niblett, G. B. F.
Ionization processes in shock waves, *Fundamental Data Obtained from Shock Tube Experiments* (A. Ferri, ed.), pp. 221–241. AGARDograph No. 41, Pergamon Press, New York, 1961.

80. Lin, S. C.
Rate of ionization behind shock waves in air, *Planetary Space Sci.* **6**, 94–99 (1961).

81. Lamb, L., and Lin, S. C.
Electrical conductivity of thermally ionized air produced in a shock tube, *J. Appl. Phys.* **28**, 754–759 (1957).

82. Sisco, W. B., and Fiskin, J. M.
Basic hypersonic plasma data of equilibrium air for electromagnetic and other requirements, *Planetary Space Sci.* **6**, 47–73 (1961).

83. Viegas, J. R., and Peng, T. C.
Electrical conductivity of ionized air in thermodynamic equilibrium, *ARS J.* **31**, 654–657 (1961).

84. Sherman, A.
Calculation of electrical conductivity of ionized gases, *ARS J.* **30**, 559–560 (1960).

85. Pikel'ner, S. B.
Spectrophotometric study of the mechanism of excitation of filamentary nebulae, *Izv. Krymsk. Astrofiz. Observ.* **12**, 93–117 (1954).
Principles of Cosmic Electrodynamics. Fizmatgiz, Moscow, 1961. English transl., Gordon and Breach, New York, 1967.

86. Lin, S. C., and Teare, J. D.
Rate of ionization behind shock waves in air. II. Theoretical interpretations, *Phys. Fluids* **6**, 355–375 (1963).

87. Lin, S. C., Neal, R. A., and Fyfe, W. I.
Rate of ionization behind shock waves in air. I. Experimental results, *Phys. Fluids* **5**, 1633–1648 (1962).

88. Imshennik, V. S., and Morozov, Yu. I.
Shock wave structure taking into account momentum and energy transfer by radiation, *Zh. Prikl. Mekhan. i Tekhn. Fiz.* 1964, No. 2, 8–21.

89. Jaffrin, M. Y., and Probstein, R. F.
Structure of a plasma shock wave, *Phys. Fluids* **7**, 1658–1674 (1964).
90. Stupochenko, E. V., Losev, S. A., and Osipov, A. I.
Relaxation Processes in Shock Waves. Nauka, Moscow, 1965.
91. Wray, K. L., and Freeman, T. S.
Shock front structure in O_2 at high Mach numbers, *J. Chem. Phys.* **40**, 2785–2789 (1964).
92. Nelson, W. C. (ed.)
The High Temperature Aspects of Hypersonic Flow. AGARDograph No. 68, Pergamon Press, New York, 1964.
93. Biberman, L. M., and Yakubov, I. T.
Approach to ionization equilibrium behind the front of a shock wave in an atomic gas, *Soviet Phys.–Tech. Phys.* (*English Transl.*) **8**, 1001–1007 (1964).
94. Gloersen, P.
Precursor signals from shock waves in xenon, *Bull. Am. Phys. Soc.* **4**, 283 (1959).
95. Kornegay, W. M., and Johnston, H. S.
Kinetics of thermal ionization. II. Xenon and krypton, *J. Chem. Phys.* **38**, 2242–2247 (1963).
96. Kuznetsov, N. M.
The influence of radiation on the ionization structure of the front of a shock wave, *Soviet Phys.–Tech. Phys.* (*English Transl.*) **9**, 483–487 (1965).
97. Biberman, L. M., and Yakubov, I. T.
The state of a gas behind a strong shock-wave front, *High Temp.* (*English Transl.*) **3**, 309–320 (1965).
98. Bronshten, V. A.
Problems on the Motion of Large Meteorites in the Atmosphere. Izdat. Akad. Nauk SSSR, Moscow, 1963.
Bronshten, V. A., and Chigorin, A. N.
Establishment of equilibrium ionization in a strong shock wave in air, *High Temp.* (*English Transl.*) **2**, 774–781 (1964).
99. Biberman, L. M., and Ul'yanov, K. N.
The effect of the emission of radiation on deviation from thermodynamic equilibrium, *Opt. Spectr.* (*USSR*) (*English Transl.*) **16**, 216–220 (1964).
100. Kohler, M.
Reibung in mässig verdünnten Gasen als Folge verzögerter Einstellung der Energie, *Z. Physik* **125**, 715–732 (1949).
101. Tamm, I. E.
On the thickness of a strong shock wave, *Tr. Fiz. Inst. Akad. Nauk SSSR* **29**, 239–249 (1965). (Work completed in 1947.)

Chapter VIII

1. Kantrowitz, A.
Effects of heat capacity lag in gas dynamics, *J. Chem. Phys.* **10**, 145 (1942).
Heat-capacity lag in gas dynamics, *J. Chem. Phys.* **14**, 150–164 (1946).
2. Bloom, M. H., and Steiger, M. H.
Inviscid flow with nonequilibrium molecular dissociation for pressure distributions encountered in hypersonic flight, *J. Aerospace Sci.* **27**, 821–835, 840 (1960).
2a. Li, Ting Y.
Recent advances in nonequilibrium dissociating gasdynamics, *ARS J.* **31**, 170–178 (1961).

3. Kneser, H. O.
Zur Dispersionstheorie des Schalles, *Ann. Physik* **11** (5th Series), 761–776 (1931).
4. Kneser, H. O.
Die Dispersion hochfrequenter Schallwellen in Kohlensäure, *Ann. Physik* **11** (5th Series), 777–801 (1931).
5. Einstein, A.
Schallausbreitung in teilweise dissoziierten Gasen, *Sitzber. Berliner Akad. Wiss.* 1920, 380–385.
6. Nozdrev, V. F.
Application of Ultrasonics in Molecular Physics. Fizmatgiz, Moscow, 1958. English transl., Gordon and Breach, New York, 1963.
7. Gorelik, G. S.
Vibrations and Waves. An Introduction in Acoustics, Radiophysics, and Optics. Fizmatgiz, Moscow, 2nd edition, 1959.
8. Mandel'shtam, L. I., and Leontovich, M. A.
On the theory of sound absorption in fluids, *Zh. Eksperim. i Teor. Fiz.* **7**, 438–449 (1937).
9. Landau, L. D., and Lifshitz, E. M.
Fluid Mechanics. Addison-Wesley, Reading, Mass., 1959.
10. Landau, L. D., and Teller, E.
Zur Theorie der Schalldispersion, *Physik. Z. Sowjetunion* **10**, 34–43 (1936).
11. Ginzburg, V. L.
On a general relation between absorption and dispersion of sound waves, *Akust. Zh.* **1**, 31–39 (1955).
12. U.S. Dept. of Defense
The Effects of Atomic Weapons. McGraw-Hill, New York, 1950.
13. Raizer, Yu. P.
The formation of nitrogen oxides in the shock wave of a strong explosion in air, *Zh. Fiz. Khim.* **33**, 700–709 (1959).
14. Zel'dovich, Ya. B., Sadovnikov, P. Ya., and Frank-Kamenetskii, D. A.
The Oxidation of Nitrogen by Combustion. Izdat. Akad. Nauk SSSR, Moscow, 1947.
15. Tsukerman, V. A., and Manakova, M. A.
Sources of short X-ray pulses for investigating fast processes, *Soviet Phys.–Tech. Phys.* (*English Transl.*) **2**, 353–363 (1957).
15a. Molmud, P.
Expansion of a rarefied gas cloud into a vacuum, *Phys. Fluids* **3**, 362–366 (1960).
16. Belokon', V. A.
Tr. Mosk. Fiz. Tekhn. Inst., 1963, No. 11.
17. Raizer, Yu. P.
Residual ionization of a gas expanding in vacuum, *Soviet Phys. JETP* (*English Transl.*) **10**, 411–412 (1960).
18. Landau, L. D., and Lifshitz, E. M.
Statistical Physics. Addison-Wesley, Reading, Mass., 1958.
19. Raizer, Yu. P.
Condensation of a cloud of vaporized matter expanding in vacuum, *Soviet Phys. JETP* (*English Transl.*) **10**, 1229–1235 (1960).
20. Zel'dovich, Ya. B., and Raizer, Yu. P.
Physical phenomena that occur when bodies compressed by strong shock waves expand in vacuo, *Soviet Phys. JETP* (*English Transl.*) **8**, 980–982 (1959).
21. Frenkel, J.
Kinetic Theory of Liquids. Oxford Univ. Press, London, 1946. Republished, Dover, New York, 1955.

22. Zel'dovich, Ya. B.
Theory of the formation of a new phase. Cavitation, *Zh. Eksperim. i Teor. Fiz.* **12**, 525–538 (1942).
23. Fesenkov, V. G.
Meteoric Material in Interplanetary Space. Izdat. Akad. Nauk SSSR, Moscow, 1947.
24. Narasimha, R.
Collisionless expansion of gases into vacuum, *J. Fluid Mech.* **12**, 294–308 (1962).
25. Pressman, A. Ya.
On the flow of a rarefied gas into a vacuum from a point source, *Soviet Phys. "Doklady"* (*English Transl.*) **6**, 451–453 (1961).
26. Raizer, Yu. P.
Note on the sudden expansion of a gas cloud into vacuum, *Zh. Prikl. Mekhan. i Tekhn. Fiz.*, 1964, No. 3, 162–163.
27. Raizer, Yu. P.
The deceleration and energy conversions of a plasma expanding in a vacuum in the presence of a magnetic field, *Zh. Prikl. Mekhan. i Tekhn. Fiz.*, 1963, No. 6, 19–28. Transl. as *NASA* (*Nat. Aeron. Space Admin.*) *Tech. Transl.* No. TTF-239 (1964).
28. Kuznetsov, N. M., and Raizer, Yu. P.
On the recombination of electrons in a plasma expanding into vacuum, *Zh. Prikl. Mekhan. i Tekhn. Fiz.*, 1965, No. 4, 10–20.

Chapter IX

1. Model', I. Sh.
Measurement of high temperatures in strong shock waves in gases, *Soviet Phys. JETP* (*English Transl.*) **5**, 589–601 (1957).
2. Zel'dovich, Ya. B.
Shock waves of large amplitude in air, *Soviet Phys. JETP* (*English Transl.*) **5**, 919–927 (1957).
Zel'dovich, Ya. B., and Raizer, Yu. P.
Strong shock waves in gases, *Usp. Fiz. Nauk* **63**, 613–641 (1957).
3. Raizer, Yu. P.
On the structure of the front of strong shock waves in gases, *Soviet Phys. JETP* (*English Transl.*) **5**, 1242–1248 (1957).
4. Raizer, Yu. P.
On the brightness of strong shock waves in air, *Soviet Phys. JETP* (*English Transl.*) **6**, 77–84 (1958).
5. Vanyukov, M. P., and Mak, A. A.
High-intensity pulsed light sources, *Soviet Phys.–Usp.* (*English Transl.*) **1**, 137–155 (1958).
6. Schneider, E. G.
An estimate of the absorption of air in the extreme ultraviolet, *J. Opt. Soc. Am.* **30**, 128–132 (1940).
7. Aglintsev, K. K.
Dosimetry of Ionizing Radiation. Gostekhizdat, Moscow, 2nd edition, 1957.
8. Landolt, H. H.
Landolt-Börnstein Zahlenwerte und Funktionen aus Physik, Chemie, Astronomie, Geophysik und Technik. Vol. I. Atom-und Molekularphysik, p. 316. Springer, Berlin, 6th edition, 1950.

9. Messner, R. H.
Der Einfluss der chemischen Bindung auf den Absorptionskoeffizienten leichter Elemente im Gebiete ultraweicher Röntgenstrahlen, *Z. Physik* **85**, 727–740 (1933).
10. Dershem, E., and Schein, M.
The absorption of the $K\alpha$ line of carbon in various gases and its dependence upon atomic number, *Phys. Rev.* **37**, 1238–1245 (1931).
11. U.S. Dept. of Defense
The Effects of Atomic Weapons. McGraw-Hill, New York, 1950.
12. Glasstone, S. (ed.)
The Effects of Nuclear Weapons. U.S. Atomic Energy Comm., Washington, revised edition, 1962 (1st edition, 1957).
13. Sedov, L. I.
Similarity and Dimensional Methods in Mechanics. Gostekhizdat, Moscow, 4th edition, 1957. English transl. (M. Holt, ed.), Academic Press, New York, 1959.
14. Raizer, Yu. P.
The formation of nitrogen oxides in the shock wave of a strong explosion in air, *Zh. Fiz. Khim.* **33**, 700–709 (1959).
15. Raizer, Yu. P.
Glow of air during a strong explosion, and the minimum brightness of a fireball, *Soviet Phys. JETP* (*English Transl.*) **7**, 331–339 (1958).
16. Zel'dovich, Ya. B., Kompaneets, A. S., and Raizer, Yu. P.
Radiation cooling of air. I. General description of the phenomenon and the weak cooling wave, *Soviet Phys. JETP* (*English Transl.*) **7**, 882–889 (1958).
17. Zel'dovich, Ya. B., Kompaneets, A. S., and Raizer, Yu. P.
Cooling of air by radiation. II. Strong cooling wave, *Soviet Phys. JETP* (*English Transl.*) **7**, 1001–1006 (1958).
18. Imshennik, V. S., and Nadezhin, D. K.
Gas dynamical model of a type II supernova outburst, *Soviet Astron.–AJ* (*English Transl.*) **8**, 664–673 (1965).
19. Abramson, I. S., Gegechkori, N. M., Drabkina, S. I., and Mandel'shtam, S. L.
The passage of a spark discharge, *Zh. Eksperim. i Teor. Fiz.* **17**, 862–867 (1947).
20. Drabkina, S. I.
The theory of the development of a spark discharge column, *Zh. Eksperim. i Teor. Fiz.* **21**, 473–483 (1951).
21. Gegechkori, N. M.
Experimental investigation of a spark discharge column, *Zh. Eksperim. i Teor. Fiz.* **21**, 493–506 (1951).
22. Dolgov, G. G., and Mandel'shtam, S. L.
Density and temperature of a gas in a spark discharge, *Zh. Eksperim. i Teor. Fiz.* **24** 691–700 (1953).
23. Mandel'shtam, S. L., and Sukhodrev, N. K.
Elementary processes in a spark discharge column, *Zh. Eksperim. i Teor. Fiz.* **24**, 701–707 (1953).
24. Sukhodrev, N. K.
On excited spectra in a spark discharge, *Tr. Fiz. Inst., Akad. Nauk SSSR* **15**, 123–177 (1961).
25. Braginskii, S. N.
Theory of the development of a spark channel, *Soviet Phys. JETP* (*English Transl.*) **7**, 1068–1074 (1958).
26. Zhivlyuk, Yu. N., and Mandel'shtam, S. L.
On the temperature of lightning and the force of thunder, *Soviet Phys. JETP* (*English Transl.*) **13**, 338–340 (1961).

27. Taylor, G. I.
The formation of a blast wave by a very intense explosion. II. The atomic explosion of 1945, *Proc. Roy. Soc. (London), Ser. A* **201**, 175–186 (1950).

Chapter X

1. Zel'dovich, Ya. B., and Kompaneets, A. S.
On the propagation of heat for nonlinear heat conduction, *Collection Dedicated to the Seventieth Birthday of Academician A. F. Ioffe* (P. I. Lukirskii, ed.), pp. 61–72. Izdat. Akad. Nauk SSSR, Moscow, 1959.
2. Barenblatt, G. I.
On some unsteady motions of a liquid and a gas in a porous medium, *Prikl. Mat. i Mekh.* **16**, 67–78 (1952).
3. Andriankin, E. I., and Ryzhov, O. S.
Propagation of an almost-spherical thermal wave, *Dokl. Akad. Nauk SSSR* **115**, 882–885 (1957).
4. Andriankin, E. I.
Propagation of a non-self-similart hermal wave, *Soviet Phys. JETP (English Transl.)* **8** 295–298 (1959).
5. Barenblatt, G. I.
On the approximate solution of problems of uniform unsteady filtration in a porous medium, *Prikl. Mat. i Mekh.* **18**, 351–370 (1954).
6. Barenblatt, G. I., and Zel'dovich, Ya. B.
On the dipole-type solution in problems of unsteady gas filtration in the polytropic regime, *Prikl. Mat. i Mekh.* **21**, 718–720 (1957).
7. Marshak, R. E.
Effect of radiation on shock wave behavior, *Phys. Fluids* **1**, 24–29 (1958).
8. Nemchinov, I. V.
Some unsteady radiative heat transfer problems, *Zh. Prikl. Mekhan. i Tekhn. Fiz.*, 1960, No. 1, 36–57.
9. Zel'dovich, Ya. B., and Barenblatt, G. I.
The asymptotic properties of self-modelling solutions of the nonstationary gas filtration equations, *Soviet Phys. "Doklady" (English Transl.)* **3**, 44–47 (1958).
10. Kompaneets, A. S., and Lantsburg, E. Ya.
The heating of gas by radiation, *Soviet Phys. JETP (English Transl.)* **14**, 1172–1176 (1962).
11. Kompaneets, A. S., and Lantsburg, E. Ya.
Propagation of a nonequilibrium heat wave with account of the finite velocity of light, *Soviet Phys. JETP (English Transl.)* **16**, 167–171 (1963).

Chapter XI

1. Al'tshuler, L. V., Krupnikov, K. K., Ledenev, B. N., Zhuchikhin, V. I., and Brazhnik, M. I.
Dynamic compressibility and equation of state of iron under high pressure, *Soviet Phys. JETP (English Transl.)* **7**, 606–614 (1958).
2. Al'tshuler, L. V., Krupnikov, K. K., and Brazhnik, M. I.
Dynamic compressibility of metals under pressures from 400,000 to 4,000,000 atmospheres, *Soviet Phys. JETP (English Transl.)* **7**, 614–619 (1958).

3. Al'tshuler, L. V., Kormer, S. B., Bakanova, A. A., and Trunin, R. F.
Equation of state for aluminum, copper, and lead in the high pressure region, *Soviet Phys. JETP* (*English Transl.*) **11**, 573–579 (1960).
4. Al'tshuler, L. V., Kormer, S. B., Brazhnik, M. I., Vladimirov, L. A., Speranskaya, M. P., and Funtikov, A. I.
The isentropic compressibility of aluminum, copper, lead, and iron at high pressures, *Soviet Phys. JETP* (*English Transl.*) **11**, 766–775 (1960).
5. Al'tshuler, L. V., Kuleshova, L. V., and Pavlovskii, M. N.
The dynamic compressibility, equation of state, and electrical conductivity of sodium chloride at high pressures, *Soviet Phys. JETP* (*English Transl.*) **12**, 10–15 (1961).
6. Shnirman, G. L., Dubovik, A. S., and Kevlishvili, P. V.
High-speed photorecording device for SFR (photographic scanning, *eds.*). Izdat. Inst. Tekhn.-Ekonom. Inform. Akad. Nauk SSSR, Moscow, 1957.
7. Dubovik, A. S.
Elements of the theory of mirror scanning, *Zh. Nauchn. i Prikl. Fotogr. i Kinematogr.* **2**, 293–303 (1957).
Mirror compensator of the displacement of photographic film, *Zh. Nauchn. i Prikl Fotogr. i Kinematogr.* **4**, 226–233 (1959).
8. Dubovik (Dubowik), A. S., Kevlishvili, P. V., and Shnirman, G. L.
Zeitlupe mit Mehrfach-Reflexion, *Kurzzeitphotographie Bericht über den IV. Internationalen Kongress für Kurzzeitphotographie und Hochfrequenzkinematographie* (H. Schardin and O. Helwich, eds.), pp. 196–201. Verlag Dr. Othmar Helwich, Darmstadt, 1959.
9. Shnirman, G. L.
Some problems of developing time magnification and photochronographs with a mirror scanner, *Usp. Nauchn. Fotogr., Akad. Nauk SSSR, Otd. Khim. Nauk* **6**, 93–101 (1959).
10. Dubovik, A. S.
Some problems in the theory of mirror scanning, *Usp. Nauchn. Fotogr., Akad. Nauk SSSR, Otd. Khim. Nauk* **6**, 102–112 (1959).
11. Tsukerman (Zuckermann), V. A., and Manakova, M. A.
Röntgen-Blitzquellen zur Untersuchung schnellverlaufender Vorgänge, *Kurzzeitphotographie: Bericht über den IV. Internationalen Kongress für Kurzzeitphotographie und Hochfrequenzkinematographie* (H. Schardin and O. Helwich, eds.), pp. 118–122. Verlag Dr. Othmar Helwich, Darmstadt, 1959.
12. Butslov, M. M., Zavoiskii, E. K., Plakhov, A. G., Smolkin, G. E., and Fanchenko, S. D.
Electron-optical method for studying short-duration phenomena, *Kurzzeitphotographie: Bericht über den IV. Internationalen Kongress für Kurzzeitphotographie und Hochfrequenzkinematographie* (H. Schardin and O. Helwich, eds.), pp. 230–242. Verlag Dr. Othmar Helwich, Darmstadt, 1959.
13. Gombàs, P.
Die statistische Theorie des Atoms und ihre Anwendungen. Springer, Wien, 1949.
14. Kormer, S. B., and Urlin, V. D.
Interpolation equations of state of metals for the region of ultrahigh pressures, *Soviet Phys. "Doklady"* (*English Transl.*) **5**, 317–320 (1960).
15. Kormer, S. B., Urlin, V. D., and Popova, L. T.
Interpolation equation of state and its application to experimental data on impact compression of metals, *Soviet Phys.–Solid State* (*English Transl.*) **3**, 1547–1553 (1962).
16. Landau, L. D., and Lifshitz, E. M.
Statistical Physics. Addison-Wesley, Reading, Mass., 1958.
17. Slater, J. C.
Introduction to Chemical Physics. McGraw-Hill, New York, 1st edition, 1939.

18. Landau, L. D., and Stanyukovich, K. P.
On a study of the detonation of condensed explosives, *Compt. Rend. (Doklady) Acad. Sci. URSS* **46**, 362–364 (1945).
19. Gilvarry, J. J.
Thermodynamics of the Thomas-Fermi atom at low temperature, *Phys. Rev.* **96**, 934–943 (1954).
Solution of the temperature-perturbed Thomas-Fermi equation, *Phys. Rev.* **96**, 944–948 (1954).
Gilvarry, J. J., and Peebles, G. H.
Solutions of the temperature-perturbed Thomas-Fermi equation, *Phys. Rev.* 99, 550–552 (1955).
20. Latter, R.
Temperature behavior of the Thomas-Fermi statistical model for atoms, *Phys. Rev.* **99**, 1854–1870 (1955).
21. Baum, F. A., Stanyukovich, K. P., and Shekhter, B. I.
Explosion Physics. Fizmatgiz, Moscow, 1959.
22. Walsh, J. M., and Christian, R. H.
Equation of state of metals from shock wave measurements, *Phys. Rev.* **97**, 1544–1556 (1955).
23. Walsh, J. M., Rise, M. H., McQueen, R. G., and Yarger, F. L.
Shock-wave compressions of twenty-seven metals. Equations of state of metals, *Phys. Rev.* **108**, 196–216 (1957).
24. Goranson, R. W., Bancroft, D., Blendin, L. B., Blechar, T., Houston, E. E., Gittings, E. F., and Landeen, S. A.
Dynamic determination of the compressibility of metals, *J. Appl. Phys.* **26**, 1472–1479 (1955).
25. Mallory, H. D.
Propagation of shock waves in aluminum, *J. Appl. Phys.* **26**, 555–559 (1955).
26. McQueen, R. G., and Marsh, S. P.
Equation of state for nineteen metallic elements from shock-wave measurements to two megabars, *J. Appl. Phys.* **31**, 1253–1269 (1960).
27. Dugdale, J. S., and McDonald, D. K. C.
The thermal expansion of solids, *Phys. Rev.* **89**, 832–834 (1953).
28. Landau, L. D., and Lifshitz, E. M.
Theory of Elasticity. Addison-Wesley, Reading, Mass., 1959.
29. Rakhmatulin, Kh. A., and Shapiro, G. S.
Propagation of disturbances in nonlinear-elastic and inelastic media, *Izv. Akad. Nauk SSSR, Otd. Tekhn. Nauk*, 1955, No. 2, 68–89.
30. Bancroft, D., Peterson, E. L., and Minshall, S.
Polymorphism of iron at high pressures, *J. Appl. Phys.* **27**, 291–298 (1956).
31. Duff, R. E., and Minshall, F. S.
Investigation of a shock-induced transition in bismuth, *Phys. Rev.* **108**, 1207–1212 (1957).
32. Drummond, W. E.
Multiple shock production, *J. Appl. Phys.* **28**, 998–1001 (1957).
33. Dremin, A. N., and Adadurov, G. A.
Shock adiabatic for marble, *Soviet Phys.* "*Doklady*" (*English Transl.*) **4**, 970–973 (1960).
34. Dremin, A. N., and Karpukhin, I. A.
Method of determining the Hugoniot curves for dispersive media, *Zh. Prikl. Mekhan. i Tekhn. Fiz.*, 1960, No. 3, 184–187.

35. Alder, B. J., and Christian, R. H.
Destruction of diatomic bonds by pressure, *Phys. Rev. Letters* **4**, 450–452 (1960).
36. Lifshitz, I. M.
Anomalies of electron characteristics of a metal in the high pressure region, *Soviet Phys. JETP* (*English Transl.*) **11**, 1130–1135 (1960).
37. Gandel'man, G. M.
Quantum-mechanical derivation of an equation of state of iron, *Soviet Phys. JETP* (*English Transl.*) **16**, 94–103 (1963).
38. Ivanov, A. G., and Novikov, S. A.
Rarefaction shock waves in iron and steel, *Soviet Phys. JETP* (*English Transl.*) **13**, 1321–1323 (1961).
39. Zadumkin, S. N.
Approximate estimate of the critical temperatures of liquid metals, *Inzh.-Fiz. Zh., Akad. Nauk Belorussk.*, 1960, No. 10, 63–65.
40. *Handbook of Chemistry, Vol. 1.* Goskhimizdat, Moscow, 1951.
41. Zel'dovich, Ya. B., Kormer, S. B., Sinitsyn, M. V., and Kuryapin, A. I.
Temperature and specific heat of Plexiglas under shock wave compression, *Soviet Phys. "Doklady"* (*English Transl.*) **3**, 938–939 (1958).
42. Zel'dovich, Ya. B.
Investigations of the equation of state by mechanical measurements, *Soviet Phys. JETP* (*English Transl.*) **5**, 1287–1288 (1957).
43. Zel'dovich, Ya. B., and Raizer, Yu. P.
Physical phenomena that occur when bodies compressed by strong shock waves expand in vacuo, *Soviet Phys. JETP* (*English Transl.*) **8**, 980–982 (1959).
44. Urlin, V. D., and Ivanov, A. A.
Melting under shock-wave compression, *Soviet Phys. "Doklady"* (*English Transl.*) **8**, 380–382 (1963).
45. Brish, A. A., Tarasov, M. S., and Tsukerman, V. A.
Electric conductivity of the explosion products of condensed explosives, *Soviet Phys. JETP* (*English Transl.*) **10**, 1095–1100 (1960).
46. Brish, A. A., Tarasov, M. S., and Tsukerman, V. A.
Electric conductivity of dielectrics in strong shock waves, *Soviet Phys. JETP* (*English Transl.*) **11**, 15–17 (1960).
47. Alder, B. J., and Christian, R. H.
Metallic transition in ionic and molecular crystals, *Phys. Rev.* **104**, 550–551 (1956).
48. Zel'dovich, Ya. B., and Landau, L. D.
On the relation between the liquid and gaseous states in metals, *Zh. Eksperim. i Teor. Fiz.* **14**, 32–34 (1944).
49. Abrikosov, A. A.
Equation of state of hydrogen at high pressures, *Astron. Zh.* **31**, 112–123 (1954).
50. Bridgman, P. W.
The Physics of High Pressure. Macmillan, New York, 1931.
Recent work in the field of high pressures, *Rev. Mod. Phys.* **18**, 1–93 (1946).
51. Zel'dovich, Ya. B., Kormer, S. B., Sinitsyn, M. V., and Yushko, K. B.
A study of the optical properties of transparent materials under high pressure, *Soviet Phys. "Doklady"* (*English Transl.*) **6**, 494–496 (1961).
52. Landau, L. D., and Lifshitz, E. M.
Electrodynamics of Continuous Media. Addison-Wesley, Reading, Mass., 1960.
53. Cowan, G. R., and Hornig, D. F.
The experimental determination of the thickness of a shock front in a gas, *J. Chem. Phys.* **18**, 1008–1018 (1950).

54. Ginzburg, V. L., and Motulevich, G. P.
Optical properties of metals, *Usp. Fiz. Nauk* **55**, 469–535 (1955).
55. Al'tshuler, L. V.
Use of shock waves in high-pressure physics, *Soviet Phys.–Usp.* (*English Transl.*) **8**, 52–91 (1965).
56. Kormer, S. B., Funtikov, A. I., Urlin, V. D., Kolesnikova, A. N.
Dynamic compression of porous metals and the equation of state with variable specific heat at high temperatures, *Soviet Phys. JETP* (*English Transl.*) **15**, 477–488 (1962).
57. Kuznetsov, N. M.
The break in a Hugoniot curve in a phase transition of the first kind, *Dokl. Akad. Nauk SSSR* **155**, 156–159 (1964).
58. Kuznetsov, N. M.
On the kinetics of shock melting of polycrystals, *Zh. Prikl. Mekhan. i Tekhn. Fiz.*, 1965, No. 1, 112–114. Also *J. Appl. Mech. and Tech. Phys.* (*English Transl.*), 1965, No. 1, 104–106.
59. Urlin, V. D.
Melting at ultra high pressures in a shock wave, *Soviet Phys. JETP* (*English Transl.*) **22** 341–346 (1966).
60. Duvall, G. E.
Some properties and application of shock waves, *Response of Metals to High Velocity Deformation* (P. G. Shewmon and V. F. Zackay, eds.), pp. 165–203. Wiley (Interscience), New York, 1961.
Duvall, G. E., and Fowles, G. R.
Shock waves, *High Pressure Physics and Chemistry, Vol. 2* (R. S. Bradley, ed.), pp. 209–291. Academic Press, New York, 1963.
61. Donnell, L. H.
Longitudinal wave transmission and impact, *Trans. ASME* (*Am. Soc. Mech. Eng.*) **52**, APM 153–167 (1930).
62. Bethe, H. A.
Theory of shock waves for an arbitrary equation of state, *Off. Sci. Res. Dev. Rept.* No. 545, 1942.

Chapter XII

1. Stanyukovich, K. P.
Unsteady Motion of Continuous Media. Gostekhizdat, Moscow, 1955. English transl. (M. Holt, ed.), Academic Press, New York, 1960.
2. Sedov, L. I.
Similarity and Dimensional Methods in Mechanics. Gostekhizdat, Moscow, 4th edition, 1957. English transl. (M. Holt, ed.), Academic Press, New York, 1959.
3. Guderley, G.
Starke kugelige und zylindrische Verdichtungstösse in der Nähe des Kugelmittelpunktes bzw. der Zylinderische, *Luftfahrtforschung* **19**, 302–312 (1942).
4. Lord Rayleigh
On the pressure developed in a liquid during the collapse of a spherical cavity, *Phil. Mag.* **34** (6th Series), 94–98 (1917).
5. Hunter, C.
On the collapse of an empty cavity in water, *J. Fluid Mech.* **8**, 241–263 (1960).
6. Zababakhin, E. I.
The collapse of bubbles in a viscous liquid, *Appl. Math. Mech., PMM* (*English Transl.*) **24**, 1714–1717 (1960).

7. Frank-Kamenetskii, D. A.
Nonadiabatic pulsations in stars, *Dokl. Akad. Nauk SSSR* **80**, 185–188 (1951).
8. Gandel'man, G. M., and Frank-Kamenetskii, D. A.
Shock wave emergence at a stellar surface, *Soviet Phys. "Doklady" (English Transl.)* **1**, 223–226 (1956).
9. Sakurai, A.
On the problem of a shock wave arriving at the edge of a gas, *Commun. Pure Appl. Math.* **13**, 353–370 (1960).
10. Ginzburg, V. L., and Syrovatskii, S. I.
Present status of the question of the origin of cosmic rays, *Soviet Phys.–Usp. (English Transl.)* **3**, 504–541 (1961).
11. Colgate, S. A., and Johnson, M. H.
Hydrodynamic origin of cosmic rays, *Phys. Rev. Letters* **5**, 235–238 (1960).
12. Zel'dovich, Ya. B.
Motion of a gas under the action of an impulsive pressure (load), *Akust. Zh.* **2**, 28–38 (1956).
13. Adamskii, V. B.
Integration of the system of self-similar equations in the problem of an impulsive load on a cold gas, *Akust. Zh.* **2**, 3–9 (1956).
14. Zhukov, A. I., and Kazhdan, Ya. M.
On the motion of a gas under the action of a short duration impulse, *Akust. Zh.* **2** 352–357 (1956).
15. Häfele, W.
Zur analytischen Behandlung ebener, starker, instationärer Stosswellen, *Z. Naturforsch.* **10a**, 1006–1016 (1955).
16. von Hoerner, S.
Lösungen der hydrodynamischen Gleichungen mit linearem Verlauf der Geschwindigkeit, *Z. Naturforsch.* **10a**, 687–692 (1955).
17. von Weizsäcker, C. F.
Genäherte Darstellung starker instationärer Stosswellen durch Homologie-Lösungen, *Z. Naturforsch.* **9a**, 269–275 (1954).
18. Adamskii, V. B., and Popov, N. A.
The motion of a gas under the action of a pressure on a piston varying according to a power law, *Appl. Math. Mech., PMM (English Transl.)* **23**, 793–806 (1959).
19. Krasheninnikova, N. L.
On the unsteady motion of a gas displaced by a piston, *Izv. Akad. Nauk SSSR, Otd. Tekhn. Nauk*, 1955, No. 8, 22–36.
20. Raizer, Yu. P.
Motion of a gas under the action of a concentrated impact along its surface (as a result of an explosion on the surface), *Zh. Prikl. Mekhan. i Tekhn. Fiz.*, 1963, No. 1, 57–66.
21. Astapovich, I. S.
Second conference on comet and meteor astronomy, Moscow 29–31 January 1937, *Astron. Zh.* **14**, 248–250 (1937).
Stanyukovich, K. P., and Fedynskii, V. V.
On the destructive effect of meteor impacts, *Dokl. Akad. Nauk SSSR* **57**, 129–132 (1947).
Stanyukovich, K. P.
Elements of the physical theory of meteors and the formation of meteor craters, *Meteoritika*, 1950, No. 7, 39–62.
Elements of the theory of the impact of solid bodies with high (cosmic) velocities, *Iskusstvenyie Sputniki Zemli* **4**, 86–117 (1960). English transl. *Artificial Earth Satellites, Vols. 3–5* (L. V. Kurnosova, ed.), pp. 292–333. Plenum Press, New York, 1961.

22. Stanyukovich, K. P.
On an effect in the area of the aerodynamics of meteors, *Izv. Akad. Nauk SSSR, Otd. Tekh. Nauk, Mekh. i Mashinostr.*, 1960, No. 5, 3–8.
23. Lavrent'ev, M. A.
The problem of piercing at cosmic velocities, *Iskusstvenyie Sputniki Zemli* **3**, 61–65 (1959). English transl. *Artificial Earth Satellites, Vols. 3–5* (L. V. Kurnosova, ed.), pp. 85–91. Plenum Press, New York, 1961.
24. Kompaneets, A. S.
Shock waves in a plastic compacting medium, *Dokl. Akad. Nauk SSSR* **109**, 49–52 (1956).
25. Andriankin, E. I., and Koryavov, B. P.
Shock waves in a variable compacting plastic medium, *Soviet Phys. "Doklady" (English Transl.)* **4**, 966–969 (1960).
26. Zel'dovich, Ya. B.
Cylindrical self-similar acoustical waves, *Soviet Phys. JETP (English Transl.)* **6**, 537–541 (1958).
27. Zababakhin, E. I., and Nechaev, M. N.
Electromagnetic-field shock waves and their cumulation, *Soviet Phys. JETP (English Transl.)* **6**, 345–351 (1958).
28. Kompaneets, A. S.
A point explosion in an inhomogeneous atmosphere, *Soviet Phys. "Doklady" (English Transl.)* **5**, 46–48 (1960).
29. Andriankin, E. I., Kogan, A. M., Kompaneets, A. S., and Krainov, V. P.
Propagation of a strong explosion in an inhomogeneous atmosphere, *Zh. Prikl. Mekhan. i Tekhn. Fiz.*, 1962, No. 6, 3–7.
30. Raizer, Yu. P.
Motion produced in an inhomogeneous atmosphere by a plane shock of short duration, *Soviet Phys. "Doklady" (English Transl.)* **8**, 1056–1058 (1964).
31. Raizer, Yu. P.
Propagation of a shock wave in an inhomogeneous atmosphere in the direction of decreasing density, *Zh. Prikl. Mekhan. i Tekhn. Fiz.*, 1964, No. 4, 49–56.
32. Raizer, Yu. P.
The deceleration and energy conversions of a plasma expanding in a vacuum in the presence of a magnetic field, *Zh. Prikl. Mekhan. i Tekhn. Fiz.*, 1963, No. 6, 19–28. Transl. as *NASA (Nat. Aeron. Space Admin.) Tech. Transl.* No. TTF-239 (1964).
33. Hayes, W. D.
Self-similar strong shocks in an exponential medium, *J. Fluid Mech.*, to appear.
34. Hayes, W. D.
The propagation upward of the shock wave from a strong explosion in the atmosphere, *J. Fluid Mech.*, to appear.

Appendix

Some often used constants, relations between units, and formulas*

Fundamental constants

Speed of light	$c = 2.998 \cdot 10^{10}$ cm/sec
Planck constant	$h = 6.625 \cdot 10^{-27}$ erg · sec
	$\hbar = h/2\pi = 1.054 \cdot 10^{-27}$ erg · sec
Electron charge	$e = 4.803 \cdot 10^{-10}$ esu
Electron mass	$m = 9.108 \cdot 10^{-28}$ g
Proton mass	$m_p = 1.673 \cdot 10^{-24}$ g
Mass of unit atomic weight	$M_0 = 1.660 \cdot 10^{-24}$ g
Boltzmann constant	$k = 1.380 \cdot 10^{-16}$ erg/deg
Universal gas constant	$\mathscr{R} = 8.317 \cdot 10^{7}$ erg/deg · mole
	$= 1.987$ cal/deg · mole
Avogadro number	$N_0 = 6.023 \cdot 10^{23}$ mole^{-1}
Loschmidt number	$n_0 = 2.687 \cdot 10^{19}$ cm^{-3}

Relations between units

Energy $E_0 = 1$ ev $= 1.602 \cdot 10^{-12}$ erg corresponds to:

temperature	$E_0/k = 11{,}605°\mathrm{K}$
frequency	$E_0/h = 2.418 \cdot 10^{14}$ sec^{-1}
wavelength	$hc/E_0 = 1.240 \cdot 10^{-4}$ cm $= 12{,}400$ Å
wave number	$E_0/hc = 8066$ cm^{-1}

* Values of the constants are taken from C. W. Allen, *Astrophysical Quantities*. (Athlone Press) Oxford Univ. Press, New York, 2nd edition, 1963. *Editors' note*. Some of the constants and numerical values in this appendix may differ slightly in the last significant figure from those used in the body of the text, which were based on constants given in the first edition (1955) of Allen's book.

In spectroscopy wave number is often used in place of frequency.

Wave number $1/\lambda = 1\ \text{cm}^{-1}$ corresponds to:

wavelength	$\lambda = 10^8$ Å
frequency	$\nu = 2.998 \cdot 10^{10}\ \text{sec}^{-1}$
temperature	$T = h\nu/k = 1.439°\text{K}$
photon energy	$h\nu = 1.240 \cdot 10^{-4}\ \text{ev} = 1.986 \cdot 10^{-16}\ \text{erg}$

$1\ \text{cal} = 4.185 \cdot 10^7\ \text{erg}$, $1\ \text{kcal} = 10^3\ \text{cal}$

1 ev per molecule corresponds to 23.05 kcal/mole

1 volt = 1/300 units of potential in esu

Constants and relations between them

Bohr radius $$a_0 = \frac{h^2}{4\pi^2 me^2} = \frac{\hbar^2}{me^2} = 0.529 \cdot 10^{-8}\ \text{cm}$$

Ionization potential of hydrogen atom $$I_\text{H} = \frac{e^2}{2a_0} = \frac{2\pi^2 e^4 m}{h^2} = \frac{e^4 m}{2\hbar^2} = 13.60\ \text{ev}$$

Rydberg constant $$Ry = \frac{I_\text{H}}{h} = \frac{2\pi^2 e^4 m}{h^3} = 3.290 \cdot 10^{15}\ \text{sec}^{-1}$$

Electron speed in first Bohr orbit $$v_0 = \frac{2\pi e^2}{h} = \frac{e^2}{\hbar} = 2.188 \cdot 10^8\ \text{cm/sec}$$

Classical electron radius $$r_0 = \frac{e^2}{mc^2} = 2.818 \cdot 10^{-13}\ \text{cm}$$

Compton wavelength $$\lambda_0 = \frac{h}{mc} = 2.426 \cdot 10^{-10}\ \text{cm}$$

$$\lambda\!\!\!^{-}_0 = \frac{\lambda_0}{2\pi} = \frac{\hbar}{mc} = 3.862 \cdot 10^{-11}\ \text{cm}$$

Rest mass energy of electron $$mc^2 = 511\ \text{kev} = 8.186 \cdot 10^{-7}\ \text{erg}$$

The number "137" = (fine structure constant)$^{-1}$ $\quad \dfrac{\hbar c}{e^2} = \dfrac{hc}{2\pi e^2} = 137.0$

Length ratio $\quad a_0 = \text{“}137\text{”}\,\lambda\!\!\!^{-}_0 = \text{“}137\text{”}^2 r_0$

Energy ratio $\quad mc^2 = 2I_H \cdot \text{“}137\text{”}^2$

Thomson cross section $\quad \varphi_0 = \dfrac{8}{3}\pi r_0^2 = 6.65 \cdot 10^{-25}\ \text{cm}^2$

Mass ratio proton/electron $\quad m_p/m = 1836$

Electric field of a proton at a distance of the first Bohr radius $\quad \dfrac{e^2}{a_0^2} = 1.715 \cdot 10^7\ \text{esu} = 5.145 \cdot 10^9\ \text{volt/cm}$

Area of spectral line with unit oscillator strength $\quad \dfrac{\pi e^2}{mc} = 0.0265\ \text{cm}^2/\text{sec}$

Atomic unit cross section $\quad \pi a_0^2 = 0.880 \cdot 10^{-16}\ \text{cm}^2$

Formulas

Radiant energy flux from surface of a perfect black body

$$S = \sigma T^4 = 5.67 \cdot 10^{-5} T_{\text{deg}}^4 = 1.03 \cdot 10^{12} T_{\text{ev}}^4\ \text{erg/cm}^2 \cdot \text{sec}$$

(σ = Stefan-Boltzmann constant)

Equilibrium radiant energy density

$$U_p = \frac{4\sigma T^4}{c} = 7.56 \cdot 10^{-15} T_{\text{deg}}^4 = 1.37 \cdot 10^2 T_{\text{ev}}^4\ \text{erg/cm}^3$$

Spectral equilibrium radiant energy density

$$U_{\nu p}\,d\nu = \frac{8\pi h\nu^3}{c^3}\,\frac{1}{e^{h\nu/kT}-1}\,d\nu \text{ erg/cm}^3$$

(maximum at the frequency $h\nu = 2.822\ kT$)

Spectral equilibrium radiation intensity

$$I_{\nu p}\,d\nu = \frac{cU_{\nu p}\,d\nu}{4}$$

$$= \frac{2h\nu^3}{c^2}\,\frac{d\nu}{e^{h\nu/kT}-1} \text{ erg/cm}^2 \cdot \text{sec} \cdot \text{sterad}$$

Saha equation

$$\frac{N_e N_+}{N_a} = A\,\frac{g_+}{g_a}\,T^{3/2}\,e^{-I/kT}$$

where

$$A = 2\left(\frac{2\pi mk}{h^2}\right)^{3/2} = 4.83 \cdot 10^{15}\ \text{cm}^{-3} \cdot \text{deg}^{-3/2}$$

$$= 6.04 \cdot 10^{21}\ \text{cm}^{-3} \cdot \text{ev}^{-3/2}$$

Maxwell distribution function normalized to unity

$$f(v)\,dv = 4\pi\left(\frac{m}{2\pi kT}\right)^{3/2} \exp\left(-\frac{mv^2}{2kT}\right) v^2\,dv$$

$$f(\varepsilon)\,d\varepsilon = \frac{2}{\pi^{1/2}}\,\frac{\varepsilon^{1/2}}{(kT)^{3/2}}\,e^{-\varepsilon/kT}\,d\varepsilon$$

Electron speed

$$v_e = 5.93 \cdot 10^7 \varepsilon_{\text{ev}}^{1/2} \text{ cm/sec}$$

Speed of particle with atomic weight A

$$v = 1.38 \cdot 10^6 (\varepsilon_{\text{ev}}/A)^{1/2} \text{ cm/sec}$$

Electron mean thermal speed

$$\bar{v}_e = \left(\frac{8kT}{\pi m}\right)^{1/2} = 6.21 \cdot 10^5 T_{\text{deg}}^{1/2}$$

$$= 6.69 \cdot 10^7 T_{\text{ev}}^{1/2} \text{ cm/sec}$$

Particle mean thermal speed

$$\bar{v} = 1.45 \cdot 10^4 \left(\frac{T_{\text{deg}}}{A}\right)^{1/2}$$

$$= 1.56 \cdot 10^6 \left(\frac{T_{\text{ev}}}{A}\right)^{1/2} \text{ cm/sec}$$

Classical damping constant

$$\gamma = \frac{8\pi^2 e^2 \nu^2}{3mc^3} = 2.47 \cdot 10^{-22} \nu_{\text{sec}}^2$$

$$= \frac{0.222 \cdot 10^{16}}{\lambda_{\text{Å}}^2} \text{ sec}^{-1}$$

Cross section σ in terms of P_c = average number of collisions per cm at 1 mm Hg and 0°C

$$\sigma = 2.83 \cdot 10^{-17} P_c \text{ cm}^2$$

Specific energy

$$1 \text{ ev/molecule} = \frac{9.65 \cdot 10^{11}}{M} \text{ erg/g}$$

where

M = molecular weight

Author Index

Volumes I and II

Numbers in brackets are reference numbers and are included to assist in locating references in which the authors' names are not mentioned in the text. Italicized numbers indicate the pages on which the references are listed, and those in parentheses the number of citations for the given page.

Volume I ends with page 464

Subject Index

Volumes I and II

Volume I ends with page 464